BEILSTEIN JOURNAL OF ORGANIC CHEMISTRY

Lipids: fatty acids and derivatives, polyketides and isoprenoids

Edited by Jeroen S. Dickschat

Imprint

Beilstein Journal of Organic Chemistry
www.bjoc.org
ISSN 1860-5397
Email: journals-support@beilstein-institut.de

The *Beilstein Journal of Organic Chemistry* is published by the Beilstein-Institut zur Förderung der Chemischen Wissenschaften.

Beilstein-Institut zur Förderung der Chemischen Wissenschaften
Trakehner Straße 7–9
60487 Frankfurt am Main
Germany
www.beilstein-institut.de

BEILSTEIN JOURNAL OF ORGANIC CHEMISTRY

Lipids: fatty acids and derivatives, polyketides and isoprenoids

Jeroen S. Dickschat

Editorial

Open Access

Address:
Kekulé-Institut für Organische Chemie und Biochemie, Rheinische Friedrich-Wilhelms-Universität Bonn, Gerhard-Domagk-Straße 1, D-53121 Bonn, Germany

Email:
Jeroen S. Dickschat - dickschat@uni-bonn.de

Keywords:
fatty acids; isoprenoids; polyketides

Beilstein J. Org. Chem. **2017,** *13,* 793–794.
doi:10.3762/bjoc.13.78

Received: 05 April 2017
Accepted: 21 April 2017
Published: 27 April 2017

This article is part of the Thematic Series "Lipids: fatty acids and derivatives, polyketides and isoprenoids".

Guest Editor: J. S. Dickschat

Lipids fulfill various functions in life as membrane constituents, for energy storage, or as signaling molecules. If the human lipid metabolism is disturbed, this may lead to serious illnesses such as adipositas and its subsequent complications including cardiovascular diseases or diabetes mellitus. Other consequences of a disordered lipid metabolism include brain dysfunctions, especially if the sphingolipid metabolism is affected, which can often be related to a specific genetic mutation. Sensu stricto, lipids are defined as apolar natural products that can be classified as fatty acids, whose derivatives are waxes, triacylglycerides, phospholipids, sphingolipids and glycolipids. Lipids also constitute important post-translational protein modifications in lipoproteins. The amphiphilic nature of compounds such as phospholipids with a polar headgroup and a long apolar chain results in the spontaneous formation of lipid bilayers in aqueous environments. This was likely a crucial process for the origin of life – and certainly still is for all existing living systems that necessarily contain lipid membranes with their interesting and finely balanced biophysical properties. In prokaryotes, these membranes define the outer surface of individual cells, while in addition to that in eukaryotic organisms membranes are of utmost importance also for cell compartmentation, i.e., the inner structure of a cell. A large portion of these membranes is composed of steroids that influence membrane properties, such as fluidity and permeability, but have a fundamentally different biosynthetic origin from fatty acids since they are made via terpene biosynthetic pathways. Nevertheless, steroids are highly apolar yet may contain a polar headgroup such as a 3-hydroxy function (as in lanosterol). Besides membrane formation, the highly apolar character of lipids has another important consequence for signaling compounds that travel with high speed in aqueous environments – an effect that is immediately recognizable if a drop of oil is spilled on a water surface. An impressive example is reported in this Thematic Series with the use of highly apolar lactones from the African reed frog that are likely amphibian signaling compounds [1]. Sensu lato, and this is the definition relevant to this Thematic Series: lipids include all kinds of apolar (or less polar) primary and secondary metabolites, including molecules that are formed via fatty acid biosynthesis, the biosynthetically related polyketide pathways, and

terpenoid biosynthesis. I hope that the present Thematic Series of the *Beilstein Journal of Organic Chemistry* on the interdisciplinary topic of "Lipids" will cover many topics of high interest to readers from chemistry, biochemistry, biophysics, medicine, pharmacy and related disciplines.

Jeroen S. Dickschat

Bonn, April 2017

Reference

1. Menke, M.; Peram, P. S.; Starnberger, I.; Hödl, W.; Jongsma, G. F. M.; Blackburn, D. C.; Rödel, M.-O.; Vences, M.; Schulz, S. *Beilstein J. Org. Chem.* **2016,** *12,* 2731–2738. doi:10.3762/bjoc.12.269

License and Terms

BEILSTEIN JOURNAL OF ORGANIC CHEMISTRY

Identification, synthesis and mass spectrometry of a macrolide from the African reed frog *Hyperolius cinnamomeoventris*

Markus Menke[1,§], Pardha Saradhi Peram[1,§], Iris Starnberger[2], Walter Hödl[2], Gregory F.M. Jongsma[3], David C. Blackburn[3], Mark-Oliver Rödel[4], Miguel Vences[5] and Stefan Schulz[*1]

Full Research Paper

Open Access

Address:
[1]Technische Universität Braunschweig, Institute of Organic Chemistry, Hagenring 30, 38106 Braunschweig, Germany, [2]Department for Integrative Zoology, Althanstraße 14, 1090 Vienna, Austria, [3]Florida Museum of Natural History, University of Florida, Gainesville, Florida 32611, United States of America, [4]Museum für Naturkunde, Leibniz Institute for Evolution and Biodiversity Science, Invalidenstr. 43, 10115 Berlin, Germany and [5]Technische Universität Braunschweig, Institute of Zoology, 38106 Braunschweig, Germany

Email:
Stefan Schulz[*] - stefan.schulz@tu-bs.de

* Corresponding author
§ Both authors share first authorship.

Keywords:
chemical communication; chiral gas chromatography; macrocyclic lactones; ring-closing metathesis; pheromones

Beilstein J. Org. Chem. **2016,** *12,* 2731–2738.
doi:10.3762/bjoc.12.269

Received: 28 September 2016
Accepted: 02 December 2016
Published: 13 December 2016

This article is part of the Thematic Series "Lipids: fatty acids and derivatives, polyketides and isoprenoids".

Guest Editor: J. S. Dickschat

Abstract

The contents of the gular glands of the male African reed frog *Hyperolius cinnamomeoventris* consist of a mixture of aliphatic macrolides and sesquiterpenes. While the known macrolide gephyromantolide A was readily identified, the structure of another major component was suggested to be a tetradecen-13-olide. The synthesis of the two candidate compounds (Z)-5- and (Z)-9-tetradecen-13-olide revealed the former to be the naturally occurring compound. The synthesis used ring-closing metathesis as key step. While the Hoveyda–Grubbs catalyst furnished a broad range of isomeric products, the (*Z*)-selective Grubbs catalyst lead to pure (*Z*)-products. Analysis by chiral GC revealed the natural frog compound to be (5*Z*,13*S*)-5-tetradecen-13-olide (**1**). This compound is also present in the secretion of other hyperoliid frogs as well as in femoral glands of male mantellid frogs such as *Spinomantis aglavei*. The mass spectra of the synthesized macrolides as well as their rearranged isomers obtained during ring-closing metathesis showed that it is possible to assign the location of the double bond in an unsaturated macrolide on the basis of its EI mass spectrum. The occurrence of characteristic ions can be explained by the fragmentation pathway proposed in the article. In contrast, the localization of a double bond in many aliphatic open-chain compounds like alkenes, alcohols or acetates, important structural classes of pheromones, is usually not possible from an EI mass spectrum. In the article, we present the synthesis and for the first time elucidate the structure of macrolides from the frog family Hyperoliidae.

Introduction

The lactone motif is found in many compounds that are used in chemical communication. Among them, macrocyclic lactones are an important class because of their biosynthetic availability and their inherent compound properties. During the biosynthesis of macrocyclic lactones, a fatty acid precursor is often oxidized near the end of the chain to form a polar hydroxy acid. The following ring-closure reduces the hydrophilicity of the compound and increases its vapor pressure, making the resulting macrocycle well-suited to serve as a signal [1]. Fatty acid derived macrolactones were therefore repeatedly invented during evolution and are used by different animals such as bees, beetles, butterflies, cockroaches, or frogs as pheromones [1].

Finding and choosing mates in frogs is usually regarded as being primarily acoustically mediated. Nevertheless, some families like the Mantellidae from Madagascar also use chemical cues. Macrocyclic lactones such as phoracantholide I (**3**), phoracantholide J (**4**) or gephyromantolide A (**5**), are released by males from femoral glands to serve as signals, often accompanied by secondary alcohols (Figure 1) [2-4]. Another frog family most likely using volatile compounds during courtship are the African reed frogs, Hyperoliidae. The males of most species emit acoustic cues to attract females. During the call, an often conspicuously colored gland on their vocal sac (the gular gland), only innervated during the mating season in at least some species, releases a complex blend of volatiles when exposed [5]. A first analysis revealed the presence of mostly unknown terpenes, macrolides and other components in species specific compositions [5].

Detailed exploration of the function of these frog volatiles requires the analysis of the secretion and the synthesis of the identified compounds for biological testing. Because of the small amount of natural material available, only GC–MS investigations can be used to identify the compounds. The analysis revealed unsaturated macrocyclic lactones to be major constituents of the secretion of the cinnamon-bellied reed frog, *Hyperolius cinnamomeoventris*. The location and configuration of the double bond might be relevant for their function, as it is the case in many insect pheromones. In typical pheromone components of insects, including long chain alkenes, alkenols, or unsaturated aldehydes, the location of the double bond can usually not be determined by analysis of their mass spectra. Positional isomers often exhibit almost identical spectra [6] and derivatization or special mass spectrometric techniques are needed to localize double bonds [7-9]. Because this might also be the case for macrolides [10], it is of interest for their identification to compare mass spectra of positional isomers of unsaturated macrolactones. Furthermore, a fast synthetic strategy is needed to synthesize various isomers. In the present work we describe 1) the identification of macrolides from *H. cinnamomeoventris*, 2) discuss EI mass spectra of unsaturated macrolactones, and 3) show how ring-closing metathesis reaction conditions can be selected to obtain either pure compounds or a library of compounds useful for evaluation of their mass spectra.

Results and Discussion

The GC–MS analysis of a gular gland extract of *Hyperolius cinnamomeoventris* showed the presence of several unknown compounds, sesquiterpenes and macrolides (Figure 2).

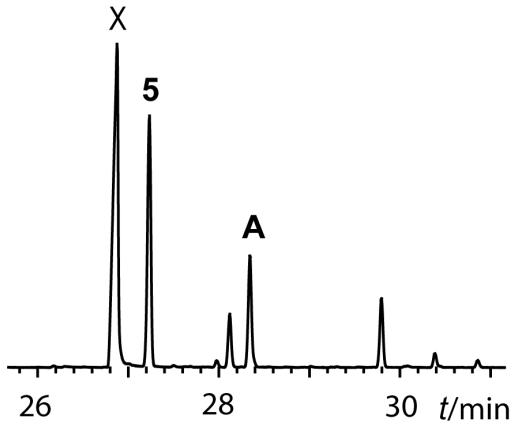

Figure 2: Total ion chromatogram of the gular gland extract of *Hyperolius cinnamomeoventris*. X: frog anaesthetic ethyl 3-aminobenzoate.

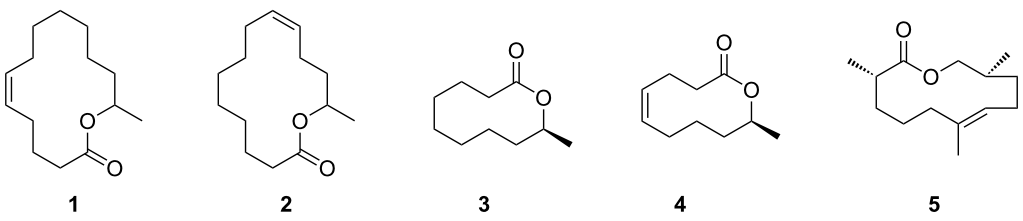

Figure 1: Macrolactones produced in scent glands of frogs: (*Z*)-Tetradec-5-en-13-olide (**1**) or (*Z*)-tetradec-9-en-13-olide (**2**), phoracantolide I (**3**), phoracantolide J (**4**), gephyromantolide A (**5**).

Gephyromantolide A (**5**), known from the mantellid frog *Gephyromantis boulengeri* [4], was readily identified. A second macrolide (**A** in Figure 2) showed a mass spectrum similar to that reported for (*Z*)-tetradec-5-en-13-olide (**1**) by Millar et al. [11], exhibiting a molecular ion at *m/z* 224. This macrolide, called cucujolide III, is used by the flat grain beetle *Cryptolestes pusillus* as pure (*S*)-enantiomer and by *C. turcicus* as a 33:67 *R*/*S* mixture [12], and acts as a synergist to the respective pheromones [11,13]. Microhydrogenation of the frog extract furnished 13-tetradecanolide, thus confirming compound **A** to be a 13-tetradecenolide. The double bond position in this macrolide likely is at C-5, because of the similarity of the mass spectrum to that of the beetle macrolide. Nevertheless, because locating double bonds in such compounds based on the mass spectrum alone seemed not to be reliable, we opted to synthesize two positional isomers.

Compound **1** is biosynthetically formed by the *Cryptolestes* beetles starting from oleic acid [14] that is shortened to 5-tetradecenoic acid, followed by ω − 1 oxidation and ring closure [15]. Another possibility would be that a common saturated acid such as stearic acid is chain-shortened first to tetradecanoic acid, on which a common Δ9-desaturase is acting, leading after ω − 1 oxidation and ring closure to tetradec-9-en-13-olide (**2**). Therefore, we opted to synthesize **2** as well.

To allow later enantiomer determination of **A**, an enantioselective synthetic strategy was followed. Several synthetic routes for the synthesis of **1** have been reported [16-20]. These syntheses were performed before the advent of ring-closing metathesis (RCM), requiring more than 10 steps each. RCM can shorten the synthesis remarkably, but requires careful selection of the RCM catalyst to control the double bond configuration. For example, Fürstner and Langemann obtained *rac*-**1** in 31:69 (*E*/*Z*)-mixture using a Ru-carbene type catalyst similar to a Grubbs I catalyst [21].

The synthesis of (*R*)-**2** using RCM as key step is shown in Scheme 1. Enantiomerically pure 1,2-epoxyhex-5-ene (**6**) was obtained by Jacobsen hydrolytic kinetic resolution on commercially available **6** (Scheme 1) [22,23]. Surprisingly, the yield of 69% of the (*R*)-enantiomer was higher than the theoretically upper limit of 50%. We discovered that **6**, sold by Acros Organics as racemic compound, was actually enriched in the

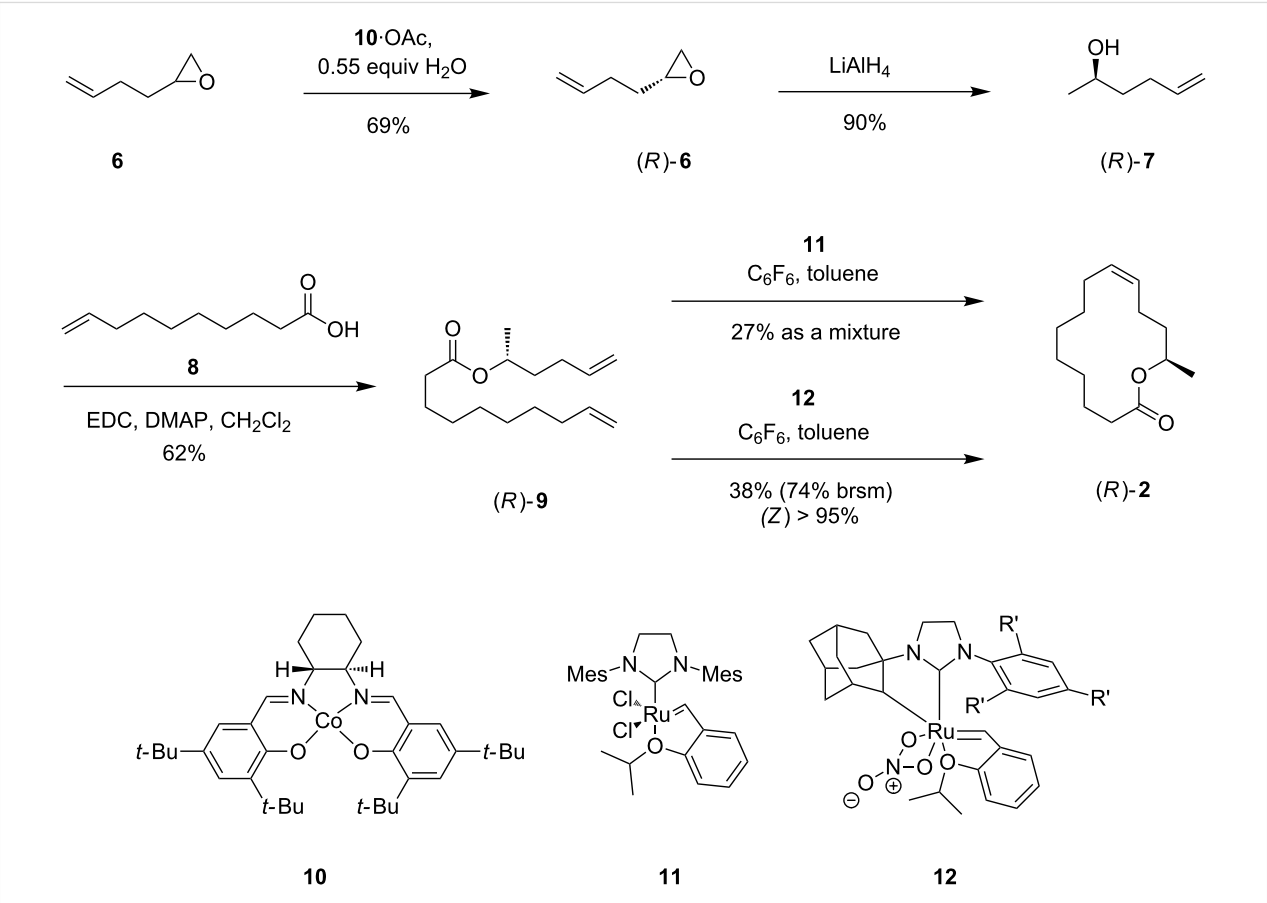

Scheme 1: Synthesis of (9*Z*,13*R*)-tetradec-9-en-13-olide (**2**).

desired (*R*)-enantiomer (see Supporting Information File 1 for optical rotation values). Diene (*R*)-**9** was obtained by reduction of the epoxide **6** with $LiAlH_4$ to form alcohol (*R*)-**7**, followed by esterification with 9-decenoic acid (**8**) using 1-ethyl-3-(3-dimethylaminopropyl)carbodiimide (EDC) and 4-(dimethylamino)pyridine (DMAP) [24,25]. The following RCM was performed using Grubbs–Hoveyda II catalyst (**11**) and hexafluorobenzene as an additive [26]. During the reaction isomerization occurred, leading to a mixture of positional isomers and chain shortened as well as elongated products. Addition of *p*-benzoquinone [27] and improved purification methods [28] suppressed isomer formation only partially. Replacing catalyst **11** with the Grubbs second generation catalyst (1,3-bis(2,4,6-trimethylphenyl)-2-imidazolidinylidene)dichloro(phenylmethylene)(tricyclohexylphosphine)ruthenium reduced the isomerization, leading to an (*E*/*Z*)-mixture of **2**. Finally, the (*Z*)-selective Grubbs catalyst **12** furnished the best results [29,30]. This catalyst yielded only the desired product (*R*)-**2** with a (*Z*)-configured double bond, although in moderate yield (see Supporting Information File 1 for full experimental data).

A similar synthetic strategy was applied for the synthesis of macrolide **1** (Scheme 2). The stereogenic center was introduced using commercially available (*R*)-propylene oxide (**13**) as starting material. After copper-catalyzed opening of the epoxide with 6-heptenylmagnesium bromide obtained from 7-bromo-1-heptene (**14**) and Steglich esterification with 5-hexenoic acid (**16**), RCM using (*Z*)-selective Grubbs catalyst **12** was used to synthesize macrolide (*R*)-**1** without any isomerization. Comparison of the mass spectra (Figure 3) and gas chromatographic retention times of pure (*Z*)-**1**, the (*E*/*Z*)-mixture obtained by the Hoyveda–Grubbs II catalyst, and **2** with those of the natural compound proved the frog compound to be (*Z*)-tetradec-5-en-13-olide (**1**).

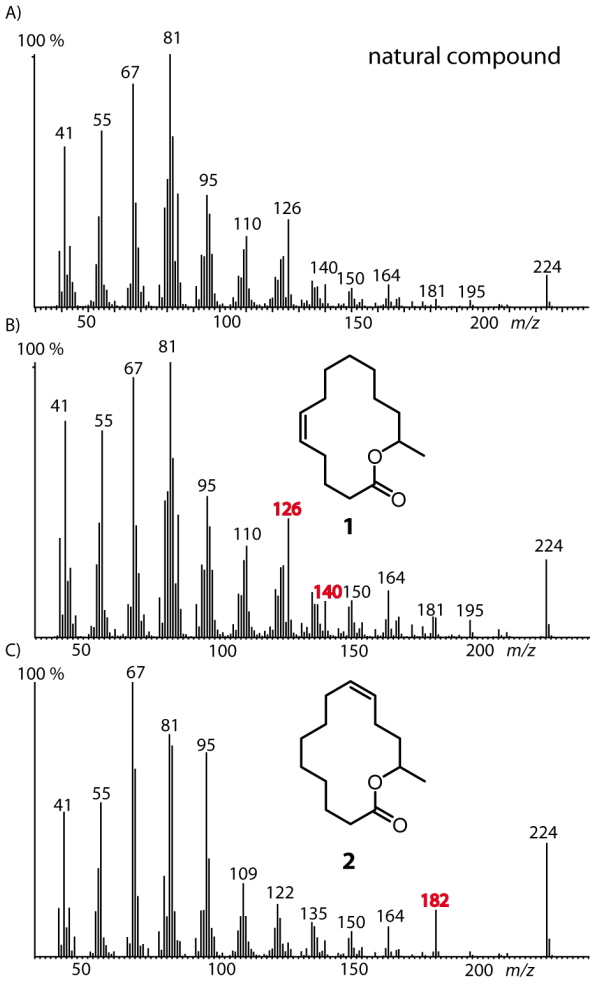

Figure 3: Mass spectra of A) the natural compound **A**, B) (*Z*)-tetradec-5-en-13-olide (**1**), and C) (*Z*)-tetradec-9-en-13-olide (**2**). Characteristic ions useful for location of the double bond are marked in red.

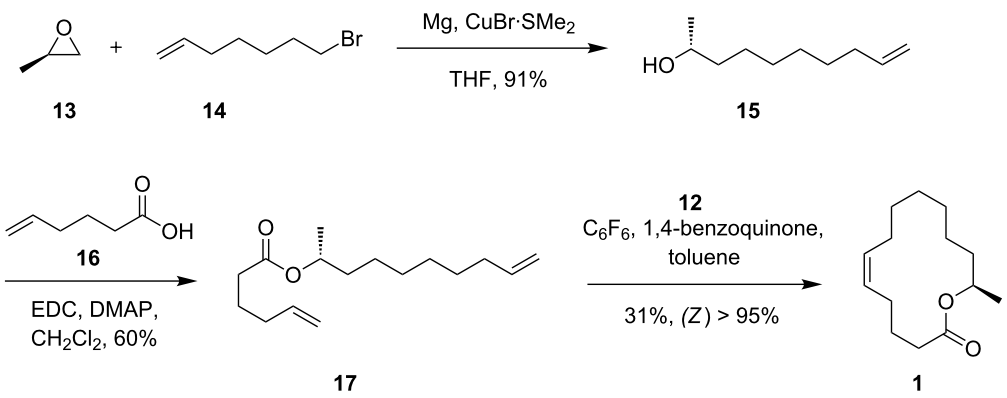

Scheme 2: Synthesis of (5*Z*,13*R*)-tetradec-5-en-13-olide ((*R*)-**1**). The enantiomer was obtained in a similar sequence, starting from (*S*)-propylene oxide instead of **13**.

For the determination of the absolute configuration of the natural compound, the other enantiomer (*S*)-**1** was needed as well. It was synthesized according to the synthesis shown in Scheme 2, starting from (*S*)-propylene oxide instead of the (*R*)-enantiomer **13**. The stereochemistry was determined by chiral gas chromatography as shown in Figure 4. The coinjection of pure (*S*)-**1** with the racemic mixture proved the first eluting peak to be this enantiomer. Injection of the natural sample as well as (*S*)-**1** showed both compounds to be enantiomerically pure. Finally, coinjection of both samples showed their identity.

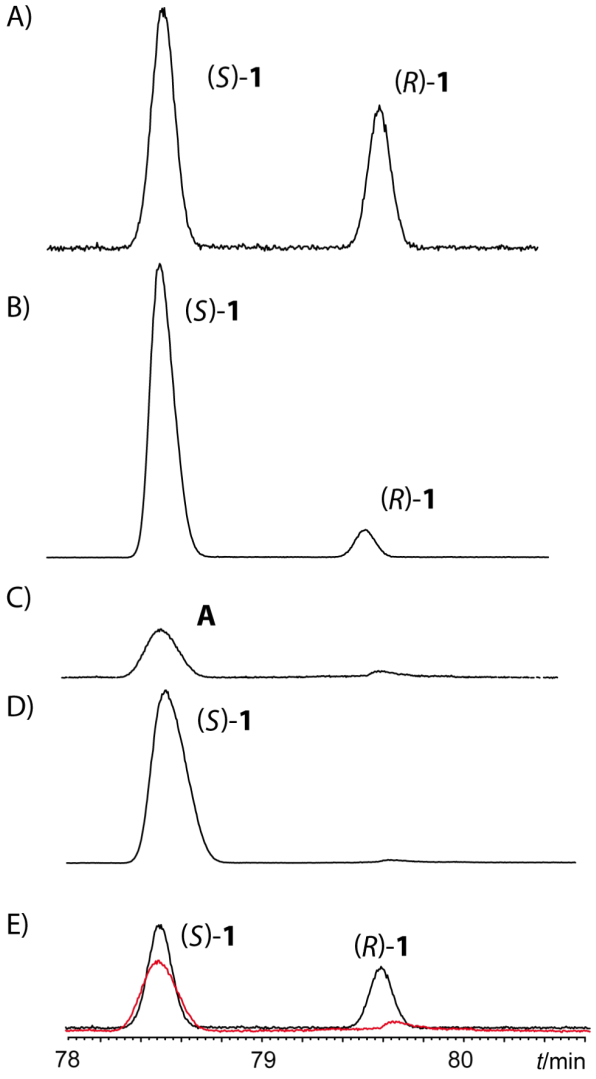

Figure 4: Total ion chromatogram of the enantiomer separation of (*Z*)-**1** on a chiral β-TBDMS- Hydrodex phase. Temperature program: isothermal for 60 min at 110 °C, then with 2 °C/min to 160 °C, followed by a sharp ramp with 25 °C/min to 220 °C. A) Racemic mixture, B) coinjection of racemic mixture and (*S*)-**1**, C) natural extract, D) coinjection of the natural extract and (*S*)-**1**, E) Overlay of A and C showing that the minor peak present in the extract is not the (*R*)-enantiomer of **1**. Black: racemate, red: natural extract. Peak identities were confirmed by mass spectrometry.

With the synthetic material in hand, we analyzed the EI mass spectra of **1** and **2**. No significant differences were detectable between the *E*/*Z*-isomers of each compound. Nevertheless, contrary to open chain compounds, characteristic differences could be found for the positional isomers. While most ions are similar in both spectra, the prominent ion *m/z* 126 present in **1** is shifted to *m/z* 182 in **2**. These ions can be used to assign the location of the double bond in the macrocyclic ring.

A possible fragmentation pathway leading to these ions is shown in Figure 5. One can speculate that after ionization of the double bond in **1** an allylic cleavage occurs, leading to the radical cation **18** along pathway a. An additional bond cleavage of a C–O single bond releases a neutral molecule, e.g., methylcyclohexane, giving rise to ion *m/z* 126 (**20**). High-resolution mass spectral data support the hypothesis because the ions *m/z* 126 as well as *m/z* 182 (**25**) formed from **2** have a molecular composition of $C_7H_{10}O_2$ (HRMS: 126.07005 found, calcd. 126.0681) or $C_{11}H_{18}O_2$ (HRMS: found 182.13206, calcd. 182.1307), respectively. Ion **20** is accompanied by the ion *m/z* 140 (HRMS: found 140.08545, calcd. 140.08373) of the same ion series $C_nH_{2n-4}O_2$ that occurs in lower abundance. Its formation along pathway b can be explained by homoallylic cleavage of **18** into **21** and further fragmentation into **22**. The formation of the ions of this series is obviously determined by the position of the double bond in the chain. Therefore, ion *m/z* 182 of **2** arises by the same mechanism, indicating the location of the double bond at C-9 (Figure 5). A b-type ion cannot be formed, because pathway b is not operative due to the close proximity of the C–O group. The pathways shown in Figure 5 are speculative. Another possible mechanisms leading to the same ions and starting with ionization of the C–O oxygen atom instead of the double bond is shown in Supporting Information File 1 (see Figure S1). Nevertheless, the proposal is useful to predict the position of double bonds in mono-unsaturated macrolides. This position can be deduced from the ion $C_{n+4}H_{2n+4}O_2$, generated by a double bond in the $n + 2$ position, as shown in **26**.

We subsequently tested our method with mass spectra of other macrolides previously reported or present in our compound library. In the mass spectra of (*Z*)-octadec-9-en-13-olide [31] and octadec-9-en-17-olide peaks at *m/z* 182 with higher and *m/z* 196 with lower intensity are present, consistent with a C-9 double bond. In contrast, (*Z*)-octadec-11-en-13-olide does not show such ions, because the close proximity of the double bond and the C–O group does not allow fragmentation along pathway a or b. The spectra of 4-methyl-5-decen-9-olide and 8-methyl-5-decen-9-olide [3] exhibit the expected ions *m/z* 140 and *m/z* 126, respectively. Pathway b is not operative because of the proximity of the C–O group. A slight alteration of the frag-

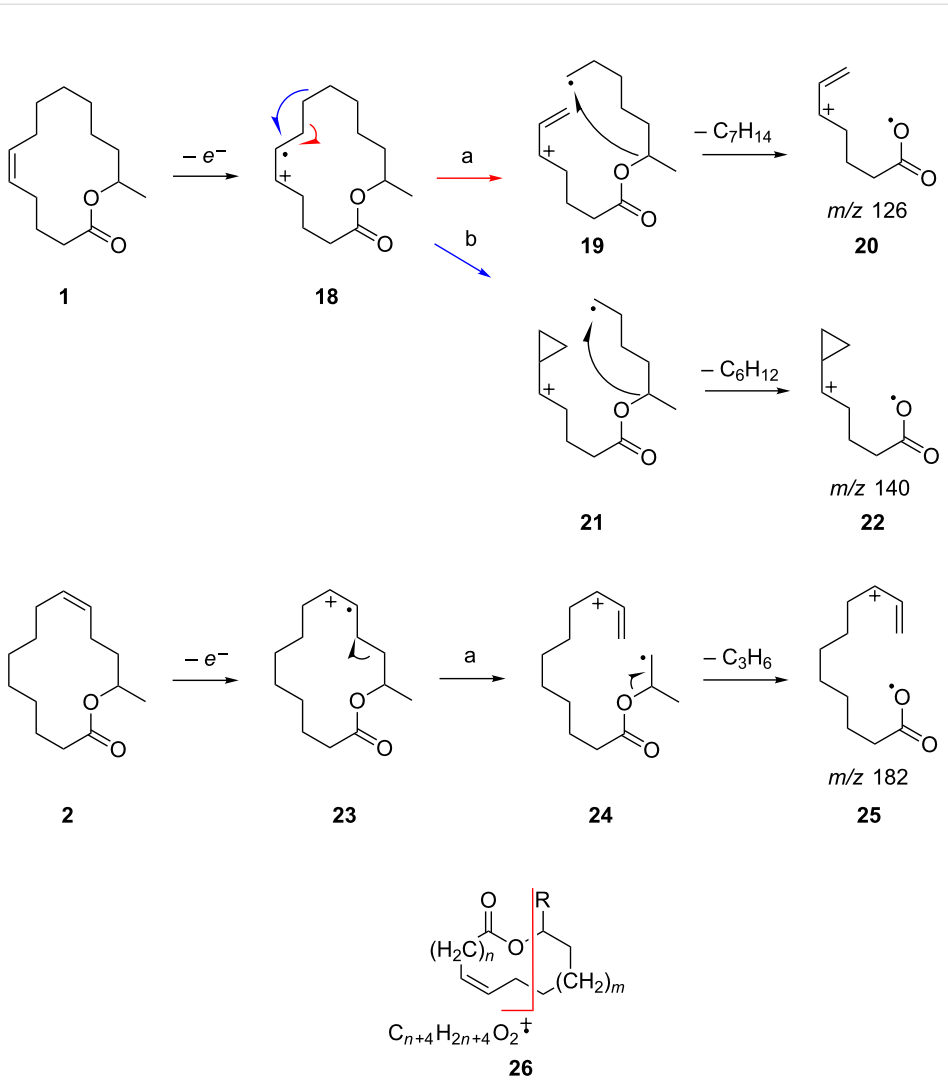

Figure 5: Proposed mass spectrometric fragmentation of macrolides **1** and **2** leading to diagnostic ions of the ion series $C_nH_{2n-4}O_2$ ($C_{n+4}H_{2n+4}O_2$ in the figure), indicating the position of the double bond in the ring.

mentation can be observed if the double bond is located at C-4, as in phoracantholide J, 4-decen-9-olide [32]. Now in pathway a, additionally an H-atom is transferred leading to the uneven ion $C_nH_{2n-3}O_2$, *m*/*z* 113, while pathway b remains unchanged, furnishing *m*/*z* 126. In the methylated analog 6-methyl-4-decen-9-olide [3], these ions shift to *m*/*z* 127 and 140. If the double bond moves closer to the C=O group as in 3-dodecen-11-olide [33], both ions a and b are visible, but their abundance is so low that their diagnostic value is largely decreased. Another limitation is that mass spectra of unsaturated unbranched macrolactones, formally derived from ω-hydroxy acids, do not show the characteristic ions generated by pathways a or b. Obviously, the primary C–O bond is not attacked by intermediates like **19**. Nevertheless, the mass spectrometric interpretation presented here will largely ease the identification of a broad range of unsaturated macrolides. The procedure may also be applicable for di- or triunsaturated compounds.

We then focused on the products of the RCM using the Hoveyda–Grubbs II catalyst **11**. It is well known that during RCM isomerization of the double bond might occur, especially with the Grubbs second generation catalysts, leading to products with migrated double bonds or smaller ring size [27,34-36]. Both types of products, 11-dodecenolides, 12-tridecenolides and isomerized 13-tetradecenolides were obtained. In addition, ring expanded 14-pentadecenolides were observed. The latter can be explained by dimerization of esters **9** or **17**, isomerization of the double bond, and final ring closure, leading to either ring-contracted or expanded products. Such processes have been reported before in polymerization experiments using Grubbs cata-

lysts [36-38]. While the isomerization is usually regarded as a negative side reaction in RCM, it turned out to be advantageous for the identification of naturally occurring macrolides in our hands. The isomerized mixtures constitute a library of closely related macrolides differing slightly in position of double bonds and ring size. With the diagnostic mass spectrometric ions discussed above, each compound can be assigned a structure after GC–MS analysis. These mass spectra together with the gas chromatographic retention index are stored in our EIMS database, easing identification of similar compounds in the future. Using this approach, we could collect mass spectra of 5-dodecen-11-olide, 5- and 6-tridecen-12-olide, 5- to 9-tetradecen-13-olide, as well as 5- and 6-pentadec-14-olide (see Supporting Information File 1 for some spectra). This set of mass spectra allowed the identification of macrolides in other frog species.

We also found macrolide **1** in the gular glands of other hyperoliids including *H. concolor*, *H. adametzi*, and *Afrixalus dorsalis*. It occurs also outside this frog family. It is a major constituent of the femoral gland of the mantellid frog *Spinomantis aglavei,* again in (*S*)-configuration. Minor amounts of **1** were also present in the glands of an undescribed species of *Guibemantis* similar to *G. bicalcaratus* as well as in *Gephyromantis ceratophrys*, accompanied by the isomer 8-tetradecen-13-olide in the latter species.

Conclusion

RCM using the (*Z*)-selective Grubbs catalyst **12** is a convenient strategy to prepare unsaturated macrocyclic lactones in a short sequence. Although isomerization is usually regarded as a disadvantage of RCM, it can be used to allow fast access to mass spectra of several isomers, helpful for the structure elucidation of natural compounds, e.g., in chemical ecology or fragrance research. The mass spectral fragmentation of macrolides differs markedly from that of open-chain esters, because initial bond cleavage often does not lead to the release of an uncharged radical, but to the formation of a distonic cationic radical prone to further fragmentation. The analysis of the fragmentation led to a rationale for the determination of the bound bond position in unsaturated macrolides. The identification of **1** and **5** in the gular gland of *H. cinnamomeoventris* and other species underlines the importance of macrolides for the chemical ecology of hyperoliid and mantellid frogs. On the contrary, other compounds such as the terpenes commonly found in hyperoliids remain largely unknown. Their identification and synthesis are a priority and would constitute a major step towards a biological evaluation of the gland secretion and its compounds to understand their real function in the behavior of the frogs. Although no experimental evidence has been obtained so far, the close association of the innervation of the gland with the mating period, its location and use during calling, and its male-specific occurrence strongly hint to a function of **1** and **5** as signaling compounds and a role in the chemical ecology of this species.

Supporting Information

Supporting Information File 1

Experimental procedures, mass spectra of macrolides, alternative fragmentation pathway, enantiomer separation by GC–MS, ^{1}H and ^{13}C NMR spectra.
[http://www.beilstein-journals.org/bjoc/content/supplementary/1860-5397-12-269-S1.pdf]

Acknowledgements

Work in Madagascar was carried out in the framework of a collaboration accord between TU Braunschweig and the Université d'Antananarivo, Département de Biologie Animale. We are grateful to the Malagasy authorities for research and export permits. Specimen collection in Rwanda was conducted within a collaboration between the University of Vienna and the University of Koblenz-Landau, Germany. We would like to particularly thank M. Dehling and P. M. Maier for their support. Specimen collection and export was authorized by the Rwanda Development Board. The Cameroon Ministry of Forests and Wildlife (MINFOF) and Ministry of Scientific Research and Innovation (MINRESI) provided necessary permits for conducting research and exportation in Cameroon.

Our study received financial support from the Deutsche Forschungsgemeinschaft (DFG Schu984/10-1, MM, PP, SS), the Austrian Science Fund (FWF): P25612 (IS, WH), and the US National Science Foundation (DEB-1202609, DCB), and under the approval of the Institutional Animal Care and Use Committee (2014-2) at the California Academy of Sciences.

References

1. Schulz, S.; Hötling, S. *Nat. Prod. Rep.* **2015,** *32,* 1042–1066. doi:10.1039/C5NP00006H
2. Hötling, S.; Haberlag, B.; Tamm, M.; Collatz, J.; Mack, P.; Steidle, J. L. M.; Vences, M.; Schulz, S. *Chem. – Eur. J.* **2014,** *20,* 3183–3191. doi:10.1002/chem.201304414
3. Poth, D.; Peram, P. S.; Vences, M.; Schulz, S. *J. Nat. Prod.* **2013,** *76,* 1548–1558. doi:10.1021/np400131q
4. Poth, D.; Wollenberg, K. C.; Vences, M.; Schulz, S. *Angew. Chem., Int. Ed.* **2012,** *51,* 2187–2190. doi:10.1002/anie.201106592
5. Starnberger, I.; Poth, D.; Peram, P. S.; Schulz, S.; Vences, M.; Knudsen, J.; Barej, M. F.; Rödel, M.-O.; Walzl, M.; Hödl, W. *Biol. J. Linn. Soc.* **2013,** *110,* 828–838. doi:10.1111/bij.12167
6. Ando, T.; Yamakawa, R. *TrAC, Trends Anal. Chem.* **2011,** *30,* 990–1002. doi:10.1016/j.trac.2011.03.010

7. Buser, H. R.; Arn, H.; Guerin, P.; Rauscher, S. *Anal. Chem.* **1983,** *55,* 818–822. doi:10.1021/ac00257a003
8. Jham, G. N.; Attygalle, A. B.; Meinwald, J. *J. Chromatogr. A* **2005,** *1077,* 57–67. doi:10.1016/j.chroma.2005.01.073
9. Kroiss, J.; Svatoš, A.; Kaltenpoth, M. *J. Chem. Ecol.* **2011,** *37,* 420–427. doi:10.1007/s10886-011-9933-4
10. Francke, W. *Chemoecology* **2010,** *20,* 163–169. doi:10.1007/s00049-010-0048-0
11. Millar, J. G.; Pierce, H. D., Jr.; Pierce, A. M.; Oehlschlager, A. C.; Borden, J. H.; Barak, A. V. *J. Chem. Ecol.* **1985,** *11,* 1053–1070. doi:10.1007/BF01020675
12. Oehlschlager, A. C.; King, G. G. S.; Pierce, H. D., Jr.; Pierce, A. M.; Slessor, K. N.; Millar, J. G.; Borden, J. H. *J. Chem. Ecol.* **1987,** *13,* 1543–1554. doi:10.1007/BF01012296
13. Millar, J. G.; Pierce, H. D., Jr.; Pierce, A. M.; Oehlschlager, A. C.; Borden, J. H. *J. Chem. Ecol.* **1985,** *11,* 1071–1081. doi:10.1007/BF01020676
14. Vanderwel, D.; Pierce, H. D., Jr.; Oehlschlager, A. C.; Borden, J. H.; Pierce, A. M. *Insect Biochem.* **1990,** *20,* 567–572. doi:10.1016/0020-1790(90)90068-6
15. Vanderwel, D.; Johnston, B.; Oehlschlager, A. C. *Insect Biochem. Mol. Biol.* **1992,** *22,* 875–883. doi:10.1016/0965-1748(92)90114-T
16. Millar, J. G.; Oehlschlager, A. C.; Wong, J. W. *J. Org. Chem.* **1983,** *48,* 4404–4407. doi:10.1021/jo00171a055
17. Sakai, T.; Hamamoto, H.; Mori, K. *Agric. Biol. Chem.* **1986,** *50,* 1621–1627.
18. Naoshima, Y.; Nakamura, A.; Munakata, Y.; Kamezawa, M.; Tachibana, H. *Bull. Chem. Soc. Jpn.* **1990,** *63,* 1263–1265. doi:10.1246/bcsj.63.1263
19. Hamada, T.; Daikai, K.; Irie, R.; Katsuki, T. *Synlett* **1995,** 407–408. doi:10.1055/s-1995-5001
20. Mori, K.; Tomioka, H. *Liebigs Ann. Chem.* **1992,** 1011–1017. doi:10.1002/jlac.1992199201167
21. Fürstner, A.; Langemann, K. *J. Org. Chem.* **1996,** *61,* 3942–3943. doi:10.1021/jo960733v
22. Breinbauer, R.; Jacobsen, E. N. *Angew. Chem., Int. Ed.* **2000,** *39,* 3604–3607. doi:10.1002/1521-3773(20001016)39:20<3604::AID-ANIE3604>3.0.CO;2-9
23. Schaus, S. E.; Brandes, B. D.; Larrow, J. F.; Tokunaga, M.; Hansen, K. B.; Gould, A. E.; Furrow, M. E.; Jacobsen, E. N. *J. Am. Chem. Soc.* **2002,** *124,* 1307–1315. doi:10.1021/ja016737l
24. Neises, B.; Steglich, W. *Angew. Chem., Int. Ed. Engl.* **1978,** *17,* 522–524. doi:10.1002/anie.197805221
25. Searles, S., Jr.; Pollart, K. A.; Lutz, E. F. *J. Am. Chem. Soc.* **1957,** *79,* 948–951. doi:10.1021/ja01561a046
26. Rost, D.; Porta, M.; Gessler, S.; Blechert, S. *Tetrahedron Lett.* **2008,** *49,* 5968–5971. doi:10.1016/j.tetlet.2008.07.161
27. Hong, S. H.; Sanders, D. P.; Lee, C. W.; Grubbs, R. H. *J. Am. Chem. Soc.* **2005,** *127,* 17160–17161. doi:10.1021/ja052939w
28. Maynard, H. D.; Grubbs, R. H. *Tetrahedron Lett.* **1999,** *40,* 4137–4140. doi:10.1016/S0040-4039(99)00726-1
29. Herbert, M. B.; Grubbs, R. H. *Angew. Chem., Int. Ed.* **2015,** *54,* 5018–5024. doi:10.1002/anie.201411588
30. Marx, V. M.; Herbert, M. B.; Keitz, B. K.; Grubbs, R. H. *J. Am. Chem. Soc.* **2013,** *135,* 94–97. doi:10.1021/ja311241q
31. Schulz, S.; Yildizhan, S.; Stritzke, K.; Estrada, C.; Gilbert, L. E. *Org. Biomol. Chem.* **2007,** *5,* 3434–3441. doi:10.1039/b710284d
32. Moore, B. P.; Brown, W. V. *Aust. J. Chem.* **1976,** *29,* 1365–1374. doi:10.1071/CH9761365
33. Wong, J. W.; Verigin, V.; Oehlschlager, A. C.; Borden, J. H.; Pierce, H. D., Jr.; Pierce, A. M.; Chong, L. *J. Chem. Ecol.* **1983,** *9,* 451–474. doi:10.1007/BF00990219
34. Fürstner, A.; Thiel, O. R.; Ackermann, L.; Schanz, H.-J.; Nolan, S. P. *J. Org. Chem.* **2000,** *65,* 2204–2207. doi:10.1021/jo9918504
35. Lehman, S. E., Jr.; Schwendeman, J. E.; O'Donnell, P. M.; Wagener, K. B. *Inorg. Chim. Acta* **2003,** *345,* 190–198. doi:10.1016/S0020-1693(02)01307-5
36. van Lierop, B. J.; Lummis, J. A. M.; Fogg, D. E. Ring-closing metathesis. In *Olefin Metathesis: Theory and Practice;* Grela, K., Ed.; Wiley: Hoboken, 2014; pp 85–152. doi:10.1002/9781118711613.ch3
37. Courchay, F. C.; Sworen, J. C.; Wagener, K. B. *Macromolecules* **2003,** *36,* 8231–8239. doi:10.1021/ma0302964
38. Petkovska, V. I.; Hopkins, T. E.; Powell, D. H.; Wagener, K. B. *Macromolecules* **2005,** *38,* 5878–5885. doi:10.1021/ma050480k

License and Terms

BEILSTEIN JOURNAL OF ORGANIC CHEMISTRY

Benzothiadiazole oligoene fatty acids: fluorescent dyes with large Stokes shifts

Lukas J. Patalag and Daniel B. Werz*

Full Research Paper

Open Access

Address:
Institut für Organische Chemie, Technische Universität Braunschweig, Hagenring 30, 38106 Braunschweig, Germany

Email:
Daniel B. Werz* - d.werz@tu-braunschweig.de

* Corresponding author

Keywords:
fatty acid; fluorescence; lipid; membrane; Stokes shift

Beilstein J. Org. Chem. **2016,** *12,* 2739–2747.
doi:10.3762/bjoc.12.270

Received: 27 October 2016
Accepted: 01 December 2016
Published: 14 December 2016

This article is part of the Thematic Series "Lipids: fatty acids and derivatives, polyketides and isoprenoids".

Guest Editor: J. S. Dickschat

Abstract

Herein, we report on the synthesis and characterization of novel fluorescent fatty acids with large Stokes shifts. Three examples consisting of the same number of carbon atoms and thus of similar chain length are presented differing in their degree of unsaturation. As major fluorogenic contributor at the terminus benzo[*c*][1,2,5]thiadiazole was used. Respective syntheses based on Wittig reactions followed by iodine-mediated isomerization are presented. The absorption properties are modulated by the number of conjugated C=C double bonds of the oligoene chain ranging from one to three. Large Stokes shifts of about 4900–5700 cm^{-1} and fluorescence quantum yields of up to 0.44 were observed.

Introduction

The membrane of living cells consists of a variety of lipids. More than 40 years ago, biological membranes were first described as Fluid Mosaic in which proteins were embedded [1]. During recent decades it became more and more clear that such a simple model is not sufficient to understand membrane dynamics and function. Often membrane domains are formed in which certain lipids, glycolipids or proteins are enriched [2-4]. Such domains – also called lipid rafts – do not only differ in their chemical composition, but also show different physical properties (e.g., differences in membrane thickness and stiffness, different diffusion coefficients etc.) [5,6]. Tools to investigate lipid membranes are multifaceted; however, all optical methods are hampered by the missing absorption and fluorescence properties of natural occurring lipid components. Therefore, indirect methods are commonly employed. Either unnatural fluorescent dyes are inserted into the membrane (e.g., pyrene) or the hydrophilic part of lipids is utilized for the covalent attachment of fluorophores. Another possibility is the use of fluorescently labelled antibodies which bind membrane components such as the carbohydrate part of glycolipids [7,8]. A further alternative is to render the lipid and especially the fatty acid part fluorescently active by the introduction of

fluorescent moieties (Figure 1). Prominent examples in this area are NBD- (**n**itro**b**enzoxa**d**iazole) [9,10], BODIPY- (**bo**ron-**dipy**rromethene) [11,12], BOIMPY- (bis(**bo**rondifluoride)-8-**im**idazodi**py**rromethene) [13] and pyrene-labeled fatty acids [14]. Of course, all these alterations might also affect the membrane structure and its dynamics. While the NBD-fluorophore suffers from unsuitable polarity, a pyrene motif disrupts the unpolar membrane core with high bulkiness. BODIPY and BOIMPY scaffolds on the other hand expose fluoride residues which might be able to interact with polarized H–X bonds. Therefore, we synthesized pentaene and hexaene fatty acids which bear five or six double bonds at the terminus or in the middle of the acyl chain [15]. Their slim shape mimics the natural geometry of a saturated hydrocarbon chain and should therefore only lead to minimal disturbances [16]. Nevertheless, we found that their stability with respect to both, oxygen and strong laser beams, is relatively low. The design of novel fluorescent fatty acids is therefore a challenging tightrope walk between advantageous spectroscopic properties, overall stability and a non-interfering molecular shape. As a promising contribution we designed alternative fatty acids which are constructed as a combination of double bonds and benzo[*c*][1,2,5]thiadiazole as a relatively unpolar terminal headgroup (Figure 1). Its electron-withdrawing strength adds on the one hand significant stability towards acidic environments and should furthermore trigger a red-shift in absorption. As another strategic goal the fluorescent fatty acids were supposed to be equipped with very similar geometrical parameters differing only in their absorption and emission wavelengths. The grade of unsaturation as the sole geometrical difference thus provides a set of probes to study the effect of rigidified ethene moieties as straight-chain alkane surrogates within biological membranes.

Results and Discussion

Synthesis

The most prominent methods to access oligoene structures are either cross-coupling reactions [17-19] or Wittig-type reactions [20-22]. The advantage of the latter ones is that they are often conducted at low temperatures and therefore are employed for sensitive compounds. However, a drawback of Wittig reactions

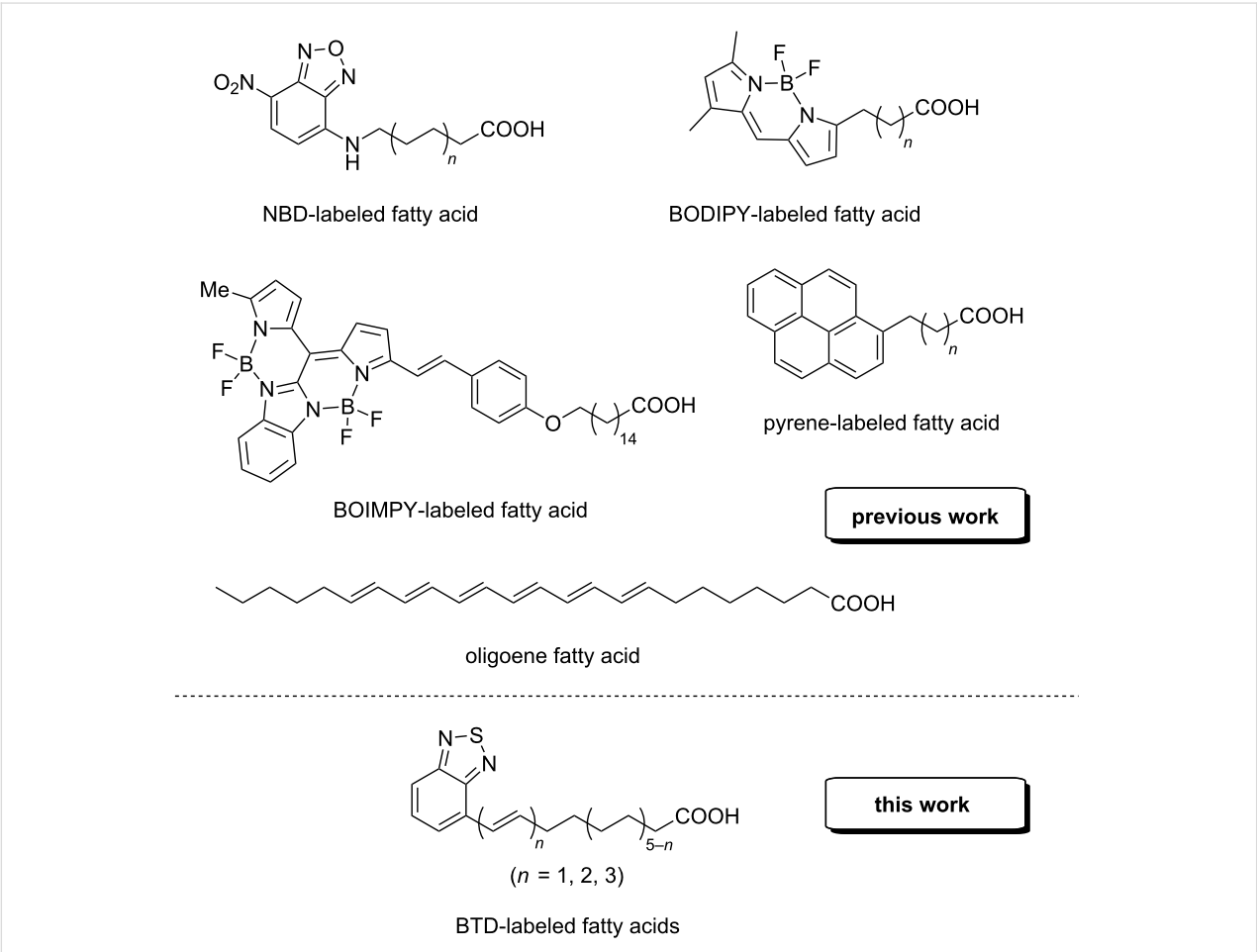

Figure 1: Examples for previously prepared fluorescent fatty acids and our present work.

is the fact that the stereochemistry of the emerging double bond strongly depends on the type of substituent used. Aliphatic residues tend to give the (*Z*)-isomer. If the thermodynamically more stable (*E*)-isomer is needed, a subsequent isomerization has to take place.

To access the benzothiadiazole (BTD) fatty acid **3** with just one conjugated double bond we made use of the Wittig reaction starting with commercially available aldehyde **1**. As expected, the (*Z*)-isomer was the major product; thus, we performed a subsequent *cis–trans* isomerization with traces of iodine as catalyst (Scheme 1). It proved to be crucial to employ degassed hexane and to ensure a strict exclusion of oxygen. Considering both, the isomerization was finished just by removing the solvent while the yield of compound **3** was not hampered.

For a BTD fatty acid analogue of the same length, but of more extended conjugation we made use of the Horner–Wadsworth–Emmons (HWE) reaction. Phosphonate **4** was reacted with the respective aldehyde **1**. In a facile three-step one-pot process the emerging α,β-unsaturated ester **5** was immediately converted to the alcohol **6** in 87% yield in the presence of a Lewis acid and DIBAL at low temperatures. MnO_2-mediated oxidation afforded the respective aldehyde that was immediately transformed by Wittig reaction. Iodine-catalyzed *cis–trans* isomerization yielded the desired fatty acid **7** in 35% over three steps (Scheme 2).

The analogue with three conjugated double bonds was accessed by a similar route that differs only in the type of the phosphonate being employed as starting material. Since three double bonds are required a tailor-made α,β-unsaturated phosphonate **8** was used, which we already employed successfully in former oligoene syntheses [15]. Whereas the second double bond is the result of the HWE reaction the third one is generated in the final Wittig reaction furnishing BTD-equipped triene fatty acid **11c** in an overall yield of 32% (Scheme 3). Notably, the ester intermediate **9** showed already a strong fluorescence at ambient

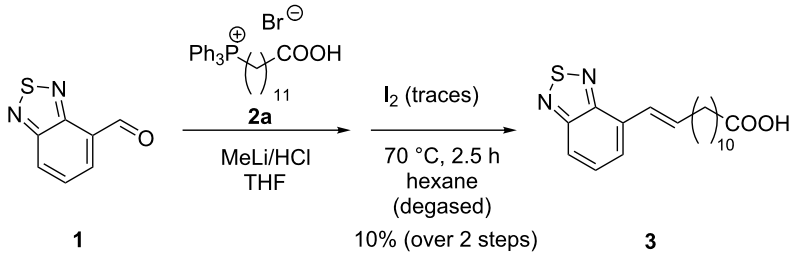

Scheme 1: Synthesis of fatty acid **3** with one olefinic unit.

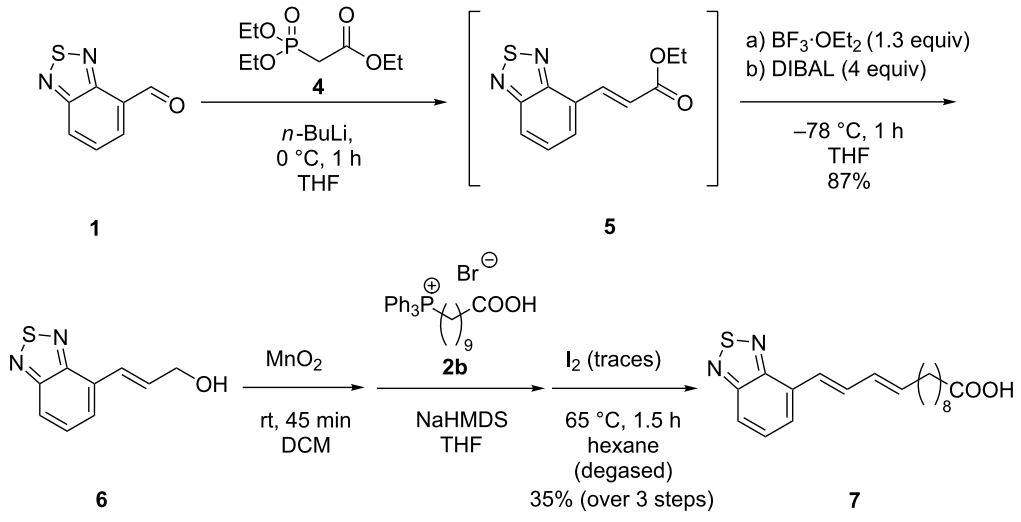

Scheme 2: Synthesis of fatty acid **7** with two olefinic units.

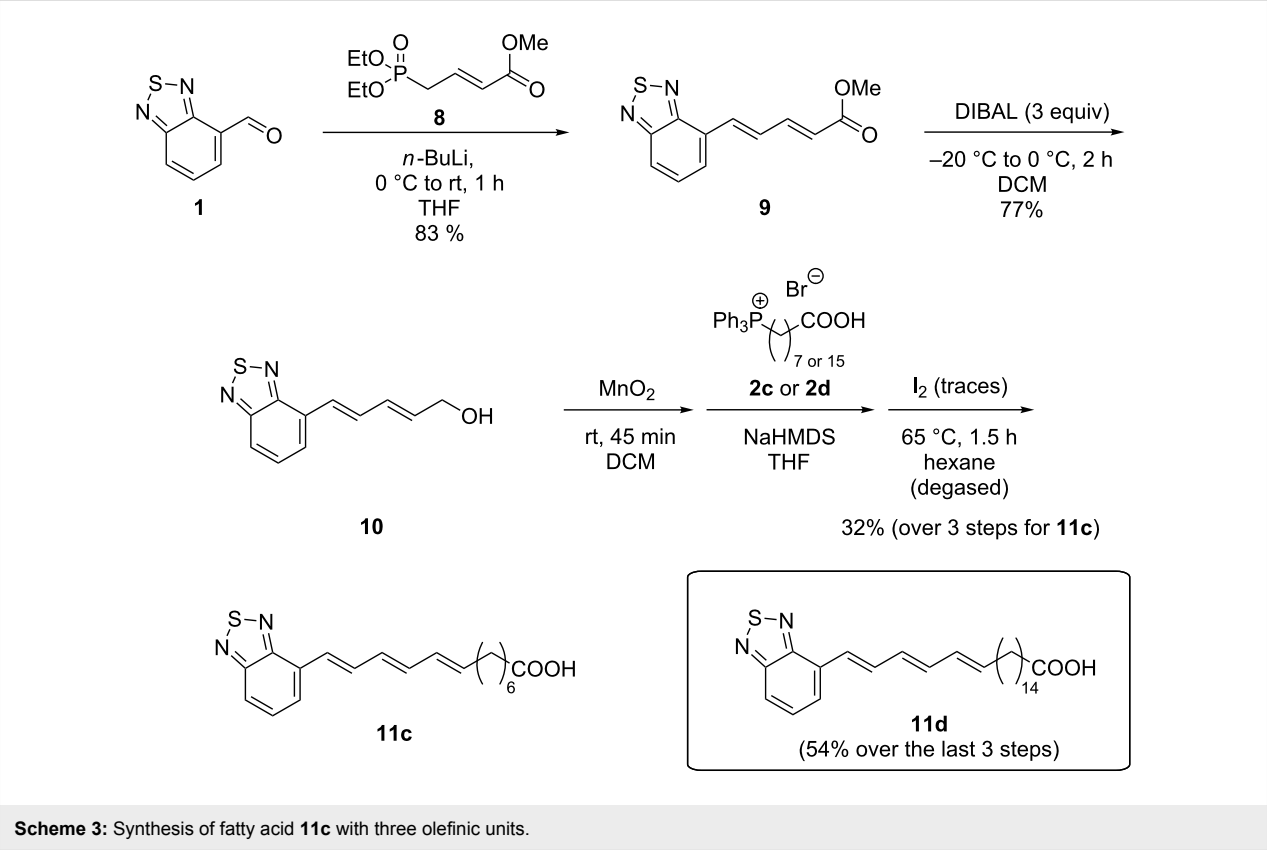

Scheme 3: Synthesis of fatty acid **11c** with three olefinic units.

light. By choosing a Wittig salt with a longer alkyl chain the synthesis of the fatty acid **11d** with a chain of 21 carbon atoms in addition to the BTD unit was equally feasible.

Spectroscopic properties and quantum chemical calculations

If one follows the oligoene chain and includes the two s-*cis*-shaped double bonds of the BTD headgroup one could regard the fluorogenic core as an oligoene with a geminal diimine acceptor group. Since oligoene absorptions are well-known we anticipated here to access a somehow red-shifted level of excitation energy. Indeed, a bathochromic shift of more than 60 nm relative to a corresponding underivatized oligoene moiety was observed in each case. As anticipated, λ_{max} values increase with a growing number of double bonds from **3** via **7** to **11** (Figure 2).

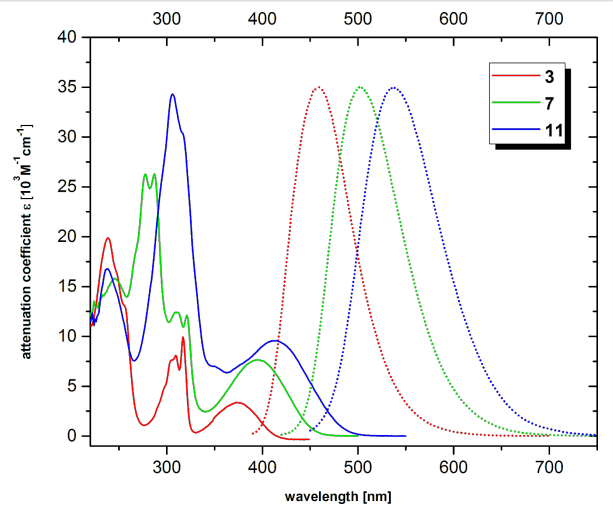

Figure 2: Absorption spectra of fatty acids **3**, **7** and **11**. Solid lines show the UV absorption while dashed lines show fluorescence emission. Excitation was performed at the longest wavelength in each case.

Concomitantly, the rather low attenuation coefficient at the longest wavelength absorption rises from 3.400 $M^{-1}cm^{-1}$ (**7**) to 11.000 $M^{-1}cm^{-1}$ for fatty acid **11** with three conjugated double bonds (Table 1). Fluorescence excitation spectra (not shown) for all three fluorophores pretty much coincide with the corresponding absorption spectra in Figure 2, which allows the fluorescence to be switched on at the longest wavelengths respectively.

Stokes shifts are large (≈5000 cm^{-1}) and increase in the same manner with the size of the π-system albeit to a smaller extent. These findings can be quite consistently rationalized when the frontier orbitals of the chromophoric cores (cc3, cc7, cc11) are taken into account. DFT calculations (B3LYP/6-311G(d,p)) reveal that the HOMO is predominantly located at the oligoene

Table 1: Spectroscopic data of synthesized fatty acids in THF at room temperature. Attenuation coefficients ε refer to the longest wavelength absorption peaks respectively.

	λ^{A}_{max} [nm]	λ^{F}_{max} [nm]	ε [10^3 $M^{-1}cm^{-1}$]	$\Delta\tilde{\nu}$ [cm^{-1}]	φ_F (rt)	Brightness [10^3 $M^{-1}cm^{-1}$]
3	374	459	3.4	4950	0.44	1.5
7	395	501	7.6	5360	0.33	2.5
11c	412	537	9.6	5650	0.18	1.7
11d	412	537	11.0	5650	0.18	2.0

chain while the LUMO is rather spread over the BTD terminus (Figure 3).

Indeed, further TD-DFT calculations (not shown) assign the longest wavelength absorptions of all three compounds to a high contribution of a HOMO–LUMO transition. Thus, the low overlap between both wavefunctions results in a small transition dipole moment and subsequently a quite weak absorption. The situation is even aggravated by the specific small angle (≈64°) between the oligoene and the longitudinal axis of the BTD moiety, which diminishes the dipole moment of the electronic shift additionally. However, the large displacement of electron density from one part of the π-system to another enforces a geometrical equilibration of the nuclei which triggers the emission event to take place from a considerably relaxed excited state. As a consequence, the fluorescence is significantly red-shifted, Stokes shifts are large and fluorescence efficiencies decrease when the expansion of the oligoene moiety

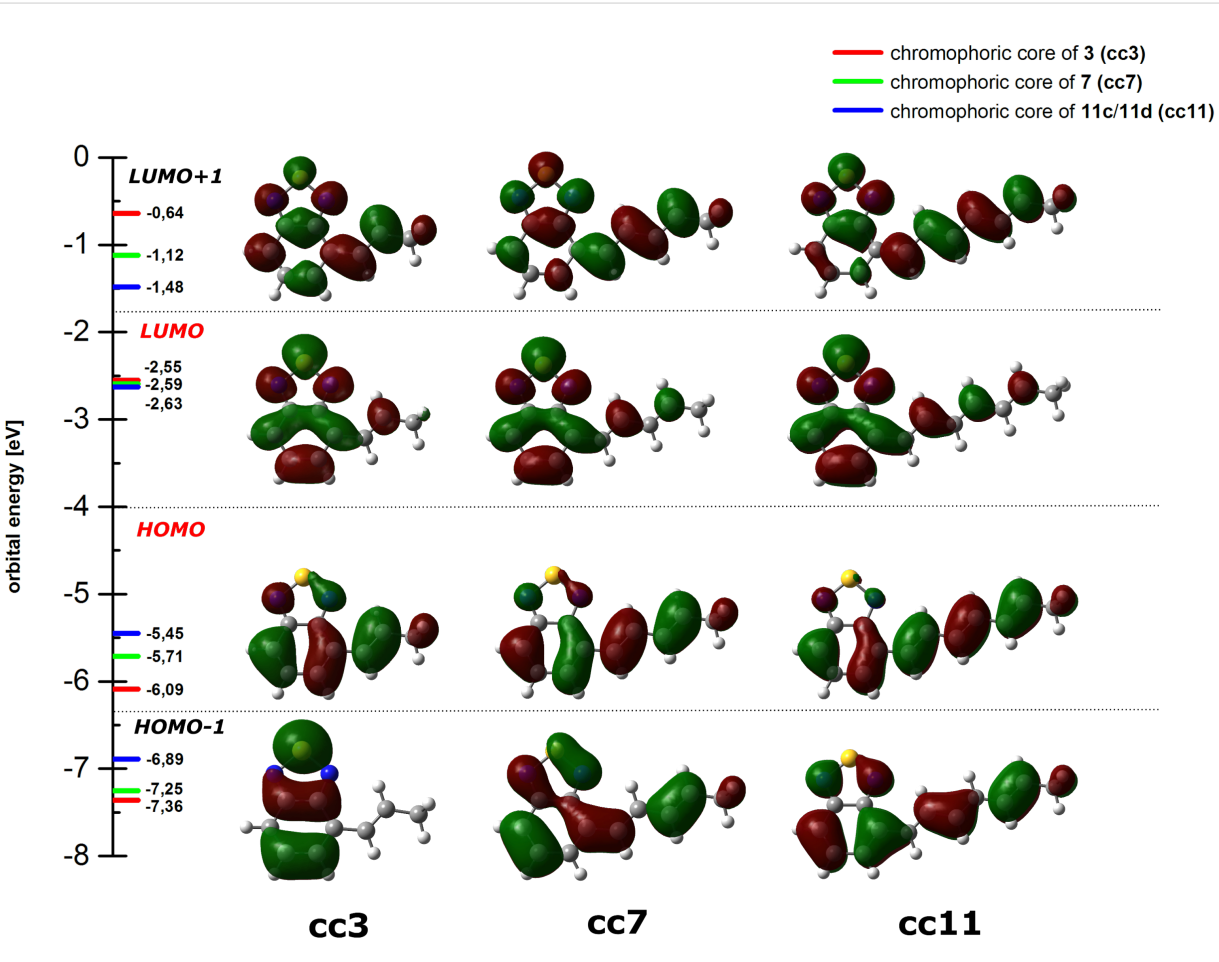

Figure 3: Frontier orbital energies (DFT) and their pictorial representation for the chromophoric cores (cc) of **3**, **7**, and **11**.

induces a pronounced geometrical relaxation upon excitation. Furthermore, as double bonds are added, the structure starts to resemble polyene systems whose fluorescence quantum yields are known to be quite modest. For comparison, a prototypical pentaene motif exhibits a fluorescence quantum yield of 0.06 in EtOH [23]. Our fatty acids **11c** and **11d**, however, which can be regarded as terminally substituted pentaene derivatives, can still reach values of 0.18 in THF.

Conclusion

In conclusion, we have developed a robust approach to three oligoene-shaped fluorescent fatty acids whose fluorescence efficiency is markedly boosted by an unpolar benzo[*c*][1,2,5]thiadiazole (BTD) moiety as terminal headgroup. Wittig reactions in combination with Horner–Wadsworth–Emmons reactions proved to be the method of choice to access the desired structures, which vary only in the grade of unsaturation while the length of their hydrocarbon chain is maintained. The absorption properties were thus modulated by the number of double bonds ranging from λ^{A}_{max} = 374 nm (one double bond) to λ^{A}_{max} = 412 nm (three double bonds) which matches the requirements for modern laser equipments to trigger efficient excitation. All three variants show remarkably large Stokes shifts ranging from 4900–5700 cm^{-1} and fluorescence quantum yields in the range of 0.18 to 0.44. As a set of geometrically similar, but spectroscopically different fluorescent probes we believe that these fatty acids might find interest as useful candidates to study the sensitive hydrophobic area of membranes in terms of domain formation or as labeling agents in general.

Experimental

General. All solvents for column chromatography were distilled before use unless otherwise stated. Tetrahydrofuran (THF) and diethyl ether (Et_2O) were distilled from sodium/benzophenone under an argon atmosphere. Dichloromethane (CH_2Cl_2) and tetrachloromethane (CCl_4) were distilled from $CaCl_2$ under an argon atmosphere. All other solvents were used as analytical grade and were stored over suitable molecular sieves (3 Å or 4 Å). Air and moisture sensitive reactions were carried out in oven-dried or flame-dried glassware, septum-capped under atmospheric pressure of argon. Commercially available compounds were used without further purification unless otherwise stated. Absolute fluorescence quantum yields were determined using a PTI QuantaMaster 40 UV–vis spectrofluorometer equipped with an integrating sphere. The provided corrections for excitation and emission were applied.

(*E*)-13-(Benzo[*c*][1,2,5]thiadiazol-4-yl)tridec-12-enoic acid (3): The corresponding Wittig salt (165 mg, 0.305 mmol, 1.0 equiv) was suspended in THF (1 mL). Methyllithium (1.5 M in diethyl ether, 0.44 mL, 0.670 mmol, 2.2 equiv) was added at −78 °C and the reaction mixture was warmed to rt over 30 min. A solution of aldehyde **1** in THF (1 mL) was added at −78 °C while the solution turns nearly colourless. After 15 min methyllithium (1.5 M in diethyl ether, 0.22 mL, 0.336 mmol, 1.1 equiv) was added again at −78 °C and the reaction mixture was warmed to −30 °C for 90 min. HCl was added (1 M in diethyl ether, 0.67 mL, 0.670 mmol, 2.2 equiv) and the reaction was warmed to rt for 2 h. The reaction was quenched with excess of HCOOH and the crude product was adsorbed directly on silica. Column chromatography (5% EtOAc, 0.1% HCOOH → 6% EtOAc, 0.15% HCOOH in pentane) gave 11 mg of *trans*-fatty acid with still 10% of the corresponding *cis*-isomer. The crude product was suspended in 80 mL of degassed *n*-hexane and treated with 6 µL of saturated solution of I_2 in *n*-hexane. The reaction mixture was heated to 70 °C for 2.5 h. After removal of solvent fatty acid **3**, a pale yellow solid, was obtained as *trans*-isomer without loss of material. It should be mentioned that the compound is first dissolved in tiny amounts of THF before hexane is added to yield a fine suspension. ^{1}H NMR (300 MHz, THF-d_8) δ 1.20–1.65 (m, 16H), 2.20 (t, J = 7.3, 2H, CH_2COOH), 2.34 (m, 2H), 6.92 (m, 1H), 7.17 (m, 1H), 7.55 (m, 2H), 7.83 (dd, J = 7.3, 2.6 Hz, 1H): ^{13}C NMR (75 MHz, THF-d_8) δ 29.58, 29.69, 29.75, 29.79, 29.94, 29.99, 33.72, 34.12, 119.7, 126.0, 126.5, 129.9, 131.5, 137.1, 153.7, 156.1, 173.9); IR (ATR) $\tilde{\nu}$ (cm^{-1}): 2919, 2850, 1696, 1532, 1466, 1428, 1302, 1263, 1237, 1209, 967, 907, 756; HRMS (ESI) *m*/*z*: calcd for $C_{19}H_{26}N_2O_2SNa^+$, 369.16072; found, 369.16088.

(*E*)-3-(Benzo[*c*][1,2,5]thiadiazol-4-yl)prop-2-en-1-ol (6): To a solution of triethyl phosphonoacetate (266 mg, 1.18 mmol, 1.3 equiv) in THF (5 mL) was added *n*-butyllithium (2.5 M, 0.48 mL, 1.18 mmol, 1.3 equiv) dropwise at 0 °C. After 15 min aldehyde **1** was added as solid. Stirring was continued for 1 h at 0 °C. At −78 °C $BF_3{\cdot}OEt_2$ (0.15 mL, 1.18 mmol, 1.3 equiv) was added and directly afterwards DIBAL (1 M in hexane, 3.7 mL, 3.65 mmol, 4 equiv) was added. Stirring was continued at −78 °C for 1 h. The reaction was quenched with excess of MeOH at −78 °C, warmed to rt and treated with excess of Rochelle salt solution. Stirring continued vigorously at rt for 1 h. After an aqueous work-up with EtOAc the crude product was submitted to column chromatography on silica gel (30% EtOAc in pentane) to give 153 mg (0.80 mmol, 87%) of pure alcohol **6**, a pale yellow solid, as *trans*-isomer. ^{1}H NMR (300 MHz, $CDCl_3$) δ 1.95 (s, 1H, O*H*), 4.48 (dd, J = 5.3, 1.4 Hz, 2H, CH_2OH), 7.11 (m, 1H), 7.26 (m, 1H), 7.54 (m, 2H), 7.88 (dd, J = 7.8, 2.0 Hz, 1H); ^{13}C NMR (75 MHz, $CDCl_3$) δ 63.8, 120.3, 126.3, 126.8, 129.5, 130.0, 134.4, 153.1, 155.4; IR (ATR) $\tilde{\nu}$ (cm^{-1}): 3315, 3067, 2898, 2854, 1533, 1084, 1044, 996, 969, 908, 754; HRMS (EI) *m*/*z*: calcd for $C_9H_8N_2OS$, 192.03573; found, 192.03451.

(10*E*,12*E*)-13-(Benzo[*c*][1,2,5]thiadiazol-4-yl)tridec-10,12-dienoic acid (7): To a solution of alcohol **6** (160 mg, 0.832 mmol, 1.0 equiv) in DCM (8 mL) was added MnO_2 (1.5 g, 16.6 mmol, 20 equiv) at rt. Stirring was continued for 45 min. A mixture of SiO_2/Al_2O_3 (1:1) was added and the solvent removed to obtain the adsorbed crude product. A short column filtration (20% EtOAc in pentane) gave 102 mg of the corresponding aldehyde which was used directly in the next step. The corresponding Wittig salt (363 mg, 0.707 mmol, 1.3 equiv) was suspended in THF (5 mL). NaHMDS (1 M in THF, 1.40 mL, 1.40 mmol, 2.6 equiv) was added at rt. Stirring was continued until a red solution was established (10 min). At 0 °C freshly prepared aldehyde dissolved in THF (2 mL) was added and stirring continued for 1 h at 0 °C. The reaction was quenched with some excess of HCOOH and the reaction mixture was directly adsorbed on silica. Column chromatography (5% EtOAc, 0.1% HCOOH → 7% EtOAc, 0.1% HCOOH in pentane) gave 100 mg (0.290 mmol, 54%) of fluorescent fatty acid **7** as *cis–trans* mixture (≈15% *cis*-isomer). Isomerization in 300 mL of degassed *n*-hexane with 30 µL of saturated I_2 solution in *n*-hexane at 65 °C for 90 min gave compound **7**, a yellow solid, as pure all-*trans*-isomer after removal of solvents. It should be mentioned that the compound is first dissolved in tiny amounts of THF before hexane is added to yield a fine suspension. ^{1}H NMR (300 MHz, THF-d_8) δ 1.20–1.65 (m, 12H), 2.13–2.25 (m, 4H, CH_2COOH, -C=CCH_2), 5.99 (dd, *J* = 14.7, 7.1 Hz, 1H), 6.34 (m, 1H), 6.96 (d, *J* = 15.7 Hz, 1H), 7.50–7.63 (m, 2H), 7.72 (dd, *J* = 15.7, 10.6 Hz, 1H), 7.78–7.88 (m, 1H); ^{13}C NMR (75 MHz, THF-d_8) δ 30.11, 30.13, 30.23, 30.28, 30.33, 33.84, 34.25, 120.3, 126.9, 126.9, 130.5, 132.1, 132.4, 135.8, 138.3, 154.1, 156.7, 174.5; IR (ATR) $\tilde{\nu}$ (cm^{-1}): 3031, 2994, 2919, 2851, 1703, 1469, 1415, 1310, 1287, 1257, 1219, 988, 897, 829, 747; HRMS (ESI) *m*/*z*: calcd for $C_{19}H_{24}N_2O_2SNa^+$, 367.14507; found, 369.14518.

Methyl (2*E*,4*E*)-5-(benzo[*c*][1,2,5]thiadiazol-4-yl)penta-2,4-dienoate (9): To a solution of conjugated phosphonate **8** (189 mg, 0.792 mmol, 1.3 equiv) in THF (5 mL) was added *n*-butyllithium (2.5 M, 0.32 mL, 0.792 mmol, 1.3 equiv) at 0 °C. Stirring was continued at this temperature for 15 min. A solution of aldehyde **1** (100 mg, 0.609 mmol, 1 equiv) in THF (2 mL) was added dropwise at 0 °C and strirring continued for 1 h. The reaction was then quenched with aqueous saturated NH_4Cl solution and worked-up with DCM. Column chromatography on silica gel (5% EtOAc, 20% DCM in pentane) gave 124 mg (0.503 mmol, 83%) of highly fluorescent ester **9** as a yellow solid. ^{1}H NMR (300 MHz, $CDCl_3$) δ 3.80 (s, 3H, OMe), 6.16 (m, 1H), 7.31 (m, 1H), 7.45–7.65 (m, 3H), 7.80–8.00 (m, 2H); ^{13}C NMR (75 MHz, $CDCl_3$) δ 51.65, 121.7, 122.4, 128.9, 129.4, 129.5, 131.7, 136.0, 145.0, 152.9, 155.5, 167.4; IR (ATR) $\tilde{\nu}$ (cm^{-1}): 2993, 2956, 1711, 1619, 1528, 1462, 1330, 1244, 1225, 1137, 990, 837, 750; HRMS (ESI) *m*/*z*: calcd for $C_{12}H_{10}N_2O_2SNa^+$, 269.03552; found, 269.03557.

(2*E*,4*E*)-5-(Benzo[*c*][1,2,5]thiadiazol-4-yl)penta-2,4-dien-1-ol (10): To a solution of ester **9** (124 mg, 0.503 mmol, 1.0 equiv) in DCM (3 mL) was added DIBAL (1 M in hexane, 1.51 mL, 1.51 mmol, 3 equiv) at −20 °C. Stirring continued for 1 h at −20 °C and for 1 h at 0 °C. MeOH was added, then Rochelle salt solution and vigorous stirring continued for 1 h at rt. After an aqueous work-up the crude product was submitted to column chromatography on silica gel (20% EtOAc, 30% DCM → 30% EtOAc, 30% DCM in pentane) to give 85 mg (0.390 mmol, 77%) of the pure alcohol **10** as a yellow solid. ^{1}H NMR (300 MHz, $CDCl_3$) δ 1.75 (s, 1H, OH), 4.31 (d, *J* = 5.5 Hz, 2H, CH_2OH), 6.14 (m, 1H), 6.54 (m, 1H), 7.03 (d, *J* = 15.7 Hz, 1H), 7.48–7.58 (m, 2H) 7.67 (dd, *J* = 15.7, 10.4 Hz, 1H), 7.85 (dd, *J* = 7.8, 2.0 Hz, 1H); ^{13}C NMR (75 MHz, $CDCl_3$) δ 63.34, 120.1, 126.6, 128.4, 129.6, 130.6, 131.7, 133.5, 134.6, 153.1, 155.5); IR (ATR) $\tilde{\nu}$ (cm^{-1}): 3416, 3358, 3014, 2991, 1529, 1483, 1275, 1155, 1094, 1066, 980, 905, 837, 742; HRMS (ESI) *m*/*z*: calcd for $C_{11}H_{10}N_2OSNa^+$, 241.04060; found, 241.04071.

(8*E*,10*E*,12*E*)-8-(Benzo[*c*][1,2,5]thiadiazol-4-yl)tridec-8,10,12-trienoic acid (11c): To a solution of **10** (40 mg, 0.183 mmol, 1.0 equiv) in DCM (1.5 mL) was added MnO_2 (318 mg, 3.66 mmol, 20 equiv) at rt. Stirring was continued for 45 min. A mixture of SiO_2/Al_2O_3 (1:1) was added and the solvent removed to obtain the adsorbed crude product. A short column filtration (20% EtOAc in pentane) gave 34 mg of the corresponding aldehyde (86%) which was used directly in the next step. The corresponding Wittig salt (116 mg, 0.238 mmol, 1.3 equiv) was suspended in THF (2 mL). NaHMDS (1 M in THF, 0.78 mL, 0.480 mmol, 2.6 equiv) was added at rt. Stirring was continued until a red solution was established (10 min). At 0 °C freshly prepared aldehyde dissolved in THF (1 mL) was added and stirring continued for 1 h at 0 °C. The reaction was quenched with HCOOH (3 equiv) and directly adsorbed on silica/Al_2O_3 (1:1). Column chromatography (10% EtOAc in pentane to remove rests of aldehyde, then 5% EtOAc, 0.1% HCOOH → 6% EtOAc, 0.15% HCOOH in pentane) gave 20 mg (0.058 mmol, 37%) of fatty acid. In some cases size exclusion chromatography in $CHCl_3$ was helpful to remove rests of Wittig salt. Isomerization was performed in *n*-hexane (200 mL, degassed) with 15 µL of saturated I_2-solution in *n*-hexane for 90 min at 65 °C. It should be mentioned that the compound was first dissolved in tiny amounts of THF before hexane was added to yield a fine suspension. After removal of solvents fatty acid **11c**, a yellow solid, was obtained as pure all-*trans* isomer. ^{1}H NMR (300 MHz, THF-d_8) δ 1.20–1.65 (m, 8H), 2.06–2.26 (m, 4H, CH_2COOH, -C=CCH_2), 5.83 (dd, *J* = 15.1, 7.1 Hz, 1H), 6.21 (m, 1H), 6.45 (m, 2H), 7.03 (d,

J = 15.6 Hz, 1H), 7.50–7.66 (m, 2H), 7.72–7.86 (m, 2H); ^{13}C NMR (75 MHz, THF-d_8) δ 25.78, 29.88, 29.94, 30.11, 33.75, 34.21, 120.4, 127.1, 128.2, 130.5, 131.8, 132.0, 132.4, 135.7, 136.5, 137.2, 154.1, 156.7, 174.4; IR (ATR) $\tilde{\nu}$ (cm^{-1}): 3009, 2927, 2853, 1695, 1526, 1265, 993, 906, 750; HRMS (ESI) m/z: calcd for $C_{19}H_{24}N_2O_2SNa^+$, 365.12942; found, 365.12956.

(16*E*,18*E*,20*E*)-21-(Benzo[*c*][1,2,5]thiadiazol-4-yl)henicos-16,18,20-trienoic acid (11d): To a solution of alcohol **10** (40 mg, 0.183 mmol, 1.0 equiv) in DCM (1.5 mL) was added MnO_2 (318 mg, 3.66 mmol, 20 equiv) at rt. Stirring was continued for 45 min. A mixture of SiO_2/Al_2O_3 (1:1) was added and the solvent was removed to obtain the adsorbed crude product. A short column filtration (20% EtOAc in pentane) gave 31 mg of the corresponding aldehyde (78%) which was used directly in the next step. The corresponding Wittig salt (111 mg, 0.186 mmol, 1.3 equiv) was suspended in THF (1.5 mL). NaHMDS (1 M in THF, 0.37 mL, 0.372 mmol, 2.6 equiv) was added at rt. Stirring was continued until a red solution was established (10 min). At 0 °C freshly prepared aldehyde dissolved in THF (1 mL) was added and stirring continued for 1 h at 0 °C. The reaction was quenched with HCOOH (3 equiv) and directly adsorbed on silica/Al_2O_3 (1:1). Column chromatography (10% EtOAc in pentane to remove rests of aldehyde, then 5% EtOAc, 0.1% HCOOH → 7% EtOAc, 0.1% HCOOH in pentane) gave 45 mg (0.099 mmol, 54%) of fatty acid. Isomerization was performed in *n*-hexane (300 mL, degassed) with 20 µL of saturated I_2-solution in *n*-hexane for 90 min at 65 °C. It should be mentioned that the compound was first dissolved in tiny amounts of THF before hexane was added to yield a fine suspension. After removal of solvents fatty acid **11d**, a yellow solid, is usually obtained as pure all-*trans*-isomer. ^{1}H NMR (300 MHz, THF-d_8) δ 1.20–1.65 (m, 8H), 2.06–2.26 (m, 4H, CH_2COOH, -C=CCH_2), 5.82 (dd, J = 15.1, 7.1 Hz, 1H), 6.20 (m, 1H), 6.45 (m, 2H), 7.03 (d, J = 15.6 Hz, 1H), 7.50–7.66 (m, 2H), 7.72–7.86 (m, 2H); ^{13}C NMR (75 MHz, THF-d_8) δ 29.59, 29.65, 29.74, 29.80, 29.93, 29.95, 30.05, 30.08, 33.28, 33.72, 119.8, 126.6, 127.7, 123.0, 131.3, 131.5, 131.9, 135.2, 135.9, 136.8, 153.6, 156.2, 173.9; IR (ATR) $\tilde{\nu}$ (cm^{-1}): 3010, 2920, 2849, 1696, 1527, 1464, 1260, 993, 927, 802, 750, 725; HRMS (ESI) m/z: calcd for $C_{27}H_{38}N_2O_2SNa^+$, 477.25462; found, 477.25542.

Supporting Information

Supporting Information File 1

Copies of ^{1}H and ^{13}C NMR spectra.
[http://www.beilstein-journals.org/bjoc/content/supplementary/1860-5397-12-270-S1.pdf]

Acknowledgements

We are grateful to the Deutsche Forschungsgemeinschaft (DFG, SFB 803 “Functionality controlled by organization in and between membranes”, project A05) and the Fonds der Chemischen Industrie (FCI) for financial support (Dozentenstipendium to D.B.W.). We thank Martin Bröring (TU Braunschweig) for the possibility of measuring quantum yields by the instrument in his labs.

References

1. Simons, K.; Ikonen, E. *Nature* **1997,** *387,* 569–572. doi:10.1038/42408
2. Sonnino, S.; Prinetti, A.; Mauri, L.; Chigorno, V.; Tettamanti, G. *Chem. Rev.* **2006,** *106,* 2111–2125. doi:10.1021/cr0100446
3. Brown, D. A.; London, E. *J. Biol. Chem.* **2000,** *275,* 17221–17224. doi:10.1074/jbc.R000005200
4. Silvius, J. R. *Biochim. Biophys. Acta, Biomembr.* **2003,** *1610,* 174–183. doi:10.1016/S0005-2736(03)00016-6
5. Windschiegl, B.; Orth, A.; Römer, W.; Berland, L.; Stechmann, B.; Bassereau, P.; Johannes, L.; Steinem, C. *PLoS One* **2009,** *4,* e6238. doi:10.1371/journal.pone.0006238
6. Ross, M.; Steinem, C.; Galla, H.-J.; Janshoff, A. *Langmuir* **2001,** *17,* 2437–2445. doi:10.1021/la001617x
7. Schütte, O. M.; Ries, A.; Orth, A.; Patalag, L. J.; Römer, W.; Steinem, C.; Werz, D. B. *Chem. Sci.* **2014,** *5,* 3104–3114. doi:10.1039/c4sc01290a
8. Schütte, O. M.; Patalag, L. J.; Weber, L. M. C.; Ries, A.; Römer, W.; Werz, D. B.; Steinem, C. *Biophys. J.* **2015,** *108,* 2775–2778. doi:10.1016/j.bpj.2015.05.009
9. Lipsky, N. G.; Pagano, R. E. *Proc. Natl. Acad. Sci. U. S. A.* **1983,** *80,* 2608–2612. doi:10.1073/pnas.80.9.2608
10. Lipsky, N. G.; Pagano, R. E. *Science* **1985,** *228,* 745–747. doi:10.1126/science.2581316
11. Pagano, R. E.; Martin, O. C.; Kang, H. C.; Haugland, R. P. *J. Cell Biol.* **1991,** *113,* 1267–1279. doi:10.1083/jcb.113.6.1267
12. Kaiser, R. D.; London, E. *Biochim. Biophys. Acta* **1998,** *1375,* 13–22. doi:10.1016/S0005-2736(98)00127-8
13. Patalag, L. J.; Jones, P. G.; Werz, D. B. *Angew. Chem.* **2016,** *128,* 13534–13539. doi:10.1002/ange.201606883
Angew. Chem., Int. Ed. **2016,** *55,* 13340–13344. doi:10.1002/anie.201606883
14. Somerharju, P. *Chem. Phys. Lipids* **2002,** *116,* 57–74. doi:10.1016/S0009-3084(02)00020-8
15. Patalag, L. J.; Werz, D. B. *J. Org. Chem.* **2012,** *77,* 5297–5304. doi:10.1021/jo300624h
16. Kuerschner, L.; Ejsing, C. S.; Ekroos, K.; Shevchenko, A.; Anderson, K. I.; Thiele, C. *Nat. Methods* **2005,** *2,* 39–45. doi:10.1038/nmeth728
17. Negishi, E.; Alimardanov, A.; Xu, C. *Org. Lett.* **2000,** *2,* 65–67. doi:10.1021/ol990336h
18. Zeng, F.; Negishi, E. *Org. Lett.* **2001,** *3,* 719–722. doi:10.1021/ol000384y
19. Zeng, F.; Negishi, E. *Org. Lett.* **2002,** *4,* 703–706. doi:10.1021/ol0102794
20. Ley, S. V.; Smith, S. C.; Woodward, P. R. *Tetrahedron Lett.* **1988,** *29,* 5829–5832. doi:10.1016/S0040-4039(00)82204-2
21. Wittig, G.; Schöllkopf, U. *Chem. Ber.* **1954,** *87,* 1318–1330. doi:10.1002/cber.19540870919

22. Wadsworth, W. S.; Emmons, W. D. *J. Am. Chem. Soc.* **1961,** *83,* 1733–1738. doi:10.1021/ja01468a042
23. Nieves, I.; Artetxe, I.; Abad, J. L.; Alonso, A.; Busto, J. V.; Fajarí, L.; Montes, L. R.; Sot, J.; Delgado, A.; Goñi, F. M. *Langmuir* **2015,** *31,* 2484–2492. doi:10.1021/la505017x

License and Terms

BEILSTEIN JOURNAL OF ORGANIC CHEMISTRY

Synthesis and evaluation of anti-oxidant and cytotoxic activities of novel 10-undecenoic acid methyl ester based lipoconjugates of phenolic acids

Naganna Narra[1,2], Shiva Shanker Kaki[*1,2,§], Rachapudi Badari Narayana Prasad[1,2], Sunil Misra[2,3], Koude Dhevendar[2,3], Venkateshwarlu Kontham[1,2] and Padmaja V. Korlipara[*1,2,§]

Full Research Paper

Open Access

Address:
[1]Centre for Lipid Research, CSIR-Indian Institute of Chemical Technology, Uppal Road, Hyderabad 500007, India, [2]Academy of Scientific and Innovative Research, New Delhi, India and [3]Biology Division, CSIR-Indian Institute of Chemical Technology, Uppal Road, Hyderabad 500007, India

Email:
Shiva Shanker Kaki[*] - shivashanker.kaki@iict.res.in;
Padmaja V. Korlipara[*] - kvpadmaja@iict.res.in

* Corresponding author
§ Tel/Fax +91-40-27193370

Keywords:
anticancer; anti-oxidants; caffeic acid; coumaric acid; ferulic acid; phenolic lipids; sinapic acid; undecenoic acid

Beilstein J. Org. Chem. **2017,** *13,* 26–32.
doi:10.3762/bjoc.13.4

Received: 24 October 2016
Accepted: 19 December 2016
Published: 04 January 2017

This article is part of the Thematic Series "Lipids: fatty acids and derivatives, polyketides and isoprenoids".

Guest Editor: J. S. Dickschat

Abstract

The synthesis of five novel methyl 10-undecenoate-based lipoconjugates of phenolic acids from undecenoic acid was carried out. Undecenoic acid was methylated to methyl 10-undecenoate which was subjected to a thiol–ene reaction with cysteamine hydrochloride. Further amidation of the amine was carried out with different phenolic acids such as caffeic, ferulic, sinapic, coumaric and cinnamic acid. All synthesized compounds were fully characterized and their structures were confirmed by spectral data. The anti-oxidant activity of the synthesized lipoconjugates of phenolic acids was studied by the 2,2-diphenyl-1-picrylhydrazyl (DPPH) radical scavenging assay and also by the inhibition of linoleic acid oxidation in micellar medium by differential scanning calorimetry (DSC). The prepared compounds were also screened for their cytotoxic activity against five cell lines. It was observed that the lipoconjugates of caffeic acid, sinapic acid, ferulic acid, and coumaric acid displayed anticancer and anti-oxidant properties. The anticancer properties of these derivatives have been assessed by their IC_{50} inhibitory values in the proliferation of MDA-MB231, SKOV3, MCF7, DU 145 and HepG2 cancer cell lines.

Introduction

Phenolic compounds are a class of natural compounds which are found ubiquitously in the plant kingdom. They are reported to possess a wide range of biological properties like anti-oxidant, antimicrobial, anti-inflammatory, anticarcinogenic and antiviral activities [1]. The phenolic acids are also reported to show in vitro anti-oxidant activity against many reactive oxygen

species and to protect neuronal cells against various types of oxidative damage [2,3]. To increase the effectiveness of phenolic compounds, their lipophilization has been the choice of derivatization as it provides beneficial effects of both the phenolics and the lipid involved in one chemical entity [4,5]. Lipids, especially fatty acids and their derivatives are known for their broad spectrum of activity which expands their application in developing new hybrid biomolecules which help in host defenses against potential pathogenic microbes. Research interest in producing new phenolipids has been increasing due to the potential applications of such products in biomedical fields. Earlier reports on the production of phenolipids were focused on the incorporation of phenolic compounds into triglycerides where a number of phenolic acids were transesterified with different oils or triglycerides [6]. Apart from these structured phenolipids, different fatty acids were esterified with phenolic compounds to produce novel esters which were evaluated for anti-oxidant and antimicrobial activities [7,8]. However, there are very few reports where the phenolic acids have been derivatized with other functionalities apart from esters. The reported compounds other than esters were amides where bioconjugates of fatty acids and amino acids were prepared and evaluated for their anti-oxidant activity by a DPPH radical assay [9]. In view of developing new conjugates of phenolic lipids, we have synthesized novel derivatives of phenolic lipids from undecenoic acid where the phenolic acids were linked to the olefinic group of undecenoic acid via a thioamide spacer. Among the various fatty acids reported, 10-undecenoic acid is unique due to its bifunctional nature with an odd-numbered carbon atom chain length derived from castor oil. There have been several reports on the synthesis and evaluation of undecenoic acid-based derivatives due to its wide applicability ranging from biological activity, natural products and polymer applications [10,11]. This type of compounds could be useful as potential novel lipid derivatives because of the presence of lipophilic chain and the phenolic amide conjugate.

Results and Discussion

Synthesis

10-Undecenoic acid was chosen as the lipid part as the derivatives of undecenoic acid have been reported to be potent bioactive compounds [12,13]. Additionally the terminal double bond of undecenoic acid provides a reactive group for further derivatization for producing potential functional derivatives. The synthetic route followed for the synthesis of the phenolipids is shown in Scheme 1. Initially, undecenoic acid was treated with sulfuric acid in methanol to obtain methyl undecenoate (**1**) in quantitative yield. Next, ester **1** was treated with 1,1′-azobis(cyclohexanecarbonitrile) (ABCN) and 2-mercaptoethylamine hydrochloride in dioxane/ethanol 70:30 (v:v) to obtain

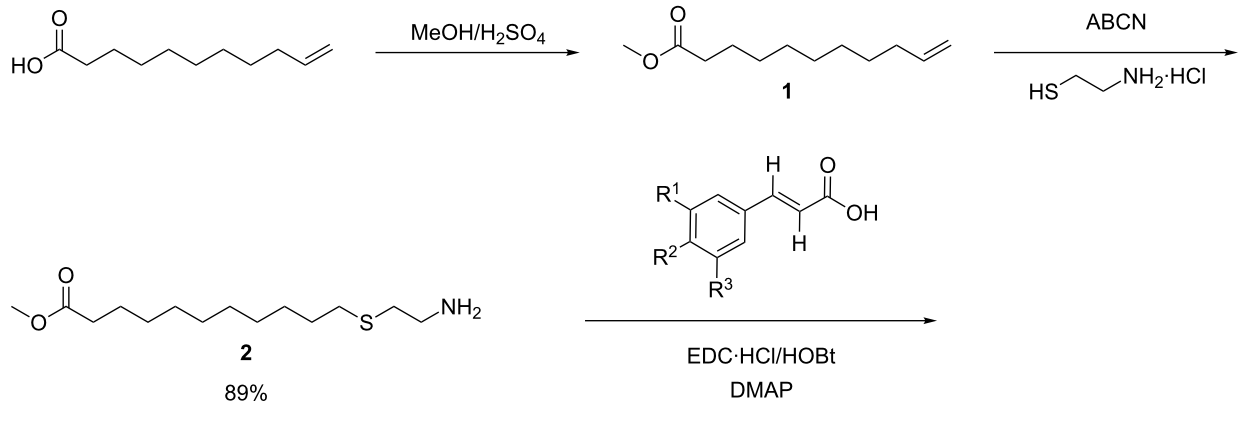

	R1	R2	R3
3a	H	H	H
3b	H	OH	H
3c	OH	OH	H
3d	OCH_3	OH	H
3e	OCH_3	OH	OCH_3

Scheme 1: Synthetic procedure for the preparation of 10-undecenoic acid methyl ester-based lipoconjugates of phenolic acids.

methyl 11-(2-aminoethylthio)undecanoate (**2**) in 89% yield. The structures of compounds **1** and **2** were in agreement with the reported literature data [14,15].

Finally, amine **2** was reacted with different phenolic acids in the presence of EDC·HCl and HOBt to give amides **3a**–**3e** with reproducible yields in the range of 84–86%.

Anti-oxidant activity

The anti-oxidant activities of the prepared derivatives were studied by the well-established DPPH radical scavenging assay and also by studying the oxidation of linoleic acid using DSC. The DPPH radical is a commercially available stable free radical which is widely used to preliminarily determine the radical scavenging potential of compounds. The results for the ability of the prepared compounds to scavenge the DPPH radical are shown in Table 1 along with reference anti-oxidants α-tocopherol (α-TP) and *tert*-butylhydroquinone (TBHQ). As can be seen, all synthesized derivatives exhibit radical scavenging ability except the cinnamic acid derivative **3a**. This could be due to the absence of a phenolic hydroxy group which is responsible for the anti-oxidant activity of most of the natural phytochemicals. Among all compounds, **3c** was found to be the most efficient free radical scavenger which showed a value closest to the standard anti-oxidant, α-TP. Compounds **3d** and **3e** also showed free radical scavenging activity (FRSA) of 68% and 67%, respectively, whereas compound **3b** showed only moderate activity with 30% FRSA.

Table 1: DPPH radical scavenging activity of the synthesized 10-undecenoic acid methyl ester-based lipoconjugates.

Compound	FRSA (%) at 1.0 mM concentration
3a	–[a]
3b	30.23
3c	87.05
3d	67.68
3e	66.57
α-TP	90.23
TBHQ	92.34

[a]no activity.

In another study, the ability of the prepared derivatives in inhibiting the oxidation of linoleic acid was studied by differential scanning calorimetry (DSC). DSC is a sensitive technique and has been used for investigating the thermotropic properties of several compounds including biological macromolecules, drugs and lipid-based materials for their stability and other characteristics [16]. In the present study, pure linoleic acid and linoleic acid containing the synthesized compounds were subjected to DSC analysis. The results of the assay are shown in Table 2 and α-TP and TBHQ were included as standard anti-oxidants.

Table 2: DSC study of the synthesized 10-undecenoic acid methyl ester–based lipoconjugates **3a–e**.

Compound[a]	OIT[b] (°C)
LA + **3a**	116
LA + **3b**	130
LA + **3c**	136
LA + **3d**	141
LA + **3e**	142
LA + α-TP	130
LA +TBHQ	126
LA	116

[a]LA: linoleic acid, [b]OIT: oxidative induction temperature.

Pure linoleic acid showed an oxidative induction temperature (OIT) of 116 °C which was found to increase when anti-oxidants were added. It can be observed that the prepared derivatives had a positive influence on the oxidation of linoleic acid except for derivative **3a** which did not show any anti-oxidant activity (see Supporting Information File 1, Figure S20 for DSC curves). All other derivatives were found to exhibit very good protective activity against oxidation of linoleic acid and the OITs were found to be similar or in case of compounds **3c**, **3d** and **3e** even higher compared to the reference anti-oxidants TBHQ and α-TP. The OIT for TBHQ and α-TP were observed to be 126 and 130 °C, respectively, whereas compound **3b** showed an OIT of 130 °C. As the anti-oxidant activity has been reported [17] to depend on several factors such as the medium of an assay, number and position of phenolic hydroxy groups, etc. the differences in the anti-oxidant potentials of the prepared phenolipids could be due to different media used for the assays; the DPPH assay is conducted in a polar medium but the linoleic acid oxidation study is conducted in a non-polar environment.

Cytotoxic activity

As there were studies reported on the cytotoxicity of phenolic lipids, we have further screened the prepared compounds for their anticancer activity [18]. The anticancer activity of compounds **3a**–**e** was tested against five cell lines along with doxorubicin as positive control and all of them showed moderate to good anticancer effects. The results are collected in Table 3. The compounds whose IC_{50} values are observed to be lower and closer to the reference drug are considered as having good anticancer potential.

Table 3: Anticancer activity of 10-undecenoic acid methyl ester–based lipoconjugates.[a]

Entry	Compound	IC_{50} values (μM)				
		MDA-MB-231	SKOV3	MCF7	DU145	HepG2
1	**3a**	21.2 ± 0.31	99.2 ± 0.79	17.2 ± 0.23	25.4 ± 0.31	38.2 ± 0.42
2	**3b**	14.5 ± 0.26	31.5 ± 0.41	39.2 ± 0.45	81.6 ± 0.77	58.3 ± 0.61
3	**3c**	12.0 ± 0.28	38.9 ± 0.37	10.55 ± 0.27	13.0 ± 0.26	67.4 ± 0.59
4	**3d**	29.0 ± 0.36	32.2 ± 0.32	28.8 ± 0.36	56.7 ± 0.62	93.9 ± 0.85
5	**3e**	12.5 ± 0.25	38.3 ± 0.40	13.9 ± 0.22	28.8 ± 0.39	141.4 ± 0.98
	doxorubicin	0.8 ± 0.14	0.7 ± 0.16	0.8 ± 0.12	0.8 ± 0.15	0.7 ± 0.14

[a]Cell lines: MDA-MB-231, breast cancer (ATCC® HTB-26™); SKOV3, ovarian cancer (ATCC® HTB-77™); MCF7, breast cancer (ATCC® HTB-22™); DU 145, prostate cancer (ATCC® HTB-81™); HepG2, liver hepatocellular carcinoma (ATCC® HB-8065™).

Specifically compounds **3c**, **3b** and **3e** were found to show promising anticancer activity according to their IC_{50} values, whereas **3d** and **3a** exhibited only moderate activity. Among all tested derivatives, compound **3c** was found to exhibit best anticancer activity against MCF7, DU145 and MDA-MB-231 cell lines with IC_{50} values of 10.55, 13.0 and 12.0 μM, respectively. It was found that the anticancer activity against some cell lines was much better compared to our previous reports on phenolic lipids [19]. However, all prepared derivatives were observed to exhibit lower anticancer activity when compared to the reference drug doxorubicin which showed IC_{50} values in the range of 0.7 to 0.8 μM against the tested cell lines.

Conclusion

In conclusion, the synthesis of five novel methyl 10-undecenoate-based lipoconjugates of phenolic acids is reported. The synthetic route was simple with product yields in the range of 84–86% over three steps. The lipid part, methyl 10-undecenoate was subjected to a thiol–ene reaction with cysteamine hydrochloride and the resulting intermediate was conjugated with the phenolic acid via amidation. The evaluation of the five novel phenolic lipids as anti-oxidants was studied using the DPPH radical scavenging assay and DSC studies where some compounds showed excellent anti-oxidant activity. Finally the compounds were further screened for anticancer activity where a few derivatives showed interesting activity.

Experimental

Materials

10-Undecenoic acid, 1,1'-azobis(cyclohexanecarbonitrile) (ABCN), hydroxybenzotriazole (HOBt) and 1-ethyl-3-(3'-dimethylaminopropyl)carbodiimide hydrochloride (EDC·HCl), cysteamine hydrochloride, cinnamic acid, sinapic acid, ferulic acid, *p*-coumaric acid, caffeic acid, α-tocopherol (α-TP), *tert*-butylhydroquinone (TBHQ), linoleic acid (LA) and 2,2-diphenyl-1-picrylhydrazyl (DPPH) radical were purchased from Sigma–Aldrich (St.Louis, USA), and pre-coated TLC plates (silica gel 60 F254) were purchased from Merck (Darmstadt, Germany). All solvents were purchased from Sd Fine Chemicals (Mumbai, India) and were of the highest grade of purity available.

Instruments

^{1}H and ^{13}C NMR spectra were recorded on a Bruker Avance operating at 700/500 MHz and 175/125 MHz. The NMR spectra were referenced to δ 7.26 ppm and δ 77.0 ppm in $CDCl_3$ solvent for ^{1}H and ^{13}C, respectively. Coupling constants (*J*) patterns in the ^{1}H NMR spectra are given as follows: s = singlet, d = doublet, t = triplet, q = quartet, m = multiplet protons. Mass spectra were recorded using electron spray ionization (ESI) on a Waters e2695 Separators module (Waters, Milford, MA, USA) mass spectrometer. FTIR spectra were recorded in chloroform on a Perkin–Elmer Fourier Transform (FTIR) spectrum BX instrument (Model: Spectrum BX; Connecticut, USA). HRMS spectra were obtained from an Exactive Orbitrap mass spectrometer (Thermo Scientific, Waltham, MA, USA). Melting points of lipoconjugates of phenolic molecules were determined with a capillary tube melting point apparatus. Gas chromatography (GC) was performed on an Agilent 6890N gas chromatograph (Delaware, USA) equipped with a flame ionization detector using a HP-1 capillary column (30 m × 0.25 mm × 0.25 μm). The injector and detector temperatures were set at 280 and 300 °C, respectively. The oven temperature was programmed at 150 °C for 2 min and then increased to 300 °C at 10 °C/min and final temperature hold for 20 min. The carrier gas used was nitrogen at a flow rate of 1.0 mL/min.

Methods

Synthesis of methyl undec-10-enoate (1): 10-Undecenoic acid (10 g, 54.34 mmol), was added to methanol (17.6 mL) and sulfuric acid (0.1 mL, 2 wt % 10-undecenoic acid) and stirred at

refluxing temperature of methanol for 6 h. After completion of the reaction as shown by TLC (hexane/ethyl acetate 80:20, v/v), excess methanol was removed under reduced pressure and the product was diluted with ethyl acetate (30 mL), washed with 5% aqueous $NaHCO_3$ solution (3 × 30 mL), and dried over anhydrous Na_2SO_4. The organic solvent was removed under reduced pressure to afford crude methyl ester of 10-undecenoic acid. The product was purified by column chromatography with basic alumina and hexane as the eluent to get 99% pure methyl undec-10-enoate (**1**) as indicated by GC. The product was analyzed by ^{1}H NMR, ^{13}C NMR, ESIMS, and FTIR and the structure was confirmed by comparing the data with those reported in the literature [14].

Synthesis of methyl 11-(2-aminoethylthio) undecanoate (2): For the synthesis of compound **2**, a reported protocol was followed with slight modifications [20]. Briefly, methyl undecenoate (**1**, 6 g, 30.3 mmol) and ABCN (0.18 g, 3 wt % of **1**) were dissolved in 40 mL chloroform. Then, 2-mercaptoethylamine hydrochloride (6.8 g, 60 mmol) and 40 mL of 1,4-dioxane/ethanol (70:30; v/v) were added and the mixture was stirred at 85 °C for 48 h. The progress of the reaction was monitored by TLC (hexane/ethyl acetate 80:20, v/v). After maximum conversion, the reaction mixture was extracted with dichloromethane (2 × 40 mL) and the combined organic phases were washed with saturated K_2CO_3, brine and finally with water and dried over anhydrous Na_2SO_4. This crude product mixture was concentrated and purified by column chromatography with hexane/ethyl acetate (92:8, v/v) to obtain pure methyl 11-(2-aminoethylthio)undecanoate (**2**) in 89% yield (7.41 g). The purified product was characterized by ^{1}H and ^{13}C NMR, IR and ESIMS spectral studies and the structure was confirmed by comparing the data with those reported in the literature [15].

Synthesis of methyl 11-((2-(cinnamamido)ethyl)sulfanyl)undecanoate (3a): The amidation reaction was performed following a reported protocol with slight modifications [21]. Briefly, compound **2** (0.58 g, 2.1 mmol) and cinnamic acid (0.4 g, 3.1 mmol) were dissolved in dichloromethane (30 mL) and the mixture was stirred at 0–5 °C under a nitrogen atmosphere. EDC·HCl (0.4 g, 2.52 mmol) and HOBt (0.3 g, 3.1 mmol) were added and the contents were stirred at 0–5 °C for 10 min. After the addition, the mixture was stirred for 12 h at rt under a nitrogen atmosphere and the progress of reaction was monitored by TLC using the solvent system chloroform/methanol (80:20, v/v). After maximum conversion, the reaction mixture was extracted with dichloromethane, washed with water and dried over anhydrous Na_2SO_4 and concentrated to obtain the crude product. The crude product was purified by column chromatography (chloroform/methanol 90:10, v/v) to obtain the thioamide of cinnamic acid in 86% yield (0.73 g). The product was characterized by ^{1}H and ^{13}C NMR, IR, ESIMS and HRMS spectral studies. Mp 55–56 °C; ^{1}H NMR (500 MHz, $CDCl_3$) δ 7.64 (d, J = 15.6 Hz, 1H), 7.54–7.46 (m, 5H), 6.24 (d, J = 15.6 Hz, 1H), 3.66 (s, 3H), 3.56 (q, 2H), 2.73 (t, 2H), 2.58 (t, 2H), 2.30 (t, 2H), 1.24–1.62 (m, 12H, CH_2); ^{13}C NMR (75 MHz, $CDCl_3$) δ 174.37 (-*C*(O)-OCH$_3$), 165.50 (-NH-*C*(O)-), 141.25 (-NH-C(O)-CH=*C*H-),134.81–127.83, 120.52 (-NH-C(O)-*C*H=CH-), 51.47 (-C(O)-O*C*H$_3$-), 38.49 (-*C*H$_2$-NH-), 29.44 (-S-*C*H$_2$-), 29.36 (-*C*H$_2$-S-), 29.22 (-*C*H$_2$-CH$_2$-S-), 29.19–24.96 (-CH$_2$-CH$_2$-); IR (cm^{-1}, KBr): 2853, 2853, 1720, 1654, 1599, 1527, 1441, 1365; ESIMS (*m*/*z*): 406 [M + H]$^+$, 428 [M + Na]$^+$; HRMS (*m*/*z*): [M + H]$^+$ calcd for $C_{23}H_{36}O_3NS$, 406.24104; found, 406.24077.

Synthesis of methyl 11-((2-((*E*)-3-(4-hydroxyphenyl)acrylamido)ethyl)sulfanyl)undecanoate (3b): Similarly, methyl 11-((2-((*E*)-3-(4-hydroxyphenyl)acrylamido)ethyl)sulfanyl)undecanoate (**3b**) was prepared from **2** (0.6 g, 2.1 mmol) and coumaric acid (0.5 g, 3.2 mmol) in 85% yield (0.78 g) and the product was characterized by ^{1}H and ^{13}C NMR, IR, ESIMS and HRMS spectral studies. Mp 64–65 °C; ^{1}H NMR (500 MHz, $CDCl_3$) δ 7.57 (d, J = 15.6 Hz, 1H), 7.39 (d, J = 8.6 Hz, 1H), 6.85 (d, J = 8.6 Hz, 1H), 6.26 (d, J = 15.6 Hz, 1H), 3.67 (s, 3H), 3.58 (q, 2H), 2.73 (t, 2H), 2.58 (t, 2H), 2.30 (t, 2H), 1.24–1.62 (m, 12H, CH_2); ^{13}C NMR (75 MHz, $CDCl_3$) δ 174.71 (-*C*(O)-OCH$_3$), 166. 84 (-NH-*C*(O)-), 158.33, 141.51 (-NH-C(O)-CH=*C*H-),129.64, 128.99, 117.32 (-NH-C(O)-*C*H=CH-), 115.98, 51.58 (-C(O)-O*C*H$_3$-), 38.63 (-*C*H$_2$-NH-), 34.16 (-S-*C*H$_2$-), 31.89 (-*C*H$_2$-S-), 31.84 (-*C*H$_2$-CH$_2$-S-), 29.69–24.96 (-CH$_2$-CH$_2$-); IR (cm^{-1}, KBr): 3409, 2923, 2853, 1729, 1652, 1595, 1519, 1452, 1373; ESIMS (*m*/*z*): 422 [M + H]$^+$, 444 [M + Na]$^+$; HRMS (*m*/*z*): [M + H]$^+$ calcd for $C_{26}H_{36}O_4NS$, 422.23596; found, 422.23491.

Synthesis of methyl 11-((2-((*E*)-3-(3,4-dihydroxyphenyl)-acrylamido)ethyl)sulfanyl)undecanoate (3c): Similarly, methyl 11-((2-((*E*)-3-(3,4-dihydroxyphenyl)acrylamido)-ethyl)sulfanyl)undecanoate was prepared from **2** (0.6 g, 2.1 mmol) and caffeic acid (0.5 g, 3.2 mmol) in 85% yield (0.81 g) and the product was characterized by ^{1}H and ^{13}C NMR, IR, ESIMS and HRMS spectral studies. ^{1}H NMR (500 MHz, $CDCl_3$) δ 7.55 (d, J = 15.6 Hz, 1H), 7.12 (d, J = 8.6 Hz, 1H), 6.95 (s, 1H) 6.87 (d, J = 8.6 Hz, 1H), 6.24 (d, J = 15.6 Hz, 1H), 3.68 (s, 3H), 3.56 (q, 2H), 2.73 (t, 2H), 2.58 (t, 2H), 2.30 (t, 2H), 1.24–1.62 (m, 12H, CH_2); ^{13}C NMR (75 MHz, $CDCl_3$) δ 174.74 (-*C*(O)-OCH$_3$), 167. 38 (-NH-*C*(O)-), 146.87, 144.53, 142.53 (-NH-C(O)-CH=*C*H-), 127.07, 121.33, 117.12 (-NH-C(O)-*C*H=CH-), 115.46, 114.71, 51.60 (-C(O)-O*C*H$_3$-), 39.05 (-*C*H$_2$-NH-), 38.88 (-S-*C*H$_2$-), 38.76 (-*C*H$_2$-S-), 34.16 (-*C*H$_2$-CH$_2$-S-), 29.59–24.96 (-CH$_2$-CH$_2$-); IR (cm^{-1}, KBr): 3359, 2953, 2854, 1721, 1654, 1599, 1527, 1441, 1365; ESIMS

(*m*/*z*): 438 $[M + H]^+$, 460 $[M + Na]^+$; HRMS (*m*/*z*): $[M + H]^+$ calcd for $C_{23}H_{36}O_5NS$, 438.23087; found, 438.23023.

Synthesis of methyl 11-((2-((*E*)-3-(4-hydroxy-3-methoxyphenyl)acrylamido)ethyl)sulfanyl)undecanoate (3d): Similarly, methyl 11-((2-((*E*)-3-(4-hydroxy-3-methoxyphenyl)acrylamido)ethyl)sulfanyl)undecanoate was prepared from **2** (0.6 g, 2.1 mmol) and ferulic acid (0.6 g, 3.2 mmol) in 84% yield (0.82 g) and the product was characterized by ^1H and ^{13}C NMR, IR, ESIMS and HRMS spectral studies. ^1H NMR (500 MHz, $CDCl_3$) δ 7.55 (d, *J* = 15.5 Hz, 1H), 7.06 (dd, *J* = 8.2, 1.5 Hz, 1H), 7.00 (d, *J* = 1.6 Hz, 1H), 6.91 (d, *J* = 8.2 Hz, 1H), 6.27 (d, *J* = 15.5 Hz, 1H), 3.92 (s, 3H), 3.67 (s, 3H), 3.58 (q, 2H), 2.73 (t, 2H), 2.58 (t, 2H), 2.30 (t, 2H), 1.24–1.62 (m, 12H, CH_2); ^{13}C NMR (75 MHz, $CDCl_3$) δ 174.36 (-*C*(O)-OCH_3), 166. 21 (-NH-*C*(O)-), 147.48, 146.76, 141.26 (-NH-C(O)-CH=*C*H-), 127.33, 122.22, 118.06 (-NH-C(O)-*C*H=CH-), 114.76, 109.64, 55.95 (-OCH_3-), 51.45 (-C(O)-O*C*H_3-), 38.42 (-*C*H_2-NH-), 34.11 (-S-*C*H_2-), 31.97 (-*C*H_2-S), 31.74 (-*C*H_2-CH_2-S-), 29.47–24.95 (-CH_2-CH_2-); IR (cm^{-1}, KBr): 3375, 2926, 2853, 1730, 1656, 1596, 1516, 1433, 1273; ESIMS (*m*/*z*): 452 $[M + H]^+$, 474 $[M + Na]^+$; HRMS (*m*/*z*): $[M + H]^+$ calcd for $C_{24}H_{38}O_5NS$, 452.24652; found, 452.24475.

Synthesis of methyl-11-((2-((*E*)-3-(4-hydroxy-3,5-dimethoxyphenyl)acrylamido)ethyl)sulfanyl)undecanoate (3e): Similarly, methyl 11-((2-((*E*)-3-(4-hydroxy-3,5-dimethoxyphenyl)-acrylamido)ethyl)sulfanyl)undecanoate was prepared from **2** (0.6 g, 2.1 mmol) and sinapic acid (0.7 g, 3.2 mmol) in 85% yield (0.89 g) and the product was characterized by ^1H and ^{13}C NMR, IR, ESIMS and HRMS spectral studies. Mp 69–70 °C; ^1H NMR (500 MHz, $CDCl_3$) δ 7.53 (d, *J* = 15.5 Hz, 1H), 6.76 (s, *J* = 8.2, 1.5 Hz, 2H), 6.28 (d, *J* = 15.5 Hz, 1H), 3.93 (s, 6H), 3.67 (s, 3H), 3.58 (q, 2H), 2.73 (t, 2H), 2.58 (t, 2H), 2.30 (t, 2H), 1.24–1.62 (m, 12H, CH_2); ^{13}C NMR (75 MHz, $CDCl_3$) δ 174.37 (-*C*(O)-OCH_3), 166.07 (-NH-*C*(O)-), 147.22, 141.43 (-NH-C(O)-CH=*C*H-),136.64, 126.29, 118.44 (-NH-C(O)-*C*H=CH-), 104.82, 56.34 (-OCH_3-), 51.48 (-C(O)-O*C*H_3-), 38.39 (-*C*H_2-NH-), 34.11 (-S-*C*H_2-), 31.96 (-*C*H_2-S-), 31.69 (-*C*H_2-CH_2-S-), 29.65–24.95 (-CH_2-CH_2-); IR (cm^{-1}, KBr): 3371, 2926, 2852, 1730, 1658, 1612, 1514, 1455 1285; ESIMS (*m*/*z*): 482 $[M + H]^+$, 504 $[M + Na]^+$; HRMS (*m*/*z*): $[M + H]^+$ calcd for $C_{25}H_{40}O_6NS$, 482.25709; found, 482.25532.

Anti-oxidant activity

DPPH radical scavenging assay

The anti-oxidant activity was determined by the radical scavenging ability using the stable DPPH radical method as reported [22]. Briefly, 200 µL of a methanolic solution of the synthesized phenolic lipoconjugates (1 mM concentrations) were added to 2 mL of a methanolic solution of the DPPH radical (1 mM concentration) and the total volume was made up to 3 mL with methanol. After 40 min of standing, the absorbance of the mixture was measured at 517 nm against methanol as blank sample. TBHQ and α-TP (1 mM concentration) were used as a positive control. The radical-scavenging activities (%) of the tested samples were evaluated by comparison with the control (2 mL DPPH radical solution and 1 mL methanol). Each sample was measured in triplicate and averaged. The free-radical scavenging activity (FRSA) was calculated using the following formula: FRSA = [(*A*c − *A*s)/*A*c] × 100 where *A*c is the absorbance of the control and *A*s is the absorbance of the tested sample after 40 min.

DSC measurements

The anti-oxidant activity was also evaluated by differential scanning calorimetry using pure linoleic acid as a lipid model system [23,24]. All studied anti-oxidants were dissolved in methanol to prepare 1 mM solutions. Samples of linoleic acid (2.5–3.0 mg) were placed in standard aluminum pans and spiked with 10 µL of the anti-oxidant solution. A blank run of linoleic acid, spiked with 10 µL of methanol was also carried out simultaneously to find the oxidative induction temperature (OIT) of linoleic acid. OIT is determined from the first exothermal peak of the plot of heat flow (mW/g) vs temperature. All measurements for each compound were run in triplicate and the results were averaged.

Cytotoxicity test (MTT assay)

The cytotoxicity assay (MTT) was evaluated for all test compounds as described in our earlier work [25]. Five different cancer cell lines viz., MDA-MB-231, breast cancer (ATCC® HTB-26™); SKOV3, ovarian cancer (ATCC® HTB-77™); MCF7, breast cancer (ATCC® HTB-22™); DU 145, prostate cancer (ATCC® HTB-81™); HepG2, liver hepatocellular carcinoma (ATCC® HB-8065™) were obtained from the ATCC (Bethesda, MD, USA) and maintained in DMEM supplemented with 10% FBS, 2 mM L-glutamine, 100 U/mL penicillin, and 100 µg/mL streptomycin at 37 °C in a 5% CO_2 incubator. After seeding of cells in 96 well culture plates, they were allowed to attach properly. Test compounds of different concentrations ranging from 1 to 50 µM were added in triplicates and incubated for 24 h. The cells were then incubated with MTT (0.5 mg/mL) for 3 h and, to dissolve the insoluble formazan crystals, 100 µL DMSO was added to each well. Finally the absorbance of the plates was measured using a Synergy H1 multi-mode plate reader (USA). Doxorubicin was used as the positive control for comparison.

Supporting Information

Supporting Information File 1

Copies of ^{1}H NMR, ^{13}C NMR, HRMS and DSC spectra.
[http://www.beilstein-journals.org/bjoc/content/supplementary/1860-5397-13-4-S1.pdf]

Acknowledgements

Naganna Narra thanks the University Grants Commission (UGC), New Delhi, India, for financial support through a Senior Research Fellowship (UGC-SRF).

References

1. Figueroa-Espinoza, M.-C.; Villeneuve, P. *J. Agric. Food Chem.* **2005,** *53,* 2779. doi:10.1021/jf0484273
2. Shahidi, F.; Chandrasekara, A. *Phytochem. Rev.* **2010,** *9,* 147. doi:10.1007/s11101-009-9142-8
3. Garrido, J.; Gaspar, A.; Garrido, E. M.; Miri, R.; Tavakkoli, M.; Pourali, S.; Saso, L.; Borges, F.; Firuzi, O. *Biochimie* **2012,** *94,* 961. doi:10.1016/j.biochi.2011.12.015
4. Crauste, C.; Rosell, M.; Durand, T.; Vercauteren, J. *Biochimie* **2016,** *120,* 62. doi:10.1016/j.biochi.2015.07.018
5. Mbatia, B.; Kaki, S. S.; Mattiasson, B.; Mulaa, F.; Adlercreutz, P. *J. Agric. Food Chem.* **2011,** *59,* 7021. doi:10.1021/jf200867r
6. Sun, S.; Zhu, S.; Bi, Y. *Food Chem.* **2014,** *158,* 292. doi:10.1016/j.foodchem.2014.02.146
7. Yasa, S. R.; Kaki, S. S.; Bhaskara Rao, B.; Jain, N.; Penumarthy, V. *Med. Chem. Res.* **2016,** *25,* 1299. doi:10.1007/s00044-016-1564-4
8. Kaki, S. S.; Kunduru, K. R.; Kanjilal, S.; Prasad, R. B. N. *J. Oleo Sci.* **2015,** *64,* 845. doi:10.5650/jos.ess15035
9. Hunneche, C. S.; Lund, M. N.; Skibsted, L. H.; Nielsen, J. *J. Agric. Food Chem.* **2008,** *56,* 9258. doi:10.1021/jf8024826
10. Van der Steen, M.; Stevens, C. V. *ChemSusChem* **2009,** *2,* 692. doi:10.1002/cssc.200900075
11. Sammaiah, A.; Kaki, S. S.; Sai Manoj, G. N. V. T.; Poornachandra, Y.; Kumar, C. G.; Prasad, R. B. N. *Eur. J. Lipid Sci. Technol.* **2015,** *117,* 692. doi:10.1002/ejlt.201400471
12. Doležalová, M.; Janiš, R.; Svobodová, H.; Kašpárková, V.; Humpolíček, P.; Krejčí, J. *Eur. J. Lipid Sci. Technol.* **2010,** *112,* 1106. doi:10.1002/ejlt.200900295
13. Tokiwa, Y.; Kitagawa, M.; Raku, T.; Yanagitani, S.; Yoshino, K. *Bioorg. Med. Chem. Lett.* **2007,** *17,* 3105. doi:10.1016/j.bmcl.2007.03.039
14. Jacobson, C. E.; Martinez-Muñoz, N.; Gorin, D. J. *J. Org. Chem.* **2015,** *80,* 7305. doi:10.1021/acs.joc.5b01077
15. Türünç, O.; Firdaus, M.; Klein, G.; Meier, M. A. R. *Green Chem.* **2012,** *14,* 2577. doi:10.1039/C2GC35982K
16. Chiu, M. H.; Prenner, E. J. *J. Pharm. BioAllied Sci.* **2011,** *3,* 39. doi:10.4103/0975-7406.76463
17. Silva, F. A. M.; Borges, F.; Guimarães, C.; Lima, J. L. F. C.; Matos, C.; Reis, S. *J. Agric. Food Chem.* **2000,** *48,* 2122. doi:10.1021/jf9913110
18. Stasiuk, M.; Kozubek, A. *Cell. Mol. Life Sci.* **2010,** *67,* 841. doi:10.1007/s00018-009-0193-1
19. Kaki, S. S.; Gopal, S. C.; Rao, B. V. S. K.; Poornachandra, Y.; Kumar, C. G.; Prasad, R. B. N. *Eur. J. Lipid Sci. Technol.* **2013,** *115,* 1123. doi:10.1002/ejlt.201300179
20. Sammaiah, A.; Padmaja, K. V.; Prasad, R. B. N. *Eur. J. Lipid Sci. Technol.* **2016,** *118,* 495. doi:10.1002/ejlt.201500119
21. Kaki, S. S.; Arukali, S.; Padmaja, K. V.; Prasad, R. B. N.; Yedla, P.; Kumar, C. G. *Bioorg. Med. Chem. Lett.* **2016,** *26,* 209. doi:10.1016/j.bmcl.2015.10.086
22. Akowuah, G. A.; Zhari, I.; Norhayati, I.; Mariam, A. *J. Food Compos. Anal.* **2006,** *19,* 118. doi:10.1016/j.jfca.2005.04.007
23. Gaspar, A.; Martins, M.; Silva, P.; Garrido, E. M.; Garrido, J.; Firuzi, O.; Miri, R.; Saso, L.; Borges, F. *J. Agric. Food Chem.* **2010,** *58,* 11273. doi:10.1021/jf103075r
24. Reis, B.; Martins, M.; Barreto, B.; Milhazes, N.; Garrido, E. M.; Silva, P.; Garrido, J.; Borges, F. *J. Agric. Food Chem.* **2010,** *58,* 6986. doi:10.1021/jf100569j
25. Bollu, V. S.; Nethi, S. K.; Dasari, R. K.; Shiva Nageshwara Rao, S.; Misra, S.; Patra, C. R. *Nanotoxicology* **2015,** *10,* 413. doi:10.3109/17435390.2015.1073398

License and Terms

BEILSTEIN JOURNAL OF ORGANIC CHEMISTRY

Posttranslational isoprenylation of tryptophan in bacteria

Masahiro Okada*, Tomotoshi Sugita and Ikuro Abe

Review

Open Access

Address:
Graduate School of Pharmaceutical Sciences, The University of Tokyo, Bunkyo-ku, Tokyo 113-0033, Japan

Email:
Masahiro Okada* - okadam@mol.f.u-tokyo.ac.jp

* Corresponding author

Keywords:
Bacillus subtilis; isoprenylation; post-translational modification; quorum sensing; tryptophan

Beilstein J. Org. Chem. **2017,** *13,* 338–346.
doi:10.3762/bjoc.13.37

Received: 10 January 2017
Accepted: 10 February 2017
Published: 22 February 2017

This article is part of the Thematic Series "Lipids: fatty acids and derivatives, polyketides and isoprenoids".

Guest Editor: J. S. Dickschat

Abstract

Posttranslational isoprenylation is generally recognized as a universal modification of the cysteine residues in peptides and the thiol groups of proteins in eukaryotes. In contrast, the *Bacillus* quorum sensing peptide pheromone, the ComX pheromone, possesses a posttranslationally modified tryptophan residue, and the tryptophan residue is isoprenylated with either a geranyl or farnesyl group at the gamma position to form a tricyclic skeleton that bears a newly formed pyrrolidine, similar to proline. The post-translational dimethylallylation of two tryptophan residues of a cyclic peptide, kawaguchipeptin A, from cyanobacteria has also been reported. Interestingly, the modified tryptophan residues of kawaguchipeptin A have the same scaffold as that of the ComX pheromones, but with the opposite stereochemistry. This review highlights the biosynthetic pathways and posttranslational isoprenylation of tryptophan. In particular, recent studies on peptide modifying enzymes are discussed.

Introduction

Posttranslational modification is the chemical modification of proteins after their translation from mRNAs to the corresponding polypeptide chains synthesized by ribosomes. Since a post-translational modification generates a novel amino acid residue in ribosomally synthesized proteins consisting of the twenty normal amino acid residues, it increases the structural diversity of ordinary proteins. In addition, newly synthesized proteins lacking the modification often cannot perform the functions of the mature proteins. Therefore, posttranslational modifications dynamically regulate the biological activities of proteins. Novel modifications have been discovered over the last several decades, revealing numerous post-translational modification patterns, including isoprenylation [1,2]. This review will discuss the posttranslational isoprenylation of tryptophan in bacteria. In particular, this review will focus on current findings which have not been available at the time we published a review on this topic previously [3].

Review

Posttranslational isoprenylation of cysteine

Posttranslational isoprenylation is generally referred to as the farnesylation or geranylgeranylation of the thiol group of the

C-terminal cysteine residue in peptides and proteins [4-7]. The isoprenylation of cysteine was first found in the peptide pheromones of basidiomycetous yeast [8-10]. Two peptide pheromones, tremerogen A-10 and tremerogen a-13, are secreted by the yeast-form haploid A-type and a-type cells of *Tremella mesenterica*, respectively (Figure 1A). Tremerogen A-10 is a decapeptide containing a hydroxyfarnesylated C-terminal cysteine methyl ester, whereas tremerogen a-13 is a tridecapeptide containing a farnesylated C-terminal cysteine (Figure 1B) [9,10]. Each pheromone causes the opposite type of cell to induce the reciprocal conjugation of the heterothallic cells, through the formation of a conjugation tube for mating. A structure–activity relationship study on tremerogen A-10 demonstrated that both the amino acid sequence and the hydrophobic side chain were essential for the initiation of the conjugation tube formation [11]. Soon thereafter, the consensus sequence for the isoprenylation of the cysteine in the precursor peptide was identified as the CaaX motif, in which "a" refers to an aliphatic amino acid and "X" refers to an appropriate amino acid, depending on the types of modifying enzymes (Figure 1C) [4-7]. Therefore, in the process of isoprenylated peptide and protein biosynthesis, the cysteine residue of the CaaX motif is isoprenylated by isoprenyltransferase, and then the last three amino acids are processed, often with methyl esterification of the resulting C-terminal isoprenylcysteine. Considering the consensus sequence, a variety of organisms may produce

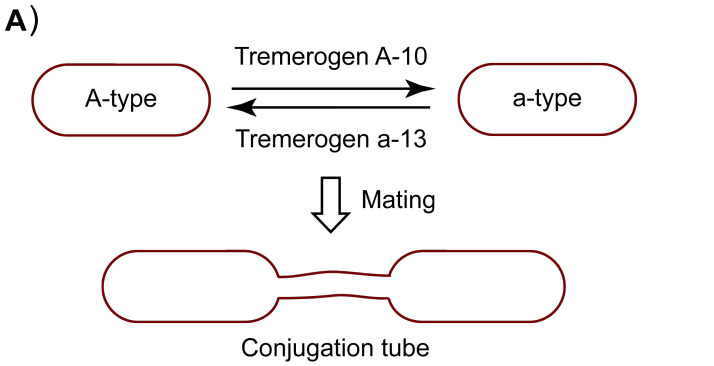

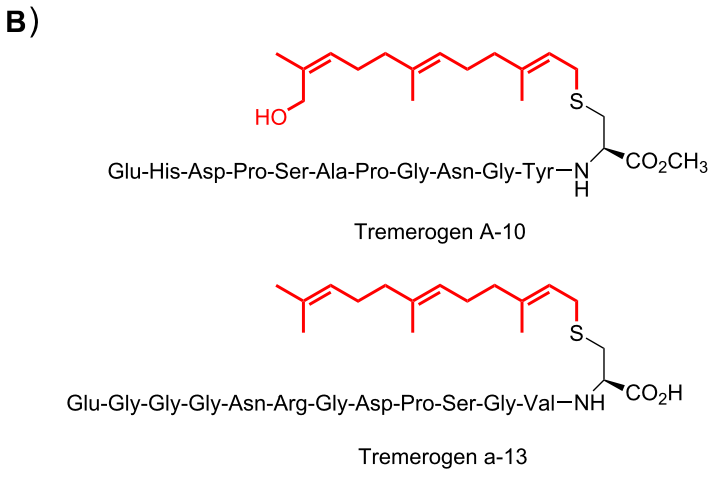

C)

Precursor	Amino acid sequence	Modification
Tremerogen a-13	EGGGNRGDPSGV**C**VIA	Farnesylation
G-protein γ6 (bovine)	ASENPFREKKFF**C**AIL	Geranylgeranylation
K-Ras 4A (human)	EEKTPGCVKIKK**C**IIM	Farnesylation
Consensus sequence	••••••••••••**CaaX**	

Figure 1: (A) Schematic representation of pheromone-induced conjugation tube formation for mating in *Tremella mesenterica*. (B) Chemical structures of tremerogens A-10 and a-13. The isoprenyl side chains are shown in red. (C) C-terminal amino acid sequences of the precursors of isoprenylated peptides and proteins. The CaaX motifs are shown in red.

isoprenylated peptides and proteins. Subsequently, numerous isoprenylated peptides and proteins, such as G-proteins including the human oncogene product K-Ras, were identified from various organisms based on the consensus sequence (Figure 1C). Since the tumor growth induced by K-Ras is highly dependent on the farnesylation, the K-Ras farnesyltransferase has attracted keen attention as a target protein for anticancer therapy [12]. Posttranslational isoprenylation is now recognized as being universal in eukaryotes, and playing an essential role in protein functions.

ComX pheromone

In contrast to eukaryotes, cysteine isoprenylation has not been detected in prokaryotes. Posttranslational isoprenylation in prokaryotes was first found in a tryptophan residue of the quorum sensing pheromone from *Bacillus subtilis*, the ComX pheromone [13]. Quorum sensing is a specific gene expression system dependent on the cell density [14]. In terms of a competition for survival, the cell population density is one of the largest factors for microorganisms because of a high proliferation rate. In the quorum sensing process, bacteria constitutively secrete specific extracellular signaling molecules, called quorum sensing pheromones, to gather information about their cell population density [15-18]. Various phenomena are stimulated by an increase in the bacterial population density, or in other words, the concentration of the specific secreted pheromone. The ComX pheromone induces natural genetic competence under the control of quorum sensing in *B. subtilis*. Specifically, the ComX pheromone induces competent cell formation for DNA transformation at a high population cell density in *B. subtilis* [19,20]. In addition, the ComX pheromone promotes the production of surfactin A, a cyclic lipopeptide with antibiotic and biological surfactant activities (Figure 2A) [21,22]. Furthermore, the $ComX_{natto}$ pheromone from *B. subtilis* subsp. *natto* contributes to the phenotypic characteristics involved in biofilm formation by *B. subtilis* subsp. *natto*, which is closely related to the *Bacillus* laboratory strains and renowned as the producer strain for the quite sticky, traditional Japanese food natto, made from fermented soybeans [23]. *B. subtilis* subsp. *natto* is obviously distinct from the other laboratory strains with respect to the biofilm formation. The biofilm mainly consists of the highly sticky poly-γ-glutamic acid (γ-PGA) polymer (Figure 2B), and the $ComX_{natto}$ pheromone activates γ-PGA biosynthesis in *B. subtilis* subsp. *natto* at nanomolar levels [24].

The ComX pheromones are oligopeptides, and their amino acid sequences and lengths vary widely among *Bacillus* strains (Figure 3A) [13,21,25]. However, each ComX pheromone possesses an invariant tryptophan residue as a single common denominator, and the tryptophan residue is isoprenylated with either a geranyl or farnesyl group at the gamma position to form tricyclic skeleton that bears a newly formed pyrrolidine, which is similar to proline (Figure 3A) [26-28]. The posttranslational modification of ComX pheromones with an isoprenoid plays an essential role for specific quorum sensing responses in *B. subtilis* and related bacilli [3]. Structure–activity relationship studies on the $ComX_{RO\text{-}E\text{-}2}$ pheromone derived from *Bacillus* strain RO-E-2, which is a hexapeptide with a geranyl-modified tryptophan residue, revealed that the exact chemical structure of the geranyl group and the absolute configurations of the tricyclic core scaffold were essential and more critical for its pheromonal activity than the amino acid sequence of the $ComX_{RO\text{-}E\text{-}2}$ pheromone [29-32]. In addition, a previous study using a conditioned medium with *Bacillus* strains suggested that the chemical structure of the isoprenyl side chain is an influential factor of the group- (or species-) specific pheromonal activity [25]. Intriguingly, the same applies for group- (or species-) specificity in Gram negative bacteria because the chemical structure and length of the acyl side chain in acylhomoserine lactones, which are quorum sensing pheromones secreted by Gram negative bacteria, have a great effect on the group specificity (Figure 3B) [33,34]. Modifications of the lipophilic side

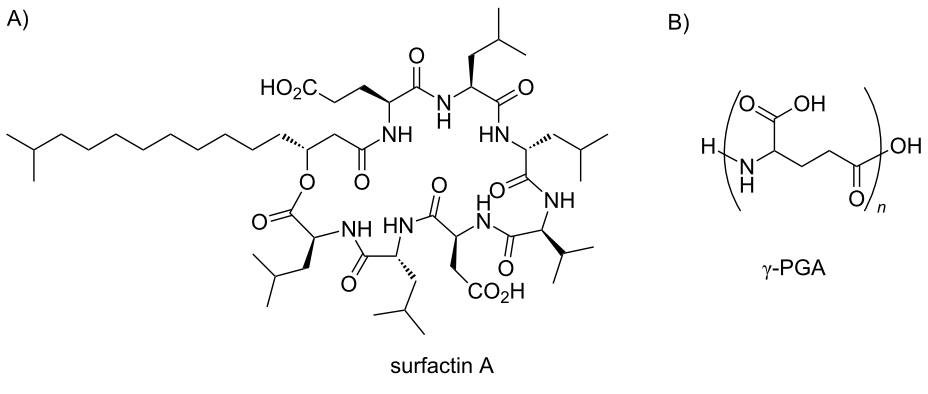

Figure 2: Chemical structures of (A) surfactin A and (B) poly-γ-glutamic acid.

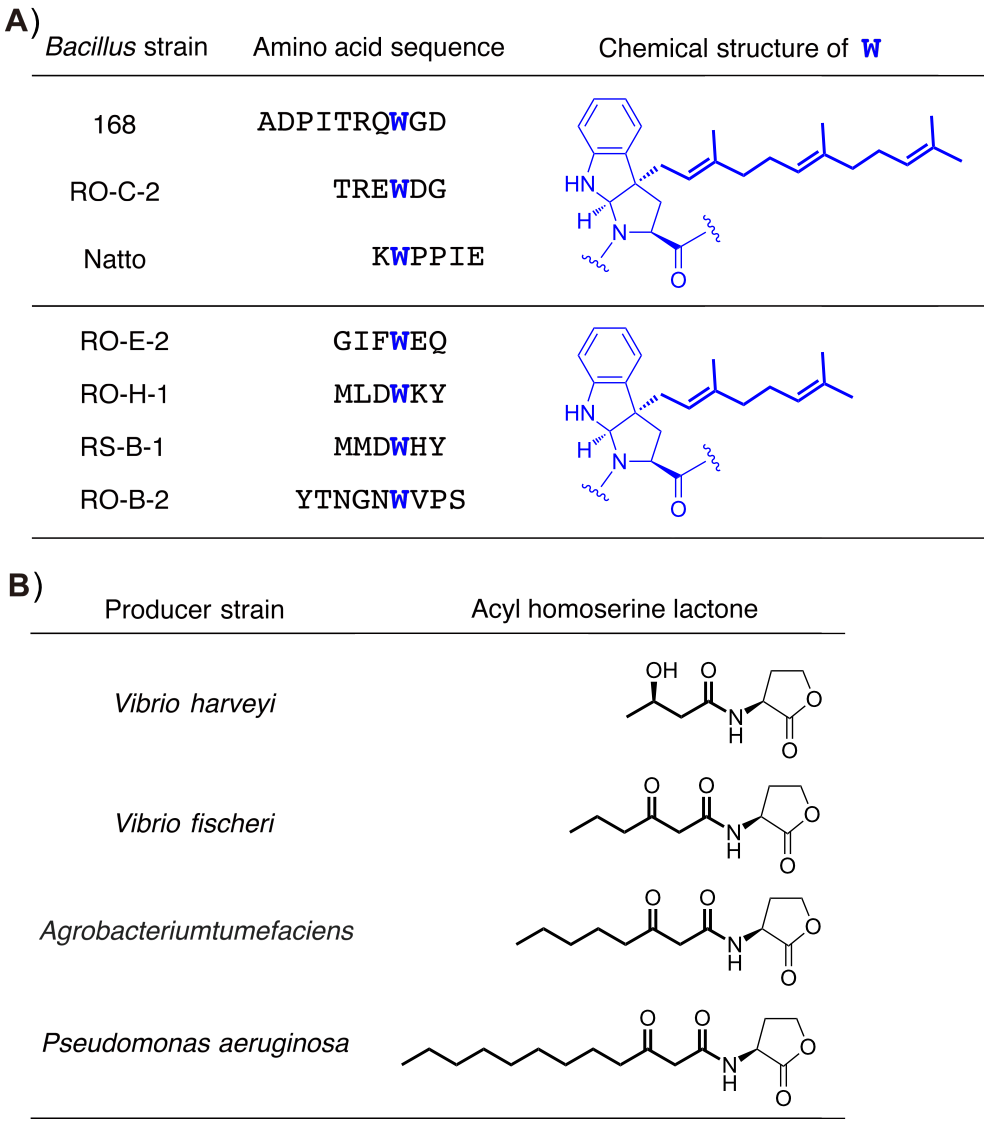

Figure 3: (A) Two types of posttranslational isoprenylations of ComX variants. The modified tryptophan residues are colored blue. The isoprenyl side chains are shown in boldface and colored blue. (B) Chemical structures of acyl homoserine lactones. The acyl side chains are shown in boldface.

chain in quorum sensing pheromones are probably a common strategy to acquire group specificity in bacteria.

ComQ

Molecular genetic analyses of the natural competence of *B. subtilis* revealed that the *comQXPA* gene cluster was responsible for *B. subtilis* to induce the genetic competence involved in the secretion of the ComX pheromone (Figure 4A) [13,21,25]. ComQ, the first protein encoded in the cluster, functions as an isoprenyltransferase for the ComX peptide, which is encoded next in the cluster [35]. The downstream ComP is homologous to transmembrane histidine kinase, and ComA is homologous to a response regulator [36]. Therefore, the two proteins constitute the large family of two-component regulatory systems widely found in bacteria. ComP becomes autophosphorylated in response to the secreted ComX signaling molecule as a receptor, and donates a phosphate group to ComA. The phosphorylated ComA subsequently transmits the signal for activating the surfactin synthase *srfA* operon and mediates the genetic competence in *B. subtilis*. ComQ lacks homology to cysteine isoprenyltransferases, tryptophan dimethylallyltransferases for cyanobactins [2,37,38] or prenyltransferases for indole alkaloids [39-42]. However, ComQ shares some homology with farnesyl diphosphate (FPP) synthases and geranylgeranyl diphosphate (GGPP) synthases, which catalyze the condensation of isopentenyl diphosphate (IPP) with geranyl diphosphate (GPP) or FPP to form C5-extended isoprenyl diphosphates FPP or GGPP (Figure 4B)

[43,44]. In the both typical diphosphate synthases, two aspartate-rich motifs containing "DDxxD" residues, in which x refers to any amino acid, are highly conserved. The two "DDxxD" motifs, named the first and second aspartate-rich motifs (FARM and SARM), function as the binding sites for the two substrates, GPP or FPP and IPP, through Mg^{2+} and play a crucial role in the FPP and GGPP syntheses. FARM is also conserved in ComQ, and a previous study demonstrated that the mutation of the first or fifth aspartate of FARM in ComQ to alanine resulted in the elimination of the downstream pheromonal signaling [21]. This result suggested that FARM of ComQ is necessary for the production of the ComX pheromone and possibly functions as a binding site for the extension substrate, GPP or FPP. In contrast to FARM, the amino acid residues corresponding to SARM in ComQ are quite different from those in the typical FPP and GGPP synthases (Figure 4B). Since only the second aspartate is preserved in the corresponding region of ComQ, the region is thus no longer aspartate-rich, and so hereafter it is referred to as a pseudo-SARM. A site-directed mutagenesis analysis of the $ComQ_{RO\text{-}E\text{-}2}$ from strain RO-E-2 with an in vitro geranylation reaction revealed that the lone-conserved second aspartate residue in the pseudo-SARM of ComQ is also critical for the isoprenylation activity, similar to the second aspartate residue in SARM in the FPP and GGPP synthases [45,46]. In addition, the first amino acid residue of the pseudo-SARM in ComQ, asparagine (or glycine), is crucial for the ComQ function. Particularly, the mutation from asparagine to aspartate drastically decreased the geranylation activity. In contrast, the last three amino acid residues of the pseudo-SARM in ComQ are replaceable, without the loss of ComQ function. Thus, for tryptophan isoprenylation the ComQ must have the sequence NDxxx (or GDxxx) in the pseudo-SARM. Although most FPP

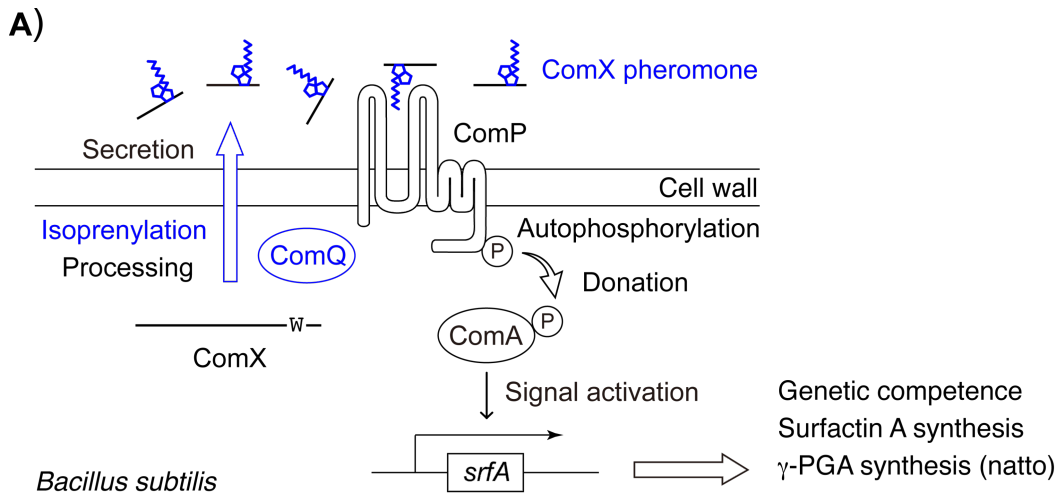

B)

Enzyme	Amino acid sequence of aspartate rich motifs	
	FARM	SARM
ComQ_168	SSDIM**D**DLE**D**EDN	GIIAQIS**GD**YYVLL
ComQ_ROC2	SSDIM**D**DLE**D**EDN	GIVAQIS**GD**YHVLF
ComQ_Natto	SADIF**D**DIE**D**KDN	GIVEQIA**ND**HYGLY
ComQ_ROE2	AFDIF**D**DLE**D**EDN	GIIKQLE**ND**YYGLV
ComQ_ROH1	SFDIY**D**DLQ**D**KDN	GIMSQID**ND**YKGLF
ComQ_RSB1	SFDIY**D**DLE**D**KDN	GIMSQID**ND**YKGLF
ComQ_ROB2	SFDIY**D**DLE**D**KDN	GIIAQIE**ND**YQGLY
EcGGPPS	AT**L**LH**DD**VV**D**ESD	G**T**A**FQ**LI**DD**LL**D**YS

Figure 4: (A) Schematic representation of the signal transduction cascade of quorum sensing stimulated by the ComX pheromone in *B. subtilis*. (B) Amino acid sequences of the aspartate-rich motif and the pseudo aspartate-rich motif in ComQ from seven *Bacillus* strains. Essential amino acid residues for function are shown in bold and colored blue. EcGGPPS is a geranylgeranyl diphosphate synthase derived from *Escherichia coli* ISC56. It's essential amino acid residues for function are shown in boldface, and the aspartate-rich motifs are underlined.

and GGPP synthases possess the DDxx(D) amino acid sequence in the SARM, the sequence is unsuitable for the isoprenylation of tryptophan.

ComX

The ComX precursor peptide possesses 53 to 58 amino acid residues in six *Bacillus* strains, except for subsp. *natto* [25,26]. The tryptophan residue isoprenylated by ComQ is located at either the 3rd or 4th position from the C-terminal end, and the cleavage of the N-terminal residues leads to the production of the mature ComX pheromone with six to ten amino acid residues (Figure 5). In most ribosomally synthesized and post-translationally modified peptides (RIPPs), a conserved recognition motif in the N-terminal leader region of the precursor peptide enables the enzymatic modification of the C-terminal core peptide, and then the leader amino acids are frequently cleaved [2]. However, there is no obvious sequence within the N-terminal region of the ComX peptide for ComQ recognition, because the truncated C-terminal dodecapeptide of $ComX_{RO\text{-}E\text{-}2}$ ([47-58]$ComX_{RO\text{-}E\text{-}2}$, LSKKCKGIFWEQ) showed significant activity for geranyl modification by $ComQ_{RO\text{-}E\text{-}2}$, although the activity was approximately 10-fold weaker than that of full length $ComX_{RO\text{-}E\text{-}2}$ [47]. Among the twelve amino acid residues, the N-terminal leucine residue and the modified tryptophan residue were the only conserved amino acids in the ComX variants. Therefore, a common consensus sequence for tryptophan isoprenylation does not seem to exist. In addition, the tryptophan residue modified with a geranyl group must be located at the 2nd, 3rd, or 4th position from the C-terminal end of $ComX_{RO\text{-}E\text{-}2}$ for geranylation by $ComQ_{RO\text{-}E\text{-}2}$, based on the in vitro reactions of C-terminal sequence analogs with either a deletion of the two residues or an alanine extension at the C-terminal end. Therefore, the undecapeptide [47-57]$ComX_{RO\text{-}E\text{-}2}$ from the 47th to the 57th residues of the $ComX_{RO\text{-}E\text{-}2}$, LSKKCKGIFWE, is the minimum substrate unit for geranylation by $ComQ_{RO\text{-}E\text{-}2}$. These results are consistent with the fact that the ComX pheromone variants among six *Bacillus* strains possess a modified tryptophan residue at the 3rd or 4th position from the C-terminal end, except for the $ComX_{natto}$ pheromone from subsp. *natto*. Unlike the six ComX pheromone variants, the $ComX_{natto}$ pheromone possesses a modified tryptophan residue with a farnesyl group at the 5th position from the C-terminal end, which corresponds to the 54th residue in the 73 amino acid residues of $ComX_{natto}$; namely, at the 20th position from the C-terminal end. In addition, the C-terminal amino acid residues of $ComX_{natto}$ as well as the N-terminal amino acid residues are processed to form the $ComX_{natto}$ pheromone, corresponding to the 53rd to 58th residues of the $ComX_{natto}$ precursor peptide [24,48]. Although it is presently not clear which step occurs first, the farnesylation of the tryptophan residue or the truncation of the C-terminal amino acid residues, the posttranslational farnesylation was not necessarily limited to a tryptophan near the C-terminus, but also has occurred at an internal tryptophan residue of the precursor peptide.

Kawaguchipeptin A

Apart from the ComX pheromones, post-translational dimethylallylations of the tyrosine, threonine, serine, and tryptophan residues of cyclic peptides from cyanobacteria were reported [49-51]. The RiPPs derived from cyanobacteria, including dimethylallylated cyclic peptides, are called cyanobactins [2,37,38]. Although several cyanobactins exhibit significant biological activities, such as antibacterial and enzyme inhibitory properties, the actual biological role of prenylation in cyanobactins is still unknown at this time. Kawaguchipeptins A and B are members of the cyanobactin family and are macrocyclic undecapeptides with the cyclic amino acid sequence of [WLNGDNNWSTP]. They are produced by *Microcystis aeruginosa* NIES-88 (Figure 6) [52,53]. Kawaguchipeptin A contains one D-leucine and two prenylated tryptophan residues, while kawaguchipeptin B consists only of L-amino acid residues. Interestingly, kawaguchipeptin A possesses two dimethylallylated tryptophan residues, which are modified with a dimethylallyl group at the gamma position, resulting in the formation of

Strain	Amino acid sequence of ComX (Underlined: ComX pheromone, **W**: isoprenylated)
168	MQDLINYFLNYPEALKKLKNKEACLIGFDVQETETIIKAYNDYYLADPITRQ**W**GD
RO-C-2	MQDLINYFLSYPEVLKKLKNREACLIGFSSNETETIIKAYNDYHLSSPTTRE**W**DG
Natto	MKHIDKIISHLVNNPEAFDQFKNGNLTLLNINEKEKKAILYAFEQGEVPRTSK**W**PPIEAISNFFEDDKRKSLI
RO-E-2	MKQDMIDYLMKNPQVLTKLENGEASLIGIPDKLIPSIVDIFNKKMT**LSKKCKGIF****W****E**Q
RO-H-1	MQEMVGYLIKYPNVLREVMEGNACLLGVDKDQSECIINGFKGLEIYSMLD**W**KY
RS-B-1	MQEMVGYLIKYPNVLREVMEGNACLLGVDKDQSECIINGFKGLEIYSMMD**W**HY
RO-B-2	MQEIVGYLVKNPEVLDEVMKGRASLLNIDKDQLKSIVDAFGGLQIYTNGN**W**VPS

Figure 5: Amino acid sequences of ComX from seven *Bacillus* strains. The sequences of the mature pheromones are underlined, and the isoprenylated tryptophan residues are shown in bold and colored blue.

a tricyclic structure with the same scaffold as that of the ComX pheromones, but with the opposite stereochemistry [54]. The *KgpA* to *G* gene cluster was identified as encoding the kawaguchipeptins synthase in *M. aeruginosa* NIES-88 [55]. KgpF is a member of the ABBA prenyltransferase family, which shares a common structural motif known as the ABBA fold and exhibits some similarity to other dimethylallyltransferases for cyanobactins and prenyltransferases for indole alkaloids, but lacks similarity to cysteine isoprenyltransferases and ComQs [2,37-44]. Considering the in vitro prenylation analysis of KgpF together with other biosynthetic studies on prenylated cyanobactins, KgpF functions at the end of the biosynthesis, and recognizes two tryptophan residues in the precursor cyclic peptide to form kawaguchipeptin A. In contrast to typical post-translational modifications, a specific amino acid motif adjacent to the core peptide sequence for directing KgpF is unlikely to be required. In addition, the prenylation reaction by KgpF does not seem to need a specific amino acid motif within the core cyclic peptide, because there is no similarity between the sequences surrounding the two tryptophan residues (PWL and NWS) in kawaguchipeptin A. Consistently, KgpF exhibits relaxed substrate specificity toward diverse tryptophan residues in peptides, as KgpF can even accept a single derivatized amino acid, Fmoc-tryptophan, as a substrate and mediate its regioselective and stereoselective dimethylallylation at the C-3 position of its indole ring.

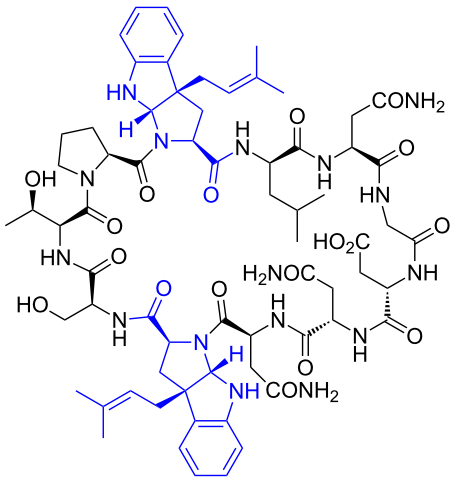

kawaguchipeptin A

Figure 6: Chemical structure of kawaguchipeptin A. Dimethylallylated tryptophan residues are colored blue.

Conclusion

The posttranslational isoprenylation of tryptophan involving pyrrolidine ring formation was first discovered in a *B. subtilis* peptide pheromone, as a crucial modification for the pheromonal function. In addition, the discovery of the $ComX_{natto}$ pheromone revealed that a tryptophan residue modified with an isoprenyl group is not always restricted to a location near the C-terminal end. The broad substrate tolerance of the modifying enzyme ComQ may attract attention as an enzyme engineering target for the synthesis of prenylated tryptophan derivatives. However, since the consensus sequences for tryptophan isoprenylation in the ComX precursor peptide and the ComX pheromone homologues have yet to be identified, it is presently considered that the post-translational geranylation or farnesylation of tryptophan is a special modification in several *Bacillus* species. In contrast, numerous peptides and proteins post-translationally modified with farnesyl or geranylgeranyl groups on the cysteine residues were identified in a variety of organisms. However, the isoprenylation was not considered to be universal at first. The isoprenylation of cysteine was also first found in peptide pheromones from a specific microorganism, as an essential modification for the pheromonal activity. Thus, it is conceivable that the posttranslational isoprenylation of tryptophan is actually widespread. Therefore, more research should be focused on the details and the diversity of the post-translational isoprenylation of tryptophan.

Acknowledgements

This work was supported in part by JSPS KAKENHI Grant Number 24688011 and a Grant-in-Aid for the Cooperative Research Project from Joint Usage/Research Center (Joint Usage/Research Center for Science-Based Natural Medicine). This work was also supported in part by Takeda Science Foundation, Kobayashi International Scholarship Foundation, and Suzuken Memorial Foundation.

References

1. Krishna, R. G.; Wold, F. Posttranslational Modifications. In *Proteins-Analysis and Design;* Angeletti, R. H., Ed.; Academic Press: San Diego, USA, 1998; pp 121–206.
2. Arnison, P. G.; Bibb, M. J.; Bierbaum, G.; Bowers, A. A.; Bugni, T. S.; Bulaj, G.; Camarero, J. A.; Campopiano, D. J.; Challis, G. L.; Clardy, J.; Cotter, P. D.; Craik, D. J.; Dawson, M.; Dittmann, E.; Donadio, S.; Dorrestein, P. C.; Entian, K.-D.; Fischbach, M. A.; Garavelli, J. S.; Göransson, U.; Gruber, C. W.; Haft, D. H.; Hemscheidt, T. K.; Hertweck, C.; Hill, C.; Horswill, A. R.; Jaspars, M.; Kelly, W. L.; Klinman, J. P.; Kuipers, O. P.; Link, A. J.; Liu, W.; Marahiel, M. A.; Mitchell, D. A.; Moll, G. N.; Moore, B. S.; Müller, R.; Nair, S. K.; Nes, I. F.; Norris, G. E.; Olivera, B. M.; Onaka, H.; Patchett, M. L.; Piel, J.; Reaney, M. J. T.; Rebuffat, S.; Ross, R. P.; Sahl, H.-G.; Schmidt, E. W.; Selsted, M. E.; Severinov, K.; Shen, B.; Sivonen, K.; Smith, L.; Stein, T.; Sussmuth, R. D.; Tagg, J. R.; Tang, G. L.; Truman, A. W.; Vederas, J. C.; Walsh, C. T.; Walton, J. D.; Wenzel, S. C.; Willey, J. M.; van der Donk, W. A. *Nat. Prod. Rep.* **2013,** *30,* 108–160. doi:10.1039/C2NP20085F
3. Okada, M. *Biosci., Biotechnol., Biochem.* **2011,** *75,* 1413–1417. doi:10.1271/bbb.110087

4. Clarke, S. *Annu. Rev. Biochem.* **1992,** *61,* 355–386. doi:10.1146/annurev.bi.61.070192.002035
5. Tamanoi, F.; Hrycyna, C. A.; Bergo, M. O., Eds. *The Enzymes. Protein Prenylation Part A,,* 1st ed.; Academic Press: San Diego, USA, 2011; Vol. 29.
6. Glomset, J. A.; Farnsworth, C. C. *Annu. Rev. Cell Biol.* **1994,** *10,* 181–205. doi:10.1146/annurev.cb.10.110194.001145
7. Zhang, F. L.; Casey, P. J. *Annu. Rev. Biochem.* **1996,** *65,* 241–269. doi:10.1146/annurev.bi.65.070196.001325
8. Kamiya, Y.; Sakurai, A.; Tamura, S.; Takahashi, N.; Abe, K.; Tsuchiya, E.; Fukui, S.; Kitada, C.; Fujino, M. *Biochem. Biophys. Res. Commun.* **1978,** *83,* 1077–1083. doi:10.1016/0006-291X(78)91505-X
9. Sakagami, Y.; Isogai, A.; Suzuki, A.; Tamura, S.; Kitada, C.; Fujino, M. *Agric. Biol. Chem.* **1979,** *43,* 2643–2645. doi:10.1271/bbb1961.43.2643
10. Sakagami, Y.; Yoshida, M.; Isogai, A.; Suzuki, A. *Science* **1981,** *212,* 1525–1527. doi:10.1126/science.212.4502.1525
11. Fujino, M.; Kitada, C.; Sakagami, Y.; Isogai, A.; Tamura, S.; Suzuki, A. *Naturwissenschaften* **1980,** *67,* 406–408. doi:10.1007/BF00405487
12. Winter-Vann, A. M.; Casey, P. J. *Nat. Rev. Cancer* **2005,** *5,* 405–412. doi:10.1038/nrc1612
13. Magnuson, R.; Solomon, J.; Grossman, A. D. *Cell* **1994,** *77,* 207–216. doi:10.1016/0092-8674(94)90313-1
14. Fuqua, W. C.; Winans, S. C.; Greenberg, E. P. *J. Bacteriol.* **1994,** *176,* 269–275. doi:10.1128/jb.176.2.269-275.1994
15. Bassler, B. L.; Losick, R. *Cell* **2006,** *125,* 237–246. doi:10.1016/j.cell.2006.04.001
16. Camilli, A.; Bassler, B. L. *Science* **2006,** *311,* 1113–1116. doi:10.1126/science.1121357
17. Williams, P.; Winzer, K.; Chan, W. C.; Cámara, M. *Philos. Trans. R. Soc., B* **2007,** *362,* 1119–1134. doi:10.1098/rstb.2007.2039
18. Dickschat, J. S. *Nat. Prod. Rep.* **2010,** *27,* 343–369. doi:10.1039/b804469b
19. Tortosa, P.; Dubnau, D. *Curr. Opin. Microbiol.* **1999,** *2,* 588–592. doi:10.1016/S1369-5274(99)00026-0
20. Hamoen, L. W.; Venema, G.; Kuipers, O. P. *Microbiology* **2003,** *149,* 9–17. doi:10.1099/mic.0.26003-0
21. Bacon Schneider, K.; Palmer, T. M.; Grossman, A. D. *J. Bacteriol.* **2002,** *184,* 410–419. doi:10.1128/JB.184.2.410-419.2002
22. Tran, L.-S. P.; Nagai, T.; Itoh, Y. *Mol. Microbiol.* **2000,** *37,* 1159–1171. doi:10.1046/j.1365-2958.2000.02069.x
23. Jung, J.; Yu, K. O.; Ramzi, A. B.; Choe, S. H.; Kim, S. W.; Han, S. O. *Biotechnol. Bioeng.* **2012,** *109,* 2349–2356. doi:10.1002/bit.24524
24. Hayashi, S.; Usami, S.; Nakamura, Y.; Ozaki, K.; Okada, M. *Biosci., Biotechnol., Biochem.* **2015,** *79,* 1567–1569. doi:10.1080/09168451.2015.1032884
25. Ansaldi, M.; Marolt, D.; Stebe, T.; Mandic-Mulec, I.; Dubnau, D. *Mol. Microbiol.* **2002,** *44,* 1561–1573. doi:10.1046/j.1365-2958.2002.02977.x
26. Okada, M.; Sato, I.; Cho, S. J.; Iwata, H.; Nishio, T.; Dubnau, D.; Sakagami, Y. *Nat. Chem. Biol.* **2005,** *1,* 23–24. doi:10.1038/nchembio709
27. Okada, M.; Yamaguchi, H.; Sato, I.; Tsuji, F.; Qi, J.; Dubnau, D.; Sakagami, Y. *Biosci., Biotechnol., Biochem.* **2007,** *71,* 1807–1810. doi:10.1271/bbb.70245
28. Okada, M.; Yamaguchi, H.; Sato, I.; Tsuji, F.; Dubnau, D.; Sakagami, Y. *Biosci., Biotechnol., Biochem.* **2008,** *72,* 914–918. doi:10.1271/bbb.80006
29. Okada, M.; Sato, I.; Cho, S. J.; Suzuki, Y.; Ojika, M.; Dubnau, D.; Sakagami, Y. *Biosci., Biotechnol., Biochem.* **2004,** *68,* 2374–2387. doi:10.1271/bbb.68.2374
30. Okada, M.; Sato, I.; Cho, S. J.; Dubnau, D.; Sakagami, Y. *Tetrahedron* **2006,** *62,* 8907–8918. doi:10.1016/j.tet.2006.06.074
31. Okada, M.; Yamaguchi, H.; Sato, I.; Cho, S. J.; Dubnau, D.; Sakagami, Y. *Bioorg. Med. Chem. Lett.* **2007,** *17,* 1705–1707. doi:10.1016/j.bmcl.2006.12.070
32. Tsuji, F.; Kobayashi, K.; Okada, M.; Yamaguchi, H.; Ojika, M.; Sakagami, Y. *Bioorg. Med. Chem. Lett.* **2011,** *21,* 4041–4044. doi:10.1016/j.bmcl.2011.04.123
33. Zhang, R.-g.; Pappas, K. M.; Brace, J. L.; Miller, P. C.; Oulmassov, T.; Molyneaux, J. M.; Anderson, J. C.; Bashkin, J. K.; Winans, S. C.; Joachimiak, A. *Nature* **2002,** *417,* 971–974. doi:10.1038/nature00833
34. Geske, G. D.; O'Neill, J. C.; Miller, D. M.; Mattmann, M. E.; Blackwell, H. E. *J. Am. Chem. Soc.* **2007,** *129,* 13613–13625. doi:10.1021/ja074135h
35. Weinrauch, Y.; Msadek, T.; Kunst, F.; Dubnau, D. *J. Bacteriol.* **1991,** *173,* 5685–5693. doi:10.1128/jb.173.18.5685-5693.1991
36. Weinrauch, Y.; Penchev, R.; Dubnau, E.; Smith, I.; Dubnau, D. *Genes Dev.* **1990,** *4,* 860–872. doi:10.1101/gad.4.5.860
37. McIntosh, J. A.; Donia, M. S.; Schmidt, E. W. *Nat. Prod. Rep.* **2009,** *26,* 537–559. doi:10.1039/b714132g
38. Czekster, C. M.; Ge, Y.; Naismith, J. H. *Curr. Opin. Chem. Biol.* **2016,** *35,* 80–88. doi:10.1016/j.cbpa.2016.08.029
39. Tello, M.; Kuzuyama, T.; Heide, L.; Noel, J. P.; Richard, S. B. *Cell. Mol. Life Sci.* **2008,** *65,* 1459–1463. doi:10.1007/s00018-008-7579-3
40. Yu, X.; Li, S.-M. *Methods Enzymol.* **2012,** *516,* 259–278. doi:10.1016/B978-0-12-394291-3.00005-8
41. Walsh, T. *ACS Chem. Biol.* **2014,** *9,* 2718–2728. doi:10.1021/cb500695k
42. Tanner, M. E. *Nat. Prod. Rep.* **2015,** *32,* 88–101. doi:10.1039/C4NP00099D
43. Wang, K.; Ohnuma, S.-i. *Trends Biochem. Sci.* **1999,** *24,* 445–451. doi:10.1016/S0968-0004(99)01464-4
44. Poulter, C. D. *Phytochem. Rev.* **2006,** *5,* 17–26. doi:10.1007/s11101-005-4887-1
45. Tsuji, F.; Ishihara, A.; Kurata, K.; Nakagawa, A.; Okada, M.; Kitamura, S.; Kanamaru, K.; Masuda, Y.; Murakami, K.; Irie, K.; Sakagami, Y. *FEBS Lett.* **2012,** *586,* 174–179. doi:10.1016/j.febslet.2011.12.012
46. Okada, M.; Ishihara, A.; Yamasaki, R.; Tsuji, F.; Hayashi, S.; Usami, S.; Sakagami, Y. *Biosci., Biotechnol., Biochem.* **2014,** *78,* 550–555. doi:10.1080/09168451.2014.891932
47. Tsuji, F.; Ishihara, A.; Nakagawa, A.; Okada, M.; Kitamura, S.; Kanamaru, K.; Masuda, Y.; Murakami, K.; Irie, K.; Sakagami, Y. *Biosci., Biotechnol., Biochem.* **2012,** *76,* 1492–1496. doi:10.1271/bbb.120206
48. Okada, M.; Nakamura, Y.; Hayashi, S.; Ozaki, K.; Usami, S. *Bioorg. Med. Chem. Lett.* **2015,** *25,* 4293–4296. doi:10.1016/j.bmcl.2015.07.083
49. Donia, M. S.; Ravel, J.; Schmidt, E. W. *Nat. Chem. Biol.* **2008,** *4,* 341–343. doi:10.1038/nchembio.84
50. McIntosh, J. A.; Donia, M. S.; Nair, S. K.; Schmidt, E. W. *J. Am. Chem. Soc.* **2011,** *133,* 13698–13705. doi:10.1021/ja205458h
51. Sardar, D.; Lin, Z.; Schmidt, E. W. *Chem. Biol.* **2015,** *22,* 907–916. doi:10.1016/j.chembiol.2015.06.014
52. Ishida, K.; Matsuda, H.; Murakami, M.; Yamaguchi, K. *Tetrahedron* **1996,** *52,* 9025–9030. doi:10.1016/0040-4020(96)00452-8

53. Ishida, K.; Matsuda, H.; Murakami, M.; Yamaguchi, K. *J. Nat. Prod.* **1997,** *60,* 724–726. doi:10.1021/np970146k
54. Okada, M.; Sugita, T.; Akita, K.; Nakashima, Y.; Tian, T.; Li, C.; Mori, T.; Abe, I. *Org. Biomol. Chem.* **2016,** *14,* 9639–9644. doi:10.1039/C6OB01759B
55. Parajuli, A.; Kwak, D. H.; Dalponte, L.; Leikoski, N.; Galica, T.; Umeobika, U.; Trembleau, L.; Bent, A.; Sivonen, K.; Wahlsten, M.; Wang, H.; Rizzi, E.; De Bellis, G.; Naismith, J.; Jaspars, M.; Liu, X.; Houssen, W.; Fewer, D. P. *Angew. Chem., Int. Ed.* **2016,** *55,* 3596–3599. doi:10.1002/anie.201509920

License and Terms

BEILSTEIN JOURNAL OF ORGANIC CHEMISTRY

Biosynthetic origin of butyrolactol A, an antifungal polyketide produced by a marine-derived *Streptomyces*

Enjuro Harunari[1], Hisayuki Komaki[2] and Yasuhiro Igarashi[*1]

Full Research Paper

Open Access

Address:
[1]Biotechnology Research Center and Department of Biotechnology, Toyama Prefectural University, 5180 Kurokawa, Imizu, Toyama 939-0398, Japan and [2]Biological Resource Center, National Institute of Technology and Evaluation (NBRC), 2-5-8 Kazusakamatari, Kisarazu, Chiba 292-0818, Japan

Email:
Yasuhiro Igarashi* - yas@pu-toyama.ac.jp

* Corresponding author

Keywords:
biosynthesis; butyrolactol; contiguous polyol; hydroxymalonyl-ACP; polyketide; *Streptomyces*; *tert*-butyl

Beilstein J. Org. Chem. **2017,** *13,* 441–450.
doi:10.3762/bjoc.13.47

Received: 17 January 2017
Accepted: 20 February 2017
Published: 08 March 2017

This article is part of the Thematic Series "Lipids: fatty acids and derivatives, polyketides and isoprenoids".

Guest Editor: J. S. Dickschat

Abstract

Butyrolactol A is an antifungal polyketide of *Streptomyces* bearing an uncommon *tert*-butyl starter unit and a polyol system in which eight hydroxy/acyloxy carbons are contiguously connected. Except for its congener butyrolactol B, there exist no structurally related natural products to date. In this study, inspired by our previous genomic analysis, incorporation of ^{13}C- and ^{2}H-labeled precursors into butyrolactol A was investigated. Based on the labeling pattern and sequencing analytical data, we confirmed that the *tert*-butyl group is derived from valine and its *C*-methylation with methionine and the polyol carbons are derived from a glycolysis intermediate, possibly hydroxymalonyl-ACP.

Introduction

Actinomycetes produce structurally diverse secondary metabolites with pharmaceutically useful bioactivities. Importantly, members of the genus *Streptomyces* have been the main source of drug discovery programs due to their high capacity in secondary metabolism including polyketides, peptides, terpenoids, alkaloids, and amino acid/carbohydrate/nucleic acid derivatives [1,2]. One of the largest groups of bacterial secondary metabolites is polyketide from which a range of clinically used drugs have been developed. Polyketides still remain in the focus of drug development because of their structural complexity that can provide attractive templates for new pharmacophores [3]. While the frequency of discovering new skeletons from actinomycetes seems declining, biosynthetic analysis of structurally unique known compounds and the following bioengineering of biosynthetic genes are currently becoming an essential part of the creation of new drug-like structures [4-8].

Butyrolactol A (**1**) is an antifungal polyketide first isolated from *Streptomyces rochei* S785-16 [9] (Figure 1). The left half of **1** is the hydrophobic unconjugated tetraene system including one

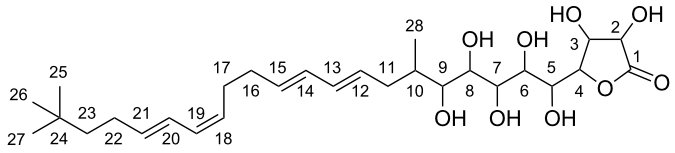

Figure 1: The structure of butyrolactol A (**1**).

Z-olefin with a terminal *tert*-butyl group, whereas the hydrophilic polyol system bearing a γ-lactone terminus constitutes the right half of the molecule. To date, no structurally related natural products are known except for its demethyl congener butyrolactol B that was also isolated from the same strain and has an isopropyl group instead of the *tert*-butyl terminus [9]. Very recently, isolation of butyrolactols C and D was presented but the details are not available in public domains [10]. **1** has a broad antimicrobial activity against fungi ranging from *Candida albicans* to *Trichophyton mentagrophytes* with comparative activity to nystatin [9]. Despite the uniqueness of the structure and the antifungal potency, no further research has been reported for **1**.

There are two interesting aspects in the structure of butyrolactol A (**1**). First, among the polyketides, a *tert*-butyl group has been found exclusively in metabolites of marine cyanobacteria except for **1** [11-14] (Figure 2). Although no experimental evi-

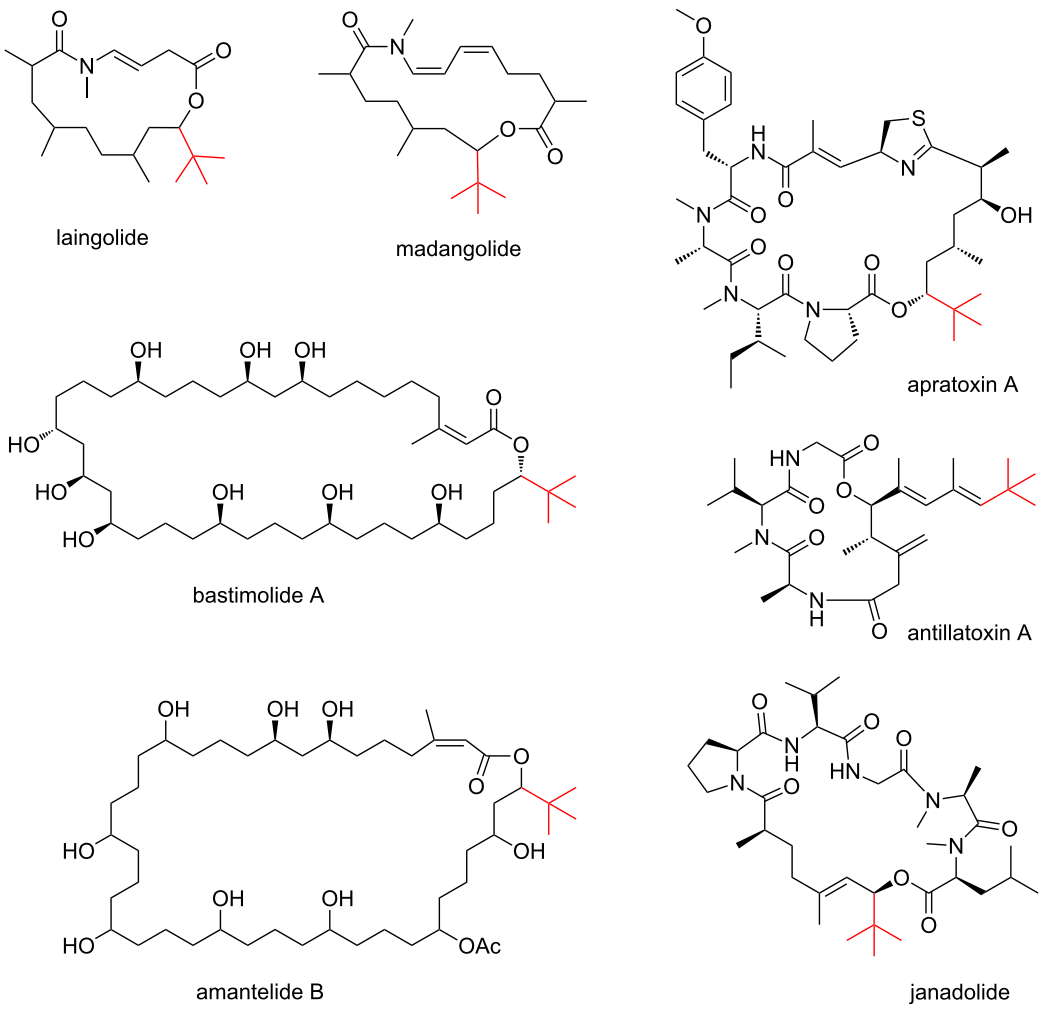

Figure 2: Cyanobacterial polyketides bearing a *tert*-butyl group.

dence is available, pivaloyl-CoA (2,2-dimethylpropanoyl-CoA) is supposed to be a starter for its biosynthesis [15]. Additionally, trimethylation of malonyl-CoA is proposed for the synthesis of the *tert*-butyl starter in the biosynthesis of apratoxin A [16]. Another intriguing feature of this molecule is the highly oxygenated carbon chain in which eight hydroxy groups, one of which is used for lactone formation, are contiguously aligned. A 1,3-diol is a common structural element in aliphatic polyketides because the incorporation of malonate-precursors gives rise to the alternative alignment of the methylene and the oxygenated carbons. Meanwhile, a 1,2-diol in polyketides is known to be formed by hydroxylation of methylene carbons as seen in the biosynthesis of erythromycin or amphotericin B [17,18]. The contiguously hydroxylated carbon chain of **1** is quite unusual as a polyketide. Examples of similar but shorter polyol carbon chains are ossamycin [19], IB-96212 [20], and antifungalmycin [21], all of which are the secondary metabolites of actinomycetes (Figure 3).

In our investigation on secondary metabolites of marine actinomycetes, butyrolactol A (**1**) was found to be produced by a *Streptomyces* strain collected from deep sea water of the Toyama Bay, Japan. In order to get insight into the construction of the above-mentioned unusual structures, we performed an in silico analysis of the biosynthetic genes of **1** through draft genome sequencing and proposed its biosynthetic pathway [22]. In this study, biosynthetic precursors of **1** were investigated for further genetic and enzymatic studies.

Results and Discussion

It was obvious from its structure that **1** was synthesized through the malonate pathway. First, [1,2-$^{13}C_2$]acetate was fed to the culture to ensure the alignment of malonate units. In the ^{13}C NMR spectrum, split signals arising from ^{13}C–^{13}C couplings were observed for six pairs of carbons: C-11/C-12, C-13/C-14, C-15/C-16, C-17/C-18, C-19/C-20, and C-21/C-22 (Table 1, Figure S1 in Supporting Information File 1). In the 2D-INADEQUATE spectrum of ^{13}C-labeled **1** obtained with a parameter set optimized for $^1J_{CC}$ 50 Hz, cross peaks derived from the intact $^{13}C_2$ acetate units were detected for the carbon pairs mentioned above (Table 1, Figure 4a).

According to the incorporation result of the doubly labeled acetate, malonyl-CoA is not the extender unit for the lactone (C-1 to C-4) and the pentaol (C-5 to C-9) moieties (Figure 3), suggesting that the contiguous polyol system is not formed by methylene hydroxylation. Another possible pathway for 1,2-diol formation is the incorporation of hydroxymalonyl-ACP from a

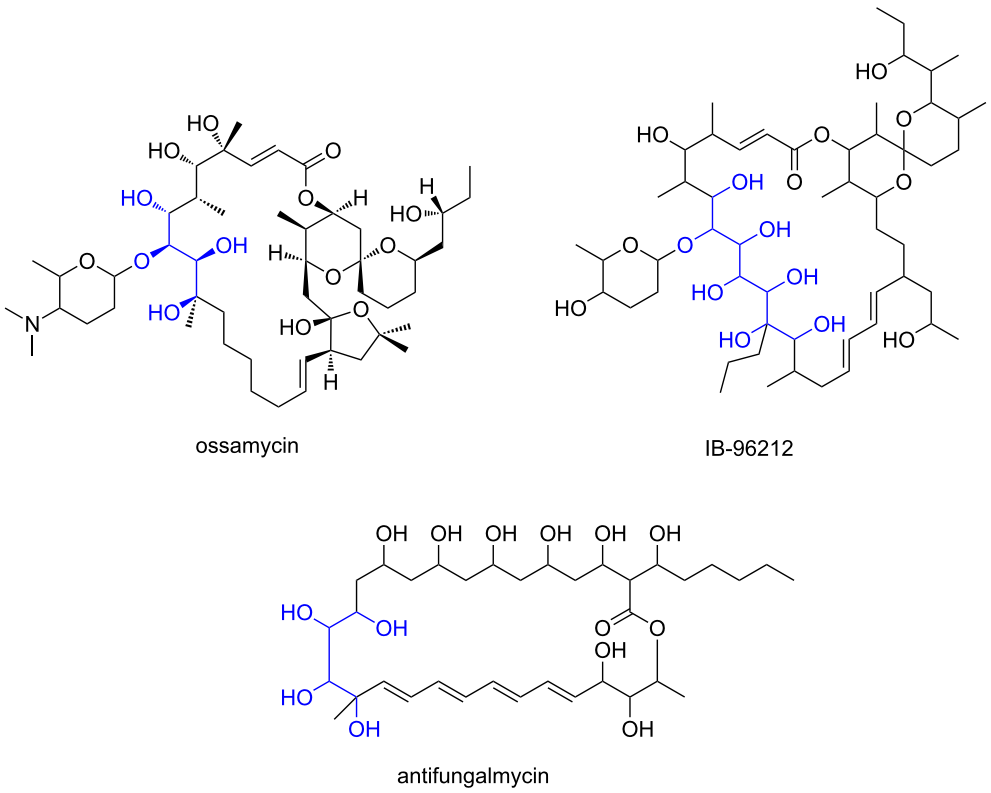

Figure 3: Actinomycete metabolites possessing a contiguous 1,2-diol system.

Table 1: Incorporation of ^{13}C-labeled precursors into **1**.

Position	δ_C	[1,2-$^{13}C_2$]acetate		[U-$^{13}C_6$]glucose		[1-^{13}C]propionate	L-[*methyl*-^{13}C]methionine
		$^1J_{CC}$ (Hz)	2D-INADEQUATE	$^1J_{CC}$ (Hz)	2D-INADEQUATE	relative enrichments[a]	
1	175.3			56	2	0.9	0.9
2	74.7			56	1	1.0	1.0
3	72.9			39	4	0.9	1.0
4	80.0			39	3	1.0	1.1
5	66.9			44	6	1.0	1.0
6	68.9			44	5	0.9	0.9
7	68.9			45	8	1.0	1.1
8	69.7			45	7	1.0	1.1
9	73.1					**4.8**	1.2
10	36.2					1.1	1.1
11	36.6	41	12	40	12	1.2	1.2
12	131.9	41	11	40	11	1.3	1.2
13	131.9	55	14	57	14	1.3	1.2
14	131.3	55	13	57	13	1.2	1.0
15	131.3	43	16	43	16	1.2	1.0
16	32.6	43	15	43	15	1.2	1.3
17	27.5	42	18	43	18	1.4	1.3
18	129.2	42	17	43	17	1.2	1.0
19	129.6	55	20	55	20	1.4	1.1
20	125.7	55	19	55	19	1.3	1.1
21	135.9	43	22	43	22	1.3	1.0
22	28.1	43	21	43	21	1.2	1.1
23	43.7					1.6	1.2
24	30.6					1.2	1.0
25	29.7					0.9	**7.1**
26	29.7					0.9	**7.1**
27	29.7					0.9	**7.1**
28	16.2					1.1	1.2

[a]The ^{13}C signal intensity of each peak in labeled **1** divided by that of the corresponding signal in unlabeled **1**, respectively, normalized to give an enrichment ratio of **1** for the unenriched C-2 peak.

glycolytic intermediate for chain elongation [23]. To investigate this possibility, we conducted a feeding experiment of [U-$^{13}C_6$]glucose which could label carbons derived from malonyl-CoA and hydroxymalonyl-ACP. In the ^{13}C NMR spectrum, ^{13}C–^{13}C couplings were observed for C-1/C-2, C-3/C-4, C-5/C-6, C-7/C-8 in addition to the carbon pairs C-11/C-12, C-13/C-14, C-15/C-16, C-17/C-18, C-19/C-20, and C-21/C-22 (Table 1, Figure S3 in Supporting Information File 1). The 2D-INADEQUATE spectrum showed cross peaks for the above-mentioned two-carbon units derived from the glycolytic degradation of [U-$^{13}C_6$]glucose (Table 1, Figure 4b). Combined with the acetate-labeling result, this labeling pattern suggested that the carbons from C-1 to C-8 are derived from hydroxymalonyl-ACP. This conclusion is supported by the sequencing analysis of the gene cluster for butyrolactol biosynthesis (Figure 5, Table 2). Four genes coding homologues of enzymes involved in hydroxymalonyl-ACP formation in the zwittermicin biosynthesis (ZmaN, ZmaD, ZmaG, and ZmaE) (Figure 6) [24] are present in the downstream of the butyrolactol PKS cluster. Genes coding for *O*-methyltransferase homologues responsible for *O*-methylation of hydroxymalonyl-ACP were not found near the cluster. Hydroxymalonyl-ACP was first identified as an unusual polyketide extender for zittermicin from *Bacillus cereus* [25]. The occurrence of this uncommon extender unit is limited to some bacterial species *Bacillus* [25,26], *Xenorhabdus* [27], *Paenibacillus* [28], and *Streptomyces* [29,30].

Methylmalonyl-CoA was readily predicted as the origin of the methyl-branched three-carbon fragment (C-9/C-10/C-28). Actu-

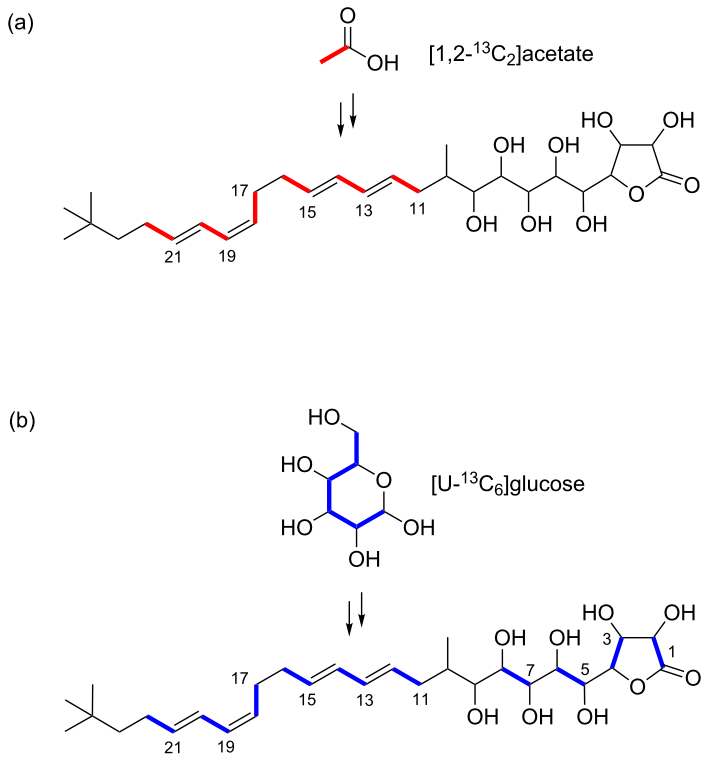

Figure 4: Feeding experiments of ^{13}C-labeled precursors into **1** detected by 2D-INADEQUATE NMR experiments. (a) [1,2-$^{13}C_2$]acetate; (b) [U-$^{13}C_6$]glucose.

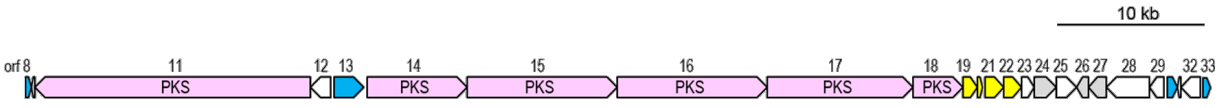

Figure 5: Organization of the biosynthesis gene cluster for **1**. Blue, transcriptional regulator; pink, PKS for polyketide backbone of **1**; yellow, genes for biosynthesis of hydroxymalonyl-ACP; gray, transporter.

ally, intense enhancement of the C-9 carbon signal was observed by feeding of [1-^{13}C]propionate (Table 1). The remaining carbons not labeled by malonate-type precursors were the terminal *tert*-butyl carbons (C-23 to C-27). The origin of the *tert*-butyl group in polyketide biosynthesis is still unknown, however, the *tert*-butyl functionality of bottromycin and polytheonamide was shown to be produced by radical *C*-methylation of the isopropyl group of valine [31,32]. By analogy, the *tert*-butyl portion of **1** was most likely supplied through the *C*-methylation of valine. To examine this possibility, feeding experiments of L-[*methyl*-^{13}C]methionine and L-valine-d_8 were carried out. As expected, the *tert*-butylmethyl carbons (C-25, C-26, C-27) were labeled as a result of L-[*methyl*-^{13}C]methionine incorporation (Table 1). In addition, the ^{2}H (deuterium) NMR spectrum showed deuterium signals for the methyl group (H-25, H-26, H-27) of L-valine-d_8-labeled **1** (Figure 7a). The mass spectrum of the L-valine-d_8-labeled **1** displayed the molecular ion with a mass increment of 6 Da (Figure 7b), corresponding to the incorporation of six deuterium atoms into the terminal methyl groups. Based on these results from precursor-feeding experiments, we concluded that the *tert*-butyl group and the adjacent methylene carbon (C-23) are derived from valine and the *S*-methyl carbon of methionine. It is controversial whether pivaloyl CoA is loaded onto the ACP as a starter or isobutyl-CoA is used as a starter and *C*-methylation takes place afterwards. The signature sequence region of the acyltransferase domain of the PKS starter loading module for butyrolactol biosynthesis (FAGHS) shares some amino acid residues with the known loading module of isobutyl CoA (bafilomycin: LAAHS [33], α-lipomycin: LAAHS [34], tautomycin: LAAHS [35]). Meanwhile, it is known that the substrate recognition is not strict for the loading module of aver-

Table 2: Annotated putative ORFs in biosynthetic gene cluster and neighboring genes of **1**.

Orf10-	Accession no.	Size (aa)	Proposed function	BLAST search	
				Protein homolog, Origin, Accession number	%[a]
8	WP_055469543	127	HxlR family transcriptional regulator	HxlR family transcriptional regulator, *Streptomyces* sp. NRRL F-7442, KOX41174	99/100
10[b]	WP_030405160	71	acetyl-CoA carboxylase biotin carboxyl carrier protein subunit	acetyl-CoA carboxylase, *Streptomyces* sp. NRRL F-7442, KOX41173	100/100
11[b]	WP_055469545	6,065	PKS	FscE, *Streptomyces cattleya*, AEW99638	76/82
12[b]	WP_055469546	473	propionyl-CoA carboxylase subunit beta	propionyl-CoA carboxylase subunit beta, *Streptomyces* sp. NRRL F-7442, KOX41172	99/99
13	WP_055469547	676	helix-turn-helix transcriptional regulator	regulator, *Streptomyces* sp. NRRL F-7442, KOX41171	99/99
14	WP_055469666	2,075	PKS	polyketide synthase type I, *Streptomyces cattleya*, AEW99622	71/80
15	WP_055469548	3,365	PKS	FscC, *Streptomyces cattleya*, AEW99623	71/79
16	WP_055469549	3,462	PKS	polyketide synthase (fragment), *Streptomyces cattleya*, KOX46585	99/99
17	WP_055469550	3,135	PKS	polyketide synthase, *Streptomyces* sp. NRRL F-7442, KOX46586	99/99
18	WP_055469551	1,169	PKS	short-chain dehydrogenase, *Streptomyces* sp. NRRL-7442, KOX46587	99/99
19	WP_055469552	301	3-hydroxyacyl-CoA dehydratase	3-hydroxybutyryl-CoA dehydrogenase, *Streptomyces* sp. NRRL F-7442, KOX46623	98/99
20	WP_030403675	88	ACP	Acyl carrier protein, *Streptomyces* sp. NRRL F-7442, KOX46588	100/100
21	WP_055469553	381	acyl-CoA dehydratase	acyl-CoA dehydrogenase, *Streptomyces* sp. NRRL F-7442, KOX46589	99/99
22	WP_055469554	356	glyceroyl-ACP biosynthesis protein	FkbH, *Streptomyces* sp. NRRL F-7442, KOX46590	99/99
23	WP_030403672	261	thioesterase	thioesterase, *Streptomyces* sp. NRRL F-7442, KOX46591	100/100
24	WP_055469555	448	MFS transporter	major facilitator superfamily permease, *Streptomyces cattleya*, AEW99632	78/84
25	WP_055469556	408	hypothetical protein	uncharacterized protein, *Streptomyces* sp. NRRL F-7442, KOX46624	99/100
26[b]	WP_055469557	253	multidrug ABC transporter permease	multidrug ABC transporter permease, *Streptomyces* sp. NRRL F-7442, KOX46592	99/99
27[b]	not registered in GenBank	373	ABC transporter ATP-binding protein	ABC transporter related protein, *Streptomyces cattleya*, AEW99635	82/89
28[b]	WP_055469558	868	hypothetical protein	beta-ketoacyl synthase, *Streptomyces* sp. NRRL F-7442, KOX46593	99/99
29[b]	WP_055469559	290	ketopantoate reductase	ketopantoate reductase, *Streptomyces* sp. NRRL F-7442, KOX46594	98/99
30	WP_055469560	209	TetR family transcriptional regulator	TetR family transcriptional regulator, *Streptomyces* sp. NRRL F-7442, KOX46595	99/99
31	WP_059296555	65	chitinase	secreted chitinase, *Streptomyces coelicolor*, NP_733504	83/87
32[b]	WP_055469561	407	FAD-dependent oxidoreductase	FAD-dependent oxidoreductase, *Streptomyces* sp. NRRL F-7442, KOX46596	98/99
33	WP_030403663	168	MarR family transcriptional regulator	MarR family transcriptional regulator, Streptomyces sp. NRRL F-7442, KOX46597.1	100/100

[a]Identity/similarity; [b]encoded in complementary strand.

mectin (VPAHS) [36] and myxalamide (VAVHS) [37] which accept both isobutyl-CoA and 2-methylbutyl-CoA. In addition, genes coding for *C*-methyltransferase are not present near the butyrolactol PKS genes. Further enzymatic studies are necessary to establish the order of the starter loading/*C*-methylation events.

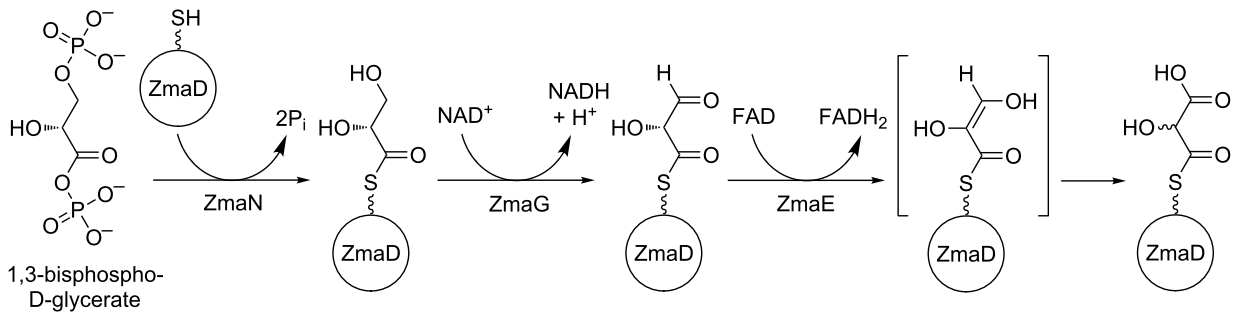

Figure 6: Biosynthetic pathway of hydroxymalonyl-ACP. Adapted from [24].

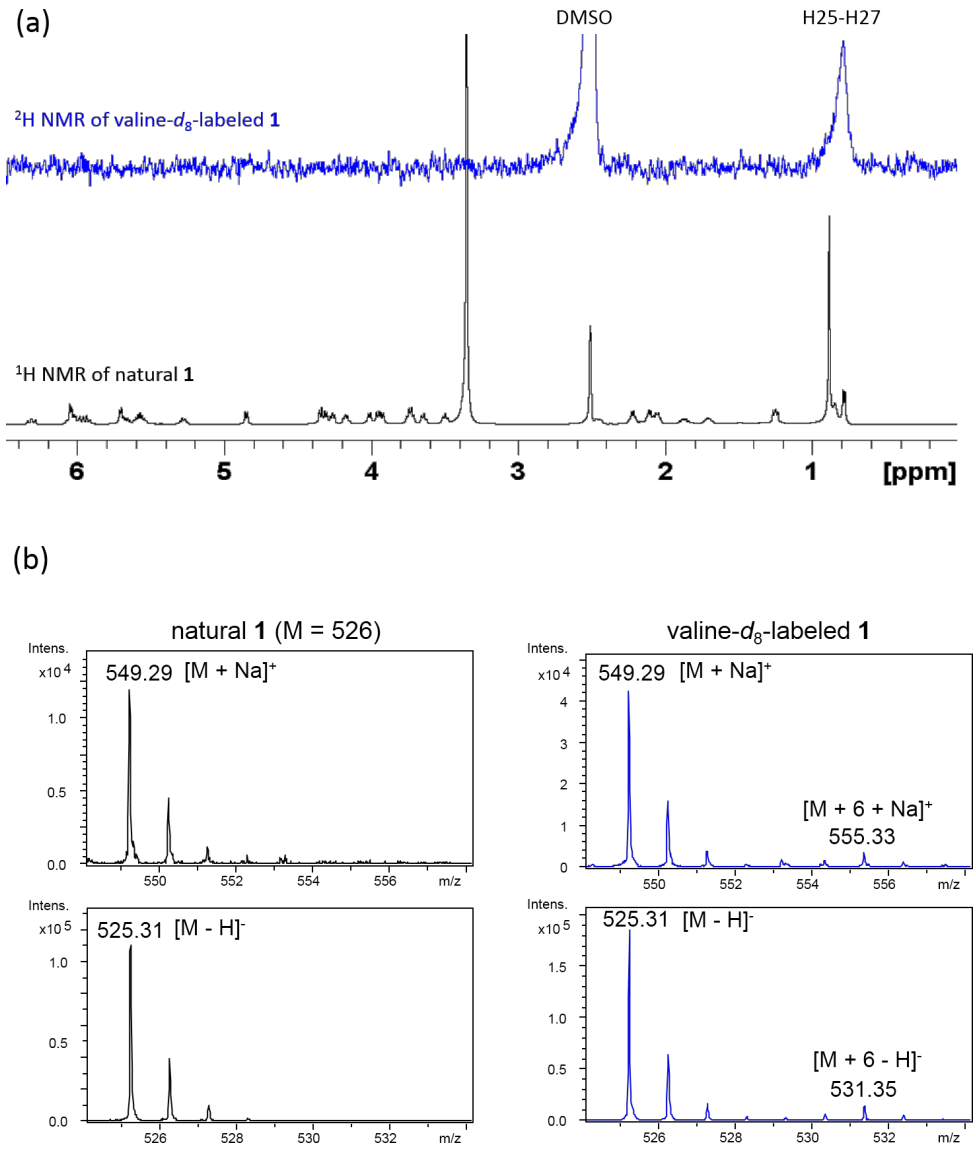

Figure 7: Incorporation of L-valine-d_8 into **1**. (a) ^{1}H NMR spectrum of natural **1** and ^{2}H NMR spectrum of L-valine-d_8-labeled **1**. (b) ESIMS spectra of natural **1** and L-valine-d_8-labeled **1**.

Conclusion

In summary, we elucidated the biosynthetic origin of butyrolactol A (**1**) on the basis of the feeding experiments of isotope-labeled precursors in combination with the bioinformatics analysis of its biosynthetic genes. The overall result of labeling experiments is summarized in Figure 8. The *tert*-butyl group was shown to be derived from the *C*-methylated isopropyl group of valine. This is the first study that experimentally identified the precursor of a *tert*-butyl group in a polyketide backbone. The unusual contiguous polyol system comprising eight hydroxylated carbons was proved to be arising from the chain extension using hydroxymalonyl-ACP by labeling experiments of [1,2-$^{13}C_2$]acetate and [U-$^{13}C_6$]glucose. This conclusion is consistent with our previous bioinformatic prediction that suggested the presence of genes necessary for the supply of hydroxymalonyl-ACP adjacent to the PKS gene cluster of the butyrolactol biosynthesis. The results obtained in this study provide useful information for further biosynthetic studies and genome mining of structurally unique/novel secondary metabolites.

Experimental

General experimental procedures

Sodium [1,2-$^{13}C_2$]acetate and L-valine-d_8 were purchased from Cambridge Isotope Laboratories, Inc. [U-$^{13}C_6$]Glucose, sodium [1-^{13}C]propionate, and L-[*methyl*-^{13}C]methionine were purchased from Sigma-Aldrich Co. LLC. ^{1}H and ^{13}C NMR spectra were obtained on a Bruker AVANCE 500 spectrometer in DMSO-d_6 using the signal of the residual solvent signals (δ_H 2.50, δ_C 40.0) as an internal standard. The ^{2}H NMR spectrum was obtained on a Bruker AVANCE 500 spectrometer in DMSO. Chemical shifts were referenced to the solvent signal ($\delta_{H(D)}$ 2.50). ESITOFMS were recorded on a Bruker microTOF focus.

Microorganism

Streptomyces sp. strain TP-A0882 was isolated from a deep seawater collected in the Toyama Bay, Japan. The strain was identified as a member of the genus *Streptomyces* on the basis of 99.9% 16S rRNA gene sequence identity (1533 nucleotides; NCBI GneBank number BBOK01000029.1) with *Streptomyces diastaticus* subsp. *ardesiacus* NRRL B-1773^T (accession number DQ026631).

Fermentation

Strain TP-A0882 growing on a plate culture was inoculated into a 500 mL K-1 flask containing 100 mL of the V-22 seed medium consisting of soluble starch 1.0%, glucose 0.5%, NZ-case (Wako Pure Chemical Industries, Ltd.) 0.3%, yeast extract (Kyokuto Pharmaceutical Industrial Co., Ltd.), 0.2%, Tryptone (Difco Laboratories) 0.5%, K_2HPO_4 0.1%, $MgSO_4{\cdot}7H_2O$ 0.05%, and $CaCO_3$ 0.3% (pH 7.0). The flask was placed on a rotary shaker (200 rpm) at 30 °C for 4 days. Then, the seed culture (3 mL) was transferred into 500 mL K-1 flasks each containing 100 mL of the A-3M production medium consisting of soluble starch 2.0%, glycerol 2.0%, glucose 0.5%, Pharma-

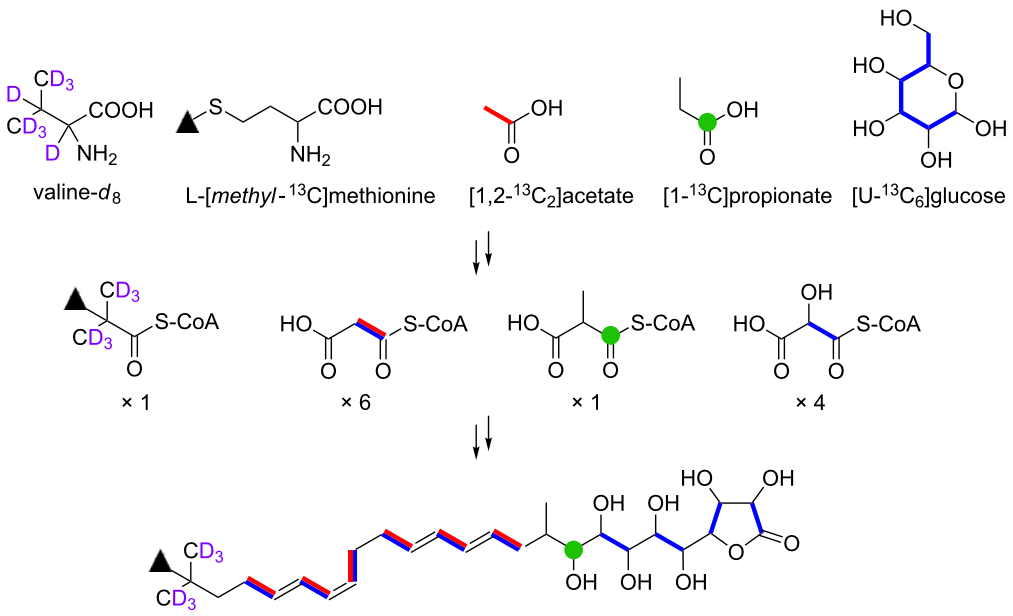

Figure 8: Incorporation of ^{13}C- and ^{2}H-labeled precursors into **1**.

media (Traders Protein) 1.5%, yeast extract 0.3%, and Diaion HP-20 resin (Mitsubishi Chemical Corporation) 1%. The pH of the medium was adjusted to 7.0 before sterilization. The inoculated flasks were placed on a rotary shaker (200 rpm) at 30 °C for 6 days.

Extraction and isolation

After incubation, 100 mL of 1-butanol was added to each flask, and the flasks were allowed to shake for an hour. The mixture was centrifuged at 6,000 rpm for 10 min and the organic layer was collected from the aqueous layer. The solvent was removed by evaporation to give 1.6 g of a crude extract from 1 L of culture. This crude extract was fractionated using silica gel column chromatography with a step gradient of $CHCl_3$–MeOH (1:0, 20:1, 10:1, 4:1, 2:1, 1:1, and 0:1 v/v). Fraction 4 (4:1) containing **1** was concentrated to give 16.2 mg of dark yellow gum. The final purification was achieved by preparative HPLC (Cosmosil 5C18-AR-II, 10 × 250 mm, 4 mL/min) using a gradient of MeCN/0.1% HCO_2H (MeCN concentration: 50–100% for 0–30 min) at 4 mL/min, yielding **1** (2.7 mg) with a retention time of 26.7 min.

Incorporation of ^{13}C- and ^{2}H-labeled precursors

Feeding experiments were performed for sodium [1,2-$^{13}C_2$]acetate, [U-$^{13}C_6$]glucose, sodium [1-^{13}C]propionate, L-[*methyl*-^{13}C]methionine, and L-valine-d_8. Inoculation, cultivation, and purification were performed in the same manner as described above. Addition of ^{13}C- and ^{2}H-labeled precursors was initiated at 48 h after inoculation and periodically carried out every 24 h for four times. After further incubation for 24 h, the cultures were extracted with 1-butanol.

1. Sodium [1,2-$^{13}C_2$]acetate: After feeding of sodium [1,2-$^{13}C_2$]acetate (total 800 mg; 20 mg × 10 flasks × 4 days), 3.6 mg of ^{13}C-labeled **1** was obtained from 1 L of culture.
2. [U-$^{13}C_6$]Glucose: After feeding of [U-$^{13}C_6$]glucose (total 800 mg; 20 mg × 10 flasks × 4 days), 2.5 mg of ^{13}C-labeled **1** was obtained from 1 L of culture.
3. Sodium [1-^{13}C]propionate: After feeding of sodium [1-^{13}C]propionate (total 800 mg; 20 mg × 10 flasks × 4 days), 2.1 mg of ^{13}C-labeled **1** was obtained from 1 L of culture.
4. L-[*Methyl*-^{13}C]methionine: After feeding of L-[*methyl*-^{13}C]methionine (total 80 mg; 2.0 mg × 10 flasks × 4 days), 3.2 mg of ^{13}C-labeled **1** was obtained from 1 L of culture.
5. L-Valine-d_8: After feeding of L-valine-d_8 (total 80 mg; 2.0 mg × 10 flasks × 4 days), 2.1 mg of deuterated **1** was obtained from 1 L of culture.

Supporting Information

Supporting Information File 1

NMR spectra of ^{13}C- and ^{2}H-labeled **1**.
[http://www.beilstein-journals.org/bjoc/content/supplementary/1860-5397-13-47-S1.pdf]

Acknowledgement

This work was supported by the Japan Society for the Promotion of Science (JSPS) for Young Scientists (15K18692) to E. H. and Institute for Fermentation, Osaka (IFO) for Young Scientists to E. H.

References

1. Bérdy, J. *J. Antibiot.* **2005,** *58,* 1–26. doi:10.1038/ja.2005.1
2. Bérdy, J. *J. Antibiot.* **2012,** *65,* 385–395. doi:10.1038/ja.2012.27
3. Hertweck, C. *Angew. Chem., Int. Ed.* **2009,** *48,* 4688–4716. doi:10.1002/anie.200806121
4. Sánchez, C.; Méndez, C.; Salas, J. A. *J. Ind. Microbiol. Biotechnol.* **2006,** *33,* 560–568. doi:10.1007/s10295-006-0092-5
5. Salas, J. A.; Méndez, C. *Trends Microbiol.* **2007,** *15,* 219–232. doi:10.1016/j.tim.2007.03.004
6. Wilkinson, B.; Micklefield, J. *Nat. Chem. Biol.* **2007,** *3,* 379–386. doi:10.1038/nchembio.2007.7
7. Kim, W.; Lee, D.; Hong, S. S.; Na, Z.; Shin, J. C.; Roh, S. H.; Wu, C.-Z.; Choi, O.; Lee, K.; Shen, Y.-M.; Paik, S.-G.; Lee, J. J.; Hong, Y.-S. *ChemBioChem* **2009,** *10,* 1243–1251. doi:10.1002/cbic.200800763
8. Kong, D.; Lee, M.-J.; Lin, S.; Kim, E.-S. *J. Ind. Microbiol. Biotechnol.* **2013,** *40,* 529–543. doi:10.1007/s10295-013-1258-6
9. Kotake, C.; Yamasaki, T.; Moriyama, T.; Shinoda, M.; Komiyama, N.; Furumai, T.; Konishi, M.; Oki, T. *J. Antibiot.* **1992,** *45,* 1442–1450. doi:10.7164/antibiotics.45.1442
10. Ko, K.; Ge, H. M.; Shin, J.; Oh, D. C. *Planta Med.* **2016,** *82* (Suppl. Suppl.1), S1–S381. doi:10.1055/s-0036-1596637
11. Dembitsky, V. M. *Lipids* **2006,** *41,* 309–340. doi:10.1007/s11745-006-5103-9
12. Shao, C.-L.; Linington, R. G.; Balunas, M. J.; Centeno, A.; Boudreau, P.; Zhang, C.; Engene, N.; Spadafora, C.; Mutka, T. S.; Kyle, D. E.; Gerwick, L.; Wang, C.-Y.; Gerwick, W. H. *J. Org. Chem.* **2015,** *80,* 7849–7855. doi:10.1021/acs.joc.5b01264
13. Salvador-Reyes, L. A.; Sneed, J.; Paul, V. J.; Luesch, H. *J. Nat. Prod.* **2015,** *78,* 1957–1962. doi:10.1021/acs.jnatprod.5b00293
14. Ogawa, H.; Iwasaki, A.; Sumimoto, S.; Kanamori, Y.; Ohno, O.; Iwatsuki, M.; Ishiyama, A.; Hokari, R.; Otoguro, K.; Omura, S.; Suenaga, K. *J. Nat. Prod.* **2016,** *79,* 1862–1866. doi:10.1021/acs.jnatprod.6b00171
15. Mander, L.; Liu, H.-W. *Comprehensive Natural Products II: Chemistry and Biology,* 1st ed.; Elsevier B.V.: Kidlington, UK, 2010.
16. Grindberg, R. V.; Ishoey, T.; Brinza, D.; Esquenazi, E.; Coates, R. C.; Liu, W.-t.; Gerwick, L.; Dorrestein, P. C.; Pevzner, P.; Lasken, R.; Gerwick, W. H. *PLoS One* **2011,** *6,* No. e18565. doi:10.1371/journal.pone.0018565
17. Staunton, J.; Wilkinson, B. *Chem. Rev.* **1997,** *97,* 2611–2630. doi:10.1021/cr9600316

18. Caffrey, P.; Lynch, S.; Flood, E.; Finnan, S.; Oliynyk, M. *Cell Chem. Biol.* **2001,** *8,* 713–723. doi:10.1016/S1074-5521(01)00046-1
19. Kirst, H. A.; Mynderse, J. S.; Martin, J. W.; Baker, P. J.; Paschal, J. W.; Steiner, J. L. R.; Lobkovsky, E.; Clardy, J. *J. Antibiot.* **1996,** *49,* 162–167. doi:10.7164/antibiotics.49.162
20. Fernández-Chimeno, R. I.; Cañedo, L.; Espliego, F.; Grávalos, D.; De La Calle, F.; Fernández-Puentes, J. L.; Romero, F. *J. Antibiot.* **2000,** *53,* 474–478. doi:10.7164/antibiotics.53.474
21. Wang, Y.-F.; Wei, S.-J.; Zhang, Z.-P.; Zhan, T.-H.; Tu, G.-Q. *Nat. Prod. Bioprospect.* **2012,** *2,* 41–45. doi:10.1007/s13659-011-0037-1
22. Komaki, H.; Ichikawa, N.; Hosoyama, A.; Fujita, N.; Igarashi, Y. *FEMS Microbiol. Lett.* **2015,** *362,* fnv155. doi:10.1093/femsle/fnv155
23. Chan, Y. A.; Boyne, M. T.; Podevels, A. M.; Klimowicz, A. K.; Handelsman, J.; Kelleher, N. L.; Thomas, M. G. *Proc. Natl. Acad. Sci. U. S. A.* **2006,** *39,* 14349–14354. doi:10.1073/pnas.0603748103
24. Park, H.; Kevany, B. M.; Dyer, D. H.; Thomas, M. G.; Forest, K. T. *PLoS One* **2014,** *9,* No. e110965. doi:10.1371/journal.pone.0110965
25. Emmert, E. A. B.; Klimowicz, A. K.; Thomas, M. G.; Handelsman, J. *Appl. Environ. Microbiol.* **2004,** *70,* 104–113. doi:10.1128/AEM.70.1.104-113.2004
26. Li, Y.; Li, Z.; Yamanaka, K.; Xu, Y.; Zhang, W.; Vlamakis, H.; Kolter, R.; Moore, B. S.; Qian, P.-Y. *Sci. Rep.* **2015,** *5,* No. 9383. doi:10.1038/srep09383
27. Park, D.; Ciezki, K.; van der Hoeven, R.; Singh, S.; Reimer, D.; Bode, H. B.; Forst, S. *Mol. Microbiol.* **2009,** *73,* 938–949. doi:10.1111/j.1365-2958.2009.06817.x
28. Müller, S.; Garcia-Gonzalez, E.; Genersch, E.; Süssmuth, R. D. *Nat. Prod. Rep.* **2015,** *32,* 765–778. doi:10.1039/C4NP00158C
29. Sakuda, S.; Ono, M.; Ikeda, H.; Inagaki, Y.; Nakayama, J.; Suzuki, A.; Isogai, A. *Tetrahedron Lett.* **1997,** *38,* 7399–7402. doi:10.1016/S0040-4039(97)01734-6
30. Ono, M.; Sakuda, S.; Ikeda, H.; Furihata, K.; Nakayama, J.; Suzuki, A.; Isogai, A. *J. Antibiot.* **1998,** *51,* 1019–1028. doi:10.7164/antibiotics.51.1019
31. Huo, L.; Rachid, S.; Stadler, M.; Wenzel, S. C.; Müller, R. *Chem. Biol.* **2012,** *19,* 1278–1287. doi:10.1016/j.chembiol.2012.08.013
32. Parent, A.; Guillot, A.; Benjdia, A.; Chartier, G.; Leprince, J.; Berteau, O. *J. Am. Chem. Soc.* **2016,** *138,* 15515–15518. doi:10.1021/jacs.6b06697
33. Hwang, J. Y.; Kim, H. S.; Kim, S. H.; Oh, H. R.; Nam, D. H. *AMB Express* **2013,** *3,* No. 24. doi:10.1186/2191-0855-3-24
34. Bihlmaier, C.; Welle, E.; Hofmann, C.; Welzel, K.; Vente, A.; Breitling, E.; Müller, M.; Glaser, S.; Bechthold, A. *Antimicrob. Agents Chemother.* **2006,** *50,* 2113–2121. doi:10.1128/AAC.00007-06
35. Zhao, C.; Ju, J.; Christenson, S. D.; Smith, W. C.; Song, D.; Zhou, X.; Shen, B.; Deng, Z. *J. Bacteriol.* **2006,** *188,* 4142–4147. doi:10.1128/JB.00173-06
36. Ikeda, H.; Nonomiya, T.; Usami, M.; Ohta, T.; Ōmura, S. *Proc. Natl. Acad. Sci. U. S. A.* **1999,** *96,* 9509–9514. doi:10.1073/pnas.96.17.9509
37. Silakowski, B.; Nordsiek, G.; Kunze, B.; Blöcker, H.; Müller, R. *Cell Chem. Biol.* **2001,** *8,* 59–69. doi:10.1016/S1074-5521(00)00056-9

License and Terms

BEILSTEIN JOURNAL OF ORGANIC CHEMISTRY

Secondary metabolome and its defensive role in the aeolidoidean *Phyllodesmium longicirrum*, (Gastropoda, Heterobranchia, Nudibranchia)

Alexander Bogdanov[1], Cora Hertzer[1], Stefan Kehraus[1], Samuel Nietzer[2], Sven Rohde[2], Peter J. Schupp[2], Heike Wägele[3] and Gabriele M. König[*1]

Full Research Paper

Open Access

Address:
[1]Institute for Pharmaceutical Biology, University of Bonn, Nussallee 6, 53115 Bonn, Germany, [2]Institute for Chemistry and Biology of the Marine Environment (ICBM), Carl-von-Ossietzki University Oldenburg, Schleusenstraße 1, 26382 Wilhelmshaven, Germany and [3]Zoologisches Forschungsmuseum Alexander Koenig, Adenauerallee 160, 53113 Bonn, Germany

Email:
Gabriele M. König[*] - g.koenig@uni-bonn.de

* Corresponding author

Keywords:
chemical defense; chemoecology; natural compounds; Nudibranchia; *Phyllodesmium longicirrum*

Beilstein J. Org. Chem. **2017,** *13,* 502–519.
doi:10.3762/bjoc.13.50

Received: 16 December 2016
Accepted: 08 February 2017
Published: 13 March 2017

This article is part of the Thematic Series "Lipids: fatty acids and derivatives, polyketides and isoprenoids".

Guest Editor: J. S. Dickschat

Abstract

Phyllodesmium longicirrum is the largest aeolidoidean species known to date, and extremely rich in terpenoid chemistry. Herein we report the isolation of a total of 19 secondary metabolites from a single specimen of this species, i.e., steroids **1–4**, cembranoid diterpenes **5–13**, complex biscembranoids **14** and **15**, and the chatancin-type diterpenes **16–19**. These compounds resemble those from soft corals of the genus *Sarcophyton*, of which to date, however, only *S. trocheliophorum* is described as a food source for *P. longicirrum*. Fish feeding deterrent activity was determined using the tropical puffer fish *Canthigaster solandri*, and showed activity for (2*S*)-isosarcophytoxide (**10**), cembranoid bisepoxide **12** and 4-oxochatancin (**16**). Determining the metabolome of *P. longicirrum* and its bioactivity, makes it evident that this seemingly vulnerable soft bodied animal is well protected from fish by its chemical arsenal.

Introduction

Marine gastropods, of which approximately 150.000 are known, mostly are protected by a shell. However, shell reduction or even loss is common within several marine Heterobranchia clades, which were united under the name Opisthobranchia in former times [1]. To compensate this lack of physical protection, alternative defensive strategies, such as the production of

calcareous needles or acidic sulfates, and sequestration or de novo synthesis of toxic metabolites emerged within the opisthobranch taxa [2-5]. Adaptations and mimicry, which help to hide in habitats is frequent in marine gastropods, as obvious from very diverse and spectacular phenotypes [1,6].

A most intriguing defense strategy, the incorporation of intact stinging cells (cnidocysts) from hydrozoan food sources, is used by animals belonging to the Aeolidoidea [7]. One of the aeolidoidean genera, i.e., *Phyllodesmium*, however, switched to cnidocyst poor Octocorallia as a food source. From there, some *Phyllodesmium* species, including *P. longicirrum* incorporate algal unicellular symbionts. These so-called zooxanthellae are stored in branches of the digestive glands which reach into the so-called cerata. *P. longicirrum* is able to maintain the symbionts for over 6 months and is believed to benefit from additional nutrients produced via photosynthesis [8,9]. The greenish-brownish color of the dinoflagellates offers additional camouflage, while being exposed grazing on soft coral surfaces. Most importantly, the octocorallian food also offers a wide spectrum of terpenoid chemistry, which is incorporated and stored by *Phyllodesmium*.

Only few chemical investigations were undertaken on *Phyllodesmium* species [10-15], describing mostly terpenoid secondary metabolites. Indirect evidence suggests that these compounds are sequestered from the respective octocorallian prey organisms. In rare cases, the ecological function of some of these metabolites as deterrent agents was demonstrated, e.g., acetoxypukalide from *P. guamensis* [15] and 4-oxochatancin (**16**) in *P. longicirrum* [12] were shown to cause a significant feeding deterrence under laboratory conditions at concentration levels below natural abundance in the sea slug bodies.

Herein we report on the secondary metabolome of a single specimen of *P. longicirrum*, including the structure elucidation of the new metabolites **1**, **5**, **9**, **14** and **15**, and show the fish feeding deterrent activity of the major metabolites **10** and **12**.

Results

UPLC–HRMS metabolome analysis

From the ethanolic extract of *P. longicirrum* the ethyl acetate-soluble organic compounds were analyzed. A first fractionation was achieved by vacuum liquid chromatography (VLC) on reversed-phase material yielding 11 fractions. ^{1}H NMR analysis of these indicated the presence of chemically diverse secondary metabolites in the major fractions 3–8, whereas the hydrophilic fractions 1 and 2 merely contained sugars and the lipophilic ones, i.e., 9–11 simple lipids.

Detailed UPLC–HRMS investigation was thus performed with the VLC fractions 3–8. The resulting UPLC chromatograms (Supporting Information File 1, Figures S47–52) were extremely complex and gave an impression on the multi-faceted metabolome of this animal. The majority (except **4** and **17**) of the subsequently isolated and characterized secondary metabolites (**1**–**19**, Figure 1) could be assigned to the detected *m*/*z* values (Supporting Information File 1, Table S7A), e.g., prominent MS data were associated with the presence of metabolites with a molecular weight of 362 Da, relating to 4-oxochatancin (**16**) or 1-oxo-9-hydroisochatancin (**18**). Peaks with retention times around 14 min in the chromatograms of VLC 5 and 6 contained a metabolite showing an *m*/*z* of 319.23 (M + H) and 341.21 (M + Na), which indicated the presence of bisepoxide **12**, having a molecular weight of 318.45 Da. A mass charge ratio of 475.39 (M + H − H_2O) and 493.39 (M + H), found for the peak with a retention time of 14.7 min of the UPLC-chromatogram of VLC fraction 7, is characteristic for the secosteroid **1** or the polyhydroxylated steroid **4**, both with a molecular weight of 492 Da.

More importantly, UPLC–HRMS investigations produced also some peaks with *m/z* values that cannot be linked to isolated compounds **1**–**19**. Thus, in VLC fraction 7 and 8 an *m/z* value of 287.24 (M + H) indicates most probably the presence of the instable sarcophytonin A with a molecular weight of 286.23 Da [16]. VLC fractions 7 and 8 also contain *m/z* values characteristic for steroid constituents of *Sarcophyton* soft corals that could not be isolated in the current study, e.g., *m/z* 397.35 (M + H) suggests the presence of a steroid compound reported by Kobayashi et al. from *Sarcophyton glaucum* [17] with a molecular mass of 396 Da as outlined in Table S7B (Supporting Information File 1). Detailed analysis of the UPLC–HRMS data also revealed the presence of *m*/*z* 711.39 (M + H) and 669.44 (M + H) in VLC fractions 6 and 7. These values would fit to not yet reported biscembranoids, containing compound **5** as a possible biogenetic precursor, with a suggested molecular mass of 710 and 668 Da (see Supporting Information File 1, Table S7B).

Notable is the occurrence of numerous peaks containing *m*/*z* values attributable to isomers of the isolated metabolites. Besides the isosarcophines **8** and **9** with a molecular weight of 316 Da, *m*/*z* values 317.21 (M + H) were also detected in the chromatograms of the fractions VLC 6 and 7 in different chromatographic peaks (t_R: 12.0, 12.7, 14.0, 15.9 min) indicating the presence of further possible cembranoid isomers as shown in Table S7A (Supporting Information File 1). The *m*/*z* values (M + H, 739.44) attributable to the isobisglaucumlides B (**14**) and C (**15**) are also found at four different retention times of the UPLC chromatograms, suggesting the presence of the further

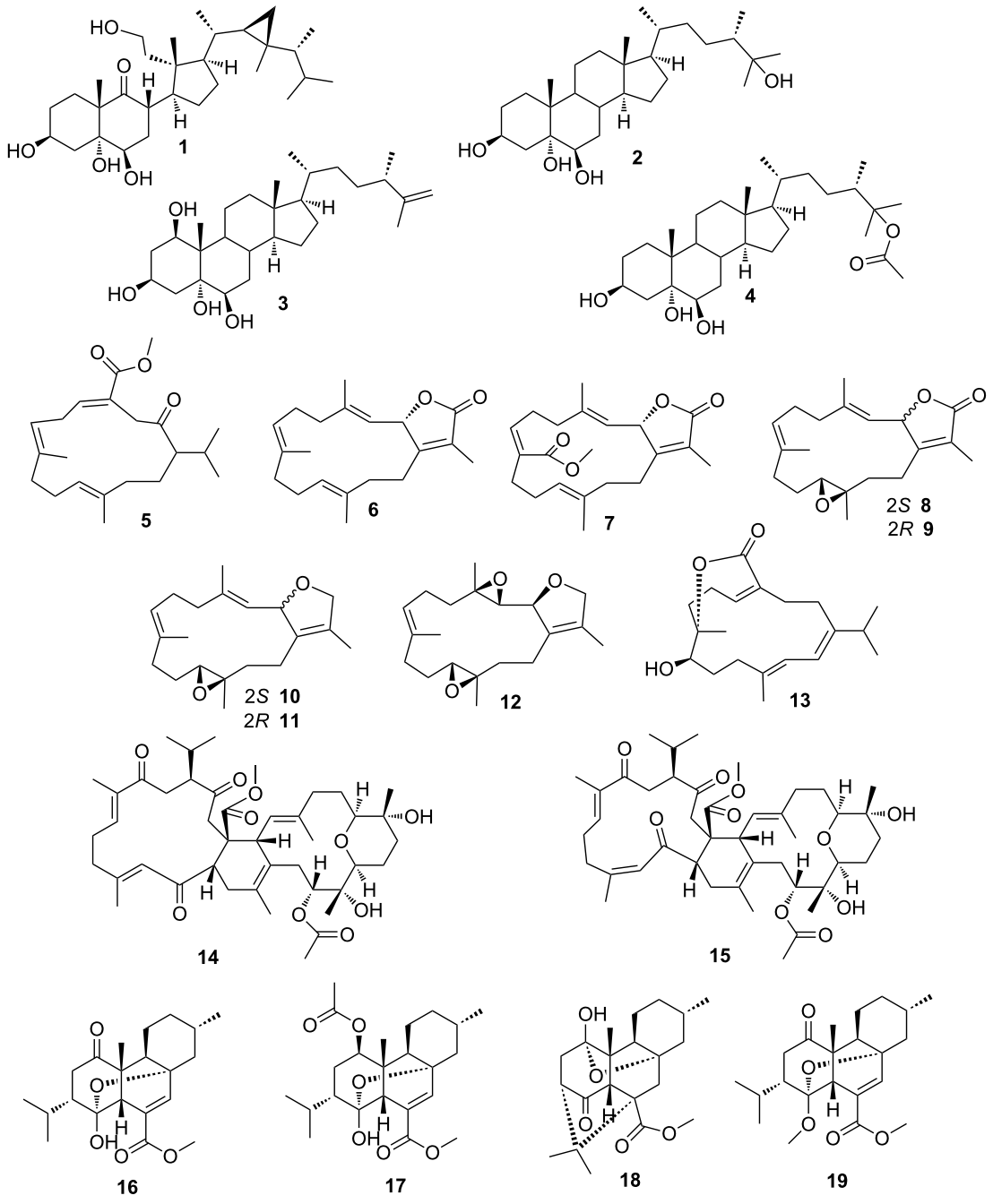

Figure 1: Secondary metabolites isolated in this study from *P. longicirrum*.

isomeric metabolites. These findings highlight the amazingly complex and diverse metabolome of *P. longicirrum*.

Regarding the reported secondary metabolites of *P. longicirrum* **20**–**22**, Figure 2 by Coll et al. [13], only compound **22** with a molecular weight of 304 Da resulting in an *m/z* of 305.25 (M + H) may be present in VLC 8 (see Supporting Information File 1, Figure S7B). However, there are about 20 further cembranoids described from *Sarcophyton* spp. with a molecular weight of 304 Da, making this assessment very tentative. It can, however be stated that the *P. longicirrum* specimen investigated in this study either belongs to a different chemotype or has different food preference than the one investigated by Coll and co-workers [13].

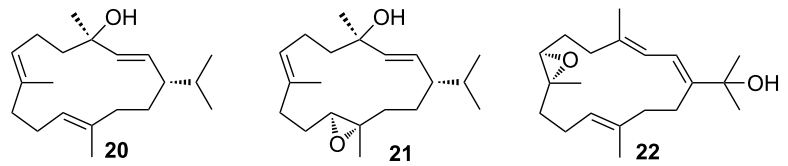

Figure 2: Structures of secondary metabolites from *P. longicirrum* as described by Coll et al. in 1985 [13].

Detailed chemical investigation of *P. longicirrum* including structure elucidation of the new metabolites **1**, **5**, **9**, **14**, **15** and stereochemical assignment of **12**

Repeated fractionation of VLC fractions 5–8 resulted in the isolation of a range of secondary metabolites, i.e., four steroids **1–4**, nine cembranoid diterpenes **5–13** and two biscembranoids **14** and **15**, as well as four polycyclic diterpenes of the chatancin type **16–19** [12]. Compounds **1** and **5** are new chemical structures. The same applies to the biscembranoids **14** and **15**, which however show close resemblance to bisglaucumlides B and C [18], but differ in their stereochemistry from the latter. Since no studies regarding the stereochemical features of the cembranoid bisepoxide **12** were published to date, we propose here its relative configuration. Figure 1 summarizes all metabolites found during this investigation. It is noteworthy, that the previously reported cembranoid diterpenes (see Figure 2, compounds **20–22**) from *P. longicirrum* by Coll et al. [13] were not isolated from the complex secondary metabolome of the investigated specimen, although the UPLC–HRMS data (see above) suggest that cembranoid alcohol **22** may be present.

Compound **1** was isolated as amorphous white solid. The specific optical rotation was measured in chloroform (*c* 0.1), giving $[\alpha]_D^{20}$ −21.0. The molecular formula $C_{30}H_{52}O_5$ was established by a HRMS measurement, which yielded *m/z* 515.3694 [M + Na] for the molecular ion. The ring double bond equivalent (RDE) was calculated to be five. The IR spectrum revealed the presence of hydroxy groups (broad band at 3360 cm^{-1}) and a keto function (sharp band at 1697 cm^{-1}).

The planar structure of **1** was established by extensive NMR experiments (^{1}H, ^{13}C NMR, COSY, DEPT, HSQC and HMBC (see Supporting Information File 1, Table S1). The ^{13}C NMR spectrum showed 30 resonances attributable to 7 methyl, 9 methylene and 8 methine groups. A ^{13}C NMR resonance at 218.4 ppm confirmed the keto group (C-9), whereas a primary alcohol moiety was evident from a ^{13}C NMR resonance at δ_C 59.1 (C-11). Further oxygenated carbons, i.e., C-3, C-5 and C-6 gave rise to ^{13}C NMR resonances at δ_C 68.0, 80.7 and 75.7, respectively. Proton carbon assignments were done according to correlations obtained in a HSQC experiment. The absence of ^{13}C NMR resonances for sp^2 hybridized carbons for C=C bonds, together with a RDE of five indicated the presence of several rings in **1**, likely of steroid origin. The latter is supported by characteristically shielded ^{1}H NMR resonances at δ_H 0.54 and δ_H −0.05 (both dd, H_2-30) as well as a multiplet at δ_H 0.32 (H-22) for a cyclopropyl group, as typically found in gorgosterols [19,20].

A ^{1}H,^{1}H COSY experiment led to partial structures which could be combined using HMBC correlations. Spin system **A** included H_2-1 to H_2-4, whereas H-6 through to H-30 formed spin system **B** (see Figure 3). The connection of partial structures **A** and **B** was established from HMBC correlations, i.e., from the resonances of H-4 to C-5 and C-6, as well as H-6 to C-5. The position of the C-9 ketone function was established due to HMBC correlations from resonances of H_2-7 and H-8 to C-9. The decaline system was finally confirmed by the heteronuclear long range correlations of the resonances from H_3-19. Of the five degrees of unsaturation one is ascribed to a keto function, another one to the cyclopropane ring in the side chain, and two further ones to the decaline ring, thus requiring a further ring in **1**. Considering this, a secosterol backbone was likely. Also, the ^{13}C NMR resonance of the oxygenated methylene at δ_C 59.1 (C-11) is characteristic for marine-derived secosterols [21]. The ^{1}H-^{1}H spin system **C** only including H_2-11 and H_2-12 was connected to the partial structure **B** via long range correlations from H_3-18 to C-12, C-13, C-14 and C-17. This also established the still required ring D. Finally, the complete gorgosterol side chain could be elucidated by connection of the ^{1}H,^{1}H

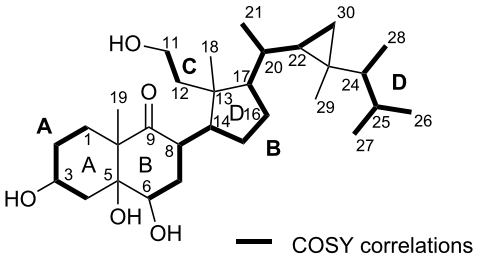

Figure 3: Significant ^{1}H,^{1}H COSY correlations as found in compound **1**.

spin system **D** with **B** using HMBC correlations from H_3-28 to C-23 and from H_3-29 to C-22, C-23, C-24 and C-30 (see Figure 3).

The NMR data (Supporting Information File 1, Table S1) of compound **1** resembled most closely those of epoxy-secosterols isolated from the gorgonian *Pseudopterogorgia americana* [22] and from the soft coral *Pachyclavularia violacea* (now *Briareum violaceum* [23]) by Anta et al. ([24], Figure 4). However, the ^{13}C NMR chemical shifts of C-5 and C-6 in compound **1** (δ_C 80.7 and δ_C 75.7, respectively) differ from shifts for the equivalent carbons in epoxy-secogorgosterol reported by Naz et al. (δ_C 61.0 and δ_C 60.4, respectively; [22]) and from those of the epoxy-secosterol reported by Anta et al. (δ_C 65.5 and δ_C 58.1, respectively; [24]). The downfield shift, observed for these carbons in **1**, results from the cleavage of the epoxide ring, and ^{13}C values around δ_C 70–80 as observed for **1** are characteristic for hydroxylated carbons.

The relative stereochemistry of the secogorgosterol **1** was established by analysis of $^1H,^1H$ coupling constants, NOESY data, and comparison of NMR spectral data with those of similar compounds [22,24]. An equatorial orientation of the OH-group at C-3 was evident, since H-3 displayed $^1H,^1H$ coupling constants to the vicinal axial H-2β and H-4β of 12 Hz and to the equatorial H-2α and H-4α of 6 Hz. NOE correlations of H-3 to H-1α, H-2α and H-4α indicate thus an α-orientation of axial H-3 and a β-orientation of the equatorial hydroxy group at C-3. The identical ^{13}C NMR shift of C-3 (δ_C 68.0) with the reported value [24] supports this orientation.

^1H NMR measurements in pyridine-d_5 led to a further downfield shift of the deshielded H-3 resonance to δ_H 4.81 (compared with δ_H 4.00 in MeOH-d_4). This shift is explained by a 1,3 axial–axial interaction with the 5α hydroxy group [25,26], demonstrating the α-orientation of the substituent at the bridge head carbon C-5. NOEs between the resonances for H-2β as well as H-1β to H_3-19 showed the latter to be β-orientated, and thus the trans configuration of the decaline system. The ^1H NMR signal at δ_H 3.66 for H-6 exhibited NOE correlation with H-4α (δ_H 1.70, m) indicating β-orientation of the equatorial OH-group at C-6. Contrary to the reported epoxy-secosteroid by Naz et al. [22], no NOE was observed between the resonances of H-6 and β-oriented H_3-19 confirming the β-orientation of the hydroxy group at C-6 (see Figure 5).

NOE correlations between H_3-19 and H-8, as well as between H-8 and H_3-18 showed the β-orientation of the methyl groups CH_3-18, CH_3-19 and of the proton at C-8, which is in accordance with reported stereochemistry for the related metabolites of this compound-class [21,22]. Free rotation along the bond between C-8 and C-14 is unlikely because of the bulky substituents on ring D. NOE correlations were observed between α-oriented H-14 and H-17 demonstrating β-orientation of the gorgosterol side chain. ^{13}C NMR shifts for the carbons of the side chain (C-20 to C-30: δ_C 36.3, 21.4, 33.3, 26.9, 52.2, 33.4, 22.7, 21.9, 15.8, 14.7, 22.2) were almost identical with those reported by Naz et al. (C-20 to C-30: δ_C 34.9, 20.8, 31.9, 25.9, 50.5, 31.4, 22.3, 21.5, 15.2, 14.2, 21.2) [22]. The relative stereochemistry of the gorgosterol side chain was thus suggested to be the same. For the compound **1** we propose the name 3β,5α,6β-trihydroxy-9-oxo-9,11-secogorgostan-11-ol.

Chemical structures of the polyhydroxylated steroids **2**–**4** were established by comparison of the NMR and MS data obtained in our laboratory (Supporting Information File 1, Figures S6–11) with the reported values [27,28].

Compound **5** was isolated as colorless oil (1.5 mg). The specific optical rotation was measured in chloroform (*c* 0.09), and yielded $[\alpha]_D^{20}$ +3.5. The molecular formula of compound **5** was deduced by HRMS–ESI (M + Na 355.2244 Da) to be $C_{21}H_{32}O_3$. Ring double bond equivalents (RDE) were calculated to be six. The IR spectrum of compound **5** showed absorptions for carbonyl bonds at 1700 cm^{-1} and 1679 cm^{-1}, indicating the presence of ketone and/or ester functions.

Extensive NMR measurements (^1H, ^{13}C NMR, COSY, DEPT, HSQC and HMBC, see Supporting Information File 1, Table S2) revealed the presence of a methoxy group (δ_H 3.71 3H,

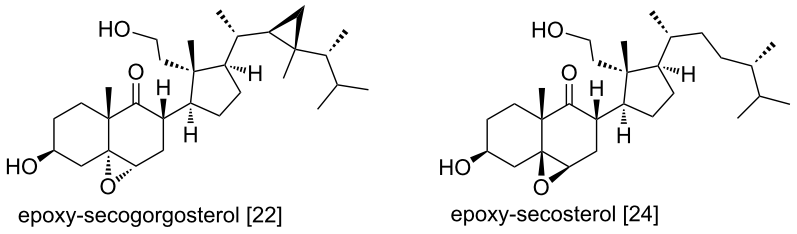

Figure 4: Secosterols [22,24] related to 3β,5α,6β-trihydroxy-9-oxo-9,11-secogorgostan-11-ol (**1**) from *P. longicirrum*.

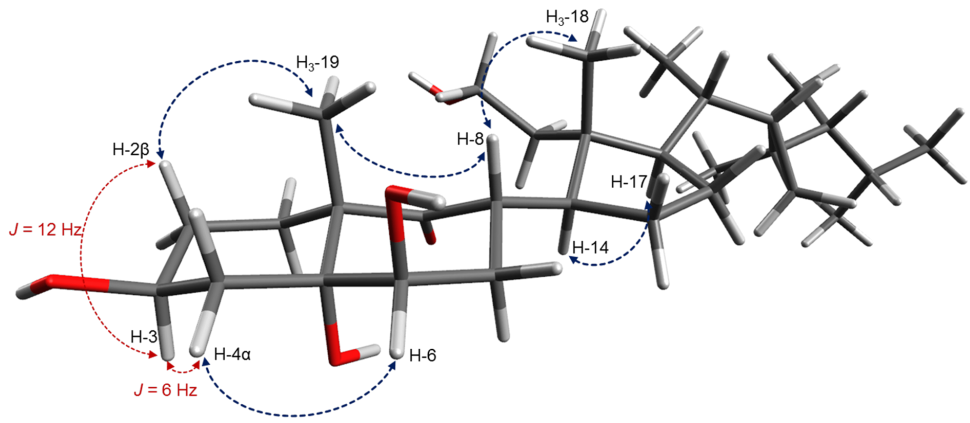

Figure 5: Conformational structure of **1** (key NOESY correlations are indicated with blue arrows; coupling constants crucial for the determination of the orientation of the 3-OH group are shown).

δ_C 52.1), an ester carbonyl (δ_C 170.0 , C-18) and a keto group (δ_C 211.3 , C-2). The ^{13}C NMR spectrum of compound **5** contained a total of 21 resonances attributable to 5 methyl, 6 methylene, 5 methine and 5 quaternary carbons as indicated by a DEPT 135 experiment. Six characteristic shifts in the ^{13}C NMR spectrum at δ_C 130.5 (C-4) and 142.8 (C-5), 121.6 (C-7) and 136.9 (C-8), 127.0 (C-11) and 135.4 (C-12) pointed towards three carbon–carbon double bonds. Together with two carbonyls (at C-2 and C-18) one RDE accountable to a ring remained, and suggested a cembrane-class diterpene.

The proton resonances could be unambiguously assigned to those of directly attached carbons by a HSQC measurement, and afterwards the fragments of the molecule were elucidated using a COSY experiment. Thus, the COSY data showed correlations of the resonances H_3-16, H_3-17 and H-1 to H-15, forming an isopropyl moiety. Together with COSY correlations from H-1 over H_2-14 to H_2-13 spin system **A** was established . Two further smaller fragments were established via COSY correlations from H-5 to H-7 (**B**), and from H-9 to H-11 (**C**). These subunits could be assigned to a 14-membered cembrane skeleton according to couplings detected in the HMBC experiment. Key heteronuclear long range correlations for assembling the complete structure were from H_3-20 to C-11, C-12 and C-13 connecting fragments **A** and **C**. The fragments **B** and **C** were then connected according to HMBC cross peaks of the methyl group resonance H_3-19 with quaternary C-8 and with C-7 and C-9 (see Figure 6).

The absence of a further ^{1}H,^{1}H spin system required heteronuclear long range correlations for the elucidation of the remaining structural features and the closure of the cembrane ring. Methylene group CH_2-3 exhibited HMBC correlations with resonances of the keto at C-2, sp^2 quaternary carbon C-4

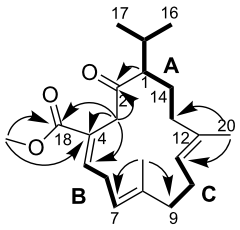

Figure 6: Structure of cembranoid **5**. ^{1}H,^{1}H spin systems (**A**, **B** and **C**) are indicated in bold, arrows show key HMBC correlations.

and tertiary carbon C-5 and with the ester carbonyl C-18. Due to the deshielded nature and large ^{1}H-coupling constant (signals of both protons appear as doublets, J = 17.7 Hz at δ_H 3.49 and 3.64) of the ^{1}H NMR resonance of the H_2-3, the position of the methylene group between keto carbonyl C-2 and the quaternary sp^2 carbon C-4 was very likely. The methyl ester moiety could be localized at C-4 due to long range correlation of the -OCH_3 resonance with ester carbonyl C-18 and quaternary C-4. A HMBC cross peak between the resonances of H-1 and C-2 established the 14-membered cembranoid ring.

The *E*-geometries at olefinic double bonds $\Delta^{7,8}$ and $\Delta^{11,12}$ were easily deduced from the ^{13}C NMR upfield shifts of the methyl group resonances CH_3-19 (δ_C 16.0) and CH_3-20 (δ_C 15.2). The deshielded resonance of H-5 (δ_H 7.08) indicated *E*-geometry of the olefinic double bond $\Delta^{4,5}$ [29].

Compound **5** resembled most closely the recently reported cembranoid pavidolide A isolated from the soft coral *Sinularia pavida* [30] and a metabolite from *Sarcophyton glaucum* – methyl sarcoate reported by Ishitsuka et al. [29] (see Figure 7). Obvious differences, however were the smaller number of keto

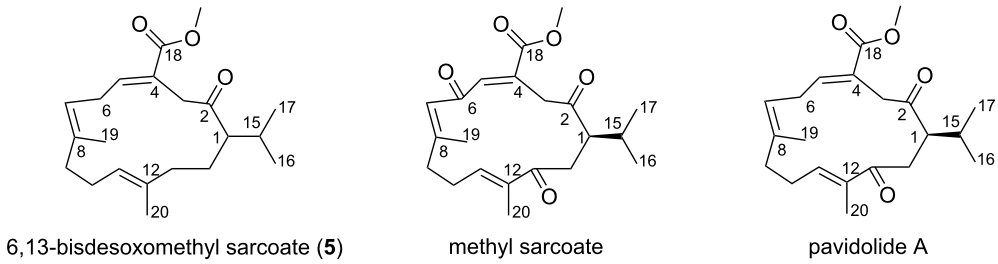

Figure 7: Compound **5** and the most closely related cembranoids from soft corals.

groups in compound **5** (only one at C-2 instead of two at C-2 and C-13 as in pavidolide A or three at C-2, C-6 and C-13 in methyl sarcoate). Both related molecules and compound **5** have only one stereogenic center, i.e., at C-1. The reported absolute configuration of pavidolide A ($[\alpha]_D^{20}$ +124, *c* 0.25, $CHCl_3$) at C-1 is *R* [30]. The specific rotation value of **5** is +3.5 and does not allow indicating any configuration for C-1 in compound **5**. Due to the instability of the substance and its rapid degradation, it was not possible to determine the absolute configuration unambiguously. Structural similarity of the compound **5** with pavidolide A and close relationship between *Sinularia* and *Sarcophyton* (food source of *P. longicirrum*) soft corals makes similar biosynthetic pathways involved into the synthesis of the cembranoid **5**, methyl sarcoate and pavidolide very likely. Thus, the configuration at C-1 in the compound **5** is proposed to be also *R*, although detailed studies are necessary to determine the stereochemistry unambiguously. Due to the close relationship to the first discovered methyl sarcoate we propose the trivial name 6,13-bisdesoxomethyl sarcoate for **5**.

Known compounds **6–8**, **10**, **11** and **13** were unambiguously identified comparing the obtained ^{1}H and ^{13}C NMR spectral data with the literature reports [31-36].

Repeated HPLC separation of VLC fraction 7 firstly led to two metabolites, which could not be structurally analyzed due to their instability. It was noted however, that two stable degradation products resulted and could be isolated, i.e., compounds **8** and **9**. The planar structure of **8** and **9** was established as that of isosarcophine by 1D and 2D NMR data (^{1}H, ^{13}C, COSY, HSQC and HMBC). Specific optical rotation measurements in chloroform (*c* 0.1 each substance) yielded $[\alpha]_D^{20}$ values of +92.0 for **8** and −38.0 for **9**. Due to the close similarity of the ^{1}H and ^{13}C NMR data (Supporting Information File 1, Table S3) compounds **8** and **9** were supposed to be stereoisomers. NMR spectral data of compound **8** were identical with those of (+)-isosarcophine ($[\alpha]_D^{20}$ +235.3) reported by Kusumi et al. [32], so **8** is established as (+)-isosarcophine. The configuration at C-2 for **8** and **9** was established with the help of CD experiments (Supporting Information File 1, Figures S22 and S27). According to Kobayashi et al. [31] (*S*) configuration at C-2 in furanocembranoids causes a negative Cotton effect at 246 nm like we obtained for compound **8**, which is thus (2*S*)-isosarcophine. The CD spectrum of **9** was the inverse of **8** and displayed a positive Cotton effect at 246 nm demonstrating that **8** and **9** are diastereomers. Thus, compound **9** is 2*R*-isosarcophine.

The cembranoid bisepoxide **12** was isolated as colorless oil, with a specific optical rotation of $[\alpha]_D^{20}$ −44.6 (*c* 3.3 in chloroform). The planar structure was deduced by the interpretation of the experimental data. The obtained ^{1}H and ^{13}C NMR data resembled those of closely related isosarcophytoxides **10** and **11**. An obvious difference between the isosarcophytoxides and compound **12** in the ^{13}C NMR spectrum was the absence of two downfield resonances resulting from the lack of a carbon–carbon double bond. Instead, two characteristic ^{13}C NMR shifts at δ_C 66.4 and 62.3, attributable to an epoxide moiety were present. ^{13}C NMR data of **12** and the specific optical rotation were identical with those reported by Bowden et al. [37], ($[\alpha]_D^{20}$ –46.7, *c* 0.9 in chloroform) for the cembranoid bisepoxide isolated from the soft coral *Sarcophyton* sp., pointing towards the same structure for this secondary metabolite. However, no 2D NMR data or stereochemistry of this molecule was reported up to now. Here we include the results of 2D NMR (COSY, HMBC and NOESY; all NMR spectral data in Supporting Information File 1, Figures S32–36 and Table S4) experiments and propose the absolute configuration of bisepoxide **12**.

Bisepoxide **12** has five stereogenic centers, found at the epoxide moieties between C-3 and C-4, and C-11 and C-12, as well as C-2 of the dihydrofuran ring. Previous studies on the stereochemistry of furanocembranoids [31,36,38,39] stated a relation between the value of the specific optical rotation, the CD Cotton effect and the configuration at C-2. Thus, a large posi-

tive specific rotation value corresponds with *S* configuration at C-2, whereas negative rotation values are found for 2*R* furanocembranoids. Likewise, a negative Cotton effect at ~250 nm is observed for (2*S*)-furanocembranoids. Kobayashi et al. reported a 2*S* configuration for sarcophytonin B (**6**) which exhibited a negative Cotton effect at 247 nm and a specific optical rotation of $[\alpha]_D^{20}$ +160 [31]. X-ray structure determination performed by Bernstein et al. for the closely related sarcophine (epoxide function at C-7, C-8) revealed also 2*S* configuration [38]. Sarcophine exhibited a negative Cotton effect at 246 nm. A CD measurement of bisepoxide **12** in acetonitrile did not yield any significant Cotton effect at 250 nm. However, NOE correlations are observed between the resonances of H-2, H-3 and H_3-18 indicating the orientation of the proton H-3 and the methyl group to the same side (see Figure 8). Due to the negative optical rotation of **12** ($[\alpha]_D^{20}$ −44.6), we propose the relative configuration at C-2 to be *S* (due to the additional epoxide at carbons C-3 and C-4 the CIP priority has changed) and thus, at C-3 and C-4 to be *R*. In addition, NOE correlations between H-11 and H_3-20 indicated a cis configured epoxide at carbons C-11 and C-12. The ^{1}H NMR resonance of H-11 (δ_H 2.88, dd, J = 3.3, 9.9 Hz in MeOH-d_4) in the bisepoxide **12** is very similar with the resonance of H-11 measured for 2*R*-isosarcophytoxide (**11**) (δ_H 2.88, dd, J = 3.3, 9.0, Hz), indicating that **11** and **12** have the same spatial orientation at carbons C-2, C-11 and C-12 [36]. Thus, we propose the relative configuration of **12** to be 2*S**, 3*R**, 4*R**, 11*R**, 12*R**. A study on a closely related cembranoid, the 3,4-epoxysarcophytoxide [40], revealed the absolute configuration at C-2, C-3 and C-4 to be *S*, *R* and *R*, respectively. According to a similar specific optical rotation measured for 3,4-epoxysarcophytoxid ($[\alpha]_D^{20}$ −52.8) the absolute configuration of **12** is likely to be the same. We propose the trivial name isosarcophytobisepoxide for compound **12**.

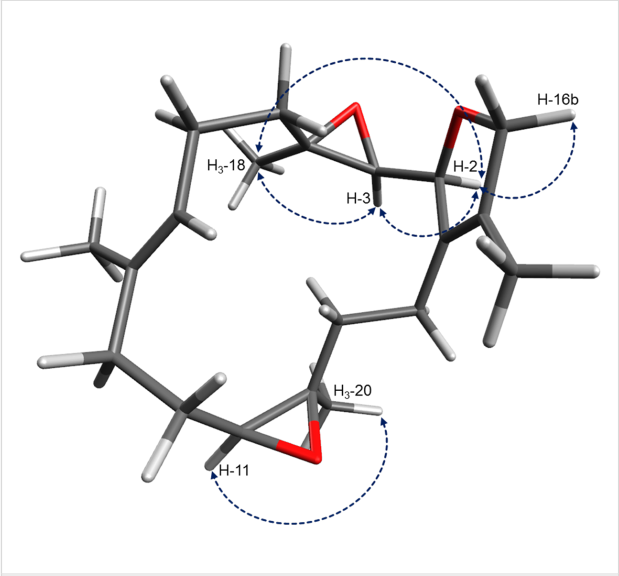

Figure 8: Proposed configuration and selected NOE correlations of bisepoxide **12** (key NOE correlations are indicated with blue arrows).

Biscembranoid **14** was isolated as an amorphous solid, with a specific optical rotation of $[\alpha]_D^{20}$ −5.0 (*c* 0.3 in MeOH). The NMR spectral data showed close resemblance with the known compounds, bisglaucumlides (**23**–**25**) isolated by Iwagawa et al. (see Figure 9) from the Pacific soft coral *Sarcophyton glaucum* [41]. The planar structure of compound **14** was established to be the same as that of bisglaucumlide B (**24**) by interpretation of the NMR data (^{1}H NMR, ^{13}C NMR, COSY, HSQC and HMBC) and comparison with the data published by Iwagawa et al. [41]. However, some ^{13}C NMR resonances of the carbons in ring C and D (NMR data in Table S5, Supporting Information File 1) of **14** were significantly different from those reported for bisglaucumlide B (**24**).

In biscembranoid **14** the ^{13}C NMR resonance of C-30 was shifted downfield to δ_C 82.1 compared with the reported value of δ_C 69.2 for the same carbon in bisglaucumlide B (**24**). The ^{13}C NMR shift of the methyl group CH_3-38 was more shielded (δ_C 16.6) than the reported resonance (δ_C 20.0) for **24**. The ^{13}C NMR shifts of C-2 and C-21 in **14** (δ_C 52.4 and 43.9) also differed from **24** (δ_C 46.8 and 40.3, respectively). Moreover, the specific optical rotation of $[\alpha]_D^{20}$ −5.0 measured for compound **14** differed significantly from the value published by Iwagawa et al. ($[\alpha]_D$ +126, *c* 0.22 in MeOH) for bisglaucumlide B (**24**) [41]. The absolute configuration of the bisglaucumlides was proposed by Iwagawa et al. according to the results of CD experiments and comparison with previously reported related molecules methyl sarcophytoate and nyalolide [29,42]. Different stereochemistry of biscembranoid **14** in the eastern part of the molecule (rings B, C and D) was thus suggested.

A ROESY experiment showed a distinct correlation of the resonances H-26 and H-30 (see conformational fragment structure, Figure 10). The lack of an ROE correlation between H-26 and the resonance of the vicinal methyl group CH_3-39, as well as the different ^{13}C NMR shift of C-30 from the reported value for bisglaucumlide B (**24**) indicated that **14** differed in the configuration at C-30, and that both protons H-26 and H-30 are oriented to the α-face of the molecule, and the proton H-30 is axial. The methyl group CH_3-40 is oriented to the β-face of the molecule since no ROE correlation could be observed between the latter and the α-oriented H-30. H_3-40 has a ROESY interaction with H-29b, since the latter has a ^{1}H-coupling to H-30 of 13.9 Hz it must be axial and β and this way proves the β and axial orientation of CH_3-40. A ROE correlation between the resonance of H-32 and the H_3-40 indicated the β-orientation of H-32, and due to the ^{1}H-coupling constant of 13.9 Hz this

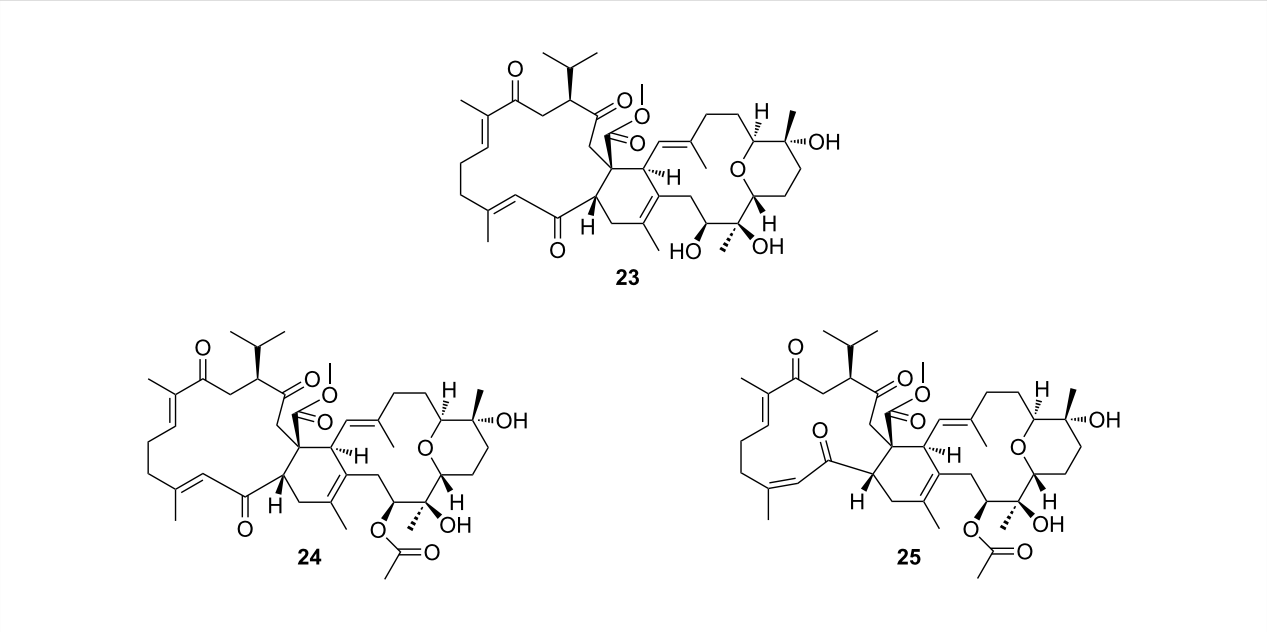

Figure 9: Structures of bisglaucumlids A–C (**23**–**25**).

proton must be axial. We propose the configurations in compound **14** to be *S* at C-30 and C-31, and *R* at C-32.

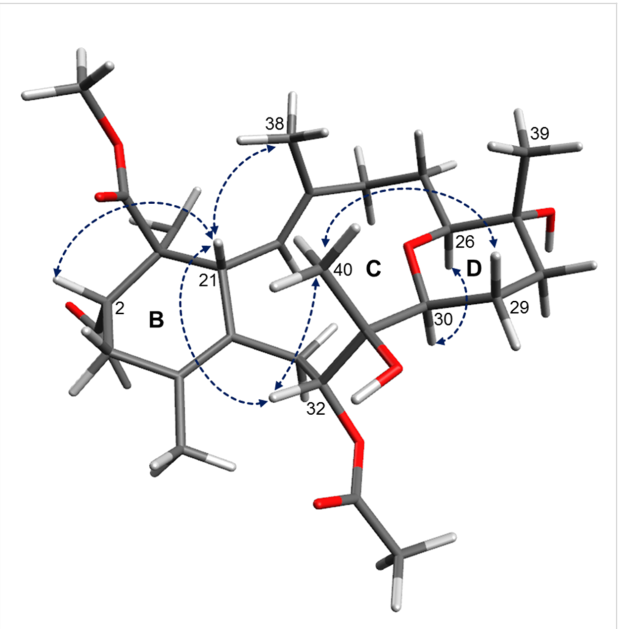

Figure 10: Proposed configuration of the eastern part (rings B, C and D) of isobisglaucumlides B and C (**14** and **15**; ROESY correlations are indicated with blue arrows).

A further discrepancy of the biscembranoid **14** with the reported bisglaucumlide B is a ROE correlation between H-2 and H-21 indicating the β-orientation of both protons and the configuration change at C-21 from *S* to *R*.

The related biscembranoid **15** was isolated as an amorphous solid with a specific optical rotation of $[\alpha]_D^{20}$ −14.0 (*c* 0.2 in MeOH). The NMR data (^{1}H NMR, ^{13}C NMR, COSY, HSQC, HMBC and ROESY, see Supporting Information File 1, Table S6) of **15** were very similar to those of **14**. The obvious difference was found at the ^{13}C NMR resonance of the methyl group CH_3-19. The chemical shift of δ_C 24.9 (compared with δ_C 18.6 in **14**) indicated the *Z* geometry at the carbon-carbon double bond between C-4 and C-5 in the biscembranoid **15**. This was also in accordance with the reported value by Iwagawa et al. [18] for bisglaucumlide C (**25**). The stereochemistry of the biscembranoid **15** in the eastern part of the molecule is suggested to be the same as that found in compound **14** due to the similar ROE experimental results. The difference in the specific rotation of the compound **15** $[\alpha]_D^{20}$ −14.0 with the reported value for bisglaucumlide C ($[\alpha]_D^{20}$ +32, in MeOH) supports the proposed stereochemistry.

We propose trivial names isobisglaucumlides B and C for compounds **14** and **15**, respectively.

Investigation of defensive properties of isolated metabolites

Subsequent experiments showed the feeding deterrent activity of the major secondary metabolites in *P. longicirrum* using the omnivorous fish *Canthigaster solandri* as model predator. In preliminary assays VLC fractions 5–7 proved to have significant deterrent effects (Supporting Information File 1, Figure S57). After the isolation of pure metabolites the deterrent properties could be traced down to few metabolites. (2*S*)-isosarco-

phytoxide (**10**) and bisepoxide **12** were already deterrent at 0.5% of dry mass, and higher concentrations (1.0% and 2.0% of dry mass) resulted in stronger effects (see Figure 11). Surprisingly, the stereoisomer of **10**, 2*R*-isosarcophytoxide (**11**) showed no significant deterrence at concentrations up to 2.0% of dry mass. No significant activity could be attributed to the structurally related sarcophytonin B (**6**) at a concentration up to 1.0% of dry mass. Polyhydroxylated steroid **2** also showed no antifeedant activity at the concentration 2.0% of dry mass.

Discussion

1. Chemical constituents of *P. longicirrum*

In this study a wide range of secondary metabolites was isolated from a single specimen of *P. longicirrum*. These belong to the polyhydroxylated steroids **1**–**4**, cembranoid diterpenoids **5**–**13** and biscembranoid tetraterpenes **14** and **15**, as well as the rare chatancin-type diterpenes **16**–**19**.

Noteworthy is the new unusual secosteroid **1** with a side chain as found in gorgosterol. Steroids with such a side chain were first described from the gorgonian coral *Plexaura flexuosa* [43]. Later on, the so-called gorgosterols were isolated from marine sediments, diatoms and most importantly from dinoflagellate cultures [44-46]. Besides inhabiting the water column, dinoflagellates of the genus *Symbiodinium* live in symbiosis as the so named zooxanthellae with various soft corals, i.e., *Sarcophyton* spp. and are also hosted by *P. longicirrum*. The secosteroid **1** isolated in this study could possibly originate either from the dinoflagellate symbionts of *Sarcophyton*, or is a product of the biosynthetic activity of the dinoflagellates within *P. longicirrum*. One possibility to explain the occurrence of chemically closely related gorgosterols in different soft coral clades is the presence of the same putative gorgosterol-producing *Symbiodinium* within their body. Overall, only few secosterols with gorgosterol side chain were reported, e.g., by Morris et al. [21], Naz et al. [22] and Anta et al. [24] and the ecological role of these compounds remains to be explored.

It cannot be ruled out completely that secosteroid **1** is an oxidation product, i.e., artifact of the secosteroid reported by Naz et al. [22] (see Figure 4). In this case, the epoxide ring at C-5 and C-6 would have undergone a cleavage to yield **1** during chromatographic procedures. The analysis of HRMS–UPLC data however, showed the presence of signals attributable to the secosteroid **1** prior the extensive HPLC (see Supporting Information File 1, Figure S53). This observation provides evidence

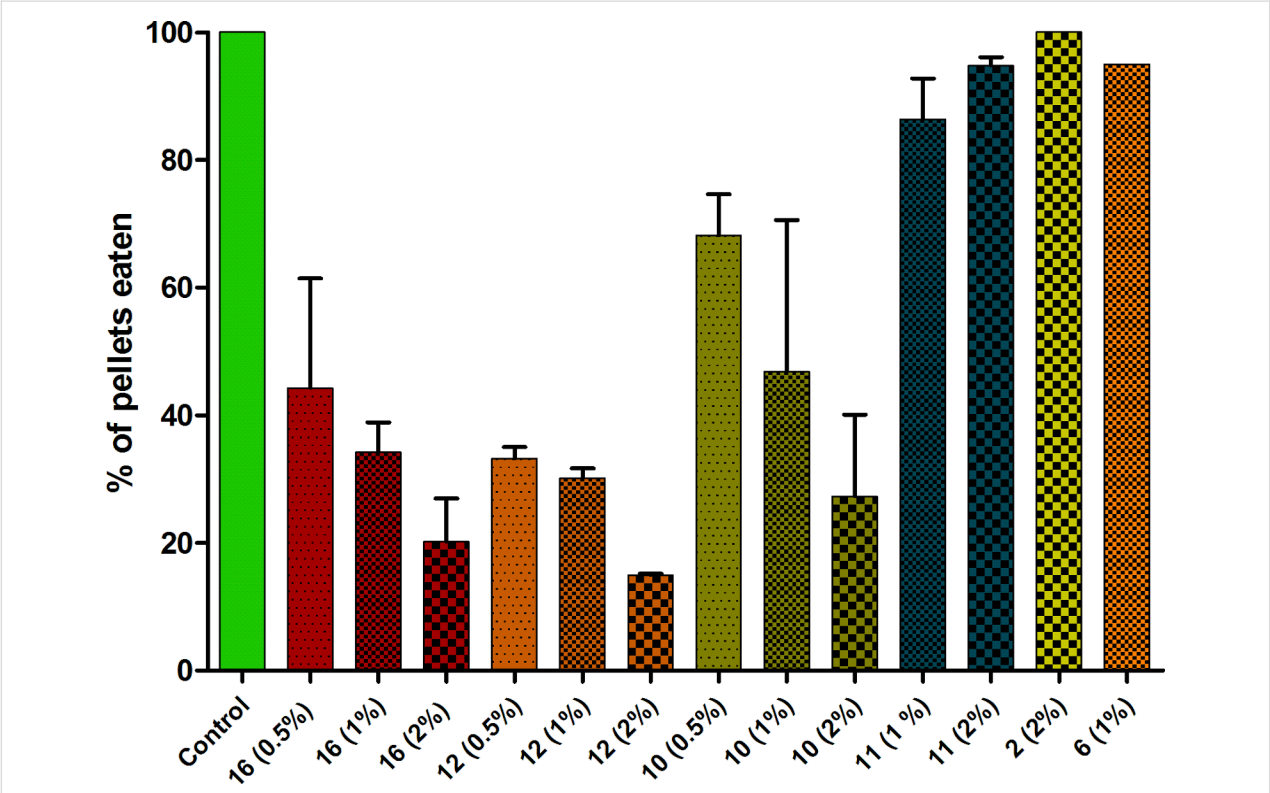

Figure 11: Effect of *Phyllodesmium* metabolites in different concentrations on predation by *Canthigaster solandri* (*n* = 8–40, depending on availability). Experiments were repeated twice with compounds **10–12** in all tested concentrations, twice with **16** at 1% and 2% and three times at 0.5%. Mean values with SD are displayed. Significance of deterrence was shown with Fisher´s exact test ($P < 0.05$ for **10**, **12** and **16**, calculated for each trial separately). Control pellets were 100% eaten for each trial.

that compound **1** is indeed a natural product, if not the epoxide moiety was cleaved already during the storage of the specimen in ethanol.

The new cembranoid 6,13-bisdesoxomethyl sarcoate (**5**) resembles most closely the methyl sarcoate described by Ishitsuka et al. [29] from soft coral *Sarcophyton glaucum* and the pavidolide A (6-desoxomethyl sarcoate) isolated from *Sinularia pavida* [30]. Methyl sarcoate is reported to be a possible biosynthetic precursor of several biscembranoids, e.g., methyl sarcophytoate [47], a metabolite from *S. glaucum* and methyl neosartortuate from *S. tortuosum* [48]. The biscembranoids are believed to originate as products from Diels–Alder cycloaddition between two cembranoid units. Besides methyl sarcoate, only methyl tetrahydrosarcoate and isosarcophytonolide D are reported to act as dienophile (western part) in over 60 described biscembranoids [49]. The western parts in the bisglaucumlides [18,41] and isobisglaucumlides isolated in this study (**14** and **15**) correspond with the structure of methyl sarcoate. To our best knowledge, there are no literature reports on biscembranoids having 6,13-bisdesoxomethyl sarcoate (**5**) or pavidolide A as building blocks. First evidence pointing towards the existence of such biscembranoids provides the UPLC–HRMS investigation in this study. As mentioned in the results part, characteristic *m*/*z* values were detected in the chromatograms of the fractions VLC 6 and 7 (Supporting Information File 1, Figures S54–56) attributable to biscembranoids incorporating compound **5** as the western part and the eastern part as found in the isobisglaucumlides **14** and **15** (M + H *m*/*z* 711.39). A further possible metabolite with *m*/*z* of 669.44 (M + H) would be one with the eastern part bearing a hydroxy instead of the acetate moiety at C-32 (as found in bisglaucumlide A (**23**) [18]). This assignment relying on the MS data only is surely somewhat speculative.

In our former study in 2014, relying on UPLC-HRMS data only, we assumed that isosarcophines **8** and **9** and sarcophytonin B (**6**) could be present in the *P. longicirrum* extract. In the current investigation we were able to isolate these metabolites and demonstrate the informative value of the preliminary UPLC–HRMS analysis. Further investigations on Alcyonacean and/or *Phyllodesmium* chemistry may thus lead to the isolation and full characterization of the putative biscembranoids.

Furanocembranoids are reported to be unstable and to quickly autoxidize in the presence of light [16]. In our study, isosarcophines **8** and **9** were isolated after repeated chromatography of purified, but labile compounds, which thus remained unidentified. Additionally, during the purification of the isosarcophytoxides **10** and **11** peaks most probably attributable to the isosarcophines **8** and **9** appeared in the chromatograms, demonstrating the oxidation of the isosarcophytoxides to the isosarcophines. Reports on such conversions are found in the literature, e.g., Kusumi et al. described the isolation of isosarcophine **8** from *Sinularia mayi* and chemical conversion of the isosarcophytoxide **10** into **8** by exposing the DCM solution of **10** to light, supporting our assumption that the isosarcophines **8** and **9** are artifacts [32].

2. Secondary metabolome of *P. longicirrum* with regard to metabolites known from *Sarcophyton*, especially in *S. glaucum*

Several *Sarcophyton* species (Octocorallia) were reported to contain the identical metabolites as isolated in this study from *P. longicirrum*. Indeed, the majority of the known compounds was firstly found in *S. glaucum* (**2**, **4**, **10**–**11**, **13** [27,35,36]). Other *Sarcophyton* species reported to contain *P. longicirrum* metabolites are *S. subviride*, i.e., compound **3** [28] and *S. cherbonnieri*, i.e., compound **7** [33]. However, two of our *P. longicirrum* compounds, sarcophytonin B (**6**) and isosarcophytobisepoxide (**12**) were first described from unidentified *Sarcophyton* species [31,37]. Concerning the new natural products from *P. longicirrum*, they can be regarded as derivatives of *S. glaucum* secondary metabolites, e.g., **1**, **5**, **14**, **15** and the chatancin-type diterpenes **16**–**19**.

Samples of the same *Sarcophyton* species collected at different times and habitats can differ greatly in their chemistry [39,50]. Other closely related soft corals, such as *Lobophytum* spp., also contain cembranoids, e.g., the isosarcophytoxides **10** and **11** [36] as well as a numerous biscembranoid compounds [51]. Distinct patterns of chemotypes in *Sarcophyton* species were demonstrated in a study by Tanaka et al. [52]. In this latter study, the largest diversity of secondary metabolites was found for *S. glaucum*, compared with the moderate chemical diversity found in *S. trocheliophorum*. The latter was the observed soft coral preyed upon by *P. longicirrum* and investigated by Coll et al. [13]. The isolation of only three metabolites **20**–**22** (Figure 2) in their study would correlate with the results of Tanaka et al. [52], showing the less complex metabolome of *S. trocheliophorum*. Exact identification of soft corals is, however still difficult and misidentification cannot be ruled out.

An explanation for the highest metabolome diversity of *S. glaucum* can lie in the taxonomic impediment of this particular species. The phylogenetic analysis by McFadden et al. clearly showed that the relationship and systematics of the soft coral genus *Sarcophyton* is not resolved (see Figure 12) [53]. *S. glaucum* seems to be a species complex with at least 6 different clades. Furthermore one of the former investigated species (*S. subviride*, compound **3**) is considered to be synonymous with *S. glaucum* [53]. A retrospective assignment of the investi-

gated *S. glaucum* specimens and the identified metabolites mentioned above is not possible. Interestingly, *S. cherbonnieri* wherefrom compound **7** was first described, shows no genetic difference to four specimens identified as *S. glaucum*. The available studies on *S. cherbonnieri* secondary metabolites [33,34,52] resulted in the isolation of a range of secondary metabolites, some of which were previously described from *S. glaucum*. These results show that chemotaxonomy might help in effective species delimitation.

The occurrence of the secosteroid **1** which is a derivative of a compound isolated from the Gorgonian *Pseudopterogorgia americana* may raise further questions about the food preferences of *P. longicirrum*. The soft corals (Alcyonacea) comprise several suborders and families including Alcyoniidae within Alcyoniina, and Gorgoniidae within Holaxonia. Phylogenetic analyses based on molecular markers and applying maximum likelihood methods, as well as parsimony analyses by McFadden et al. [54] do not clarify the relationship of the mor-

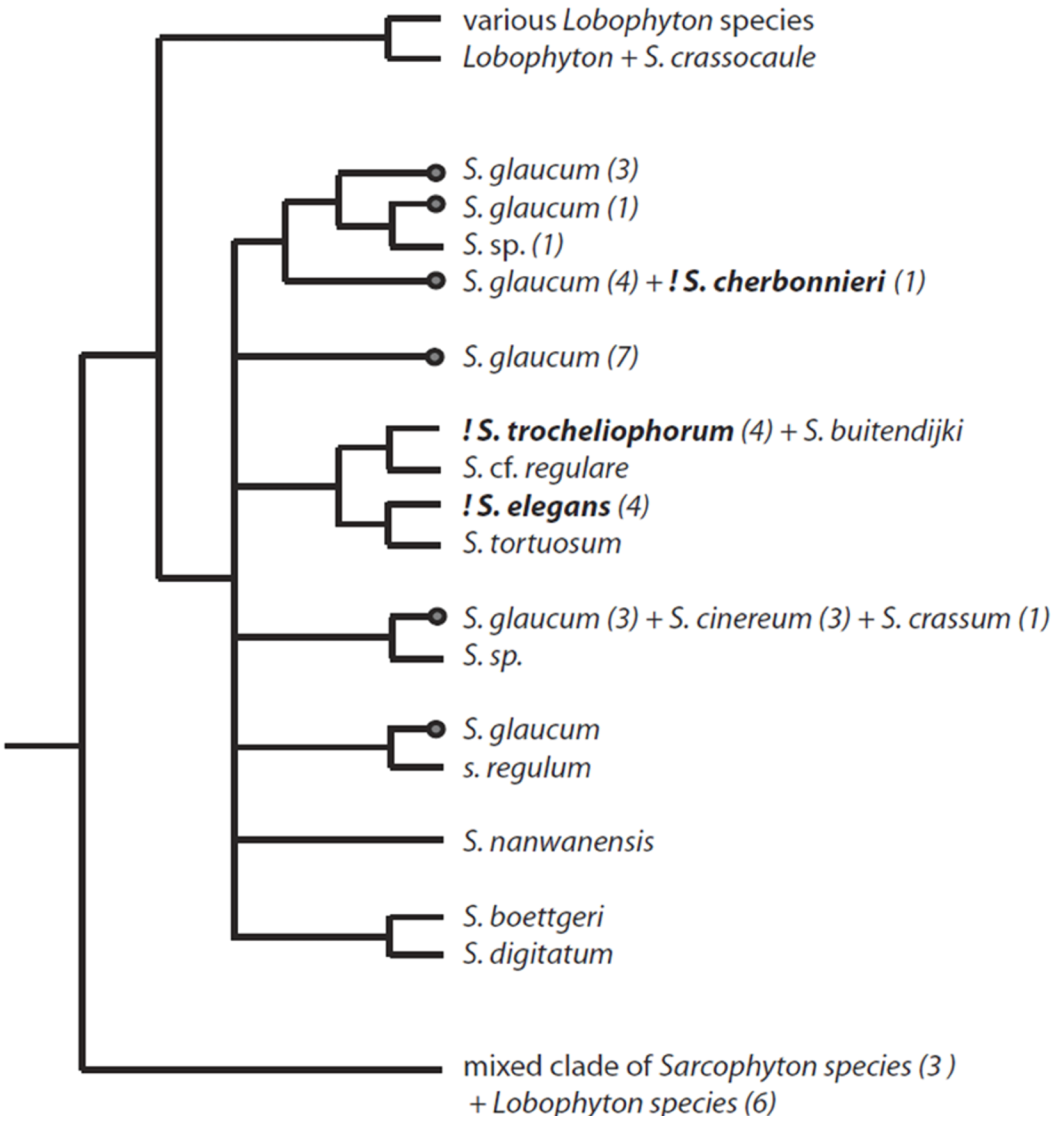

Figure 12: Phylogenetic tree of octocorals relevant as putative food sources for *Phyllodesmium* spp. Phylogram of *Sarcophyton* and *Lobophytum*, based on a consensus phylogram of McFadden et al. [54]. Only the *Sarcophyton* clade with species investigated with regard to secondary metabolites are given in detail. The two other clades from the original phylogram are only indicated; *Lobophytum* and the mixed clade consisting of *Sarcophyton* and *Lobophytum* species. Numbers indicate the number of specimens that represent the respective branch. Note that the single specimen of *S. cherbonnieri* groups with 4 specimens of *S. glaucum*. *S. glaucum* is not monophyletic, but is represented with several independent clades. The dots at the terminal branches of *S. glaucum* in the tree indicate that secondary metabolites are described from this species, but it is not known, from which clade. Species in bold indicate that secondary metabolites were described.

phologically, as well as chemically different Alcyoniidae (including *Sarcophyton*) and Gorgoniidae (including *Pseudopterogorgia* within Alcyonacea). Nevertheless, feeding on *Pseudopterogorgia* by *P. longicirrum* seems extraordinary and very unusual. The habitus of this gorgoniid is so different – fragile with very narrow branches – compared to the mushroom shape of *Sarcophyton*. Moreover, no typical gorgonian diterpenes (e.g., pseudopterosines, [55]) were isolated from *P. longicirrum*. As stated before, it is more likely that the secosterol is produced by zooxanthellae independently from its host and/or the *Sarcophyton* soft corals produce a wider variety of secondary metabolites as known.

Altogether, the types of the majority of the isolated metabolites provide circumstantial evidence that the investigated *P. longicirrum* specimen fed mainly, if not exclusively, on *S. glaucum* which is a common soft coral in the Indo-West Pacific coral reefs and has been observed at Lizard Island. In contrast, the animal collected from a different place in the GBR and studied by Coll et al. [13] preyed upon *S. trocheliophorum*, which is according to McFaddens and co-workers phylogenetic research [53] found in the different clade from the *S. glaucum* species complex (see Figure 12). We can state that the highly diverse metabolome of the herein studied *P. longicirrum* probably results from the different chemotypes among *S. glaucum* which might reflect the cryptic speciation as well as the wide metabolite spectrum of the *S. glaucum* complex. Whether a cryptic speciation also occurs in *P. longicirrum* by specializing on certain chemotypes within *Sarcophyton* clades remains to be clarified.

3. Defensive role of *P. longicirrum* metabolites

The coral reef is a harsh environment with a high predation pressure, especially for slow moving and soft bodied animals like *P. longicirrum*. In the past, studies were conducted trying to shed light on the ecology of soft corals, especially with regard to the protection against predators. A pioneering work was done by Neeman and coworkers in 1974 [56]. There, one of the first isolated cembranoid diterpenes from *S. glaucum* – sarcophine – was reported to be a defensive agent in *Sarcophyton* colonies. Sarcophine, the main toxic substance of the investigated soft coral, was shown to be ichthyotoxic in lethality assays using the freshwater fish *Gambusia affinis*, and therefore believed to be at least involved in the chemical defense. Later investigations provided toxicity ranking among the Alcyonarian soft corals. *Sarcophyton* species together with *Sinularia*, *Lemnalia*, *Lobophytum* and *Nephthea* soft corals showed the highest ichthyotoxicity levels [57,58]. The study on the defensive strategies of soft corals carried out by La Barre et al. focused on feeding deterrence of aqueous coral extracts against *G. affinis* [59]. The remarkable result was that the fish deterrent activity and ichthyotoxicity not necessarily correlated, demonstrating the complexity of such ecological studies. The comprehensive article by Pawlik provides deeper insights into the problematics concerning the determination of the defensive role of marine natural products [60].

Defense strategy using sequestered soft coral metabolites has been discussed for the members of the genus *Phyllodesmium*, however, there are only few studies supporting this hypothesis. Besides our earlier study [12] reporting a feeding deterrent activity of 4-oxochatancin (**16**), only a study by Slattery et al. [15] could show an antifeedant effect of a secondary metabolite sequestered by *Phyllodesmium*. In the latter study, acetoxypukalide, which was sequestered by *P. guamensis* from its prey corals *Sinularia* spp., successfully deterred the omnivorous pufferfish *Canthigaster solandri* under laboratory conditions at 0.5% of dry mass in artificial food. The concentration chosen was at least an order of magnitude lower, than found in the body tissues of *P. guamensis*.

Determination of the exact percentage of secondary metabolites in the body tissues of *P. longicirrum* in our study was experimentally not possible, since the single specimen investigated herein was stored in ethanol (90%) immediately after collection. Taking into account the comparable physiology and the close relationship of *P. guamensis* and *P. longicirrum*, we have chosen a concentration of 0.5% of the respective substance in the dry weight of the artificial food as lowest level (according to the study by Slattery et al. [15]) for pure compounds in laboratory feeding assays using *C. solandri*.

The major metabolites (2*S*)-isosarcophytoxide (**10**) and bisepoxide **12** were significant deterrent at 0.5% of the fish diet calculated for the dry mass. The deterrence was more pronounced at higher concentrations (1 and 2%) (see Figure 11). 4-oxochatancin (**16**), as reported earlier showed comparable activity [12]. Remarkable, however, is the inactivity of the (2*R*)-isosarcophytoxide (**11**) up to 2% of dry pellet mass, a mere stereoisomer of the active metabolite **10**. Such a dependence on stereochemistry may result from a specific interaction with taste receptors in *C. solandri* lips, oral cavity and pharyngeal part. The importance of stereochemistry for taste response was shown in studies using alanine as a ligand for taste receptors from fish [61,62]. Investigations on the effects of cembranoid diterpenes on receptors are published, e.g., nicotinic receptors by Ferchmin et al. [63].

An important chemical feature of deterrent cembranoid metabolites is the epoxy-moiety. Among the tested cembranoids the strongest deterrent effect was found for the isosarcophytobise-

poxide **12**, following by (2*S*)-isosarcophytoxide (**10**). The assayed furanocembranoid sarcophytonin B (**6**) could not exhibit reproducible effect, even though one probe was highly deterrent. Probable spontaneous oxidation of **6** to potentially active epoxide-bearing metabolites, e.g., (2*S*)-isosarcophytoxide (**10**) or isosarcophines **8** and **9** may have led to this observation. Deterrent abilities of the latter, however, are still not determined due to insufficiently available amounts.

Isolated steroid compounds **1**–**4** in this study are minor metabolites compared to the diterpenes present in the investigated specimen (e.g., **10**–**12** and **16**). The ecological role (defensive or ichthyotoxic) of polyhydroxylated steroids could not yet been assigned in the marine environment [59]. Here, the only assayed steroidal compound was **2**, but found to be inactive at 2% of dry mass. The ecological significance or role of this compound class in *P. longicirrum* remains unexplored.

Fish may represent the main, however not the only potential predation threat to slugs. The omnivorous Echinodermata, Crustacea and Cephalopoda could also consider *Phyllodesmium* as possible prey. Whether the compounds, proven defensive against fish predation in this study function as deterrents towards other organisms, has yet to be shown. Even if the furanocembranoids represent the protection against omnivorous fish, it is possible that some of the numerous secondary metabolites found in this study could be useful against a wider range of predators.

In summary, chemical investigation of a single large *P. longicirrum* specimen resulted in isolation of 19 secondary metabolites of terpenoid origin. Taking the metabolites detected by UPLC–HRMS analysis also into account, *P. longicirrum* demonstrates an unprecedented level of secondary metabolite diversity. The herein studied *P. longicirrum* sequesters its secondary metabolites most probably from the chemistry-rich *S. glaucum* species complex, in contrary to a previously reported investigated *P. longicirrum*. The defensive role of the major diterpenoid constituents (**10**, **12** and **16**) as feeding deterrent agents against tropical omnivorous fish *C. solandri* was shown in laboratory assays, providing further strong evidence for the use of chemical protection strategy within the scarcely investigated aeolidoidean genus *Phyllodesmium*.

Experimental

General experimental procedures

Optical rotations were measured with a Jasco DIP 140 polarimeter. ECD spectra were taken on a Jasco J-810 CD spectropolarimeter. UV and IR spectra were obtained using Perkin-Elmer Lambda 40 and Perkin-Elmer Spectrum BX instruments, respectively. All NMR spectra were recorded in MeOH-d_4 using Bruker Avance 300 DPX, Bruker Avance 500 DRX or Bruker Ascend 600 (with cryoprobe Prodigy) spectrometers, respectively. Spectra were referenced to residual solvent signals with resonances at $\delta_{H/C}$ 3.35/49.0. LC–ESIMS was performed using an Agilent 1100 system with an API 2000 Triple Quadrupole LC/MS/MS with ESI source (Applied Biosystems/MDS Sciex) and a photodiode array detector (PDA). HRMS–ESI were recorded on a LTQ Orbitrap mass spectrometer. UPLC–HRMS analysis was performed on a Thermo Scientific Qexactive mass spectrometer with HESI source, Phenomenex Kinetex C_{18} column (150 mm × 4.6 mm, 2.6 µm, 100 Å).

A Grace Reveleris X2 system equipped with 12 g Reveleris C_{18} column was used for flash chromatography. HPLC was performed either on a Merck Hitachi HPLC system equipped with a L-6200A pump, a L-4500A PDA detector, a D-6000A interface with D-7000A HSM software, a Rheodyne 7725i injection system or on a Waters HPLC system equipped with a 1525µ dual pump, a 2996 PDA detector, Breeze software and a Rheodyne 7725i injection system. A Waters Atlantis T3 C_{18} column (250 mm × 4.6 mm; 5 µm), Macherey-Nagel Nucleoshell C_{18} column (250 mm × 4.6 mm; 5 µm), Knauer Eurospher C_{18} column (250 mm × 8 mm; 5 µm) and Phenomenex Luna 5 µm C_{18}(2) 100A column (250 mm × 10 mm; 5µm) were used.

Sample

The sample of *P. longicirrum* was collected 2008 during a field trip to Lizard Island (Great Barrier Reef, Australia) by H. Wägele. The specimen (Phlo08-LI) was stored in ethanol (96%) until further extraction and processing in the laboratories at the University of Bonn.

Extraction and isolation

The extraction procedure was analogous as described in [11]. The ethanolic storage solution was combined with the MeOH extract (3 × 150 mL) of the slug biomass and the solvents were evaporated. After liquid–liquid separation of the methanolic crude extract (4.5 g) between 100 mL H_2O and 3 × 100 mL ethyl acetate (EtOAc), EtOAc solubles (2.2 g) were fractionated by vacuum liquid chromatography (VLC) over Polygoprep 60–50 C_{18} stationary phase (Macherey-Nagel) using gradient elution from 20:80 (MeOH/H_2O) to 100% MeOH to yield 11 fractions. 100 mL of the mobile phase was used for each fraction. Fractions 3–8 (6 mg, 16 mg, 207 mg, 763 mg, 696 mg, 150 mg, respectively) were analyzed with the UPLC–HRMS system using the following solvent gradient program: A. water + 0.1% formic acid and B. acetonitrile + 0.1% formic acid; 5% B 0–2 min, 5–95% B 2–14 min, 95% B 14–17 min, 95–5% B 17–22 min. The column oven was adjusted to 30 °C. Complex chromatograms obtained from VLC fractions 5–8 by

UPLC–HRMS analysis indicated the presence of a wide range of secondary metabolites. These VLC fractions were thus subsequently submitted for further chromatographic separation.

VLC fraction 7 (690 mg) was further separated by normal phase VLC using silica gel (60Å, 70–230 mesh, 63–200 µm) and dichloromethane (DCM):acetone gradient from 100% DCM to 100% acetone (100 mL of eluent each fraction, 20% steps) to yield 6 fractions (7.1–7.6). HPLC of fractions 7.5 and 7.6 ($MeOH/H_2O$ 83:17, 0.9 mL/min, column: Waters Atlantis T3) resulted in the isolation of the new secosterol **1** (1.4 mg) along with the known steroid compounds **2** (2.5 mg), **3** (1.0 mg) and **4** (1.5 mg).

The new cembranoid diterpene **5** was isolated after RP–HPLC separation of VLC fraction 8 ($MeOH/H_2O$ 90:10, Phenomenex Luna column, 2 mL/min). Seven fractions (8.1–8.7) were obtained, fraction 8.2 (17.4 mg) was further purified using Atlantis T3 column ($MeOH/H_2O$ 78:22, 0.9 mL/min) yielding 1.5 mg of **5**.

Sarcophytonin B (**6**) (14.0 mg), furanocembranoid **7** (2.0 mg), isosarcophines **8** and **9** (each 2.0 mg), isosarcophytoxides **10** (13.0 mg) and **11** (12.0 mg) were isolated from fraction VLC 7.2 (530 mg) after repeated normal phase VLC with a silica gel having a smaller particle size (60 Å, particle size < 63 µm, mesh < 230; DCM/acetone gradient from 100% DCM to 100% acetone in 10% steps, 50 mL of eluent each fraction) and subsequent RP–HPLC separation ($MeOH/H_2O$ 75:25, 0.9 mL/min, Macherey-Nagel Nucleoshell column).

VLC fraction 6 was separated on a Sephadex LH-20 column with MeOH as eluent to yield 11 fractions S1–11, using 100 mL MeOH per fraction. The major fraction S7 (412 mg) was separated on RP flash chromatography ($MeOH:H_2O$ 60:40, 30 mL/min; Reveleris C_{18} column, 12 g) to yield 28 mg of cembranoid bisepoxide **12**. Cembranoid **13** (1.0 mg) was obtained after the separation of fraction S8 (24 mg) on RP–HPLC (Waters Atlantis T3 C_{18} column; 70:30 $MeOH/H_2O$ mobile phase, 0.8 mL/min). Separation of fraction S5 (60 mg) using RP–HPLC ($MeOH/H_2O$ 70:30, Macherey-Nagel Nucleoshell column, 0.9 mL/min) led to the isolation of two biscembranoids **14** (4.0 mg) and **15** (2.0 mg).

(3β,5α,6β)-Trihydroxy-9-oxo-9,11-secogorgostan-11-ol (**1**): amorphous solid; $[\alpha]_D^{20}$ −21.0 (*c* 0.1, $CHCl_3$); UV (MeOH) λ_{max} (ε): 245 (190) nm; IR (ATR) ν_{max}: 3360, 2958, 2925, 2871, 1697, 1468, 1370, 1165, 1029, 974, 669 cm^{-1}; ^1H and ^{13}C NMR (Supporting Information File 1, Table S1); HRMS–ESI (*m*/*z*): $[M + Na]^+$ calcd for $C_{30}H_{52}O_5Na$, 515.3712; found, 515.3694.

6,13-Bisdesoxomethyl sarcoate (**5**): colorless oil; $[\alpha]_D^{20}$ +3.5 (*c* 0.09, $CHCl_3$); UV (MeOH) λ_{max} (ε): 204 (510) nm; IR (ATR) ν_{max}: 3360, 2853, 1700, 1679, 1459, 1377, 1205, 1137, 633 cm^{-1}; ^1H and ^{13}C NMR (Supporting Information File 1, Table S2); HRMS–ESI (*m*/*z*): $[M + Na]^+$ calcd for $C_{21}H_{32}O_3Na$, 355.2249; found, 355.2244.

(2*R*,11*R*,12*R*)-Isosarcophine (**9**): colorless oil, $[\alpha]_D^{20}$ −38.0 (*c* 0.1 in $CHCl_3$); UV (MeOH) λ_{max} (ε): 204 (11587), 260 (sh) (1587) nm; IR (ATR) ν_{max}: 3445, 2924, 1748, 1677, 1440, 1385, 1093, 997 cm^{-1}; ^1H and ^{13}C NMR (Supporting Information File 1, Table S3); ESIMS (*m*/*z*): $[M + H]^+$ 317.1.

(2*S*,3*R*,4*R*,11*R*,12*R*)-Isosarcophytobisepoxide (**12**): colorless oil, $[\alpha]_D^{20}$ −44.6 (*c* 3.3 in $CHCl_3$); UV (MeOH) λ_{max} (ε): 206 (5716) nm; IR (ATR) ν_{max}: 3431, 2925, 2854, 1711, 1457, 1378, 1267, 1247, 1205, 1142, 995 cm^{-1}; ^1H and ^{13}C NMR (Supporting Information File 1, Table S4); HRMS–ESI (*m*/*z*): $[M + H]^+$ calcd for $C_{20}H_{31}O_3$, 319.2268; found, 319.2222.

Isobisglaucumlide B (**14**): amorphous solid, $[\alpha]_D^{20}$ −5.0 (*c* 0.3 in MeOH); UV (MeOH) λ_{max} (ε): 230 (1148) nm; IR (ATR) ν_{max}: 3420, 2927, 2361, 1706, 1669, 1436, 1373, 1205, 1087, 761 cm^{-1}; ^1H and ^{13}C NMR (Supporting Information File 1, Table S5); HRMS–ESI (*m*/*z*): $[M + Na]^+$ calcd for $C_{43}H_{62}O_{10}Na$, 761.4235; found, 761.4194.

Isobisglaucumlide C (**15**): amorphous solid, $[\alpha]_D^{20}$ −14.0 (*c* 0.2 in MeOH); UV (MeOH) λ_{max} (ε): 231 (1407) nm; IR (ATR) ν_{max}: 3424, 2928, 2359, 1707, 1614, 1435, 1372, 1204, 1085, 1027, 773 cm^{-1}; ^1H and ^{13}C NMR (Supporting Information File 1, Table S6); HRMS–ESI (*m*/*z*): $[M + Na]^+$ calcd for $C_{43}H_{62}O_{10}Na$, 761.4235; found, 761.4177.

Spectral data of literature reported metabolites **2–4**, **6–8** and **13** are found in Supporting Information File 1.

Isolation and structure elucidation of four new unusual chatancin-type diterpenes **16–19** from the same *P. longicirrum* specimen was reported in our recent publication [13].

Chemical defense

To evaluate defensive properties of *P. longicirrum* secondary metabolites, feeding assays with the pufferfish *Canthigaster solandri* were carried out under laboratory conditions. This fish is a generalist feeder in the tropical Pacific living sympatric with the main food of *P. longicirrum* and thus being a putative predator of *P. longicirrum*. It was also used previously as a model predator by Rohde et al. [64], Rohde and Schupp [65]. The *C. solandri* were kept in separate 70 L flow-through tanks and fed regularly days before feeding assay in order not to

change the feeding preference patterns. The artificial diet was made of 0.3 g sodium alginate and 0.5 g squid powder (if available) or commercial dry fish food filled up with purified water up to 10 g. The mixture was stirred vigorously and shortly heated up in the microwave oven. The tested fractions or pure compounds were pre-solved in a drop of ethanol in an Eppendorf tube and homogenized subsequently with 1 mL of artificial diet. After pouring the semi-liquid diet into 0.25 M calcium chloride solution using a syringe, the solidified strip was washed with sea water and cut into suitable pellets. For control only a drop of ethanol was mixed with the artificial diet. Since any color differences between control and treated pellets were detectable, no additional coloring was necessary. A control and treated pellet were offered sequentially to each *C. solandri*. If the treated pellet was rejected or spit out at least three times, a second control pellet was offered to confirm that fish had not ceased feeding. A rejection was only scored when both controls were eaten. *Fisher's exact test* was used to show the significance of the reduced palatability of treated pellets compared to control pellets. Preliminary experiments with fractions VLC 5–7 were performed with concentration levels below estimated natural occurrence in living *P. longicirrum* (VLC 5 at 2.5%, VLC 6 at 5%, VLC 7 at 1.2% of dry artificial food mass).

After obtaining and characterizing the pure metabolites from the VLC fractions tested previously, the feeding assays were repeated. Isolated secondary metabolites were chosen for the assays depending on the amounts and compound class. Major metabolites were tested twice or three times at each different concentration to enhance the statistical power. The assays were performed with compounds **2** (at 2% of dry mass), **6** (three times at 0.5%, twice at 1% of dry mass), **10** (2× at 0.5%, 1% and 2% of dry mass), **11** (2× at 1% and 2% of dry mass), **12** (twice at 0.5%, 1% and 2% of dry mass) and as previously published with **16** (3× at 0.5%, 2× at 1% and 2% of dry mass). The number of available fish individuals involved in the assays varied from 8 to 50.

Supporting Information

Supporting Information File 1

Spectroscopic data and other relevant information.
[http://www.beilstein-journals.org/bjoc/content/supplementary/1860-5397-13-50-S1.pdf]

Acknowledgements

We thank the German Science Foundation for support to two authors: HW (Wa618/10-1) and GK (Ko 902/8-1), as well as the Indobio BMBF project. The animal material was collected and exported legally with permits provided to H.W. The picture of *P. longicirrum* in its natural habitat was provided with permission by L. Vail from Lizard Island research station.

References

1. Wägele, H.; Klussmann-Kolb, A.; Verbeek, E.; Schrödl, M. *Org. Divers. Evol.* **2013,** *14,* 133–149. doi:10.1007/s13127-013-0151-5
2. Cattaneo-Vietti, R.; Angelini, S.; Bavestrello, G. *Boll. Malacol.* **1993,** *29,* 173–180.
3. Edmunds, M. J. B. *Mar. Sci.* **1968,** *18,* 203–219.
4. Edmunds, M. J. A. *Malacol. Bull.* **1987,** *5,* 185–196.
5. Wägele, H.; Ballesteros, M.; Avila, C. *Oceanogr. Mar. Biol.* **2006,** *44,* 197–276. doi:10.1201/9781420006391.ch5
6. Klussmann-Kolb, A.; Dinapoli, A.; Kuhn, K.; Streit, B.; Albrecht, C. *BMC Evol. Biol.* **2008,** *8,* No. 57. doi:10.1186/1471-2148-8-57
7. Greenwood, P. G. *Toxicon* **2009,** *54,* 1065–1070. doi:10.1016/j.toxicon.2009.02.029
8. Burghardt, I.; Schrödl, M.; Wägele, H. *J. Molluscan Stud.* **2008,** *74,* 277–292. doi:10.1093/mollus/eyn016
9. Wägele, H.; Raupach, M. J.; Burghardt, I.; Grzymbowski, Y.; Händeler, K. Solar powered seaslugs (Opisthobranchia, Gastropoda, Mollusca): incorporation of photosynthetic units: a key character enhancing radiation?. In *Evolution in Action;* Glaubrecht, M., Ed.; Springer: Berlin-Heidelberg, 2010; pp 263–282. doi:10.1007/978-3-642-12425-9_13
10. Affeld, S.; Kehraus, S.; Wägele, H.; König, G. M. *J. Nat. Prod.* **2009,** *72,* 298–300. doi:10.1021/np800583e
11. Bogdanov, A.; Kehraus, S.; Bleidissel, S.; Preisfeld, G.; Schillo, D.; Piel, J.; Brachmann, A. O.; Wägele, H.; König, G. M. *J. Chem. Ecol.* **2014,** *40,* 1013–1024. doi:10.1007/s10886-014-0496-z
12. Bogdanov, A.; Hertzer, C.; Kehraus, S.; Nietzer, S.; Rohde, S.; Schupp, P. J.; Wägele, H.; König, G. M. *J. Nat. Prod.* **2016,** *79,* 611–615. doi:10.1021/acs.jnatprod.5b00860
13. Coll, J. C.; Bowden, B. F.; Tapiolas, D. M.; Willis, R. H.; Djura, P.; Streamer, M.; Trott, L. *Tetrahedron* **1985,** *41,* 1085–1092. doi:10.1016/S0040-4020(01)96476-2
14. Mao, S.-C.; Gavagnin, M.; Mollo, E.; Guo, Y.-W. *Biochem. Syst. Ecol.* **2011,** *39,* 408–411. doi:10.1016/j.bse.2011.05.018
15. Slattery, M.; Avila, C.; Starmer, J.; Paul, V. J. *J. Exp. Mar. Biol. Ecol.* **1998,** *226,* 33–49. doi:10.1016/S0022-0981(97)00240-2
16. Kobayashi, M.; Nakagawa, T.; Mitsuhashi, H. *Chem. Pharm. Bull.* **1979,** *27,* 2382–2387. doi:10.1248/cpb.27.2382
17. Kobayashi, M.; Ishizaka, T.; Mitsuhashi, H. *Steroids* **1982,** *40,* 209–221. doi:10.1016/0039-128X(82)90034-4
18. Iwagawa, T.; Hashimoto, K.; Okamura, H.; Kurawaki, J.-i.; Nakatani, M.; Hou, D.-X.; Fujii, M.; Doe, M.; Morimoto, Y.; Takemura, K. *J. Nat. Prod.* **2006,** *69,* 1130–1133. doi:10.1021/np058115+
19. Hale, R. L.; Leclerq, J.; Tursch, B.; Djerassi, C.; Gross, R. A., Jr.; Weinheimer, A. J.; Gupta, K. C.; Scheuer, P. J. *J. Am. Chem. Soc.* **1970,** *92,* 2179–2180. doi:10.1021/ja00710a089
20. He, H.; Kulanthaivel, P.; Baker, B. J.; Kalter, K.; Darges, J.; Cofield, D.; Wolff, L.; Adams, L. *Tetrahedron* **1995,** *51,* 51–58. doi:10.1016/0040-4020(94)00962-T
21. Morris, L. A.; Christie, E. M.; Jaspars, M.; van Ofwegen, L. P. *J. Nat. Prod.* **1998,** *61,* 538–541. doi:10.1021/np9705118
22. Naz, S.; Kerr, R. G.; Narayanan, R. *Tetrahedron Lett.* **2000,** *41,* 6035–6040. doi:10.1016/S0040-4039(00)01015-7
23. Samimi-Namin, K.; van Ofwegen, L. *ZooKeys* **2016,** *557,* 1–44. doi:10.3897/zookeys.557.6298

24. Anta, C.; González, N.; Rodríguez, J.; Jiménez, C. *J. Nat. Prod.* **2002,** *65,* 1357–1359. doi:10.1021/np010592e
25. Kobayashi, M.; Hayashi, T.; Nakajima, F.; Mitsuhashi, H. *Steroids* **1979,** *34,* 285–293. doi:10.1016/0039-128X(79)90080-1
26. Demarco, P. V.; Farkas, E.; Doddrell, D.; Mylari, B. L.; Wenkert, E. *J. Am. Chem. Soc.* **1968,** *90,* 5480–5486. doi:10.1021/ja01022a027
27. Kobayashi, M.; Kanda, F.; Rao, C. V. L.; Kumar, S. M. D.; Trimurtulu, G.; Rao, C. B. *Chem. Pharm. Bull.* **1990,** *38,* 1724–1726. doi:10.1248/cpb.38.1724
28. Raju, B. L.; Subbaraju, G. V.; Reddy, M. C.; Rao, D. V.; Rao, C. B.; Raju, V. S. *J. Nat. Prod.* **1992,** *55,* 904–911. doi:10.1021/np50085a009
29. Ishitsuka, M. O.; Kusumi, T.; Kakisawa, H. *Tetrahedron Lett.* **1991,** *32,* 2917–2918. doi:10.1016/0040-4039(91)80648-P
30. Shen, S.; Zhu, H.; Chen, D.; Liu, D.; van Ofwegen, L.; Proksch, P.; Lin, W. *Tetrahedron Lett.* **2012,** *53,* 5759–5762. doi:10.1016/j.tetlet.2012.08.049
31. Kobayashi, M.; Hirase, T. *Chem. Pharm. Bull.* **1990,** *38,* 2442–2445. doi:10.1248/cpb.38.2442
32. Kusumi, T.; Yamada, K.; Ishitsuka, M. O.; Fujita, Y.; Kakisawa, H. *Chem. Lett.* **1990,** *19,* 1315–1318. doi:10.1246/cl.1990.1315
33. Gross, H.; Kehraus, S.; Nett, M.; König, G. M.; Beil, W.; Wright, A. D. *Org. Biomol. Chem.* **2003,** *1,* 944–949. doi:10.1039/b210039h
34. Gross, H.; Wright, A. D.; Beil, W.; König, G. M. *Org. Biomol. Chem.* **2004,** *2,* 1133–1138. doi:10.1039/B314332E
35. Bowden, B. F.; Coll, J. C.; Willis, R. H. *Aust. J. Chem.* **1982,** *35,* 621–627. doi:10.1071/CH9820621
36. Bowden, B. F.; Coll, J. C.; Heaton, A.; König, G. M.; Bruck, M. A.; Cramer, R. E.; Klein, D. M.; Scheuer, P. J. *J. Nat. Prod.* **1987,** *50,* 650–659. doi:10.1021/np50052a013
37. Bowden, B. F.; Coll, J. C.; Mitchell, S. J.; Stokie, G. J. *Aust. J. Chem.* **1979,** *32,* 653–659. doi:10.1071/CH9790653
38. Bernstein, J.; Shmeuli, U.; Zadock, E.; Kashman, Y.; Néeman, I. *Tetrahedron Lett.* **1974,** *30,* 2817–2824. doi:10.1016/S0040-4020(01)97451-4
39. Kashman, Y.; Zadock, E.; Néeman, I. *Tetrahedron* **1974,** *30,* 3615–3620. doi:10.1016/S0040-4020(01)97044-9
40. Miyaoka, H.; Taira, S.; Mitome, H.; Iguchi, K.; Matsumoto, K.; Yokoo, C.; Yamada, Y. *Chem. Lett.* **1996,** *25,* 239–240. doi:10.1246/cl.1996.239
41. Iwagawa, T.; Hashimoto, K.; Yokogawa, H.; Okamura, H.; Nakatani, M.; Doe, M.; Morimoto, Y.; Takemura, K. *J. Nat. Prod.* **2009,** *72,* 946–949. doi:10.1021/np8003485
42. Feller, M.; Rudi, A.; Berer, N.; Goldberg, I.; Stein, Z.; Benayahu, Y.; Schleyer, M.; Kashman, Y. *J. Nat. Prod.* **2004,** *67,* 1303–1308. doi:10.1021/np040002n
43. Bergmann, W.; McLean, M. J.; Lester, D. *J. Org. Chem.* **1943,** *8,* 271–282. doi:10.1021/jo01191a008
44. Ciereszko, L. S.; Johnson, M. A.; Schmidt, R. W.; Koons, C. B. *Comp. Biochem. Physiol.* **1968,** *24,* 899–904. doi:10.1016/0010-406X(68)90801-3
45. Wardroper, A. M. K.; Maxwell, J. R.; Morris, R. J. *Steroids* **1978,** *32,* 203–221. doi:10.1016/0039-128X(78)90006-5
46. Rampen, S. W.; Volkman, J. K.; Hur, S. B.; Abbas, B. A.; Schouten, S.; Jameson, I. D.; Holdsworth, D. G.; Bae, J. H.; Damsté, J. S. S. *Org. Geochem.* **2009,** *40,* 144–147. doi:10.1016/j.orggeochem.2008.09.002
47. Kusumi, T.; Igari, M.; Ishitsuka, M. O.; Ichikawa, A.; Itezono, Y.; Nakayama, N.; Kakisawa, H. *J. Org. Chem.* **1990,** *55,* 6286–6289. doi:10.1021/jo00313a014
48. Leone, P. A.; Bowden, B. F.; Carroll, A. R.; Coll, J. C.; Meehan, G. V. *J. Nat. Prod.* **1993,** *56,* 521–526. doi:10.1021/np50094a011
49. Huang, C.-Y.; Sung, P.-J.; Uvarani, C.; Su, J.-H.; Lu, M.-C.; Hwang, T.-L.; Dai, C.-F.; Wu, S.-L.; Sheu, J.-H. *Sci. Rep.* **2015,** *5,* No. 15624. doi:10.1038/srep15624
50. Koh, M.; Iwanaga, T.; Hatanaka, M.; Nakano, A.; Morihara, K.; Takemura, K. *Biosci., Biotechnol., Biochem.* **2000,** *64,* 858–861. doi:10.1271/bbb.64.858
51. Yan, P.; Deng, Z.; van Ofwegen, L.; Proksch, P.; Lin, W. *Chem. Biodiversity* **2011,** *8,* 1724–1734. doi:10.1002/cbdv.201000244
52. Tanaka, J.; Yoshida, T.; Benayahu, Y. *Galaxea* **2005,** *7,* 1–9. doi:10.3755/jcrs.2005.1
53. McFadden, C. S.; Alderslade, P.; van Ofwegen, L. P.; Johnsen, H.; Rusmevichientong, A. *Invertebr. Biol.* **2006,** *125,* 288–305. doi:10.1111/j.1744-7410.2006.00070.x
54. McFadden, C. S.; France, S. C.; Sanchez, J. A.; Alderslade, P. *Mol. Phylogenet. Evol.* **2006,** *41,* 513–527. doi:10.1016/j.ympev.2006.06.010
55. Fenical, W. *J. Nat. Prod.* **1987,** *50,* 1001–1008. doi:10.1021/np50054a001
56. Ne'eman, I.; Fishelson, L.; Kashman, Y. *Toxicon* **1974,** *12,* 593–594. doi:10.1016/0041-0101(74)90192-5
57. Coll, J. C.; La Barre, S.; Sammarco, P. W.; Williams, W. T.; Bakus, G. J. *Mar. Ecol. Prog. Ser.* **1982,** *8,* 271–278. doi:10.3354/meps008271
58. Coll, J. C. *Chem. Rev.* **1992,** *92,* 613–631. doi:10.1021/cr00012a006
59. La Barre, S. C.; Coll, J. C.; Sammarco, P. W. *Biol. Bull. (Woods Hole, MA, U. S.)* **1986,** *171,* 565–576. doi:10.2307/1541624
60. Pawlik, J. R. Antipredatory defensive roles of natural products from marine invertebrates.. In *Handbook of Marine Natural Products;* Fattorusso, E.; Gerwick, W. H.; Tagliatella-Scarfati, O., Eds.; Springer: New York, 2012; pp 677–710. doi:10.1007/978-90-481-3834-0_12
61. Brand, J. G.; Bryant, B. P.; Cagan, R. H.; Kalinoski, D. L. *Brain Res.* **1987,** *416,* 119–128. doi:10.1016/0006-8993(87)91503-4
62. Oike, H.; Nagai, T.; Furuyama, A.; Okada, S.; Aihara, Y.; Ishimaru, Y.; Marui, T.; Matsumoto, I.; Misaka, T.; Abe, K. *J. Neurosci.* **2007,** *27,* 5584–5592. doi:10.1523/JNEUROSCI.0651-07.2007
63. Ferchmin, P. A.; Pagán, O. R.; Ulrich, H.; Szeto, A. C.; Hann, R. M.; Eterović, V. A. *Toxicon* **2009,** *54,* 1174–1182. doi:10.1016/j.toxicon.2009.02.033
64. Rohde, S.; Schupp, P. J. *J. Exp. Mar. Biol. Ecol.* **2011,** *399,* 76–83. doi:10.1016/j.jembe.2011.01.012
65. Rohde, S.; Gochfield, D. J.; Ankisetty, S.; Avula, B.; Schupp, P. J.; Slattery, M. *J. Chem. Ecol.* **2012,** *38,* 463–475. doi:10.1007/s10886-012-0124-8

BEILSTEIN JOURNAL OF ORGANIC CHEMISTRY

Membrane properties of hydroxycholesterols related to the brain cholesterol metabolism

Malte Hilsch[1], Ivan Haralampiev[1], Peter Müller[1], Daniel Huster[2] and Holger A. Scheidt[*2,§]

Full Research Paper

Open Access

Address:
[1]Department of Biology, Humboldt University Berlin, Invalidenstraße 43, D-10115 Berlin, Germany and [2]Institute for Medical Physics and Biophysics, Leipzig University, Härtelstr. 16–18, D-04107 Leipzig, Germany

Email:
Holger A. Scheidt[*] - holger.scheidt@medizin.uni-leipzig.de

* Corresponding author
§ Tel: +49 (0) 341 97-15726; Fax: +49 (0) 341 97-15709

Keywords:
cholesterol; fluorescence; hydroxycholesterol; membrane structure; NMR

Beilstein J. Org. Chem. **2017,** *13,* 720–727.
doi:10.3762/bjoc.13.71

Received: 10 February 2017
Accepted: 04 April 2017
Published: 18 April 2017

This article is part of the Thematic Series "Lipids: fatty acids and derivatives, polyketides and isoprenoids".

Guest Editor: J. S. Dickschat

Abstract

Compared to cholesterol, hydroxycholesterols contain an additional hydroxy group in the alkyl chain and are able to efficiently cross the brain–blood barrier. Therefore, they are responsible for the sterol transfer between brain and circulation. The current study compares the membrane properties of several hydroxycholesterols with those of cholesterol using ^{2}H NMR spectroscopy, a membrane permeability assay, and fluorescence microscopy experiments. It is shown that hydroxycholesterols do not exert the unique impact on membrane properties characteristic for cholesterol with regard to the influence on lipid chain order, membrane permeability and formation of lateral domains.

Introduction

Cholesterol is a major component of mammalian cell membranes with various biological functions. It plays a key role in maintaining the membrane's barrier function by increasing the bilayer packing density through condensing the phospholipids. Furthermore, cholesterol is an important player in the dynamic domain structure of the plasma membrane and the formation of lateral lipid domains with relevance to membrane protein function, protein trafficking, and intramembrane proteolysis [1-3]. A large amount of cholesterol in the human body is located in the brain, where it constitutes an integral part of myelin membranes acting as electrical insulators [4]. Cholesterol is also a major component of the plasma membranes of astrocytes and neurons [5]. The tight control of the cholesterol concentration and homeostasis is of paramount importance for the functions of all cells of the body but particularly for the brain. More so as the rate of cholesterol accumulation and synthesis is subject to subtle alterations over the lifetime of a human being [4,6].

Insoluble cholesterol is transported in the blood in small lipoprotein particles of varying density and the rate, at which cholesterol crosses the lipid membrane, is extremely low [7]. To overcome the blood–brain barrier, nature has developed effi-

cient mechanisms to convert cholesterol into metabolites, which can easily diffuse into the brain. These metabolites are primarily the oxysterols (24*S*)-hydroxycholesterol (24*S*-HC) for the transport from the brain to the bloodstream and 27-hydroxycholesterol (27-HC) for the transport in the opposite direction [4,6,8]. These molecules are modified by a hydroxy group at the alkyl chain end of the cholesterol molecule, introducing a second polar center to the hydrophobic tetracyclic ring system in addition to the OH moiety of cholesterol (Figure 1). This putatively simple modification is responsible for the better membrane penetrability (see below, [7]). A very interesting finding is that the plasma level of 24*S*-HC, which is nearly exclusively produced in the brain [6], can be used as a marker for neurodegenerative and neurological diseases including Alzheimer's diseases [4,6,8,9].

The biophysical properties of cholesterol and their influence on lipid membranes have been widely investigated as a basis for the understanding of the cell biological importance of the molecule. It has been shown that the membrane properties of cholesterol are extremely well adapted to exert a very specific influence on the other membrane constituents, resulting in highly characteristic effects on the packing and lateral organization of the membrane lipids and proteins [1,10-13]. Even very small alterations in the molecular structure of cholesterol cause large differences in the interaction with phospholipids and its membrane's barrier function. Interestingly, not only modifications in the tetracyclic sterol ring system lead to pronounced changes of the molecular membrane architecture and of the interactions between the respective sterol and membrane lipids and proteins [14-17], but also the *iso*-branched side chain of cholesterol has an important impact on the membrane properties [18-20].

For the hydroxysterols 24*S*-HC and 27-HC, little experimental data on their influence on membrane properties are available. So far, only slightly altered lipid mobility was observed in the presence of both hydroxysterols using fluorescence techniques [21]. Also, a decreased but still significant effect of the hydroxysterols on lipid condensation compared to native cholesterol was found in molecular dynamics simulations, which is probably caused by an increased tilt angle of the sterols to the membrane normal [8,21]. However, using ^{2}H NMR measurements, only a very small increase of acyl chain order was observed in the presence of 24*S*-HC [8]. Surprisingly, in the same study, 24*S*-HC and 27-HC exhibited a comparable effect on the acyl chain order compared to endogenous cholesterol measuring the diphenylhexatriene (DPH) anisotropy. Furthermore, high exchange rates of the molecules between erythrocytes and plasma were found [7], indicating that 24*S*-HC and 27-HC can – contrary to cholesterol – rapidly cross plasma membranes. Also for other oxysterols, like 7-ketocholesterol and 25-hydroxycholesterol, a lower tendency to form lateral lipid domains and an attenuated phospholipid condensation effect was found. These properties, which depend on

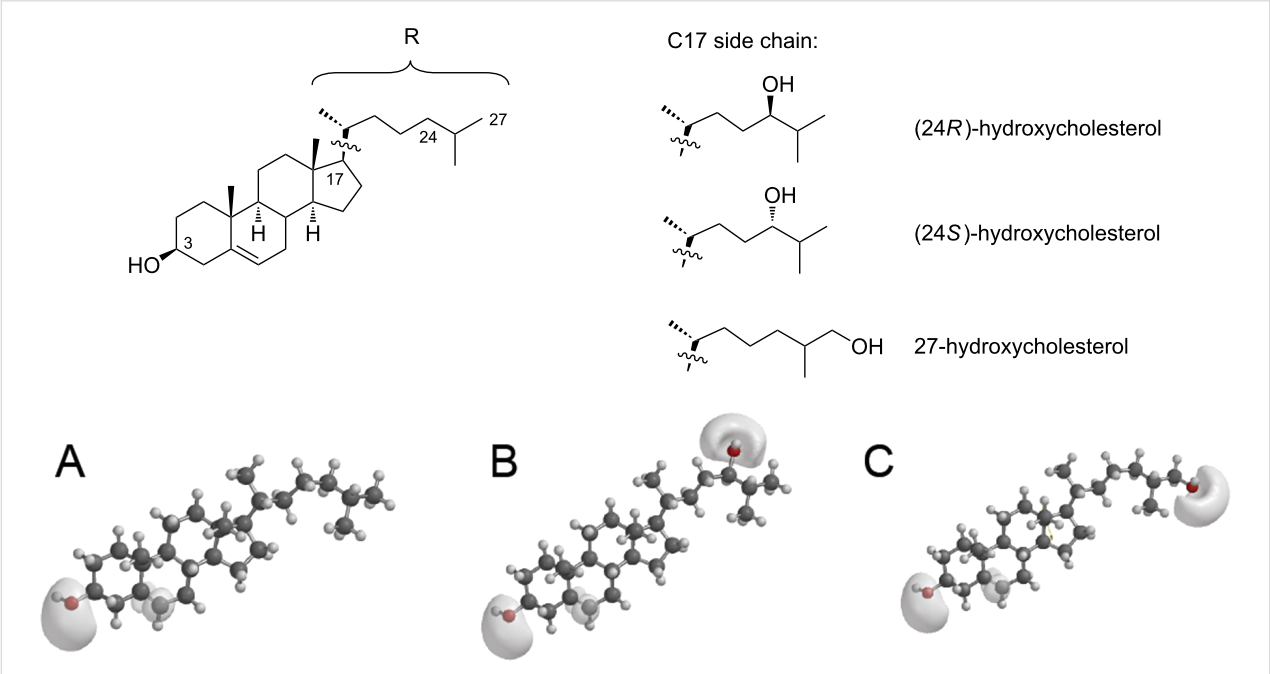

Figure 1: Top: Chemical structures of cholesterol and hydroxycholesterols with selected numbering for the carbon atoms. The investigated hydroxycholesterols are modified with an OH-group bound to the carbon in position 24 (either in *R*- or *S*-configuration) or in position 27, respectively. Bottom: Molecular models and isosurfaces of the electrostatic potential of cholesterol (A), (24*R*)-hydroxycholesterol (B) and 27-hydroxycholesterol (C).

the molecular position of the hydroxy group, were correlated with cytotoxic effects of the respective molecules [22,23].

In the current study, the influence of hydroxycholesterols on membrane properties such as lipid chain packing, membrane permeability, and membrane domain formation is investigated. These parameters are compared with those obtained for cholesterol by using various biophysical techniques such as NMR and fluorescence spectroscopy as well as fluorescence microscopy.

Results

Lipid chain order of hydroxycholesterol-containing membranes

The influence of the hydroxycholesterols on the lipid chain order and the degree of lipid condensation was investigated by ^{2}H NMR measurements on lipid membranes of chain deuterated 1-palmitoyl-d_{31}-2-oleoyl-*sn*-glycero-3-phosphocholine (POPC-d_{31}) in the presence of 20 mol % of the respective hydroxysterols or cholesterol. The ^{2}H NMR spectra (not shown) exhibited for all samples the typical superposition of Pake doublets with varying quadrupolar splittings as well-known for a lamellar bilayer membrane in the liquid-crystalline phase. From the ^{2}H NMR spectra, chain order parameter plots were calculated, which are displayed in Figure 2A. As well-known from the literature, the presence of 20 mol % cholesterol leads to a pronounced increase in the 1-palmitoyl-2-oleoyl-*sn*-glycero-3-phosphocholine (POPC) chain order parameters [13,24]. In contrast, all three hydroxycholesterols did not induce such a cholesterol-like increase in POPC lipid chain order; in contrast, they caused a small decrease in lipid chain order compared with pure POPC membranes. While this decrease was insignificant for 24*S*-HC, it was more pronounced for 24*R*-HC, especially in the middle chain region, and quite substantial and out of the experimental error for 27-HC. These results are also reflected in the calculated lipid chain extent calculated using the mean torque model [25,26] (Table 1). Similar effects were observed in the lipid mixture, *N*-palmitoyl-d_{31}-D-sphingomyelin (PSM-d_{31})/1,2-dioleoyl-*sn*-glycero-3-phosphocholine (DOPC)/hydroxycholesterol (molar ratio 1:1:1), which forms lateral membrane domains (Figure 2B), where all three hydroxycholesterols were not able to increase the lipid chain order parameters as observed for cholesterol. While for 24*S*-HC a very small

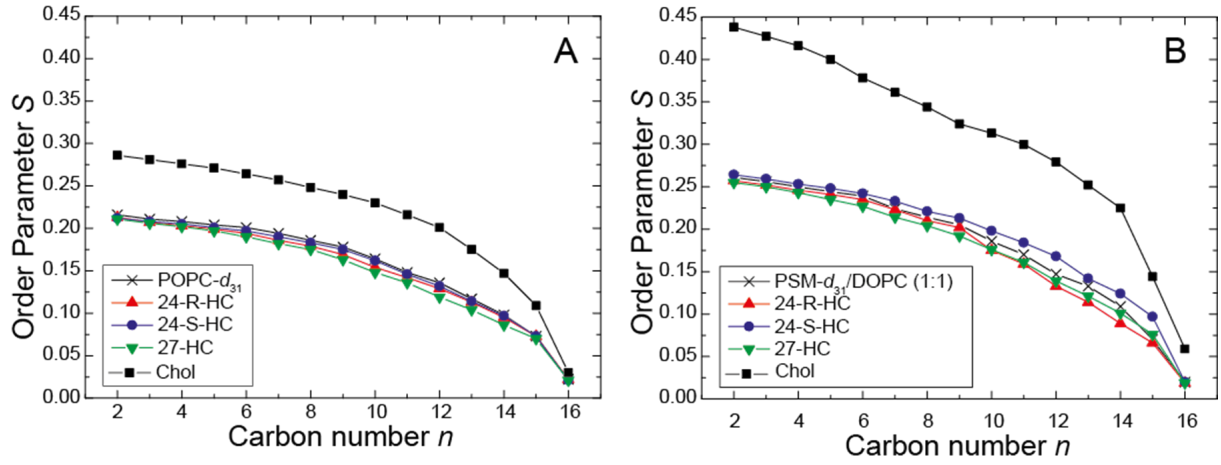

Figure 2: ^{2}H NMR chain order parameter of the *sn*-1 chain of (A) POPC-d_{31} in the absence and in the presence of the respective sterol (molar ratio 0.8:0.2) and (B) PSM-d_{31} in PSM-d_{31}/DOPC/sterol membranes (molar ratio 1:1:1), (24*R*)-hydroxycholesterol (red), (24*S*)-hydroxycholesterol (blue) and 27-hydroxycholesterol (green) at a temperature of 30 °C. For comparison, the chain order parameters of a lipid membrane without any sterol and in the presence of the respective amount of cholesterol are shown in black [18]. Experimental errors are smaller than the symbol size.

Table 1: The lipid chain extent of membranes consisting of POPC-d_{31} without and with the given cholesterols (molar ratio 0.8:0.2) and PSM-d_{31} in PSM-d_{31}/DOPC/sterol membranes (molar ratio 1:1:1) were calculated using the mean torque model [25,26]. The values for pure POPC-d_{31} and in the presence of cholesterol are taken from the literature [19].

Sample	Chain extent [Å] for POPC-d_{31}	Chain extent [Å] for PSM-d_{31}/DOPC (1:1)
pure lipids	11.7 ± 0.1	12.3 ± 0.1
+ (24*R*)-hydroxycholesterol	11.5 ± 0.1	12.1 ± 0.2
+ (24*S*)-hydroxycholesterol	11.6 ± 0.1	12.6 ± 0.1
+ 27-hydroxycholesterol	11.3 ± 0.1	12.1 ± 0.1
+ cholesterol	13.2 ± 0.1	15.0 ± 0.2

increase compared to a pure lipid membrane without any cholesterol was observed, 24*R*-HC and 27-HC exhibited a decrease in lipid chain order again which was most pronounced in the middle chain region. Accordingly, the calculated lipid chain extents (Table 1) for the three hydroxycholesterols were close to the pure lipid membrane but significant smaller for a cholesterol containing membrane.

Influence of hydroxylcholesterols on membrane permeability

The permeability of POPC membranes in the absence and in the presence of the respective sterol (molar ratio 0.8:0.2) was measured by using a fluorescence assay, which determines the permeation of dithionite ion across membranes (see Experimental, [18,27]). The rate constants of dithionite permeation in large unilamellar vesicles (LUVs) of varying lipid composition are shown in Figure 3 revealing that the rate constants of cholesterol-containing vesicles were lower than those of pure POPC LUVs. It is well-known that this sterol decreases the permeability toward polar molecules [28]. The rate constants in the presence of hydroxycholesterols were similar (24*R*-HC, 24*S*-HC) or even higher (27-HC) compared to those of pure POPC membranes indicating that these sterols are not able to seal a phospholipid membrane like endogenous cholesterol.

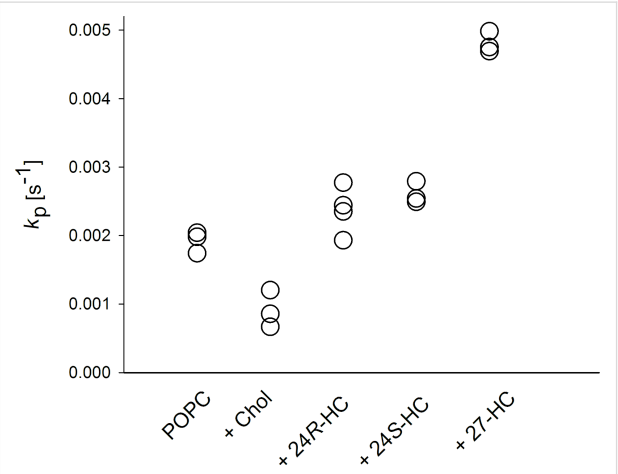

Figure 3: Rate constants for the permeation of dithionite across LUV membranes composed of POPC in the absence or in the presence of cholesterol or (24*R*)-hydroxycholesterol (24*R*-HC), (24*S*)-hydroxycholesterol (24*S*-HC) or 27-hydroxycholesterol (27-HC) (molar ratios 0.8:0.2) at 37 °C. All single values of the rate constants are shown which were determined from independent measurements.

Influence of hydroxycholesterols on the formation of lateral domains in giant unilamellar vesicles (GUVs)

GUVs were prepared consisting of DOPC, PSM, and cholesterol at a molar ratio of 1:1:1. This lipid mixture is known for the formation and coexistence of lateral disordered (ld) and ordered (lo) domains. The domain structure was visualized by labeling the membrane with the ld marker 1,2-dioleoyl-*sn*-glycero-3-phosphoethanolamine-*N*-(lissamine rhodamine B sulfonyl) (ammonium salt) (N-Rh-DOPE) and recording z-stacks of the vesicles. The fluorescence microscopy images of cholesterol-containing GUVs show large membrane regions of low and of high fluorescence intensity, representing the lo and ld phase, respectively (Figure 4A). Note, that the vesicle shown in Figure 4A probably forms another dark lo domain on the back side. When cholesterol was substituted by hydroxycholesterols, the GUVs showed a different pattern of lateral domains (Figure 4B–D). These vesicles revealed a multitude of small ordered domains within the bright fluorescent disordered domains. We note that the GUVs shown in Figure 4 represent the majority of vesicles of the respective sample. A low percentage of vesicles were also observed having a different pattern of domains with respect to the shape and to the size.

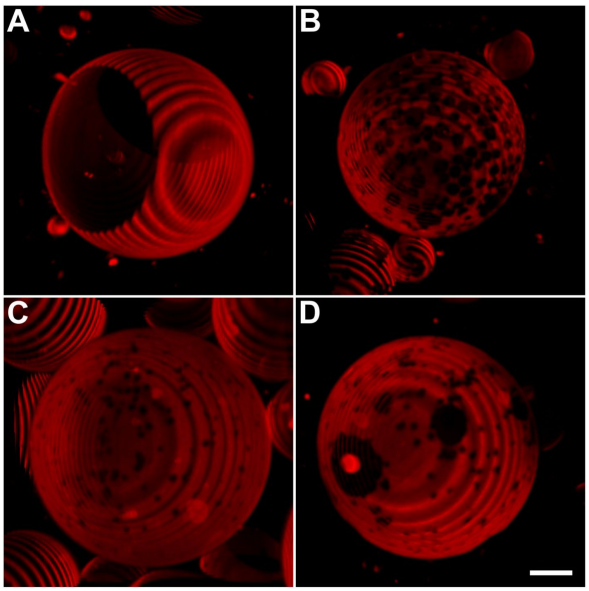

Figure 4: Confocal fluorescence images of GUVs containing DOPC/PSM/cholesterol (A), DOPC/PSM/24*R*-HC (B), DOPC/PSM/24*S*-HC (C), or DOPC/PSM/27-HC (D) (molar ratios 1:1:1). The GUV membranes were labeled with N-Rh-DOPE (0.5 mol %) that sorts preferentially into liquid disordered (ld) domains and z-stacks of the vesicles were recorded as described in the Experimental. Bar corresponds to 10 µm. The ring-like structures of the vesicles are caused by the assembly of the z-stacks having a step-size of 1 µm.

Discussion

Cholesterol is the main sterol of mammalian cell membranes and has a unique impact on membrane properties by that influencing important membrane functions. A special situation is encountered in the human brain, which contains a large amount of the body cholesterol. Almost all brain cholesterol is produced by local synthesis. It is the blood–brain barrier, which effectively protects the brain from the exchange with cholesterol pro-

vided from lipoproteins in the circulation, the cholesterol homeostasis in the brain is as far as possible self-contained. Regardless, a certain amount of cholesterol has to cross the blood–brain barrier in both directions. This transport function is fulfilled by hydroxycholesterols, which contain an additional hydroxy group in the alkyl chain compared to cholesterol, introducing a second polar moiety into the molecule rendering hydroxycholesterols more polar. It can be assumed that this modification alters the membrane properties of these molecules, which have been investigated so far only in a few studies (see Introduction). Therefore, the present study characterizes the impact of various hydroxycholesterols on membranes using various biophysical methods.

Our data show, that the influence of selected hydroxycholesterols on membrane properties differs from that of cholesterol with regard to (i) lipid chain order, (ii) membrane permeability and (iii) formation of lateral lipid domains.

Investigating their effect on the lipid chain order by ^{2}H NMR, it was found that the three investigated hydroxycholesterols did not cause the typical lipid chain condensation mediated by endogenous cholesterol. Rather, some hydroxysterols caused a small decrease of lipid chain order. A similar tendency was observed for 24*S*-HC also using ^{2}H NMR measurements [21]. This membrane behavior of the hydroxycholesterols can be rationalized in that the additional hydroxy moiety in these molecules diminishes their interaction with surrounding phospholipids. Such modifications can severely alter the orientation of a sterol in the membrane [29]. A similar situation has been encountered for estradiol, which also contains one hydroxy group on either end of the sterol [29]. In this work, a significant amount of the estradiol was found in the lipid water interface of the membrane with an orientation perpendicular to the membrane normal. By that, the molecules act disturbing rather than ordering. Notably, MD simulations found an opposite effect of the hydroxycholesterols [21]. The additional polarity of hydroxycholesterol also influences their impact on membrane permeability. For cholesterol, the induced membrane condensation causes a decreased penetration of polar molecules, e.g., water, across the membrane. This was proven here by measuring the permeation of dithionite across LUV membranes. The rate constant of dithionite permeation in POPC membranes containing cholesterol was reduced to about 50% compared to pure POPC vesicles. Replacing cholesterol by hydroxycholesterol, this effect was completely lost. The rate constants in the presence of 24*R*-HC and 24*S*-HC were similar to those of POPC membranes. For 27-HC, even an increase in permeation was observed, in these membranes dithionite permeated about 2.5 more rapidly than in pure POPC membranes. We note, that the changes of rate constants can also be explained by changes of lipid analogue flip-flop. However, in any case, they reflect membrane packing density towards the transbilayer permeation of a polar moiety.

As a third parameter, the impact of hydroxycholesterols on the formation of lateral membrane domains was investigated. Principally, these sterols are also able to trigger the formation of disordered and ordered domains, although they do not condense lipid chains as cholesterol does. Lipid condensation leads to thicker lo domains in membranes that are segregated from ld phase patches. However, it has also been shown that sterols that do not order lipid chains can induce lateral domain formation [14,30,31]. This can be rationalized by preferential interactions between sterols and saturated lipid chains, that represent the driving force for membrane domain formation even in the absence of a lipid condensation effect [32,33]. However, the pattern of domain formation was different with regard to their size and the number of domains per vesicle. This suggests that subtle differences in the interaction energies of the oxysterols and the other lipids of the mixture must exist. GUVs containing hydroxycholesterols show numerous small lo domains between the large ld domains. This indicates a different intermolecular interaction between the respective sterol and sphingomyelin being the basis for lipid segregation and, finally, domain formation.

What is the physiological consequence of the data presented? We could show that hydroxycholesterols at similarly large membrane concentrations like endogenous cholesterol do not disturb the bilayer structure of the membrane. Although, physiological membrane concentrations of hydroxycholesterols are not known, one can assume that these are much lower than those of cholesterol. However, due to the additional hydroxy group in the alkyl chain the interaction between the respective sterol and surrounding lipids (and proteins) is impacted. MD simulations for 27-HC have shown, that this molecule adopts compared to cholesterol different orientations within the membrane, which are upside-down, largely tilted and/or inter-leaflet positions [21].

These properties indicate that the molecules are less strongly anchored within the membrane bilayer, which guides their ability to cross the blood–brain barrier. This process consists of three steps at the membrane level, (i) incorporation of sterols into the plasma membrane, (ii) their transbilayer diffusion and (iii) their release from the membrane. With regard to the transfer of sterols to and from membranes, this can be principally realized via vesicular traffic or via monomeric transfer. The latter mechanism requires the presence of donors and acceptors, respectively, due to the low water solubility of sterols. Nevertheless, the import and export of cholesterol is

rather slow [34], wherefore membrane proteins have been proposed to facilitate these processes. One putative function of those proteins could be to relieve the presentation of cholesterol molecules on the membrane surface for a better binding to extracellular acceptors (see [35]). It can be hypothesized, that the lower membrane embedding of hydroxycholesterols facilitates their membrane incorporation and/or release. Indeed, it was found that the transfer of hydroxycholesterols between erythrocytes and blood plasma is much faster than that of cholesterol [7].

With regard to the transbilayer mobility of sterols, it is generally assumed that cholesterol traverses the bilayer very rapidly by passive diffusion, although at certain conditions, e.g., special membrane compositions, its transbilayer movement could be compounded (see [35]). For hydroxycholesterols, the transbilayer movement has not been investigated so far. However, the studies measuring the transfer of those sterols between erythrocytes and plasma also indicate a rapid translocation of hydroxycholesterols across membranes [7].

Conclusion

Our data show that, compared with endogenous cholesterol, hydroxycholesterols have a different influence on important membrane parameters which reflects an attenuated embedding of these sterols within the membrane.

Experimental

Materials

All lipids, POPC, DOPC, 1-palmitoyl-2-(12-[*N*-(7-nitrobenz-2-oxa-1,3-diazol-4-yl)amino]dodecanoyl]-*sn*-glycero-3-phosphocholine (NBD-PC), N-Rh-DOPE, POPC-d_{31}, PSM-d_{31} as well as cholesterol and the three investigated hydroxycholesterols (structure see Figure 1) were purchased from Avanti Polar Lipids, Inc. (Alabaster, AL, USA). All other chemicals were purchased from Sigma-Aldrich (Taufkirchen, Germany) and were used without further purification.

Preparation of NMR samples

The respective amounts of hydroxycholesterols and phospholipids were dissolved in chloroform at the respective molar ratios. The solvent was evaporated and the samples were re-dissolved in cyclohexane. After overnight lyophilization at high vacuum, the obtained fluffy powder was hydrated with 40 wt % deuterium-depleted water. The samples were equilibrated by ten freeze-thaw cycles and transferred into 5 mm glass vials and sealed.

^{2}H NMR measurements

The ^{2}H NMR experiments were performed on a Bruker DRX300 NMR spectrometer (Bruker BioSpin, Rheinstetten, Germany) at a resonance frequency of 46.1 MHz for ^{2}H using a solid probe with a 5 mm solenoid coil. ^{2}H NMR spectra were acquired using a quadrupolar echo pulse sequence [36] with a relaxation delay of 1 s. The two $\pi/2$ pulses with a typical length of around 3.2 µs were separated by a 50 µs delay. The spectral width was 500 kHz. ^{2}H NMR spectra were dePaked and smoothed order parameters were determined as described in [37]. From these order parameters, the lipid chain extent was calculated according the mean torque model [25,26].

Preparation of LUVs

LUVs were prepared using the extrusion method [38]. Aliquots of lipids dissolved in chloroform were combined in a glass vial and the solvent was evaporated in a rotating round-bottom flask under vacuum. Lipids were resuspended in a small volume of ethanol (final ethanol concentration was below 1% (v/v)), followed by the addition of HBS (HEPES buffered saline, 145 mM NaCl and 10 mM Hepes, pH 7.4, final lipid concentration 1 mM) and the mixture was vortexed. To prepare LUVs, this suspension was subjected to five freeze-thaw cycles followed by extrusion of the lipid suspension 10 times through 0.1 µm polycarbonate filters at 40 °C (extruder from Lipex Biomembranes Inc., Vancouver, Canada; filters from Costar, Nucleopore, Tübingen, Germany).

Preparation of GUVs

GUVs were prepared using the electroswelling method [39]. Lipid mixtures were prepared from stock solutions in chloroform. Finally, 100 nmol of the domain forming lipid mixture of DOPC, PSM and cholesterol or the respective hydroxycholesterol (1:1:1, molar ratio) including 0.5 mol % of the liquid disordered (ld) domain marker N-Rh-DOPE were dissolved in chloroform and spotted onto custom-built titan chambers. These were placed on a heater plate at 50 °C to facilitate solvent evaporation, and subsequently subjected to high vacuum for at least 1 h for evaporation of remaining traces of the solvent. Lipid-coated slides were assembled using a spacer of Parafilm (Pechiney Plastic Packaging, Chicago, IL, USA) for insulation. The electroswelling chamber was filled with 1 mL sucrose buffer (250 mM sucrose, 15 mM NaN_3, osmolarity of 280 mOsm/kg) and sealed with plasticine. An alternating electrical field of 10 Hz rising from 0.02 V to 1.1 V in the first 56 min was applied for 3 h at 55 °C.

Permeation assay

For characterizing the permeation of polar molecules across the lipid membrane, an assay was applied which measures the transmembrane diffusion of dithionite [18,19,27]. The assay was performed in a similar manner to the procedure described in [19]. Briefly, LUVs containing POPC and 0.5 mol % NBD-PC without or with cholesterol or the respective hydroxycholes-

terol (molar ratio 0.8:0.2) were prepared. The NBD fluorescence intensity of 33 μM LUVs was recorded in a cuvette at 540 nm (λ_{ex} = 470 nm, slit width for excitation and emission 4 nm) at 37 °C using an Aminco Bowman Series 2 spectrofluorometer (Urbana, IL). After 30 s, sodium dithionite was added from a 1 M stock solution in 100 mM Tris (pH 10.0) to give a final concentration of 50 mM. Dithionite ions rapidly quench the fluorescence of the lipid analogs localized in the outer leaflet, which is reflected by a rapid initial decrease of fluorescence intensity (kinetics not shown). Subsequently, the fluorescence intensity decreased slowly caused by a slow permeation of dithionite ions across the bilayer. By that process, dithionite reacted with the NBD-PC molecules in the inner leaflet. After 300 s, Triton X-100 (0.5% (w/v) final concentration) was added, enabling complete reaction of dithionite with NBD-PC, resulting in a complete loss of fluorescence. The curves were normalized to the fluorescence intensities before addition of dithionite and were fitted to a bi-exponential equation. From the fittings, the rate constants for the rapid fluorescence decrease (representing reduction of NBD-PC in the outer leaflet) and those for the slow decrease (representing permeation of dithionite across the bilayer) were determined. The latter ones were used as the parameter for membrane permeability.

Confocal laser scanning microscopy

For microscopy, a Visitron VisiScope scanning disk confocal laser microscope (Visitron Systems, Puchheim, Germany) with a 60× oil objective and an Andor iXon 888 EMCCD camera (1024 × 1024 pixels, Andor, Belfast, Northern Ireland) were used. N-Rh-DOPE was excited by a 561 nm diode laser.

Fife μL GUVs were mixed with 15 μL 250 mM glucose buffer (5.8 mM NaH_2PO_4, 5.8 mM Na_2HPO_4, osmolarity of 300 mOsm/kg, pH 7.2) in tissue culture treated microscopy suitable plastic dishes (ibiTreat μ-Slides Angiogenesis, ibidi, Martinsried, Germany). Vesicles were allowed to settle down some minutes before acquisition of z-stacks with 1 μm step size.

References

1. Simons, K.; Ikonen, E. *Nature* **1997,** *387,* 569–572. doi:10.1038/42408
2. Leslie, M. *Science* **2011,** *334,* 1046–1047. doi:10.1126/science.334.6059.1046-b
3. Maxfield, F. R.; van Meer, G. *Curr. Opin. Cell Biol.* **2010,** *22,* 422–429. doi:10.1016/j.ceb.2010.05.004
4. Björkhem, I. *J. Intern. Med.* **2006,** *260,* 493–508. doi:10.1111/j.1365-2796.2006.01725.x
5. Björkhem, I.; Meaney, S. *Arterioscler., Thromb., Vasc. Biol.* **2004,** *24,* 806–815. doi:10.1161/01.ATV.0000120374.59826.1b
6. Moutinho, M.; Nunes, M. J.; Rodrigues, E. *Biochim. Biophys. Acta* **2016,** *1861,* 1911–1920. doi:10.1016/j.bbalip.2016.09.011
7. Meaney, S.; Bodin, K.; Diczfalusy, U.; Björkhem, I. *J. Lipid Res.* **2002,** *43,* 2130–2135. doi:10.1194/jlr.M200293-JLR200
8. Kulig, W.; Cwiklik, L.; Jurkiewicz, P.; Rog, T.; Vattulainen, I. *Chem. Phys. Lipids* **2016,** *199,* 144–160. doi:10.1016/j.chemphyslip.2016.03.001
9. Krištofiková, Z.; Kopecký, V., Jr.; Hofbauerová, K.; Hovorková, P.; Řipová, D. *Neurochem. Res.* **2008,** *33,* 412–421. doi:10.1007/s11064-007-9443-5
10. Kusumi, A.; Suzuki, K. G. N.; Kasai, R. S.; Ritchie, K.; Fujiwara, T. K. *Trends Biochem. Sci.* **2011,** *36,* 604–615. doi:10.1016/j.tibs.2011.08.001
11. Jacobson, K.; Mouritsen, O. G.; Anderson, R. G. W. *Nat. Cell Biol.* **2007,** *9,* 7–14. doi:10.1038/ncb0107-7
12. Levental, I.; Grzybek, M.; Simons, K. *Proc. Natl. Acad. Sci. U. S. A.* **2011,** *108,* 11411–11416. doi:10.1073/pnas.1105996108
13. Oldfield, E.; Meadows, M.; Rice, D.; Jacobs, R. *Biochemistry* **1978,** *17,* 2727–2740. doi:10.1021/bi00607a006
14. Wang, J.; Megha; London, E. *Biochemistry* **2004,** *43,* 1010–1018. doi:10.1021/bi035696y
15. Scheidt, H. A.; Müller, P.; Herrmann, A.; Huster, D. *J. Biol. Chem.* **2003,** *278,* 45563–45569. doi:10.1074/jbc.M303567200
16. Róg, T.; Pasenkiewicz-Gierula, M.; Vattulainen, I.; Karttunen, M. *Biochim. Biophys. Acta* **2009,** *1788,* 97–121. doi:10.1016/j.bbamem.2008.08.022
17. Shaghaghi, M.; Chen, M.-T.; Hsueh, Y.-W.; Zuckermann, M. J.; Thewalt, J. L. *Langmuir* **2016,** *32,* 7654–7663. doi:10.1021/acs.langmuir.6b01401
18. Scheidt, H. A.; Meyer, T.; Nikolaus, J.; Baek, D. J.; Haralampiev, I.; Thomas, L.; Bittman, R.; Müller, P.; Herrmann, A.; Huster, D. *Angew. Chem., Int. Ed.* **2013,** *52,* 12848–12851. doi:10.1002/anie.201306753
19. Meyer, T.; Baek, D. J.; Bittman, R.; Haralampiev, I.; Müller, P.; Herrmann, A.; Huster, D.; Scheidt, H. A. *Chem. Phys. Lipids* **2014,** *184,* 1–6. doi:10.1016/j.chemphyslip.2014.08.002
20. Robalo, J. R.; Ramalho, J. P. P.; Huster, D.; Loura, L. M. S. *Phys. Chem. Chem. Phys.* **2015,** *17,* 22736–22748. doi:10.1039/C5CP03097H
21. Kulig, W.; Olżyńska, A.; Jurkiewicz, P.; Kantola, A. M.; Komulainen, S.; Manna, M.; Pourmousa, M.; Vazdar, M.; Cwiklik, L.; Rog, T.; Khelashvili, G.; Harries, D.; Telkki, V.-V.; Hof, M.; Vattulainen, I.; Jungwirth, P. *Free Radical Biol. Med.* **2015,** *84,* 30–41. doi:10.1016/j.freeradbiomed.2015.03.006
22. Massey, J. B. *Curr. Opin. Lipidol.* **2006,** *17,* 296–301. doi:10.1097/01.mol.0000226123.17629.ab
23. Mintzer, E.; Charles, G.; Gordon, S. *Chem. Phys. Lipids* **2010,** *163,* 586–593. doi:10.1016/j.chemphyslip.2010.05.001
24. McMullen, T. P. W.; Lewis, R. N. A. H.; McElhaney, R. N. *Curr. Opin. Colloid Interface Sci.* **2004,** *8,* 459–468. doi:10.1016/j.cocis.2004.01.007
25. Petrache, H. I.; Tu, K.; Nagle, J. F. *Biophys. J.* **1999,** *76,* 2479–2487. doi:10.1016/S0006-3495(99)77403-5
26. Petrache, H. I.; Dodd, S. W.; Brown, M. F. *Biophys. J.* **2000,** *79,* 3172–3192. doi:10.1016/S0006-3495(00)76551-9
27. Pomorski, T.; Herrmann, A.; Zachowski, A.; Devaux, P. F.; Müller, P. *Mol. Membr. Biol.* **1994,** *11,* 39–44. doi:10.3109/09687689409161028
28. Szabo, G. *Nature* **1974,** *252,* 47–49. doi:10.1038/252047a0
29. Vogel, A.; Scheidt, H. A.; Feller, S. E.; Metso, J.; Badeau, R. M.; Tikkanen, M. J.; Wähälä, K.; Jauhiainen, M.; Huster, D. *Biophys. J.* **2014,** *107,* 114–125. doi:10.1016/j.bpj.2014.04.060

30. Brown, D. A.; London, E. *J. Biol. Chem.* **2000,** *275,* 17221–17224. doi:10.1074/jbc.R000005200
31. Xu, X.; Bittman, R.; Duportail, G.; Heissler, D.; Vilchèze, C.; London, E. *J. Biol. Chem.* **2001,** *276,* 33540–33546. doi:10.1074/jbc.M104776200
32. Almeida, P. F. F.; Pokorny, A.; Hinderliter, A. *Biochim. Biophys. Acta* **2005,** *1720,* 1–13. doi:10.1016/j.bbamem.2005.12.004
33. Tsamaloukas, A.; Szadkowska, H.; Heerklotz, H. *Biophys. J.* **2006,** *90,* 4479–4487. doi:10.1529/biophysj.105.080127
34. Lange, Y.; Molinaro, A. L.; Chauncey, T. R.; Steck, T. L. *J. Biol. Chem.* **1983,** *258,* 6920–6926.
35. Müller, P.; Plazzo, A. P.; Herrmann, A. Transbilayer movement and distribution of cholesterol. In *Transbilayer dynamics of lipids;* Devaux, P. F.; Hermann, A., Eds.; John Wiley & Sons Inc.: Hoboken, New Jersey, 2011; pp 75–96. doi:10.1002/9781118120118.ch5
36. Davis, J. H.; Jeffrey, K. R.; Bloom, M.; Valic, M. I.; Higgs, T. P. *Chem. Phys. Lett.* **1976,** *42,* 390–394. doi:10.1016/0009-2614(76)80392-2
37. Huster, D.; Arnold, K.; Gawrisch, K. *Biochemistry* **1998,** *37,* 17299–17308. doi:10.1021/bi980078g
38. Mayer, L. D.; Hope, M. J.; Cullis, P. R. *Biochim. Biophys. Acta* **1986,** *858,* 161–168. doi:10.1016/0005-2736(86)90302-0
39. Angelova, M. I.; Soléau, S.; Méléard, P.; Faucon, F.; Bothorel, P. *Prog. Colloid Polym. Sci.* **1992,** *89,* 127–131. doi:10.1007/BFb0116295

License and Terms

BEILSTEIN JOURNAL OF ORGANIC CHEMISTRY

Opportunities and challenges for the sustainable production of structurally complex diterpenoids in recombinant microbial systems

Katarina Kemper, Max Hirte, Markus Reinbold, Monika Fuchs and Thomas Brück*

Review

Open Access

Address:
Professorship for Industrial Biocatalysis, Department of Chemistry, Technical University of Munich, Lichtenbergstraße 4, 85748 Garching, Germany

Email:
Thomas Brück* - brueck@tum.de

* Corresponding author

Keywords:
enzyme engineering; heterologous production in *E. coli*; metabolic pathway optimization; modular biosynthesis; plant diterpenes

Beilstein J. Org. Chem. **2017,** *13,* 845–854.
doi:10.3762/bjoc.13.85

Received: 15 February 2017
Accepted: 11 April 2017
Published: 08 May 2017

This article is part of the Thematic Series "Lipids: fatty acids and derivatives, polyketides and isoprenoids".

Guest Editor: J. S. Dickschat

Abstract

With over 50.000 identified compounds terpenes are the largest and most structurally diverse group of natural products. They are ubiquitous in bacteria, plants, animals and fungi, conducting several biological functions such as cell wall components or defense mechanisms. Industrial applications entail among others pharmaceuticals, food additives, vitamins, fragrances, fuels and fuel additives. Central building blocks of all terpenes are the isoprenoid compounds isopentenyl diphosphate and dimethylallyl diphosphate. Bacteria like *Escherichia coli* harbor a native metabolic pathway for these isoprenoids that is quite amenable for genetic engineering. Together with recombinant terpene biosynthesis modules, they are very suitable hosts for heterologous production of high value terpenes. Yet, in contrast to the number of extracted and characterized terpenes, little is known about the specific biosynthetic enzymes that are involved especially in the formation of highly functionalized compounds. Novel approaches discussed in this review include metabolic engineering as well as site-directed mutagenesis to expand the natural terpene landscape. Focusing mainly on the validation of successful integration of engineered biosynthetic pathways into optimized terpene producing *Escherichia coli*, this review shall give an insight in recent progresses regarding manipulation of mostly diterpene synthases.

Introduction

Isoprenoid natural products are one of the most structurally diverse groups of primary and secondary metabolites in all kinds of organisms. Moreover, they represent an invaluable source of bioactive natural products. Prominent representatives of these compounds are taxol [1] (paclitaxel, anticancer drug), artemisinin [2] (antimalarial agent) and α-pinene [3] (antibiotic,

anti-inflammatory). Apart from bioactive compounds with applications as drugs/pharmaceuticals [4] or in the nutrition or agricultural sector, isoprenoids of minor structural complexity are used as bulk chemicals or fuel additives [5,6]. To identify new isoprenoids of industrial relevance essential oil extracts are screened for bioactive properties that may furnish future drugs [7,8]. Harnessing isoprenoid compounds for large-scale industrial purposes can be hampered due to low natural occurrence. Being mostly secondary metabolites isoprenoid titers in plants may be low in dependence to seasonal [9] or circadian expression [10]. On the other hand for some members simply the number of available plants may be limited like the pacific yew *Taxus brevifolia* from which paclitaxel was first extracted [11]. The chemical synthesis can be an alternative for the delivery of simpler isoprenoid structures such as carotenoids [12]. Industrially relevant total synthesis of highly oxygenated terpenes comprising several chiral centers is often more complex since usually various different reaction steps have to be performed that regularly involve cost- and workup-intensive metal-organic catalysts [13-16]. The work of McKerrall et al. on ingenol [17,18] sets an example for the difficulty of stereoselective synthesis of complex diterpenes. Additionally, semi-synthetic approaches are tainted with the equivalent issues of economic efficiency and sustainability akin to total chemical synthesis, which is often associated with toxic metal-organic chemistry, low product yields and/or insufficient purity [19,20].

A promising route for sufficient supply of industrially relevant products or their precursors is the heterologous production of plant diterpenes in well-established recombinant hosts, such as *Escherichia coli* [21-23]. Recent developments in this field will be reviewed in this work.

Review

Biosynthesis of diterpenes and transfer to heterologous production system

Integration of biosynthetic gene clusters from plants into a bacterial host is often not trivial due to complex metabolic coherences. The essential steps in establishing successful production of diterpenoid carbohydrate backbones in heterologous systems can be partitioned into three following areas:

1: formation of central isoprenoid precursors,

2: combination of C5-building blocks to linear isoprenyl diphosphates and

3: cyclization or condensation reaction by synthase enzyme(s).

General catalytic processes involved in these steps will be presented briefly in the following section. Selected elements of the distinct pathways will be discussed in more detail when describing the metabolic engineering of a bacterial host.

Precursor formation

All terpenes derive from the ubiquitous central metabolites isopentenyl diphosphate (IPP) and dimethylallyl diphosphate (DMAPP) [24] (see Scheme 1). Interestingly, only two metabolic pathways (MEP and MEV) have been identified for the diverse biosynthesis of the structurally highly diverse family of isoprenoids. Both pathways use intermediate products of the central sugar metabolism as carbon sources [25]. In most eukaryotes (all mammals, yeast, fungi, archaea and plants (more precisely in the cytosol and mitochondria)) the isoprenoid precursors are synthesized via the mevalonate pathway (MVA) starting from acetyl-CoA [26]. Alternatively, in the majority of eubacteria, cyanobacteria, green algae and in the plastids of plants isoprenoid biosynthesis originates from glyceraldehyde-3-phosphate (G3P) and pyruvate [26,27]. Eponymous intermediate of this pathway is the product of the second enzymatic step where 1-deoxy-D-xylulose-5-phosphate (DXP) is reduced to 2-*C*-methyl-D-erythritol-4-phosphate (see Scheme 1).

Parallel occurrence of both pathways in higher plants is regulated through compartmentalization [30] with localization of diterpene biosynthesis in the plastids [31]. Metabolic engineering of plants to produce diterpenes remains challenging due to the required direction of biosynthetic enzymes into the specific organelles [32] and feedback inhibition of the 1-deoxy-D-xylulose-5-phosphate synthase (DXS) that can prevent accumulation of the desired lead structures [33].

Isoprenyl diphosphate formation

Downstream of precursor formation condensation of IPP and DMAPP to longer-chain polyprenyls precedes subsequent metabolization to linear or mono- and polycyclic products, respectively, by the terpene synthases [24]. One exception to this standard sequence is presented by the hemiterpenes like isoprene which are directly derived from DMAPP [34].

In order to obtain mono-(C10), sesqui-(C15), di-(C20)terpenes and those harboring larger carbon skeletons, IPP and DMAPP are linked together by isoprenyl diphosphate synthases (IDSs) which are well-reviewed by Wang and Ohnuma [35]. Members of prenyltransferases are distinguished according to length and stereochemistry of their products [36,37].

Z-Isoprenyl diphosphate synthases are involved in the synthesis of very long-chain polyprenols like natural rubber [38] and the comparably short chains of dolichols [39]. The vast majority of terpenes, steroids and other isoprenoids like cholesterols and carotenoids are obtained from *E*-condensations [35].

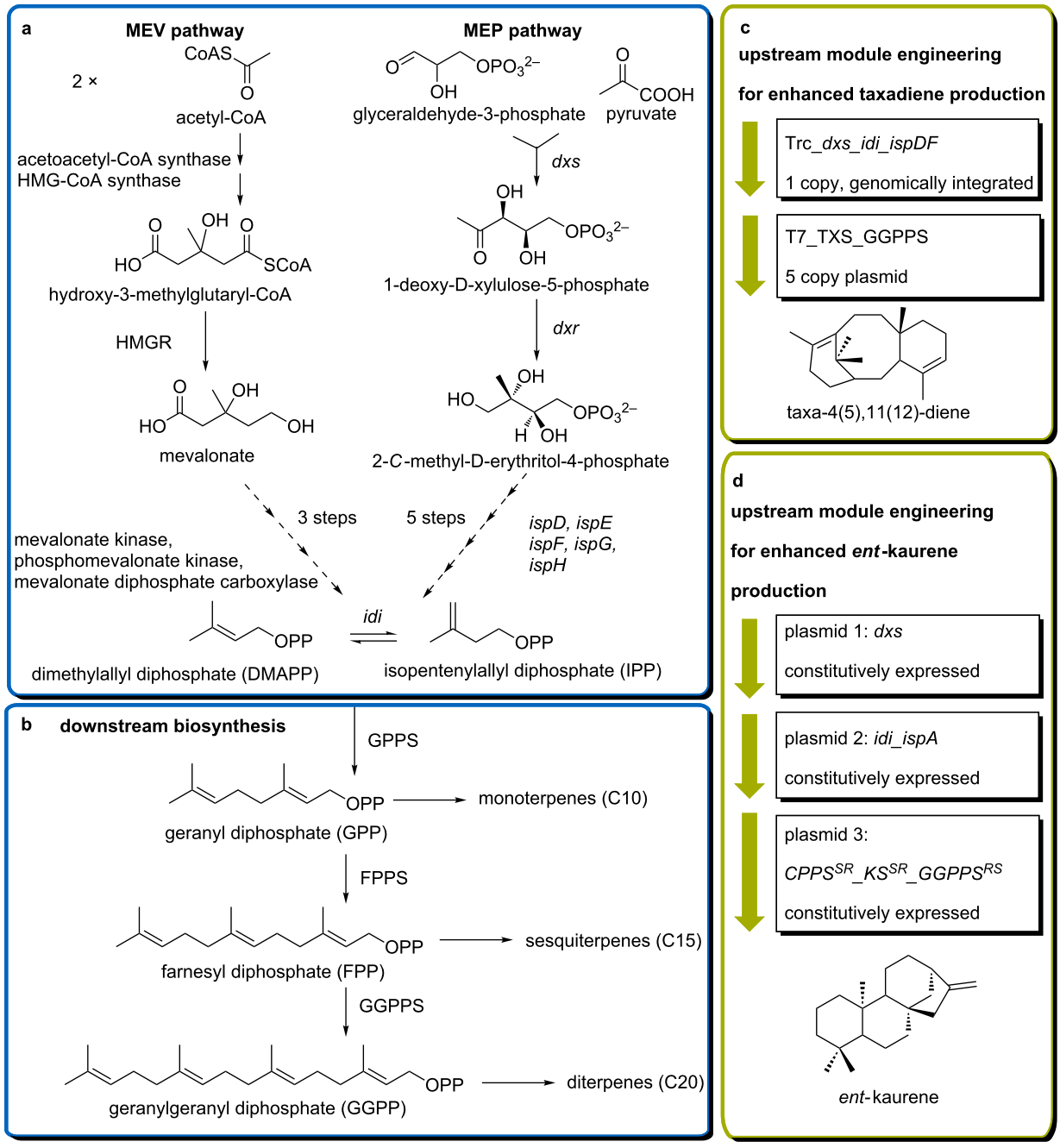

Scheme 1: Isoprenoid biosynthetic pathways and examples for their engineering in heterologous production systems. a) Formation of central isoprenoid metabolites isopentenyl diphosphate (IPP) and dimethylallyl diphosphate (DMAPP) occurs via two distinct natural pathways. Designations MEV and MEP derive from significant intermediates: MEV = mevalonate-dependent and MEP= methylerythritol phosphate-dependent. b) Subsequent condensation of IPP and DMAPP by isoprenyl diphosphate synthases provides specific terpene synthases with their linear substrates. Terpenes are classified according to the carbon atom number in their basic scaffold, beginning with hemiterpenes (C5) and continuing in multiples of five. c) A possible strategy for MEP-pathway optimization for the improved production of the diterpene taxadiene reported by Ajikumar et al. [28]; targeted elements of the biosynthetic pathways and their expression manipulations are given. d) Selection of overexpression targets for the production of *ent*-kaurene reported by Kong et al. [29]; HMGR = hydroxymethylglutaryl(HMG)-CoA-reductase; *dxs* = 1-deoxy-D-xylulose-5-phosphate synthase; *dxr* = 1-deoxy-D-xylulose-5-phosphate reductoisomerase; *ispD* = 2-C-methyl-D-erythritol(ME)-4-phosphate cytidylyltransferase; *ispE* = 4-(cyt-5'-diphospho)-ME kinase; *ispF* = ME-2,4-cyclodiphosphate synthase; *ispG* = hydroxylmethylbutenyl(HMB)-4-diphosphate synthase; *ispH* = HMB-4-diphosphate reductase; *ispA* = farnesyl diphosphate synthase from *Escherichia coli*; *idi* = IPP isomerase; GPPS = geranyl diphosphate synthase; FPPS = farnesyl diphosphate synthase, GGPPS = geranylgeranyl diphosphate synthase; $GGPPS^{RS}$ = GGPPS from *Rhodobacter sphaeroides*; KS^{SR} = *ent*-kaurene synthase from *Stevia rebaudiana*, $CPPS^{SR}$ = *ent*-copalyl diphosphate synthase from *Stevia rebaudiana*, Trc = Trc promoter; T7 = T7 promoter.

Head-to-tail connection of single IPP and DMAPP by geranyl diphosphate synthase (GPPS) results in geranyl diphosphate, GPP, the universal precursor for all monoterpenes [40]. Subsequent *cis*-addition of further IPP-units to geranyl diphosphate by farnesyl diphosphate synthase (FPPS) and geranylgeranyl diphosphate synthase (GGPPS) yield in the respective precursors for sesquiterpenes (farnesyl diphosphate, FPP) and diterpenes (geranylgeranyl diphosphate, GGPP) [35].

Terpene synthases

Interestingly, plant metabolism can convert the universal aliphatic diterpene precursor GGPP into thousands of different terpene structures with high structural complexity and elaborately functional decorations [41]. While the structural diversity of terpene products is obtained by precise modulation of cyclization and rearrangement steps performed by terpene cyclase enzymes [31], initial functional groups are introduced by hydroxylation of the carbon backbone with highly specific P450 monooxygenases [42-44].

At present, terpene synthases (TPS) are classified into three groups which mainly comprise α-helical structures that are designated as α-, β- and γ-domains [45]. Structural and catalytic diversity, especially of plant terpene synthases, originate in various combinations of these domains [46]. The three groups of terpene synthases are classed according to their intron/exon pattern [47] and their diverse reaction initiation mechanisms [48]. Genomic analyses of plant terpene synthases by Trapp and co-workers [47] revealed general organization of 12–14 introns for Class I terpene cyclases, 9 introns for Class II and 6 introns for Class III cyclases. Class III-type terpene synthases appear to be exclusively responsible for angiosperm secondary metabolites of mono-, sesqui- and diterpene structure and contain a highly conserved RR(x)8W-motif [47,49]. The terpene formation performed by Class I-type enzymes occurs via coordination of the isoprenyl diphosphate substrate by a three-ion cluster of divalent metal ions [48]. More specifically, Mg^{2+}- or Mn^{2+}-ions are bound by two conserved amino acid sequences, termed the DDXX(XX)D/E ("aspartate rich") and NSE/DTE [(N,D)D(L,I,V)X(S,T)XXXE] motif, respectively [48]. The first committed step in synthesis of these Class I enzymes is the abstraction of the diphosphate group from the isoprenyl diphosphate substrate [50] at what the diphosphate group is postulated to remain inside the active site of the enzyme [51,52]. Class II terpene synthases harbor a distinct DXDD-motif [52] and the cyclization is generally initiated by protonation of the terminal carbon double bond of the substrate [53]. Since the diphosphate group is preserved during substrate activation by this type of synthases, products from Class II TPS can serve as substrates for Class I TPS which has been reported for example in the biosynthesis of labdane- and clerodane type diterpenes [41]. This close collaboration is performed either in one single bifunctional enzyme containing structure motifs of both types or sets of two different monofunctional synthases of both classes [54,55].

Engineering measures can directly target the primary structure of the terpene synthases or indirectly aim to alter or optimize the product spectrum by changing the tertiary or quaternary structure, respectively [23]. The following paragraphs should give an overview of selected current developments in the areas of mutational engineering, combinatorial enzyme design and microbial engineering.

Mutational engineering of terpene synthases

Site-directed mutagenesis of diterpene cyclases is conventionally applied to elucidate structure–function relationships and mostly targets the active site of the enzyme in order to change the polarity or dimension of the substrate coordinating cavity. Recently reported targeted engineering [51] of the Class I taxadiene synthase from *Taxus brevifolia* (TXS) enabled new understanding of the mechanistic procedures that are carried out by this enzyme on the substrate GGPP. Quenching the carbocation cascade that naturally leads to the formation of tricyclic taxadiene [56] was achieved by exchanging a valin in position 584 with methionine. The resulting product was identified as a bicyclic diterpene of the verticillene type [51] (Scheme 2). A single residue switch in position 753 (W753H) presumably causes premature deprotonation of a cembrene-15-yl cation intermediate in the cyclization mechanism of TXS leading to the monocyclic cembrene A [51] (Scheme 2).

Hence reprogramming the catalytic cascade of diterpene synthases and subsequent functional expression of enzyme variants in a microbial host can not only provide insights into cyclization mechanism but also lead to novel products or changes in the product spectra. This has also been demonstrated for the bacterial diterpene cyclooctat-9-en-7-ol synthase (CotB2) [57], also a putative Class I TPS. Mutation of tryptophan 288 to glycine in CotB2 resulted in the stereoselective synthesis of (1*R*,3*E*,7*E*,11*S*,12*S*)-3,7,18-dolabellatriene, a bicyclic diterpene (Scheme 2). Dollabellanes derive mostly from marine organisms and display bioactivities such as antiviral and cytotoxic effects [59]. Dolabellatriene from a reprogrammed CotB2 contribute with antimicrobial activity against multidrug resistant *Staphylococcus aureus* to this family of natural products [57]. Other mutations on this enzyme generated one cembrane-type monocycle (F107A) (Scheme 2) and two non-natural fusicoccane-type diterpenes (F107Y and F149L) [57]. The latter are putative intermediates in novel routes to phytotoxic

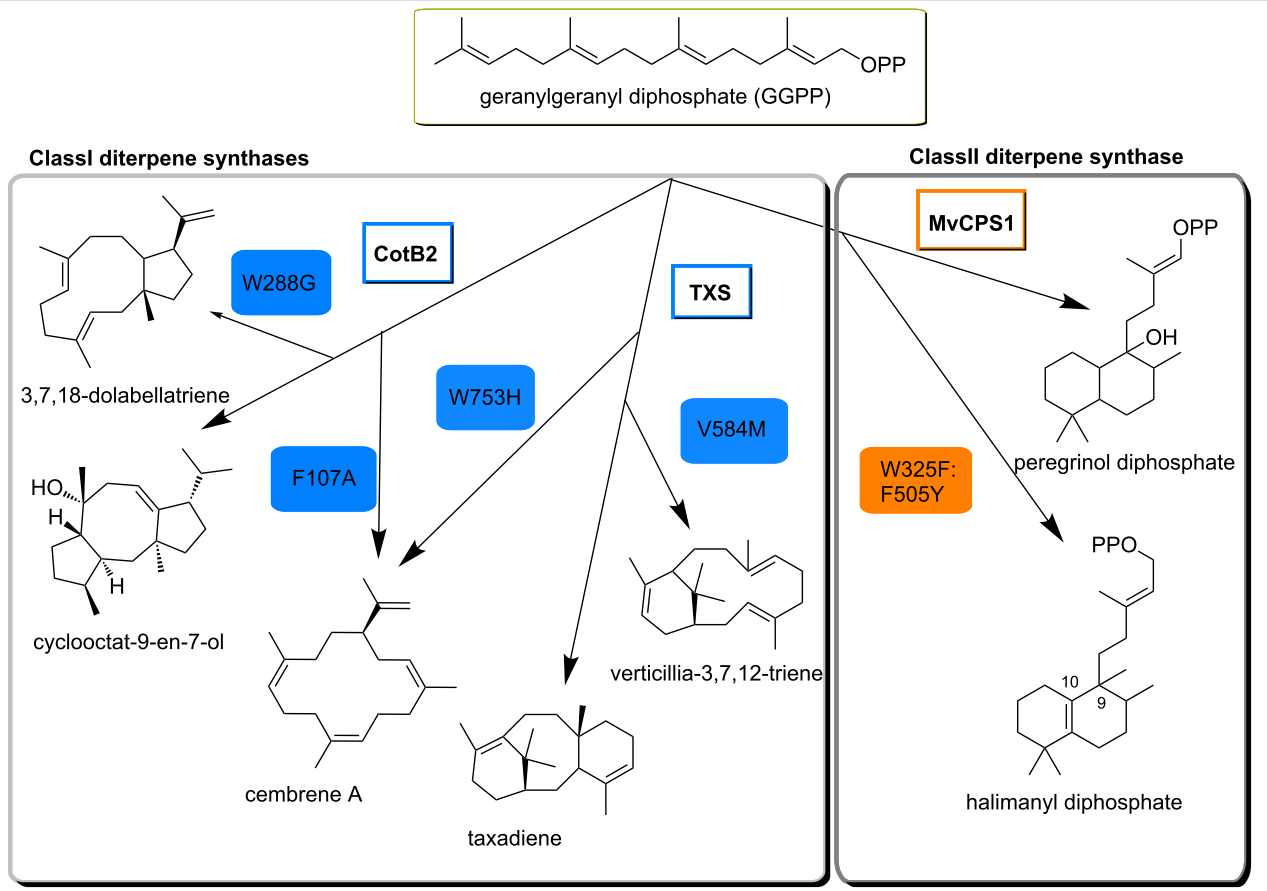

Scheme 2: Mutational engineering of different classes of terpene synthases. Left side: The natural product of wild-type cyclooctat-9-en-7-ol-synthase (CotB2) is a tricyclic diterpene whereas mutations in positions 107 and 288 yield in monocyclic cembrene A and bicyclic 3,7,18-dolabellatriene [57]. Changing the main product specificity of taxadiene synthase from *Taxus brevifolia* (TXS) without significant loss in synthase activity was realized in bicyclic verticillia-3,7,12-triene production through mutation of valin584. Another mutation (W753H) resulted in 100% product specificity for cembrene A but TXS activity was reduced by half in comparison to the wild-type [51]. Right side: Methyl group shifts in Class II peregrinol diphosphate synthase from *Marrubium vulgare* (MvCPS1) were drastically rearranged by introduction of two mutations leading to a previously undescribed halimadane type diphosphate [58], a possible new precursor for valuable halimadane diterpenes with antimicrobial or anti-allergic potential.

fusicoccin A [60] and its derivative with presumably anticancer potential [61].

Exchange of two amino acid residues in the active site of the Class II peregrinol diphosphate synthase from the horehound *Marrubium vulgare* (MvCPS1) [58] resulted in an altered neutralization mechanism of a labda-13-en-8-yl diphosphate carbocation intermediate and the formation of halima-5(10),13-dienyl diphosphate (Scheme 2). In wild-type Class II diterpene synthases, the labda-13-en-8-yl diphosphate carbocation undergoes either single deprotonation or a cascade of hydride and methyl group shifts prior to deprotonation with occasional hydration at the C8 position of the carbocation intermediate which yields hydroxylated diphosphate products [62]. MvCPS1, however, catalyzes a C9–C8 hydride shift preceding hydration resulting in the labdane-type diterpene precursor for the antidiabetic marrubiin [63]. Double mutations of MvCPS1, W323L:F505Y, and W323F:F505Y completely changed the product specificity towards a novel, so far uncharacterized halimadane type diterpene [58] (Scheme 2).

Combinatorial biosynthesis – enzyme design for manufactured terpenes

Conventional identification of new enzyme activities involved in diterpene biosynthetic routes entail time-consuming genome-mining and high-throughput screening technologies [64,65]. Additionally, the number of currently available, even partly annotated plant genomes and crystal structures of diterpene synthases is still limited. Yet, in order to establish heterologous production systems for known diterpenes or to obtain new compounds, deep understanding and accessibility to structural information of this enzyme class can be crucial.

In the last few years, modular approaches encompassing metabolomics and transcriptomics-based methods opened up new avenues for the rapid identification of (di)terpenes.

Andersen-Ranberg and co-workers reported recently on the creation of a synthetic collection of monofunctional Class I/Class II diterpene synthase combinations, which lead to high stereoselective syntheses of an impressive number of previously unknown or unamenable diterpenes with labdane- and clerodane-type structures [66]. Additional findings were provided by Jia and co-workers [67], who demonstrated high substrate promiscuity of a plant and a fungal Class I diterpene synthase. This study involved general substrates of diterpene cyclases like GGPP and its *cis*-isomer nerylneryl diphosphate (NNPP) [68] but also new combinations with 12 known and available products of plant Class II diterpene synthases. Consequently, they obtained 13 previously undescribed diterpenes of the labdane family in addition to previously described diterpenes like manool [69], sclareol [69] and *cis*-abienol [64].

A biosynthesis study of salvinorin A (a psychotrophic agent with potential application as neuropsychiatric drug and for addiction treatment) in *Salvia divinorum* [70] resulted in the identification of five new Class I and Class II diterpene synthases. Moreover, this study performed in vivo substrate promiscuity tests following a combinatorial approach [41,66]. The resulting products entailed pimarane- and abietane-type diterpenes as well as the *trans*-clerodane type diterpene kolavenol, a putative intermediate in the salvinorin A biosynthesis.

Other bifunctional diterpene synthases do not comprise combinations of Class I/Class II domains but contain both a prenyltransferase domain and a terpene synthase moiety. This combination of catalytic modules allows the direct formation of the isoprenyl diphosphate substrate for the terpene synthase in a single biocatalyst. An unusual example of these bifunctional enzymes was published by Chen and coworkers [60], who managed to crystalize catalytic domains of PaFS, a diterpene synthase from *Phomopsis amygdali*. The formation of GGPP is located in a C-terminal α-domain with very low sequence identity to the N-terminal Class I terpene synthase domain indicating different catalytical properties. The natural product of PaFS is fusicocca-2,10(14)-diene, an intermediate in the biosynthesis of the phytotoxin fusicoccin A by *P. amygdali*. Interestingly, a recent work by Qin and co-workers [71] even revealed the conversion of a fungal diterpene synthase into a sesterterpene synthase by interchanging the prenyltransferase domain.

Combining these structural insights and newly created biosynthetic routes with functional expression in bacterial production hosts, industrial scale synthesis of fragrance compound (+)-sclareol, (13*R*)-(+)-manoyl oxide (precursor for pharmaceutic forskolin) or miltiradiene (precursor for antioxidants and tanshinones) may be within reach [66]. Additionally, genetic engineering of diterpene synthases enhances the knowledge of structure–function relationships alongside with increasing supply of novel potentially bioactive diterpenes.

Reprogramming the catalytic activities of (plant) diterpene synthases may also be an alternative to extensive genome-mining and screening strategies since this technique can potentially close or circumvent knowledge gaps in biosynthetic pathways to bioactive products which were previously inaccessible. A good example is the mutagenesis of the bacterial diterpene synthase CotB2 that resulted in dolabellatriene-type scaffolds, which were by then mostly found in marine organisms [59]. To that end, these new routes can provide substantial and environmentally friendly alternatives for sourcing natural diterpenes from rare resources like corals [72].

Microbial engineering

The genetically readily accessible engineering hosts *Escherichia coli* and *Saccharomyces cerevisiae* are suitable for heterologous terpene production. Established culture conditions are completed by the availability of metabolic databases and computational tools [73] that enable model-based optimization such as flux-balance analyses [74]. Taking advantage of natural presence and manipulability of distinct isoprenoid pathways in both organisms (MEP in *E. coli* and MEV in *S. cerevisiae*), heterologous production of several isoprenoid natural products has been accomplished with industrially relevant production titers [75-77]. However, at present there is no clear preference for one microbial production host as each engineering endeavor requires a de novo benchmarking for a specific terpenoid product, indicating that even minimal introduction of heterologous genes for terpene production lead to unpredictable metabolic feedback reactions that currently can only be counteracted by empirical approaches. Monoterpenes, for example, can have toxic effects on microorganisms, though *E. coli* seems to be more tolerant towards products like α-pinene or limonene [78].

At present, 27.4 g/L of amorphadiene is the highest published titer for any reported terpenoid produced in *E. coli.* This result is of particular industrial relevance as amorphadiene constitutes the sesquiterpenoid scaffold of the antimalarial drug artemisinin [79]. In comparison, production of amorphadiene in *S. cerevisiae* did yield in excess titer of 40 g/L [80].

The opposite result to amorphadiene was observed for the model diterpene taxadiene where heterologous production in *S. cerevisiae* resulted in 8.7 mg/L, while yields of 1 g/L taxadiene could be obtained in *E. coli* [28,81]. Different approaches

of terpene product increase involved targeting specific elements of the MEP pathway [28] or introducing heterologous MEV pathway from yeast [82,83]. A high level of taxadiene production in *E. coli* was achieved by Ajikumar and co-workers through overexpression of bottleneck enzymes of the endogenous MEP pathway (*dxs*, *idi*, *ispD*, *ispF*, Scheme 1) together with GGPP-synthase (GGPPS) and taxadiene-synthase (TXS) from *Taxus brevifolia* [28]. Elevation of product titers of the important diterpene intermediate *ent*-kaurene (precursor for the gibberellin biosynthesis [84]) was reported from Kong et al. [29]. Their strategy involved overexpression of the MEP-Elements *dxs, idi* and *ispA* (see Scheme 1) in an engineered *E.coli* strain co-expressing recombinant *ent*-copalyl diphosphate synthase (CPPS) and *ent*-kaurene synthase (KS) from *Stevia rebaudiana* as well as a GGPPS from *Rhodobacter sphaeroides*.

With an increasing number of integrated recombinant enzymes balanced (over)expression gains importance in order to sustain optimal carbon flux in the production host from cultivation medium feed to the desired product. In this respect, determining the optimal strength of the ribosomal binding site (RBS) may be as crucial as the correct arrangement of the genetic elements on designed operons [85-87]. To this end, the lycopene reporter system represents a valuable tool in determining balanced expression of terpene centered heterologous pathways in *E. coli* [88,89]. Furthermore, a significant obstacle in large scale bacterial diterpene production is the functional expression of engineered terpene synthases in the heterologous host. Similarly, the downstream functionalization of the hydrocarbon scaffold, which is a prerequisite for biological activity [90], remains challenging in any recombinant host. The vast majority of modifications accomplished in the downstream biosynthesis of diterpenes comprise introduction of oxygen moieties by cytochrome-P450 enzymes, which are commonly not sourced from bacterial systems. In fact the functional reconstitution of eukaryotic terpene synthases or oxidoreductases requires significant enzyme modifications. Specifically, codon optimization and the truncation of distinct domains which are responsible for, e.g., membrane localization can improve the enzyme activity. To date, identifying the necessary sequence segment for soluble expression in the bacterial host alongside with finding the optimal redox partner for P450 enzymes is still a matter of empirical work [44,91,92]. Furthermore, integration of every additional enzyme to the production system will eventually result in a significant decrease in the final yield, which makes very complex biosyntheses involving multiple oxygenation steps challenging [93]. Even highly optimized systems for the production of just the first hydroxylated intermediate in taxol biosynthesis, 5-α-hydroxytaxadiene [91], show a product loss of over 40% in comparison to previously reported titers for the undecorated taxadiene macrocycle [28]. Engineering one host alone can therefore sometimes be insufficient since there are specific elements of biosynthetic pathways that may have different production capacities in one organism or another. Zhou et al. [94] reported stable co-culture fermentation of specifically engineered *E. coli* and *S. cerevisiae* strains for the production of different sesqui- and diterpenes. Although, the final yield for the taxane product was in very low mg scale, first microbial production of deoxygenated monoacetylated taxadiene could be realized.

Optimization of the up-scaled fermentative process generally involves selection of the carbon source, media composition and in situ or post-fermentational product removal. Some terpene products have cytotoxic effects against the production host and separation from the cells is recommended already during fermentation. Ajikumar et al. also reported in-process-accumulation of the inhibitory metabolite indole [28]. A suitable method for most fermentations is an overlay with apolar alkanes such as dodecane [28,79,95] although subsequent product extraction from this phase may be challenging and oxygenation capacity is reduced. Engineering efflux transporters to enhance extracellular product secretion can be a viable support for this apolar-phase-capture [96]. However, these methods are no longer applicable as soon as further engineering steps involve polarization of the product backbone.

A summary of the various areas that have to be covered for successful establishment of heterologous terpene production in a bacterial host is given in Figure 1.

Conclusion

Over the last years, countless and in some cases groundbreaking studies about terpenes and heterologous terpene biosynthesis have been published, and it still seems like just the tip of the iceberg. Potentially, modular biosynthesis that has resources to fast expanding databases will widen the amenable targets for large scale production to unforeseen extend. As a prerequisite, strain optimization of heterologous hosts has to be developing with equal progress although continuous reporting about engineering the native pathway for isoprenoid precursor formation in *E. coli*, MEP, proves its complexity. Computational approaches that involve flux-balance analyses can redirect empirical screening for optimized systems towards guided engineering to overcome metabolic bottlenecks and identify feedback inhibition loops. Heterologous production of several diterpenes could already be realized in stable systems with moderate yields, validating the established approaches of enzyme engineering for terpene synthases. Yet this success could not be transferred in full extend to heterologous expression of P450 enzymes. Solubility together with substrate and product specificity remains important targets for further engineering.

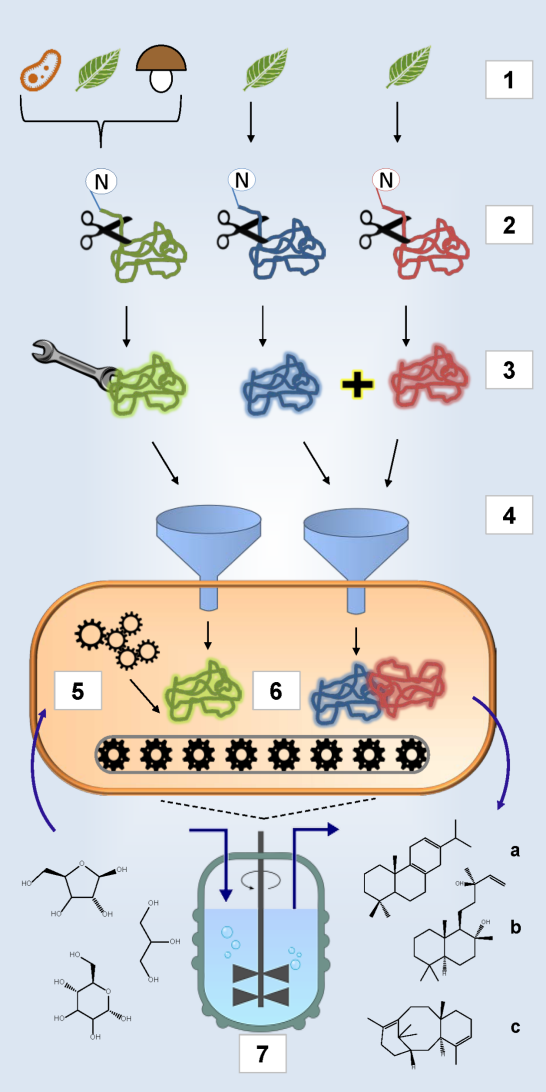

Figure 1: Implementation of a microbial cell factory. 1: Selection of enzymes from different species. P450 and related reductase enzymes (indicated with blue and red knots respectively) derive almost exclusively from plants; terpene synthases and other enzymes that are involved in precursor formation (indicated with green knot) can be obtained from various organisms (indicated through symbolic bacteria, leaf (representing plants in general) and fungi). 2: Eukaryotic enzymes have to be engineered for functional and soluble expression in prokaryotic hosts like *E. coli*, Removal of the N-terminal and thereby the cell-wall-localization domain (indicated through scissors) is a standard procedure in engineering plant enzymes; 3: Further engineering steps are not mandatory but often entail site-directed mutagenesis (indicated through wrench) of TPS (green) for product modulation or introduction of a linker-coding sequence for co-expression of P450 monooxygenase and reductase (blue and red); 4: Heterologous expression in *E. coli* (depicted in orange). Construction of synthetic operons and screening for highest yield of plasmid systems generally precedes genomic integration; 5: Isoprenoid precursor supply: precursor flux has to be balanced carefully to avoid metabolic overload and accumulation of unwanted byproducts; 6: Downstream terpenoid biosynthesis using heterologous enzymes; 7: Upscaling of terpene production in fermentation systems using different carbon sources (left) for optimally engineered *E. coli* strains is a potential future source for valuable diterpenes like miltiradiene (a), sclareol (b) or taxadiene (c).

Acknowledgements

KK, MH, MF and TB gratefully acknowledge the support of SysBioTerp project funded by the Federal Ministry of Education and Research in the Systems Biology funding framework (BMBF; Grant number: 031A305A). MR and TB thankfully acknowledge the support of the OMCBP project by the Federal Ministry of Education and Research granted within the BMBF international call framework (Grant number: 031A276A).

References

1. Wani, M. C.; Taylor, H. L.; Wall, M. E.; Coggon, P.; McPhail, A. T. *J. Am. Chem. Soc.* **1971,** *93,* 2325–2327. doi:10.1021/ja00738a045
2. Klayman, D. L. *Science* **1985,** *228,* 1049–1055. doi:10.1126/science.3887571
3. Lis-Balcnin, M.; Ochocka, R. J.; Deans, S. G.; Asztemborska, M.; Hart, S. *J. Essent. Oil Res.* **1999,** *11,* 393–397. doi:10.1080/10412905.1999.9701162
4. Cragg, G. M.; Kingston, D. G. I.; Newman, D. J. *Anticancer agents from natural products,* 2nd ed.; CRC press: Boca Raton, 2012. doi:10.1201/b11185
5. Beller, H. R.; Lee, T. S.; Katz, L. *Nat. Prod. Rep.* **2015,** *32,* 1508–1526. doi:10.1039/C5NP00068H
6. Schwab, W.; Fuchs, C.; Huang, F.-C. *Eur. J. Lipid Sci. Technol.* **2013,** *115,* 3–8. doi:10.1002/ejlt.201200157
7. Yagi, S.; Babiker, R.; Tzanova, T.; Schohn, H. *Asian Pac. J. Trop. Med.* **2016,** *9,* 763–770. doi:10.1016/j.apjtm.2016.06.009
8. Teixeira, B.; Marques, A.; Ramos, C.; Neng, N. R.; Nogueira, J. M. F.; Saraiva, J. A.; Nunes, M. L. *Ind. Crops Prod.* **2013,** *43,* 587–595. doi:10.1016/j.indcrop.2012.07.069
9. Alves, E. G.; Jardine, K.; Tota, J.; Jardine, A.; Yãnez-Serrano, A. M.; Karl, T.; Tavares, J.; Nelson, B.; Gu, D.; Stavrakou, T.; Martin, S.; Artaxo, P.; Manzi, A.; Guenther, A. *Atmos. Chem. Phys.* **2016,** *16,* 3903–3925. doi:10.5194/acp-16-3903-2016
10. Loivamäki, M.; Louis, S.; Cinege, G.; Zimmer, I.; Fischbach, R. J.; Schnitzler, J.-P. *Plant Physiol.* **2007,** *143,* 540–551. doi:10.1104/pp.106.092759
11. Gibson, D. M.; Ketchum, R. E. B.; Vance, N. C.; Christen, A. A. *Plant Cell Rep.* **1993,** *12,* 479–482. doi:10.1007/BF00236091
12. Shen, R.; Jiang, X.; Ye, W.; Song, X.; Liu, L.; Lao, X.; Wu, C. *Tetrahedron* **2011,** *67,* 5610–5614. doi:10.1016/j.tet.2011.05.104
13. Zhu, L.; Luo, J.; Hong, R. *Org. Lett.* **2014,** *16,* 2162–2165. doi:10.1021/ol500623w
14. Schmidt, J.; Khalil, Z.; Capon, R. J.; Stark, C. B. W. *Beilstein J. Org. Chem.* **2014,** *10,* 1228–1232. doi:10.3762/bjoc.10.121
15. Frija, L. M. T.; Frade, R. F. M.; Afonso, C. A. M. *Chem. Rev.* **2011,** *111,* 4418–4452. doi:10.1021/cr100258k
16. Vasas, A.; Hohmann, J. *Chem. Rev.* **2014,** *114,* 8579–8612. doi:10.1021/cr400541j
17. McKerrall, S. J.; Jørgensen, L.; Kuttruff, C. A.; Ungeheuer, F.; Baran, P. S. *J. Am. Chem. Soc.* **2014,** *136,* 5799–5810. doi:10.1021/ja501881p
18. McKerrall, S. J.; Jørgensen, L.; Kuttruff, C. A.; Ungeheuer, F.; Baran, P. S. *J. Am. Chem. Soc.* **2015,** *137,* 14545. doi:10.1021/jacs.5b11112
19. Justicia, J.; Rosales, A.; Buñuel, E.; Oller-López, J. L.; Valdivia, M.; Haïdour, A.; Oltra, J. E.; Barrero, A. F.; Cárdenas, D. J.; Cuerva, J. M. *Chem. – Eur. J.* **2004,** *10,* 1778–1788. doi:10.1002/chem.200305647

20. Kusama, H.; Hara, R.; Kawahara, S.; Nishimori, T.; Kashima, H.; Nakamura, N.; Morihira, K.; Kuwajima, I. *J. Am. Chem. Soc.* **2000,** *122,* 3811–3820. doi:10.1021/ja9939439
21. Klein-Marcuschamer, D.; Ajikumar, P. K.; Stephanopoulos, G. *Trends Biotechnol.* **2007,** *25,* 417–424. doi:10.1016/j.tibtech.2007.07.006
22. Peralta-Yahya, P. P.; Zhang, F.; del Cardayre, S. B.; Keasling, J. D. *Nature* **2012,** *488,* 320–328. doi:10.1038/nature11478
23. King, J. R.; Edgar, S.; Qiao, K.; Stephanopoulos, G. *F1000Research* **2016,** *5,* 397. doi:10.12688/f1000research.7311.1
24. Dewick, P. M. *Nat. Prod. Rep.* **2002,** *19,* 181–222. doi:10.1039/b002685i
25. Lange, B. M.; Rujan, T.; Martin, W.; Croteau, R. *Proc. Natl. Acad. Sci. U. S. A.* **2000,** *97,* 13172–13177. doi:10.1073/pnas.240454797
26. Kuzuyama, T. *Biosci., Biotechnol., Biochem.* **2002,** *66,* 1619–1627. doi:10.1271/bbb.66.1619
27. Kirby, J.; Keasling, J. D. *Annu. Rev. Plant Biol.* **2009,** *60,* 335–355. doi:10.1146/annurev.arplant.043008.091955
28. Ajikumar, P. K.; Xiao, W.-H.; Tyo, K. E. J.; Wang, Y.; Simeon, F.; Leonard, E.; Mucha, O.; Phon, T. H.; Pfeifer, B.; Stephanopoulos, G. *Science* **2010,** *330,* 70–74. doi:10.1126/science.1191652
29. Kong, M. K.; Kang, H.-J.; Kim, J. H.; Oh, S. H.; Lee, P. C. *J. Biotechnol.* **2015,** *214,* 95–102. doi:10.1016/j.jbiotec.2015.09.016
30. Lichtenthaler, H. K.; Rohmer, M.; Schwender, J. *Physiol. Plant.* **1997,** *101,* 643–652. doi:10.1111/j.1399-3054.1997.tb01049.x
31. Chen, F.; Tholl, D.; Bohlmann, J.; Pichersky, E. *Plant J.* **2011,** *66,* 212–229. doi:10.1111/j.1365-313X.2011.04520.x
32. Lange, B. M.; Ahkami, A. *Plant Biotechnol. J.* **2013,** *11,* 169–196. doi:10.1111/pbi.12022
33. Banerjee, A.; Wu, Y.; Banerjee, R.; Li, Y.; Yan, H.; Sharkey, T. D. *J. Biol. Chem.* **2013,** *288,* 16926–16936. doi:10.1074/jbc.M113.464636
34. Bohlmann, J.; Keeling, C. I. *Plant J.* **2008,** *54,* 656–669. doi:10.1111/j.1365-313X.2008.03449.x
35. Wang, K. C.; Ohnuma, S.-i. *Biochim. Biophys. Acta* **2000,** *1529,* 33–48. doi:10.1016/S1388-1981(00)00136-0
36. Jia, Q.; Chen, F. *Mol. Plant* **2016,** *9,* 189–191. doi:10.1016/j.molp.2015.12.020
37. Tarshis, L. C.; Proteau, P. J.; Kellogg, B. A.; Sacchettini, J. C.; Poulter, C. D. *Proc. Natl. Acad. Sci. U. S. A.* **1996,** *93,* 15018–15023. doi:10.1073/pnas.93.26.15018
38. Asawatreratanakul, K.; Zhang, Y.-W.; Wititsuwannakul, D.; Wititsuwannakul, R.; Takahashi, S.; Rattanapittayaporn, A.; Koyama, T. *Eur. J. Biochem.* **2003,** *270,* 4671–4680. doi:10.1046/j.1432-1033.2003.03863.x
39. Akhtar, T. A.; Matsuba, Y.; Schauvinhold, I.; Yu, G.; Lees, H. A.; Klein, S. E.; Pichersky, E. *Plant J.* **2013,** *73,* 640–652. doi:10.1111/tpj.12063
40. Dong, L.; Jongedijk, E.; Bouwmeester, H.; Van Der Krol, A. *New Phytol.* **2016,** *209,* 679–690. doi:10.1111/nph.13629
41. Zerbe, P.; Bohlmann, J. *Trends Biotechnol.* **2015,** *33,* 419–428. doi:10.1016/j.tibtech.2015.04.006
42. Toyomasu, T. *Biosci., Biotechnol., Biochem.* **2008,** *72,* 1168–1175. doi:10.1271/bbb.80044
43. Guerra-Bubb, J.; Croteau, R.; Williams, R. M. *Nat. Prod. Rep.* **2012,** *29,* 683–696. doi:10.1039/c2np20021j
44. Morrone, D.; Chen, X.; Coates, R. M.; Peters, R. J. *Biochem. J.* **2010,** *431,* 337–347. doi:10.1042/BJ20100597
45. Cao, R.; Zhang, Y.; Mann, F. M.; Huang, C.; Mukkamala, D.; Hudock, M. P.; Mead, M. E.; Prisic, S.; Wang, K.; Lin, F.-Y.; Chang, T.-K.; Peters, R. J.; Oldfield, E. *Proteins: Struct., Funct., Bioinf.* **2010,** *78,* 2417–2432. doi:10.1002/prot.22751
46. Gao, Y.; Honzatko, R. B.; Peters, R. J. *Nat. Prod. Rep.* **2012,** *29,* 1153–1175. doi:10.1039/c2np20059g
47. Trapp, S. C.; Croteau, R. B. *Genetics* **2001,** *158,* 811–832.
48. Aaron, J. A.; Christianson, D. W. *Pure Appl. Chem.* **2010,** *82,* 1585–1597. doi:10.1351/PAC-CON-09-09-37
49. Dornelas, M. C.; Mazzafera, P. *Genet. Mol. Biol.* **2007,** *30,* 832–840. doi:10.1590/S1415-47572007000500011
50. Mafu, S.; Potter, K. C.; Hillwig, M. L.; Schulte, S.; Criswell, J.; Peters, R. J. *Chem. Commun.* **2015,** *51,* 13485–13487. doi:10.1039/C5CC05754J
51. Schrepfer, P.; Buettner, A.; Goerner, C.; Hertel, M.; van Rijn, J.; Wallrapp, F.; Eisenreich, W.; Sieber, V.; Kourist, R.; Brück, T. *Proc. Natl. Acad. Sci. U. S. A.* **2016,** *113,* E958–E967. doi:10.1073/pnas.1519680113
52. Prisic, S.; Xu, J.; Coates, R. M.; Peters, R. J. *ChemBioChem* **2007,** *8,* 869–874. doi:10.1002/cbic.200700045
53. Gong, H.-Y.; Zeng, Y.; Chen, X.-Y. *Nat. Prod. Bioprospect.* **2014,** *4,* 59–72. doi:10.1007/s13659-014-0012-8
54. Peters, R. J.; Carter, O. A.; Zhang, Y.; Matthews, B. W.; Croteau, R. B. *Biochemistry* **2003,** *42,* 2700–2707. doi:10.1021/bi020492n
55. Zerbe, P.; Hamberger, B.; Yuen, M. M. S.; Chiang, A.; Sandhu, H. K.; Madilao, L. L.; Nguyen, A.; Hamberger, B.; Bach, S. S.; Bohlmann, J. *Plant Physiol.* **2013,** *162,* 1073–1091. doi:10.1104/pp.113.218347
56. Hong, Y. J.; Tantillo, D. J. *J. Am. Chem. Soc.* **2011,** *133,* 18249–18256. doi:10.1021/ja2055929
57. Görner, C.; Häuslein, I.; Schrepfer, P.; Eisenreich, W.; Brück, T. *ChemCatChem* **2013,** *5,* 3289–3298. doi:10.1002/cctc.201300285
58. Mafu, S.; Fischer, E.; Addison, J. B.; Riberio Barbosana, I.; Zerbe, P. *ChemBioChem* **2016,** *17,* 2304–2307. doi:10.1002/cbic.201600419
59. Görner, C.; Hirte, M.; Huber, S.; Schrepfer, P.; Brück, T. *Front. Microbiol.* **2015,** *6,* 1115. doi:10.3389/fmicb.2015.01115
60. Chen, M.; Chou, W. K. W.; Toyomasu, T.; Cane, D. E.; Christianson, D. W. *ACS Chem. Biol.* **2016,** *11,* 889–899. doi:10.1021/acschembio.5b00960
61. Miyake, T.; Honma, Y.; Urano, T.; Kato, N.; Suzumiya, J. *Int. J. Oncol.* **2015,** *47,* 315–324. doi:10.3892/ijo.2015.2979
62. Peters, R. J. *Nat. Prod. Rep.* **2010,** *27,* 1521–1530. doi:10.1039/c0np00019a
63. Mnonopi, N.; Levendal, R.-A.; Mzilikazi, N.; Frost, C. L. *Phytomedicine* **2012,** *19,* 488–493. doi:10.1016/j.phymed.2011.12.008
64. Zerbe, P.; Chiang, A.; Yuen, M.; Hamberger, B.; Hamberger, B.; Draper, J. A.; Britton, R.; Bohlmann, J. *J. Biol. Chem.* **2012,** *287,* 12121–12131. doi:10.1074/jbc.M111.317669
65. Lauchli, R.; Rabe, K. S.; Kalbarczyk, K. Z.; Tata, A.; Heel, T.; Kitto, R. Z.; Arnold, F. H. *Angew. Chem., Int. Ed.* **2013,** *52,* 5571–5574. doi:10.1002/anie.201301362
66. Andersen-Ranberg, J.; Kongstad, K. T.; Nielsen, M. T.; Jensen, N. B.; Pateraki, I.; Bach, S. S.; Hamberger, B.; Zerbe, P.; Staerk, D.; Bohlmann, J.; Møller, B. L.; Hamberger, B. *Angew. Chem., Int. Ed.* **2016,** *55,* 2142–2146. doi:10.1002/anie.201510650
67. Jia, M.; Potter, K. C.; Peters, R. J. *Metab. Eng.* **2016,** *37,* 24–34. doi:10.1016/j.ymben.2016.04.001
68. Zi, J.; Matsuba, Y.; Hong, Y. J.; Jackson, A. J.; Tantillo, D. J.; Pichersky, E.; Peters, R. J. *J. Am. Chem. Soc.* **2014,** *136,* 16951–16953. doi:10.1021/ja508477e

69. Ignea, C.; Ioannou, E.; Georgantea, P.; Loupassaki, S.; Trikka, F. A.; Kanellis, A. K.; Makris, A. M.; Roussis, V.; Kampranis, S. C. *Metab. Eng.* **2015,** *28,* 91–103. doi:10.1016/j.ymben.2014.12.001
70. Pelot, K. A.; Mitchell, R.; Kwon, M.; Hagelthorn, D. M.; Wardman, J. F.; Chiang, A.; Bohlmann, J.; Ro, D.-K.; Zerbe, P. *Plant J.* **2017,** *89,* 885–897. doi:10.1111/tpj.13427
71. Qin, B.; Matsuda, Y.; Mori, T.; Okada, M.; Quan, Z.; Mitsuhashi, T.; Wakimoto, T.; Abe, I. *Angew. Chem., Int. Ed.* **2016,** *55,* 1658–1661. doi:10.1002/anie.201509263
72. Berrue, F.; Kerr, R. G. *Nat. Prod. Rep.* **2009,** *26,* 681–710. doi:10.1039/b821918b
73. Fernández-Castané, A.; Fehér, T.; Carbonell, P.; Pauthenier, C.; Faulon, J.-L. *J. Biotechnol.* **2014,** *192,* 302–313. doi:10.1016/j.jbiotec.2014.03.029
74. Biggs, B. W.; De Paepe, B.; Santos, C. N. S.; De Mey, M.; Kumaran Ajikumar, P. *Curr. Opin. Biotechnol.* **2014,** *29,* 156–162. doi:10.1016/j.copbio.2014.05.005
75. Li, Y.; Pfeifer, B. A. *Curr. Opin. Plant Biol.* **2014,** *19,* 8–13. doi:10.1016/j.pbi.2014.02.005
76. Chang, M. C. Y.; Keasling, J. D. *Nat. Chem. Biol.* **2006,** *2,* 674–681. doi:10.1038/nchembio836
77. Vickers, C. E.; Bongers, M.; Liu, Q.; Delatte, T.; Bouwmeester, H. *Plant, Cell Environ.* **2014,** *37,* 1753–1775. doi:10.1111/pce.12316
78. Himejima, M.; Hobson, K. R.; Otsuka, T.; Wood, D. L.; Kubo, I. *J. Chem. Ecol.* **1992,** *18,* 1809–1818. doi:10.1007/BF02751105
79. Tsuruta, H.; Paddon, C. J.; Eng, D.; Lenihan, J. R.; Horning, T.; Anthony, L. C.; Regentin, R.; Keasling, J. D.; Renninger, N. S.; Newman, J. D. *PLoS One* **2009,** *4,* e4489. doi:10.1371/journal.pone.0004489
80. Westfall, P. J.; Pitera, D. J.; Lenihan, J. R.; Eng, D.; Woolard, F. X.; Regentin, R.; Horning, T.; Tsuruta, H.; Melis, D. J.; Owens, A.; Fickes, S.; Diola, D.; Benjamin, K. R.; Keasling, J. D.; Leavell, M. D.; McPhee, D. J.; Renninger, N. S.; Newman, J. D.; Paddon, C. J. *Proc. Natl. Acad. Sci. U. S. A.* **2012,** *109,* E111–E118. doi:10.1073/pnas.1110740109
81. Engels, B.; Dahm, P.; Jennewein, S. *Metab. Eng.* **2008,** *10,* 201–206. doi:10.1016/j.ymben.2008.03.001
82. Morrone, D.; Lowry, L.; Determan, M. K.; Hershey, D. M.; Xu, M.; Peters, R. J. *Appl. Microbiol. Biotechnol.* **2010,** *85,* 1893–1906. doi:10.1007/s00253-009-2219-x
83. Yang, L.; Wang, C.; Zhou, J.; Kim, S.-W. *Microb. Cell Fact.* **2016,** *15,* 14. doi:10.1186/s12934-016-0409-7
84. Su, P.; Tong, Y.; Cheng, Q.; Hu, Y.; Zhang, M.; Yang, J.; Teng, Z.; Gao, W.; Huang, L. *Sci. Rep.* **2016,** *6,* No. 23057. doi:10.1038/srep23057
85. Nowroozi, F. F.; Baidoo, E. E. S.; Ermakov, S.; Redding-Johanson, A. M.; Batth, T. S.; Petzold, C. J.; Keasling, J. D. *Appl. Microbiol. Biotechnol.* **2014,** *98,* 1567–1581. doi:10.1007/s00253-013-5361-4
86. Salis, H. M. *Methods Enzymol.* **2011,** *498,* 19–42. doi:10.1016/B978-0-12-385120-8.00002-4
87. Levin-Karp, A.; Barenholz, U.; Bareia, T.; Dayagi, M.; Zelcbuch, L.; Antonovsky, N.; Noor, E.; Milo, R. *ACS Synth. Biol.* **2013,** *2,* 327–336. doi:10.1021/sb400002n
88. Yoon, S.-H.; Lee, Y.-M.; Kim, J.-E.; Lee, S.-H.; Lee, J.-H.; Kim, J.-Y.; Jung, K.-H.; Shin, Y.-C.; Keasling, J. D.; Kim, S.-W. *Biotechnol. Bioeng.* **2006,** *94,* 1025–1032. doi:10.1002/bit.20912
89. Bongers, M.; Chrysanthopoulos, P. K.; Behrendorff, J. B. Y. H.; Hodson, M. P.; Vickers, C. E.; Nielsen, L. K. *Microb. Cell Fact.* **2015,** *14,* 193. doi:10.1186/s12934-015-0381-7
90. Lipinski, C. A.; Lombardo, F.; Dominy, B. W.; Feeney, P. J. *Adv. Drug Delivery Rev.* **2001,** *46,* 3–26. doi:10.1016/S0169-409X(00)00129-0
91. Biggs, B. W.; Lim, C. G.; Sagliani, K.; Shankar, S.; Stephanopoulos, G.; De Mey, M.; Ajikumar, P. K. *Proc. Natl. Acad. Sci. U. S. A.* **2016,** *113,* 3209–3214. doi:10.1073/pnas.1515826113
92. Görner, C.; Schrepfer, P.; Redai, V.; Wallrapp, F.; Loll, B.; Eisenreich, W.; Haslbeck, M.; Brück, T. *Microb. Cell Fact.* **2016,** *15,* 86. doi:10.1186/s12934-016-0487-6
93. Marienhagen, J.; Bott, M. *J. Biotechnol.* **2013,** *163,* 166–178. doi:10.1016/j.jbiotec.2012.06.001
94. Zhou, K.; Qiao, K.; Edgar, S.; Stephanopoulos, G. *Nat. Biotechnol.* **2015,** *33,* 377–383. doi:10.1038/nbt.3095
95. Kim, E.-M.; Eom, J.-H.; Um, Y.; Kim, Y.; Woo, H. M. *J. Agric. Food Chem.* **2015,** *63,* 4606–4612. doi:10.1021/acs.jafc.5b01334
96. Zhang, C.; Chen, X.; Stephanopoulos, G.; Too, H.-P. *Biotechnol. Bioeng.* **2016,** *113,* 1755–1763. doi:10.1002/bit.25943

License and Terms

BEILSTEIN JOURNAL OF ORGANIC CHEMISTRY

Aggregation behaviour of a single-chain, phenylene-modified bolalipid and its miscibility with classical phospholipids

Simon Drescher*[1], Vasil M. Garamus[2], Christopher J. Garvey[3], Annette Meister[4,5] and Alfred Blume[4]

Full Research Paper

Open Access

Address:
[1]Institute of Pharmacy, Martin Luther University (MLU) Halle-Wittenberg, Wolfgang-Langenbeck-Str. 4, 06120 Halle (Saale), Germany, [2]Helmholtz-Zentrum Geesthacht (HZG), Centre for Materials and Costal Research, Max-Planck-Str. 1, 21502 Geesthacht, Germany, [3]Australian Nuclear Science and Technology Organisation (ANSTO), Kirrawee DC, NSW, Australia, [4]Institute of Chemistry, MLU Halle-Wittenberg, von-Danckelmann-Platz 4, 06120 Halle (Saale), Germany and [5]Institute of Biochemistry and Biotechnology, MLU Halle-Wittenberg, Kurt-Mothes-Str. 3, 06120 Halle (Saale), Germany

Email:
Simon Drescher* - simon.drescher@pharmazie.uni-halle.de

* Corresponding author

Keywords:
aggregation behaviour; bolaamphiphiles; bolalipids; membrane lipids; mixing behaviour; nanofibres; self-assembly

Beilstein J. Org. Chem. **2017,** *13,* 995–1007.
doi:10.3762/bjoc.13.99

Received: 15 March 2017
Accepted: 28 April 2017
Published: 23 May 2017

This article is part of the Thematic Series "Lipids: fatty acids and derivatives, polyketides and isoprenoids". Dedicated to Prof. Dr. Bodo Dobner on the occasion of his 65th birthday.

Guest Editor: J. S. Dickschat

Abstract

In the present work, we describe the synthesis of a single-chain, phenylene-modified bolalipid with two phosphocholine headgroups, PC-C18pPhC18-PC, using a Sonogashira cross-coupling reaction as a key step. The aggregation behaviour was studied as a function of temperature using transmission electron microscopy (TEM), differential scanning calorimetry (DSC), Fourier-transform infrared (FTIR) spectroscopy, and small angle neutron scattering (SANS). We show that our new bolalipid self-assembles into nanofibres, which transform into flexible nanofibres at 27 °C and further to small elongated micelles at 45 °C. Furthermore, the miscibility of the bolalipid with bilayer-forming phosphatidylcholines (DMPC, DPPC, and DSPC) was investigated by means of DSC, TEM, FTIR, and small angle X-ray scattering (SAXS). We could show that the PC-C18pPhC18-PC is partially miscible with saturated phosphatidylcholines; however, closed lipid vesicles with an increased thermal stability were not found. Instead, bilayer fragments and disk-like aggregates are formed.

Introduction

Bolalipids are amphiphilic molecules consisting of two hydrophilic headgroups attached to both ends of a long hydrocarbon spacer [1]. The hydrophobic spacer is composed of either a single alkyl chain or two chains connected via a glycerol moiety. These bolalipids originate in membranes of some species of archaea, e.g., thermoacidophiles and these archaeal membranes can withstand extreme living conditions, such as high temperatures or low pH values [2-4]. Archaea are quite different from bacteria and eukaryotes [5-9], which is also reflected in the chemical structure of those archaeal membrane

lipids: the alkyl chains are connected via ether linkages in the inverse *sn*-2,3 configuration to the glycerol, the alkyl chains sometimes contain a varying number of cyclopentane rings or several methyl branches [2,3], and some of the archaeal lipids consist of two transmembrane alkyl chains (caldarchaeol-type). Especially this type of bolalipids is of great interest for applications in material sciences, biotechnology, and pharmaceuticals [10-15]. Since these bolalipids are able to span the membrane of classical phospholipid bilayers, they can be used to stabilize liposomes for drug delivery purposes. The applicability of this approach was already tested for a large variety of natural and artificial bolalipids [12,16-22].

The isolation of archaeal bolalipids from natural sources is expensive and often leads to mixtures of bolalipids with different alkyl chain pattern. But also the synthesis of natural as well as artificial bolalipids is elaborate and time-consuming and, hence, present research tries to simplify the chemical structure of bolalipids by keeping up their membrane-stabilizing properties [23]. This simplification strategy led in our group to the synthesis of dotriacontane-1,32-diylbis[2-(trimethylammonio)-ethylphosphate] (PC-C32-PC) [24,25], the simplest bola model lipid consisting of two phosphocholine (PC) headgroups connected by a long, unmodified C32 alkyl chain. If PC-C32-PC is suspended in water, the formation of a dense network of nanofibres and, as a consequence, a clear and transparent hydrogel is observed [25]. The nanofibres have a thickness of about 6 nm, corresponding to the length of a PC-C32-PC molecule. Due to the bulky PC headgroup, the PC-C32-PC molecules are arranged side by side within the fibrous aggregate but slightly twisted relative to each other leading to a helical super structure of the fibres. This helicity was previously confirmed by cryo-transmission electron microscopy (cryo-TEM), high resolution atomic force microscopy (AFM) [26], and Monte Carlo simulations [27]. A temperature increase leads to a transformation of the nanofibres into small micelles and the gel character is lost. This reversible gel/sol transformation is accompanied by a cooperative endothermic transition at T_m = 48 °C, which can be followed by differential scanning calorimetry (DSC) [24].

However, the use of PC-C32-PC as "stabilizer" of phospholipid bilayers failed. In mixtures of PC-C32-PC with classical phospholipids, such as 1,2-dipalmitoyl-*sn*-glycero-3-phosphocholine (DPPC) or 1-palmitoyl-2-oleoyl-*sn*-glycero-3-phosphocholine (POPC), no significant insertion of the bolalipid into the bilayer was observed [28]. The reason for this behaviour is that packing problems due to the mismatch between the large space requirement of the PC headgroup of PC-C32-PC and the small cross-sectional area of its single alkyl chain arise. The insertion of a PC-C32-PC molecule in a stretched conformation into phospholipid bilayers is energetically unfavourable as it produces void volume, which can be filled by neither bolalipid nor phospholipid. Consequently, the self-assembly of PC-C32-PC into nanofibres is preferred.

To evade these packing problems, we expanded the cross-sectional area of the alkyl chain of the bolalipid in order to fill the void volume. Besides heteroatoms [29,30], acetylene [31] or diacetylene groups [32], or methyl branches [31,33], also phenyl- or biphenyl rings were inserted into the long alkyl chain [34-37]. The insertion of a phenylene group led to PC-C16pPhC16-PC [36], which self-assembles at room temperature into small ellipsoidal micelles, and to PC-C17pPhC17-PC [35] that forms nanofibres with a significantly reduced thermal stability compared to PC-C32-PC. Unfortunately, the insertion of PC-C17pPhC17-PC into phospholipid bilayers composed of, e.g., DPPC did not result in the formation of stabilized lipid vesicles and elongated micelles as well as bilayer fragments were found instead. We have now synthesized a bolalipid with phenyl modification and a slightly longer alkyl chain, PC-C18pPhC18-PC (Figure 1), to investigate a possible chain length dependency on both the aggregation behaviour of the pure bolalipid and the miscibility with bilayer-forming phospholipids.

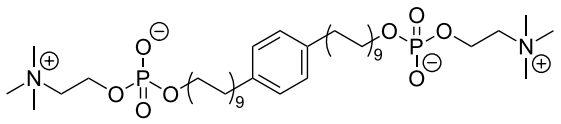

Figure 1: Chemical structure of PC-C18pPhC18-PC.

In this study, we investigated the aggregation behaviour of PC-C18pPhC18-PC in aqueous suspension by means of DSC, TEM, Fourier-transform infrared (FTIR) spectroscopy, and small angle neutron scattering (SANS). Moreover, the mixing behaviour of PC-C18pPhC18-PC with saturated phosphatidylcholines 1,2-dimyristoyl-*sn*-glycero-3-phosphocholine (DMPC), DPPC, and 1,2-distearoyl-*sn*-glycero-3-phosphocholine (DSPC) was studied by means of DSC and TEM. Additionally, one mixture was exemplarily investigated by FTIR and small angle X-ray scattering (SAXS).

Results and Discussion

Synthesis of PC-C18pPhC18-PC and its temperature-dependent aggregation behaviour

Synthesis

The phenylene-modified bolalipid 18,18'-(1,4-phenylene)bis-{octadec-1-yl[2-(trimethylammonio)ethylphosphate]} (PC-C18pPhC18-PC) was synthesised from the corresponding diol (HO-C18pPhC18-OH) by established phosphorylation and

quarternisation reactions described previously [38]. The long-chain, phenylene-modified 1,ω-diol in turn was prepared using a bis-Sonogashira cross-coupling reaction [37] with $PdCl_2(PPh_3)_2$ as catalyst and tetra-*n*-butylammonium fluoride (TBAF) as solvent as well as 1,4-dibromobenzene and octadec-17-yn-1-ol (Ac-C16-OH) [32,39] as starting material. Following, both triple bonds were converted into single bonds by hydrogenation. The bolalipid was finally purified by middle pressure liquid chromatography (MPLC) using $CHCl_3$/MeOH/H_2O as eluent and the gradient technique. The synthetic pathway is summarised in Scheme 1. Details of synthetic procedures and analytical data can be found in Supporting Information File 1.

Aggregation behaviour

The aggregation behaviour of this novel bolalipid was investigated as a function of temperature by means of TEM, DSC, FTIR, and SANS. The results obtained were compared to PC-C17pPhC17-PC [35] and PC-C16pPhC16-PC [36], structural analogues with slightly shorter alkyl chains, and the homologous series of phenylene-free PC-Cn-PC, with n = 22–36 [24-26,38,40].

The first observation is a gelation of the suspension when the bolalipid PC-C18pPhC18-PC is dissolved in water at a concentration of c = 1 mg mL^{-1}. This behaviour indicates the formation of nanofibres, which in turn immobilize the solvent molecules and allow the formation of a transparent hydrogel. A similar observation was found for PC-C17pPhC17-PC [35] and also for phenylene-free analogues, such as PC-Cn-PC with alkyl chain lengths ranging from n = 22–36 [24-26,38,40].

DSC and FTIR

The DSC heating curve of PC-C18pPhC18-PC (c = 1 mg mL^{-1} in H_2O) shows two endothermic transitions (Figure 2): the first one at T_m = 27.4 °C ($\Delta H \approx$ 12 kJ mol^{-1}) and a second broad peak at about 45 °C ($\Delta H \approx$ 6 kJ mol^{-1}). The corresponding cooling curve depicts also two but very broad peaks with a hysteresis, which is an indication for a hindered reorganisation of bola molecules within the aggregates.

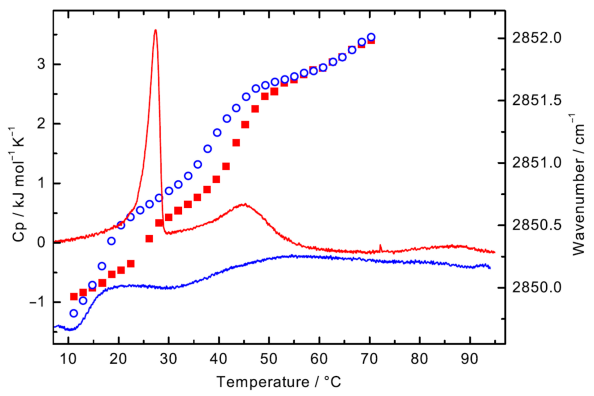

Figure 2: DSC curves for PC-C18pPhC18-PC (c = 1 mg mL^{-1} in H_2O, solid lines, heating: red, cooling: blue). FTIR: wavenumber of the symmetric methylene stretching vibration (symbols, c = 50 mg mL^{-1} in H_2O, heating: filled red squares, cooling: open blue circles).

Both transition temperatures in the DSC heating scan are about 5 K higher compared to T_m-values of the lipid analogue PC-C17pPhC17-PC with a slightly shorter alkyl chain (two methylene units) [35]. The increase in T_m is caused by the elongation of the alkyl chain, which leads to an increase in van-der-Waals contacts of neighbouring bola molecules. This effect has been observed before with other bolalipids [38]. When the alkyl chain becomes too short, as in PC-C16pPhC16-PC whose alkyl chain is again two methylene units shorter, no fibre formation is observed but the bolalipid molecules self-assemble at room temperature into small micellar aggregates. Consequently, no endothermic transition was observed between 2–95 °C for this bolalipid [31,35,36].

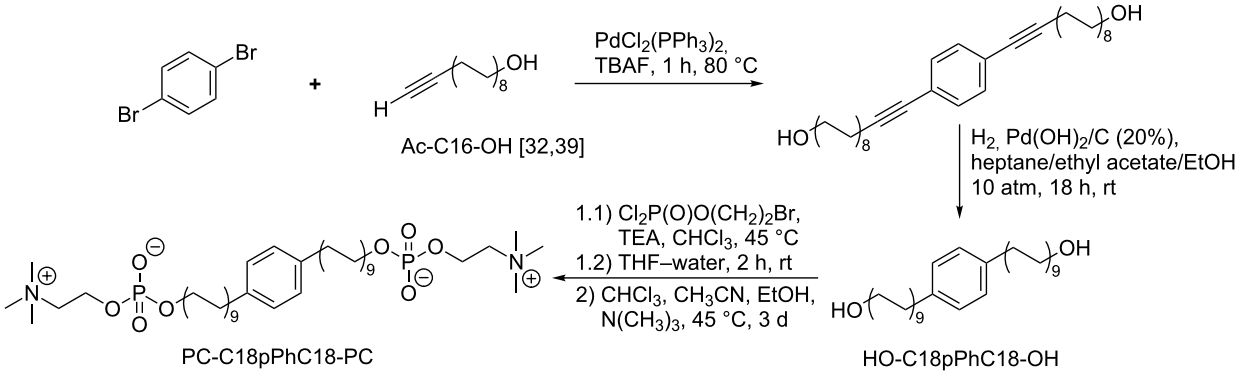

Scheme 1: Synthesis of PC-C18pPhC18-PC; TBAF: tetra-*n*-butylammonium fluoride, TEA: triethylamine, rt: room temperature.

To obtain information on the conformation and the mobility of the alkyl chain of PC-C18pPhC18-PC molecules within the aggregates, IR measurements of a bolalipid suspension (c = 50 mg mL^{-1} in H_2O) were conducted. The position of the symmetric methylene stretching vibrational band ($\nu_s CH_2$) gives information about the order of the alkyl chain, whether *gauche* conformers are present or not [41,42]. The wavenumber of the $\nu_s(CH_2)$ vibrational band as a function of temperature is shown in Figure 2.

At T = 11.1 °C, the frequency of $\nu_s(CH_2)$ is at 2849.9 cm^{-1} indicating ordered alkyl chains in all-*trans* conformation. Within the temperature range of the first transition observed in DSC, the wavenumber of this band increases to 2850.6 cm^{-1} at T = 30.0 °C, which is attributed to a slightly increased amount of *gauche* conformers and a more flexible alkyl chain. However, this increase in wavenumber is not as pronounced as for PC-C17pPhC17-PC within its main DSC transition, where the wavenumber of $\nu_s(CH_2)$ jumps to 2851.5 cm^{-1} [35]. If we compare the increase in frequency of $\nu_s(CH_2)$ of phenylene-free bolalipids at their first DSC transition, e.g., PC-C32-PC [38] (2849.5 cm^{-1} → 2851.3 cm^{-1}; fibres → micelles) and PC-C34-PC [40] (2849.6 cm^{-1} → 2850.8 cm^{-1}; fibres → fibres), the increase is in our case relatively small and comparable to PC-C34-PC. This shows that the chain order in the intermediate structures of PC-C18pPhC18-PC present at 30 °C, between both DSC transitions, is still relatively high.

With a further increase in temperature, the frequency of $\nu_s(CH_2)$ increases to 2851.5 cm^{-1} at T = 53.0 °C and finally to 2852.0 cm^{-1} at T = 70.3 °C. This increase is again attributed to an increased amount of *gauche* conformers and a higher flexibility of the alkyl chains. The corresponding cooling curve shows the same pattern except for a hysteresis of 5–7 K, which is indicative for a hindered reformation of the ordered fibrous aggregates. A comparable hysteresis is visible in the DSC scan.

TEM

To analyse the structure of aggregates, samples for TEM were prepared below the first transition as well as between the first and the second transition of PC-C18pPhC18-PC. At about 7 °C, the TEM image depicts a dense network of long nanofibres (A). The morphology of these fibres changes with increasing temperature. At 36 °C, the TEM image shows the presence of flexible nanofibres; no small micellar aggregates were found (B) (Figure 3). This means, the first endothermic transition of PC-C18pPhC18-PC is connected to a fibre–fibre transformation and not to a fibre–micelle transformation as found for PC-C17pPhC17-PC [35] and also for unmodified, phenylene-free bolalipids PC-Cn-PC with alkyl chain lengths (n) up to 32 carbon atoms [24,38]. But, bolalipids with very long alkyl chain, namely PC-C34-PC and PC-C36-PC, show an additional fibre–fibre transition, where the flexibility of bolalipid molecules is slightly increased. However, due to the very long alkyl chains, the remaining van-der-Waals contacts are sufficient for the formation of fibrous aggregates above the first transition [26,40]. This seems to be also the case for PC-C18pPhC18-PC.

SANS

In order to ensure the results obtained with TEM and IR, SANS measurements were performed (c = 1 mg mL^{-1} in D_2O). SANS data follows the structural changes of bolalipid aggregates with varying temperature and shows firstly an increase of scattering intensities with temperature change from 4 °C to 32 °C, accompanied with an increase of slope (α) of scattering intensities approximated by power law, i.e., $I(q) \sim q^{-\alpha}$ at lower q-range from 1 to 2 (Figure 4). A further increase in temperature to 60 °C leads to a decrease of scattering intensities and a decrease of α almost to zero. The observation of slope α equals −1 is a signature of scattering from elongated and rigid objects of length L and radius R in an interval of scattering vectors $1/L < q < 1/R$. Scattering data have been analysed via indirect Fourier transformation (IFT) method (Figure 4, solid lines) for infinitely long

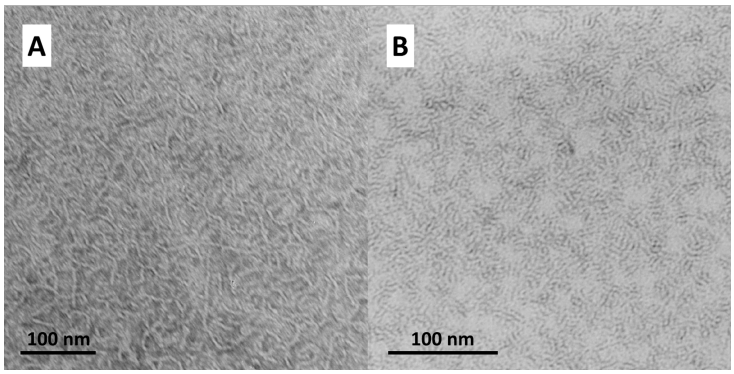

Figure 3: TEM image of an aqueous suspension (c = 0.05 mg mL^{-1}) of PC-C18pPhC18-PC. The samples were prepared at about 7 °C (A) or at 36 °C (B) and stained with uranyl acetate before drying.

cylinder described previously [43-46] and the cross section pair distance distribution function, $p_{CS}(r)$, has been obtained (Supporting Information File 1, Figure S1). This distribution function gives values of the diameter of cross section of ≈ 50–55 Å and an aggregation number N_{agg} of about 9 ± 1 bolalipid molecules per 1 nm length of cylinder at T = 4 °C.

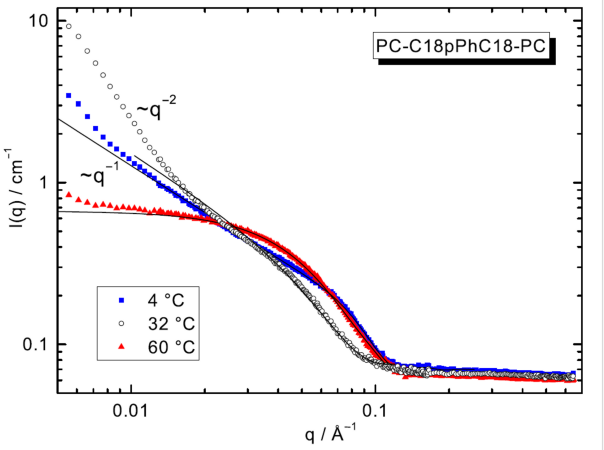

Figure 4: SANS data of a suspension of PC-C18pPhC18-PC (c = 1 mg mL^{-1} in D_2O, scattered data) with IFT analysis (solid lines) at different temperatures.

At 32 °C – a temperature between the first transition and the second transition of PC-C18pPhC18-PC – SANS intensities are proportional to q^{-2} and, hence, suggest the scattering from flexible chains. Here, the q-value measured is $L_{cont}^{-1} < q < l_p^{-1}$, where l_p is the persistence length of flexible aggregates and L_{cont} is the contour length of the aggregate. The crossover between the region of rigid cylinder, i.e., the plateau of Holtzer [47] $qI(q)$ versus q (Supporting Information File 1, Figure S3), to increase at lowest q (flexibility region) takes place around q = 0.02 Å^{-1}, which suggests that aggregates become flexible in length scale above 100 Å. It can be concluded that an increase of temperature from 4 °C to 32 °C shifts system from long and rigid fibres to flexible chains. Additionally, also the cross-sectional parameters of flexible chain changes, i.e., the diameter increases up to 70 Å (Supporting Information File 1, Figure S1) and N_{agg} slightly increases to 10 ± 1 bolalipid molecules per 1 nm length of flexible chain.

At 60 °C, the scattering intensities at lowest q-range are typical for scattering from small globular objects such as micelles. Mean diameter D of these objects ($q << 1/D$) and p(r) has been obtained in approximation of 3D-objects, where all three axes of the object have the same order of magnitude. At 60 °C bolalipid molecules form small, elliptical-like micelles of maximal diameter of 200 Å (Supporting Information File 1, Figure S2). The radius of gyration (R_g) is around 32 ± 2 Å, which equals a diameter of 83 Å, and N_{agg} is about 121 ± 5 bolalipid molecules per micelle. Modelling of the scattering curves by ellipsoids of revolution yields values for the semi axes $a = b$ = 22 Å and c = 47 Å. The results of SANS measurements are summarized in Table 1.

Mixing behaviour with saturated phosphatidylcholines

In order to investigate the miscibility of our new bolalipid with bilayer-forming phospholipids, PC-C18pPhC18-PC was mixed with the double-chain phospholipids DMPC, DPPC, and DSPC, i.e., phosphatidylcholines with saturated alkyl chains of different length. In a previous study we showed that unmodified bolalipids, such as PC-C32-PC, could not be incorporated into bilayers of DMPC or POPC [28]. In contrast, bolalipids with an alkyl chain modification, e.g., PC-C17pPhC17-PC, were partially miscible with DPPC and DSPC. But, closed lipid vesicles (liposomes) and a pronounced stabilization of the lamellar

Table 1: SANS data obtained from IFT analysis for aqueous suspensions of PC-C18pPhC18-PC in D_2O at different temperatures.[a]

T [°C]	aggregate shape	D_{max} [Å]	$I(0)$ [cm g^{-1}] or $I_{CS}(0)$ [Å^{-1} cm g^{-1}]	M [g] or M_L [g cm^{-1}]	N_{agg} or N_{agg} [nm^{-1}]	R_g [Å] or $R_{CS,g}$ [Å]	R [Å]	a [Å]	b [Å]	L [Å] or c [Å]
4	fibres (stiff cylinders)	45	3.96 ± 0.01	1.37 × 10^{-13}	8.7 ± 1	16.40 ± 0.02	23.2	22 ± 2	22 ± 2	>2000
32	flexible fibres	70	4.61 ± 0.01	1.59 × 10^{-13}	10 ± 1	24.25 ± 0.03	34.3	30 ± 3	30 ± 3	>2000
60	micelles	100	590 ± 10	1.91 × 10^{-19}	121 ± 5	32 ± 2	41.3	22 ± 2	22 ± 2	47 ± 4

[a]D_{max}: maximal size or cross section of aggregate; $I(0)$: scattering at "zero angle"; $I_{CS}(0)$: scattering at "zero angle" of cylindrical cross section; M: mass; M_L: mass per unit length; N_{agg}: aggregation number of micelles or number of molecules per unit length of rod-like object; R_g: radius of gyration; $R_{CS,g}$: radius of gyration of cross-section; R and R_{CS} are effective radius of aggregate or radius of cylindrical cross section in homogeneous approximation; a, b, c, and L: values for semi axes a and b, and estimated length L for fibres with circular cross-section and for semi axes of ellipsoid of revolution of micelles $a = b$, and c.

structure – prerequisites for the use as drug delivery vehicle – could not be observed, and bilayer fragments as well as elongated micelles were formed instead [35]. The isomers PC-C17mPhC17-PC and PC-C17oPhC17-PC, bearing a *meta* or *ortho* substitution at the central phenyl ring, showed the formation of disk-like aggregates in mixtures with DPPC and DSPC, respectively, with partly increased thermal stability [34]. The mixing behaviour of PC-C18pPhC18-PC with phosphatidylcholines was now studied by means of DSC and TEM. Additionally, one example of a bolalipid/phospholipid mixture was further investigated by FTIR and SAXS measurements.

DSC

We firstly investigated the thermotropic behaviour of aqueous suspensions of PC-C18pPhC18-PC:phospholipid mixtures (c = 3 mM) with different molar ratios, namely 1:10, 1:5, 1:2, and 1:1 (n:n). The heating scans are depicted in the left-hand column of Figure 5, the corresponding cooling scans are shown in the right-hand column of Figure 5.

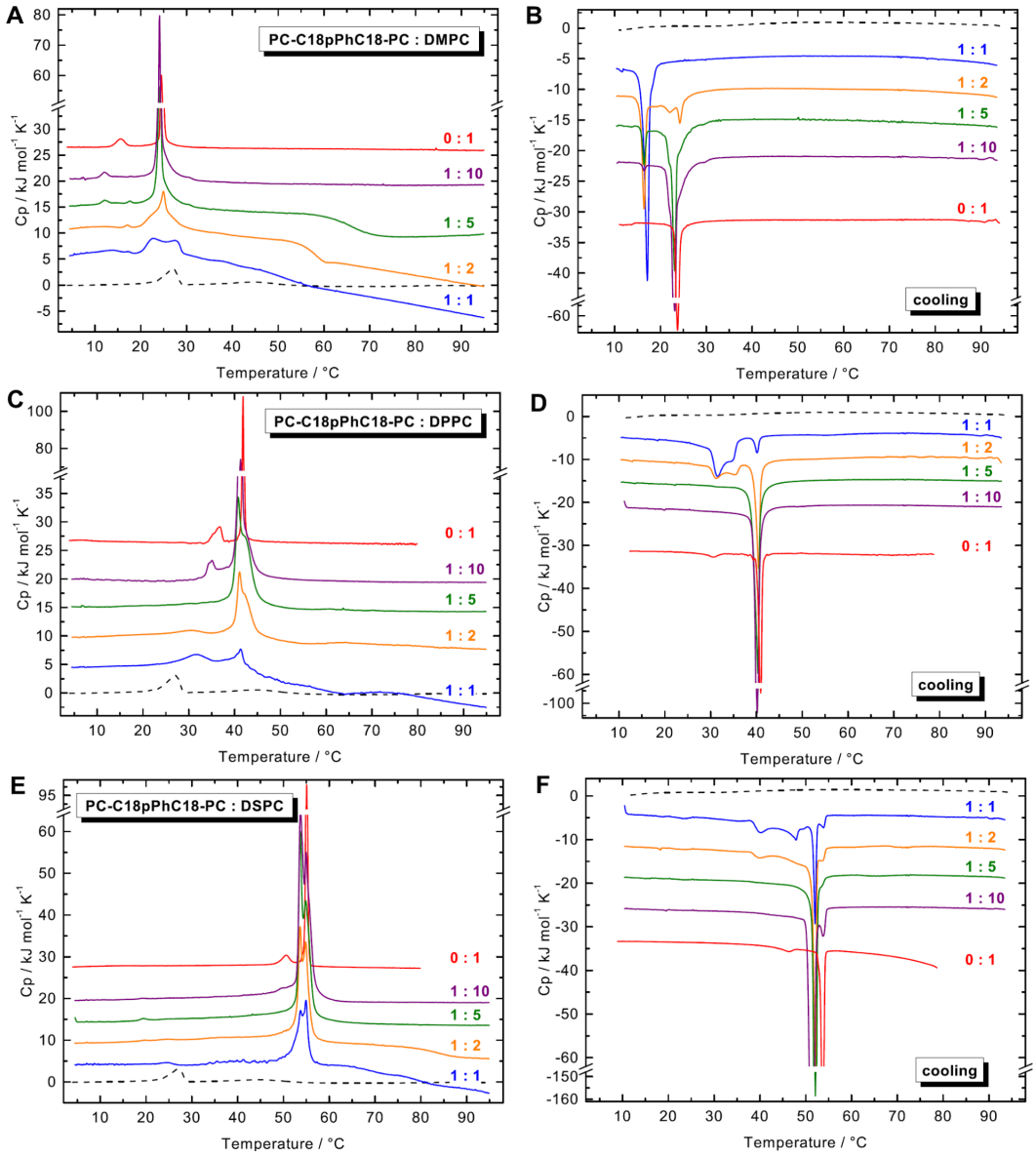

Figure 5: DSC heating (left-hand column) and cooling (right-hand column) scans of different PC-C18pPhC18-PC:phospholipid mixtures (c = 3 mM in phosphate buffer, pH 7.6): DMPC (A,B), DPPC (C,D), and DSPC (E,F). The molar ratios are displayed in the graph. The DSC data of pure PC-C18pPhC18-PC (black dashed line, c = 1 mg mL^{-1}) and pure phospholipids (red solid line, c = 1 mg mL^{-1}) are shown for comparison. The heating and cooling rate was 60 K h^{-1}. The curves are shifted vertically for clarity.

The DSC heating scans of the pure, bilayer-forming phospholipids show the two well-known endothermic transitions (see red solid lines in Figure 5): the pre-transition from the $L_{\beta'}$-phase to the ripple-phase ($P_{\beta'}$) and the very cooperative main transition to the L_{α}-phase, where the alkyl chains are fluidized due to an increased amount of *gauche* conformers.

The DSC heating scan of a 1:10 mixture of PC-C18pPhC18-PC and DMPC (Figure 5A) shows a sharp peak at T = 24.1 °C, below T_m of the pure DMPC. With increasing amount of bolalipid, this peak stays nearly at the same temperature but gets broader. In the equimolar mixture of PC-C18pPhC18-PC and DMPC, the DSC scan shows a broad transition with two peaks at T = 22.8 °C and T = 27.3 °C. The latter one corresponds to T_m of the pure bolalipid. In addition, one or two very small pre-transitions are detectable below the main transition. In the corresponding DSC cooling scans (Figure 5B), a biphasic transition appears in most mixtures. Starting with the 1:10 mixture, the DSC scan depicts a peak at T = 23.1 °C, slightly below T_m of pure DMPC. With increasing amount of the bolalipid, this peak disappeared gradually and at the same time a second peak at T = 16.5 °C emerged, which shifts to T = 17.1 °C in the 1:1 mixture.

In the mixtures with DPPC (Figure 5C), the DSC heating scan of the 1:10 ratio shows an endothermic transition at T = 41.4 °C, 0.5 K below the T_m of pure DPPC, including a high-temperature shoulder. With increasing amount of bolalipid, this peak disappears gradually. In the 1:2 mixture and more pronounced in the 1:1 mixture, a second, broad peak emerged at $T \approx 32$ °C, which is above T_m of the pure bolalipid. The corresponding DSC cooling scans (Figure 5D) depicts a sharp transition peak at around 40.2 °C, again slightly below T_m of pure DPPC, which decreases gradually with increasing amount of bolalipid. In the 1:2 and 1:1 mixture, two additional low-temperature peaks appear at 34.7 °C and 31.5 °C, indicating a complex behaviour.

A comparable situation is found for mixtures of PC-C18pPhC18-PC with DSPC. Here, the DSC heating scan of the 1:10 mixture (bolalipid:phospholipid) shows a main transition with a splitting (53.7 °C and 54.9 °C; Figure 5E), again slightly below T_m of pure phospholipid. With increasing amount of bolalipid, both transition peaks decrease in intensity but virtually stay at the same temperature. The DSC cooling scan (Figure 5F) of the 1:10 mixture shows a peak at about 52 °C. With increasing amount of PC-C18pPhC18-PC, this peak stays at the same temperature and decreases gradually. Finally, the cooling scan of the 1:1 mixture shows again several peaks: the most distinct ones at 52.1 °C, and three smaller ones at 53.9 °C, 47.8 °C, and 40.2 °C.

In the DSC heating curve of some of our bolalipid/phospholipid mixtures, an additional exothermic peak as well as a continuous or stepwise decrease in the heat capacity is observed during heating. It is conceivable that a metastable state is reached after T_m. This kinetically stable state transforms within the timescale of the DSC experiment (heating rate = 60 K h^{-1}) into a thermodynamically stable state, which is accompanied by an exothermic heat effect showing up as broad transition peak or as decrease in *Cp*. The notion of two different states is supported by the fact that this exothermic peak or the decrease in *Cp* disappeared using a slower heating rate of 20 K h^{-1} (data not shown). A similar effect was found previously for mixtures of PC-C17pPhC17-PC [35] and PC-C32-10,10'Me-PC, a bolalipid with two methyl groups within the long alkyl chain [48], with different saturated phosphatidylcholines.

TEM

To get an idea about the aggregate structure of the mixed systems in aqueous suspension TEM images were recorded from negatively stained samples. All specimens were prepared at about 22 °C, i.e., in the case of mixtures with DMPC at the beginning of the main transition and for mixtures with DPPC and DSPC, respectively, below the transitions observed in DSC. The images are shown in Figure 6. By comparing the images of the different phospholipid mixtures (DMPC, DPPC or DSPC) with same mixing ratio, one can see that the shape of aggregates is similar.

Starting with the lowest bolalipid content, EM images of the 1:10 mixture reveal the presence of crashed vesicles as well as disk-like aggregates (Figure 6A–C). The disks, which are particularly found in mixtures with DPPC, are nearly round shaped and they are oriented either parallel (black arrow head) or perpendicular to the grid surface (white arrow head). EM images of a bolalipid/phospholipid = 1:5 mixture show the existence of disk-like aggregates of comparable size for all three different phospholipids (Figure 6D–F). However, also some collapsed vesicles are present in the mixture with DMPC and DPPC. By increasing the bolalipid content to a 1:2 mixture (bolalipid/phospholipid), the shape of aggregates changes to small, elongated micelles (Figure 6G–I). In the case of DPPC and DSPC mixtures, another kind of larger aggregates is formed. Lastly, for the equimolar mixtures (Figure 6K–M), EM images show again the formation of small, elongated micelles. Only in the case of the DSPC mixture, some larger aggregates are found.

We conclude that PC-C18pPhC18-PC is not completely immiscible with bilayer-forming phosphatidylcholines and that the PC-C18pPhC18-PC is partially miscible with these phospholipids. When ca. 10 or 20 mol % of bolalipid is inserted in

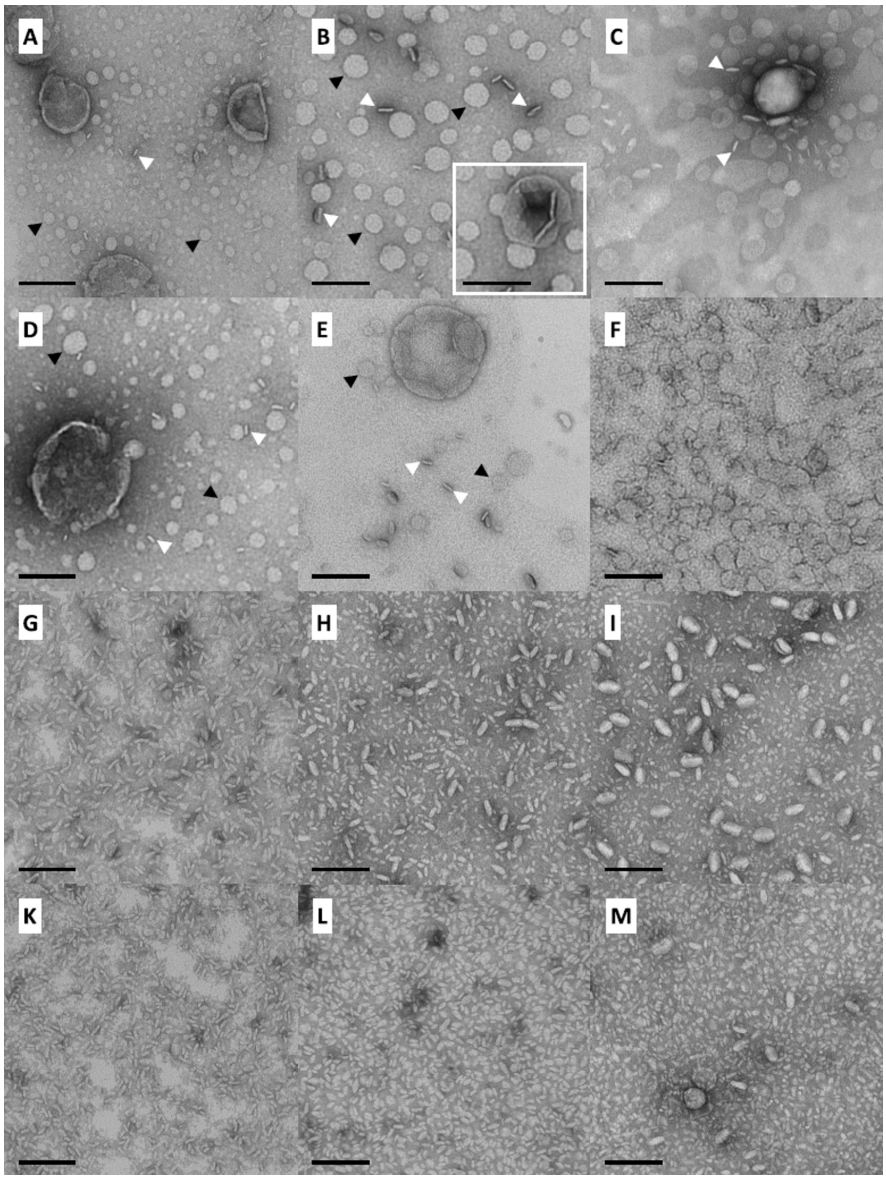

Figure 6: TEM images of aqueous suspensions (c = 60 µM or c = 30 µM for C) of PC-C18pPhC18-PC/phospholipid mixtures with DMPC (left-hand column), DPPC (middle column), or DSPC (right-hand column) in different bolalipid/phospholipid ratios: 1:10 (A–C), 1:5 (D–F), 1:2 (G–I), and 1:1 (K–M). Samples were prepared at 22 °C and stained with uranyl acetate before drying. The bar corresponds to 100 nm.

membranes of phosphatidylcholines, disk-like structures are the dominant aggregate form. We can only speculate, whether both types of lipid molecules are randomly distributed within the disks or not. It is also conceivable that a partial demixing occurs inside the disk and that bolalipid molecules are accumulated at the rim of this disk stabilizing them against fusion into larger aggregates. With increasing amount of bolalipid, micellar structures became dominant. It seems conceivable that, in the case of 1:1 and 1:2 mixtures, either both components are not homogeneously distributed within the aggregates or two different species of aggregates exists, bolalipid-rich ones and phospholipid-rich ones (see for example Figure 6H or I, showing two different sizes of micelles). This is in accordance with the DSC measurements shown above, where a very broad peak or two peaks are observed in the mixture of, e.g., PC-C18pPhC18-PC and DMPC (Figure 5A) or DPPC (Figure 5C).

Similar disk-like assemblies (bicelles) were also reported for phospholipid mixtures, for example in DPPC/DHPC systems [49], or for mixtures of phospholipids with other amphiphilic substances, e.g., in PEG-stabilized bilayer systems [50,51], for phospholipids with membrane scaffold proteins [52,53] or in combination with copolymers [54,55], or for DPPC in mixture with a T-shaped amphiphile [56].

FTIR spectroscopy and SAXS of PC-C18pPhC18-PC/DPPC (1:1)

To support the finding of disk-like aggregates seen by TEM, one mixture was exemplarily analyzed by means of FTIR and SAXS. Temperature dependent FTIR measurements were used to clarify the question whether the transition of both PC-C18pPhC18-PC and DPPC happen simultaneously. To distinguish between both components, DPPC with fully deuterated alkyl chains (d_{62}-DPPC) was used and the change in the position of the stretching vibrational band of CH_2 (from the bolalipid; Figure 7 red symbols) and CD_2 (from the phospholipid; Figure 7 green symbols) was followed. The deuteration of alkyl chains in phospholipids usually causes a shift of the main transition by about 5 K to lower temperatures, as shown by Petersen et al. [57].

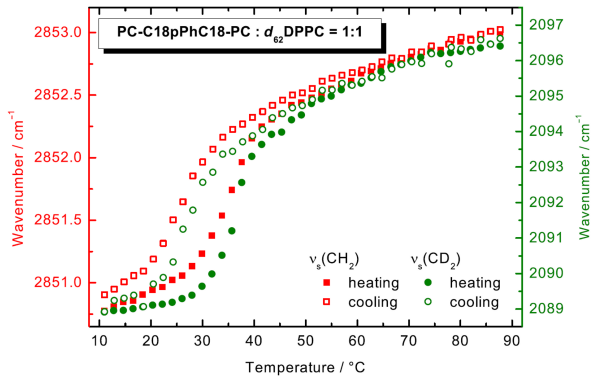

Figure 7: FTIR spectroscopic data (symmetric CH_2 stretching vibration: red squares, right axis; symmetric CD_2 stretching vibration: green circles, left axis) of an equimolar mixture of PC-C18pPhC18-PC:d_{62}-DPPC (c = 50 mg mL^{-1} in phosphate buffer, pH 7.6, heating: filled symbols, cooling: open symbols).

At T = 10.9 °C, the frequency of $\nu_s(CH_2)$ is at 2850.8 cm^{-1}, which is comparable to the frequency of $\nu_s(CH_2)$ of the pure PC-C18pPhC18-PC at T = 30 °C, above the first transition in DSC (see above). Hence, the alkyl chains of the bolalipid contain a small amount of *gauche* conformers. The frequency of $\nu_s(CD_2)$ is at 2088.9 cm^{-1} at T = 10.9 °C, indicating ordered alkyl chains in all-*trans* conformation for the deuterated phospholipid. With increasing temperature, the frequencies of both band increase with a distinct jump to 2852.3 cm^{-1} and 2093.9 cm^{-1} at 43.4 °C and further to 2853.0 cm^{-1} and 2096.4 cm^{-1} at 87.7 °C. This increase is attributed to an increased amount of *gauche* conformers within both deuterated and non-deuterated alkyl chains. However, the transition from the gel phase to the liquid-crystalline phase seems to be slightly different for both components and did not occur simultaneously. The increase in frequency for $\nu_s(CH_2)$ (bolalipid) starts at lower temperature than for $\nu_s(CD_2)$ (phospholipid), which stays nearly constant up to 30 °C. One explanation for this behaviour could be that at low temperatures, the phospholipid forms bilayer fragments that are stabilized by bolalipid molecules, possibly in a U-shaped conformation, at the rim of the disk.

To analyze the aggregates in more detail, SAXS measurements at different temperatures were performed (Figure 8A). Scattering data do not show sharp diffraction maxima, which are observed for binary DPPC/water mixtures at similar temperature and concentration range [34]. The transformation from sharp maxima to broad ones points on structural changes of the lipid system from multilamellar objects for pure DPPC to separated lamellae for the PC-C18pPhC18-PC:DPPC mixtures. Only at T = 50 °C, a very small diffraction peak has been observed (see arrow in Figure 8A), which corresponds to a lamellar repeat distance (bilayer thickness plus an interlamellar water layer) of about 67 Å.

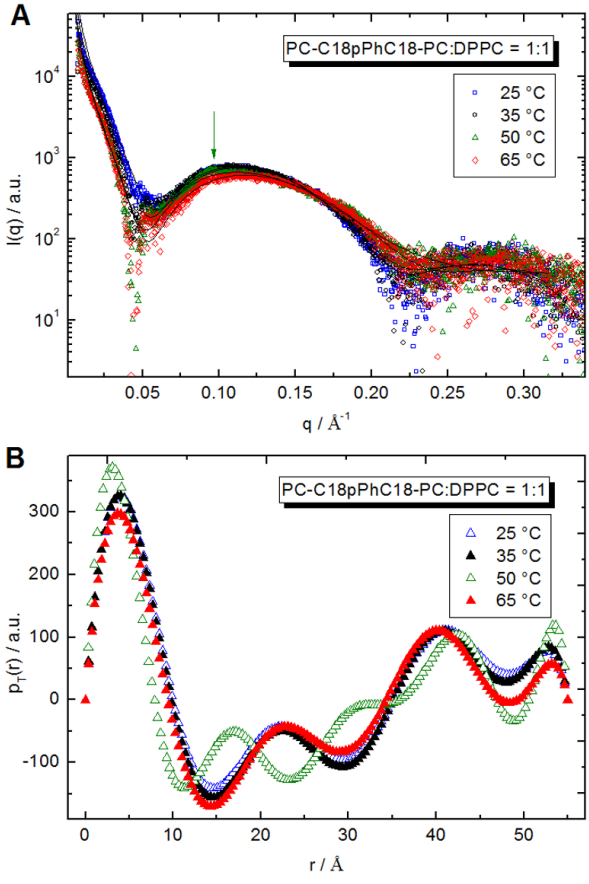

Figure 8: (A) SAXS diffractograms of an equimolar mixture of PC-C18pPhC18-PC/DPPC (c = 10 mg mL^{-1}, scattered data) in phosphate buffer (pH 7.6) at different temperatures and IFT fits (solid lines). The arrow points to diffraction maximum (at T = 50 °C) of multilayer object. (B) Pair distance distribution function of thickness of discs obtained at different temperatures of an equimolar mixture of PC-C18pPhC18-PC/DPPC (c = 10 mg mL^{-1}) in phosphate buffer (pH 7.6).

Firstly, the slope at low q-range has been determined as −2, which corresponds to the scattering from flat objects, i.e., aggregates, where the size of two dimensions is much larger than the third dimension. In order to get structural information such as a distribution of scattering length density along the smaller dimension, IFT analysis in approximation of infinitely thin objects has been applied [45,46]. The thickness pair distance distribution function $p_T(r)$ describes the scattering intensity via:

$$d\Sigma(q)/d\Omega = \left(\frac{2\pi}{q^2}\right)\pi\int_0^\infty p_T(r)\cos(qr)dr \qquad (1)$$

The $p_T(r)$ function is connected with the scattering contrast between object and solvent and is written as

$$p_T(r) = \frac{c}{2\pi M_s}\int \Delta\rho(r')\Delta\rho(r+r')dr' \qquad (2)$$

where r is the coordinate in the direction normal to the surface of the disk-like objects and M_S is connected with mass per surface unit. IFT satisfactorily describes our experimental data (solid lines in Figure 8A). The $p_T(r)$ functions for the equimolar PC-C18pPhC18-PC/DPPC mixtures versus temperature are shown in Figure 8B. The negative values of $p_T(r)$ in the intermediate r-range could be explained by different sign of the scattering contrast for alkyl chains (positive) and polar groups (negative) of DPPC in water.

IFT analysis requires as input parameter the maximal size of objects, whose numerical solution is searched for. In present analysis, the maximal thickness of disks is needed. To get a sufficient fit of experimental data and a stable shape of $p_T(r)$ function, a maximal thickness of 55 Å has been applied. The comparison with pure DPPC bilayers (without additives) confirms that an addition of PC-C18pPhC18-PC does not change the thickness of the DPPC bilayer [58]. Also, a significant decrease of bilayer thickness with increasing temperature was not observed; only a small change for large r (region of polar groups) for 65 °C has been detected. The difference found for 50 °C can be connected that in these conditions also some multilamellar objects are formed.

Conclusion

The PC-C18pPhC18-PC, a long-chain, phenylene-modified bolalipid, self-assembles at room temperature into nanofibres, which leads to a gelation of the suspension. With increasing temperature, the stiff fibres transform into more flexible ones. This transformation is accompanied with an endothermic transition observed in DSC measurements. The existence of fibrous aggregates after the first DSC transition peak is remarkable since the analogue bolalipid, PC-C17pPhC17-PC with a slightly shorter alkyl chain, shows a direct transformation from nanofibres into small micelles. For PC-C18pPhC18-PC, small micellar aggregates are only observed after the second transition observed by DSC. Hence, the elongation of the alkyl chain for two methylene units is sufficient to stabilize the flexible fibres above the first transition via van-der-Waals interactions.

The mixing of PC-C18pPhC18-PC with bilayer-forming phosphatidylcholines (DMPC, DPPC, or DSPC) leads in most cases to the formation of small elongated micelles, bilayer fragments, or disk-like aggregates. However, an increased thermal stability of these aggregates could not be observed. For PC-C18pPhC18-PC:DPPC mixtures with an excess of phospholipid, the formation of virtually uniform, disk-like aggregates is observed. The arrangement of both lipid components inside these disks is not fully understood, but it seems very likely that a partial demixing occurs and that the rims of the bilayer disks are stabilized by PC-C18pPhC18-PC molecules in a U-shaped conformation.

Experimental

Substances

DMPC and DPPC were obtained from Lipoid KG (Ludwigshafen, Germany). DSPC was purchased from Sygena AG (Switzerland). d_{62}-DPPC was obtained from Avanti Polar Lipids (Alabaster, AL, USA). The synthetic procedure and the analytical data of the newly prepared bolalipid PC-C18pPhC18-PC are described in detail in Supporting Information File 1.

Methods

Sample preparation

In a similar manner to a procedure from [34], the appropriate amount of the bolalipid PC-C18pPhC18-PC was suspended in H_2O (Milli-Q). Homogeneous suspensions were obtained by heating to 90 °C and vortexing. Binary lipid mixtures were prepared from lipid stock solutions in $CHCl_3$/MeOH (2/1, v/v) as solvent by mixing appropriate volumes of the stock solutions. The organic solvent was then removed in a stream of N_2. The resulting lipid films were kept in an evacuated flask for 24 h to remove residual traces of solvent. The suspensions were then prepared by adding a certain volume of aqueous phosphate buffer (10 mM, pH 7.6) to obtain a total lipid concentration of 3 mM. The samples were vigorously vortexed at 60 °C to obtain a homogeneous suspension.

Transmission electron microscopy (TEM)

The samples were prepared by spreading 5 µL of the bolalipid suspension (c = 0.05 mg mL^{-1} in case of pure bolalipid, c = 60 µM in case of lipid mixtures) onto a copper grid coated with a Formvar film. After 1 min, excess liquid was blotted off

with filter paper and 5 µL of 1% aqueous uranyl acetate solution were placed onto the grid and drained off after 1 min. Specimens prepared below ambient temperature ($T \approx 7$ °C) were dried for 2 days at this temperature and kept in an desiccator at ambient temperature. Specimens, which were prepared in a modified drying oven above ambient temperature, were further dried for 1 h at the appropriate temperature and finally kept in an desiccator at room temperature. All specimens were examined with a Zeiss EM 900 transmission electron microscope (Carl Zeiss Microscopy GmbH, Jena, Germany).

Differential scanning calorimetry (DSC)

DSC measurements were performed using a MicroCal VP-DSC differential scanning calorimeter (MicroCal Inc. Northampton, MA, USA). Before the measurements, the sample suspension and the water (or phosphate buffer) used as a reference were degassed under vacuum while stirring. A heating rate of 60 K h^{-1} was used, and the measurements were performed in the temperature interval from 5 °C to 95 °C. To check the reproducibility, three consecutive scans were recorded for each sample. The water–water and buffer–buffer baseline, respectively, was subtracted from the thermogram of the sample, and the DSC scans were evaluated using MicroCal Origin 8.0 software.

Fourier-transform infrared spectroscopy (FTIR)

Infrared spectra were collected using a Bruker Vector 22 Fourier transform spectrometer with DTGS detector operating at 2 cm^{-1} resolution. The bolalipid suspension (PC-C18pPhC18-PC: c = 50 mg mL^{-1} in H_2O; PC-C18pPhC18-PC/d_{62}-DPPC, 1:1, n/n, c = 100 mg mL^{-1} in phosphate buffer 300 mM, pH 7.7) was placed between two CaF_2 windows, separated by a 6 µm spacer. IR spectra were recorded in steps of 2 K in the temperature range 9 °C to 71 °C or 9 °C to 89 °C. After an equilibration time of 8 min, 64 scans were recorded and accumulated. The corresponding spectra of the solvent (H_2O or D_2O) were subtracted from the sample spectra using the OPUS software supplied by Bruker.

Small angle neutron scattering (SANS)

SANS measurements were made on the steady state reactor based pin-hole SANS instrument Quokka [59] which is found on a cold guide at the Australian Nuclear Science and Technology Organization's (ANSTO) research reactor OPAL (Lucas Heights, Australia). Sample (PC-C18pPhC18-PC, c = 1 mg mL^{-1} in D_2O) was placed in cylindrical quartz cuvettes of path length 2 mm. SANS spectra were recorded on a position sensitive detector consisting of 192 × 192 pixels (5 × 5 mm^2) at 3 sample-to-detector distance 1.3, 6, and 12 m using neutrons of wavelength, λ = 5.0 Å ($\Delta\lambda/\lambda$ = 10%). After correcting the raw data for the sensitivity of each detector pixel, masking the beam stop shadow, subtracting backgrounds consisting of the sample buffer in identical samples cells and normalizing to the empty beam intensity the radially averaged isotropic scattering data from each sample-to-detector distance were joined to produce a continuous q-range of 0.009 to 0.7 $Å^{-1}$, where $q = 4\pi \times \sin(2\theta)/\lambda$ and θ is the scattering angle. This was achieved using macros modified for the program IgorPro (version 6.34, WaveMetrics, Inc. 2013) from those macros written for the NIST Center for Neutron Research (Gaitherburg, USA) SANS instruments [60].

Small angle X-ray scattering (SAXS)

SAXS experiments were performed at the P12 BioSAXS beamline of the European Molecular Biology Laboratory (EMBL) at the storage ring PETRA III of the Deutsche Elektronen Synchrotron (DESY, Hamburg, Germany) using a Pilatus 2M detector (1475 × 1679 pixels; Dectris, Switzerland) and synchrotron radiation with a wavelength λ = 1 Å. The sample-to-detector distance was 4 m, allowing for measurements in the q-range interval from 0.75 $Å^{-1}$ to 5 $Å^{-1}$. The q-range was calibrated using the diffraction patterns of silver behenate. The experimental data were normalized to the incident beam intensity, corrected for non-homogeneous detector response, and the background scattering of the aqueous buffer was subtracted. Sample (PC-C18pPhC18-PC/DPPC, 1:1, n/n, c = 10 mg mL^{-1} in phosphate buffer pH 7.4) has been placed in 1 mm glass capillaries. Temperature has been controlled by Linkam heating stage HFSX 350 (Surrey, UK) with accuracy ± 0.1 °C. Twenty consecutive frames (each 0.05 s) comprising the measurement of the solvent (phosphate buffer pH 7.4) and sample were performed. In order to verify that no artefacts as a result of radiation damage occurred, all scattering curves of a recorded dataset were compared to a reference measurement (typically the first exposure) and finally integrated by automated acquisition program given by Franke et al. [61].

Supporting Information

Supporting Information File 1

Experimental procedures, characterization data for synthesized compounds and further SANS data.
[http://www.beilstein-journals.org/bjoc/content/supplementary/1860-5397-13-99-S1.pdf]

Acknowledgments

This work was financially supported by grants from the Deutsche Forschungsgemeinschaft (DFG): project DR 1024/1-1. The support of Dr. Gerd Hause (Biocenter, MLU Halle-Wittenberg) by providing us access to the electron microscope facility and the support of Dr. Clement Blanchet (EMBL, Hamburg) during SAXS measurements are greatly appreciated.

References

1. Fuhrhop, J.-H.; Wang, T. *Chem. Rev.* **2004,** *104,* 2901–2938. doi:10.1021/cr030602b
2. Langworthy, T. A. *Biochim. Biophys. Acta, Lipids Lipid Metab.* **1977,** *487,* 37–50. doi:10.1016/0005-2760(77)90042-X
3. De Rosa, M.; Esposito, E.; Gambacorta, A.; Nicolaus, B.; Bu'Lock, J. D. *Phytochemistry* **1980,** *19,* 827–831. doi:10.1016/0031-9422(80)85120-X
4. Gambacorta, A.; Gliozzi, A.; De Rosa, M. *World J. Microbiol. Biotechnol.* **1995,** *11,* 115–131. doi:10.1007/BF00339140
5. Woese, C. R.; George, E. F. *Proc. Natl. Acad. Sci. U. S. A.* **1977,** *74,* 5088–5090. doi:10.1073/pnas.74.11.5088
6. Koch, R.; Zablowski, P.; Spreinat, A.; Antranikian, G. *FEMS Microbiol. Lett.* **1990,** *71,* 21–26. doi:10.1111/j.1574-6968.1990.tb03792.x
7. Woese, C. R.; Magrum, L. J.; Fox, G. E. *J. Mol. Evol.* **1978,** *11,* 245–252. doi:10.1007/BF01734485
8. Baumeister, W.; Lembcke, G. *J. Bioenerg. Biomembr.* **1992,** *24,* 567–575. doi:10.1007/BF00762349
9. Lewalter, K.; Müller, V. *Biochim. Biophys. Acta, Bioenerg.* **2006,** *1757,* 437–445. doi:10.1016/j.bbabio.2006.04.027
10. Cornell, B. A.; Braach-Maksvytis, V. L. B.; King, L. G.; Osmann, P. D. J.; Raguse, B.; Wieczorek, L.; Pace, R. J. *Nature* **1997,** *387,* 580–583. doi:10.1038/42432
11. Bakowsky, U.; Rothe, U.; Antonopoulos, E.; Martini, T.; Henkel, L.; Freisleben, H.-J. *Chem. Phys. Lipids* **2000,** *105,* 31–42. doi:10.1016/S0009-3084(99)00131-0
12. Benvegnu, T.; Réthoré, G.; Brard, M.; Richter, W.; Plusquellec, D. *Chem. Commun.* **2005,** 5536–5538. doi:10.1039/b511440c
13. Brown, D. A.; Venegas, B.; Cooke, P. H.; English, V.; Chong, P. L.-G. *Chem. Phys. Lipids* **2009,** *159,* 95–103. doi:10.1016/j.chemphyslip.2009.03.004
14. Jain, N.; Arntz, Y.; Goldschmidt, V.; Duportail, G.; Mély, Y.; Klymchenko, A. S. *Bioconjugate Chem.* **2010,** *21,* 2110–2118. doi:10.1021/bc100334t
15. Nuraje, N.; Bai, H.; Su, K. *Prog. Polym. Sci.* **2013,** *38,* 302–343. doi:10.1016/j.progpolymsci.2012.09.003
16. Fuhrhop, J. H.; Liman, U.; Koesling, V. *J. Am. Chem. Soc.* **1988,** *110,* 6840–6845. doi:10.1021/ja00228a037
17. Moss, R. A.; Li, G.; Li, J.-M. *J. Am. Chem. Soc.* **1994,** *116,* 805–806. doi:10.1021/ja00081a066
18. Brard, M.; Richter, W.; Benvegnu, T.; Plusquellec, D. *J. Am. Chem. Soc.* **2004,** *126,* 10003–10012. doi:10.1021/ja049805n
19. Jacquemet, A.; Barbeau, J.; Lemiègre, L.; Benvegnu, T. *Biochimie* **2009,** *91,* 711–717. doi:10.1016/j.biochi.2009.01.006
20. Mahmoud, G.; Jedelská, J.; Strehlow, B.; Bakowsky, U. *Eur. J. Pharm. Biopharm.* **2015,** *95,* 88–98. doi:10.1016/j.ejpb.2015.04.009
21. Uhl, P.; Helm, F.; Hofhaus, G.; Brings, S.; Kaufman, C.; Leotta, K.; Urban, S.; Haberkorn, U.; Mier, W.; Fricker, G. *Eur. J. Pharm. Biopharm.* **2016,** *103,* 159–166. doi:10.1016/j.ejpb.2016.03.031
22. Leriche, G.; Cifelli, J. L.; Sibucao, K. C.; Patterson, J. P.; Koyanagi, T.; Gianneschi, N. C.; Yang, J. *Org. Biomol. Chem.* **2017,** *15,* 2157–2162. doi:10.1039/C6OB02832B
23. Meister, A.; Blume, A. *Curr. Opin. Colloid Interface Sci.* **2007,** *12,* 138–147. doi:10.1016/j.cocis.2007.05.003
24. Köhler, K.; Förster, G.; Hauser, A.; Dobner, B.; Heiser, U. F.; Ziethe, F.; Richter, W.; Steiniger, F.; Drechsler, M.; Stettin, H.; Blume, A. *J. Am. Chem. Soc.* **2004,** *126,* 16804–16813. doi:10.1021/ja046537k
25. Köhler, K.; Förster, G.; Hauser, A.; Dobner, B.; Heiser, U. F.; Ziethe, F.; Richter, W.; Steiniger, F.; Drechsler, M.; Stettin, H.; Blume, A. *Angew. Chem., Int. Ed.* **2004,** *43,* 245–247. doi:10.1002/anie.200351731
26. Meister, A.; Drescher, S.; Mey, I.; Wahab, M.; Graf, G.; Garamus, V. M.; Hause, G.; Mögel, H.-J.; Janshoff, A.; Dobner, B.; Blume, A. *J. Phys. Chem. B* **2008,** *112,* 4506–4511. doi:10.1021/jp710119j
27. Wahab, M.; Schiller, P.; Schmidt, R.; Mögel, H.-J. *Langmuir* **2010,** *26,* 2979–2982. doi:10.1021/la903414d
28. Meister, A.; Köhler, K.; Drescher, S.; Dobner, B.; Karlsson, G.; Edwards, K.; Hause, G.; Blume, A. *Soft Matter* **2007,** *3,* 1025–1031. doi:10.1039/B703152A
29. Graf, G.; Drescher, S.; Meister, A.; Garamus, V. M.; Dobner, B.; Blume, A. *J. Colloid Interface Sci.* **2013,** *393,* 143–150. doi:10.1016/j.jcis.2012.10.017
30. Drescher, S.; Meister, A.; Graf, G.; Hause, G.; Blume, A.; Dobner, B. *Chem. – Eur. J.* **2008,** *14,* 6796–6804. doi:10.1002/chem.200800033
31. Blume, A.; Drescher, S.; Meister, A.; Graf, G.; Dobner, B. *Faraday Discuss.* **2013,** *161,* 193–213. doi:10.1039/C2FD20102J
32. Drescher, S.; Helmis, K.; Langner, A.; Dobner, B. *Monatsh. Chem.* **2010,** *141,* 339–349. doi:10.1007/s00706-010-0255-y
33. Heiser, U. F.; Wolf, R.; Dobner, B. *Chem. Phys. Lipids* **1997,** *90,* 25–30. doi:10.1016/S0009-3084(97)00073-X
34. Drescher, S.; Meister, A.; Garamus, V. M.; Hause, G.; Garvey, C. J.; Dobner, B.; Blume, A. *Eur. J. Lipid Sci. Technol.* **2014,** *116,* 1205–1216. doi:10.1002/ejlt.201300387
35. Drescher, S.; Lechner, B.-D.; Garamus, V. M.; Almásy, L.; Meister, A.; Blume, A. *Langmuir* **2014,** *30,* 9273–9284. doi:10.1021/la501160s
36. Drescher, S.; Sonnenberger, S.; Meister, A.; Blume, A.; Dobner, B. *Monatsh. Chem.* **2012,** *143,* 1533–1543. doi:10.1007/s00706-012-0833-2
37. Drescher, S.; Becker, S.; Dobner, B.; Blume, A. *RSC Adv.* **2012,** *2,* 4052–4054. doi:10.1039/c2ra20411h
38. Drescher, S.; Meister, A.; Blume, A.; Karlsson, G.; Almgren, M.; Dobner, B. *Chem. – Eur. J.* **2007,** *13,* 5300–5307. doi:10.1002/chem.200601866
39. Menger, F. M.; Chen, X. Y.; Brocchini, S.; Hopkins, H. P.; Hamilton, D. *J. Am. Chem. Soc.* **1993,** *115,* 6600–6608. doi:10.1021/ja00068a017
40. Meister, A.; Drescher, S.; Karlsson, G.; Hause, G.; Baumeister, U.; Hempel, G.; Garamus, V. M.; Dobner, B.; Blume, A. *Soft Matter* **2010,** *6,* 1317–1324. doi:10.1039/b923066a
41. Mantsch, H. H.; McElhaney, R. N. *Chem. Phys. Lipids* **1991,** *57,* 213–226. doi:10.1016/0009-3084(91)90077-O
42. Mendelsohn, R.; Moore, D. J. *Chem. Phys. Lipids* **1998,** *96,* 141–157. doi:10.1016/S0009-3084(98)00085-1
43. Meister, A.; Drescher, S.; Garamus, V. M.; Karlsson, G.; Graf, G.; Dobner, B.; Blume, A. *Langmuir* **2008,** *24,* 6238–6246. doi:10.1021/la800166h
44. Meister, A.; Bastrop, M.; Koschoreck, S.; Garamus, V. M.; Sinemus, T.; Hempel, G.; Drescher, S.; Dobner, B.; Richtering, W.; Huber, K.; Blume, A. *Langmuir* **2007,** *23,* 7715–7723. doi:10.1021/la7003479
45. Glatter, O. *J. Appl. Crystallogr.* **1977,** *10,* 415–421. doi:10.1107/S0021889877013879
46. Pedersen, J. S. *Adv. Colloid Interface Sci.* **1997,** *70,* 171–210. doi:10.1016/S0001-8686(97)00312-6

47. Denkinger, P.; Burchard, W. *J. Polym. Sci., Part B: Polym. Phys.* **1991,** *29,* 589–600. doi:10.1002/polb.1991.090290508
48. Blume, A.; Drescher, S.; Graf, G.; Köhler, K.; Meister, A. *Adv. Colloid Interface Sci.* **2014,** *208,* 264–278. doi:10.1016/j.cis.2014.01.002
49. Rubio, L.; Rodríguez, G.; Alonso, C.; López-Iglesias, C.; Cócera, M.; Coderch, L.; De la Maza, A.; Parra, J. L.; López, O. *Soft Matter* **2011,** *7,* 8488–8497. doi:10.1039/c1sm05692a
50. Johansson, E.; Engvall, C.; Arfvidsson, M.; Lundahl, P.; Edwards, K. *Biophys. Chem.* **2005,** *113,* 183–192. doi:10.1016/j.bpc.2004.09.006
51. Zetterberg, M. M.; Reijmar, K.; Pränting, M.; Engström, Å.; Andersson, D. I.; Edwards, K. *J. Controlled Release* **2011,** *156,* 323–328. doi:10.1016/j.jconrel.2011.08.029
52. Denisov, I. G.; Grinkova, Y. V.; Lazarides, A. A.; Sligar, S. G. *J. Am. Chem. Soc.* **2004,** *126,* 3477–3487. doi:10.1021/ja0393574
53. Bayburt, T. H.; Sligar, S. G. *FEBS Lett.* **2010,** *584,* 1721–1727. doi:10.1016/j.febslet.2009.10.024
54. Lee, S. C.; Knowles, T. J.; Postis, V. L. G.; Jamshad, M.; Parslow, R. A.; Lin, Y.-p.; Goldman, A.; Sridhar, P.; Overduin, M.; Muench, S. P.; Dafforn, T. R. *Nat. Protoc.* **2016,** *11,* 1149–1162. doi:10.1038/nprot.2016.070
55. Oluwole, A. O.; Danielczak, B.; Meister, A.; Babalola, J. O.; Vargas, C.; Keller, S. *Angew. Chem., Int. Ed.* **2017,** *56,* 1919–1924. doi:10.1002/anie.201610778
56. Scholtysek, P.; Achilles, A.; Hoffmann, C.-V.; Lechner, B.-D.; Meister, A.; Tschierske, C.; Saalwächter, K.; Edwards, K.; Blume, A. *J. Phys. Chem. B* **2012,** *116,* 4871–4878. doi:10.1021/jp207996r
57. Petersen, N. O.; Kroon, P. A.; Kainosho, M.; Chan, S. I. *Chem. Phys. Lipids* **1975,** *14,* 343–349. doi:10.1016/0009-3084(75)90071-7
58. Nagle, J. F.; Zhang, R.; Tristram-Nagle, S.; Sun, W.; Petrache, H. I.; Suter, R. M. *Biophys. J.* **1996,** *70,* 1419–1431. doi:10.1016/S0006-3495(96)79701-1
59. Gilbert, E. P.; Schulz, J. C.; Noakes, T. J. *Phys. B (Amsterdam, Neth.)* **2006,** *385–386,* 1180–1182. doi:10.1016/j.physb.2006.05.385
60. Kline, S. R. *J. Appl. Crystallogr.* **2006,** *39,* 895–900. doi:10.1107/S0021889806035059
61. Franke, D.; Kikhney, A. G.; Svergun, D. I. *Nucl. Instrum. Methods Phys. Res., Sect. A* **2012,** *689,* 52–59. doi:10.1016/j.nima.2012.06.008

License and Terms

BEILSTEIN JOURNAL OF ORGANIC CHEMISTRY

Total syntheses of the archazolids: an emerging class of novel anticancer drugs

Stephan Scheeff and Dirk Menche*

Review

Open Access

Address:
Kekulé-Institut für Organische Chemie und Biochemie, Universität Bonn, Gerhard-Domagk-Strasse 1, 53121 Bonn, Germany

Email:
Dirk Menche* - dirk.menche@uni-bonn.de

* Corresponding author

Keywords:
anticancer agent; medicinal chemistry polyketides; synthetic methodology; total synthesis

Beilstein J. Org. Chem. **2017,** *13,* 1085–1098.
doi:10.3762/bjoc.13.108

Received: 07 March 2017
Accepted: 09 May 2017
Published: 07 June 2017

This article is part of the Thematic Series "Lipids: fatty acids and derivatives, polyketides and isoprenoids".

Guest Editor: J. S. Dickschat

Abstract

V-ATPase has recently emerged as a promising novel anticancer target based on extensive in vitro and in vivo studies with the archazolids, complex polyketide macrolides which present the most potent V-ATPase inhibitors known to date, rendering these macrolides important lead structures for the development of novel anticancer agents. The limited natural supply of these metabolites from their myxobacterial source renders total synthesis of vital importance for the further preclinical development. This review describes in detail the various tactics and strategies employed so far in archazolid syntheses that culminated in three total syntheses and discusses the future synthetic challenges that have to be addressed.

Introduction

The complex structures of polyketides continues to be a great challenge for synthetic chemists and has also been a key driver for the development of new methodologies [1-9]. In many cases, total synthesis is of critical importance to enhance the supply of these often scarce metabolites and even complex polyketides have been prepared on an industrial scale [10,11]. These natural products are also valuable molecular probes for the discovery and evaluation of novel biological targets and pathways [12,13]. Vacuolar-type ATPases (V-ATPases) are heteromultimeric proton translocating proteins that are localized in a multitude of eukaryotic membranes [14-16] that have been known as key mediators in a variety of biochemical pathways. They are responsible for a variety of important cellular functions, including pH-control [17,18], membrane trafficking, protein degradation, release of neurotransmitters [18], urinary acidification [19], bone resorption [20], sperm maturation [21], cholesterol biosynthesis [22] and cytokine secretion [23]. In recent years, a key role of these multimeric enzymes also in cancer development and progression was discovered and has been increasingly unraveled. The archazolids, polyketide

macrolides from the myxobacterium *Archangium gephyra*, have played a key role in these studies. They present the most potent V-ATPase inhibitors known to date with activities in the low nanomolar range [24,25], by binding to the functional transmembrane subunit c [26,27], and display highly potent growth-inhibitory activities against a range of cancer cell lines, both in vitro and in vivo [23,28-34]. In detail, archazolid inhibition of V-ATPase abrogates tumor metastasis via repression of endocytic activation [28], leads to impaired cathepsin B activation in vivo [30], modulates anoikis resistance and metastasis of cancer cells [31], overcomes trastuzumab resistance of breast cancers [32], blocks iron metabolism and thereby mediates therapeutic effects in breast cancers [33], and plays a role in tumor sensitizing in the context of the MDM2 antagonist nutlin-3a [34]. Based on these studies V-ATPases have been increasingly emerging as an extremely promising novel anticancer target [26,27,35-37] and the archazolids have become important lead structures for the development of novel anticancer agents.

As shown in Scheme 1 for the most prominent representatives archazolid A (**1**) and B (**2**) [38-40], their unique architectures are characterized by a 24-membered macrolactone ring with seven alkenes, including a characteristic (*Z*,*Z*,*E*)-triene, a thiazole side chain and a characteristic sequence of eight methyl and hydroxy-bearing stereocenters.

Synthetic chemistry is of key importance to enhance the supply of these scarce polyketides to fully evaluate the biological potential and develop them as potential drug candidates. The important biological properties in combination with their limited natural supply as well as their intriguing molecular architectures and initially unknown stereochemistry, have rendered the archazolids as highly attractive synthetic targets and so far, three total syntheses have been reported by the groups of Menche and Trauner [41-43]. Furthermore several fragment syntheses as well as methodological studies to access key structural elements have been published in the last years [44-54]. Recently, the focus has been increasingly shifted towards analog development and SAR studies [49,55-58] and the group of O'Neil has been targeting dihydroarchazolid B (**3**) as a potentially equipotent structurally simplified derivative [45,46,48]. This review covers the various tactics and strategies, employed by the Menche, Trauner and O'Neil group in archazolid syntheses and discusses the challenges for the development of a scalable route.

Review

The first total synthesis of archazolids A and B were independently developed by the Menche group and the group of Trauner in 2007 by completely independent routes. In 2009, a second total synthesis of archazolid B has been described again by the Menche group following a sequence that was related to their archazolid A synthesis.

Menche's retrosynthetic analysis and strategy

As a prelude to initiating a synthetic campaign directed towards the archazolids the Menche group first elucidated the full stereochemistry and three dimensional conformation of the archazolids by NMR methods, molecular modelling and chemical derivatizations [59,60]. During these studies, they became aware that C2–C5 diene of acyclic analogs would be very labile towards isomerization. However, such processes would be suppressed in the macrolide natural products, presumably due to conformational factors. In contrast, the *Z*,*Z*,*E*-triene system at northern part of the target molecule (i.e., C9 to C14) was stable,

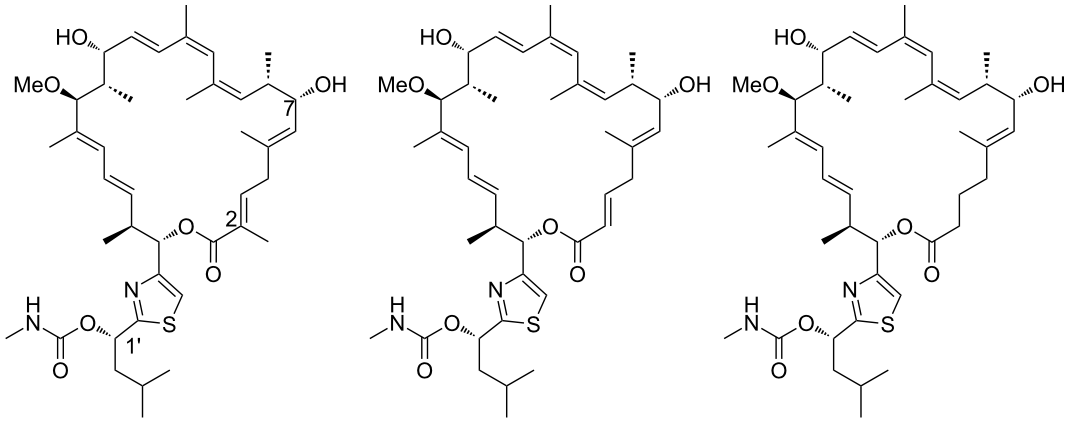

1: Archazolid A
Menche et al. [41]

2: Archazolid B
Trauner et al. [43]
Menche et al. [42]

3: Dihydroarchazolid B
Fragments:
O'Neil et al. [45,46,48]

Scheme 1: Molecular structures of the archazolids.

also in an acyclic state, presumably due to distortion of the conjugated system due to constraints exerted by the methyl groups at C10 and C12. Based on this analysis, their synthetic plan was to first build the triene, while the C2–C5 fragment should be constructed directly before or during ring closure as shown in Scheme 2. Consequently, they first planned to connect the north-eastern fragment **5** with the propionate unit **4** by a suitable olefination strategy. Subsequently, for connecting the resulting fragment to the thiazole subunit **6** a Heck reaction was envisioned as part of studies advancing this type of Palladium-catalyzed coupling strategies in complex target synthesis [61-66]. Finally, a HWE-macrocyclization was planned which would likewise set the labile C2–C5 diene and thus concomitantly stabilize this functionality by macrocyclic constraints.

Menche's total synthesis of archazolid A

Synthesis of the north-eastern fragment

As shown in Scheme 3, the construction of the north-eastern fragment **5** relied on a boron-mediated *anti*-aldol reaction [67] of lactate-derived ethyl ketone **13** with aldehyde **12**, which in turn was available from aldehyde **9** by HWE olefination. This Paterson aldol reaction and related aldol reactions, which have been amply used by the Menche group [68-70], proceeded with excellent yield and selectivity. The resulting β-hydoxyketone **14**

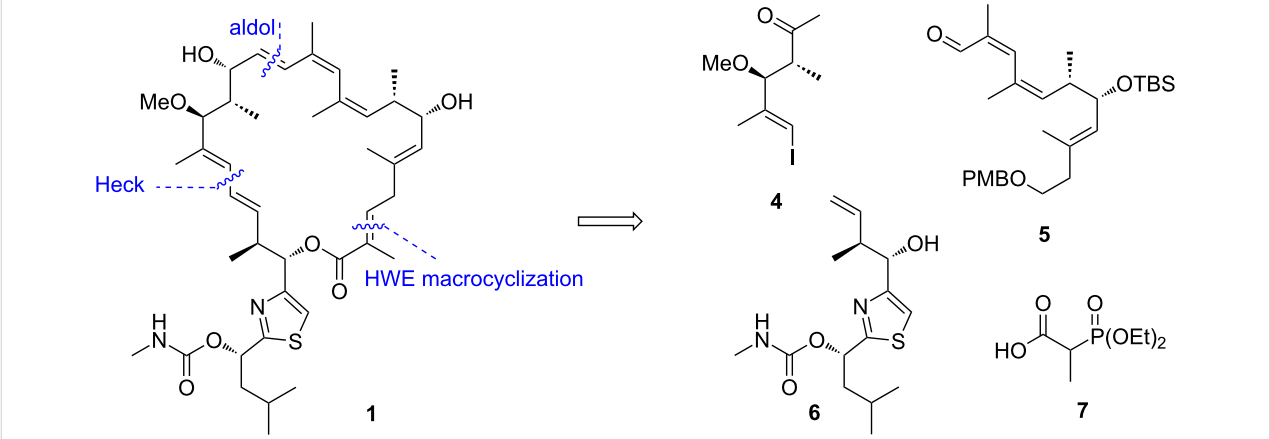

Scheme 2: Retrosynthetic analysis of archazolid A by the Menche group.

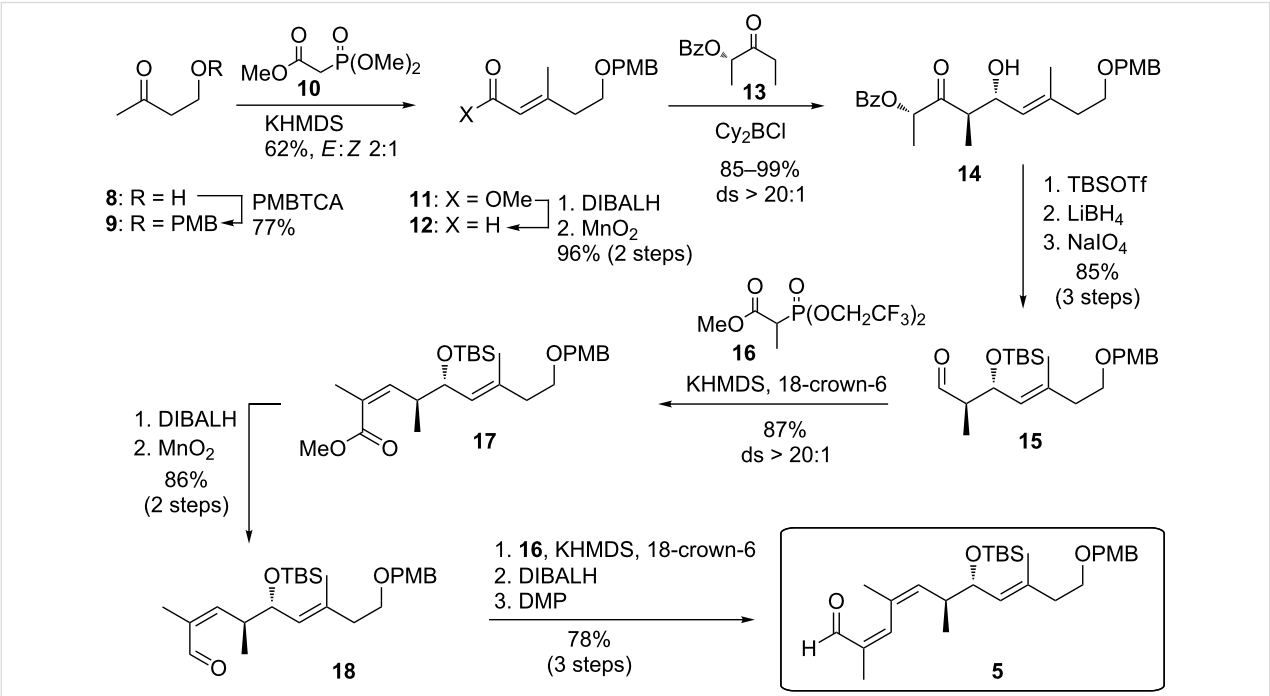

Scheme 3: Synthesis of north-eastern fragment **5** through a Paterson *anti*-aldol addition and multiple Still–Gennari olefinations.

was then protected as TBS ether and converted to aldehyde **15** by reductive removal of the benzoate group and periodate cleavage. Notably, depending on the choice of protection group, deprotection and further oxidation with $NaIO_4$ may be observed, a procedure that was further studied by the group [71]. The two vicinal *Z*-alkenes were then installed by two consecutive Still–Gennari olefinations [72] with aldehydes **15** and **18**. In both cases coupling with the Still–Gennari reagent **16** gave **17** and after reduction the final building block **5** was formed in high yields and selectivity. While the overall sequence towards **5** consequently required twice a two-step adaption of the oxidation state which renders this route quite lengthy, the authors argue that the robustness, facile conduction and scalability of each step was very high and made them decide to stick to this sequence as compared to likewise tested alternatives.

Synthesis of the north-western fragment

For the construction of the north-western fragment **4** the Menche group opted to first install the terminal *E*-configured vinyl iodide. While appearing to be a simple problem, quite some efforts had to be invested, before acid **21** could be efficiently obtained as shown in Scheme 4. Finally, after optimization of a reported procedure [73] the successful route employed a one-pot process involving a sodium hydride-mediated coupling of methyl malonate **19** with iodoform (**20**) followed by a stereoselective elimination and decarboxylation in situ. The corresponding aldehyde **22** was then homologated by an Abiko–Masamune *anti*-aldol addition [74] with ephedrine-derived ester **23**, which proceeded with excellent yield and stereoselectivity. However, the subsequent removal of the sterically hindered chiral auxiliary proved demanding. The Menche group realized that a transformation to a Weinreb amide may be realized in an effective manner by an in situ activation of **24** with iPrMgCl [75], followed by a methylation of the free hydroxy group and introduction of the methyl ketone. This procedure proved superior to an original sequence involving a reductive cleavage of the auxiliary.

Synthesis of the southern fragment

The same southern fragment **6** was independently chosen by the Menche group in their total synthesis of archazolid A and by the Trauner group in their total synthesis of archazolid B. Both groups also pursued identical routes to this subunit. As shown in Scheme 5, this sequence started from L-leucine (**26**) which was first converted with nitrous acid to the hydroxy acid **27**, which proceeds with retention of the configuration due to intermediate lactone formation after generation of the diazonium-intermediate [76]. After conversion to amide **28** and thioamide **29** the thiazole **31** was obtained by condensation with bromoester **30**. The carbamate was then introduced by activation of the deprotected hydroxy group with carbonyldiimidazole and treatment with methylamine, before the ester was selectively reduced to the aldehyde **32** with DIBALH. Finally, a Brown crotylation [77] set the two vicinal stereogenic centers of **6** with high stereoselectivity. In total this route enabled an efficient and reliable access to this key fragment. However, one drawback of this sequence was a tendency of epimerisation at C1' during thiazole formation on large scale, requiring an oxidation–reduction sequence (90%) in this case.

Completion of the total synthesis

After evaluation of several strategies, the assembly of the two northern fragments **4** and **5** could be realized by an aldol condensation, involving a boron-mediated aldol coupling, acetate protection of the newly generated hydroxy group and DBU-mediated elimination. This three-step sequence proceeded as shown in Scheme 6 with excellent yields (94%) giving the triene **33** as a single diastereomer, which demonstrates the

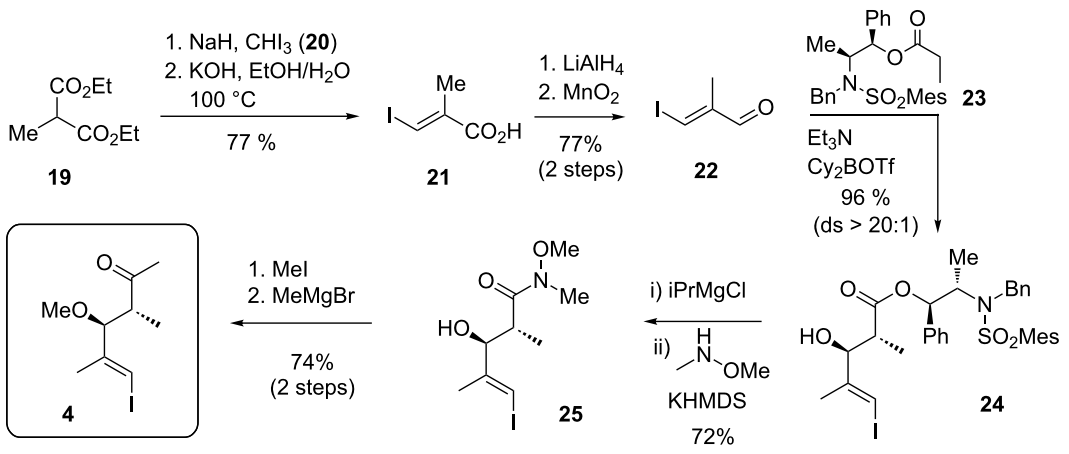

Scheme 4: Synthesis of **4** through an Abiko–Masamune *anti*-aldol addition.

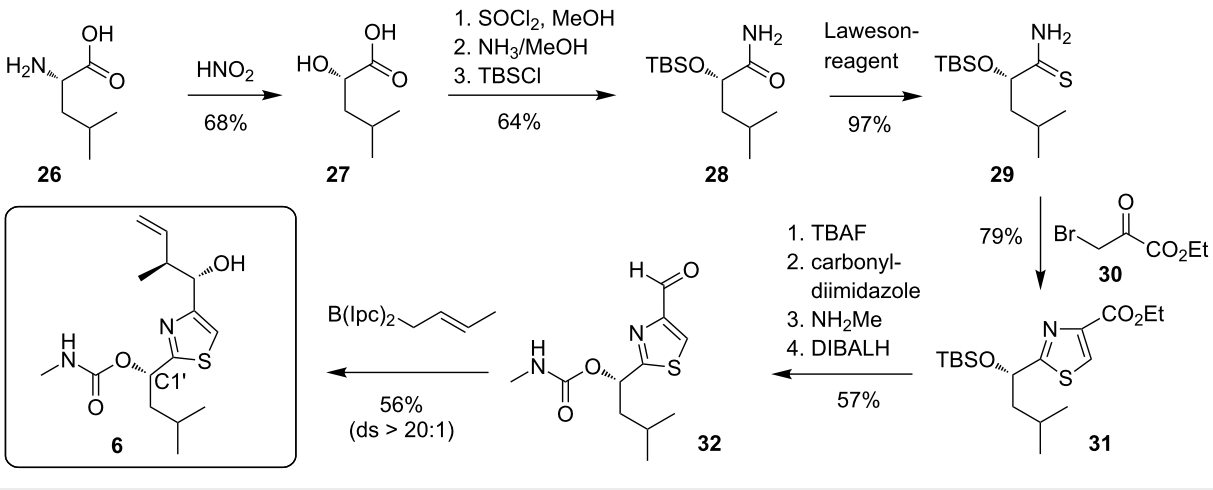

Scheme 5: Thiazol construction and synthesis of the southern fragment **6**.

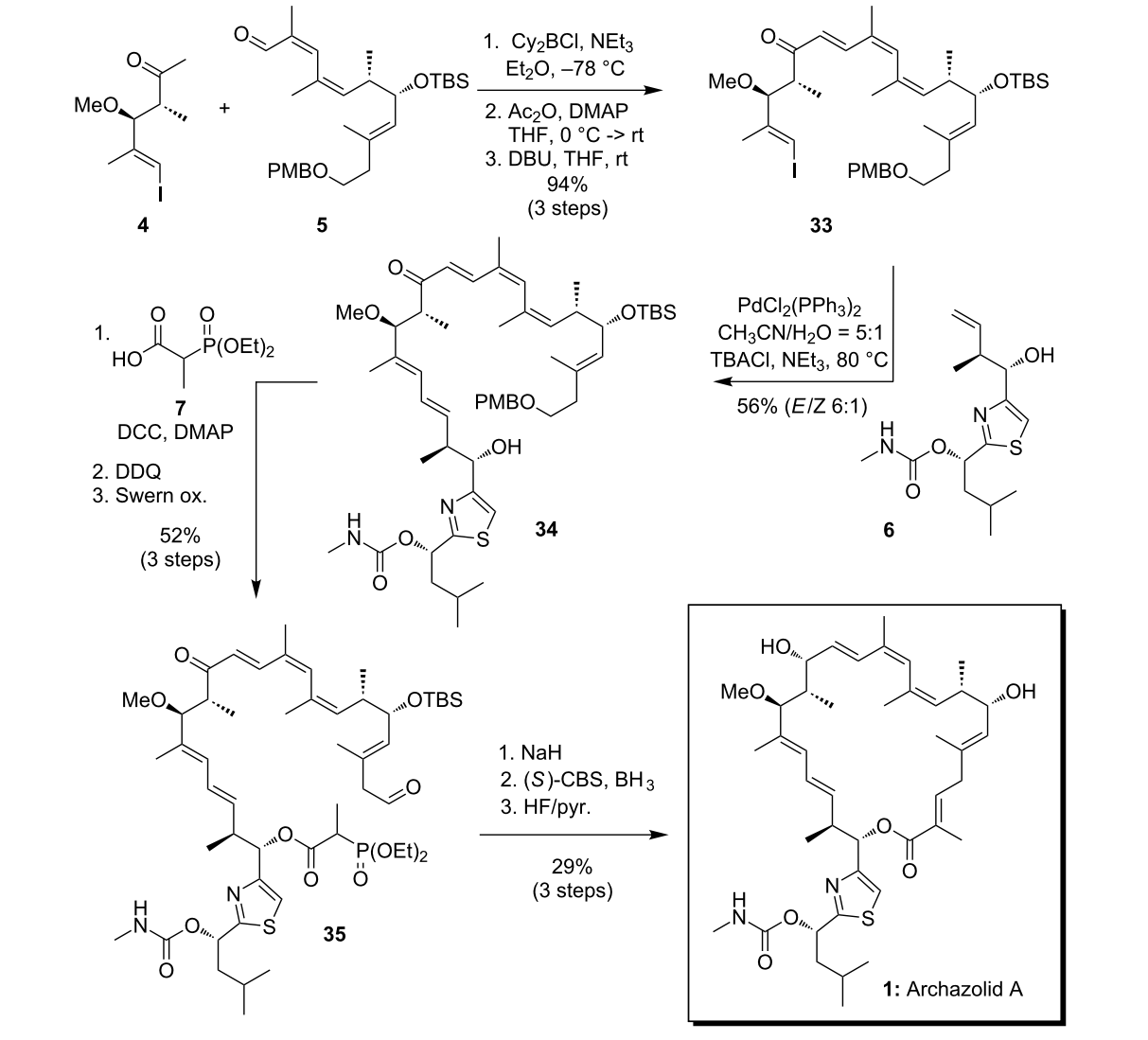

Scheme 6: Completion of the total synthesis of archazolid A.

usefulness of aldol condensations in complex target synthesis, also on highly elaborate substrates. Considerable efforts were invested before the challenging Heck coupling with the thiazole fragment **6** could be effected with useful selectivities. Besides the desired *E*,*E*-diene **34** formation of other double bond isomers both in the southern and northern part of the molecule could not be suppressed and required a tedious HPLC separation at this stage. After attachment of the phosphonate **7**, aldehyde **35** was obtained by removal of the PMB group and oxidation of the primary alcohol. The moderate yields of this sequence are mainly due to side reactions in the deprotection step. The Menche group then had considerable difficulties in closing the macrocyclic ring using an HWE reaction. Finally, the macrocylization could be realised by using NaH as a strong non-nucleophilic base. It proved essential to perform this reaction in the presence of molecular sieves to remove any traces of water which were shown to lead to unfavourable isomerization pathways. Finally, an oxazaborolidine-assisted borane reduction [78] set the stereogenic center at C15 and global deprotection gave synthetic archazolid A, which proved to be fully identical with a natural sample, thus unambiguously confirming the stereochemistry of this macrolide [59].

Menche's total synthesis of archazolid B

One the methodological incentives of the synthetic campaign of the Menche group directed towards the archazolids were the further development and application of the Heck reaction in complex target synthesis. Accordingly, they applied a Heck macrocyclization strategy for the total synthesis of archazolid B. As shown in Scheme 7, this strategy could be successfully implemented and the macrocyclic core of the target compound was obtained in useful yields by coupling of **38**, which in turn was accessible by an intermolecular HWE reaction of **36** with **37** using the procedure evaluated above. Final stereoselective CBS reduction and global deprotection liberated archazolid B in 41% yield over 3 steps [42]. This accomplishment presented the second total synthesis of this macrolide while the first total synthesis was enabled by the group of Trauner and will be discussed below.

Trauner's retrosynthetic analysis and strategy

Shortly after the total synthesis of archazolid A (**1**) by Menche et al. [41] the total synthesis of archazolid B **2** was reported by Trauner and co-workers [43]. As shown in Scheme 8, they could successfully couple the three main fragments **39**, **40** and **6** by first a Stille reaction, followed by a Kita esterification. Notably, this esterification was critical to avoid unfavorable isomerizations. For closing of the macrolide core they planned a challenging Hoye relay ring closing metathesis (RRCM) which would lead directly after deprotection to archazolid B (**2**).

Trauner's total synthesis of archazolid B

Synthesis of the north-eastern fragment

The synthesis of fragment **40** started with the literature-known protocol for generation of ynone **42** derived from (*S*)-Roche ester **41** [79] as shown in Scheme 9. After reduction the alcohol was protected with TIPS and the TBS ether was cleaved by acetic acid to get to the primary alcohol **43**. The reduction with (*S*)-alpine borane was highly diastereoselective (dr > 20:1). Following this sequence over 6 steps the two stereogenic centers at C7 and C8 were successfully built up. The primary alcohol of fragment **43** was then oxidized by the Dess–Martin reagent (DMP) and then treated with CBr_4 and PPh_3 to generate the dibromoalkene **44** in high yield of 75% over 2 steps. The group now installed the vinyliodide for the Stille coupling by treating the alkene with lithium dimethylcuprate. In comparison with the likewise attempted Stork–Zhao olefination this protocol by Tanino and Miyashita was superior in yield and

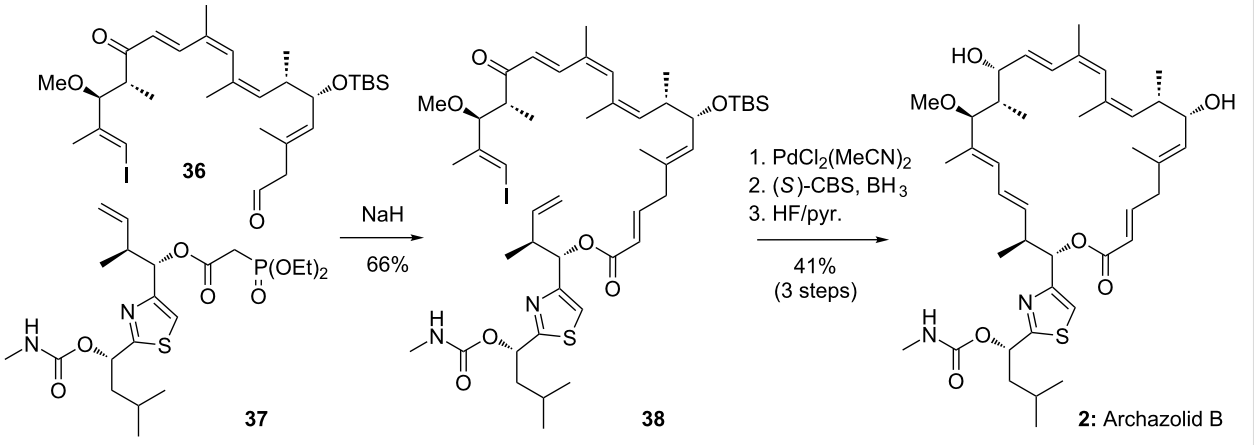

Scheme 7: Synthesis of archazolid B (**2**) by a ring closing Heck reaction of **38**.

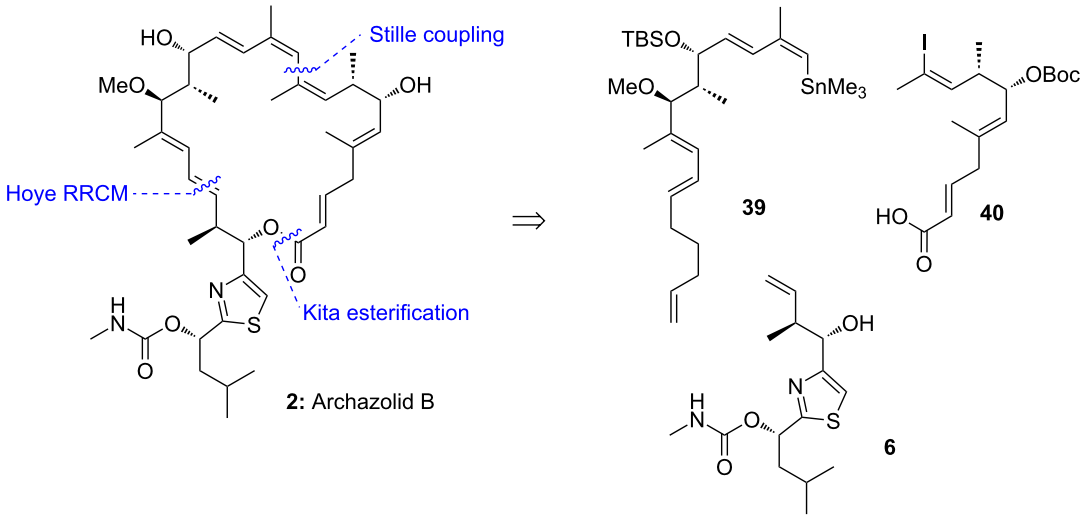

Scheme 8: Retrosynthetic analysis of archazolid B by the Trauner group.

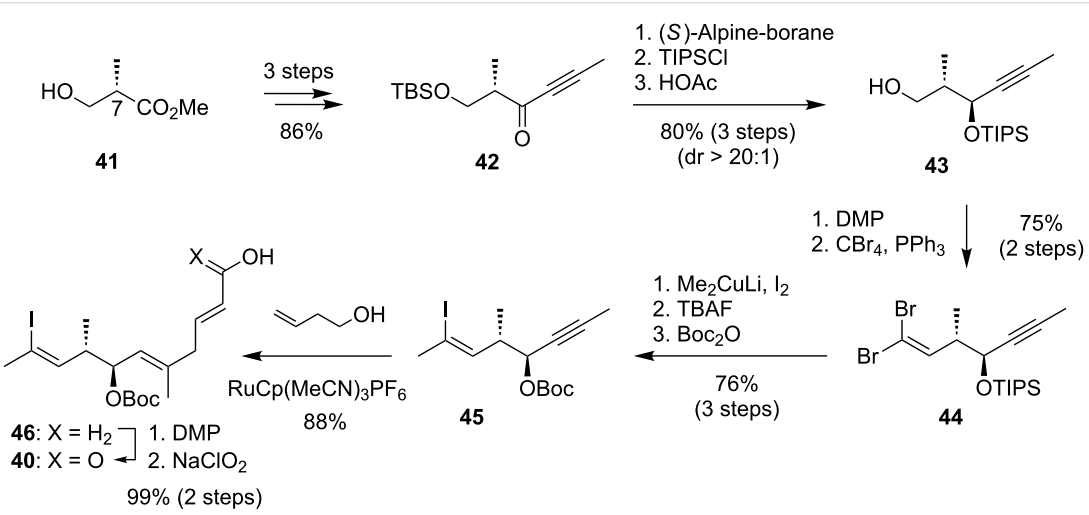

Scheme 9: Synthesis of acid **40** from Roche ester **41** involving a highly efficient Trost–Alder ene reaction.

stereoselectivity [80]. To complete the fragment synthesis the [Ru]-catalyzed Trost–Alder-ene reaction [81] generated the desired primary alcohol which was oxidized in 2 steps with DMP and $NaClO_2$/NaH_2PO_4 to the free acid **40**. The high regioselectivity of the Alder-Ene reaction is remarkable and was argued to be derived by a coordinating effect of the carbonate. Also, the overall high yield for synthesis of this elaborate vinyl iodide is impressive.

Synthesis of the north-western fragment

As shown in Scheme 10, the synthesis of stannane **39** started with aldehyde **48** which was derived from propargyl alcohol in five steps [82]. After DMP oxidation the generated aldehyde **48** underwent a *syn*-selective Evans aldol addition with oxazolidinone **47** to obtain the alcohol **49** in 76% over 2 steps [83]. Before TBS protection the Weinreb amide was generated and then conversed into the phosphonate **50** as a precursor for a Horner–Wadsworth–Emmons reaction. The olefination led to unsaturated ketone **52** in 79% yield. For the final fragment synthesis the ketone was reduced with sodium borohydride to generate all three required stereogenic centers for this fragment with excellent diasteroselectivity. Final methylation of the free alcohol was followed by conversion of the vinyl iodide into the desired stannane to get fragment **39** which was used directly for coupling.

Completion of the total synthesis

Final assembly of the fragments as shown in Scheme 11 began with an unusual [Ru]-catalyzed Kita esterification due to the instability of fragment **40** towards basic esterification ap-

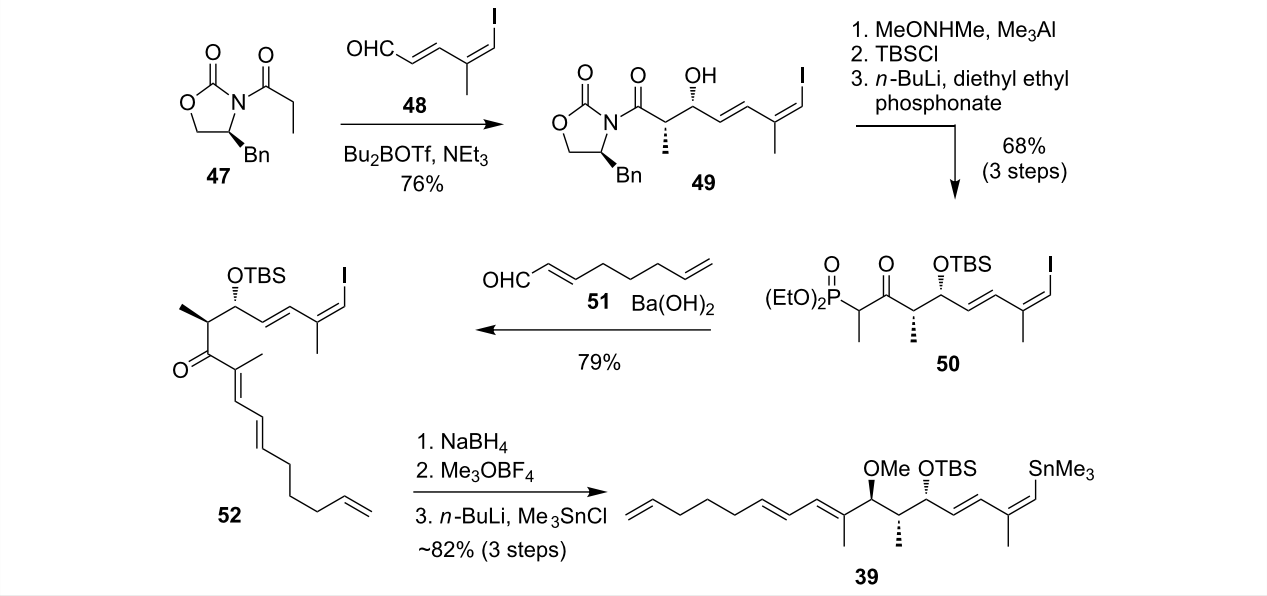

Scheme 10: Synthesis of precursor **39** for the projected relay RCM reaction.

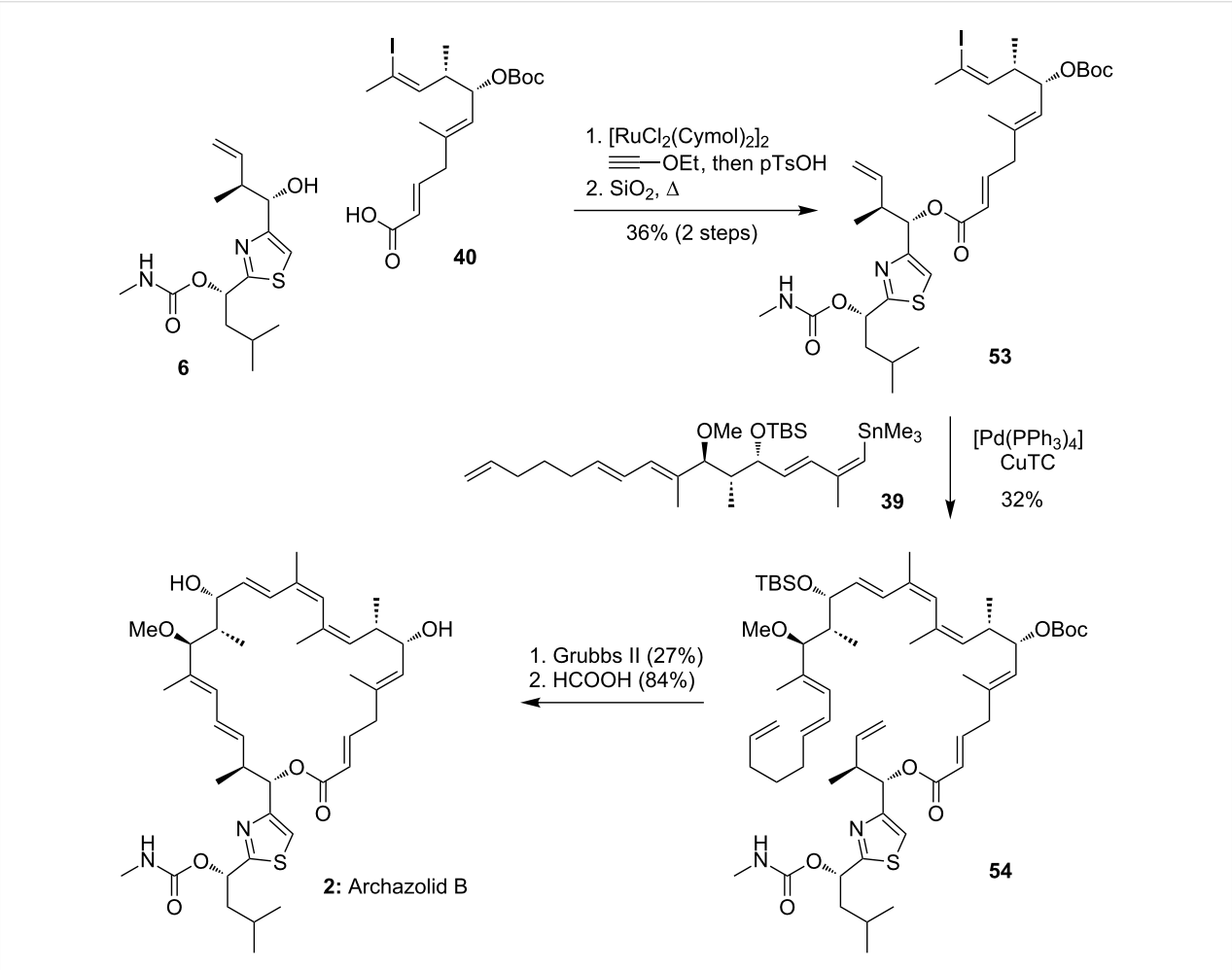

Scheme 11: Final steps of Trauner's total synthesis of archazolid B.

proaches [84]. The following Stille coupling with stannane **39** was then accomplished by CuTC co-catalysis to get the final fragment **54** in 32% yield [85,86]. The envisioned Hoye relay RCM was catalyzed by Grubbs' second generation catalyst to close the macrocycle in 27% yield. The final acid-mediated deprotection liberated finally archazolid B (**2**). Notably, no cyclization was observed in an analogous RCM reaction with a substrate without the relay tether, which underscores the usefulness of this relay tactic.

It is important to mention, that the three main fragments were coupled in only four steps, showing the highly modular approach from Trauner and co-workers. With this strategy it was possible to synthesize archazolid B (**2**) in only 19 steps from (*S*)-Roche ester **41** (longest linear sequence).

O'Neil's retrosynthetic analysis and strategy

As discussed above one of the main difficulties of any archazolid synthesis involves the labile C1 to C5-dienoate system, which is prone to isomerization. However, the similar biological potency of archazolids A and B as well as the archazolid B isomer archazolid F, which bears a 3,4- instead of the 2,3-alkene, suggest that the C2-olefin may not be essential for the biological potency. Accordingly, the group of O'Neil and co-workers has been targeted dihydroarchazolid B (**3**). They assumed a similar biological potency of the derivative with simultaneous simplification of the synthesis. While so far, they have not been able to finish this synthesis, they have reported several very instructive and efficient fragment syntheses, including the three main fragments **55**, **56** and **57** as shown in Scheme 12 [45,46,48]. The challenging ring-closing metathesis between C13 and C14 could not be established mainly due a competing backbiting process of the corresponding western fragment [46].

O'Neil's syntheses of advanced dihydroarchazolid B fragments

Synthesis of the macrocyclic skeleton

Based on this unsuccessful approach O'Neil and co-workers published a new synthetic route towards 2,3-dihydroarchazolid B (**3**) [48]. As shown in Scheme 13 they were able to synthesize the macrocyclic skeleton **68** by a Stille coupling between stannane **56** and iodide **55** as the key step. Notably, they had to switch the halide/organometallic functionality of each building block after an unsuccessful coupling between the stannane synthesized by reduction and methylation of ketone **67** and the iodine derived from fragment **62**. They assume that the steric hindrance of the methyl group in C10 position possibly lowers the reactivity of the iodine in the oxidative addition step in the catalytic cycle.

For the synthesis of stannane **56** the authors could benefit from the previous fragment synthesis. In 2010 they first published an approach to an eastern building block through an allylation-elimination sequence to form the triene system C9 to C14 [44]. In a second generation fragment synthesis building block **62** was firstly synthesized in 2014 [46]. Starting with the TBS-protected alkyne **58** [87] a zirconium-mediated carboalumination reaction [88] and subsequent coupling with aldehyde **59** gave alcohol **60**. In this $\Delta^{5,6}$-*trans*-selective reaction the desired *anti*-diastereomer could be isolated in 85% with a dr of 6:1, which presumably arises from a chelation-controlled stereoselectivity [89]. The aldehyde **59** itself can be prepared in two steps from the corresponding Roche ester [90]. After protection of the free

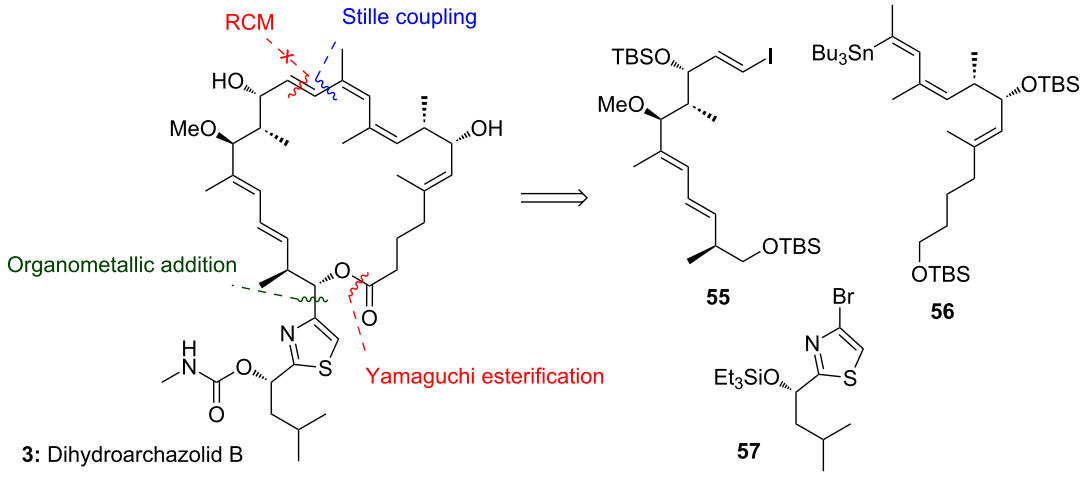

Scheme 12: Overview of the different retrosynthetic approaches for the synthesis of dihydroarchazolid B (**3**) reported by the O'Neil group.

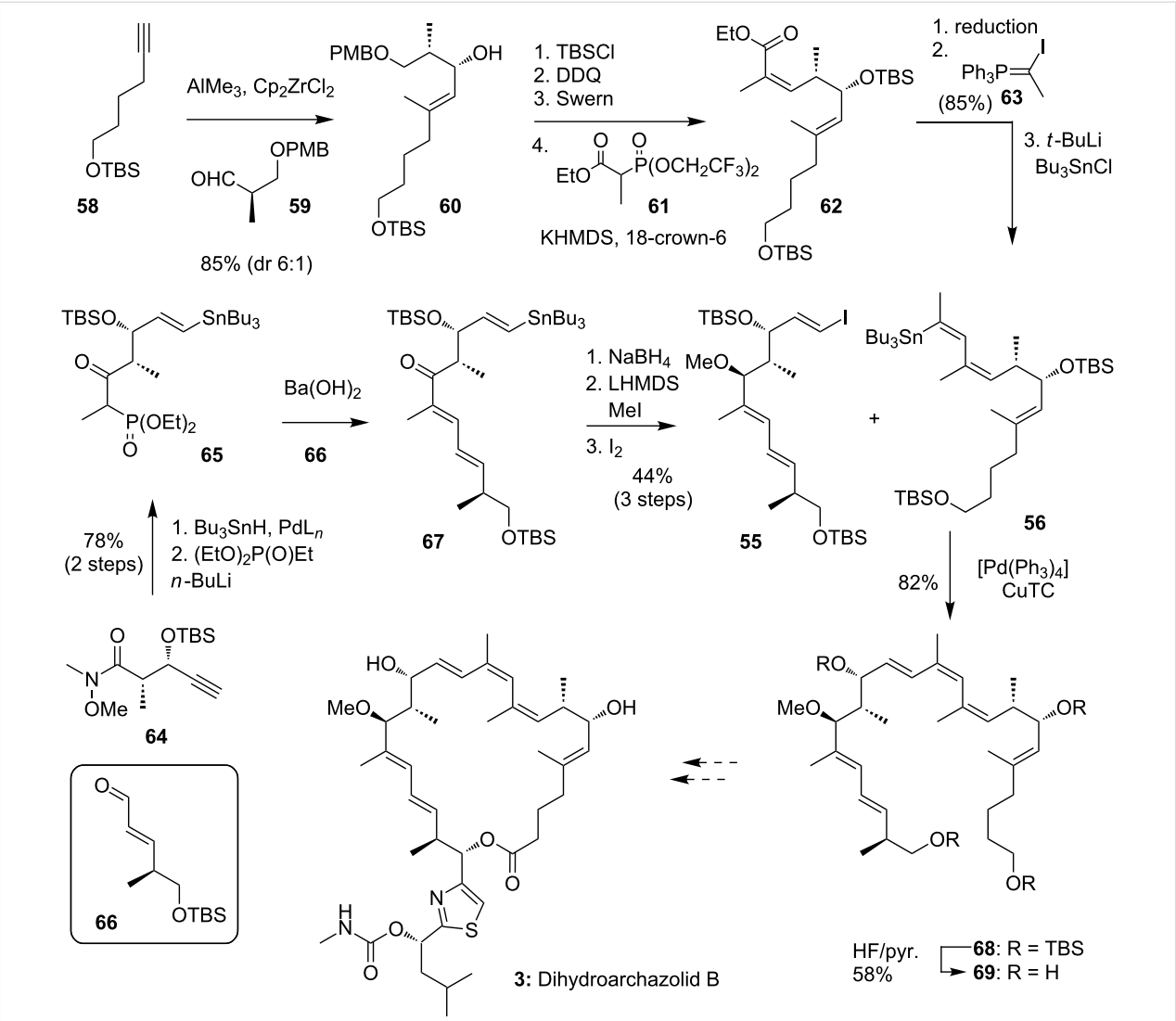

Scheme 13: Fragment synthesis of **69** towards the total synthesis of **3**.

alcohol and deprotection of the primary PMB-protected alcohol with DDQ, the resulting alcohol was oxidized to the corresponding aldehyde. The crude aldehyde was then directly transformed into the (*Z*)-α,β-unsaturated ester **62** as a single stereoisomer by a Still–Gennari [72] olefination with phosphonate **61** in an excellent yield of 93% over 4 steps. After reduction of ester **62** to the corresponding aldehyde (by a method that was not specified by the authors) phosphorane **63** was used to generate the respective *Z*-vinyl iodide in 85% yield as an 8:1 (*Z,Z)*:(*Z,E)* mixture [91] which was later switched to the stannane **56** by lithium–halogen exchange and further treatment with Bu_3SnCl [92] in 90% yield.

The synthesis of the coupling partner **55** started with known Weinreb amide **64** which underwent a *syn*-selective palladium-catalyzed hydrostannylation and was then transformed to phosphonate **65** in good yield. For coupling with known aldehyde **66** [93] the O'Neil group chose $Ba(OH)_2$ as base for the HWE-type reaction [94] to generate the α,β-unsaturated ketone **67** in 75% yield as a 10:1 mixture of isomers. Similar to the earlier discussed synthesis of Trauner and co-workers [43] reduction with sodium borohydride delivered the desired alcohol in a 10:1 diastereoselectivity. The alcohol was methylated by a protocol involving methyl iodide and LiHMDS, that had been previously used by the group [45]. The stannane was finally converted to the iodide **55** by iododestannylation [95] to complete the fragment synthesis in 44% yield over 3 steps.

For the final step the authors decided to follow a Stille coupling protocol established by Fürstner et al. [96] with CuTC as co-catalyst and $[Ph_2PO_2][NBu_4]$ as tin scavenger. Subsequently, the triene **68** could be synthesized in excellent 82%

yield. For biological studies the final fragment **68** was globally deprotected to the alcohol **69**.

To this end, the O'Neil group successfully established a route to the dihydroarchazolid B fragment **68** in only 9 steps (longest linear synthesis). This route also proved that a retrosynthetic disconnection between C12 and C13 can be useful for new approaches to the 24-membered macrolide core. For the completion of the synthesis of **3** the side chain would have to be introduced, followed by an oxidation to the acid and a ring closing esterification.

Concise synthesis of the thiazole fragment

In an earlier synthesis the O'Neil group had already coupled a similar fragment **70** with the southern fragment **57** by an organometallic addition, however, with a lack of stereoselectivity in C23 position [45]. As shown in Scheme 14, they started with the deprotection of the primary TBS ether **70** and DMP oxidation to the aldehyde **71**. The bromide **57**, derived in two steps from literature-known ketone **72** [49], was converted to an organolithium compound which attacked the aldehyde to give the free alcohol **73** in 1:2.5 diasteroselectivity in favor of the undesired *R*-isomer of **73**, which can be explained by the Felkin–Ahn model. For generation of only (*S*)-**73** the both epimers were oxidized to the ketone by DMP followed by reduction with L-selectride. Protection of the free alcohol with acetate and deprotection of the TES group was then required to install the carbamate with CDI and $MeNH_2$. After deprotection, fragment **75** was synthesized in 67% yield over 2 steps.

Having these tactics in hand it will be interesting to follow the completion of the first synthesis of dihydroarchazolid B (**3**) by the O'Neil group and the biological data of this compound.

Conclusion

The discovery of the archazolids led to important advances in the understanding of the role of V-ATPases in cancer development and progression. Based on extensive studies with these macrolides as chemical tools V-ATPases have emerged as a completely novel and highly promising novel class of anticancer targets. Along these lines synthetic chemistry has played a pivotal role, not only by providing these scarce natural products for biological evaluation, but also in supplying novel analogues with tailored functional properties to decipher the target inhibitor interactions at a molecular level. Finally, the total syntheses of the Menche and Trauner group were also of key importance to assign the full stereochemistry in the first place. The various approaches discussed within this manuscript show the various tactics and strategies that may be employed in complex polyketide synthesis. Notable features of the total synthesis by the Menche group include the robustness of boron mediated aldol reactions to set both the characteristic assemblies of neighbored methyl and hydroxy group bearing stereogenic centers. In addition, an aldol condensation was shown to enable

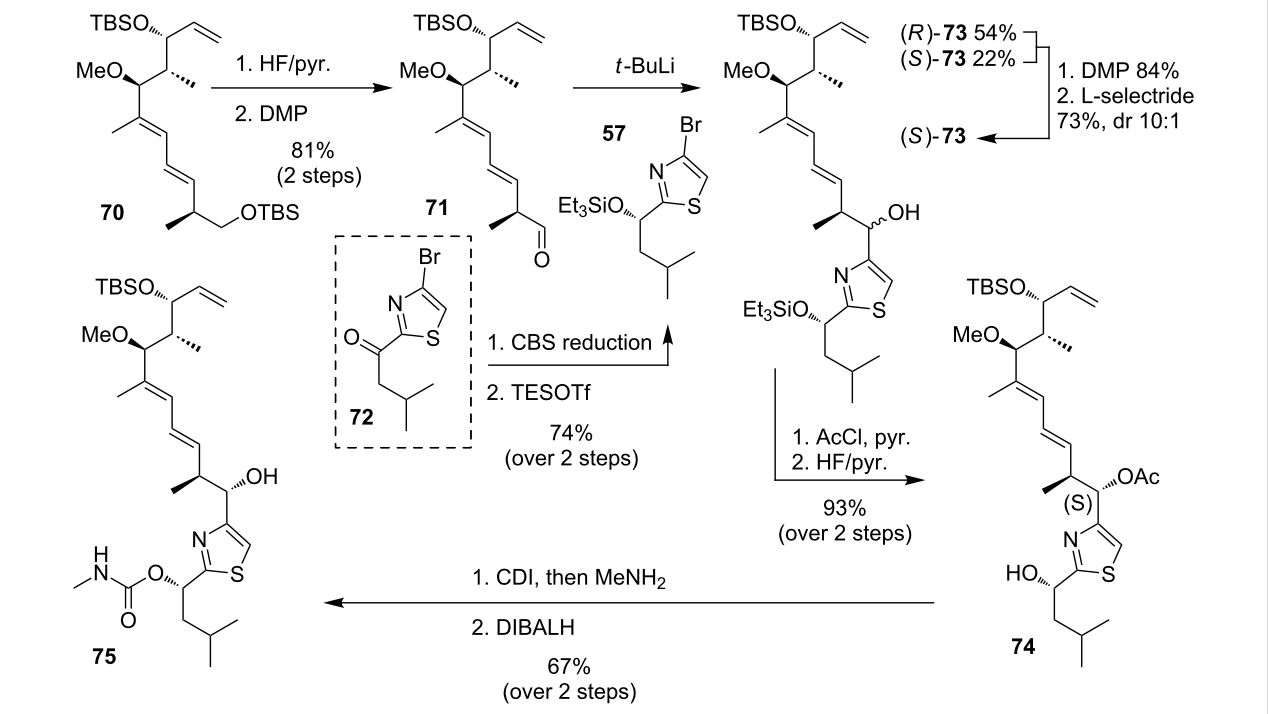

Scheme 14: Organometallic addition of the side chain to access free alcohol **75**.

an efficient route for construction of a delicate triene system. The final *E*-selective Heck coupling on a highly elaborate substrate and the subsequent HWE macrocyclization are remarkable. The Trauner group in turn effectively employed various ruthenium-catalyzed reactions, including a relay ring-closing metathesis, which demonstrates the powerfulness of such a tactic even for highly elaborate substrates with several initiation positions. However, despite these advances and impressive total syntheses the design and development of a truly reliable and scalable route that will enable an access to gram amounts of thee scarce metabolites continues to present a key scientific challenge and the O'Neil group has already demonstrated that a more concise route may be possible. Efforts are now being directed in the design and development of truly practicable and scalable routes to more stable archazolids to enhance the further preclinical development of these novel anticancer agents. Particular importance will be the development of a truly reliable and high yielding macrocyclization method, while efficient methods for fragment syntheses have been established. It will also be interesting to follow whether synthetic chemists will be successful to establish a scalable route that will enable the synthesis of gram quantities of the authentic natural products or novel archazolids with likewise potent or even improved pharmacological and pharmacokinetic properties to fully exploit the extremely promising biological profile of these polyketide macrolides.

Acknowledgements

Financial support by the Deutsche Forschungsgemeinschaft (Forschergruppe 1406), the Volkswagenstiftung and the Fonds der Chemischen Industrie is gratefully acknowledged. We greatly appreciate the dedicated work of those members of our group who have developed this field of research and the stimulating cooperations with our scientific partners – their names can be seen from the literature cited.

References

1. Yeung, K.-S.; Paterson, I. *Chem. Rev.* **2005,** *105,* 4237–4313. doi:10.1021/cr040614c
2. Schetter, B.; Mahrwald, R. *Angew. Chem., Int. Ed.* **2006,** *45,* 7506–7525. doi:10.1002/anie.200602780
3. Dalby, S. M.; Paterson, I. *Curr. Opin. Drug Discovery Dev.* **2010,** *13,* 777–794.
4. Brodmann, T.; Lorenz, M.; Schäckel, R.; Simsek, S.; Kalesse, M. *Synlett* **2009,** 174–192. doi:10.1055/s-0028-1087520
5. Li, J.; Menche, D. *Synthesis* **2009,** 2293–2315. doi:10.1055/s-0029-1216881
6. Dieckmann, M.; Menche, D. *Org. Lett.* **2013,** *15,* 228–231. doi:10.1021/ol3033303
7. Dechert-Schmitt, A.-M. R.; Schmitt, D. C.; Gao, X.; Itoh, T.; Krische, M. J. *Nat. Prod. Rep.* **2014,** *31,* 504–513. doi:10.1039/c3np70076c
8. Seiple, I. B.; Zhang, Z.; Jakubec, P.; Langlois-Mercier, A.; Wright, P. M.; Hog, D. T.; Yabu, K.; Allu, S. R.; Fukuzaki, T.; Carlsen, P. N.; Kitamura, Y.; Zhou, X.; Condakes, M. L.; Szczypiński, F. T.; Green, W. D.; Myers, A. G. *Nature* **2016,** *533,* 338–345. doi:10.1038/nature17967
9. Bredenkamp, A.; Wegener, M.; Hummel, S.; Häring, A. P.; Kirsch, S. F. *Chem. Commun.* **2016,** *52,* 1875–1878. doi:10.1039/C5CC09328G
10. Mickel, S. J. *Curr. Opin. Drug Discovery Dev.* **2004,** *7,* 869–881.
11. Klar, U.; Buchmann, B.; Schwede, W.; Skuballa, W.; Hoffmann, J.; Lichtner, R. B. *Angew. Chem., Int. Ed.* **2006,** *45,* 7942–7948. doi:10.1002/anie.200602785
12. Cragg, G. M.; Grothaus, P. G.; Newman, D. J. *Chem. Rev.* **2009,** *109,* 3012–3043. doi:10.1021/cr900019j
13. Weissman, K. J.; Müller, R. *Nat. Prod. Rep.* **2010,** *27,* 1276–1295. doi:10.1039/c001260m
14. Nishi, T.; Forgac, M. *Nat. Rev. Mol. Cell Biol.* **2002,** *3,* 94–103. doi:10.1038/nrm729
15. Jefferies, K. C.; Cipriano, D. J.; Forgac, M. *Arch. Biochem. Biophys.* **2008,** *476,* 33–42. doi:10.1016/j.abb.2008.03.025
16. Beyenbach, K. W.; Wieczorek, H. *J. Exp. Biol.* **2006,** *209,* 577–589. doi:10.1242/jeb.02014
17. Maxfield, F. R.; McGraw, T. E. *Nat. Rev. Mol. Cell Biol.* **2004,** *5,* 121–132. doi:10.1038/nrm1315
18. Hiesinger, P. R.; Fayyazuddin, A.; Mehta, S. Q.; Rosenmund, T.; Schulze, K. L.; Zhai, R. G.; Verstreken, P.; Cao, Y.; Zhou, Y.; Kunz, J.; Bellen, H. J. *Cell* **2005,** *121,* 607–620. doi:10.1016/j.cell.2005.03.012
19. Brown, D.; Paunescu, T. G.; Breton, S.; Marshansky, V. *J. Exp. Biol.* **2009,** *212,* 1762–1772. doi:10.1242/jeb.028803
20. Toyomura, T.; Murata, Y.; Yamamoto, A.; Oka, T.; Sun-Wada, G.-H.; Wada, Y.; Futai, M. *J. Biol. Chem.* **2003,** *278,* 22023–22030. doi:10.1074/jbc.M302436200
21. Pietrement, C.; Sun-Wada, G.-H.; Da Silva, N.; McKee, M.; Marshansky, V.; Brown, D.; Futai, M.; Breton, S. *Biol. Reprod.* **2006,** *74,* 185–194. doi:10.1095/biolreprod.105.043752
22. Hamm, R.; Chen, Y.-R.; Seo, E.-J.; Zeino, M.; Wu, C.-F.; Müller, R.; Yang, N.-S.; Efferth, T. *Biochem. Pharmacol.* **2014,** *91,* 18–30. doi:10.1016/j.bcp.2014.06.018
23. Scherer, O.; Steinmetz, H.; Kaether, C.; Weinigel, C.; Barz, D.; Kleinert, H.; Menche, D.; Müller, R.; Pergola, C.; Werz, O. *Biochem. Pharmacol.* **2014,** *91,* 490–500. doi:10.1016/j.bcp.2014.07.028
24. Sasse, F.; Steinmetz, H.; Höfle, G.; Reichenbach, H. *J. Antibiot.* **2003,** *56,* 520–525. doi:10.7164/antibiotics.56.520
25. Huss, M.; Sasse, F.; Kunze, B.; Jansen, R.; Steinmetz, H.; Ingenhorst, G.; Zeeck, A.; Wieczorek, H. *BMC Biochem.* **2005,** *6,* No. 13. doi:10.1186/1471-2091-6-13
26. Bockelmann, S.; Menche, D.; Rudolph, S.; Bender, T.; Grond, S.; von Zezschwitz, P.; Muench, S. P.; Wieczorek, H.; Huss, M. *J. Biol. Chem.* **2010,** *285,* 38304–38314. doi:10.1074/jbc.M110.137539
27. Gölz, J. P.; Bockelmann, S.; Mayer, K.; Steinhoff, H.-J.; Wieczorek, H.; Huss, M.; Klare, J. P.; Menche, D. *ChemMedChem* **2016,** *11,* 420–428. doi:10.1002/cmdc.201500500
28. Wiedmann, R. M.; von Schwarzenberg, K.; Palamidessi, A.; Schreiner, L.; Kubisch, R.; Liebl, J.; Schempp, C.; Trauner, D.; Vereb, G.; Zahler, S.; Wagner, E.; Müller, R.; Scita, G.; Vollmar, A. M. *Cancer Res.* **2012,** *72,* 5976–5987. doi:10.1158/0008-5472.CAN-12-1772
29. von Schwarzenberg, K.; Wiedmann, R. M.; Oak, P.; Schulz, S.; Zischka, H.; Wanner, G.; Efferth, T.; Trauner, D.; Vollmar, A. M. *J. Biol. Chem.* **2013,** *288,* 1385–1396. doi:10.1074/jbc.M112.412007

30. Kubisch, R.; Fröhlich, T.; Arnold, G. J.; Schreiner, L.; von Schwarzenberg, K.; Roidl, A.; Vollmar, A. M.; Wagner, E. *Int. J. Cancer* **2014,** *134,* 2478–2488. doi:10.1002/ijc.28562
31. Schempp, C. M.; von Schwarzenberg, K.; Schreiner, L.; Kubisch, R.; Müller, R.; Wagner, E.; Vollmar, A. M. *Mol. Cancer Ther.* **2014,** *13,* 926–937. doi:10.1158/1535-7163.MCT-13-0484
32. von Schwarzenberg, K.; Lajtos, T.; Simon, L.; Müller, R.; Vereb, G.; Vollmar, A. M. *Mol. Oncol.* **2014,** *8,* 9–19. doi:10.1016/j.molonc.2013.08.011
33. Schneider, L. S.; von Schwarzenberg, K.; Lehr, T.; Ulrich, M.; Kubisch-Dohmen, R.; Liebl, J.; Trauner, D.; Menche, D.; Vollmar, A. M. *Cancer Res.* **2015,** *75,* 2863–2874. doi:10.1158/0008-5472.CAN-14-2097
34. Schneider, L. S.; Ulrich, M.; Lehr, T.; Menche, D.; Müller, R.; von Schwarzenberg, K. *Mol. Oncol.* **2016,** *10,* 1054–1062. doi:10.1016/j.molonc.2016.04.005
35. Pérez-Sayáns, M.; Somoza-Martin, J. M.; Barros-Angueira, F.; Rey, J. M. G.; García-García, A. *Cancer Treat. Rev.* **2009,** *35,* 707–713. doi:10.1016/j.ctrv.2009.08.003
36. Hernandez, A.; Serrano-Bueno, G.; Perez-Castineira, J. R.; Serrano, A. *Curr. Pharm. Des.* **2012,** *18,* 1383–1394. doi:10.2174/138161212799504821
37. Cotter, K.; Capecci, J.; Sennoune, S.; Huss, M.; Maier, M.; Martinez-Zaguilan, R.; Forgac, M. *J. Biol. Chem.* **2015,** *290,* 3680–3692. doi:10.1074/jbc.M114.611210
38. Menche, D.; Hassfeld, J.; Steinmetz, H.; Huss, M.; Wieczorek, H.; Sasse, F. *J. Antibiot.* **2007,** *60,* 328–331. doi:10.1038/ja.2007.43
39. Menche, D.; Hassfeld, J.; Steinmetz, H.; Huss, M.; Wieczorek, H.; Sasse, F. *Eur. J. Org. Chem.* **2007,** 1196–1202. doi:10.1002/ejoc.200600912
40. Horstmann, N.; Essig, S.; Bockelmann, S.; Wieczorek, H.; Huss, M.; Sasse, F.; Menche, D. *J. Nat. Prod.* **2011,** *74,* 1100–1105. doi:10.1021/np200036v
41. Menche, D.; Hassfeld, J.; Li, J.; Rudolph, S. *J. Am. Chem. Soc.* **2007,** *129,* 6100–6101. doi:10.1021/ja071461o
42. Menche, D.; Hassfeld, J.; Li, J.; Mayer, K.; Rudolph, S. *J. Org. Chem.* **2009,** *74,* 7220–7229. doi:10.1021/jo901565n
43. Roethle, P. A.; Chen, I. T.; Trauner, D. *J. Am. Chem. Soc.* **2007,** *129,* 8960–8961. doi:10.1021/ja0733033
44. O'Neil, G. W.; Black, M. J. *Synlett* **2010,** 107–110. doi:10.1055/s-0029-1218537
45. Tran, A. B.; Melly, G. C.; Doucette, R.; Ashcraft, B.; Sebren, L. J.; Havko, N.; Young, J. C.; O'Neil, G. W. *Org. Biomol. Chem.* **2011,** *9,* 7671–7674. doi:10.1039/c1ob06446k
46. King, B. R.; Swick, S. M.; Schaefer, S. L.; Welch, J. R.; Hunter, E. F.; O'Neil, G. W. *Synthesis* **2014,** *46,* 2927–2936. doi:10.1055/s-0034-1379003
47. Swick, S. M.; Schaefer, S. L.; O'Neil, G. W. *Tetrahedron Lett.* **2015,** *56,* 4039–4042. doi:10.1016/j.tetlet.2015.05.014
48. O'Neil, G. W.; Craig, A. M.; Williams, J. R.; Young, J. C.; Spiegel, P. C. *Synlett* **2017,** *28,* 1101–1105. doi:10.1055/s-0036-1588413
49. Moulin, E.; Nevado, C.; Gagnepain, J.; Kelter, G.; Fiebig, H.-H.; Fürstner, A. *Tetrahedron* **2010,** *66,* 6421–6428. doi:10.1016/j.tet.2010.05.043
50. Xu, S.; Negishi, E.-i. *Heterocycles* **2014,** *88,* 845–877. doi:10.3987/REV-13-SR(S)5
51. Pop, L.; Lassalas, P.; Bencze, L. C.; Toşa, M. I.; Nagy, B.; Irimie, F. D.; Hoarau, C. *Tetrahedron: Asymmetry* **2012,** *23,* 474–481. doi:10.1016/j.tetasy.2012.03.014
52. de Paolis, M.; Chataigner, I.; Maddaluno, J. *Top. Curr. Chem.* **2012,** *327,* 87–146. doi:10.1007/128_2012_320
53. Negishi, E.-i.; Wang, G.; Rao, H.; Xu, Z. *J. Org. Chem.* **2010,** *75,* 3151–3182. doi:10.1021/jo1003218
54. Huang, Z.; Negishi, E.-i. *J. Am. Chem. Soc.* **2007,** *129,* 14788–14792. doi:10.1021/ja0772039
55. Menche, D.; Hassfeld, J.; Sasse, F.; Huss, M.; Wieczorek, H. *Bioorg. Med. Chem. Lett.* **2007,** *17,* 1732–1735. doi:10.1016/j.bmcl.2006.12.073
56. Persch, E.; Basile, T.; Bockelmann, S.; Huss, M.; Wieczorek, H.; Carlomagno, T.; Menche, D. *Bioorg. Med. Chem. Lett.* **2012,** *22,* 7735–7738. doi:10.1016/j.bmcl.2012.09.081
57. Dreisigacker, S.; Latek, D.; Bockelmann, S.; Huss, M.; Wieczorek, H.; Filipek, S.; Gohlke, H.; Menche, D.; Carlomagno, T. *J. Chem. Inf. Model.* **2012,** *52,* 2265–2272. doi:10.1021/ci300242d
58. Reker, D.; Perna, A. M.; Rodrigues, T.; Schneider, P.; Reutlinger, M.; Mönch, B.; Koeberle, A.; Lamers, C.; Gabler, M.; Steinmetz, H.; Müller, R.; Schubert-Zsilavecz, M.; Werz, O.; Schneider, G. *Nat. Chem.* **2014,** *6,* 1072–1078. doi:10.1038/nchem.2095
59. Hassfeld, J.; Farès, C.; Steinmetz, H.; Carlomagno, T.; Menche, D. *Org. Lett.* **2006,** *8,* 4751–4754. doi:10.1021/ol061831y
60. Farès, C.; Hassfeld, J.; Menche, D.; Carlomagno, T. *Angew. Chem., Int. Ed.* **2008,** *47,* 3722–3726. doi:10.1002/anie.200800225
61. Dieckmann, M.; Rudolph, S.; Dreisigacker, S.; Menche, D. *J. Org. Chem.* **2012,** *77,* 10782–10788. doi:10.1021/jo302134y
62. Kretschmer, M.; Dieckmann, M.; Li, P.; Rudolph, S.; Herkommer, D.; Troendlin, J.; Menche, D. *Chem. – Eur. J.* **2013,** *19,* 15993–16018. doi:10.1002/chem.201302197
63. Symkenberg, G.; Kalesse, M. *Angew. Chem., Int. Ed.* **2014,** *53,* 1795–1798. doi:10.1002/anie.201309386
64. Li, P.; Li, J.; Arikan, F.; Ahlbrecht, W.; Dieckmann, M.; Menche, D. *J. Am. Chem. Soc.* **2009,** *131,* 11678–11679. doi:10.1021/ja9056163
65. Li, P.; Li, J.; Arikan, F.; Ahlbrecht, W.; Dieckmann, M.; Menche, D. *J. Org. Chem.* **2010,** *75,* 2429–2444. doi:10.1021/jo100201f
66. Yang, Z.; Xu, X.; Yang, C.-H.; Tian, Y.; Chen, X.; Lian, L.; Pan, W.; Su, X.; Zhang, W.; Chen, Y. *Org. Lett.* **2016,** *18,* 5768–5770. doi:10.1021/acs.orglett.6b02729
67. Cowden, C. J.; Paterson, I. *Org. React.* **1997,** *51,* 1–200. doi:10.1002/0471264180.or051.01
68. Arikan, F.; Li, J.; Menche, D. *Org. Lett.* **2008,** *10,* 3521–3524. doi:10.1021/ol801292t
69. Kretschmer, M.; Menche, D. *Synlett* **2010,** 2989–3007. doi:10.1055/s-0030-1259070
70. Essig, S.; Menche, D. *Pure Appl. Chem.* **2013,** *85,* 1103–1120. doi:10.1351/PAC-CON-12-09-12
71. Li, J.; Menche, D. *Synthesis* **2009,** 1904–1908. doi:10.1055/s-0028-1088062
72. Still, W. C.; Gennari, C. *Tetrahedron Lett.* **1983,** *24,* 4405–4408. doi:10.1016/S0040-4039(00)85909-2
73. Baker, R.; Castro, J. L. *J. Chem. Soc., Perkin Trans. 1* **1990,** 47–65. doi:10.1039/p19900000047
74. Inoue, T.; Liu, J.-F.; Buske, D. C.; Abiko, A. *J. Org. Chem.* **2002,** *67,* 5250–5256. doi:10.1021/jo0257896
75. Li, J.; Li, P.; Menche, D. *Synlett* **2009,** 2417–2420. doi:10.1055/s-0029-1217819
76. Pitt, N.; Gani, D. *Tetrahedron Lett.* **1999,** *40,* 3811–3814. doi:10.1016/S0040-4039(99)00534-1
77. Brown, H. C.; Bhat, K. S.; Randad, R. S. *J. Org. Chem.* **1989,** *54,* 1570–1576. doi:10.1021/jo00268a017

78. Corey, E. J.; Helal, C. J. *Angew. Chem., Int. Ed.* **1998,** *37,* 1986–2012. doi:10.1002/(SICI)1521-3773(19980817)37:15<1986::AID-ANIE1986>3.0.CO;2-Z
79. Trost, B. M.; Gunzner, J. L. *J. Am. Chem. Soc.* **2001,** *123,* 9449–9450. doi:10.1021/ja011424b
80. Tanino, K.; Arakawa, K.; Satoh, M.; Iwata, Y.; Miyashita, M. *Tetrahedron Lett.* **2006,** *47,* 861–864. doi:10.1016/j.tetlet.2005.12.002
81. Trost, B. M.; Dean Toste, F. *Tetrahedron Lett.* **1999,** *40,* 7739–7743. doi:10.1016/S0040-4039(99)01639-1
82. Beaudry, C. M.; Trauner, D. *Org. Lett.* **2002,** *4,* 2221–2224. doi:10.1021/ol026069o
83. Evans, D. A.; Black, W. C. *J. Am. Chem. Soc.* **1993,** *115,* 4497–4513. doi:10.1021/ja00064a011
84. Kita, Y.; Maeda, H.; Omori, K.; Okuno, T.; Tamura, Y. *Synlett* **1993,** 273–274. doi:10.1055/s-1993-22428
85. Farina, V.; Kapadia, S.; Krishnan, B.; Wang, C.; Liebeskind, L. S. *J. Org. Chem.* **1994,** *59,* 5905–5911. doi:10.1021/jo00099a018
86. Allred, G. D.; Liebeskind, L. S. *J. Am. Chem. Soc.* **1996,** *118,* 2748–2749. doi:10.1021/ja9541239
87. Molander, G. A.; Fumagalli, T. *J. Org. Chem.* **2006,** *71,* 5743–5747. doi:10.1021/jo0608366
88. van Horn, D. E.; Negishi, E.-i. *J. Am. Chem. Soc.* **1978,** *100,* 2252–2254. doi:10.1021/ja00475a058
89. Reetz, M. T. *Acc. Chem. Res.* **1993,** *26,* 462–468. doi:10.1021/ar00033a002
90. Chen, T.; Altmann, K.-H. *Chemistry* **2015,** *21,* 8403–8407. doi:10.1002/chem.201501252
91. Loiseleur, O.; Koch, G.; Cercus, J.; Schürch, F. *Org. Process Res. Dev.* **2005,** *9,* 259–271. doi:10.1021/op049807s
92. Dineen, T. A.; Roush, W. R. *Org. Lett.* **2004,** *6,* 2043–2046. doi:10.1021/ol049331x
93. Mandal, A. K.; Schneekloth, J. S., Jr.; Kuramochi, K.; Crews, C. M. *Org. Lett.* **2006,** *8,* 427–430. doi:10.1021/ol052620g
94. Paterson, I.; Yeung, K.-S.; Smaill, J. B. *Synlett* **1993,** 774–776. doi:10.1055/s-1993-22605
95. Börding, S.; Bach, T. *Chem. Commun.* **2014,** *50,* 4901–4903. doi:10.1039/C4CC01338G
96. Fürstner, A.; Funel, J.-A.; Tremblay, M.; Bouchez, L. C.; Nevado, C.; Waser, M.; Ackerstaff, J.; Stimson, C. C. *Chem. Commun.* **2008,** 2873–2875. doi:10.1039/B805299A

License and Terms

BEILSTEIN JOURNAL OF ORGANIC CHEMISTRY

Correlation of surface pressure and hue of planarizable push–pull chromophores at the air/water interface

Frederik Neuhaus[1,2], Fabio Zobi[1], Gerald Brezesinski[3], Marta Dal Molin[2,4], Stefan Matile[2,4] and Andreas Zumbuehl[*1,2]

Full Research Paper

Open Access

Address:
[1]Department of Chemistry, University of Fribourg, Chemin du Musée 9, 1700 Fribourg, Switzerland, [2]National Centre of Competence in Research (NCCR) Chemical Biology, Geneva, Switzerland, [3]Max Planck Institute of Colloids and Interfaces, Science Park Potsdam-Golm, 14476 Potsdam, Germany and [4]School of Chemistry and Biochemistry, University of Geneva, Geneva, Switzerland

Email:
Andreas Zumbuehl[*] - andreas.zumbuehl@unifr.ch

* Corresponding author

Keywords:
fluorescent probes; membrane biophysics; membrane pressure; membrane probes; monolayers

Beilstein J. Org. Chem. **2017,** *13,* 1099–1105.
doi:10.3762/bjoc.13.109

Received: 15 February 2017
Accepted: 13 May 2017
Published: 08 June 2017

This article is part of the Thematic Series "Lipids: fatty acids and derivatives, polyketides and isoprenoids".

Guest Editor: J. S. Dickschat

Abstract

It is currently not possible to directly measure the lateral pressure of a biomembrane. Mechanoresponsive fluorescent probes are an elegant solution to this problem but it requires first the establishment of a direct correlation between the membrane surface pressure and the induced color change of the probe. Here, we analyze planarizable dithienothiophene push–pull probes in a monolayer at the air/water interface using fluorescence microscopy, grazing-incidence angle X-ray diffraction, and infrared reflection–absorption spectroscopy. An increase of the lateral membrane pressure leads to a well-packed layer of the 'flipper' mechanophores and a clear change in hue above 18 mN/m. The fluorescent probes had no influence on the measured isotherm of the natural phospholipid DPPC suggesting that the flippers probe the lateral membrane pressure without physically changing it. This makes the flipper probes a truly useful addition to the membrane probe toolbox.

Introduction

Physical triggers are a major regulator of biological processes. The lateral bilayer membrane pressure, e.g., influences the nucleation [1] and shape changes [2] of lipid domains, it gates mechanosensitive pores [3] and globally organizes cell shape and motility [4]. However, although the surface pressure is vitally important to all living organisms, it eludes direct measurement and remains difficult to grasp.

The field is complicated by the fact that the lateral pressures in the inner and outer membrane leaflet do not have to be the same

[5], and an indirect method of measuring the membrane pressure would only yield an averaged global value. What is needed is a probe that directly measures the local surface pressure in a single membrane leaflet. One solution to the problem are the planarizable push–pull probes that have been recently introduced. The structure of such a "flipper" probe is depicted in Figure 1 [6-9].

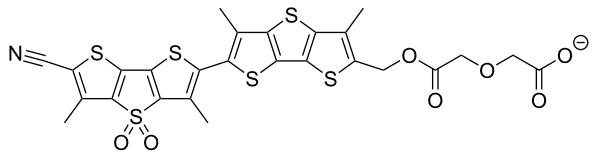

Figure 1: Structure of the (bis)dithienothiophene mechanosensitive flipper probe. Twisted out of planarity by two methyl groups next to the mechanosensitive bond, the two flipper-like heterocycles arrange themselves according to the surface pressure of the membrane.

Without going into details, the two dithienothiophene flippers are twisted out of planarity by chalcogen bond repulsion between the methyl groups and the endocyclic sulfurs next to the mechanosensitive bond [9]. Mechanical planarization in the ground state increases the conjugation of the push–pull system. As a result, the excitation (or absorption) maximum shifts up to 80 nm to the red [8]. An anionic headgroup is added to produce an amphiphile that self-assembles into monolayers and micelles and enters directionally into lipid bilayer membranes.

In order to use fluorescent flipper mechanophores for biological measurements, it is crucial to understand the exact relation between surface pressure and their spectroscopic properties. In earlier studies [8], the fluorescence was qualitatively determined in different lipid environments: the mechanosensitive probes (1.3 mol %) were added to large unilamellar vesicles (LUV) of either DPPC (dipalmitoyl-*sn*-glycero-3-phosphocholine) or DOPC (dioleoyl-*sn*-glycero-3-phosphocholine) at different temperatures. The flipper probes in DPPC, but not in DOPC, showed a red shift of the excitation maximum while emitting the same wavelength. The important difference between these two types of vesicles is their respective membrane phase: LUVs of DPPC undergo a gel to liquid crystalline phase change at the main transition temperature T_m of 41 °C, while LUVs of DOPC remain liquid crystalline over the entire temperature range measured [10]. What is missing is a quantitative correlation between the surface pressure of a membrane and the spectroscopic properties of the flipper mechanophores [4,8]. Therefore, we have performed Langmuir–Pockels monolayer experiments.

Monolayers at the air/water interface are well known models for biological membranes, avoiding trans-bilayer leaflet correlation effects [11-14]. Various techniques exist to probe the surface pressure and the lateral organization of the monolayer [14]. Using monolayers of pure flipper probes, we were able to study the fundamental questions of surface pressure–hue correlation avoiding interfering effects from other lipids or solvents. The putative lateral organization of the hydrophobic part of the flipper probes was probed by grazing-incidence angle X-ray diffraction experiments (GIXD) [15-18], as well as infrared reflection–absorption spectroscopy (IRRAS) [19].

Results and Discussion

Pressure-area isotherm measurements

All pressure-area isotherm measurements were performed on Langmuir–Pockels troughs (either a self-made computer-interfaced film balance [20] using the Wilhelmy method with a roughened glass plate or the commercial film balance from Riegler & Kierstein, Potsdam, Germany, with a Wilhelmy paper plate [12] to measure the surface tension with an accuracy of ±0.1 mN/m; the accuracy of the molecular area measurements is ±0.5 Å^2) at 295 K air and 293 K subphase temperature. Ultrapure water (18.2 MΩ·cm) has been used as subphase. A solution of the flipper mechanophore in chloroform/DMSO (8:2 vol%/vol%) was spread onto an expanded air/water interface. After evaporation and dissolution of the organic solvents, the size of the air/water interface was decreased with either one or two moving barriers (2 cm^2/min).

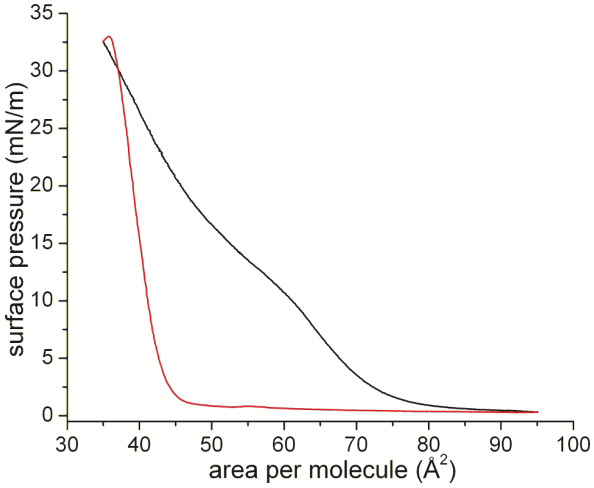

Figure 2: Langmuir–Pockels isotherm of a monolayer of flipper mechanophores during the first compression (black) and subsequent expansion (red) at the air/water interface at 20 °C subphase temperature and 22 °C air temperature.

The first compression curve is characterized by a fluid-like behavior (no lateral long-range ordering) at low pressure, and a transition range around 15 mN/m. Above this pressure range, the slope of the isotherm is smaller than expected for a

condensed layer. However, this apparently low slope is connected with the experimental problem of measuring the surface tension of stiff films and the organization of this particular flipper mechanophore. The stiffness of the layer leads to a tilting of the Wilhelmy plate (expansion leads shortly to a surface pressure increase, seen in the red curve). The tilting of the Wilhelmy plate can be remedied by slowing down the compression speed. Under these quasi-equilibrium conditions (see Figure S1, Supporting Information File 1) it is apparent that the film is slowly being organized into a condensed phase and will remain in this same condensed phase for the remainder of the experiments.

During the first compression, the film organized obviously into a condensed phase. Upon decompression, the monolayer remains in this condensed state due to strong π–π interactions. The following compression cycles reach the exact same values as before depicting a stably organized monolayer film with possible long-range order. The area per molecule of about 38 $Å^2$ is comparable to that observed for cholesterol monolayers [21,22].

Simulation

The molecular geometry of the mechanosensitive flipper probe was simulated in the gas phase at the density functional level of theory (DFT) in order to estimate an average value of the height and area of the same (details are given in the Experimental section and in Supporting Information File 1). The calculations indicate that, in its minimum energy surface structure, the probe spans a height of 24.3 Å (see Figure S2, Supporting Information File 1). From the optimized molecular geometry, the area of the probe was calculated as 37.2 $Å^2$ (see Figure S3, Supporting Information File 1). By assuming free rotation around the C–C bond connecting the two dithienothiophenes a value as high as 49.3 $Å^2$ is obtained, that mirrors the area per molecule at low surface pressure found in the Langmuir–Pockels experiments. The transition into the densely packed film due to strong π–π interactions around 15 mN/m leads to the smaller area per molecule.

Grazing incidence X-ray diffraction (GIXD)

The ordering phenomenon during the first compression can be explained by π–π interactions between the flipper mechanophores. We therefore characterized the degree of membrane ordering using synchrotron grazing incidence X-ray diffraction. The GIXD data in Supporting Information File 1 shows the absence of any long-range correlation giving rise to pronounced Bragg peaks at low surface pressures as expected from the first compression isotherm (see Figure S4, Supporting Information File 1). From the low-intensity and very broad diffraction signal, a large area per molecule of 58 $Å^2$ could be calculated for the flipper probe in the monolayer between 0 and 10 mN/m. It can be concluded that the flipper mechanophores do organize in an amorphous monolayer at low pressure (akin to an ordered liquid phase). High lateral pressures could not be reached with the present set-up. Therefore, further insights were expected from monolayer IRRAS experiments.

Infrared reflection–absorption spectroscopy (IRRAS)

The infrared reflection–absorption was recorded for a monolayer at different surface pressures (see Figures S5, S6, Supporting Information File 1). The positive peak at around 3600 cm^{-1}, indicating a higher intensity of the OH stretching vibrational band in the reference trough, is directly connected with the thickness of the monolayer in the sample trough (see Figure 3). The intensity of the OH-band increases during the first compression up to 20 mN/m, and remains constant at expansion. This is a clear hint that the thickness of the film increases markedly during the first compression and does not change afterwards during expansion. This experimental result can be explained by the transformation of an amorphous layer into a single layer of tightly packed molecules due to strong π–π interactions. This layer does not relax during expansion but remains tightly packed indicating the remarkable stability.

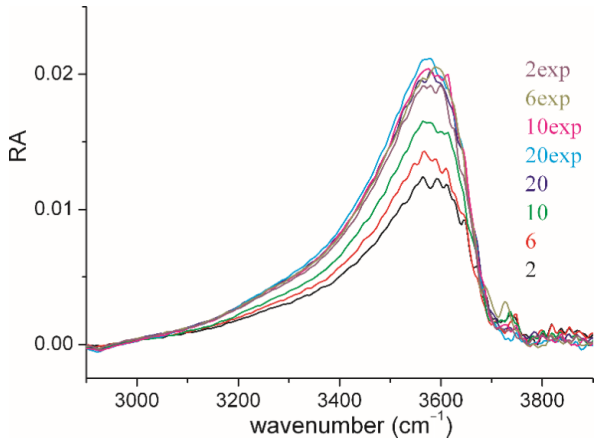

Figure 3: OH-stretching vibration (v(OH); 3600 cm^{-1}) for IRRA spectra of a flipper mechanophore monolayer during compression (2, 6, 10, and 20 mN/m) and expansion (20, 10, 6, 2 mN/m). The increase of intensity up to 20 mN/m indicates an increase of the effective layer thickness. It is important to note that the OH-band intensity does not change during expansion.

Angle dependent measurements allowed the quantification of the film thickness. The monolayer was first compressed to 20 mN/m, completely expanded and re-compressed to 10 mN/m. As shown in Figure 2, the isotherm of the expansion has the typical shape of a completely condensed film. Using a refractive index of 1.5, the value obtained from the fit of the OH

stretching vibrational band (see Figure S7, Supporting Information File 1) amounts to 24.1 Å, which is in accordance with the simulated length of the molecule, suggesting that the flipper mechanophore is standing upright on the air/water interface. The strong π–π interactions stabilize this upright orientation of the flipper molecules in the monolayer. Even the expansion to 2 mN/m does not lead to changes in the condensed monolayer thickness.

It is interesting to note that the ratio of the reflection absorbance (RA) of the $\nu_s(SO_2)$ measured with s- and p-polarized light does not change during compression indicating no change in the orientation of this transition dipole moment (see Figure S6, Supporting Information File 1).

Effect of flipper on DPPC

There is a structural similarity between the flipper probes and cholesterol with both molecules being amphiphilic and flat. This called for a closer look at the influence of both molecules on phospholipid membrane organization (see Figure 4).

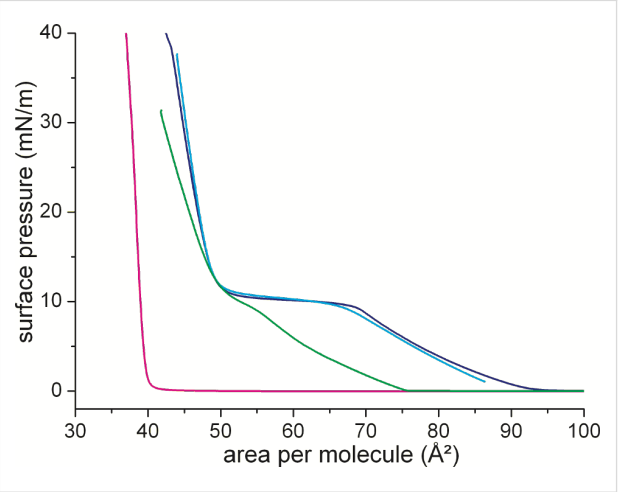

Figure 4: Isotherms of DPPC (dark blue), cholesterol (magenta), DPPC/cholesterol (8:2 mol/mol, green), and DPPC/flipper (8:2 mol/mol, blue) measured on water at 25 °C. The area in the mixture is given as area per DPPC molecule.

For DPPC, the first-order phase transition between the disordered LE and the ordered LC phase can be identified as a plateau region in which the two phases are coexisting. The phase transition pressure amounts to ≈10 mN/m. Cholesterol has a fully condensed isotherm with low compressibility of the layer. The addition of flipper probes to DPPC does not influence the shape of the isotherm. This could be an indication of a lack of interactions between the two molecules. This observation is supported by the IRRAS data ($\nu_{as}(CH_2)$) showing no influence of the 20 mol % of added mechanophore on the position of the CH_2 stretching vibration of the DPPC chains (see Figure S8, Supporting Information File 1). This is in contrast to the influence of cholesterol. There, the isotherm is shifted and the two-phase coexistence region is hardly visible anymore. This is again in complete agreement with the IRRAS data indicating the ordering effect of cholesterol on the LE phase of DPPC (shift to lower wavenumbers) and the disordering effect (shift to higher wavenumbers) on the LC phase. Overall, the lack of influence of the flipper mechanophore on the organization of the DPPC membrane is beneficial for the flipper's purpose as a membrane probe. This paves the way for testing the correlation of the flipper's fluorescent signal and the membrane lateral surface pressure.

Hue surface-pressure correlation

The flipper mechanophore shows a flexible geometry between the two heterocyclic chromophores. These two flippers can adapt to a decreasing monolayer molecular area and increasing surface pressure by decreasing the volume one molecule occupies. The flattening of the molecules should lead to a change of its spectroscopic properties [6-8]. In order to quantify this; we measured, to our knowledge, one of the first correlations between surface pressure and the hue of a fluorescent molecule. The hue is one of the main color appearance parameters and represents a digital value for color in the hue, saturation and value (HSV) color model.

In the second compression (see Figure S1, Supporting Information File 1) the correlation in Figure 5 shows a significant change in the observed hue of the monolayer starting at 18 mN/m. Although the measured areas per molecule are not fully quantitative [23], a value of 38 $Å^2$ can be assumed for the flipper chromophore in the condensed state. Upon expansion, the hue relaxes back to the initial range. Compared to compression the hue relaxation on expansion is slower. This effect can be hypothesized as follows: during the compression, defects in the monolayer organization are minimized until no defects are found anymore. A small further compression then leads to an abrupt change in hue. This creates a local energy minimum. Upon expansion, again defects are introduced into the film organization with concomitant slow adaptation by the flipper mechanophores.

The color range of the change is in the orange-yellow-region of the spectrum. The lateral pressure is in the range assumed for a natural bilayer membrane (≈30 mN/m) [24,25]. The color change is significant and represents the expected red shift. Although contributions from changes in π–π stacking on spectroscopic properties cannot be excluded, the observed red shift in compressed flipper monolayers is consistent with the earlier experiments on the planarization of monomeric flipper probes in bilayer membranes of increasing order [8]. Similar interpreta-

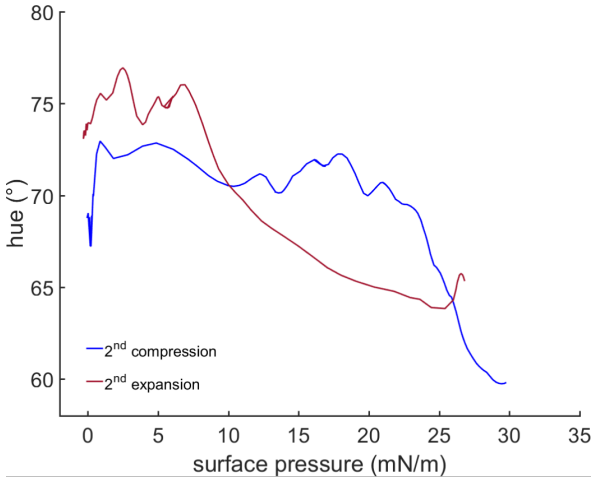

Figure 5: Correlation of the hue of a monolayer flipper probe with its measured surface pressure at the water/air interface at 20 °C subphase temperature and 22 °C air temperature.

tions have been made for the spectral changes observed upon planarization of self-assembled mechanosensitive twisted phenylethynyl polymers [26].

Conclusion

In conclusion, we have presented the first measurement correlating the hue of a mechanoresponsive fluorescent push–pull probe to the surface pressure of its monolayer. As expected, the color changed at a surface pressure of 18 mN/m. This value ranges in the 30 mN/m that are assumed for the surface pressure of an optimally packed fluid membrane [24,25]. Compared to cholesterol, the flipper probes do not influence the membrane packing of DPPC and therefore show true potential as disturbance-free mechanosensitive membrane probes.

Experimental

Grazing incidence angle X-ray diffraction (GIXD)

Grazing incidence angle X-ray diffraction measurements were performed at the PETRA III/P08 beamline at the DESY-Hamburg campus, Germany. A photon beam with 15 keV was used. The monolayers were prepared on a Langmuir–Pockels trough at 295 K air and 293 K subphase temperature. Beneath the analyzed area a glass block was placed in order to dampen any mechanically induced surface movement. The trough chamber was flushed with wet helium throughout the whole measurement. The yielded data has been processed as follows; the water-data was subtracted from the flipper data to isolate the flipper signal from that of the water molecules on the surface. The weakly correlated signal was then integrated to determine the maximum position of Q_{xy}. From the determined $d = 2\pi/Q_{xy}$ the resulting area per molecule has been calculated.

Infrared reflection–absorption spectroscopy (IRRAS)

Infrared reflection–absorption spectra were recorded on a Vertex 70 FTIR spectrometer from Bruker (Ettlingen, Germany) equipped with a liquid nitrogen cooled MCT (mercury cadmium telluride) detector attached to an external air/water reflection unit (XA-511). The IR beam was conducted out of the spectrometer and focused onto the water surface of the thermostated Langmuir trough. The measurements were carried out with p- and s-polarized light at different angles of incidence. Measurements were performed using a trough with two compartments. One compartment contained the monolayer system under investigation (sample), whereas the other was filled with the pure subphase (reference). The trough was shuttled by a computer-controlled shuttle system to illuminate either the sample or the reference [19,27,28]. The single-beam reflectance spectrum (R_0) from the reference trough was taken as background for the single-beam reflectance spectrum (R) of the monolayer in the sample trough to calculate the reflection–absorption spectrum as $-\log(R/R_0)$ in order to eliminate the water vapor signal. In order to maintain a constant water vapor content, the whole system was placed into a hermetically sealed box. The resolution and scanner speed in all experiments were 8 cm^{-1} and 20 kHz. The incident IR beam was polarized with a KRS-5 wire grid polarizer. For s-polarized light, spectra were co-added over 200 scans, and spectra with p-polarized light were co-added over 400 scans. Spectra were corrected to a common baseline to allow for comparison. IRRA spectra were simulated using a MATLAB program [29,30] on the basis of the optical model of Kuzmin and Michailov [31,32]. The intensity and shape of a reflection absorption band depend on the absorption coefficient k, the full-width of half-height (fwhh), the orientation of the transition dipole moment (TDM) within the molecule α, the molecular tilt angle θ, the polarization and the angle of incidence (AoI) of the incoming light, as well as the layer thickness d and its refractive index n. Simulated spectra were fitted to the experimental data in a global fit, where all spectra recorded at different AoI and different polarizations were fitted in one non-linear least square minimization using the Levenberg/Marquardt algorithm. The polarizer quality was set to $\Gamma = 0.01$. The optical constants of the water subphase were taken from Bertie et al. [33,34]. The layer thickness d was determined from a fit of the OH stretching vibrational band (ν(OH)) in the range of 3800–3000 cm^{-1}.

Computational simulations

Geometry optimization, as well as frequency calculations for the flipper mechanophore, were performed in the gas phase at the density functional level of theory with the Gaussian 03 program package [35] using the hybrid B3LYP functional [36] in conjunction with the LanL2DZ basis set [37-39]. The geome-

try of the flipper mechanophore was fully optimized without symmetry restrictions. The nature of the stationary points was checked by computing vibrational frequencies in order to verify true minima. The final optimized geometry shows no negative values of vibrational frequencies. The height (h) and the minimum area (A) value of the flipper mechanophore were measured on the basis of the structural parameters of the optimized geometry. These were respectively obtained by: a) measuring the distance between the oxygen and nitrogen atoms of the terminal carboxylic and ethynyl groups (h) and b) measuring the distance d between centroids of planes defined by the outmost external atoms with $A = \pi(d/2)^2$. In the gas phase optimized geometry d = 6.88 Å giving A = 37.2 Å^2. However, by assuming free rotation around the C–C bond connecting the two dithienothiophene units a maximum value of d = 7.92 Å is obtained giving A = 49.3 Å^2.

Hue measurement

The optical signal from the Langmuir–Pockels trough was recorded with a Leica DFC7000 T microscope camera. The optics was provided by a home-made fluorescence microscope (Riegler & Kierstein, Germany). The video processing was performed using a self-developed script running on MatLab® R2015a (Version: 8.5.0.197613), which also correlated the data of the pressure/area isotherms. The hue values were calculated from the RGB (red-green-blue) data recorded from the microscope camera using the following equations via the rgb2hsv functionality of MatLab® R2015a:

$$R' = \frac{\text{Red}}{255}$$

$$G' = \frac{\text{Green}}{255}$$

$$B' = \frac{\text{Blue}}{255}$$

$$C_{\max} = \max\left(R', G', B'\right)$$

$$C_{\min} = \min\left(R', G', B'\right)$$

$$\Delta = C_{\max} - C_{\min}$$

$$\text{Hue} = \begin{cases} 0^\circ & ,\Delta = 0 \\ 60^\circ \times \left(\frac{G'-B'}{\Delta} \bmod 6\right) & ,C_{\max} = R' \\ 60^\circ \times \left(\frac{B'-R'}{\Delta} + 2\right) & ,C_{\max} = G' \\ 60^\circ \times \left(\frac{R'-G'}{\Delta} + 4\right) & ,C_{\max} = B' \end{cases}$$

The curves were fitted using a Lowess regression which is a local regressiong using weighted linear least squares and a second degree polynomial model giving no weight to outliers higher than sixfold absolute mean.

Supporting Information

Supporting Information File 1

Surface pressure/area per molecule isotherms, energy minimized structures of the flipper mechanophore, GIXD heightmaps, and IRRAS data.
[http://www.beilstein-journals.org/bjoc/content/supplementary/1860-5397-13-109-S1.pdf]

Acknowledgements

Parts of this research were carried out at PETRA III at DESY, a member of the Helmholtz Association (HGF). We would like to thank Dr. Uta Ruett and Dr. Florian Bertram for assistance (in using beamline P08). The authors thank Dr. Sandor Balog (University of Fribourg) for helpful discussion on GIXD, Irina Berndt (MPI Potsdam) for the IRRAS experiments, and the Universities of Fribourg and Geneva, the National Centre of Competence in Research (NCCR) in Chemical Biology as well as the Swiss National Science Foundation for financial support.

References

1. Chen, D.; Santore, M. M. *Langmuir* **2014,** *30,* 9484–9493. doi:10.1021/la502089t
2. Komura, S.; Shimokawa, N.; Andelman, D. *Langmuir* **2006,** *22,* 6771–6774. doi:10.1021/la053135x
3. Pliotas, C.; Dahl, A. C. E.; Rasmussen, T.; Mahendran, K. R.; Smith, T. K.; Marius, P.; Gault, J.; Banda, T.; Rasmussen, A.; Miller, S.; Robinson, C. V.; Bayley, H.; Sansom, M. S. P.; Booth, I. R.; Naismith, J. H. *Nat. Struct. Mol. Biol.* **2015,** *22,* 991–998. doi:10.1038/nsmb.3120
4. Diz-Muñoz, A.; Fletcher, D. A.; Weiner, O. D. *Trends Cell Biol.* **2013,** *23,* 47–53. doi:10.1016/j.tcb.2012.09.006
5. Traïkia, M.; Warschawski, D. E.; Lambert, O.; Rigaud, J.-L.; Devaux, P. F. *Biophys. J.* **2002,** *83,* 1443–1454. doi:10.1016/S0006-3495(02)73915-5
6. Fin, A.; Jentzsch, A. V.; Sakai, N.; Matile, S. *Angew. Chem., Int. Ed.* **2012,** *51,* 12736–12739. doi:10.1002/anie.201206446
7. Doval, D. A.; Dal Molin, M.; Ward, S.; Fin, A.; Sakai, N.; Matile, S. *Chem. Sci.* **2014,** *5,* 2819–2825. doi:10.1039/c4sc00939h
8. Dal Molin, M.; Verolet, Q.; Colom, A.; Letrun, R.; Derivery, E.; Gonzalez-Gaitan, M.; Vauthey, E.; Roux, A.; Sakai, N.; Matile, S. *J. Am. Chem. Soc.* **2015,** *137,* 568–571. doi:10.1021/ja5107018
9. Soleimanpour, S.; Colom, A.; Derivery, E.; Gonzalez-Gaitan, M.; Roux, A.; Sakai, N.; Matile, S. *Chem. Commun.* **2016,** *52,* 14450–14453. doi:10.1039/C6CC08771J
10. Lewis, R. N. A. H.; McElhaney, R. N. The Mesomorphic Phase Behavior of Lipid Bilayers. In *The Structure of Biological Membranes,* 3rd ed.; Yeagle, P. L., Ed.; CRC Press: Boca Raton, 2012; pp 19–89. doi:10.1201/b11018-5
11. Brezesinski, G.; Möhwald, H. *Adv. Colloid Interface Sci.* **2003,** *100–102,* 563–584. doi:10.1016/S0001-8686(02)00071-4

12. Weinberger, A.; Tanasescu, R.; Stefaniu, C.; Fedotenko, I. A.; Favarger, F.; Ishikawa, T.; Brezesinski, G.; Marques, C. M.; Zumbuehl, A. *Langmuir* **2015,** *31,* 1879–1884. doi:10.1021/la5041745
13. Moehwald, H.; Brezesinski, G. *Langmuir* **2016,** *32,* 10445–10458. doi:10.1021/acs.langmuir.6b02518
14. Stefaniu, C.; Brezesinski, G.; Möhwald, H. *Adv. Colloid Interface Sci.* **2014,** *208,* 197–213. doi:10.1016/j.cis.2014.02.013
15. Stefaniu, C.; Brezesinski, G. *Adv. Colloid Interface Sci.* **2014,** *207,* 265–279. doi:10.1016/j.cis.2014.01.005
16. Stefaniu, C.; Brezesinski, G. *Curr. Opin. Colloid Interface Sci.* **2014,** *19,* 216–227. doi:10.1016/j.cocis.2014.01.004
17. Levine, J. R.; Cohen, J. B.; Chung, Y. W.; Georgopoulos, P. *J. Appl. Crystallogr.* **1989,** *22,* 528–532. doi:10.1107/S002188988900717X
18. Chason, E.; Mayer, T. M. *Crit. Rev. Solid State Mater. Sci.* **1997,** *22,* 1–67. doi:10.1080/10408439708241258
19. Mendelsohn, R.; Brauner, J. W.; Gericke, A. *Annu. Rev. Phys. Chem.* **1995,** *46,* 305–334. doi:10.1146/annurev.pc.46.100195.001513
20. Vollhardt, D. *Curr. Opin. Colloid Interface Sci.* **2014,** *19,* 183–197. doi:10.1016/j.cocis.2014.02.001
21. Shah, D. O.; Schulman, J. H. *J. Lipid Res.* **1967,** *8,* 215–226.
22. Ziblat, R.; Leiserowitz, L.; Addadi, L. *J. Am. Chem. Soc.* **2010,** *132,* 9920–9927. doi:10.1021/ja103975g
23. Stefaniu, C.; Zaffalon, P.-L.; Carmine, A.; Verolet, Q.; Fernandez, S.; Wesolowski, T. A.; Brezesinski, G.; Zumbuehl, A. *Langmuir* **2015,** *31,* 1296–1302. doi:10.1021/la5039987
24. Blume, A. *Biochim. Biophys. Acta* **1979,** *557,* 32–44. doi:10.1016/0005-2736(79)90087-7
25. Marsh, D. *Biochim. Biophys. Acta* **1996,** *1286,* 183–223. doi:10.1016/S0304-4157(96)00009-3
26. Kim, J.; Swager, T. M. *Nature* **2001,** *411,* 1030–1034. doi:10.1038/35082528
27. Flach, C. R.; Gericke, A.; Mendelsohn, R. *J. Phys. Chem. B* **1997,** *101,* 58–65. doi:10.1021/jp962288d
28. Muenter, A. H.; Hentschel, J.; Börner, H. G.; Brezesinski, G. *Langmuir* **2008,** *24,* 3306–3316. doi:10.1021/la701909m
29. Schwieger, C.; Chen, B.; Tschierske, C.; Kressler, J.; Blume, A. *J. Phys. Chem. B* **2012,** *116,* 12245–12256. doi:10.1021/jp306612k
30. Schrettl, S.; Stefaniu, C.; Schwieger, C.; Pasche, G.; Oveisi, E.; Fontana, Y.; Fontcuberta i Morral, A.; Reguera, J.; Petraglia, R.; Corminboeuf, C.; Brezesinski, G.; Frauenrath, H. *Nat. Chem.* **2014,** *6,* 468–476. doi:10.1038/nchem.1939
31. Kuzmin, V. L.; Mikhailov, A. V. *Opt. Spectrosc.* **1981,** *51,* 691–695.
32. Kuzmin, V. L.; Romanov, V. P.; Michailov, A. V. *Opt. Spectrosc.* **1992,** *73,* 1–26.
33. Bertie, J. E.; Ahmed, M. K.; Eysel, H. H. *J. Phys. Chem.* **1989,** *93,* 2210–2218. doi:10.1021/j100343a008
34. Bertie, J. E.; Lan, Z. *Appl. Spectrosc.* **1996,** *50,* 1047–1057. doi:10.1366/0003702963905385
35. Iyengar, S. S.; Frisch, M. J. *J. Chem. Phys.* **2004,** *121,* 5061–5070. doi:10.1063/1.1780157
36. Becke, A. D. *J. Chem. Phys.* **1993,** *98,* 5648–5652. doi:10.1063/1.464913
37. Hay, P. J.; Wadt, W. R. *J. Chem. Phys.* **1985,** *82,* 270–283. doi:10.1063/1.448799
38. Wadt, W. R.; Hay, P. J. *J. Chem. Phys.* **1985,** *82,* 284–298. doi:10.1063/1.448800
39. Hay, P. J.; Wadt, W. R. *J. Chem. Phys.* **1985,** *82,* 299–310. doi:10.1063/1.448975

License and Terms

BEILSTEIN JOURNAL OF ORGANIC CHEMISTRY

Strategies in megasynthase engineering – fatty acid synthases (FAS) as model proteins

Manuel Fischer and Martin Grininger*

Review

Open Access

Address:
Institute of Organic Chemistry and Chemical Biology, Buchmann Institute for Molecular Life Sciences, Cluster of Excellence for Macromolecular Complexes, Goethe University Frankfurt, Max-von-Laue-Str. 15, 60438 Frankfurt am Main, Germany

Email:
Martin Grininger* - grininger@chemie.uni-frankfurt.de

* Corresponding author

Keywords:
fatty acid synthases; megasynthases; metabolic enzyme engineering; polyketide synthases; protein design

Beilstein J. Org. Chem. **2017,** *13,* 1204–1211.
doi:10.3762/bjoc.13.119

Received: 23 March 2017
Accepted: 26 May 2017
Published: 21 June 2017

This article is part of the Thematic Series "Lipids: fatty acids and derivatives, polyketides and isoprenoids".

Guest Editor: J. S. Dickschat

Abstract

Megasynthases are large multienzyme proteins that produce a plethora of important natural compounds by catalyzing the successive condensation and modification of precursor units. Within the class of megasynthases, polyketide synthases (PKS) are responsible for the production of a large spectrum of bioactive polyketides (PK), which have frequently found their way into therapeutic applications. Rational engineering approaches have been performed during the last 25 years that seek to employ the "assembly-line synthetic concept" of megasynthases in order to deliver new bioactive compounds. Here, we highlight PKS engineering strategies in the light of the newly emerging structural information on megasynthases, and argue that fatty acid synthases (FAS) are and will be valuable objects for further developing this field.

Review

Megasynthases are proteins in natural compound synthesis

Microbial natural products represent a rich source of pharmaceutically relevant chemical entities. A major class is represented by polyketides (PK) exemplified by the antibiotics erythromycin and rifamycin, by the antineoplastic doxorubicin and by the antiparasitic avermectin (Figure 1a) [1]. PK are assembled from acyl-coenzyme A (acyl-CoA) units via a series of Claisen-type condensation reactions catalyzed by polyketide synthases (PKS) (Figure 1b). PKS occur as large multifunctional enzymes, termed megasynthases, which harbor the catalytic domains on large polypeptides that can exceed sizes of one MDa [2]. PK compounds are assembled either in a linear manner, where multiple modules successively condense precursor units to the final compound (modular systems) [3], or in a recursive manner, with the catalytic domains of a single module repeatedly condensing precursor units until the specific length/size is attained (iterative systems) [4]. In either case, the enzy-

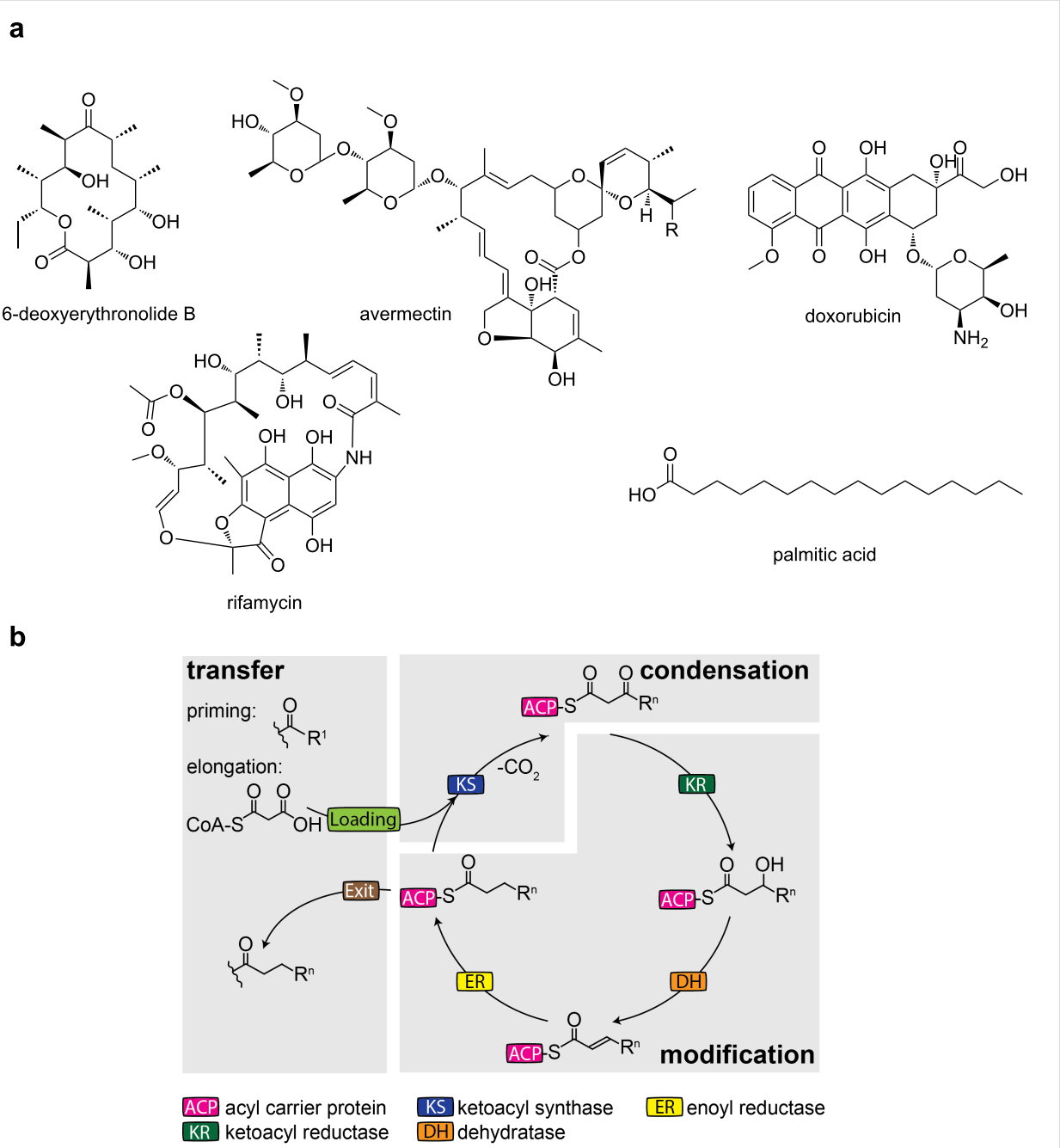

Figure 1: Megasynthases – chemistry and modes of action. a) Products of PKS and FAS megasynthases. b) Reaction cycle of iterative fatty acid biosynthesis as performed by fatty acid synthases (FAS). Synthesis by PKS is essentially similar, except a variation in the degree of β-carbon modification, and the variation in loading and exit transferases. Modular PKS perform one cycle per module before translocating the substrate to the next module.

matic functions of each module deterministically encode the chemical nature of the final product [5].

Fatty acid synthases (FAS) are a type of PKS megasynthases

The biosynthetic foundations of PKS are essentially identical to those of FAS. Whereas FAS are strictly fully reducing (Figure 1b), the nature and extent of β-carbon modification varies across the PKS [6]. Though knowledge on PKS has improved in the last decade [7], particularly aided by recent structural studies [8-10], the current insight onto PKS is still significantly built on FAS data. Since the onset of FAS research with the pioneering studies of Bloch, Lynen, Stadtman and Wakil [10-12], FAS have been subject of intense investigation and are

today relatively well understood. In recent years, a wealth of structural data on FAS multienzyme complexes (type I) has further deepened the insight into the principles of fatty acid (FA) synthesis [13-19].

Molecular mechanisms of FAS/PKS mode of action

Compartmentalization

Compartmentalization is a phenomenon seen both in FAS as well as PKS systems, but it is differing in its specific structural manifestation. In fungal FAS (and bacterial type I FAS occurring in *Corynebacterium*, *Mycobacterium* and *Nocardia* of the genus *Actinomycetales*), nature evolved a D3-symmetric barrel-shaped structure of 2.6 MDa, which encloses all synthetic processes in two reaction chambers (Figure 2a) [19,20]. The animal FAS exhibits a structurally open homodimeric fold, which shows high conformational flexibility allowing large swinging and swiveling motions (Figure 2b). In animal FAS, synthesis of FA is performed in reaction clefts rather than in enclosed chambers, as found in fungal FAS.

An approximate calculation from the dimensions of the fungal FAS (barrel structure abstracted as cylinder and considering six full sets of active sites per barrel) accounts for a virtual concentration of 1.8 mM of active sites. An analogous consideration for animal FAS (again abstracted as spanning a cylindrical reaction space, two full sets of active sites) gives a virtual active site concentration of 1.2 mM. Accordingly, both scaffolds of FA type I synthesis facilitate reactions at high virtual concentration of enzymatic domains. PKS megasynthases share basic principles with the mammalian FAS fold (Figure 2c) [6,7], and it is valid to assume that active site concentrations lie in the similar range. Bacterial and mitochondrial FA synthesis comprises separate enzymes. To compensate for the lower organizational level, key enzymes occur at copy numbers of about 10,000 (malonyl transferase FabD) to 23,000 (dehydratase FabA), as

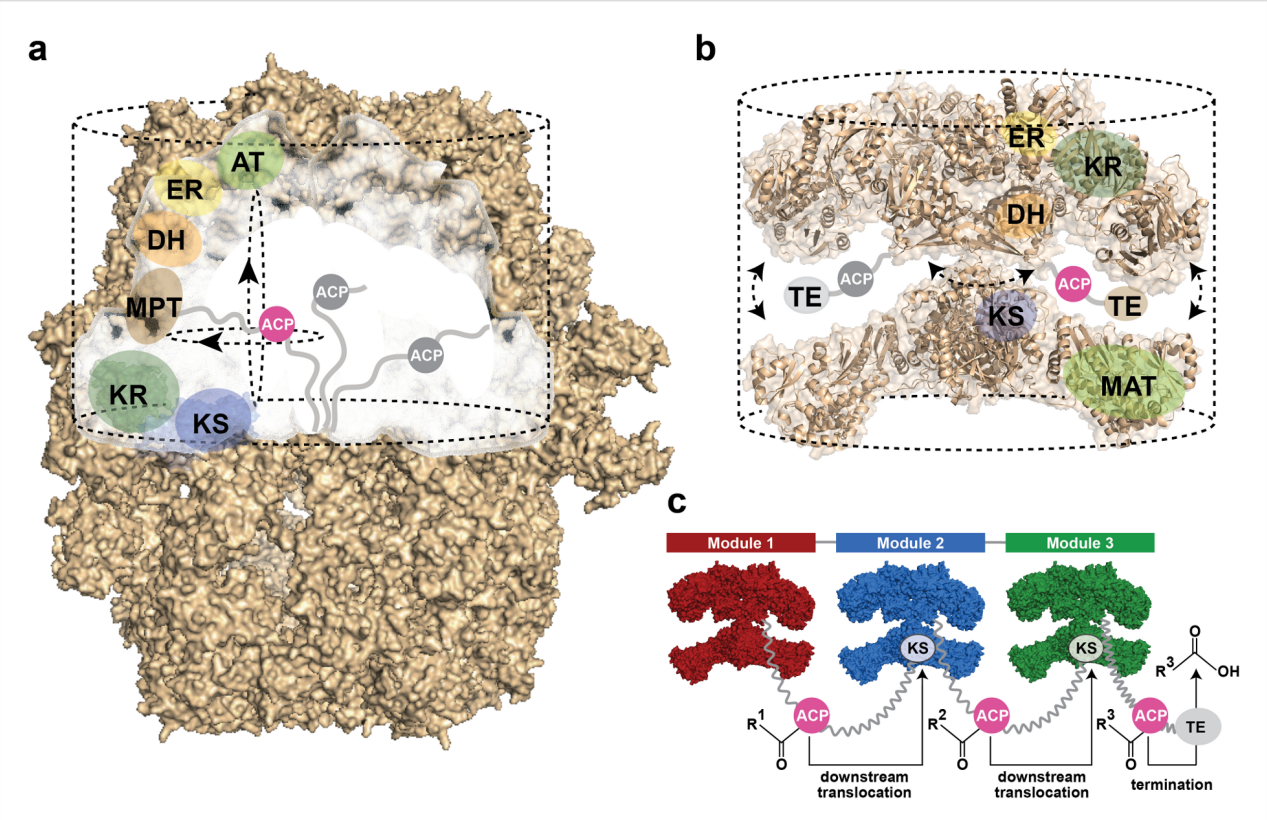

Figure 2: Compartmentalization of synthesis. a) Surface depiction of fungal FAS (PDB-code: 3hmj) with the upper reaction chamber shown without the front part of the barrel wall. One of overall three sets of catalytic domains within a reaction chamber is indicated. Abbreviations as introduced before; additionally, acetyl transferase (AT) and malonyl-/palmitoyl-transferase (MPT). Two linkers, abstracted as grey lines, flexibly bind the acyl carrier protein (ACP) domain. The reaction volume was calculated as indicated by dashed lines. b) Cartoon representation of X-shaped animal FAS I (PDB-code: 2vz8) with one of overall two sets of catalytic domains highlighted. Abbreviations as introduced before; additionally, malonyl-/acetyl-transferase (MAT) and thioesterase (TE). Conformational flexibility of animal FAS, as indicated by arrows, is largely induced by a central waist. The reaction volume was calculated as cylinder as indicated by dashed lines. c) Model of a modular PKS assembly line. Modules 1–3 are depicted in an animal FAS I-like fold. Linkers, covalently or non-covalently connecting modules in modular PKS, are abstracted with zig-zag lines carrying also ACP. Only one of the two ACP domains per homodimeric module is shown for clarity. Each ACP acts *in cis* for substrate elongation (see Figure 2b) and *in trans* for substrate translocation.

such being represented within the class of most abundant proteins in *E. coli*; in concentration directly following ribosomal proteins and proteins associated with translation [21]. Calculated with an average volume of an *E. coli* cell of 2.5 μm [3,22], copy numbers account for molar concentrations of about 0.007 to 0.016 mM.

Substrate shuttling

FA and PK syntheses generally rely on ACP that shuttles substrates and intermediates as covalently bound cargo between active sites [23]. In FAS and PKS (type I) megasynthases, ACP are embedded as domains in the large polypeptide chains (Figure 2a and b). Held in the compartment, ACP hinders the loss of the covalently attached acyl moiety, realizing high substrate concentrations. In addition to intramodular substrate shuttling, ACP is also responsible for the translocation of the cargo to the downstream modules in modular PKS, which largely accounts for the assembly-line character of these proteins (Figure 2c).

As part of the multienzyme compartment, the mode of ACP action is best described as enabling limited diffusion within a conformational space that is restricted by ACP linkers and the protein scaffold. As calculated from the reported specific activity of 2,500 mU/mg [24], *S. cerevisiae* FAS runs about 18 iterative cycles per second (per set of active sites). Given that each cycle requires six productive interactions between the ACP and the catalytic domains (ACP:KS (ping-step) → ACP:MTP → ACP:KS (pong-step) → ACP:KR → ACP:DH → ACP:ER), *S. cerevisiae* FAS performs a catalytic step every 9.2 milliseconds. This high catalytic efficiency is due to the highly evolutionarily developed architecture of fungal FAS. Enzymatic domains are rigidly embedded into the walls of the reaction chambers, while the ACP domains are held centrally in the chamber by two unstructured linkers of about 20 to 50 amino acid residues in length (40 and 25 amino acids in *S. cerevisiae* FAS). Interestingly, duplicated ACP domains have been observed in certain fungal FAS, and ACP duplication has been ranked as a rather late event during the course of evolution [25]. In the light of the key role of ACP in substrate shuttling, multiple ACP domains might be beneficial in increasing the substrate concentration at which type I synthesis is performed [26,27]. The conformationally more flexible mammalian FAS runs at 2 cycles per second (per set of active sites) calculated from specific activities reported for chicken FAS [28]. Owing to a difficult access to the purified proteins, a limited number of studies report the activity of PKS megasynthases. For example, the modular PKS 6-deoxyerythronolide B synthase (DEBS) shows a turnover number of about 1 min^{-1} over the six elongation steps for product production (accordingly roughly 0.05 elongations per second per set of active sites) [29]. For the iterative PKS 6-methylsalicylic acid synthase (MSAS), a turnover number of about 4.2 min^{-1} over the three iterations for product synthesis was reported (0.1 elongations per second per set of active sites) [30].

The function of ACP

The molecular details underlying the ACP mode of action are currently collaboratively decoded via structural, functional and computational methods, disclosing the picture of substrate shuttling being much more than just a mean to keep substrates recruited at the synthetic unit. Most of the understanding about the interaction of ACP with catalytic domains again originates from studies on FAS. Early information was received by *S. cerevisiae* FAS X-ray structures, in which ACP was found in contact with the KS domain [31]. In fungal FAS, ACP is an extended fold comprised of a bacterial-like core fold and a 4-helical extender fold, rendering ACP about twice the size of ACP occurring in mammalian FAS and PKS. The active serine, which is post-translationally phosphopantetheinylated [24,32], is located at the tip of the fold opposite to the N- and C-terminal attachment sites. This structural organization likely preserves linkers from interfering in ACP:domain interactions, and, concomitantly, may support the loading of the covalent acyl moiety by steering the acyl tail into the binding channels. A computational study, on the basis of *S. cerevisiae* FAS data, refined the understanding of ACP-mediated substrate shuttling in *S. cerevisiae* FAS by confirming steering in the sense of promoting correct orientations, as well as suggesting electrostatic steering by charge complementarity of the surfaces of binding partners [33]. Recent studies have characterized ACP of FAS megasynthases as not sequestering the covalently bound acyl moiety, which is supportive of molecular steering effects underlying substrate shuttling [34,35]. Specific structural information on the interaction of ACP with the catalytic domains is otherwise rare, hindered by the transient nature of this event. The application of specific crosslinkers aided in overcoming this difficulty for the interaction of ACP with the FAS type II dehydratase FabA [36,37]. This study was the first in tracing key events in ACP docking and acyl-moiety binding, and allowed catching an initial glimpse of the dynamic process of ACP substrate delivery. Also the interaction of ACP VinL and the acyltransferase VinK, involved in loading a PKS megasynthase, was recently resolved in structure [38]. It is reasonable to assume that the ACP mode of action in PKS is similar to FAS. The role of ACP in modular PKS is, however, complicated by the additional task of delivering the acyl moieties also to the downstream module (Figure 2c). Just rudimentary information on the nature of this translocation step is available; most importantly suggesting ACP to dock with different faces during intra- and intermodular acyl-chain delivery [39,40].

Strategies for megasynthase engineering

The concept of one multienzyme module being responsible for the incorporation of one building block in modular systems has inspired chemists and biologists for more than two decades to create engineered pipelines for the directed synthesis of bioactive compounds [41,42]. Engineering of megasynthases provides the opportunity to complement or replace synthetic chemical strategies for natural compound production with sustainable, green-chemistry approaches. Several reports on the engineering of PKS have proven the feasibility of the concept [43,44], but megasynthase design as a tool for the custom synthesis of natural compounds or complex precursor molecules has remained elusive to date [45,46].

Towards the desirable goal to produce PK by designing the respective megasynthase, the chemical/biological community has largely performed the approach of assembling modules and domains from interchangeable units. Mainly by addition, removal and/or substitution of modules and domains (Figure 3a), libraries of compounds have been generated with varying patterns of functional groups [1,47-50]. In the light of the emerging knowledge on the complex role of ACP during intramodular and intermodular interactions, as well as the yet essentially unclear principles of module–module interactions [8,51,52], the idea of an unhindered vectorial transport through such chimeric assembly line PKS may seem naive. Clearly, research over the last two decades has demonstrated that modules and domains are not interchangeable per se [45,46], and a successful mixing-and-matching approach will significantly depend on engineering clashing interfaces.

An alternative approach towards harnessing PKS for custom-product synthesis, may be built on the concept of establishing selected PKS as generic scaffolds (“chassis”). In such an engineering strategy, a PKS scaffold is first selected and then adapted to the requirement of a specific synthesis; the latter essentially requiring the engineering of active sites and binding channels for accepting and processing desired substrates and intermediates (Figure 3b). In using a related terminology as for the approach of domain and module recombination (“mix-and-match”), such an alternative approach may be termed “preserve-and-adapt”. While the adaptation of active sites will remain as a challenging task in such an approach, the generally profound description of substrate/active site complexes, the conservation of active sites beyond protein families, and their susceptibility for biophysical assays makes the engineering of substrate specificities a promising alternative to the mix-and-match approach; particularly as domain–domain and module–module interactions are comparably difficult to engineer. The benefit of a preserve-and-adapt approach lies in the non-invasive nature to

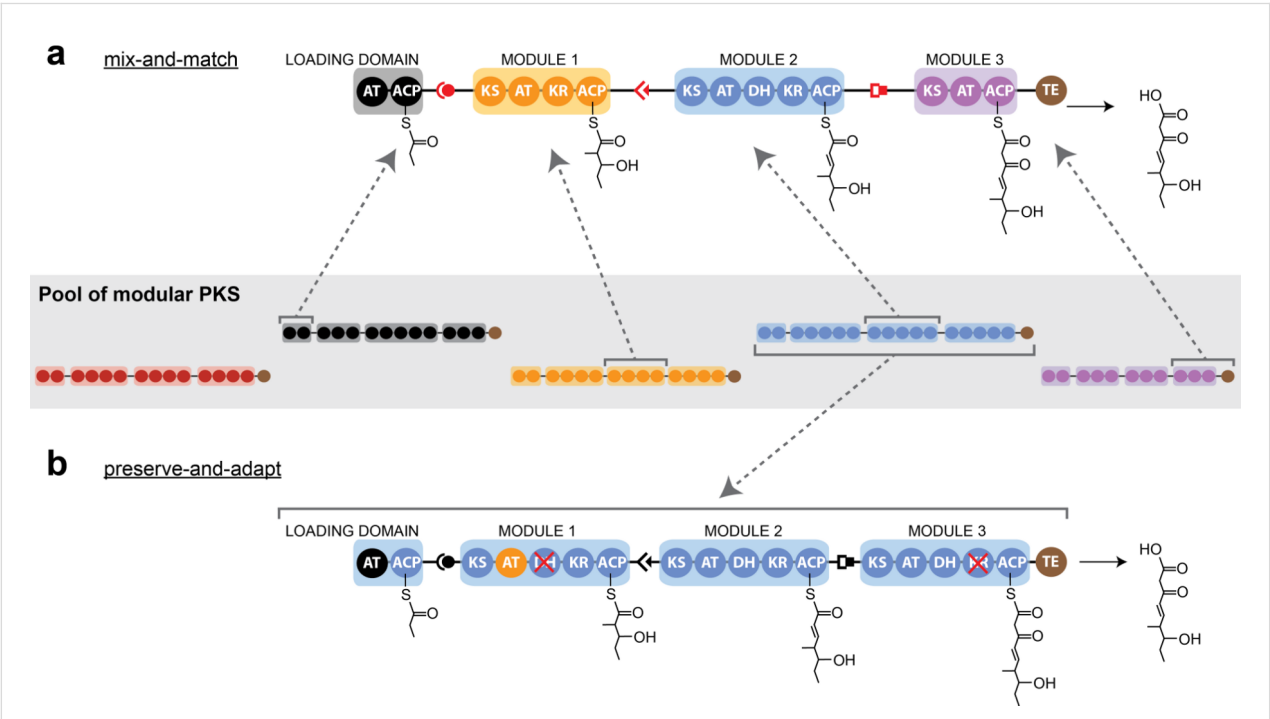

Figure 3: Strategies of megasynthase engineering. a) Mix-and-match approach: A hypothetical chimeric PKS is assembled module by module from a pool of available PKS. In such approach, docking domains (represented in red color) are adapted for coding the sequence of assembly. b) Preserve-and-adapt approach: A modular PKS, selected from the native pool by beneficial properties (see text) is used as a scaffold and adapted in catalytic functions and substrate specificities.

the overall structural frame of an assembly line, i.e., keeping module–module and domain–domain interactions as well as substrate shuttling intact. Another advantage is that such PKS scaffolds could be selected for suited properties, as, e.g., expression levels and protein quality in recombinant hosts; likely an aspect, which is underestimated in mix-and-match approaches. A preserve-and-adapt approach might moreover be aided by the evolutionary loosely developed substrate specificity of megasynthases. As megasynthase-mediated synthesis is subject to substrate shuttling, achieving high local concentrations of substrates and mediating specificity of the system via domain–domain interactions, evolution has likely not selected for strict substrate specificity as compared to diffusion-loaded proteins, and megasynthases might be inherently substrate tolerant [53-55].

Preserve-and-adapt approach on the example of FAS

Given the detailed understanding of their structural and functional properties, FAS are ideal proteins for evaluating a preserve-and-adapt engineering strategy on megasynthases in an in vitro environment. We therefore recently started the specific project of installing the synthesis of short-chain FA (SCFA) and the polyketide lactone 6-heptyl-4-hydroxypyran-2-one (6-HHP) within the scaffold of the *Corynebacterium ammoniagenes* FAS (a bacterial type I system). In an engineered reaction sequence, an initial FAS module was designed to produce SCFA as acyl esters, which are in a second FAS module elongated to the triketide and cyclized to the final lactone (Figure 4). A similar synthetic route can be found in norsolorinic acid synthesis, in which a fully reducing fungal FAS collaborates with a non-reducing PKS [4,56], as well as in resorcylic acid lactone synthesis, in which two iterative PKS systems work in sequence [57]. We selected this reaction route, as it involves the engineering of the condensation domain KS and the transferase domains AT and MPT that make up the catalytic core in PKS/FAS proteins. This approach was successful in finally obtaining the desired compound in 35% yield by overall just implementing five mutations [58].

When introducing module 1 mutations into baker's yeast, the technologically relevant SCFA were produced by C_8-CoA being hydrolyzed and exported to the culture medium [59]. Particularly in this function, module 1 is interesting for comparing the preserve-and-adapt approach with other strategies employed to date for producing SCFA. By adapting active site specificities, mutations essentially steer de novo fatty acid synthesis towards the early release of not yet fully elongated C_{16} and C_{18}-acyl-CoA, while leaving the overall molecular mechanisms intact. Indeed, evaluated on the basis of SCFA yields, the approach turned out to be highly powerful compared to other strategies that were overwriting native synthesis with a short-chain acyl-ACP specific thioesterase that is inserted as extra domain into the polypeptide chain [60-63].

Further studies on FAS can be envisioned, i.e., when considering the PKS-like mammalian FAS fold. Already at this level, the proof-of-concept performed on FAS can, however, serve as a seed for starting efforts in also making PKS amenable to de novo pathway design; being well aware that in-depth characterization of PKS with enzymological techniques is further needed to collect quantitative data that can inform rational engineering efforts.

Conclusion

Transient and static domain–domain and module–module interactions as part of an "assembly-line synthetic concept" are still poorly understood. The emerging picture from a fast growing knowledge about the structure and function of megasynthases suggests an impact of these interfaces in megasynthase-mediated natural compound synthesis that can hardly be overstated. The limited success rate of mix-and-match engineering experiments, programming the assembly of domains and modules to new megasynthases, may well be traced back to weakly cooperating domains and modules in these chimeric systems. We suggest that preserve-and-adapt approaches are valuable alternative strategies in rational megasynthase design. Instead of mixing and matching modules, a preserve-and-adapt approach is based on the intact native megasynthase scaffold, in which

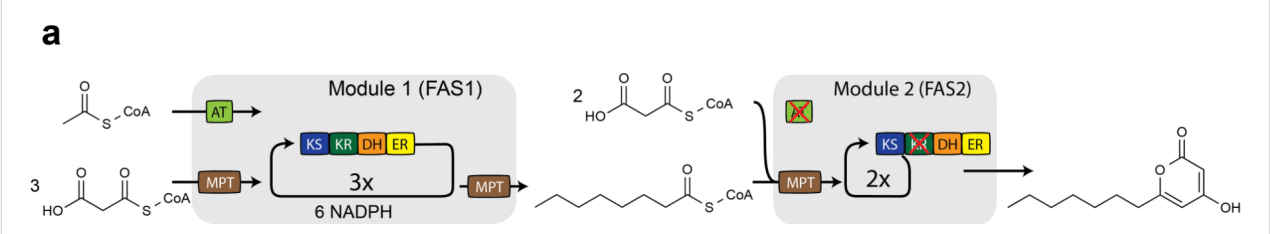

Figure 4: Preserve-and-adapt approach with FAS. *C. ammoniagenes* FAS has been engineered in two cooperatively acting modules to produce 6-heptyl-4-hydroxypyran-2-one. Module 1, mutated in domains KS and MPT, is responsible for the release of the acyl ester C_8-CoA, and module 2 for the non-reductive elongation of C_8-CoA, induced by a KR-domain functional knockout, to synthesize the final lactone PK. The knockout in the AT-domain hinders the uptake of acetyl-CoA and encodes for modules acting in sequence.

overall structural properties remain preserved, while the individual active sites are adapted for embedding custom syntheses.

Acknowledgements

M.G. thanks Dieter Oesterhelt for valuable discussions on FAS and PKS catalytic mechanisms, and continuous support during many years. We also thank Karthik S. Paithankar for carefully reading the manuscript. This work was supported by a Lichtenberg Grant of the Volkswagen Foundation awarded to M.G. (grant number 85 701), and by the LOEWE Research focus MegaSyn funded by the Hessian Ministry for Science and Arts.

References

1. Weissman, K. J.; Leadlay, P. F. *Nat. Rev. Microbiol.* **2005,** *3,* 952. doi:10.1038/nrmicro1287
2. Stinear, T. P.; Mve-Obiang, A.; Small, P. L. C.; Frigui, W.; Pryor, M. J.; Brosch, R.; Jenkin, G. A.; Johnson, P. D. R.; Davies, J. K.; Lee, R. E.; Adusumilli, S.; Garnier, T.; Haydock, S. F.; Leadlay, P. F.; Cole, S. T. *Proc. Natl. Acad. Sci. U. S. A.* **2004,** *101,* 1345. doi:10.1073/pnas.0305877101
3. Cane, D. E.; Walsh, C. T.; Khosla, C. *Science* **1998,** *282,* 63. doi:10.1126/science.282.5386.63
4. Crawford, J. M.; Thomas, P. M.; Scheerer, J. R.; Vagstad, A. L.; Kelleher, N. L.; Townsend, C. A. *Science* **2008,** *320,* 243. doi:10.1126/science.1154711
5. Hertweck, C. *Angew. Chem., Int. Ed.* **2009,** *48,* 4688. doi:10.1002/anie.200806121
6. Keatinge-Clay, A. T. *Nat. Prod. Rep.* **2012,** *29,* 1050. doi:10.1039/c2np20019h
7. Weissman, K. J. *Nat. Chem. Biol.* **2015,** *11,* 660. doi:10.1038/nchembio.1883
8. Herbst, D. A.; Jakob, R. P.; Zähringer, F.; Maier, T. *Nature* **2016,** *531,* 533. doi:10.1038/nature16993
9. Dutta, S.; Whicher, J. R.; Hansen, D. A.; Hale, W. A.; Chemler, J. A.; Congdon, G. R.; Narayan, A. R. H.; Håkansson, K.; Sherman, D. H.; Smith, J. L.; Skiniotis, G. *Nature* **2014,** *510,* 512. doi:10.1038/nature13423
10. Edwards, A. L.; Matsui, T.; Weiss, T. M.; Khosla, C. *J. Mol. Biol.* **2014,** *426,* 2229. doi:10.1016/j.jmb.2014.03.015
11. Lynen, F. *Eur. J. Biochem.* **1980,** *112,* 431. doi:10.1111/j.1432-1033.1980.tb06105.x
12. Wakil, S. J. *Biochemistry* **1989,** *28,* 4523. doi:10.1021/bi00437a001
13. Maier, T.; Leibundgut, M.; Ban, N. *Science* **2008,** *321,* 1315. doi:10.1126/science.1161269
14. Jenni, S.; Leibundgut, M.; Boehringer, D.; Frick, C.; Mikolásek, B.; Ban, N. *Science* **2007,** *316,* 254. doi:10.1126/science.1138248
15. Lomakin, I. B.; Xiong, Y.; Steitz, T. A. *Cell* **2007,** *129,* 319. doi:10.1016/j.cell.2007.03.013
16. Johansson, P.; Wiltschi, B.; Kumari, P.; Kessler, B.; Vonrhein, C.; Vonck, J.; Oesterhelt, D.; Grininger, M. *Proc. Natl. Acad. Sci. U. S. A.* **2008,** *105,* 12803. doi:10.1073/pnas.0805827105
17. Ciccarelli, L.; Connell, S. R.; Enderle, M.; Mills, D. J.; Vonck, J.; Grininger, M. *Structure* **2013,** *21,* 1251. doi:10.1016/j.str.2013.04.023
18. Maier, T.; Leibundgut, M.; Boehringer, D.; Ban, N. *Q. Rev. Biophys.* **2010,** *43,* 373. doi:10.1017/S0033583510000156
19. Grininger, M. *Curr. Opin. Struct. Biol.* **2014,** *25,* 49. doi:10.1016/j.sbi.2013.12.004
20. Bukhari, H. S. T.; Jakob, R. P.; Maier, T. *Structure* **2014,** *22,* 1775. doi:10.1016/j.str.2014.09.016
21. Ishihama, Y.; Schmidt, T.; Rappsilber, J.; Mann, M.; Hartl, F. U.; Kerner, M. J.; Frishman, D. *BMC Genomics* **2008,** *9,* No. 102. doi:10.1186/1471-2164-9-102
22. Volkmer, B.; Heinemann, M. *PLoS One* **2011,** *6,* e23126. doi:10.1371/journal.pone.0023126
23. Beld, J.; Lee, D. J.; Burkart, M. D. *Mol. BioSyst.* **2015,** *11,* 38. doi:10.1039/C4MB00443D
24. Fichtlscherer, F.; Wellein, C.; Mittag, M.; Schweizer, E. *Eur. J. Biochem.* **2000,** *267,* 2666. doi:10.1046/j.1432-1327.2000.01282.x
25. Fischer, M.; Rhinow, D.; Zhu, Z.; Mills, D. J.; Zhao, Z. K.; Vonck, J.; Grininger, M. *Protein Sci.* **2015,** *24,* 987. doi:10.1002/pro.2678
26. Jiang, H.; Zirkle, R.; Metz, J. G.; Braun, L.; Richter, L.; Van Lanen, S. G.; Shen, B. *J. Am. Chem. Soc.* **2008,** *130,* 6336. doi:10.1021/ja801911t
27. Davison, J.; Dorival, J.; Rabeharindranto, H.; Mazon, H.; Chagot, B.; Gruez, A.; Weissman, K. *J. Chem. Sci.* **2014,** *5,* 3081. doi:10.1039/c3sc53511h
28. Jayakumar, A.; Tai, M. H.; Huang, W. Y.; al-Feel, W.; Hsu, M.; Abu-Elheiga, L.; Chirala, S. S.; Wakil, S. J. *Proc. Natl. Acad. Sci. U. S. A.* **1995,** *92,* 8695. doi:10.1073/pnas.92.19.8695
29. Lowry, B.; Robbins, T.; Weng, C.-H.; O'Brien, R. V.; Cane, D. E.; Khosla, C. *J. Am. Chem. Soc.* **2013,** *135,* 16809. doi:10.1021/ja409048k
30. Moriguchi, T.; Kezuka, Y.; Nonaka, T.; Ebizuka, Y.; Fujii, I. *J. Biol. Chem.* **2010,** *285,* 15637. doi:10.1074/jbc.M110.107391
31. Leibundgut, M.; Jenni, S.; Frick, C.; Ban, N. *Science* **2007,** *316,* 288. doi:10.1126/science.1138249
32. Johansson, P.; Mulinacci, B.; Koestler, C.; Vollrath, R.; Oesterhelt, D.; Grininger, M. *Structure* **2009,** *17,* 1063. doi:10.1016/j.str.2009.06.014
33. Anselmi, C.; Grininger, M.; Gipson, P.; Faraldo-Gómez, J. D. *J. Am. Chem. Soc.* **2010,** *132,* 12357. doi:10.1021/ja103354w
34. Ploskoń, E.; Arthur, C. J.; Evans, S. E.; Williams, C.; Crosby, J.; Simpson, T. J.; Crump, M. P. *J. Biol. Chem.* **2008,** *283,* 518. doi:10.1074/jbc.M703454200
35. Perez, D. R.; Leibundgut, M.; Wider, G. *Biochemistry* **2015,** *54,* 2205. doi:10.1021/bi5014563
36. Nguyen, C.; Haushalter, R. W.; Lee, D. J.; Markwick, P. R. L.; Bruegger, J.; Caldara-Festin, G.; Finzel, K.; Jackson, D. R.; Ishikawa, F.; O'Dowd, B.; McCammon, J. A.; Opella, S. J.; Tsai, S.-C.; Burkart, M. D. *Nature* **2014,** *505,* 427. doi:10.1038/nature12810
37. Finzel, K.; Lee, D. J.; Burkart, M. D. *ChemBioChem* **2015,** *16,* 528. doi:10.1002/cbic.201402578
38. Miyanaga, A.; Iwasawa, S.; Shinohara, Y.; Kudo, F.; Eguchi, T. *Proc. Natl. Acad. Sci. U. S. A.* **2016,** *113,* 1802. doi:10.1073/pnas.1520042113
39. Kapur, S.; Lowry, B.; Yuzawa, S.; Kenthirapalan, S.; Chen, A. Y.; Cane, D. E.; Khosla, C. *Proc. Natl. Acad. Sci. U. S. A.* **2012,** *109,* 4110. doi:10.1073/pnas.1118734109
40. Kapur, S.; Chen, A. Y.; Cane, D. E.; Khosla, C. *Proc. Natl. Acad. Sci. U. S. A.* **2010,** *107,* 22066. doi:10.1073/pnas.1014081107
41. Khosla, C.; Zawada, R. J. X. *Trends Biotechnol.* **1996,** *14,* 335. doi:10.1016/0167-7799(96)10046-9
42. Leadlay, P. F. *Curr. Opin. Chem. Biol.* **1997,** *1,* 162. doi:10.1016/S1367-5931(97)80005-1

43. Menzella, H. G.; Reid, R.; Carney, J. R.; Chandran, S. S.; Reisinger, S. J.; Patel, K. G.; Hopwood, D. A.; Santi, D. V. *Nat. Biotechnol.* **2005,** *23,* 1171. doi:10.1038/nbt1128
44. Klaus, M.; Ostrowski, M. P.; Austerjost, J.; Robbins, T.; Lowry, B.; Cane, D. E.; Khosla, C. *J. Biol. Chem.* **2016,** *291,* 16404. doi:10.1074/jbc.M116.730531
45. Williams, G. J. *Curr. Opin. Struct. Biol.* **2013,** *23,* 603. doi:10.1016/j.sbi.2013.06.012
46. Robbins, T.; Liu, Y.-C.; Cane, D. E.; Khosla, C. *Curr. Opin. Struct. Biol.* **2016,** *41,* 10. doi:10.1016/j.sbi.2016.05.009
47. McDaniel, R.; Ebert-Khosla, S.; Hopwood, D. A.; Khosla, C. *Nature* **1995,** *375,* 549. doi:10.1038/375549a0
48. Bruegger, J.; Haushalter, B.; Vagstad, A. L.; Shakya, G.; Mih, N.; Townsend, C. A.; Burkart, M. D.; Tsai, S.-C. *Chem. Biol.* **2013,** *20,* 1135. doi:10.1016/j.chembiol.2013.07.012
49. Abe, I.; Oguro, S.; Utsumi, Y.; Sano, Y.; Noguchi, H. *J. Am. Chem. Soc.* **2005,** *127,* 12709. doi:10.1021/ja053945v
50. Newman, A. G.; Vagstad, A. L.; Storm, P. A.; Townsend, C. A. *J. Am. Chem. Soc.* **2014,** *136,* 7348. doi:10.1021/ja5007299
51. Whicher, J. R.; Dutta, S.; Hansen, D. A.; Hale, W. A.; Chemler, J. A.; Dosey, A. M.; Narayan, A. R. H.; Håkansson, K.; Sherman, D. H.; Smith, J. L.; Skiniotis, G. *Nature* **2014,** *510,* 560. doi:10.1038/nature13409
52. Rittner, A.; Grininger, M. *ChemBioChem* **2014,** *15,* 2489. doi:10.1002/cbic.201402432
53. Koryakina, I.; McArthur, J. B.; Draelos, M. M.; Williams, G. J. *Org. Biomol. Chem.* **2013,** *11,* 4449. doi:10.1039/c3ob40633d
54. Sundermann, U.; Bravo-Rodriguez, K.; Klopries, S.; Kushnir, S.; Gomez, H.; Sanchez-Garcia, E.; Schulz, F. *ACS Chem. Biol.* **2013,** *8,* 443. doi:10.1021/cb300505w
55. Murphy, A. C.; Hong, H.; Vance, S.; Broadhurst, R. W.; Leadlay, P. F. *Chem. Commun.* **2016,** *52,* 8373. doi:10.1039/C6CC03501A
56. Watanabe, C. M. H.; Townsend, C. A. *Chem. Biol.* **2002,** *9,* 981. doi:10.1016/S1074-5521(02)00213-2
57. Winssinger, N.; Barluenga, S. *Chem. Commun.* **2007,** 22. doi:10.1039/B610344H
58. Gajewski, J.; Buelens, F.; Serdjukow, S.; Janßen, M.; Cortina, N.; Grubmüller, H.; Grininger, M. *Nat. Chem. Biol.* **2017,** *13,* 363. doi:10.1038/nchembio.2314
59. Gajewski, J.; Pavlovic, R.; Fischer, M.; Boles, E.; Grininger, M. *Nat. Commun.* **2017,** *8,* No. 14650. doi:10.1038/ncomms14650
60. Choi, Y. J.; Lee, S. Y. *Nature* **2013,** *502,* 571. doi:10.1038/nature12536
61. Xu, P.; Qiao, K.; Ahn, W. S.; Stephanopoulos, G. *Proc. Natl. Acad. Sci. U. S. A.* **2016,** *113,* 10848. doi:10.1073/pnas.1607295113
62. Leber, C.; Da Silva, N. A. *Biotechnol. Bioeng.* **2014,** *111,* 347. doi:10.1002/bit.25021
63. Zhu, Z.; Zhou, Y. J.; Krivoruchko, A.; Grininger, M.; Zhao, Z. K.; Nielsen, J. *Nat. Chem. Biol.* **2017,** *13,* 360. doi:10.1038/nchembio.2301

License and Terms

BEILSTEIN JOURNAL OF ORGANIC CHEMISTRY

Total synthesis of elansolids B1 and B2

Liang-Liang Wang and Andreas Kirschning*

Full Research Paper

Open Access

Address:
Institute of Organic Chemistry and Center of Biomolecular Drug Research (BMWZ), Leibniz University Hannover, Schneiderberg 1b, 30167 Hannover, Germany

Email:
Andreas Kirschning* - andreas.kirschning@oci.uni-hannover.de

* Corresponding author

Keywords:
antibiotics; polyenes; polyketides; Stille reaction; Suzuki reaction; total synthesis

Beilstein J. Org. Chem. **2017,** *13,* 1280–1287.
doi:10.3762/bjoc.13.124

Received: 03 April 2017
Accepted: 17 May 2017
Published: 28 June 2017

This article is part of the Thematic Series "Lipids: fatty acids and derivatives, polyketides and isoprenoids".

Guest Editor: J. S. Dickschat

Abstract

The elansolids A1–A3, B1, and B2 are secondary metabolites formed by the gliding bacterium *Chitinophaga sancti*. They show antibacterial activity against Gram-positive bacteria. A second generation total synthesis of the antibiotic elansolid B1 (**2**) and the first synthesis of elansolid B2 (**3**) are reported. In contrast to previous work, the (*Z,E,Z)*-triene at C10–C15 was assembled by using an optimized C–C cross-coupling sequence with a Suzuki cross-coupling reaction as key step.

Introduction

The elansolids are metabolites from the gliding bacterium *Chitinophaga sancti* (formerly *Flexibacter spec.*) (Figure 1) [1,2]. Elansolid A2 (**1***), an atropisomer of elansolid A1 (**1**), showed antibiotic activity against Gram-positive bacteria in the range of 0.2 to 64 µg/mL and cytotoxicity against L929 mouse fibroblast cells with an IC_{50} value of 12 µg/mL. Besides these two macrocylic members also elansolids B1 (**2**) and B2 (**3**) along with A3 (**4**) bearing the unusual *p*-quinone methide unit were isolated from the fermentation broth. All elansolids belong to the group of *trans*-polyketides type I [3-6].

For the first generation total synthesis of elansolid B1 (**2**) we utilized an *endo*-selective intramolecular Diels–Alder (IMDA) cycloaddition as key step to construct the tetrahydroindane unit (Scheme 1) [7]. An enone, derived from allylic alcohol **8** served as precursor to yield tetrahydroindane **9** with excellent diastereocontrol at −25 °C. The major drawback of our first total synthesis of elansolid B1 (**2**) was the installation of the side chain at C1–C13. The synthesis relied on two consecutive Sonogashira–Hagihara cross-coupling reactions that provided the ene–diyne system (C10–C15) **10** in good yield. However, partial hydrogenation (only the zinc–copper couple worked) furnished the desired (*Z,E,Z*)-triene **11** in only low yield (35%) and overreduction was difficult to control. Practically, the reduction was stopped when still substantial amounts of monoreduced product (the alkyne at C10–C11 is reduced pref-

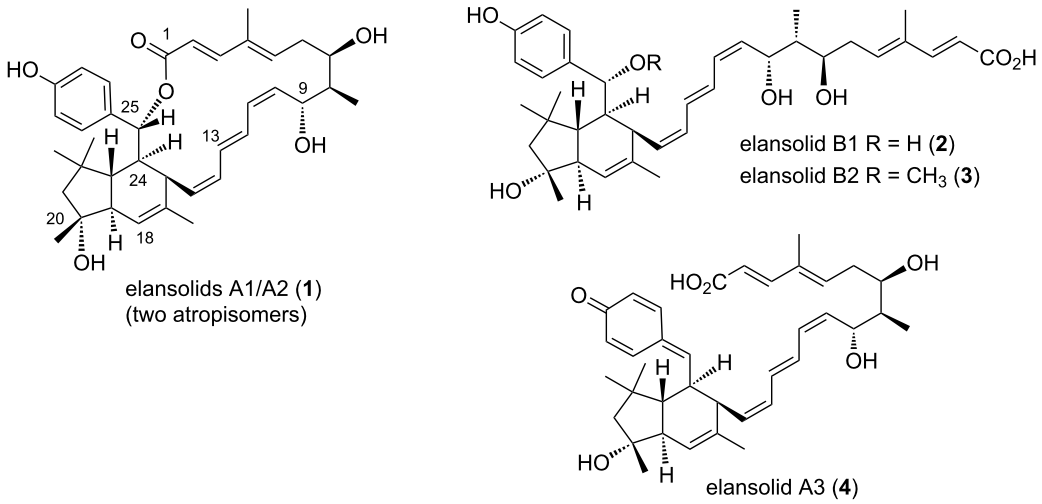

Figure 1: Elansolids A1/A2, B1, B2 and A3 (**1**–**4**).

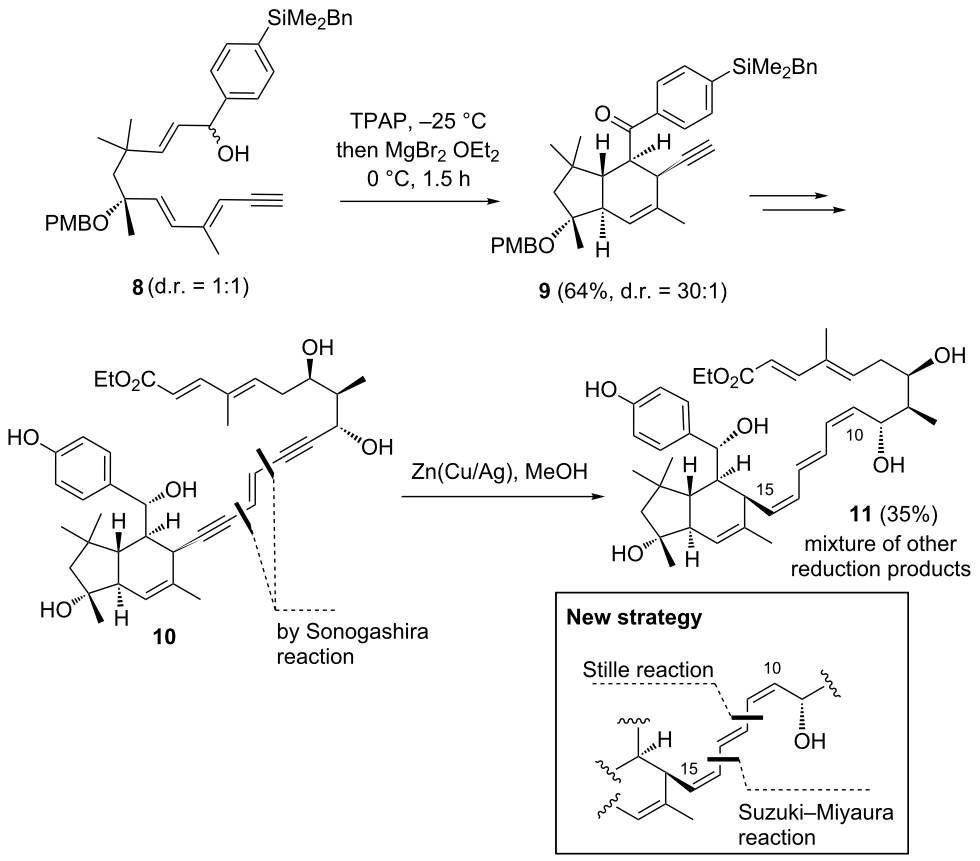

Scheme 1: IMDA to generate the tetrahydroindane unit of the elansolids by oxidation of benzyl ether **8** as precursor and construction of the (*Z*,*E*,*Z*)-triene unit at C10–C15 (TPAP = tetra-*n*-propylammonium perruthenate(VII); PMB = *p*-methoxybenzyl; Bn = benzyl).

erentially) were present. Consequently, the hydrogenation yielded a mixture of products, which in any case made the separation and isolation a very challenging task.

As continuation of our synthetic investigations on the elansolids, we report an improved second generation approach for generating the carbon chain C1–C13 [8] and for preparing elan-

solid B1 (**2**). Furthermore, we also describe the first synthesis of elansolid B2 (**3**). The key for improvement was to abandon the two Sonogashira reactions along with the *syn*-reductions of the two alkynes. Instead, we planned to utilize the Suzuki–Miyaura and the Stille reactions and two *Z*-configured vinyl iodides to assemble the (*Z,E,Z*)-triene unit.

Results and Discussion

The improved synthesis utilizes the Suzuki–Miyaura cross-coupling reaction to merge the western fragment derived from ketone **9** with the newly designed eastern building block **13**. This fragment was obtained in very good yield from vinyl iodide **12** [9] by a Stille protocol using doubly functionalized alkene **14** which is suited for a sequential cross-coupling strategy (Scheme 2). Under the catalytic conditions, we did not encounter isomerization of the alkene and diene configurations in vinyl boronate **13**.

The preparation of the newly modified western fragment started from known IMDA product **9** [7], which was first reduced at C-25 (Scheme 3). The two diastereoisomers could be separated by chromatography and the stereochemical assignment of the major isomer was based on X-ray crystallographic analysis [7]. Next, Tamao–Fleming oxidation [10] yielded phenol **15**. The alkyne was transformed into vinyl iodide **17** after *O*-acylation, iodination of the terminal alkyne and finally diimide-mediated *syn*-reduction [11].

Next, DDQ-mediated removal of the PMB protecting group yielded vinyl iodide **18**. The synthesis of both fragments **13** and **18** set the stage for the Suzuki–Miyaura coupling which delivered the desired (*Z,E,Z*)-configured triene **19**. Again, we did not encounter formation of stereoisomers in the triene unit. The configuration of the triene was unequivocally assigned by analysis of coupling constants (*J*) and by measuring nuclear Overhauser effects (nOe). Finally, desilylation and global saponification of all ester groups in the presence of isopropanol successfully yielded elansolid B1 (**2**). When isopropanol was exchanged by methanol, elansolid B2 (**3**) was generated. Its formation can be rationalized by formation of the intermediate *p*-methide quinone which selectively trapped methanol, exclusively yielding the *R*-isomer at C25. This excellent facial selectivity has been demonstrated, e.g., for anilines as nucleophiles before. It is due to the preferred conformation around the bond at C24–C25 which leads to the efficient shielding of the *si*-face by the two germinal methyl groups at C22 [4,5]. The NMR data determined for both synthetic products were identical with those of authentic samples of elansolid B1 (**2**) and elansolid B2 (**3**) (copies of spectra, see Supporting Information File 1).

Conclusion

In conclusion, we describe an improved second generation synthesis of the highly active antibiotic elansolid B1 (**2**). The improvements are mainly associated with the preparation of the triene unit at C10–C15 by utilizing the Stille and the Suzuki–Miyaura cross-coupling reactions as well as the highly versatile difunctionalized building block **14**. In principal, the synthesis sheds light on how such (*Z,E,Z*)-configured triene units are ideally be constructed, clearly demonstrating that enediynes are less preferred precursors for such structural elements. It has to be noted that there is precedence in the literature for the use of the Suzuki–Miyaura cross-coupling reaction as key step to assemble differently configured trienes present in polyketides [12-15].

Furthermore, we show how the intermediate *p*-methide quinone can be exploited to also prepare elansolid B2 (**3**). The improved synthesis allows more easily preparing analogues of the elansolids for further biological evaluation.

Experimental

General information:

^{1}H NMR spectra were recorded at 400 MHz or 500 MHz, respectively, and ^{13}C NMR spectra were recorded at 100 MHz or

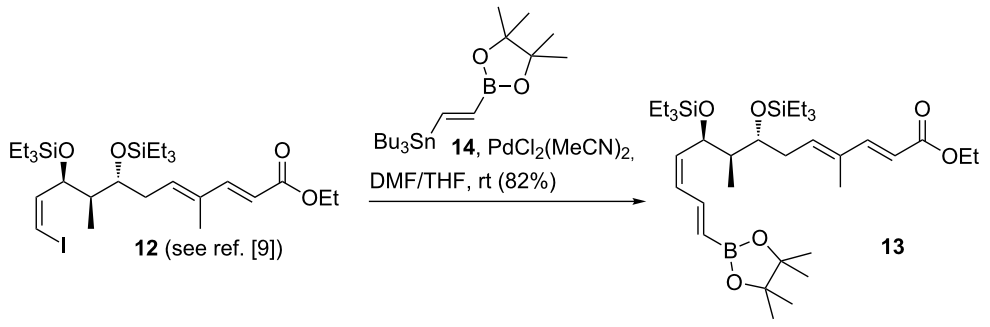

Scheme 2: Stille cross-coupling reaction and formation of eastern fragment **13**.

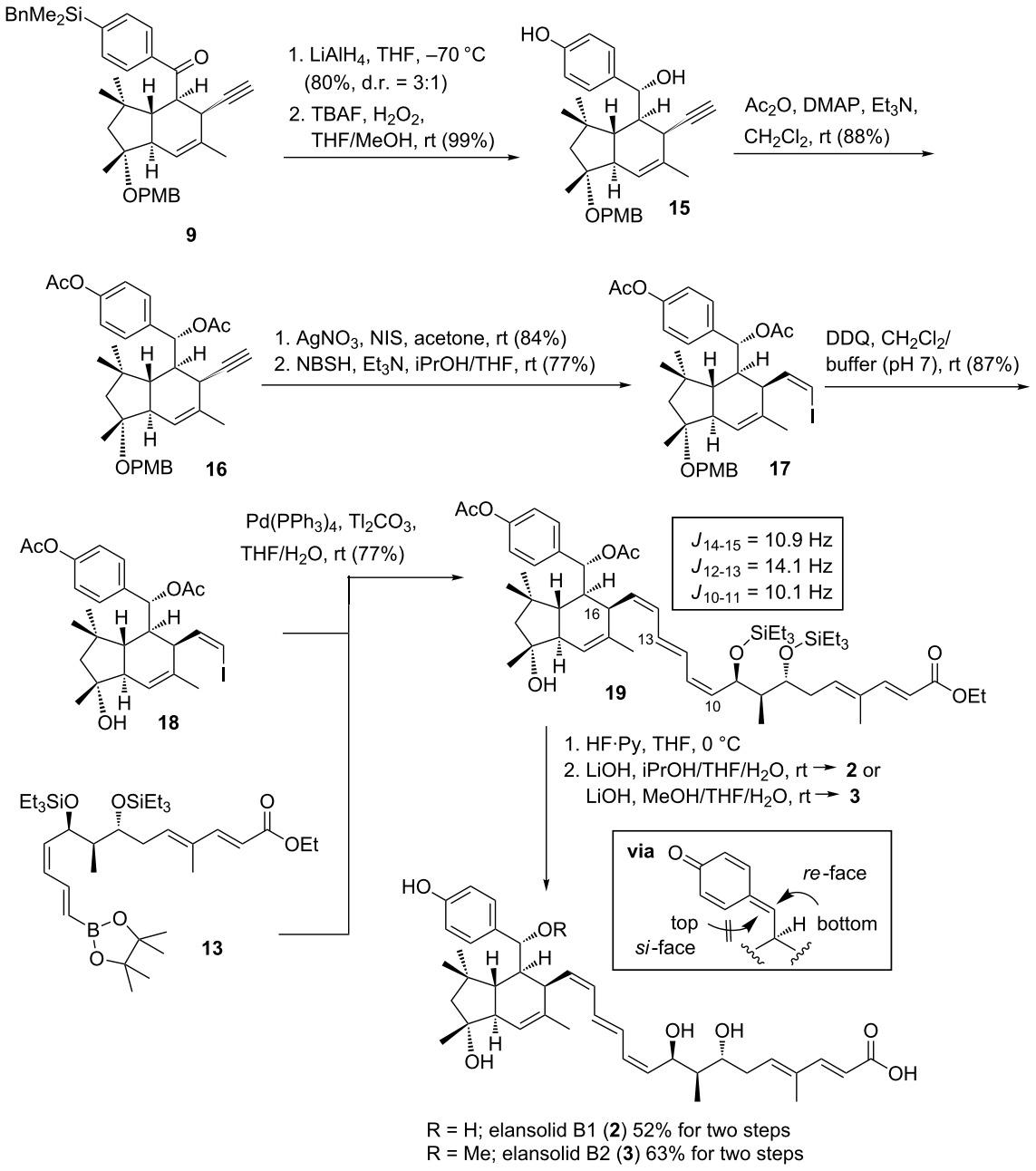

Scheme 3: Total synthesis of elansolids B1 (**2**) and B2 (**3**).

125 MHz, respectively, with a Bruker Avance 400, DPX 400 or DRX 500. Chemical shift values of NMR data are reported as values in ppm relative to the (residual undeuterated) solvent signal as internal standard. Multiplicities for ^{1}H NMR signals are described using the following abbreviations: s = singlet, d = doublet, t = triplet, q = quartet, m = multiplet; where appropriate with the addition of b = broad. Mass spectra were obtained with a type LCT (ESI) (Micromass) equipped with a lockspray dual ion source in combination with a Waters Alliance 2695 LC system, or with a type QTOF premier (Micromass) spectrometer (ESI mode) in combination with a Waters Acquity UPLC system equipped with a Waters BEH C18 1.7 µm (SN 01473711315545) column (solvent A: water + 0.1% (v/v) formic acid, solvent B: MeOH + 0.1% (v/v) formic acid; flow rate = 0.4 mL/min; gradient (*t* [min]/solvent B [%]): (0:5) (2.5:95) (6.5:95) (6.6:5) (8:5)). Ion mass signals (*m*/*z*) are reported as values in atomic mass units. Optical rotations were measured on a Perkin-Elmer polarimeter type 341 or

241 in a quartz glass cuvette at l = 589 nm (Na D-line). The optical rotation is given in [° mL·g^{-1}·dm^{-1}] with c = 1 corresponding to 10 mg mL^{-1}. Preparative HPLC was operated at a Merck Hitachi LaChrome HPLC (Pump L7150 or L7100, Interface D-7000, Diode Array Detector L-7450), respectively, at a Beckmann system Gold HPLC (Solvent Module 125, Detector 166). Solvents, columns, operating procedures and retention times are given with the corresponding experimental and analytical data.

All reactions were performed under an argon atmosphere unless otherwise stated. Glassware was dried by heating under vacuum followed by flushing with argon gas prior to use. Dry solvents were obtained after filtration through drying columns on a M. Braun solvent purification system or purchased form commercial providers. The synthesis of building blocks **9** [7] and **12** [9] was reported before.

Synthetic experiments

Synthesis of boronate **13**

A flame dried round bottom flask equipped with a stirring bar was charged with vinyl iodide **12** (10 mg, 16 µmol, 1.0 equiv) and boronate **14** (10.68 mg, 24 µmol, 1.5 equiv) in DMF (0.3 mL) and THF (0.1 mL). To this stirred solution $PdCl_2(MeCN)_2$ (1.25 mg, 4.8 µmol, 0.3 equiv) was added at room temperature and stirring was continued for 8 h. The volatiles were removed in vacuo and the residue was purified by silica gel chromatography to afford vinyl boronate **13** (8.5 mg, 12.3 µmol, 82%). R_f = 0.40 (PE/EtOAc 10:1, visualized using an anisaldehyde stain or UV), $[\alpha]_D^{20}$ = −34.5 (c 0.8, CH_2Cl_2); ^{1}H NMR (400 MHz, $CDCl_3$, $CHCl_3$ = 7.26 ppm) δ 7.32 (d, J = 15.6 Hz, 1H), 7.25 (d, J = 11.4, 17.5 Hz, 1H), 6.09 (t, J = 11.1 Hz, 1H), 5.97 (dd, J = 7.1 Hz, 1H), 5.78 (d, J = 15.5 Hz, 1H), 5.61 (d, J = 17.4 Hz, 1H), 5.57 (t, J = 10.2 Hz, 1H), 4.63 (dd, J = 6.4, 9.2 Hz, 1H), 4.22 (q, J = 7.1 Hz, 2H), 3.84–3.80 (m, 1H), 2.42–2.34 (m, 1H), 2.27–2.23 (m, 1H), 1.76 (s, 3H), 1.74–1.71 (m, 1H), 1.33 (t, J = 7.2 Hz, 3H), 1.28 (s, 12H), 0.97–0.93 (m, 21H), 0.59 (q, J = 8.0Hz, 12H); ^{13}C NMR (100 MHz, $CDCl_3$ = 77.16 ppm) δ 167.6, 149.6, 143.8, 139.6, 137.4, 133.6, 130.6, 123.3, 115.4, 83.2, 72.5, 69.8, 60.1, 47.1, 32.6, 24.8, 24.7, 14.3, 12.6, 9.7, 7.0, 6.9, 5.2, 5.1; HRMS (ESI) m/z: $[M + Na]^+$ calculated for $C_{35}H_{65}BO_6Si_2Na$, 671.4310; found, 671.4312.

Reduction of ketone **9** and formation of benzyl alcohol

A solution of ketone **9** (466.2 mg, 0.79 mmol, 1.0 equiv) in THF (3 mL) was added to a suspension of $LiAlH_4$ (599.2 mg, 15.79 mmol, 20 equiv) in THF (12 mL) at −70 °C. After stirring for 3 d at this temperature the reaction was terminated by slow addition of a saturated potassium sodium tartrate solution. The reaction mixture was vigorously stirred for 1 h at room temperature. The layers were seperated and the aqueous phase was extracted with ethyl acetate. The combined organic extracts were dried over Na_2SO_4, filtered and concentrated under reduced pressure. The resulting benzyl alcohol (371.7 mg, 0.63 mmol, 80%, d.r. = 3:1) was obtained after flash column chromatography. Separation of diastereomers was achieved by preparative HPLC (C18 ISIS-SP) (gradient H_2O/MeOH 30:70 to 0:100 {0–80 min}, 15 mL/min, t_R = 67.6 min). R_f = 0.6 (PE/EtOAc 5:1, visualized using anisaldehyde stain or UV), $[\alpha]_D^{20}$ = +28.9 (c 0.82, CH_2Cl_2); ^{1}H NMR (400 MHz, $CDCl_3$, $CHCl_3$ = 7.26 ppm) δ 7.48 (d, J = 8.0 Hz, 2H), 7.42 (d, J = 7.9 Hz, 2H), 7.30 (d, J = 9.8 Hz, 2H), 7.19 (t, J = 7.5 Hz, 2H), 7.08 (t, J = 7.3 Hz, 1H), 6.94–6.89 (m, J = 6.8 Hz, 4H), 5.60 (s, 1H), 5.29 (dd, J = 2.9, 11.0 Hz, 1H), 4.47 (d, J = 10.8 Hz, 1H), 4.40 (d, J = 10.8 Hz, 1H), 4.27 (d, J = 11.1 Hz, 1H, OH), 3.83 (s, 3H), 2.87 (d, J = 10.7 Hz, 1H), 2.57 (br, 1H), 2.48 (d, J = 2.4 Hz, 1H), 2.33 (s, 2H), 2.20 (ddd, J = 3.5, 4.6, 11.4 Hz, 1H), 2.10 (d, J = 14.0 Hz, 1H), 2.02 (dd, J = 11.8, 12.0 Hz, 1H), 1.69 (s, 3H), 1.69 (d, J = 13.6 Hz, 1H), 1.40 (s, 3H), 1.32 (s, 3H), 1.29 (s, 3H), 0.29 (s, 6H); ^{13}C NMR (100 MHz, $CDCl_3$ = 77.16 ppm) δ 158.9, 144.3, 139.7, 136.6, 133.8, 133.2, 131.8, 128.7, 128.3, 128.1, 124.7, 124.1, 123.7, 113.8, 86.7, 81.3, 73.9, 73.5, 64.9, 55.8, 55.3, 52.9, 46.6, 45.3, 38.0, 33.4, 31.1, 26.3, 24.2, 22.7, 21.3, −3.4, −3.3; HRMS (ESI) m/z: $[M + Na]^+$ calculated for $C_{39}H_{48}O_3SiNa$, 615.3270; found, 615.3270.

Synthesis of phenol **15**

To a solution of the benzyl alcohol described above (124.0 mg, 0.21 mmol, 1.0 equiv) in THF (0.75 mL) was added a solution of TBAF (c = 1.0 M in THF, 0.84 mL, 4.0 equiv) and the mixture was stirred for 15 min. Methanol (2.23 mL), $KHCO_3$ (41.85 mg, 0.42 mmol, 2.0 equiv) and H_2O_2 (35% in H_2O, 0.36 mL, 4.18 mmol, 20 equiv) were sequentially added and stirring was continued overnight. Then, the reaction was terminated by slow addition of a saturated, aqueous $Na_2S_2O_3$ solution and the aqueous layer was extracted with ethyl acetate. The combined organic extracts were dried over Na_2SO_4 filtered and concentrated in vacuo. Purification by flash column chromatography gave phenol **15** (96.0 mg, 0.20 mol, 99%) as a colorless solid. R_f = 0.20 (PE/EtOAc 3:1, visualized using an anisaldehyde stain or UV), $[\alpha]_D^{20}$ = +26.1 (c 0.7, CH_2Cl_2); ^{1}H NMR (400 MHz, $CDCl_3$, $CHCl_3$ = 7.26 ppm) δ 7.31–7.28 (m, 4H), 6.90 (d, J = 8.7 Hz, 2H), 6.86 (d, J = 8.6 Hz, 2H), 5.59 (s, 1H), 5.25 (dd, J = 3.0, 10.9 Hz, 1H), 4.97 (s, 1H, OH), 4.47 (d, J = 10.8 Hz, 1H), 4.39 (d, J = 10.8 Hz, 1H), 4.22 (d, J = 10.9 Hz, 1H), 3.82 (s, 3H), 2.85 (dd, J = 1.8, 12.4 Hz, 1H), 2.60 (br, 1H), 2.45 (d, J = 2.5 Hz, 1H), 2.13 (ddd, J = 3.8, 4.4, 11.1Hz, 1H), 2.08 (d, J = 14.0 Hz, 1H), 2.00 (t, J = 11.8 Hz, 1H), 1.68 (s, 3H), 1.67 (d, J = 13.7 Hz, 1H), 1.38 (s, 3H), 1.30 (s, 3H), 1.28

(s, 3H); ^{13}C NMR (100 MHz, $CDCl_3$ = 77.16 ppm) δ 158.9, 154.4, 135.5, 133.2, 131.8, 128.7, 126.6, 123.7, 115.2, 113.8, 86.8, 81.3, 73.9, 73.1, 64.9, 55.7, 55.3, 52.9, 46.7, 45.4, 38.0, 33.3, 31.1, 24.2, 22.7, 21.3; HRMS (ESI) *m/z*: $[M + H]^+$ calculated for $C_{30}H_{37}O_4$, 461.2692; found, 461.2693.

Synthesis of acetyl ester **16**

A round bottom flask equipped with a magnetic stirring bar was sequentially charged with alcohol **15** (89.6 mg, 0.195 mmol, 1.0 equiv), CH_2Cl_2 (2 mL), DMAP (23.82 mg, 0.196 mmol, 1.0 equiv), Et_3N (0.204 mL, 1.46 mmol, 7.4 equiv) and Ac_2O (0.092 mL, 0.973 mmol, 4.0 equiv). After stirring at ambient temperature for 2 d the reaction was terminated by addition of H_2O and extracted with Et_2O several times. The combined organic phases were dried over anhydrous Na_2SO_4, filtered, concentrated in vacuo. The residue was purified by silica gel column chromatography to give compound **16** (93 mg, 0.17 mmol, 88%). R_f = 0.5 (PE/EtOAc 3:1, visualized using an anisaldehyde or UV), $[\alpha]_D^{20}$ = +35.8 (*c* 0.5, CH_2Cl_2); ^{1}H NMR (400 MHz, $CDCl_3$, $CHCl_3$ = 7.26 ppm) δ 7.41 (d, *J* = 8.6 Hz, 2H), 7.27 (d, *J* = 9.0 Hz, 2H), 7.11 (d, *J* = 8.6 Hz, 2H), 6.89 (d, *J* = 8.7 Hz, 2H), 6.01 (d, *J* = 3.2 Hz, 1H), 5.54 (s, 1H), 4.44 (d, *J* = 10.8 Hz, 1H), 4.37 (d, *J* = 10.8 Hz, 1H), 3.82 (s, 3H), 2.84 (dd, *J* = 1.8, 12.3 Hz, 1H), 2.65 (br, 1H), 2.32 (s, 3H), 2.24 (d, *J* = 2.6 Hz, 1H), 2.14 (s, 3H), 2.10–2.06 (m, 1H), 2.03–2.00 (m, 2H), 1.73 (s, 3H), 1.60 (d, *J* = 14.0 Hz, 1H), 1.28 (s, 3H), 1.24 (s, 3H), 1.11 (s, 3H); ^{13}C NMR (100 MHz, $CDCl_3$ = 77.16 ppm) δ 170.3, 169.3, 158.9, 149.9, 137.0, 134.5, 131.7, 128.7, 126.9, 122.7, 121.5, 113.8, 85.4, 81.0, 74.9, 71.0, 64.9, 55.7, 55.3, 53.5, 46.1, 45.8, 37.9, 34.6, 29.9, 23.8, 22.8, 21.6, 21.2, 21.1; HRMS (ESI) *m/z*: $[M + Na]^+$ calculated for $C_{34}H_{40}O_6Na$, 567.2723; found, 567.2728.

Synthesis of vinyl iodide **17**

To a stirred solution of compound of **16** (88 mg, 0.162 mmol, 1.0 equiv) in acetone (4 mL) was added $AgNO_3$ (8.3 mg, 0.05 mmol, 0.3 equiv) and *N*-iodosuccinimide (40.0 mg, 0.18 mmol, 1.1 equiv) at ambient temperature. The resulting mixture was stirred for 1.5 h and concentrated in vacuo. The residue was purified by silica gel column chromatography to give the corresponding alkynyl iodide (91.0 mg, 0.136 mmol, 84%). This product (81.9 mg, 0.12 mmol, 1.0 equiv) was dissolved in a mixture of THF (1.1 mL) and iPrOH (1.1 mL). Et_3N (0.026 mL, 0.183 mmol, 1.5 equiv) and 2-nitrobenzenesulfonyl hydrazide (34.5 mg, 0.159 mmol, 1.3 equiv) were sequentially added. After stirring for 20 h, Et_3N (0.026 mL, 0.183 mmol, 1.5 equiv) and 2-nitrobenzenesulfonyl hydrazide (17.25 mg, 0.079 mmol, 0.7 equiv) were added and the reaction mixture was stirred for additional 5 h. The volatiles were then removed in vacuo at ambient temperature. The residue was purified by silica gel column chromatography to give vinyl iodide **17** (62.0 mg, 0.092 mmol, 77%). R_f = 0.60 (PE/EtOAc 3:1, visualized using an anisaldehyde stain or UV), $[\alpha]_D^{20}$ = +14.1 (*c* 0.95, CH_2Cl_2); ^{1}H NMR (400 MHz, $CDCl_3$, $CHCl_3$ = 7.26 ppm) δ 7.28 (d, *J* = 8.6 Hz, 2H), 7.17 (d, *J* = 8.6 Hz, 2H), 7.11 (d, *J* = 8.6 Hz, 2H), 6.90 (d, *J* = 8.6 Hz, 2H), 6.43 (dd, *J* = 7.8, 9.4 Hz, 1H), 6.29 (d, *J* = 7.5 Hz, 1H), 6.03 (d, *J* = 2.5 Hz, 1H), 5.56 (s, 1H), 4.45 (d, *J* = 10.8 Hz, 1H), 4.38 (d, *J* = 10.8 Hz, 1H), 3.82 (s, 3H), 2.89–2.83 (m, 2H), 2.37 (ddd, *J* = 2.9, 3.7, 10.9 Hz, 1H), 2.31 (s, 3H), 2.15 (s, 3H), 2.07 (d, *J* = 14.0 Hz, 1H), 1.79 (t, *J* = 11.8 Hz, 1H), 1.64 (s, 3H), 1.59 (d, *J* = 14.0 Hz, 1H), 1.30 (s, 3H), 1.24 (s, 3H), 1.09 (s, 3H); ^{13}C NMR (100 MHz, $CDCl_3$ = 77.16 ppm) δ 169.9, 169.3, 158.9, 149.6, 141.9, 136.1, 135.2, 131.7, 128.7, 126.7, 123.7, 121.9, 113.8, 80.9, 80.1, 75.5, 64.9, 55.9, 55.3, 53.4, 46.6, 46.1, 46.0, 38.3, 30.1, 23.5, 22.7, 22.2, 21.3, 21.2; HRMS (ESI) *m/z*: $[M + Na]^+$ calculated for $C_{34}H_{41}O_6INa$, 695.1846; found, 695.1837.

Synthesis of vinyl iodide **18**

DDQ (56.5 mg, 0.25 mmol, 3.0 equiv) was added to a stirred solution of **17** (55.8 mg, 0.083 mmol, 1.0 equiv) in CH_2Cl_2 (4.5 mL)/pH 7.0 phosphate buffer (0.45 mL) at 0 °C. After stirring for 1.5 h, the reaction mixture was terminated by addition of a saturated, aqueous $NaHCO_3$ solution. The aqueous solution was extracted with Et_2O. The combined, organic phases were dried over anhydrous Na_2SO_4, filtered, concentrated in vacuo and the crude product was purified by silica gel column chromatography to furnish the title vinyl iodide **18** (40.0 mg, 0.072 mol, 87%). R_f = 0.25 (PE/EtOAc 3:1, visualized using an anisaldehyde or UV), $[\alpha]_D^{20}$ = +36.7 (*c* 0.86, CH_2Cl_2); ^{1}H NMR (400 MHz, $CDCl_3$, $CHCl_3$ = 7.26 ppm) δ 7.17 (d, *J* = 8.6 Hz, 2H), 7.11 (d, *J* = 8.6 Hz, 2H), 6.40 (dd, *J* = 7.6, 9.6 Hz, 1H), 6.28 (d, *J* = 7.6 Hz, 1H), 6.03 (d, *J* = 2.3 Hz, 1H), 5.51 (s, 1H), 2.84 (dd, *J* = 4.1, 9.6 Hz, 1H), 2.70 (d, *J* = 12.7 Hz, 1H), 2.34 (ddd, *J* = 2.8, 4.0, 11.3 Hz, 1H), 2.31 (s, 3H), 2.15 (s, 3H), 1.84 (d, *J* = 14.2 Hz, 1H), 1.77 (d, *J* = 14.2 Hz, 1H), 1.74 (t, *J* = 11.9 Hz, 1H), 1.65 (s, 3H), 1.30 (s, 3H), 1.19 (s, 3H), 1.07 (s, 3H); ^{13}C NMR (100 MHz, $CDCl_3$ = 77.16 ppm) δ 169.9, 169.3, 149.6, 141.8, 136.1, 135.7, 126.7, 122.4, 121.9, 80.1, 76.2, 75.4, 60.1, 54.8, 46.4, 46.3, 45.9, 38.1, 30.2, 26.4, 23.9, 22.2, 21.2, 21.1; HRMS (ESI) *m/z*: $[M + Na]^+$ calculated for $C_{26}H_{33}O_5INa$, 575.1270; found, 575.1272.

Synthesis of triene **19**

To a stirred solution of vinyl iodide **18** (21 mg, 40.2 µmol, 1.0 equiv) and boronate **13** (39.12 mg, 60.0 µmol, 1.5 equiv) in THF (5 mL) and H_2O (1.25 mL) were sequentially added thallium(I) carbonate (33.92 mg, 72.0 µmol, 1.8 equiv) and $Pd(PPh_3)_4$ (13.93 mg, 12.0 µmol, 0.3 equiv) at room temperature. The reaction mixture was stirred for 4 h and then H_2O was added. The aqueous solution was extracted with Et_2O. The combined, organic phases were dried over anhydrous Na_2SO_4,

filtered, concentrated in vacuo and the crude product was purified by silica gel column chromatography to furnish the title triene **19** (29.3 mg, 31.0 µmol, 77%). R_f = 0.4 (PE/EtOAc 2:1, visualized using an anisaldehyde or UV), $[\alpha]_D^{20}$ = +77.2 (*c* 0.53, CH_2Cl_2); ^{1}H NMR (400 MHz, acetone-d_6, acetone-d_5 = 2.05 ppm) δ 7.32 (d, *J* = 15.7 Hz, 1H, H3), 7.19 (d, *J* = 8.5 Hz, 2H, H27), 7.00 (d, *J* = 8.5 Hz, 2H, H28), 6.64 (dd, *J* = 11.7, 14.1 Hz, 1H, H12), 6.17 (dd, *J* = 10.9, 11.2 Hz, 1H, H14), 6.11–6.04 (m, 3H, H5, H11, H13), 6.01 (d, *J* = 2.6 Hz, 1H, H25), 5.83 (d, *J* = 15.7 Hz, 1H, H2), 5.78 (d, *J* = 10.4, 10.7 Hz, 1H, H15), 5.55 (s,1H, H18), 5.48 (t, *J* = 10.1 Hz, 1H, H10), 4.71 (dd, *J* = 6.6, 9.2 Hz, 1H, H9), 4.14 (q, *J* = 7.1 Hz, 2H, H1'), 4.05–4.00 (m, 1H, H7), 2.87–2.88 (m, 1H, H16), 2.74 (d, *J* = 12.6 Hz, 1H, H19), 2.49 (t, *J* = 6.9 Hz, 2H, H6), 2.39 (ddd, *J* = 3.3, 3.5, 11.4 Hz, 1H, H24), 2.27 (s, 3H, H12'), 2.12 (s, 3H, H10'), 1.93 (dd, *J* = 11.8, 11.9 Hz, 1H, H23), 1.89 (s, 3H, H3'), 1.84 (d, *J* = 13.6 Hz, 1H, H21b), 1.83–1.80 (m, 1H, H8), 1.73 (d, *J* = 13.9 Hz, 1H, H21a), 1.45 (s, 3H, H5'), 1.30 (s, 3H, H6'), 1.23 (t, *J* = 7.1 Hz, 3H, H2'), 1.14 (s, 3H, H8'), 1.08 (d, *J* = 6.8 Hz, 3H, H4'), 1.07 (s, 3H, H7'), 1.04–0.99 (m, 18H, H14', H16'), 0.70–0.58 (m, 12H, H13', H15'); ^{13}C NMR (400 MHz, acetone-d_6 = 29.8 and 206.3 ppm) δ 169.4 (C9'), 168.7 (C11'), 166.4 (C1), 149.8 (C29), 148.8 (C3), 139.3 (C5), 137.1 (C26), 134.9 (C17), 134.5 (C15), 133.8 (C4), 133.2 (C10), 131.6 (C13), 129.4 (C11), 127.1 (C12), 126.5 (C27), 125.6 (C14), 122.7 (C18),121.3 (C28), 115.9 (C2), 75.0 (C25) , 74.8 (C20), 72.9 (C7), 70.1 (C9), 60.2 (C21), 59.6 (C1'), 55.1 (C19), 47.4 (C8), 46.6 (C24), 44.7 (C23), 40.8 (C16), 37.5 (C22), 32.6 (C6), 29.8 (C7'), 25.7 (C8'), 23.6 (C6'), 20.6 (C5'), 20.3 (C12'), 20.1 (C10'), 13.7 (C2'), 11.9 (C3'), 9.5 (C4'), 6.5 (C14'), 6.3 (C16'), 4.9 (C13',15'); HRMS (ESI) *m/z*: $[M + Na]^+$ calculated for $C_{55}H_{86}O_9Si_2Na$, 969.5708; found, 969.5707.

Synthesis of elansolid B1 (**2**)

Polyene **19** (2.65 mg, 2.79 µmol, 1.0 equiv) was dissolved in THF (0.5 mL) and cooled to 0 °C. A solution of hydrogen fluoride pyridine complex (0.5 mL) prepared by mixing hydrogen fluoride pyridine (2 mL; hydrogen fluoride ≈70 %) with pyridine (5.6 mL) in THF (9.8 mL) at 0 °C. The reaction mixture was stirred for 1 h at this temperature and the reaction was terminated by addition of a saturated bicarbonate solution. The aqueous solution was extracted with Et_2O for three times. The combined organic phases were dried over Na_2SO_4, filtered and concentrated under reduced pressure to afford the corresponding diol suitably pure for directly being employed in the next step. An aqueous solution of LiOH (1 M, 0.3 mL, 107 equiv) was added to crude diol in iPrOH (0.3 mL) and THF (0.3 mL) at room temperature. After stirring for 5 h, the reaction was terminated by slowly adding HCl (1 N, 0.24 mL), phosphate buffer (pH 7, 0.1 mL) and MeOH (0.3 mL). The crude mixture was directly subjected to HPLC (C18 ISIS-SP) (MeOH: H_2O/50 mM NH_4OAc 70:30 to MeOH:H_2O/50 mM NH_4OAc 100:0 {0–70 min}, 3.0 mL/min) to give elansolid B1 (**2**) (0.88 mg, 1.45 µmol, 52% over two steps, t_R = 47.8 min). $[\alpha]_D^{20}$ = +176.0 (*c* 0.05, MeOH); ^{1}H NMR (500 MHz, acetone-d_6; acetone-d_5 = 2.05 ppm) δ 7.35 (d, *J* = 15.6 Hz, 1H, H3), 7.14 (d, *J* = 8.3 Hz, 2H, H27), 6.75 (d, *J* = 8.5 Hz, 2H, H28), 6.57 (dd, *J* = 12.2, 13.6 Hz, 1H, H12), 6.17 (t, *J* = 7.23 Hz, 1H, H5), 6.09–6.02 (m, 2H, H13, H14), 5.99 (dd, *J* = 10.8, 11.0 Hz, 1H, H11), 5.84 (d, *J* = 15.7 Hz, 1H, H2), 5.70 (*t*, *J* = 10.5 Hz, 1H, H15), 5.55 (dd, *J* = 9.5, 10.9 Hz, 1H, H10), 5.52 (s, 1H, H18), 5.18 (d, *J* = 2.5 Hz, 1H, H25), 4.94 (ddd, *J* = 0.9, 3.6, 8.6 Hz, 1H, H9), 3.87–3.84 (m, 1H, H7), 2.92 (dd, *J* = 4.0, 10.8 Hz, 1H, H16), 2.69 (d, *J* = 2.6 Hz, 1H, H19), 2.59 (ddd, *J* = 4.2, 6.8, 15.3 Hz, 1H, H6a), 2.51–2.47 (m, 1H, H6b), 2.22–2.18 (m, 1H, H24), 1.99–1.95 (m, 1H, H23), 1.88 (s, 3H, H1'), 1.83–1.80 (m, 1H, H8), 1.83 (d, *J* = 13.8 Hz, 1H, H21a), 1.73 (d, *J* = 13.8 Hz, 1H, H21b), 1.44 (dd, *J* = 1.4, 2.2 Hz, 3H, H3'), 1.30 (s, 3H, H5'), 1.29 (s, 3H, H6'), 1.14 (s, 3H, H4'), 1.03 (d, *J* = 7.0 Hz, 3H, H2'); ^{13}C NMR (125 MHz, acetone-d_6 = 29.8 and 206.3 ppm) δ 167.5 (C1), 155.7 (C29), 149.4 (C3), 138.9 (C5), 135.2 (C26, C17), 134.8 (C15), 133.8 (C4), 132.9 (C10), 130.9 (C13), 129.3 (C11), 127.5 (C12), 127.0 (C27), 126.5 (C14), 122.5 (C18), 115.9 (C2), 114.5 (C28), 74.9 (C20), 73.0 (C7), 72.2 (C25), 68.5 (C9), 60.5 (C21), 55.1 (C19), 48.4 (C24), 44.5 (C23), 44.0 (C8), 40.4 (C16), 37.7 (C22), 34.1 (C6), 30.9 (C5'), 25.7 (C4'), 23.8 (C6'), 20.6 (C3'), 11.8 (C1'), 10.7 (C2'); HRMS (ESI) *m/z*: $[M + Na]^+$ calculated for $C_{37}H_{50}O_7Na$, 629.3454; found, 629.3463.

Synthesis of elansolid B2 (**3**)

In aqueous solution of LiOH (1 M, 0.3 mL, 107 equiv) was added to the crude diol (3.1 µmol) described for the synthesis of elansolid B1 (**2**) in MeOH (0.3 mL) and THF (0.3 mL) at room temperature. After stirring for 5 h, the reaction was terminated by slowly adding HCl (1 N, 0.24 mL), phosphate buffer (pH 7, 0.1 mL) and MeOH (0.3 mL). The crude mixture was directly subjected to HPLC (C18 ISIS-SP) (MeOH: H_2O/50 mM NH_4OAc 70:30 to MeOH:H_2O/50 mM NH_4OAc 100:0 {0–70 min}, 3.0 mL/min) to give elansolid B2 (**3**) (1.2 mg, 1.93 µmol, 63% over two steps, t_R = 63.4 min). $[\alpha]_D^{20}$ = +262.1 (*c* 0.087, MeOH); ^{1}H NMR (400 MHz, acetone-d_6; acetone-d_5 = 2.05 ppm) δ 7.35 (d, *J* = 15.7 Hz, 1H, H3), 7.07 (d, *J* = 8.4 Hz, 2H, H27), 6.77 (d, *J* = 8.5 Hz, 2H, H28), 6.63 (dd, *J* = 11.5, 14.6 Hz, 1H, H12), 6.34 (dd, *J* = 11.5, 14.6 Hz, 1H, H13), 6.18 (t, *J* = 7.2 Hz, 1H, H5), 6.13 (t, *J* = 11.2 Hz, 1H, H11), 6.02 (t, *J* = 11.2 Hz, 1H, H14), 5.82 (d, *J* = 15.7 Hz, 1H, H2), 5.68 (t, *J* = 10.8 Hz, 1H, H15), 5.57 (dd, *J* = 9.7, 10.1 Hz, 1H, H10), 5.48 (s, 1H, H18), 4.99 (ddd, *J* = 0.9, 3.5, 8.6 Hz, 1H, H9), 4.66 (d, *J* = 2.4 Hz, 1H, H25), 3.88–3.84 (m, 1H, H7), 3.12 (s, 3H, H7'), 2.90 (dd, *J* = 3.3, 10.6 Hz, 1H, H16), 2.64–2.62 (m, 1H, 19H), 2.60–2.58 (m, 1H, H6a), 2.52–2.44

(m, 1H, H6b), 2.01–1.97 (m, 1H, H24), 1.95–1.91 (m, 1H, H23), 1.89 (s, 3H, H1'), 1.85–1.82 (m, 1H, H8), 1.82 (d, J = 13.5 Hz, 1H, H21a), 1.72 (d, J = 13.8 Hz, 1H, H21b), 1.45 (dd, J = 1.3, 2.1 Hz, 3H, H3'), 1.29 (s, 3H, H5'), 1.21 (s, 3H, H6'), 1.12 (s, 3H, H4'), 1.03 (d, J = 7.0 Hz, 3H, H2'); ^{13}C NMR (100 MHz, acetone-d_6 = 29.8 and 206.3 ppm) δ 167.3 (C1), 156.2 (C29), 149.4 (C3), 139.0 (C5), 135.5 (C15), 135.3 (C17), 133.8 (C4), 132.5 (C10), 131.6 (C13), 131.0 (C26), 129.4 (C11), 128.3 (C27), 126.8 (C12), 124.3 (C14), 122.5 (C18), 115.7 (C2), 114.7 (C28), 82.9 (C25), 74.8 (C20), 73.0 (C7), 68.5 (C9), 60.4 (C21), 55.6 (C7'), 55.2 (C19), 48.8 (C24), 44.8 (C23), 44.0 (C8), 40.3 (C16), 37.6 (C22), 34.2 (C6), 30.4 (C6'), 25.7 (C4'), 23.7 (C5'), 20.9 (C3'), 11.8 (C1'), 10.8 (C2'); HRMS (ESI) *m/z*: $[M + Na]^+$ calculated for $C_{38}H_{52}O_7Na$, 643.3611; found, 643.3611.

Supporting Information

Supporting Information File 1

^{1}H and ^{13}C NMR spectra of synthesized compounds.
[http://www.beilstein-journals.org/bjoc/content/supplementary/1860-5397-13-124-S1.pdf]

References

1. Gerth, K.; Steinmetz, H.; Höfle, G. Elansolids, novel natural metabolites of flexibacter and antibiotically active derivatives thereof. Eur. Pat. Appl. EP 2 093 212 A1, Aug 26, 2009.
2. Steinmetz, H.; Gerth, K.; Jansen, R.; Schläger, N.; Dehn, R.; Reinecke, S.; Kirschning, A.; Müller, R. *Angew. Chem.* **2011,** *123,* 553–557. doi:10.1002/ange.201005226
3. Dehn, R.; Katsuyama, Y.; Weber, A.; Gerth, K.; Jansen, R.; Steinmetz, H.; Höfle, G.; Müller, R.; Kirschning, A. *Angew. Chem., Int. Ed.* **2011,** *123,* 3968–3973. doi:10.1002/ange.201006880
4. Jansen, R.; Gerth, K.; Steinmetz, H.; Reinecke, S.; Kessler, W.; Kirschning, A.; Müller, R. *Chem. – Eur. J.* **2011,** *17,* 7739–7744. doi:10.1002/chem.201100457
5. Steinmetz, H.; Zander, W.; Shushni, M. A. M.; Jansen, R.; Gerth, K.; Dehn, R.; Dräger, G.; Kirschning, A.; Müller, R. *ChemBioChem* **2012,** *13,* 1813–1817. doi:10.1002/cbic.201200228
6. Minami, A.; Oikawa, H. *J. Antibiot.* **2016,** *69,* 500–506. doi:10.1038/ja.2016.67
7. Weber, A.; Dehn, R.; Schläger, N.; Dieter, B.; Kirschning, A. *Org. Lett.* **2014,** *16,* 568–571. doi:10.1021/ol403441c
8. For simplification the carbon atoms are numbered as in the natural product elansolid throughout the text.
9. Wang, L. L.; Candito, D.; Dräger, G.; Hermann, J.; Müller, R.; Kirschning, A. *Chem. – Eur. J.* **2017,** *23,* 5291–5298. doi:10.1002/chem.201605884
10. Jones, G. R.; Landais, Y. *Tetrahedron* **1996,** *52,* 7599–7662. doi:10.1016/S0040-4020(96)00038-5
11. Hartmann, O.; Kalesse, M. *Org. Lett.* **2012,** *14,* 3064–3067. doi:10.1021/ol3011387
12. Gao, D.; O'Doherty, G. A. *Org. Lett.* **2010,** *12,* 3752–3755. doi:10.1021/ol101340n
13. Fuwa, H.; Sasaki, M. *Org. Lett.* **2010,** *12,* 584–587. doi:10.1021/ol902778y
14. Fuwa, H.; Suzuki, T.; Kubo, H.; Yamori, T.; Sasaki, M. *Chem. – Eur. J.* **2011,** *17,* 2678–2688. doi:10.1002/chem.201003135
15. Essig, S.; Bretzke, S.; Müller, R.; Menche, D. *J. Am. Chem. Soc.* **2012,** *134,* 19362–19365. doi:10.1021/ja309685n

License and Terms

BEILSTEIN JOURNAL OF ORGANIC CHEMISTRY

BODIPY-based fluorescent liposomes with sesquiterpene lactone trilobolide

Ludmila Škorpilová[1,2], Silvie Rimpelová[3], Michal Jurášek[1], Miloš Buděšínský[4], Jana Lokajová[4], Roman Effenberg[1], Petr Slepička[5], Tomáš Ruml[3], Eva Kmoníčková[6,7], Pavel B. Drašar[*1] and Zdeněk Wimmer[*1,2]

Full Research Paper

Open Access

Address:
[1]Department of Chemistry of Natural Compounds, University of Chemistry and Technology Prague, Technická 5, 166 28 Prague 6, Czech Republic, [2]Institute of Experimental Botany, ASCR, Vídeňská 1083, 142 20 Prague 4, Czech Republic, [3]Department of Biochemistry and Microbiology, University of Chemistry and Technology Prague, Technická 5, 166 28 Prague 6, Czech Republic, [4]Institute of Organic Chemistry and Biochemistry, ASCR, Flemingovo n. 2, 166 10 Prague 6, Czech Republic, [5]Department of Solid State Engineering, University of Chemistry and Technology Prague, Technická 5, 166 28 Prague 6, Czech Republic, [6]Institute of Experimental Medicine, ASCR, Vídeňská 1083, 142 20 Prague 4, Czech Republic and [7]Charles University, Faculty of Medicine in Pilsen, Alej Svobody 76, 323 00 Pilsen, Czech Republic

Email:
Pavel B. Drašar[*] - pavel.drasar@vscht.cz; Zdeněk Wimmer[*] - wimmer@biomed.cas.cz

* Corresponding author

Keywords:
BODIPY conjugates; cancer targeting; drug delivery; liposomes; natural compounds; sesquiterpene lactone trilobolide

Beilstein J. Org. Chem. **2017,** *13,* 1316–1324.
doi:10.3762/bjoc.13.128

Received: 20 February 2017
Accepted: 20 June 2017
Published: 04 July 2017

This article is part of the Thematic Series "Lipids: fatty acids and derivatives, polyketides and isoprenoids".

Guest Editor: J. S. Dickschat

Abstract

Like thapsigargin, which is undergoing clinical trials, trilobolide is a natural product with promising anticancer and anti-inflammatory properties. Similar to thapsigargin, it has limited aqueous solubility that strongly reduces its potential medicinal applications. The targeted delivery of hydrophobic drugs can be achieved using liposome-based carriers. Therefore, we designed a traceable liposomal drug delivery system for trilobolide. The fluorescent green-emitting dye BODIPY, cholesterol and trilobolide were used to create construct **6**. The liposomes were composed of dipalmitoyl-3-trimethylammoniumpropane and phosphatidylethanolamine. The whole system was characterized by atomic force microscopy, the average size of the liposomes was 150 nm in width and 30 nm in height. We evaluated the biological activity of construct **6** and its liposomal formulation, both of which showed immunomodulatory properties in primary rat macrophages. The uptake and intracellular distribution of construct **6** and its liposomal formulation was monitored by means of live-cell fluorescence microscopy in two cancer cell lines. The encapsulation of construct **6** into the liposomes improved the drug distribution in cancer cells and was followed by cell death. This new liposomal

trilobolide derivative not only retains the biological properties of pure trilobolide, but also enhances the bioavailability, and thus has potential for the use in theranostic applications.

Introduction

Targeted (smart) drug delivery is a method for specific delivering of an active compound preferentially to some cells or tissues in the human body. This approach has become the key issue for surpassing the bottleneck of drug discovery. With the advent of new technologies and deeper understanding of the biological processes, the concept of specific targeting has become one of the most attractive directions in the field of biomedicine. Specific drug targeting can be achieved by using, for example, antibodies, peptides, polyethylene glycol polymers, and last but not least, liposomes, which have been nowadays extensively investigated [1,2]. In general, liposomes are employed in order to enhance the therapeutic index of an applied drug by improvement of drug absorption, prolonging its biological half-life or decreasing its metabolism [3].

Since "seeing is believing", it is strongly desired to not only target a drug to the disease-affected tissue, but also image its localization and possibly its mechanism of action directly on the given site. Based on this approach, multimodal agents delivered using a vehicle containing a drug capable of both imaging and curing were developed [4]. A meaningful information about biomolecule/drug localization and action can be gained employing fluorescence imaging, since it provides non-invasiveness, sensitivity and good spatio-temporal resolution altogether [5]. From the plethora of known fluorescent compounds, there are widely used small organic fluorophores, such as BODIPY dyes.

BODIPYs are fluorescent dyes based on the 4,4-difluoro-4-bora-3a,4a-diaza-*s*-indacene scaffold, which have recently experienced increased attention in chemistry [6-10] and life science applications [11-13]. On the grounds of high fluorescence quantum yield, narrow spectral characteristics, and sufficient chemical stability, BODIPYs have been utilized for example as laser dyes, tags of small organic molecules [14-16], drugs [17], cell organelle markers, for antibody, peptide and nucleic acid labelling [18-20], for pH [21], metal [22,23] and redox potential sensing (well-reviewed in Boens et al. [24]), as well as for the development of photodynamically active agents [25,26].

In this work, we describe the synthesis and application of a fluorescent construct (further called construct **6**, depicted in Scheme 1) based on a green-emitting BODIPY dye and trilobolide–cholesterol (Tb-ChL) in a liposome formulation. Trilobolide (Tb, Figure 1) is a potent natural compound of the sesquiterpene lactone class, which causes cell death via depleting intracellular Ca^{2+} ion stores by the irreversible inhibition of sarco-/endoplasmic reticulum Ca^{2+}-ATPase (SERCA) already at nanomolar concentrations [27-30]. In our recent study, we reported the localization of fluorescent Tb-BODIPY conjugates in the endoplasmic reticulum of a number of cancer cell lines [31]. Besides that, Tb is of high interest also for the fact that it induces high production of nitric monoxide (NO) which has an immunomodulating effect on rat peritoneal cells [32]. We documented in [31] that Tb, prepared as a fluorescent conjugate with green-emitting BODIPY, induced a dose-dependent NO production in primary rat macrophages. The potency of the fluorescent Tb to express inducible NO and cytokine secretion was shifted to a low micromolar range in comparison to the submicromolar activity of Tb itself.

The introduction of cholesterol (ChL) in the proposed structure is based on its routine exploitation in production of artificial liposome vehicles. Incorporation of ChL into liposomes was shown to 'tighten' the fluid bilayers, and thus, to reduce the leakage of an active content from the liposomes [1]. Taken together, a construct **6** probe, containing Tb, ChL and BODIPY, represents a well-defined traceable system with a potentiated ability to assemble into liposomal systems.

Results and Discussion

Chemistry

In this work, Tb was connected to a pegylated BODIPY building block containing ChL. This way obtained construct **6** was used as a component for liposomal formulation. The syntheses of some of the employed molecules were previously described [24,27,28], their structures are shown in Figure 1.

The synthesis of a BODIPY-based building block is displayed in Scheme 1, part A. Methyl 4-iodo-L-phenylalaninate hydrochloride was prepared by the reaction of 4-iodo-L-phenylalanine with thionyl chloride in MeOH in quantitative yield [33]. The successive acylation of the α-amino group with 5-azidovaleric acid catalyzed by T3P (propylphosphonic anhydride) in the mixture of pyridine and AcOEt gave azidoterminated product **1** in 70% yield. Alkaline hydrolysis of methyl ester **1** with aqueous LiOH in THF and subsequent Suzuki cross-coupling with BODIPY-BA [34] catalyzed by $Pd(PPh_3)_4$ and K_2CO_3 in a mixture of toluene/MeOH/water provided the fluorescent building block **3** in 88% yield.

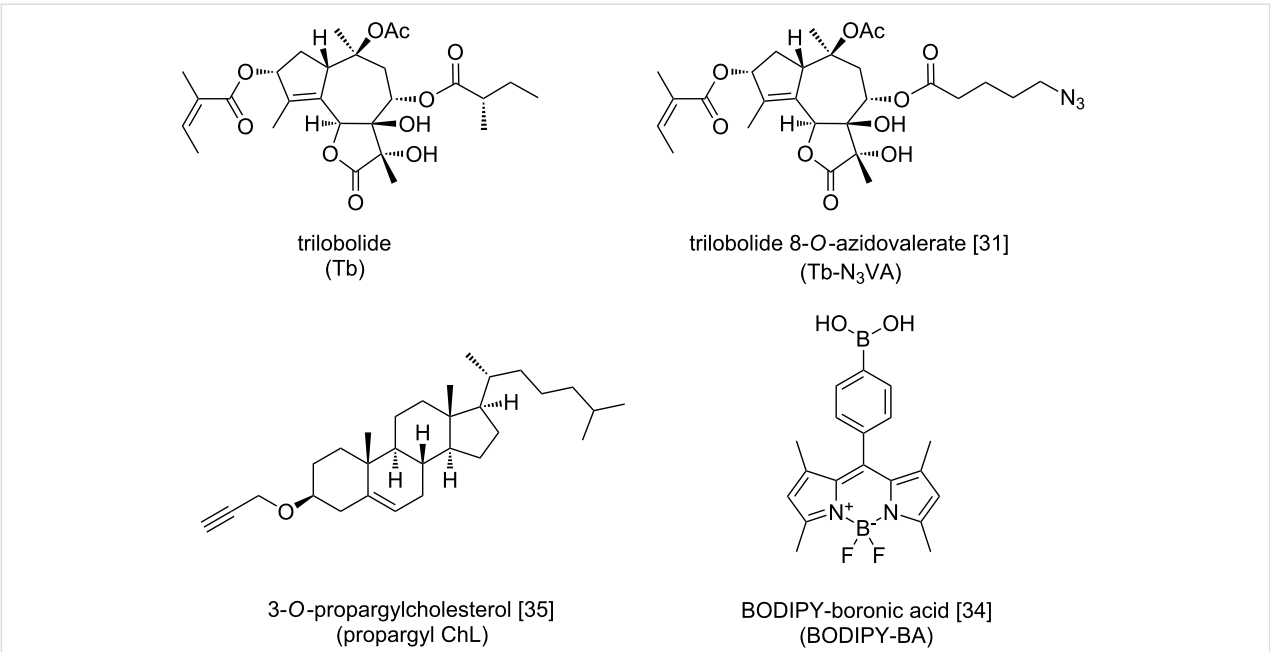

Figure 1: Chemical structures of the basic compounds used in this study.

Sequential connection of other functional components of the target compound is shown in Scheme 1, part B. Propargyl-ChL [35] was introduced into Huisgen copper-catalyzed 1,3-dipolar cycloaddition [36] (CuAAC) with BODIPY **3**. This microwave-assisted reaction catalyzed by $CuSO_4{\cdot}5H_2O$, sodium ascorbate and a catalytic amount of TBTA (tris[(1-benzyl-1*H*-1,2,3-triazol-4-yl)methyl]amine) [37] in DMF gave a cholesterol-containing clickate **4** in 49% yield. The pegylation of **4** with amino-PEG_4-alkyne in the presence of EDCI (*N*-(3-dimethylaminopropyl)-*N*′-ethylcarbodiimide hydrochloride), 4-DMAP (4-dimethylaminopyridine) and HOBt (*N*-hydroxybenzotriazole) in DMF provided an alkyne-terminated intermediate **5** in excellent yield (92%). Finally, CuAAC cycloadition of **5** and Tb-N_3VA [31] gave the target fluorescent construct **6** in good yield (84%).

The absorbance and fluorescence emission spectra of compounds **3**–**6** are depicted in Figure 2.

Compounds **3**–**6** showed absorption and emission maxima at 503 and 513 nm (excitation at 475 nm), respectively. The molar extinction coefficients of **3**–**6** in DCM ranged from 45,000 to

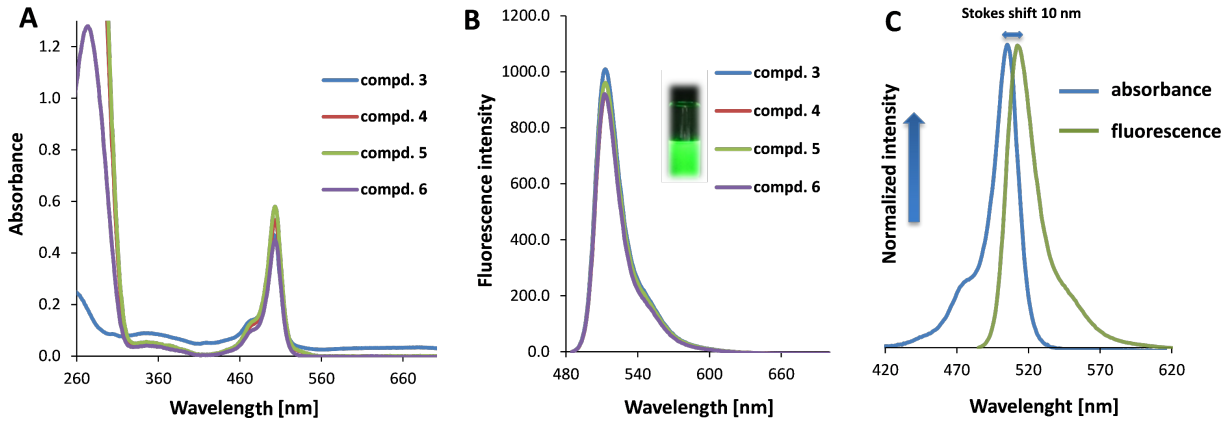

Figure 2: Absorbance and fluorescence spectra of compounds **3**–**6**. UV spectra (part A) were recorded with a concentration of 10 μM in DCM and fluorescence spectra (part B) with a concentration of 0.1 μM in DCM using an excitation wavelength of 475 nm. A typical Stokes shift (10 nm) is demonstrated for construct **6** (part C).

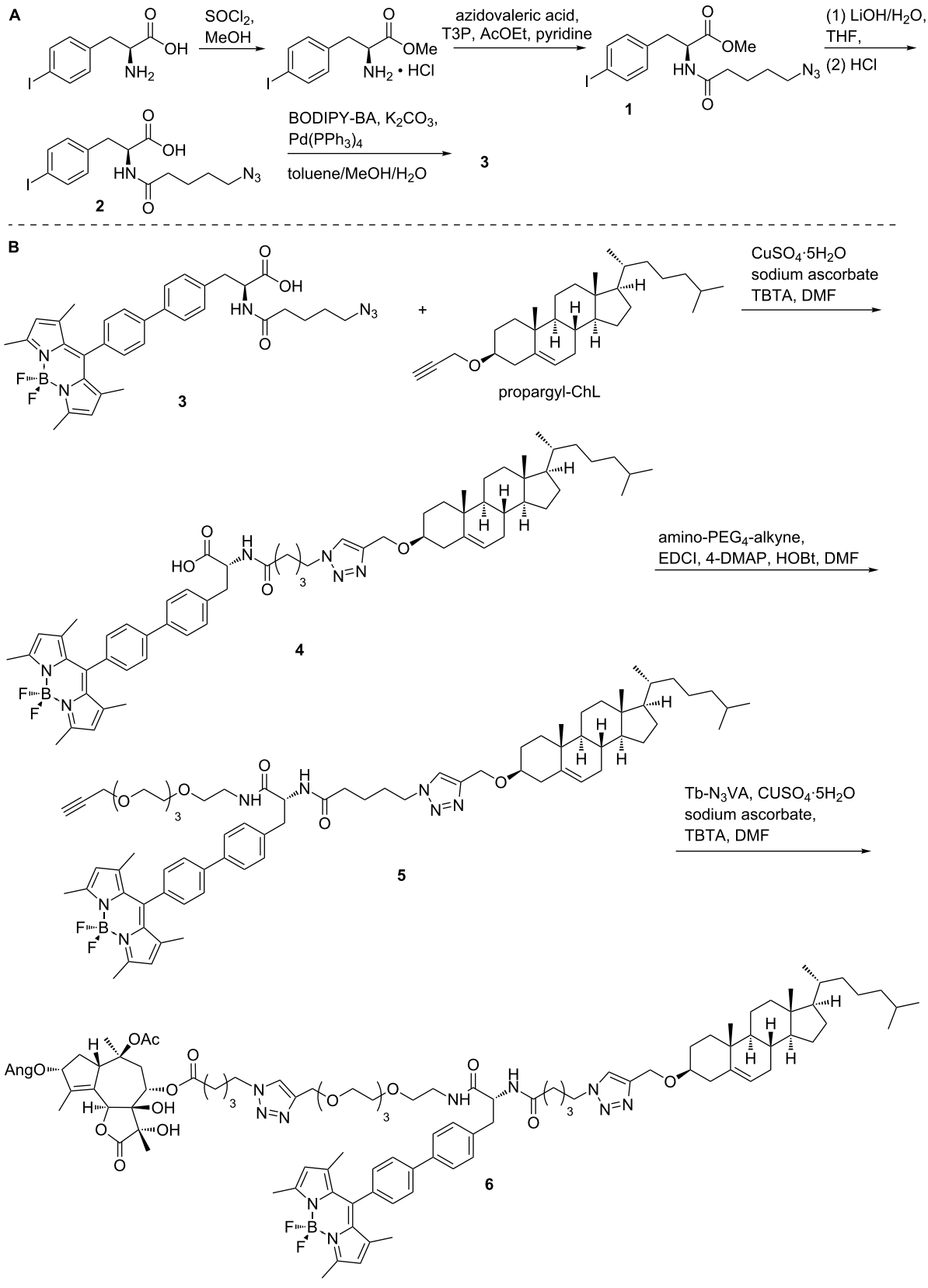

Scheme 1: Synthesis of the BODIPY building block (part A) and construct **6** (part B).

58,000 $L \cdot mol^{-1} \cdot cm^{-1}$. The purity of the target construct **6** was determined by HPLC–MS and proved to be ≥95% (Supporting Information File 1, section 5.3, Figure S15). Thereafter, construct **6** was used for liposomal formulation and biological experiments, in which the immunomodulatory, delivery and anticancer potential was evalueated.

Nitric oxide release in primary macrophages

NO (nitric oxide) is one of the most important effector molecules in the repertoire of non-specific immune defence mechanisms. This molecule is produced by macrophages and the antimicrobial and antiparasitic properties of NO have been well described [38]. Currently, the role of NO as a mediator between chronic inflammation and carcinogenesis is intensively studied [39]. The expression of inducible NO is under control of a number of cytokines. Alternatively, lipopolysaccharide (endotoxin) is known as strong inducer of NO in macrophages. Since it is known that sesquiterpene lactones, Tg, Tb, as well as Tb derivatives [31], possess strong stimulating activity for NO production by immune cells [40,41], we examined whether construct **6**, also based on Tb, exhibits similar immunobiological properties. The production of NO was evaluated after 24 h of cultivation of primary rat macrophages in the presence of increasing concentrations of Tb and construct **6**. In this study, we observed the typical activity of Tb to induce NO production in rodent macrophages which started below 0.1 μM Tb and reached an NO production of 50 μM in the presence of 4 μM Tb (the highest concentration tested, Figure 3).

The tested construct **6** induced moderate dose-dependent NO induction (methods in Supporting Information File 1, sections 4.3 and 4.4). The significant increase of NO to 21 μM was observed only at the highest concentration of 100 μM of construct **6** (*$P < 0.05$). We also investigated an eventual synergistic effect of construct **6** and lipopolysaccharide (LPS) in macrophage immunomodulation. To activate the macrophages, only a low concentration of an immunostimulator (LPS, 100 $pg \cdot mL^{-1}$) was used. In the presence of LPS, the dose-dependent curve for NO production was running higher and it was in parallel with the curve of non-stimulated cells. The synergistic effect of construct **6** with LPS on increased NO production was detected at 40 μM concentration of Tb-construct **6**, and it was significantly pronounced at 100 μM of construct **6** (*$P < 0.05$ vs LPS), upon which the level of NO reached 30 μM concentration. As expected, no effect on NO synthesis was found for **4** and **5** BODIPYs-ChL derivatives not containing Tb. No changes were detected in cell viability (WST-1 assay) for compounds **4**, **5**, and **6** (data not shown). From these and previous findings [30,31], we can summarize that the reduced immunomodulatory activity of Tb construct **6** is given by its high molecular weight (M_W equal to 1814) in comparison to Tb (M_W equal to 522), and overall shape of the molecule. Further,

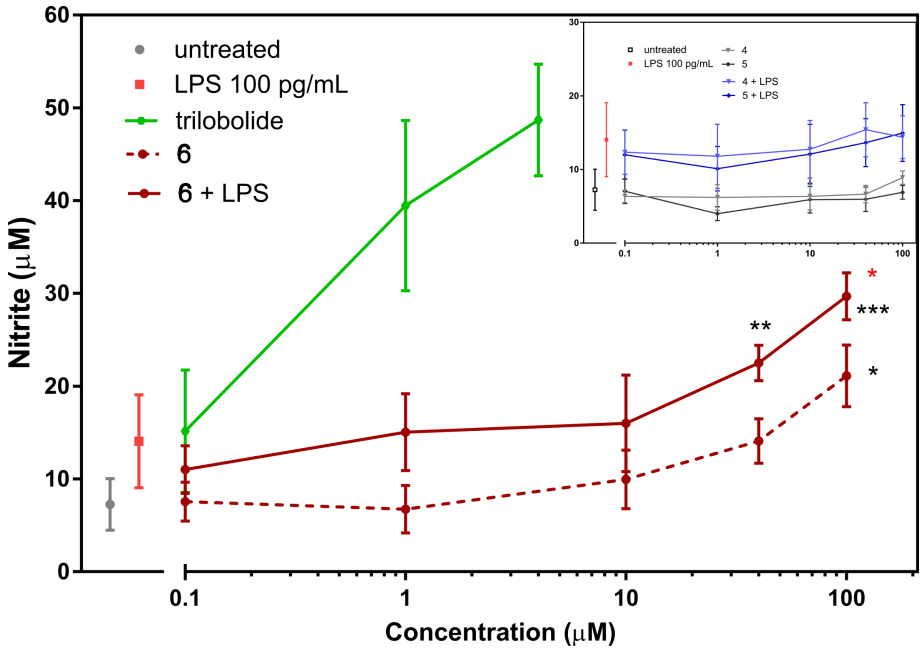

Figure 3: NO production in primary rat macrophages. The cells were treated with Tb, compounds **4**, **5**, and Tb-construct **6** for 24 h with or without lipopolysaccharide (LPS, 100 $pg \cdot mL^{-1}$). The results represent the mean ± SEM of 2 independent experiments, $n = 4$. Statistical significance: *$P < 0.05$, **$P < 0.01$, ***$P < 0.001$; black*: compounds are significantly different from untreated cells, red*: the compound is significantly different from LPS-treated cells.

cholesterol is one of the basic natural components of eukaryotic cells, thus some portion of construct **6** could be fixed in plasma membrane, which decreases the possibility of manifesting the known biological effects of Tb inside cells [42].

Liposome preparation and characterization

Liposomes were prepared by a reverse-phase evaporation method followed by homogenization (Supporting Information File 1, section 2). Dipalmitoyl-3-trimethylammonium-propane (DPTAP), phosphatidylethanolamine (DOPE) and ChL were used for implementation of fluorescent construct **6** into liposomal formulation (ratio 4:4:1:1, respectively). A hydrophobic film prepared by evaporation of a lipid–chloroform solution was hydrated with physiological solution. The desired unilamellar vesicles were obtained by homogenization of the dispersion through a 100 nm pore size polycarbonate filter. Characterization of the prepared liposomes with incorporated construct **6** was performed by atomic force microscopy (AFM) analysis in a tapping mode in 2D and 3D arrangement, see Figure 4 (Supporting Information File 1, section 3).

We confirmed the successful preparation of liposomes, the average size of which was 150 nm in width and 30 nm in height. The larger dimension of the liposomes in width, than expected, was probably caused by their adhesion to the glass surface, which was on the other hand necessary in order to perform the AFM analysis. The values of average roughness described in the Figure 4 for both (2 × 2) and (5 × 5) μm^2 are almost similar, therefore the uniformity of prepared liposomes over the surface was proven (no significant differences caused by change in the surface structure). It was confirmed, on the basis of surface roughness for both scanning areas and the evaluation of height and width of globular structures, that prepared liposomes were uniform in shape (high variability in shape or inhomogeneous peak structure would extensively increase the roughness value) and the cover over the surface was also homogeneous.

Live-cell imaging of construct **6** and its liposomal formulation

The potency of the fluorescent construct Tb-ChL and BODIPY and its liposome derivative to enter cancer cells was tested by live-cell fluorescence microscopy using two human cell line models: cells were derived from osteosarcoma (U-2 OS) and cervical carcinoma (HeLa).

Inside U-2 OS cells, construct **6** was localized from 200 nM concentration already after 1 h of incubation, the fluorescent signal was of dot-like character and persisted for at least 48 h until which, the intracellular localization was followed (Figure 5).

A similar situation was observed in HeLa cells (Supporting Information File 1, Figure S17), in which the construct **6** was also internalized and its distribution resembled the structure of the endoplasmic reticulum as well as partially the cell membrane.

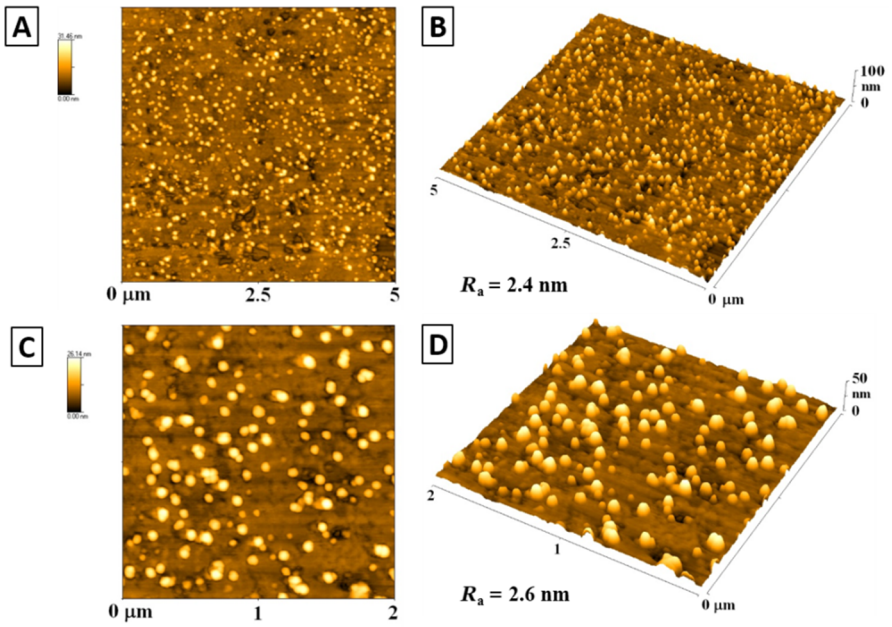

Figure 4: Atomic force microscopy images of liposomes, 5 μm area: A) 2D image, B) 3D image (R_a = 2.4 nm); 2 μm area: C) 2D image, D) 3D image (R_a = 2.6 nm). R_a represents the arithmetic average of the deviations from the centre plane of the sample.

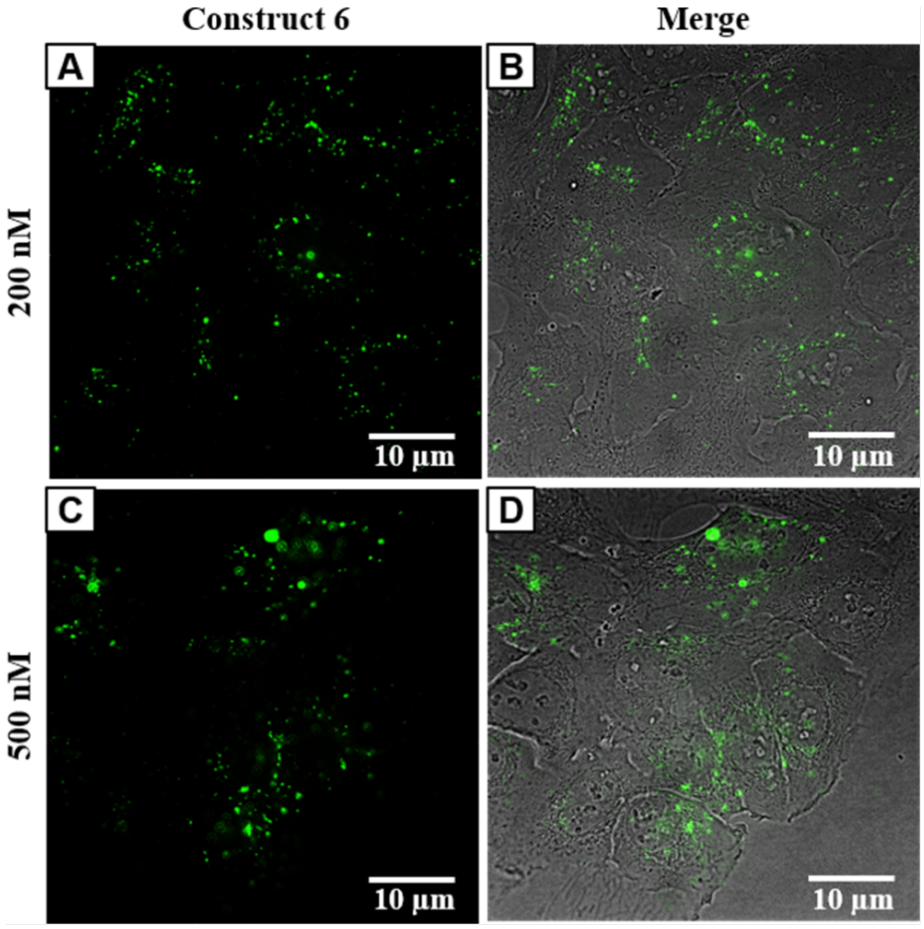

Figure 5: Panel of images from live-cell fluorescence microscopy: intracellular localization of construct **6** in U-2 OS cells after 48 h of incubation: A) 200 nM; C) 500 nM concentration of construct **6**; B) and D) merges of A and C with bright field images of U-2 OS cells, respectively.

In the case of liposomes containing construct **6**, intracellular uptake was detected already at 43 nM concentration after 1 h of incubation with U-2 OS cells (Supporting Information File 1, Figure S16), on which they were bound at the plasma membrane. After 2 h of incubation, there were two populations of cells with liposomes bound either on the plasma membrane or inside the cells (Figure 6).

The intracellular localization of liposomes was further pronounced with increased concentration up to 1.25 µM (Supporting Information File 1, Figure S18) after 2 h of incubation. With prolonged time (7 h), the U-2 OS cells were disrupted and underwent cell death (Supporting Information File 1, Figure S18), which could be caused by the release of the active construct **6** from the liposomes. Further tests are necessary to confirm this hypothesis.

Conclusion

In summary, in order to develop a drug delivery system for potential theranostic applications, we prepared a submicron liposome-based formulation of a cytotoxic agent, sesquiterpene lactone, trilobolide. More specifically, we synthesized and characterized a fluorescent construct of Tb conjugated to cholesterol and a green-emitting BODIPY dye, which was successfully incorporated into liposomes. The immunomodulatory activity tested in primary rat macrophages revealed significant dose-dependent NO production in the presence of LPS; at 100 µM concentration of construct **6**, the level of NO raised up to 30 µM. In further biological evaluation, we found that construct **6** was efficiently localized inside human U-2 OS and HeLa cancer cells. The encapsulation of construct **6** into liposomes resulted in sufficient distribution inside the cancer cells. The intracellular trafficking pattern of liposomes was characterized by two populations: the first one clearly localized on the cell membrane and the other inside the cells. With prolonged time, the population with internalized liposomes was linked to cell death, which might be caused by the release of active construct **6** from liposomes in cells. This study could be useful for further design and optimization of analogous systems for theranostic liposomal drug-delivery applications.

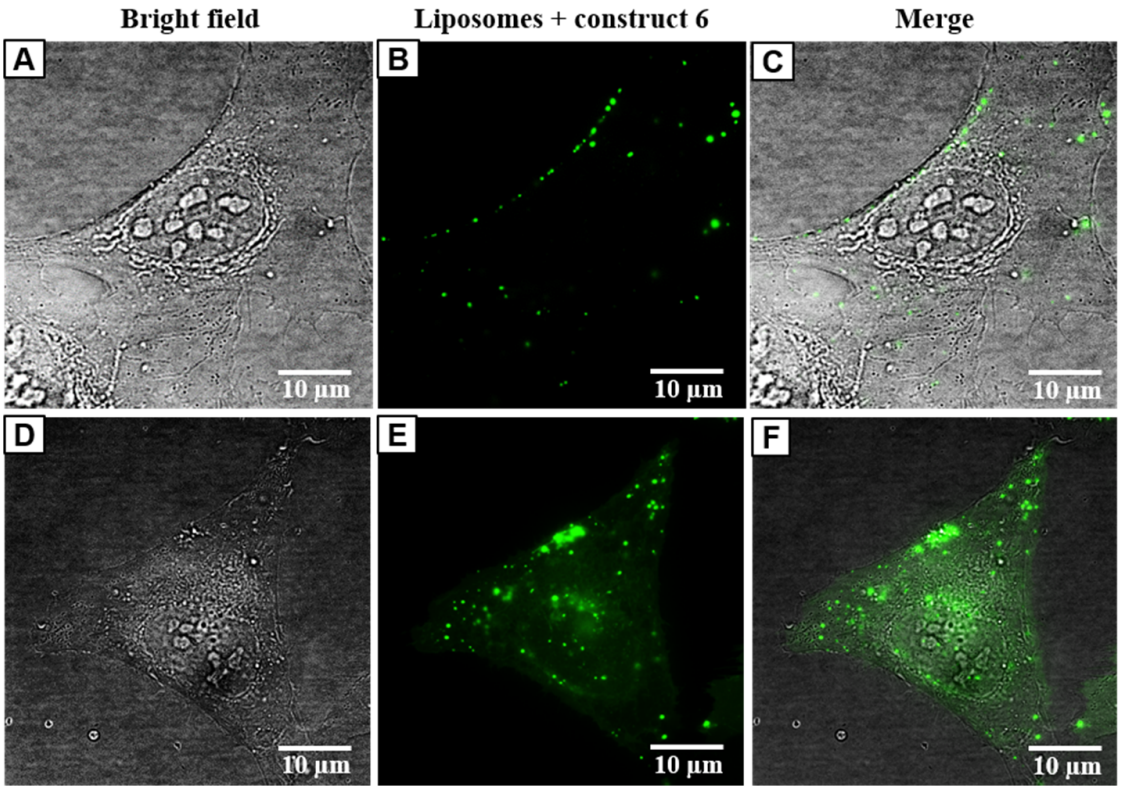

Figure 6: Panel of images from live-cell fluorescence microscopy: intracellular localization of liposomes with construct **6** (250 nM) in U-2 OS cells after 2 h of incubation: A, D) bright field; B, E) construct **6** in liposomes; C, F) merged images of A and B and D and E.

Supporting Information

Supporting Information File 1

Additional information, characterization methods, experimental, analytical data, and supporting images from live-cell fluorescence microscopy.
[http://www.beilstein-journals.org/bjoc/content/supplementary/1860-5397-13-128-S1.pdf]

Acknowledgements

The authors thank for funding of this research to MŠMT (project MSMT No 20-SVV/2017, and project COST LD15012, a part of the COST Action CM1407) and Czech Science Foundation (GAČR) 14-04329S and the Czech Republic grants no. CZ.2.16/3.1.00/24503, LO1601, LO1304 (National Program of Sustainability). The authors are grateful to Dr. Juraj Harmatha for trilobolide.

References

1. Allen, T. M.; Cullis, P. R. *Adv. Drug Delivery Rev.* **2013,** *65,* 36–48. doi:10.1016/j.addr.2012.09.037
2. Pattni, B. S.; Chupin, V. V.; Torchilin, V. P. *Chem. Rev.* **2015,** *115,* 10938–10966. doi:10.1021/acs.chemrev.5b00046
3. Çağdaş, M.; Sezer, A. D.; Bucak, S. Liposomes as Potential Drug Carrier Systems for Drug Delivery. In *Application of Nanotechnology in Drug Delivery;* Sezer, A. D., Ed.; InTech., 2014. doi:10.5772/58459
4. Kelkar, S. S.; Reineke, T. M. *Bioconjugate Chem.* **2011,** *22,* 1879–1903. doi:10.1021/bc200151q
5. Liu, Y.; Lok, C.-N.; Ko, B. C.-B.; Shum, T. Y.-T.; Wong, M.-K.; Che, C.-M. *Org. Lett.* **2010,** *12,* 1420–1423. doi:10.1021/ol902890j
6. Courtis, A. M.; Santos, S. A.; Guan, Y.; Hendricks, J. A.; Ghosh, B.; Szantai-Kis, D. M.; Reis, S. A.; Shah, J. V.; Mazitschek, R. *Bioconjugate Chem.* **2014,** *25,* 1043–1051. doi:10.1021/bc400575w
7. Verbelen, B.; Boodts, S.; Hofkens, J.; Boens, N.; Dehaen, W. *Angew. Chem., Int. Ed.* **2015,** *54,* 4612–4616. doi:10.1002/anie.201410853
8. Chong, H.; Lin, H.-A.; Shen, M.-Y.; Liu, C.-Y.; Zhao, H.; Yu, H.-h. *Org. Lett.* **2015,** *17,* 3198–3201. doi:10.1021/acs.orglett.5b00875
9. Ni, Y.; Lee, S.; Son, M.; Aratani, N.; Ishida, M.; Samanta, A.; Yamada, H.; Chang, Y.-T.; Furuta, H.; Kim, D.; Wu, J. *Angew. Chem., Int. Ed.* **2016,** *55,* 2815–2819. doi:10.1002/anie.201511151
10. Patalag, L. J.; Jones, P. G.; Werz, D. B. *Angew. Chem., Int. Ed.* **2016,** *55,* 13340–13344. doi:10.1002/anie.201606883
11. Hölttä-Vuori, M.; Uronen, R.-L.; Repakova, J.; Salonen, E.; Vattulainen, I.; Panula, P.; Li, Z.; Bittman, R.; Ikonen, E. *Traffic* **2008,** *9,* 1839–1849. doi:10.1111/j.1600-0854.2008.00801.x
12. Osati, S.; Ali, H.; van Lier, J. E. *J. Porphyrins Phthalocyanines* **2016,** *20,* 61–75. doi:10.1142/S1088424616300019
13. Lv, H.-j.; Zhang, X.-t.; Wang, S.; Xing, G.-w. *Analyst* **2017,** *142,* 603–607. doi:10.1039/C6AN02705A

14. Li, Z.; Mintzer, E.; Bittman, R. *J. Org. Chem.* **2006,** *71,* 1718–1721. doi:10.1021/jo052029x
15. Malachowska-Ugarte, M.; Sperduto, C.; Ermolovich, Y. V.; Sauchuk, A. L.; Jurášek, M.; Litvinovskaya, R. P.; Straltsova, D.; Smolich, I.; Zhabinskii, V. N.; Drašar, P.; Demidchik, V.; Khripach, V. A. *Steroids* **2015,** *102,* 53–59. doi:10.1016/j.steroids.2015.07.002
16. Jurášek, M.; Rimpelová, S.; Pavlíčková, V.; Ruml, T.; Lapčík, O.; Drašar, P. B. *Steroids* **2015,** *97,* 62–66. doi:10.1016/j.steroids.2014.10.002
17. Fishkin, N. *Mol. Pharmaceutics* **2015,** *12,* 1745–1751. doi:10.1021/mp500843r
18. Seo, T. S.; Bai, X.; Ruparel, H.; Li, Z.; Turro, N. J.; Ju, J. *Proc. Natl. Acad. Sci. U. S. A.* **2004,** *101,* 5488–5493. doi:10.1073/pnas.0401138101
19. Tram, K.; Twohig, D.; Yan, H. *Nucleosides, Nucleotides Nucleic Acids* **2011,** *30,* 1–11. doi:10.1080/15257770.2010.536798
20. Ehrenschwender, T.; Wanninger-Weiß, C.; Wagenknecht, H.-A. *Nucleic Acids Symp. Ser.* **2008,** *52,* 349–350. doi:10.1093/nass/nrn176
21. Ni, Y.; Wu, J. *Org. Biomol. Chem.* **2014,** *12,* 3774–3791. doi:10.1039/c3ob42554a
22. Niu, L.-Y.; Li, H.; Feng, L.; Guan, Y.-S.; Chen, Y.-Z.; Duan, C.-F.; Wu, L.-Z.; Guan, Y.-F.; Tung, C.-H.; Yang, Q.-Z. *Anal. Chim. Acta* **2013,** *775,* 93–99. doi:10.1016/j.aca.2013.03.013
23. Feng, L.; Li, H.; Niu, L.-Y.; Guan, Y.-S.; Duan, C.-F.; Guan, Y.-F.; Tung, C.-H.; Yang, Q.-Z. *Talanta* **2013,** *108,* 103–108. doi:10.1016/j.talanta.2013.02.073
24. Boens, N.; Leen, V.; Dehaen, W. *Chem. Soc. Rev.* **2012,** *41,* 1130–1172. doi:10.1039/C1CS15132K
25. Kamkaew, A.; Lim, S.-H.; Lee, H. B.; Kiew, L. V.; Chung, L. Y.; Burgess, K. *Chem. Soc. Rev.* **2013,** *42,* 77–88. doi:10.1039/C2CS35216H
26. Caruso, E.; Banfi, S.; Barbieri, P.; Leva, B.; Orlandi, V. T. *J. Photochem. Photobiol., B* **2012,** *114,* 44–51. doi:10.1016/j.jphotobiol.2012.05.007
27. Gibbs, J. H.; Zhou, Z.; Kessel, D.; Fronczek, F. R.; Pakhomova, S.; Vicente, M. G. H. *J. Photochem. Photobiol., B* **2015,** *145,* 35–47. doi:10.1016/j.jphotobiol.2015.02.006
28. Søhoel, H.; Lund Jensen, A.-M.; Møller, J. V.; Nissen, P.; Denmeade, S. R.; Isaacs, J. T.; Olsen, C. E.; Christensen, S. B. *Bioorg. Med. Chem.* **2006,** *14,* 2810–2815. doi:10.1016/j.bmc.2005.12.001
29. Wictome, M.; Khan, Y. M.; East, J. M.; Lee, A. G. *Biochem. J.* **1995,** *310,* 859–868. doi:10.1042/bj3100859
30. Jurášek, M.; Džubák, P.; Rimpelová, S.; Sedlák, D.; Konečný, P.; Frydrych, I.; Gurska, S.; Hajdúch, M.; Bogdanová, K.; Kolář, M.; Müller, T.; Kmoníčková, E.; Ruml, T.; Harmatha, J.; Drašar, P. B. *Steroids* **2017,** *117,* 97–104. doi:10.1016/j.steroids.2016.08.011
31. Jurášek, M.; Rimpelová, S.; Kmoníčková, E.; Drašar, P.; Ruml, T. *J. Med. Chem.* **2014,** *57,* 7947–7954. doi:10.1021/jm500690j
32. Kmoníčková, E.; Harmatha, J.; Vokáč, K.; Kostecká, P.; Farghali, H.; Zídek, Z. *Fitoterapia* **2010,** *81,* 1213–1219. doi:10.1016/j.fitote.2010.08.005
33. Yan, J.; Huang, N.; Li, S.; Yang, L.-M.; Xing, W.; Zheng, Y.-T.; Hu, Y. *Bioorg. Med. Chem. Lett.* **2012,** *22,* 1976–1979. doi:10.1016/j.bmcl.2012.01.037
34. Bai, M.; Huang, J.; Zheng, X.; Song, Z.; Tang, M.; Mao, W.; Yuan, L.; Wu, J.; Weng, X.; Zhou, X. *J. Am. Chem. Soc.* **2010,** *132,* 15321–15327. doi:10.1021/ja106637e
35. Rega, M.; Jiménez, C.; Rodriguez, J. *Steroids* **2007,** *72,* 729–735. doi:10.1016/j.steroids.2007.03.014
36. Rostovtsev, V. V.; Green, L. G.; Fokin, V. V.; Sharpless, K. B. *Angew. Chem., Int. Ed.* **2002,** *41,* 2596–2599. doi:10.1002/1521-3773(20020715)41:14<2596::AID-ANIE2596>3.0.CO;2-4
37. Hein, J. E.; Tripp, J. C.; Krasnova, L. B.; Sharpless, K. B.; Fokin, V. V. *Angew. Chem., Int. Ed.* **2009,** *48,* 8018–8021. doi:10.1002/anie.200903558
38. Mariotto, S.; Menegazzi, M.; Suzuki, H. *Curr. Pharm. Des.* **2004,** *10,* 1627–1645. doi:10.2174/1381612043384637
39. Rahat, M. A.; Hemmerlein, B. *Front. Physiol.* **2013,** *4,* No. 144. doi:10.3389/fphys.2013.00144
40. Kmoníčková, E.; Melkusová, P.; Harmatha, J.; Vokáč, K.; Farghali, H.; Zídek, Z. *Eur. J. Pharmacol.* **2008,** *588,* 85–92. doi:10.1016/j.ejphar.2008.03.037
41. Harmatha, J.; Buděšínský, M.; Vokáč, K.; Kostecká, P.; Kmoníčková, E.; Zídek, Z. *Fitoterapia* **2013,** *89,* 157–166. doi:10.1016/j.fitote.2013.05.025
42. Tomanová, P.; Rimpelová, S.; Jurášek, M.; Buděšínský, M.; Vejvodová, L.; Ruml, T.; Kmoníčková, E.; Drašar, P. B. *Steroids* **2015,** *97,* 8–12. doi:10.1016/j.steroids.2014.08.024

License and Terms

BEILSTEIN JOURNAL OF ORGANIC CHEMISTRY

An improved preparation of phorbol from croton oil

Alberto Pagani[1], Simone Gaeta[1], Andrei I. Savchenko[2], Craig M. Williams[2] and Giovanni Appendino[*1]

Full Research Paper

Open Access

Address:
[1]Dipartimento di Scienze del Farmaco, Università degli Studi del Piemonte Orientale, Largo Donegani 2, 28100 Novara, Italy and [2]School of Chemistry and Molecular Biosciences, University of Queensland, 4072, Brisbane, Australia

Email:
Giovanni Appendino[*] - giovanni.appendino@uniupo.it

* Corresponding author

Keywords:
croton oil; diterpenoids; natural products; phorbol; transesterification

Beilstein J. Org. Chem. **2017,** *13,* 1361–1367.
doi:10.3762/bjoc.13.133

Received: 10 April 2017
Accepted: 09 June 2017
Published: 11 July 2017

This article is part of the Thematic Series "Lipids: fatty acids and derivatives, polyketides and isoprenoids".

Guest Editor: J. S. Dickschat

Abstract

Background: Croton oil is the only commercial source of the diterpenoid phorbol (**1a**), the starting material for the semi-synthesis of various diesters extensively used in biomedical research to investigate cell function and to evaluate in vivo anti-inflammatory activity. While efficient chemoselective esterification protocols have been developed for phorbol, its isolation from croton oil is technically complicated, and involves extensive manipulation of very toxic materials like the oil or its native diterpenoid fraction.

Results: The preparation of a crude non-irritant phorboid mixture from croton oil was telescoped to only five operational steps, and phorbol could then be purified by gravity column chromatography and crystallization. Evidence is provided that two distinct phorboid chemotypes of croton oil exist, differing in the relative proportion of type-A and type-B esters and showing different stability to deacylation.

Conclusion: The isolation of phorbol from croton oil is dangerous because of the toxic properties of the oil, poorly reproducible because of differences in its phorboid profile, and time-consuming because of the capricious final crystallization step. A solution for these issues is provided, suggesting that the poor-reproducibility of croton oil-based anti-inflammatory assays are the result of poor quality and/or inconsistent composition of croton oil.

Introduction

Croton oil is obtained by pressing or solvent extraction from the seeds of *Croton tiglium* L., a small tree native to the Far East [1]. The oil is toxic to all living organisms, from bacteria to insects and vertebrates, and its irritancy and cathartic properties are legendary [2]. Croton oil was once used in human medicine as a topical rubefacient and in veterinarian medicine as a strong laxative [1], but nowadays its only medical use is in rejuvenating esthetic surgery in association to blepharoplasty, a prac-

tice that was mastered in the 1960s capitalizing on the potent exfoliating activity of the oil, especially in association to phenol [3].

The extraordinarily obnoxious and vesicant properties of croton oil have fostered studies aimed at the identification of its active principles since the very early developments of organic chemistry. Thus, the first chemical study on croton oil was reported by Pelletier and Caventou, the founding fathers of alkaloid chemistry, in 1818 [4], but the nature of its irritant principles remained obscure and controversial until 1930, when Flaschenträger unambiguously characterized the inflammatory fraction of the oil as a mixture of esters of a crystalline diterpene pentaol, named phorbol (Figure 1, **1a**) after the plant family to whom *C. tiglium* belongs (Euphorbiaceae) [5]. The early studies left their mark in organic chemistry in the well-known names of crotonic and tiglic acids, although, paradoxically, croton oil does not contain crotonic acid, that is only generated in the harsh conditions of the early studies [6]. The structure of phorbol eluded clarification until 1968, when it was eventually elucidated by a low-temperature (−160 °C) crystallographic study on the chloroform solvate of its 20-(5-bromofuroate) [7]. This study solved a riddle that classic degradative studies had proved unable to address because of the tendency of phorbol to skeletal rearrangement and to its idiosyncratic chemical reactivity [6]. By this time, the medicinal use of croton oil had become obsolete, but interest had been rekindled by the discovery of its co-carcinogenic properties by Berenblum in 1941 [8]. The tumor-promoting properties of the oil were associated to a specific class of phorbol diesters, exemplified by phorbol myristate acetate (PMA, TPA, **1b**), having a long-chain and a short-chain acyl residue on the vicinal hydroxy groups on ring C (Type-A esters). The molecular target of PMA was identified in a series of isoforms of PKC, a family of serine/threonine kinases involved in a host of cellular activities [9]. Because of its kinase-activating properties, PMA has become an indispensable tool in the study of cell function, with a single vendor claiming to have sold over 250,000 ampules of TPA since 1980 [10]. PMA has also been clinically investigated as an anticancer agent [11], and, in the wake of the successful development of ingenol mebutate for the management of actinic keratosis, a pre-cancerous condition [12], interest for phorboids in the area of cancer prevention and treatment remains high [13].

Phorbol occurs in croton oil as a mixture of di- and triesters, generally in a ca. 1:2 ratio [6], and therefore isolation involves a deacylation step, critical because of the sensitivity of phorbol to isomerization to 4α-phorbol (**2**) by a base-induced vinylogous retro-aldol mechanism [6]. Furthermore, phorbol strongly retains all kinds of solvents, forming crystalline solvates of limited stability with many common solvents, including ethanol

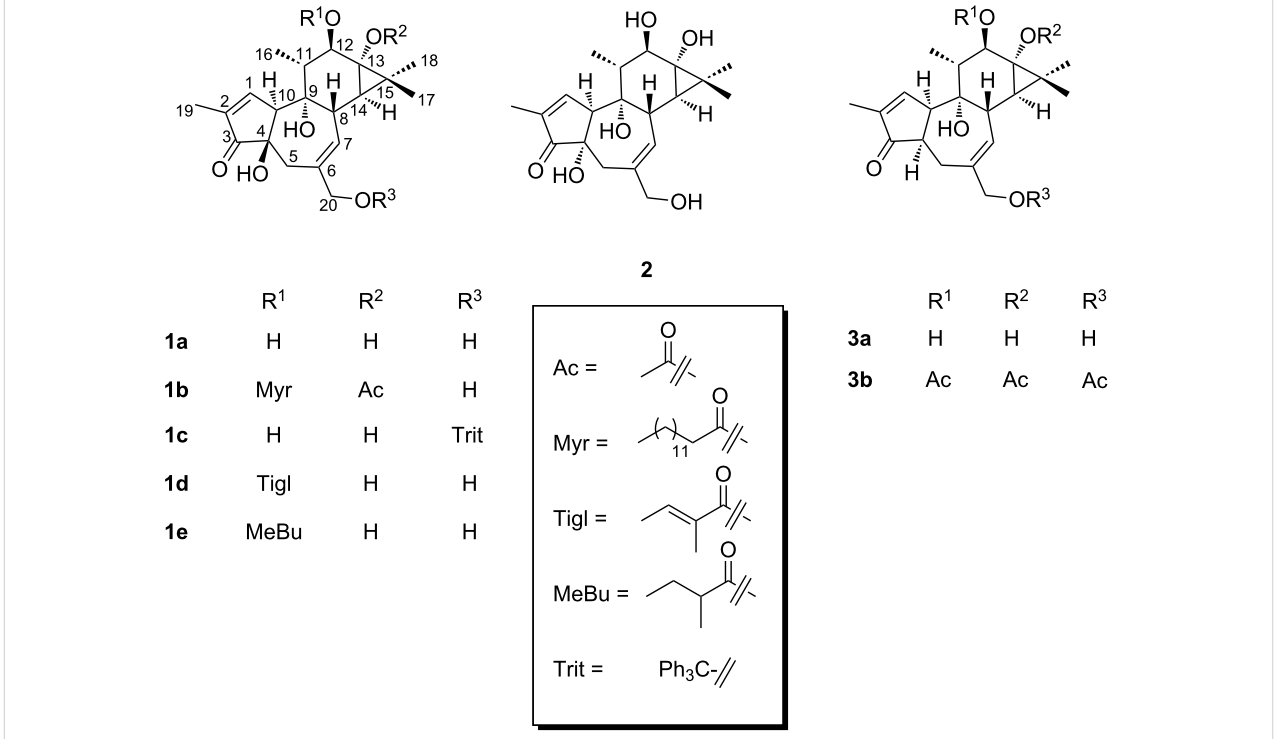

	R^1	R^2	R^3
1a	H	H	H
1b	Myr	Ac	H
1c	H	H	Trit
1d	Tigl	H	H
1e	MeBu	H	H

	R^1	R^2	R^3
3a	H	H	H
3b	Ac	Ac	Ac

Figure 1: The major diterpene polyols from croton oil [phorbol (**1a**), 4α-phorbol (**2**), 4-deoxy-4α-phorbol (**3a**)] and their derivatives.

[6,10]. Over the past three decades, we have been interested in the chemistry of phorbol, and have practiced its preparation from croton oil, evaluating various strategies to minimize the contact with this very toxic and irritant material, simplifying the purification strategy, and improving the storage of the final product. After summarizing the methods previously described in the literature, we describe in detail the protocol we have developed and its modulation according to differences in the composition of commercial croton oil.

Results and Discussion

The process developed by Flaschenträger [5] and then basically used by Hecker [6] and Crombie [14] in their classic studies on the structure of phorbol is based on the repeated extraction of croton oil with methanol to separate phorbol esters from triglycerides, and on the use of barium hydroxide as a base for the hydrolysis, using long (4–5 days) reaction times under mild basic conditions (pH ca. 8–9). After partition between ether and water, and precipitation of barium as a sulfate, the water phase is exhaustively extracted with ether and ethyl acetate, and then evaporated. Phorbol is extracted from the residue with hot methanol and, after filtration of the inorganic salts and evaporation, the methanol extract is crystallized from ethanol. There are two major issues with this protocol. The first one is the repeated handling of croton oil, a very toxic and obnoxious material, during the methanol extraction step, that requires several hours of stirring and then of resting to achieve a good phase separation, and the second one is the capricious crystallization of phorbol from the transesterification reaction mixture, a viscous oil for the presence of glycerol, that requires extended periods (four weeks according to ref. [6]). Furthermore, the unstable ethanol solvate has to be transformed into a more stable hydrate by recrystallization from hot water, a step that also requires a long time (one week according to ref. [6]). Also of concern is the overall number of operational steps (a series of over fifteen partitions, separations and evaporations), while the recovery of the more lipophilic and abundant phorbol triesters by methanol extraction of the oil is problematic, since these compounds are strongly retained in the triglyceride phase and multiple extractions are necessary to transfer them into the methanol phase, with an estimated loss of ca 50% [15]. To cope with the difficulties of the crystallization steps, protocols based on the purification of a crude mixture of ethanol solvates of phorboids by reverse-phase preparative flash chromatography or by countercurrent chromatography were developed [15-17]. The recovery of the triesters could be improved by first treating croton oil with acidic methanol to selectively remove the 20-acyl group. Partition between methanol and hexane afforded a crude mixture of phorbol diesters, that was next tritylated. After deacylation by basic treatment and chromatography, 20-tritylphorbol (**1c**) was obtained, as a hydrate, in sufficient purity to be used as starting material for the esterification [18]. This method was originally developed by Bernd Sorg of the Deutsches Krebsforschung Zentrum (Heidelberg, Germany), who kindly shared it with other researchers in the field. In our hands, it was simpler and more efficient than the original process developed by Flaschenträger, but it was, nevertheless, problematic for the multigram isolation of phorbol due to the extensive handling of the toxic croton oil and the ultra-toxic mixture of phorbol diesters obtained in the acidic transesterification step. Furthermore, the tritylation of the crude mixture of phorbol diesters suffered from interference from variable amounts of glyceryl mono- and diesters co-extracted with phorbol diesters and, presumably, already occurring in the native oil.

Since phorbol and its monoesters are not toxic, an "anticipation" of the deacylation step could afford a reaction mixture amenable to handling under normal laboratory conditions, also securing the recovery of phorbol triesters, difficult to selectively extract from the oil with a polar solvent. This strategy is not new in conception [16,19], but its implementation needs improvement in the recovery of phorbol to be practical. Thus, the water solution of phorbol and glycerol obtained after hydrolysis of the oil and washing with organic solvents must be evaporated with care, maintaining an acidic pH to minimize epimerization to 4α-phorbol [19]. Next, the recovery of phorbol from the resulting ca 10% solution of phorboids in glycerol is difficult under both normal- and reverse-phase silica gel chromatography, that fail to separate phorbol from 4α-4-deoxyphorbol (**3a**) because of their similar chromatographic behavior and of the presence of glycerol. As a result, the week-long crystallization from water was still necessary [19], a process that, tediousness aside, we found was accompanied by partial epimerization to 4α-phorbol (**2a**) and erosion of the overall final yield.

To streamline the recovery of phorbol in the deacylation step, croton oil was treated with sodium methylate. By replacing hydrolysis with transesterification, it was possible to remove fats from the detoxified reaction mixture by extraction with petroleum ether, making dilution with water unnecessary. Provided that the pH of the reaction did not exceeded 13, retroaldol epimerization was also negligible, and undetectable by TLC control. Evaporation of methanol was straightforward and gave a solution of phorboids in glycerol as a dark thick oil that was subjected to liquid–liquid partition to recover phorbol from the glyceryl matrix. After considerable experimentation, we found that glycerol could be efficiently removed from a tetrahydrofuran (THF) solution of the transesterification residue by repeated washings with acidified brine. 1-Butanol and 1,4-dioxane were far less selective, affording extracts heavily contaminated by glycerol, also giving problems of foaming during their evaporation. The rationale for the selective partition be-

tween THF, a low-boiling and easily removed solvent, and water is unclear. The use of THF was inspired by the work of Seebach on the solubility of peptides in ether-type organic solvents in the presence of certain alkaline cations [20], and it is not unconceivable that the interaction with sodium ions substantially diversifies the relative polarity of glycerol and phorbol, making it possible to selectively partition them. In this way, the preparation of the diterpene polyol fraction was telescoped to only five operational steps (treatment of croton oil with sodium methylate, extraction with petroleum ether, evaporation, partition between THF and brine, and evaporation of THF). Purification of phorbol from the THF extract by gravity column chromatography (GCC) was then straightforward, affording a semicrystalline ca. 5:1 mixture of phorbol (**1a**) and 4α-4-deoxyphorbol (**3a**). The two compounds had very similar chromatographic behavior, but could be efficiently separated by exploiting the efficient solubility of **3a** in ethyl acetate, a solvent where phorbol is insoluble. Thus, after trituration with ethyl acetate, filtration, and washing, phorbol could be obtained as an off-white powder (6.0 g, 1.2% from croton oil), sufficiently pure for further chemical modification and devoid of **3a**. The ethyl acetate solvate of phorbol is a powder with limited stability (weeks) also at low temperature, but crystallization from methanol afforded large crystals of the more stable methanol solvate. While the ethanol solvate of phorbol degrades in a few days even at low temperature [21], the methanol solvate could be stored for at least four months at 4 °C without any significant degradation.

Transesterification with sodium methylate, and presumably also with barium hydroxide under the milder conditions of the Flaschenträger protocol, could not remove the α-branched acyl group of type-B phorbol esters, and a mixture of phorbol 12-monoesters, mainly phorbol 12-tiglate (**1d**) and phorbol 12-(2-methylbutyrate) (**1e**) was obtained from the early chromatographic fractions. The mixture of 12-acyl phorbols that had resisted global transesterification could not be further hydrolyzed without epimerization to 4α-phorbol (**2**) and extensive degradation, and accounted for ca 30% of the amount of phorbol obtained from the transesterification. The recovery of phorbol from the monoesters **1d** and **1e** was, however, possible after tritylation of the primary 20-hydroxy group (vide infra).

While this method worked well with different batches of croton oil, with consistent yields of phorbol as EtOAc solvate in the range of 1%, some samples gave a lower yield (0.2–0.3%) because of incomplete transesterification. Furthermore, the crude transesterification mixture was devoid of significant amounts of 4α-4-deoxyphorbol (**3a**), and contained as major constituent a mixture of partially hydrolyzed esters, mainly phorbol 12-tiglate (**1d**) and phorbol 12-(2-methyl)butyrate (**1e**). Thus, the ^{1}H NMR spectrum (methanol-d_4) of the crude phorboid fraction, while showing the deshielded signals of the tiglate methine (δ ca. 6.80) and of H-1 of phorbol at δ ca. 7.60, lacked the singlet of H-1 of 4α-4-deoxyphorbol at δ ca. 7.20. Hydrolysis of the 12-monoesters failed under a variety of conditions, including hydrazinolysis for the tiglate residue, and required conditions too basic for the survival of phorbol. On the other hand, tritylation of the primary 20-hydroxy group had a surprising stabilizing effect toward basic degradation, making it possible to remove the remaining ester group. 20-Tritylphorbol (**1c**) [18] obtained in this way could be directly used for the synthesis of specific esters, or, alternatively, deprotected with acidic methanol (pH 3) to phorbol. The reasons for this trityl-induced stabilization are unclear, an educated guess being that the bulky trityl group could hinder oxidative reactions based on oxygen attack to the ring B double bond, a major degradation pathway for phorbol derivatives, especially under basic conditions [22].

Taken together, these observations revealed that two chemotypes of croton oil exist. The high-yielding oil contains mainly type-A phorbol di- and triesters. These phorboids have a long-chain acyl group bound to the secondary hydroxy group at C-12 and a short chain acyl group bound to the 13-hydroxy group, and are easily transesterified to phorbol. Conversely, the low-yield chemotype is dominated by type-B phorbol esters, where the long-chain ester group is located at the tertiary 13-hydroxy group, and branched acyl groups are bound to the 12-hydroxy. These branched acyl groups are not significantly removed by transesterification in the pH range of stability of phorbol, even at the more basic conditions of our protocol compared to the classic Flaschenträger method. Furthermore, 4α-4-deoxyphorbol derivatives are not contained in significant amounts in this chemotype.

Croton oil is used as a reference for in vivo anti-inflammatory assays, like the mouse-ear erythema assay, and it is tempting to suggest that the notoriously poor-reproducibility of the data from this assay [23] might be related also to differences in the composition of croton oil, since the irritancy of phorbol esters is critically dependent on their acylation profile [6]. However, the native phorboid profile of croton oil is still poorly characterized in terms of analytical profile [24], and the recovery of the native highly lipophilic phorboid esters from the lipid matrix of the oil remains a challenge. We hope that our observations will foster studies aimed at developing analytical methods to better characterize and quantify the diterpenoid profile of this oil, whose extraordinarily irritant properties have not only generated scientific interest, but also found a place in history [25] and literature [26].

Experimental

General experimental procedures: ^{1}H and ^{13}C NMR spectra for the mixtures **1d**/**1e** were measured on a Bruker 700 Anance III HD (700.43 MHz; 176.13 MHz). Chemical shifts were referenced to the residual solvent signal ($CDCl_3$: δH = 7.24, δC = 77.0). Silica gel 60 (70–230 mesh) for gravity column chromatography (GCC) was purchased from Macherey-Nagel (Düren, Gerrmay). Aluminum-coated Merck 60 F254 (0.25 mm) plates were used for TLC, visualizing the spots by UV inspection and/or staining with 5% H_2SO_4 in ethanol and heating. All solvents were of analytical grade, and were purchased from Aldrich, while croton oil was supplied by Adipogen Life Sciences (San Diego, USA). References samples of the batches used in this study are kept at the Novara laboratories.

Phorbol from croton oil

a) Croton oil rich of type-A esters: In a 2 L round-bottom flask, freshly prepared 0.3 N sodium methylate in methanol was added dropwise (ca. 10 mL/min) to a magnetically stirred mixture of croton oil (LKT Laboratories, batch number 2597837, 500 mL) and methanol (50 mL) until the pH reached a value of 12–12.5 (pH strips, 0.5 pH unit resolution). Approximatively 1 L of methylate solution was necessary to reach and stabilize this pH value, and during the addition the amber color of the oil initially faded, and next darkened to eventually become black when the pH was strongly basic (>10). The course of the transesterification was followed by TLC, monitoring the appearance of the spot of phorbol [(EtOAc/MeOH 96:4 as eluent, direct deposition from the reaction mixture, R_f (phorbol) = 0.14)], and the lack of formation of 4α-phorbol (R_f = 0.09 in the same eluent system). After stirring overnight, the reaction mixture, whose pH was now around 11.5, was transferred into a 3 L separatory funnel, neutralized with a few drops of glacial acetic acid, and extracted with petroleum ether (5 × 300 mL). The upper phase was initially deep yellow, but its color faded with the successive extractions, while the lower phase remained dark colored. Evaporation of the lower methanol phase gave a viscous black residue that was dissolved in THF (250 mL) and washed with brine until the lower water phase was almost colorless (5 × 250 mL). The combined water phases were back-extracted with THF (ca. 100 mL), and the pooled THF phases were dried with sodium sulfate and then evaporated. A semi-solid residue was obtained (ca. 30 g), then purified by GCC on silica gel (250 g). The column was packed with petroleum ether/EtOAc 5:5 and the amount of EtOAc was gradually increased. Elution with petroleum ether/EtOAc 2:8 gave a crude fraction of phorbol monoester (8.9 g, see infra or the characterization). Elution was next continued with EtOAc and finally with EtOAc/MeOH 9:1 to afford a mixture of phorbol (**1a**) and 4α-4-deoxyphorbol (**3a**) as a semi-solid orange paste (ca. 15 g). The paste was triturated with EtOAc (150 mL) and the suspension was cooled two hours at the refrigerator temperature and next suction filtered to obtain phorbol as a slightly oatmeal-colored powder (6.0 g, 1.2% from the oil). Recrystallized from hot MeOH (35 mL) afforded 1.07 g of large colorless crystals of a methanol solvate.

The mother liquors from the trituration with EtOAc were evaporated, dissolved in pyridine (20 mL), and then treated with Ac_2O (20 mL) and DMAP (cat.). After 1 h, the reaction was worked up by the addition of a few drops of methanol to destroy the excess Ac_2O and of 2 N H_2SO_4, and next extracted with EtOAc. After drying and evaporation, the residue was purified by GCC on silica gel using petroleum ether/EtOAc 8:2 as eluent to afford 12,13,20-triiacetyl-4α-4-deoxyphorbol (**3b**, 1 g) [27] and 12,13,20-triacetylphorbol (500 mg) [27].

b) Croton oil rich of type-B esters: The oil (Alexis Biochemicals, batch number 350-089-0000, 500 mL) was processed as above. The de-glycerinated THF crude phorboid mixture was separated by GCC to afford 9.0 g of a mixture of phorbol monoesters and 1.0 g crude phorbol, that, when analyzed by ^{1}H NMR was devoid of 4α-4-deoxyphorbol. A portion (1.0) of the phorbol monoesters mixture was further purified by GCC to obtain an orange powder, that was then washed with ether to afford a colorless product (400 mg). This, when analyzed by ^{1}H NMR, was a mixture of the phorbol monoesters **1d** and **1e** (ca. 2:1 ratio).

Phorbol-12-tiglate (1d): ^{1}H NMR (700.43 MHz, $CDCl_3$) δ 7.56 (s, 1H, H-1), 5.63 (m, 1H, H-7), 4.84 (d, *J* = 9.8 Hz, 1H, H-12), 4.03 (m, 1H, H-20b), 3.98 (m, 1H, H-20a), 3.17 (br d, *J* = 2.5 Hz, 1H, H-10), 3.09 (m, 1H, H-8), 2.54 (m, 1H, H-5b), 2.44 (m, 1H, H-5a), 1.77 (dd, *J* = 2.9,1.3 Hz, 3H, H-19), 2.15 (m, 1H, H-11), 1.01 (s, 3H, H-17), 1.16 (s, 3H, H-16), 1.03 (s, 3H, H-18), 0.90 (m, 1H, H-14), 6.85 (qd, *J* = 7.1, 1.3 Hz, 1H, H-3'), 1.78 (m, 3H, H-4'), 1.80 (d, *J* = 1.09 Hz, 1H, H-5'), 4.93 (br s, 1H, 9-OH); ^{13}C NMR (176.13 MHz, $CDCl_3$) δ 208.80 (s, C-3), 160.28 (s, C-1), 140.74 (s, C-6), 133.41 (s, C-2), 129.29 (d, C-7), 79.17 (s, C-9), 87.36 (d, C-12), 73.49 (s, C-4), 67.97 (t, C-20), 60.83 (s, C-13), 56.77 (d, C-10), 43.50 (d, C-11), 38.99 (d, C-8), 38.74 (t, C-5), 35.19 (d, C-14), 27.69 (s, C-15), 22.27 (q, C-16), 17.05 (q, C-17), 16.08 (q, C-18), 10.14 (q, C-19), 170.51 (s, C-1'), 138.66 (s, C-3'), 128.13 (s, C-2'), 14.51 (q, C-4'), 12.05 (q, C-5').

Phorbol-12-(2-methylbutyrate) (**1e**): ^{1}H NMR (700.43 MHz, $CDCl_3$) δ 7.55 (br s, 1H, H-1), 5.63 (br d, *J* = 5.1 Hz, 1H, H-7), 4.83 (d, *J* = 10.0 Hz, 1H, H-12), 4.03 (d, *J* = 12.9 Hz, 1H, H-20b), 3.98 (d, *J* = 12.9 Hz, 1H, H-20a), 3.16 (br d, *J* = 3.3 Hz, 1H, H-10a), 3.09 (br d, *J* = 5.6 Hz, 1H, H-8a), 2.54 (d, *J* = 19.1 Hz, 1H, H-5b), 2.44 (d, br, *J* = 16.3 Hz, 1H, H-5a), 1.80

(dd, J = 2.9, 1.3 Hz, 3H, H-19), 2.11 (dd, J = 10.0, 6.72 Hz, 1H, H-11), 1.04 (s, 3H, H-17), 1.17 (s, 3H, H-16), 1.00 (d, J = 6.5 Hz, 3H, H-18), 0.89 (d, J = 7.6 Hz, 1H, H-14a), 2.39 (td, J = 13.9, 7.0 Hz, 1H, H-2'), 1.65 (m, 1H, H-3'), 1.48 (tt, J = 13.7, 7.4 Hz, 1H, H-3'), 1.13 (d, J = 6.9 Hz, 1H, H-5'), 0.90 (t, J = 6.0 Hz, 3H, H-4'); ^{13}C NMR (176.13 MHz, $CDCl_3$) δ 208.77 (s, C-3), 160.18 (d, C-1), 140.84 (s, C-6), 133.42 (s, C-2), 129.17 (d, C-7), 79.12 (s, C-9), 87.41 (d, C-12), 73.47 (s, C-4), 67.92 (t, C-20), 60.89 (s, C-13), 56.82 (d, C-10), 43.28 (d, C-11), 38.96 (d, C-8), 38.70 (t, C-5), 35.14 (d, C-14), 27.63 (s, C-15), 22.37 (q, C-16), 17.24 (q, C-17), 15.92 (q, C-18), 10.13 (q, C-19), 179.68 (s, C-1'), 41.31 (d, C-2'), 26.90 (t, C-3'), 11. 67 (q, C-4'), 16.47 (q, C-5').

Hydrolysis of the mixture of 1d/1e: A portion of the mixture of monoesters (3.0 g) was dissolved in pyridine (30 mL) and treated with trityl chloride (11.4 g) and cat. DMAP. After stirring overnight at room temp., the reaction was worked up by dilution with EtOAc (50 mL) and washing with 2 N H_2SO_4/brine (10:1, 100 mL). After drying and evaporation, the residue was purified by GCC on silica gel (petroleum ether/EtOAc 4:6 as eluent) to afford 3.14 g of a mixture of 20-tritylphorbol monoesters. The latter was dissolved in methanol, and 0.3 N sodium methylate was added dropwise until pH reached 12.5. After stirring overnight at room temp., the reaction was worked up by neutralization with 2 N H_2SO_4, dilution with brine, and extraction with CH_2Cl_2. Evaporation of the solvent left a solid residue, that was purified by GCC on silica gel (75 g, petroleum ether/EtOAc 3:7 as eluent) to afford 930 mg of 20-trityl phorbol. The latter could be directly used for the preparation of specific 12,13-diesters. Alternatively, it was dissolved in methanol (15 mL) and acidified to pH 3 with a few drops of 70% $HClO_4$. After 30 min, the reaction was worked up by neutralization with NaOAc and evaporation. The residue was purified by GCC on silica gel (15 g) using EtOAc/MeOH 95:5 as eluent, to afford 460 mg phorbol, that was triturated with EtOAc, eventually affording 295 mg of a colorless powder.

Supporting Information

Supporting Information File 1

ESI-HRMS and ^{1}H and ^{13}C NMR spectra of compounds **1d** and **1e**.

[http://www.beilstein-journals.org/bjoc/content/supplementary/1860-5397-13-133-S1.pdf]

Acknowledgements

We acknowledge EcoBiotics Ltd, QBiotics Ltd, the University of Queensland and the Università degli Studi del Piemonte Orientale for financial support, and Adipogen Life Sciences (San Diego, USA) for providing the samples of croton oil used in this investigation.

References

1. Gläser, S.; Winter, A.; Hecker, E. *Crotonis oleum* (Crotonöl). In *Hagers Handbuch der Pharmazeutischen Praxis;* Blaschek, W.; Hänsel, R.; Keller, K.; Reichling, J.; Rimpler, H.; Schneider, G., Eds.; Springer: Berlin, 1998; pp 471–476.
2. Meyer-Bertenrath, J. G. *Experientia* **1969,** *25,* 1–5. doi:10.1007/BF01903855
3. Orra, S.; Waltzman, J. T.; Mlynek, K.; Duraes, E. F. R.; Kundu, N.; Zins, J. E. *Plast. Reconstr. Surg.* **2015,** *136,* 99–100. doi:10.1097/01.prs.0000472401.26529.67
4. Pelletier, J.; Caventou, J. B. *J. Pharm.* **1818,** *4,* 289–314.
5. Böhm, R.; Flaschenträger, B. *Naunyn-Schmiedeberg's Arch. Pharmacol.* **1930,** *157,* 115–123. doi:10.1007/BF01972119
6. Hecker, E.; Schmidt, R. *Prog. Chem. Org. Nat. Prod.* **1974,** *31,* 378–467.
7. Pettersen, R. C.; Ferguson, G.; Crombie, L.; Games, M. L.; Pointer, D. J. *Chem. Commun.* **1967,** 716–717. doi:10.1039/c19670000716
8. Berenblum, I. *Cancer Res.* **1941,** *1,* 44–48.
9. Newton, A. C. *Chem. Rev.* **2001,** *101,* 2353–2364. doi:10.1021/cr0002801
10. http://www.lclabs.com/products/P-1680?gclid=CNeX-ZP4ocwCFaoy0wodPhsAOg (accessed March 2, 2017).
11. Han, Z. T.; Zhu, X. X.; Yang, R. Y.; Sun, J. Z.; Tian, G. F.; Liu, X. J.; Cao, G. S.; Newmark, H. L.; Conney, A. H.; Chang, R. L. *Proc. Natl. Acad. Sci. U. S. A.* **1998,** *95,* 5357–5361. doi:10.1073/pnas.95.9.5357
12. Appendino, G. *Prog. Chem. Org. Nat. Prod.* **2016,** *102,* 1–90. doi:10.1007/978-3-319-33172-0_1
13. Boyle, G. M.; d'Souza, M. M. A.; Pierce, C. J.; Adams, R. A.; Cantor, A. S.; Johns, J. P.; Maslovskaya, L.; Gordon, V. A.; Reddell, P. W.; Parsons, P. G. *PLoS One* **2014,** *9,* e108887. doi:10.1371/journal.pone.0108887
14. Crombie, L.; Games, M. L.; Pointer, D. J. *J. Chem. Soc. C* **1968,** 1347–1362. doi:10.1039/j39680001347
15. Pieters, L. A.; Vlietnick, A. J. *Planta Med.* **1986,** *52,* 465–468. doi:10.1055/s-2007-969255
16. Marshall, G. T.; Douglas Kinghorn, A. *J. Chromatogr.* **1981,** *206,* 421–424. doi:10.1016/S0021-9673(00)82560-1
17. Mishra, N. C.; Estensen, R. D.; Abdel-Monem, M. M. *J. Chromatogr.* **1986,** *369,* 435–439. doi:10.1016/S0021-9673(00)90154-7
18. Bertolini, T. M.; Giorgione, J.; Harvey, D. F.; Newton, A. C. *J. Org. Chem.* **2003,** *68,* 5028–5036. doi:10.1021/jo030029w
19. Cairnes, D. A.; Mirvish, S. S.; Wallcave, L. *Cancer Lett.* **1981,** *14,* 85–91. doi:10.1016/0304-3835(81)90013-6
20. Seebach, D.; Thaler, A.; Beck, A. K. *Helv. Chim. Acta* **1989,** *72,* 857–867. doi:10.1002/hlca.19890720502
21. Tseng, S.-S.; Van Duuren, B. L.; Solomon, J. J. *J. Org. Chem.* **1977,** *42,* 3645–3649. doi:10.1021/jo00443a002
22. Schmidt, R.; Hecker, R. *Cancer Res.* **1975,** *35,* 1375–1377.
23. Tubaro, A.; Dri, P.; Delbello, G.; Zilli, C.; Della Loggia, R. *Agents Actions* **1986,** *17,* 347–349. doi:10.1007/BF01982641
24. Bauer, R.; Tittel, G.; Wagner, H. *Planta Med.* **1983,** *48,* 10–16. doi:10.1055/s-2007-969869

25. Breuer, W. B. *Deceptions of World War II;* Wiley & Sons, 2002; pp 189–190.
26. Steinbeck, J. *Dubious Battle;* Penguin Books, 2006; p 99.
27. Evans, F. I. Phorbol: Its Esters and Derivatives. In *Naturally Occurring Phorbol Esters;* Evans, F. J., Ed.; CRC Press: Boca Raton, Florida, 1986; pp 171–215.

License and Terms

BEILSTEIN JOURNAL OF ORGANIC CHEMISTRY

A new member of the fusaricidin family – structure elucidation and synthesis of fusaricidin E

Marcel Reimann[1], Louis P. Sandjo[1,2], Luis Antelo[3], Eckhard Thines[3,4], Isabella Siepe[5] and Till Opatz[*1]

Full Research Paper

Open Access

Address:
[1]Institute of Organic Chemistry, Johannes Gutenberg-University, Duesbergweg 10–14, 55128 Mainz, Germany, [2]Departamento de Ciências Farmacêuticas, Centro de Ciências da Saúde, Bloco J/K, Universidade Federal de Santa Catarina, Florianópolis 88040-900, SC, Brazil, [3]Institute of Biotechnology and Drug Research, Erwin Schrödinger-Str. 56, 66776 Kaiserslautern, Germany, [4]Institute of Molecular Physiology, Microbiology and Wine Research, Johannes Gutenberg University Mainz, Johann-Joachim-Becher-Weg 15, 55128 Mainz, Germany and [5]BASF SE, 67056 Ludwigshafen, Germany

Email:
Till Opatz* - opatz@uni-mainz.de

* Corresponding author

Keywords:
cyclodepsipeptides; fusaricidins; lipopeptides; structure elucidation; total synthesis

Beilstein J. Org. Chem. **2017,** *13,* 1430–1438.
doi:10.3762/bjoc.13.140

Received: 03 May 2017
Accepted: 07 July 2017
Published: 20 July 2017

This article is part of the Thematic Series "Lipids: fatty acids and derivatives, polyketides and isoprenoids".

Guest Editor: J. S. Dickschat

Abstract

Two hitherto unknown fusaricidins were obtained from fermentation broths of three *Paenibacillus* strains. After structure elucidation based on tandem mass spectrometry and NMR spectroscopy, fusaricidin E was synthesized to confirm the structure and the suggested stereochemistry. The synthesis was based on a new strategy which includes an efficient access to the 15-guanidino-3-hydroxypentadecanoyl (GHPD) side chain from erucamide.

Introduction

Fusaricidins are lipid-modified non-ribosomal cyclic hexadepsipeptides containing four D-amino acids and two L-amino acids. All of them carry an L-threonine linked to a unique 15-guanidino-3-hydroxypentadecanoic acid side chain through the *N*-terminus. This particular ω-functionalized lipid side chain is of key importance for the antibiotic activity of the fusaricidins and their selective inhibition of bacterial cells due to the interaction with phospholipid cell membranes [1]. Genetic analysis of the producing organisms suggests that the biosynthesis of this essential part of the fusaricidins most likely shows similarity to the fatty acid synthesis pathway [2].

All fusaricidins have three amino acids (L-Thr, D-*allo*-Thr, and D-Ala) in common and are mostly isolated in pairs which differ in a single amino acid (asparagine vs glutamine). There are several known members of the fusaricidin family which were isolated from several strains of *Paenibacillus polymyxa* [3,4]. Fusaricidins exhibit antimicrobial activity against Gram-posi-

tive bacteria and a wide range of fungi including *Leptosphaeria maculans*, a plant pathogenic fungus responsible for the blackleg disease on *Brassica* crops [5-7].

Two new compounds were obtained from fermentation of *Paenibacillus sp.* strain Lu16774 as an inseparable mixture of two homologous cyclic depsipeptides containing either glutamine (in **1**) or asparagine (in **2**). Initially, the absolute and relative configuration of the isoleucine residue was unknown (Figure 1). Thus, an assumed stereoisomer (containing D-*allo*-Ile) of the new fusaricidin member was synthesized based on analogy to known members of the series and compared to the natural product [8].

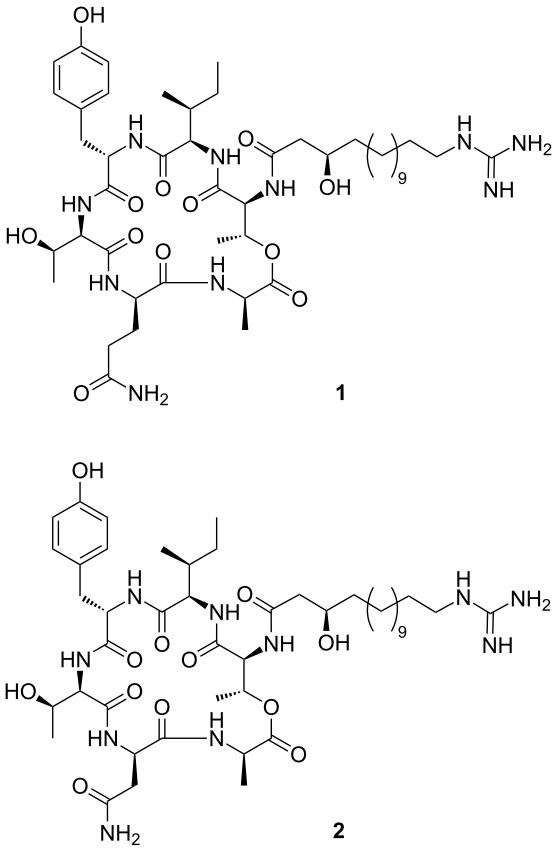

Figure 1: Structure of fusaricidins E (**1**) and F (**2**).

Results and Discussion

Isolation and structure elucidation

The *Paenibacillus* strain was cultivated on agar plates containing GYM medium (10 g/L glucose, 4 g/L yeast extract, 10 g/L malt extract; pH 5.5, adjusted before autoclaving) and 20 g/L agar. The submerged cultivation was carried out for 10 to 20 days at room temperature. For maintenance, agar slants containing the same medium were used and stored at 4 °C. Small scale liquid cultures (250 mL GYM medium in 500 mL flasks) were inoculated with 4–5 pieces of a well grown agar culture and cultivated on an orbital shaker at 120 rpm at room temperature. Large scale fermentations were carried out in 20 L fermenters with 15 L GYM medium inoculated with 250 mL well grown liquid culture at room temperature with agitation (120 rpm) and aeration (3 L/min) for 5 to 8 days. To prevent excessive foaming, a few mL of silicone antifoam were added prior to sterilization of the medium.

An equal volume of isopropanol was added to the culture. After agitation for 2 h, 200 g/L sodium chloride was added to the mixture until phase separation of the organic and aqueous phase was visible. The isopropanol layer was concentrated in vacuo. The resulting extract was dissolved in methanol, centrifuged for better precipitation of salt residues, and the organic phase was concentrated in vacuo again. This step was repeated until no further salt precipitates were visible.

A portion of the extract (30 g) was dissolved in methanol and adsorbed to silica gel (Merck, K60, 70–230 mesh, 50 g), dried at 40 °C and applied onto silica gel (1 kg, column 10 cm diameter, 30 cm height). Elution was carried out in four steps as follows: ethyl acetate, ethyl acetate/methanol (3:1, v/v), ethyl acetate/methanol (1:1, v/v) and methanol. The third fraction containing the active compounds, was dried in vacuo and dissolved in 40% methanol (MeOH) in 0.1% formic acid (FA, concentration: 100 mg/mL). The other fractions were discarded. A fraction (20 mL) of the sample was loaded onto a previously equilibrated (with 40% MeOH in 0.1% FA) Chromabond HR-X cartridge (Macherey-Nagel, 1000 mg). The cartridge was washed with 100 mL 40% MeOH in 0.1% FA and eluted with 60 mL 70% MeOH in 0.1% FA. The sample was dissolved in DMSO (concentration: 200 mg/mL) and 300 µL thereof were applied to a Sunfire C18 column (19 × 250 mm, 5 µm, Waters) and eluted as follows: 16 min at 10 mL/min, isocratic 70% 0.2% FA; 30% acetonitrile (MeCN), 1 min at 14 mL/min, gradient to 65% 0.2% FA; 35% MeCN, 5 min at 14 mL/min, isocratic 65% 0.2% FA; 35% MeCN. The five resulting fractions were dried in vacuo and re-dissolved in DMSO (concentration: 125 mg/mL). Further purification was performed using the same column and isocratic conditions (flow: 10.5 mL/min) adjusted for every fraction (12.5 mg per run). In the second fraction 68% 0.2% FA; 32% MeCN was used and a single peak was detected, consisting of an inseparable mixture of two novel fusaricidins which were named fusaricidin E (**1**) and fusaricidin F (**2**). The mixture (6.0 mg) was composed of 3 parts of **2** and 7 parts of its higher homologue **1** and had an optical rotation of $[\alpha]_D^{25}$ +20.9 (*c* 0.6, DMSO-d_6). The mass difference between both metabolites is 14 amu. This observation was supported by two ion peaks observed in the ESIMS spectrum at *m/z* 961.6 and *m/z* 975.6, respectively.

Through extensive analysis of the 1 and 2D NMR data of the major component **1**, six amino acids including tyrosine (Tyr), glutamine (Gln), alanine (Ala), two threonines (Thr1 and Thr2) and isoleucine (Ile) were identified. NMR experiments like COSY, NOESY and HMBC (Figure 2) clarified the sequence of the amino acids through two or three bonds correlation.

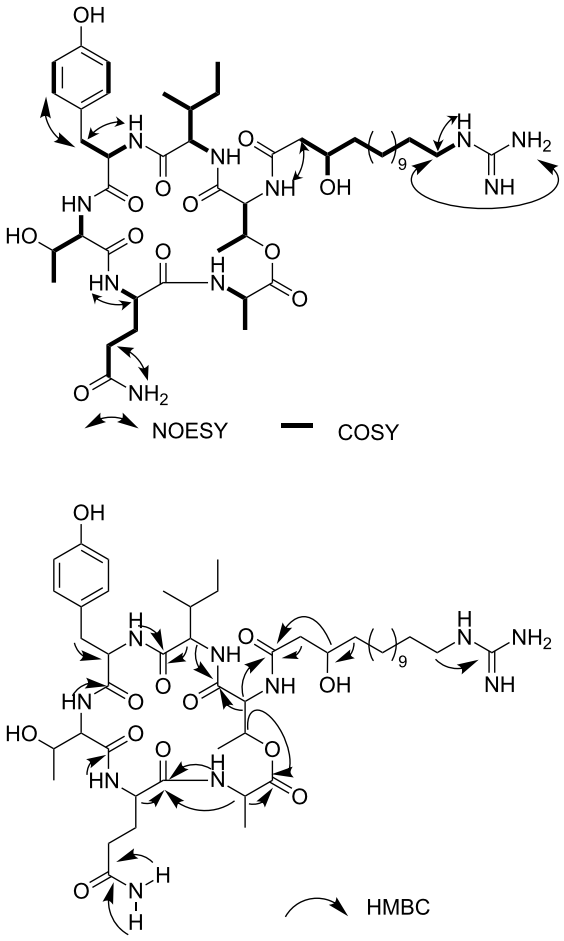

Figure 2: NOESY /COSY and HMBC correlations of compound **1**.

The spectra revealed correlations from the Thr2 NH at δ 8.50 to the α-CH of Thr2 at δ 3.94 and the carbonyl of Tyr at δ 166.7. The same correlations were found for the Tyr NH at δ 8.52, the Tyr α-CH at δ 2.60 and the carbonyl of Ile at δ 170.4. The spectra also showed a strong correlation of the Ile α-CH at δ 4.16 with the carbonyl signal of Ile at δ 170.4 and a weak correlation with the carbonyl of Thr1 at δ 168.6. Furthermore, the β-methine proton at δ 5.30 of Thr1 correlated with the carbonyl signal at δ 170.4 of Ala and additionally the NH of Ala at δ 7.27 had the expected contact with Ala's α-CH at δ 4.20. The latter proton showed correlations with the carbonyl of the same amino acid and the one of Gln. The NH proton of Gln at δ 8.20 displayed correlations with the methine hydrogen of Gln at δ 3.87 and the carbonyl of Thr2 at δ 170.6. All data suggested a cyclodepsipeptidic structure for **1**. The N-atom of Thr1 was bound to a guanidine β-hydroxy fatty acid as a key correlation was observed between the signal of its α-methine proton at δ 4.46 and the resonance of a carbonyl at δ 171.9. This carbonyl showed HMBC correlation with α-methylene protons at δ 2.35 and the β-methine proton at δ 3.77. Additionally correlations between methylene protons at δ 3.03 and the guanidine carbon at δ 157.2 were found. The length of the side chain between the β-hydroxy and the guanidine group was affirmed by the fragment ion observed in the APCI–MS–MS spectrum of the parent $[M + H]^+$ ion at *m*/*z* 256.2. Likewise, this spectrum provided information (Figure 3) which confirmed the connection sequence of amino acids and led to elucidate the structure of **1** and **2** as shown below.

Signals of geminal hydrogen atoms at δ 2.80, 2.52 revealed a direct correlation with the carbon atom δ 36.3 in the HSQC spectrum. Based on long-range H–H and H–C interactions, these resonances were assigned to the β-CH_2 group of asparagine (Asn) in the lower homologue **2**. Thus, the conclusion was supported by reported data for Asn in other fusaricidins [9] in conjunction to fragments obtained from the tandem mass of the parent peak at *m*/*z* 961.6 (Figure 3).

Retrosynthetic plan

For our synthesis, a novel and efficient access to the GHPD side chain starting from erucamide (**6**) as an inexpensive natural source for the required C_{13}-fragment was developed. After ozonolysis of the Fmoc-protected amine obtained by reduction and alkoxycarbonylation from **6**, the stereocenter should be generated by nucleophilic addition of an allyl anion equivalent to the resulting aldehyde **5**.

Guanidine formation and ozonolysis with subsequent oxidation to the carboxylic acid would then furnish the protected GHPD side chain building block **3** which can then be coupled to the cyclodepsipeptide fragment to give the desired product **1** (Scheme 1). For the synthesis of the cyclodepsipeptide portion, a convergent route was envisaged in which the complete GHPD side chain should be attached in solution after assembly of the cyclodepsipeptide on solid support. The hitherto only published synthesis of a natural fusaricidin by the Jolliffe group employed a ring closure via a lactonization in solution and subsequent attachment of the side chain to the cyclized depsipeptide [10]. Since the macrolactonization approach suffered from diastereoselectivity issues and low yield, it was decided to perform an on-resin head-to-tail macrolactamization instead [11]. A similar strategy had been used by Cudic and co-workers to synthesize analogs of fusaricidin A with an on resin coupling of a 12-aminododecanoic acid combined with a late stage guani-

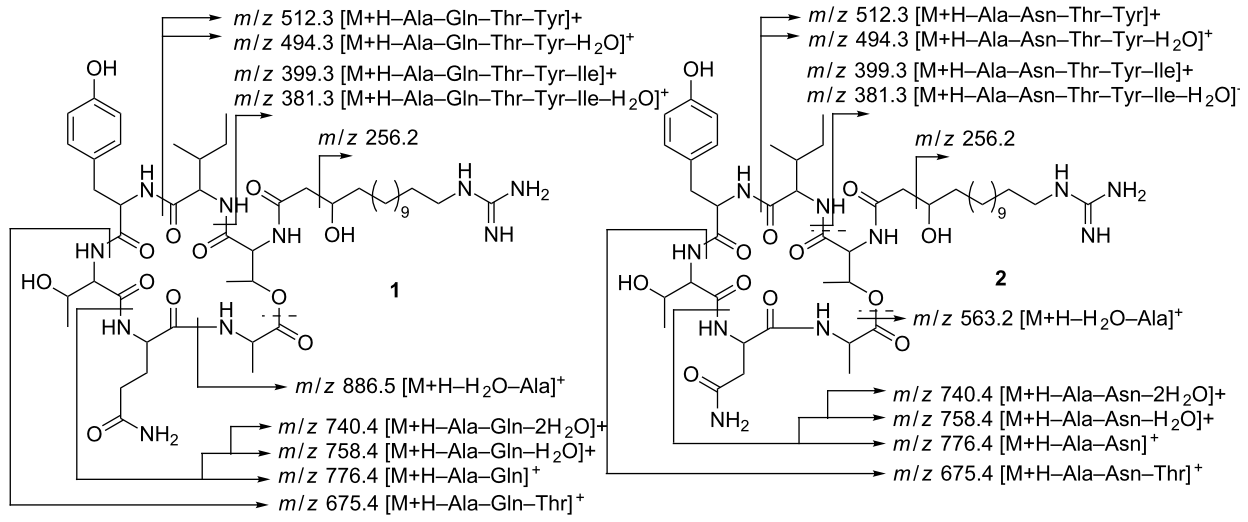

Figure 3: Fragmentation pattern of compounds **1** and **2**.

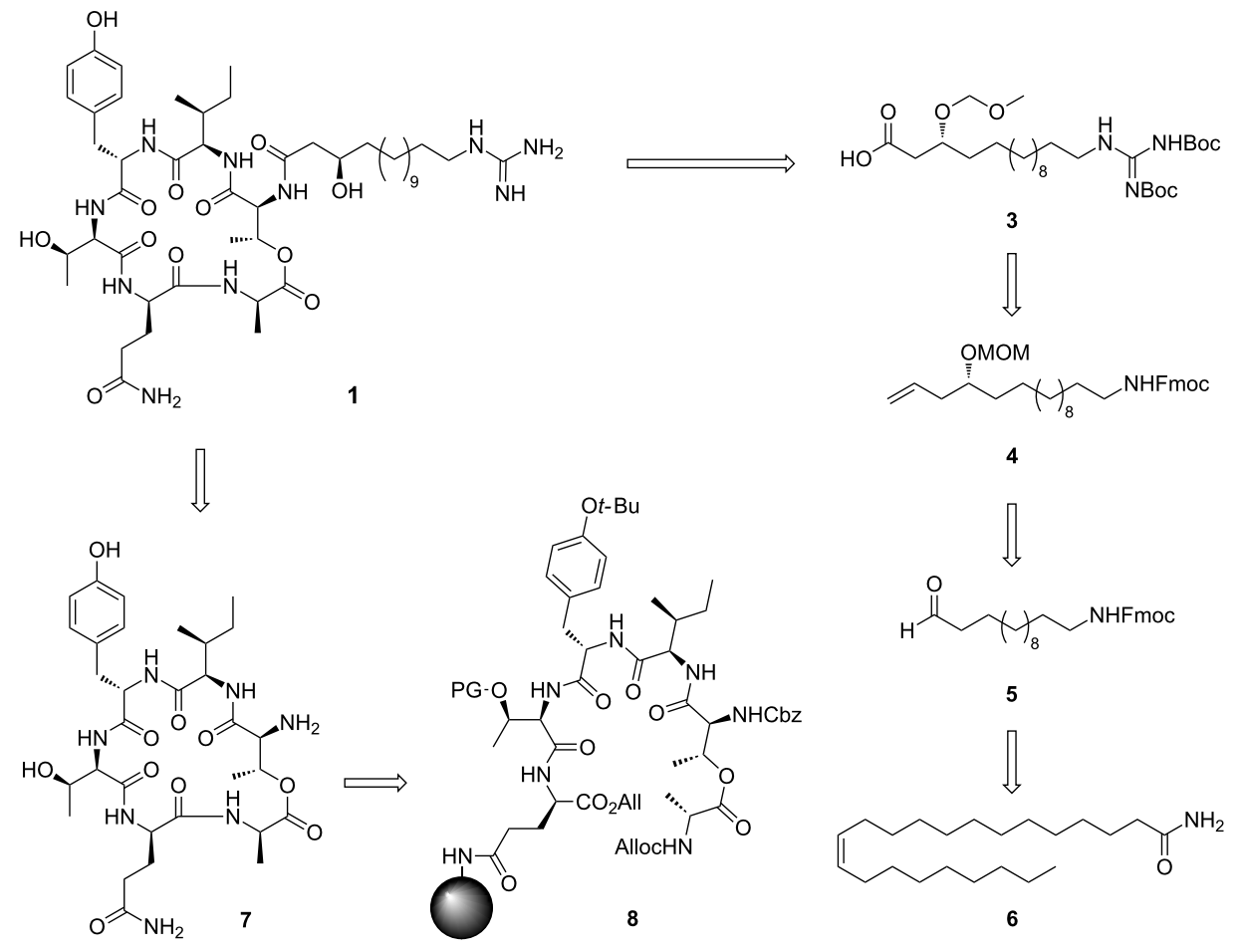

Scheme 1: Retrosynthetic plan for the depsipeptide and GHPD side chain.

dinylation to give the unnatural 12-guanidinyldodecanoic acid side chain [12]. In order to reduce the number of linear steps, the protected guanidino group was included in the side chain building block in our case. This strategy would allow to assemble the complete peptide core in a solid-phase synthesis and to perform the solution-phase coupling without a large excess of the GHPD side chain building block. Thus, Cudic's SPPS approach should be combined with the advantages of the late stage coupling employed by Jolliffe.

Synthesis

The C_{13}-fragment was prepared starting from erucamide (**6**) in three simple operations. Reduction of the amide with lithium aluminium hydride, followed by Fmoc-protection and ozonolysis furnished aldehyde **5** in 57% yield over three steps (Scheme 2).

The homoallylic alcohol was prepared by an enantioselective Duthaler–Hafner allylation [13] with the titanium-complex **15** in high yield and 94% ee. Attempts to perform a catalytic Keck allylation with BINOL-titanium catalysts failed due to low conversion [14]; however, in spite of good experience with the Maruoka–Keck allylation in another total synthesis, the conversion was not satisfying in this case [15]. After protection and guanidinylation with triflylguanidine **14**, the homoallylic alcohol **12** was subjected to ozonolysis and Pinnick oxidation to furnish the protected GHPD acid **3** in an overall yield of 14.3%.

The peptide core was synthesized manually according to a standard SPPS Fmoc protocol using HATU and NMM in NMP [16]. For protection of the threonine unit, it was converted into a 2,2-dimethylated pseudoproline ($\Psi^{Me,Me'}$Pro). This method has been reported to improve yields of macrolactamizations through stabilizing the *cis*-configuration of the amide bond and working as a turn inducer in peptides [17-20]. The $\Psi^{Me,Me'}$Pro unit turned out not to be completely stable during the esterification with DIC/DMAP [12] as the double acylation product **18** could be detected (Scheme 3).

Further investigations suggested DMAP to be responsible for the cleavage of the $\Psi^{Me,Me'}$Pro and after reduction of the amount of DMAP to 5 mol %, nearly no doubly acylated product was found.

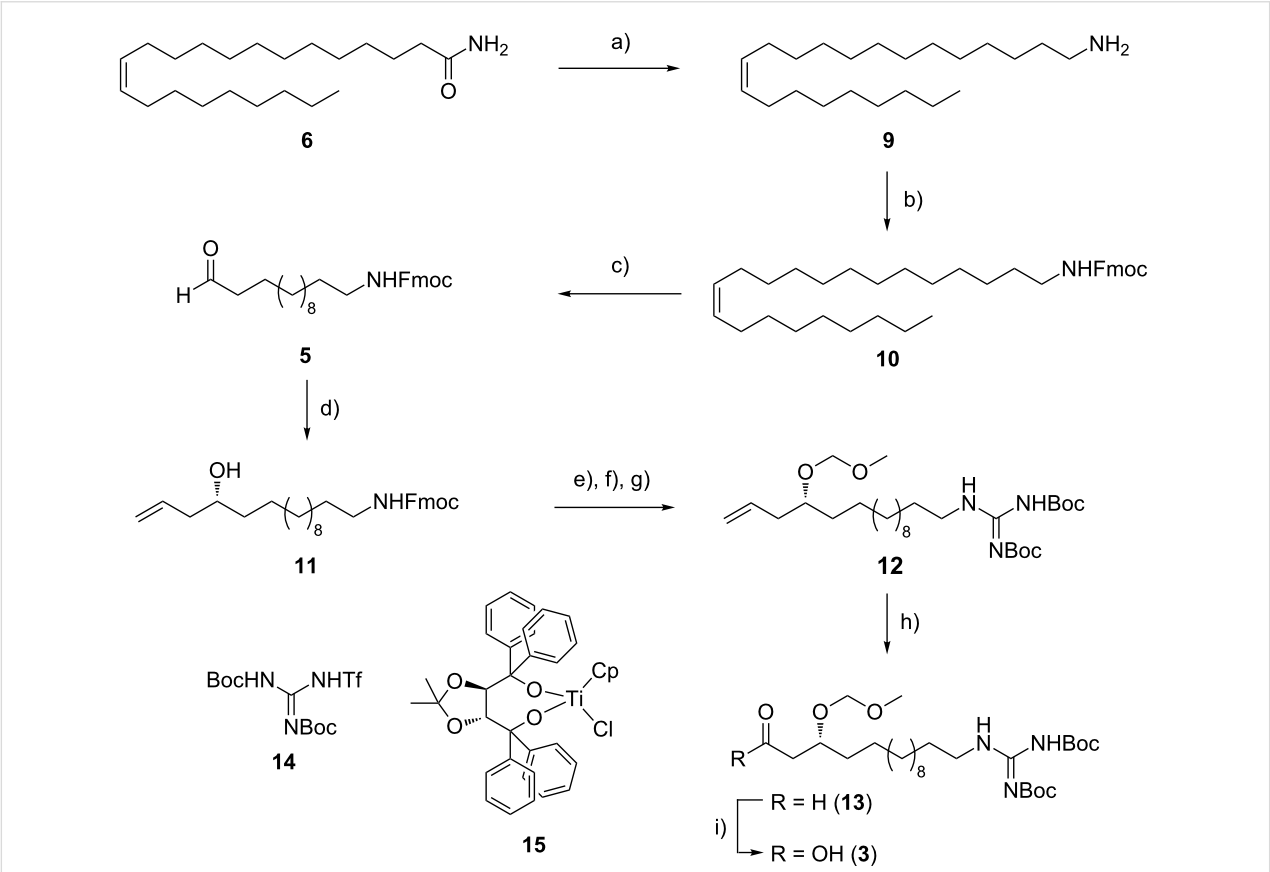

Scheme 2: a) $LiAlH_4$, THF, reflux, 12 h, quant.; b) Fmoc-OSu, $NaHCO_3$, 1,4-dioxane, H_2O, 0 °C to rt, 87%; c) 1: O_3, DCM, –78 °C, 2: Zn, HOAc, –78 °C to 10 °C, 66%; d) allylmagnesium chloride, **15**, Et_2O, –78 °C, 84%, 94% ee; e) MOMCl, DIPEA, DCM 0 °C to rt; f) piperidine, DCM, rt; g) **14**, NEt_3, DCM, 49% (over 3 steps); h) 1: O_3, DCM, –78 °C, 2: PPh_3, –78 °C → rt, 77%; i) $NaClO_2$, NaH_2PO_4, amylene, *t*-BuOH, H_2O, rt, 80%.

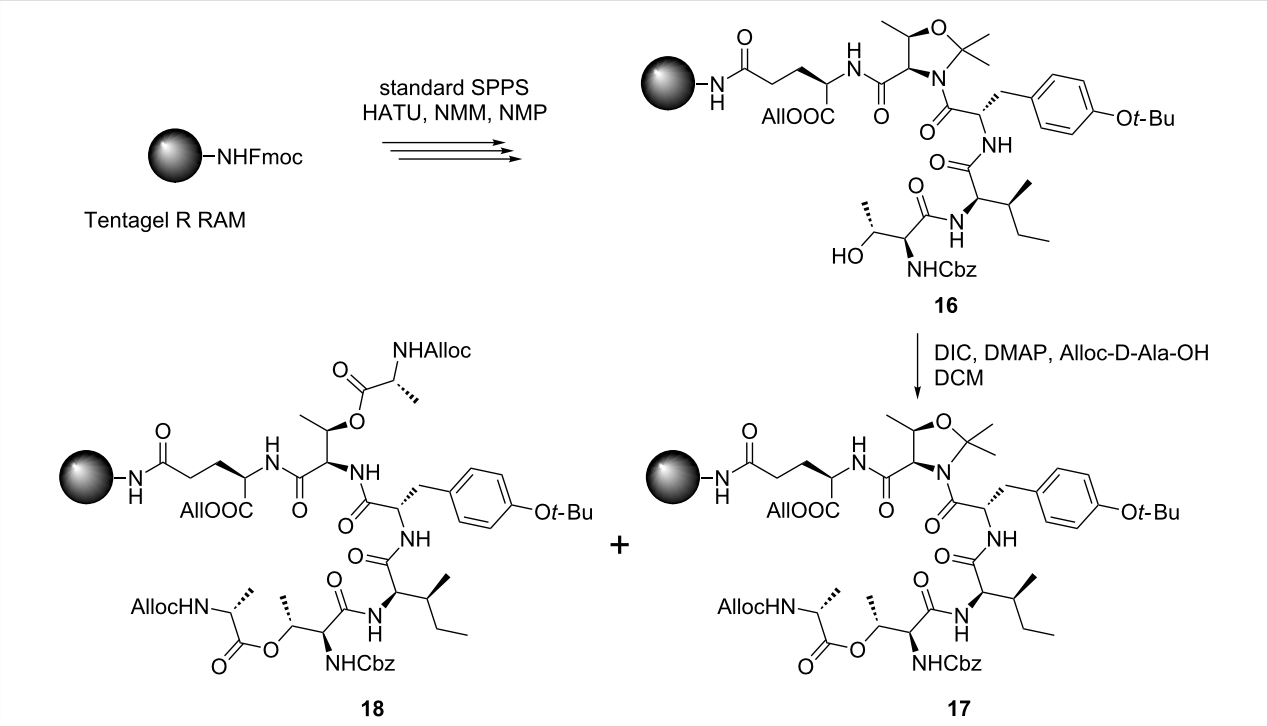

Scheme 3: Ester bond formation with 2,2-dimethylated pseudoproline including peptide **16**.

Besides the doubly acylated product, several other uncharacterized byproducts were formed. Nevertheless, *O*-deallylation with $Pd(PPh_3)_4$ and $BH_3{\cdot}NHMe_2$ gave a high conversion to the deprotected peptide [1]. The cyclization with PyBOP, HOBt and DIPEA in DMF led again to the formation of numerous byproducts. In contrast to literature reports [12], it was found that cleavage from the resin with "reagent K" [12,21] was inferior to a TFA/TIS/H_2O mixture (95:2.5:2.5). Due to the instability of $\Psi^{Me,Me'}$Pro during esterification and cyclization, the isolated yield of **19** was only 6% (Scheme 4).

To improve this, O-*tert*-butyl-protected D-*allo*-Thr was employed instead. For the O-*tert*-butyl-protected D-*allo*-Thr, clean and complete conversion was observed during both esterification and deprotection. This time, cyclization was performed with PyAOP and NMM in NMP to provide **19** in an isolated yield of 37% (Scheme 5).

Unfortunately, we observed two signal sets in NMR spectra (intensity 3:1) for the product which could not be attributed to conformers or rotamers as evidenced by variable temperature and NOESY NMR experiments.

These results, and the fact that Cochrane also reported problems due to epimerization during macrolactonization suggested that a partial loss of stereochemical integrity had taken place during either cyclization or esterification [11]. The site of epi-

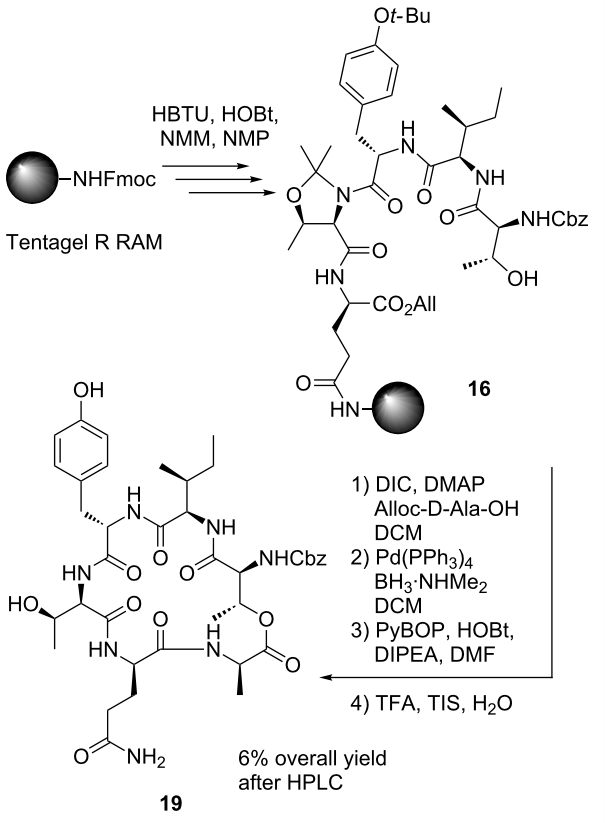

Scheme 4: Cyclization with 2,2-dimethylated pseudoproline including peptide **16**.

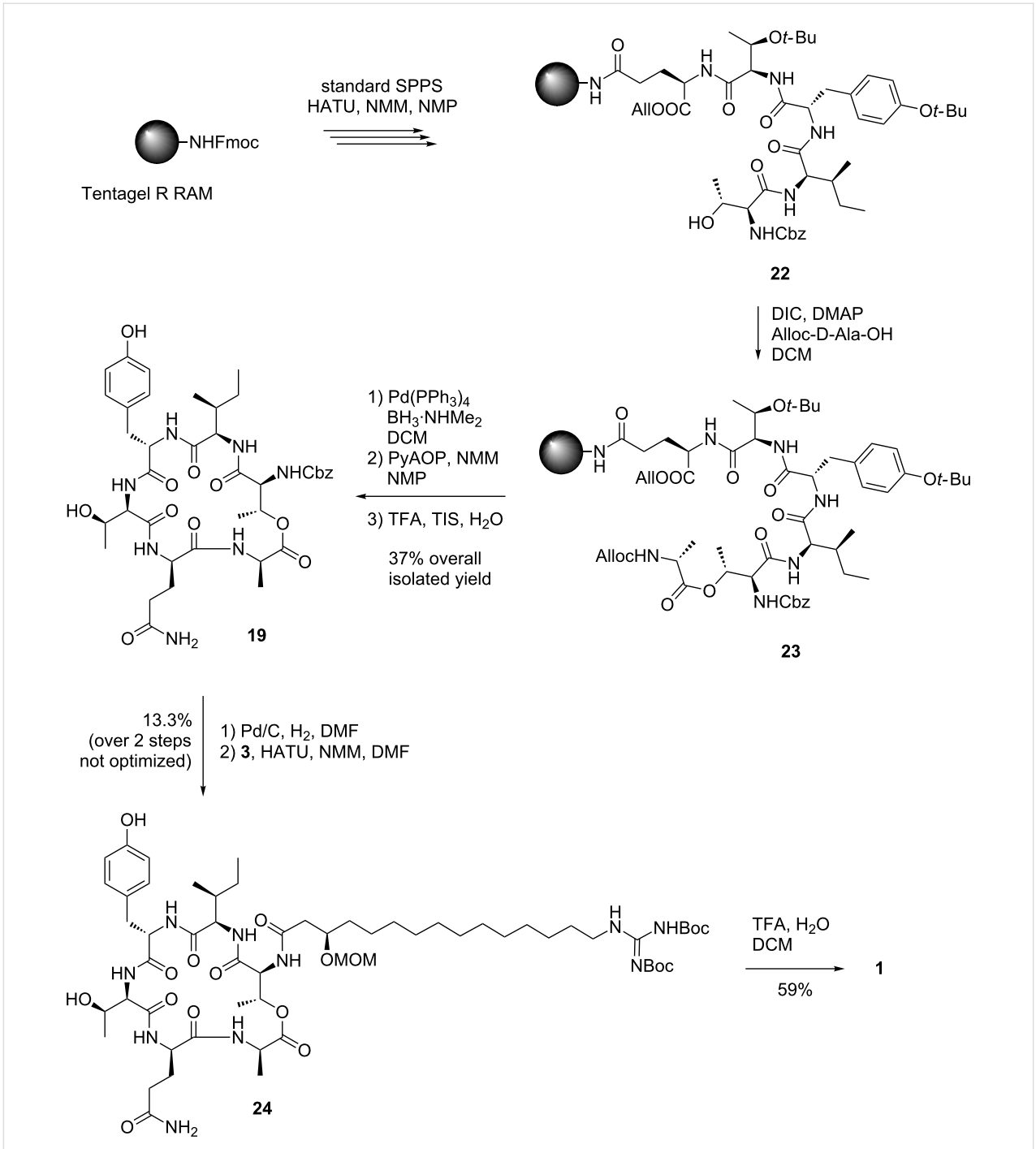

Scheme 5: Depsipeptide cyclization and coupling with GHPD side chain.

merization could not be determined with certainty, but most likely, the D-Ala residue was affected.

As the assumed diastereomers could not be observed or separated by HPLC, the next steps were performed with the mixture. Performing the removal of the Cbz group with H_2/Pd-C in THF, we encountered the formation of the *N*-(4-hydroxybutylated) product **25** resulting from a ring opening reaction of the solvent (Figure 4). This side reaction has been reported for unstabilized THF [22] while stabilized THF was used in our case.

Due to solubility problems in 1,4-dioxane and other solvents suitable for hydrogenolysis, the deprotection was thus performed in DMF [23,24]. Unfortunately, an *O*→*N* acyl shift to

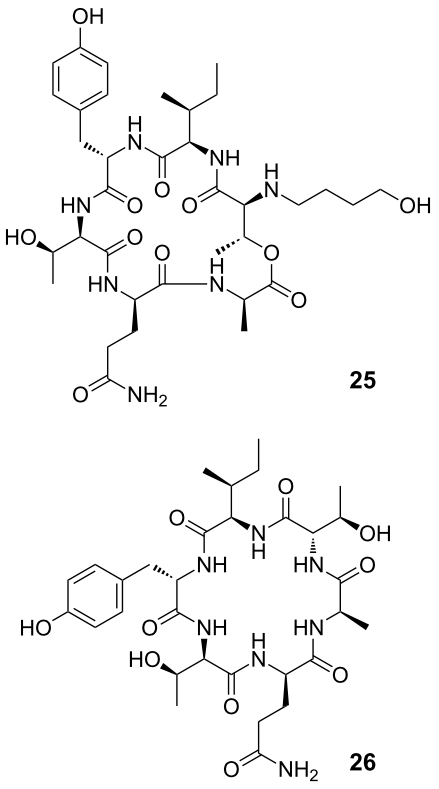

Figure 4: Byproducts from removal of Cbz group in THF and DMF.

product **26** could be observed as judged by NMR spectroscopy when aged DMF was used for this purpose. In fresh DMF, hydrogenolysis smoothly produced amine **7** instead. When the crude peptide was coupled to the GHPD side chain unit **3**, HPLC showed only a single peak with the correct *m/z* ratio. This compound **24** was isolated by preparative HPLC and NMR analysis showed a single signal set, so the fate of the assumed minor stereoisomer remains unclear and it was probably lost during HPLC purification. The analysis also revealed that the acylation with the GHPD side chain was selective for the amine and no *O*-acylated product was formed. Side chain protecting groups were removed to yield the natural product **1**. HPLC analysis showed only a single peak with the same retention time, mass and fragmentation pattern as the natural product. After purification by preparative HPLC, NMR spectroscopy confirmed that the assumed structure and stereochemistry of the natural product was correct (see pages S38 and S39 of Supporting Information File 1).

Conclusion

In summary, two new members of the fusaricidin family, fusaricidins E and F, were isolated from fermentation broths of *Paenibacillus sp.* strain Lu16774 as an inseparable mixture of homologs. Structure elucidation of both peptides was performed with extensive NMR spectroscopy and tandem mass spectrometry. The full stereostructure of the major component, fusaricidin E, could be confirmed by total synthesis. It included a macrolactamization approach combined with a late stage attachment of the GHPD side chain which was synthesized by a newly developed and efficient sequence starting from erucamide. Compared to the Jolliffe strategy, yields were improved and the number of solution phase transformations was reduced. On the other hand, the yields of the Cudic synthesis could not be reached and more steps required purification of the respective products.

Supporting Information

Supporting Information File 1

Procedures for the synthesis and characterisation data of the compounds.
[http://www.beilstein-journals.org/bjoc/content/supplementary/1860-5397-13-140-S1.pdf]

Acknowledgements

This work was supported by the Rhineland Palatinate Center for Natural Products Research as well as by BASF SE. We thank Dr. J. C. Liermann (Mainz) for NMR spectroscopy and Dr. N. Hanold (Mainz) for mass spectrometry.

References

1. Bionda, N.; Stawikowski, M.; Stawikowska, R.; Cudic, M.; López-Vallejo, F.; Treitl, D.; Medina-Franco, J.; Cudic, P. *ChemMedChem* **2012,** *7,* 871–882. doi:10.1002/cmdc.201200016
2. Li, J.; Jensen, S. E. *Chem. Biol.* **2008,** *15,* 118–127. doi:10.1016/j.chembiol.2007.12.014
3. Han, J. W.; Kim, E. Y.; Lee, J. M.; Kim, Y. S.; Bang, E.; Kim, B. S. *Biotechnol. Lett.* **2012,** *34,* 1327–1334. doi:10.1007/s10529-012-0913-8
4. Vater, J.; Niu, B.; Dietel, K.; Borriss, R. *J. Am. Soc. Mass Spectrom.* **2015,** *26,* 1548–1558. doi:10.1007/s13361-015-1130-1
5. Kurusu, K.; Ohba, K.; Arai, T.; Fukushima, K. *J. Antibiot.* **1987,** *40,* 1506–1514. doi:10.7164/antibiotics.40.1506
6. Kajimura, Y.; Kaneda, M. *J. Antibiot.* **1996,** *49,* 129–135. doi:10.7164/antibiotics.49.129
7. Kajimura, Y.; Kaneda, M. *J. Antibiot.* **1997,** *50,* 220–228. doi:10.7164/antibiotics.50.220
8. Siepe, I.; Büser, H.; Klappach, K.; Schneider, K. H.; Spröte, P.; Hage, K.; Blanz, B.; Thines, E.; Antelo, L.; Sandjo, L. P. Antifungal paenibacillus strains, fusaricidin-type compounds, and their use. WO Patent WO2016020371, Feb 2, 2016.
9. Kuroda, J.; Fukai, T.; Konishi, M.; Uno, J.; Kurusu, K.; Nomura, T. *Heterocycles* **2000,** *53,* 1533–1549. doi:10.3987/COM-00-8922
10. Cochrane, J. R.; McErlean, C. S. P.; Jolliffe, K. A. *Org. Lett.* **2010,** *12,* 3394–3397. doi:10.1021/ol101254m
11. Cochrane, J. R.; Yoon, D. H.; McErlean, C. S. P.; Jolliffe, K. A. *Beilstein J. Org. Chem.* **2012,** *8,* 1344–1351. doi:10.3762/bjoc.8.154

12. Stawikowski, M.; Cudic, P. *Tetrahedron Lett.* **2006,** *47,* 8587–8590. doi:10.1016/j.tetlet.2006.09.116
13. Hafner, A.; Duthaler, R. O.; Marti, R.; Rihs, G.; Rothe-Streit, P.; Schwarzenbach, F. *J. Am. Chem. Soc.* **1992,** *114,* 2321–2336. doi:10.1021/ja00033a005
14. Hanawa, H.; Uraguchi, D.; Konishi, S.; Hashimoto, T.; Maruoka, K. *Chem. – Eur. J.* **2003,** *9,* 4405–4413. doi:10.1002/chem.200305078
15. Götz, K.; Liermann, J. C.; Thines, E.; Anke, H.; Opatz, T. *Org. Biomol. Chem.* **2010,** *8,* 2123–2130. doi:10.1039/c001794a
16. Chan, W.; White, P. *Fmoc Solid Phase Peptide Synthesis: A Practical Approach;* Oxford University Press: Oxford, 2000.
17. Skropeta, D.; Jolliffe, K. A.; Turner, P. *J. Org. Chem.* **2004,** *69,* 8804–8809. doi:10.1021/jo0484732
18. Sayyadi, N.; Skropeta, D.; Jolliffe, K. A. *Org. Lett.* **2005,** *7,* 5497–5499. doi:10.1021/ol0522891
19. Dumy, P.; Keller, M.; Ryan, D. E.; Rohwedder, B.; Wöhr, T.; Mutter, M. *J. Am. Chem. Soc.* **1997,** *119,* 918–925. doi:10.1021/ja962780a
20. Fairweather, K. A.; Sayyadi, N.; Luck, I. J.; Clegg, J. K.; Jolliffe, K. A. *Org. Lett.* **2010,** *12,* 3136–3139. doi:10.1021/ol101018w
21. Jubilut, G. N.; Cilli, E. M.; Crusca, E., Jr.; Silva, E. H.; Okada, Y.; Nakaie, C. R. *Chem. Pharm. Bull.* **2007,** *55,* 468–470. doi:10.1248/cpb.55.468
22. Russell, H. F.; Bremner, J. B.; Bushelle-Edghill, J.; Lewis, M. R.; Thomas, S. R.; Bates, F., II. *Tetrahedron Lett.* **2007,** *48,* 1637–1639. doi:10.1016/j.tetlet.2006.12.136
23. Greven, H. M.; van Nispen, J. W.; Bijl, W. A. A. J. *Recl. Trav. Chim. Pays-Bas* **1980,** *99,* 284–286. doi:10.1002/recl.19800990909
24. Fukami, T.; Niiyama, K.; Amano, Y.; Hisaka, A.; Fujino, N.; Sawasaki, Y.; Ihara, M.; Ishikawa, K. *Chem. Pharm. Bull.* **1996,** *44,* 609–614. doi:10.1248/cpb.44.609

License and Terms

BEILSTEIN JOURNAL OF ORGANIC CHEMISTRY

The chemistry and biology of mycolactones

Matthias Gehringer and Karl-Heinz Altmann*§

Review

Open Access

Address:
Department of Chemistry and Applied Biosciences, Institute of Pharmaceutical Sciences, ETH Zürich, Vladimir-Prelog-Weg 4, 8093 Zürich, Switzerland

Email:
Karl-Heinz Altmann* - karl-heinz.altmann@pharma.ethz.ch

* Corresponding author
§ Phone: +41-44-6337390; Fax: +41-44-6331369;

Keywords:
Buruli ulcer; mode of action; mycolactones; structure–activity relationships; target elucidation; total synthesis

Beilstein J. Org. Chem. **2017,** *13,* 1596–1660.
doi:10.3762/bjoc.13.159

Received: 30 May 2017
Accepted: 21 July 2017
Published: 11 August 2017

This article is part of the Thematic Series "Lipids: fatty acids and derivatives, polyketides and isoprenoids".

Guest Editor: J. S. Dickschat

Abstract

Mycolactones are a group of macrolides excreted by the human pathogen *Mycobacterium ulcerans*, which exhibit cytotoxic, immunosuppressive and analgesic properties. As the virulence factor of *M. ulcerans*, mycolactones are central to the pathogenesis of the neglected disease Buruli ulcer, a chronic and debilitating medical condition characterized by necrotic skin ulcers. Due to their complex structure and fascinating biology, mycolactones have inspired various total synthesis endeavors and structure–activity relationship studies. Although this review intends to cover all synthesis efforts in the field, special emphasis is given to the comparison of conceptually different approaches and to the discussion of more recent contributions. Furthermore, a detailed discussion of molecular targets and structure–activity relationships is provided.

Review

I. Mycolactones and Buruli ulcer

Buruli ulcer is a chronic and debilitating disease characterized by skin ulcers and necrotic cutaneous lesions. Ulcers typically occur at the limbs and can extend to 15% of the skin surface if untreated. The disease is caused by the pathogen *Mycobacterium ulcerans* and represents the third most common mycobacterial infection after tuberculosis and leprosy [1-3].

At its outset Buruli ulcer usually occurs as painless subcutaneous swellings in the form of nodules, papules, plagues or diffuse edema [4]. Due to their inconspicuous appearance, early disease stages might be confused with insect bites, boils, lipomas or diverse subcutaneous infections [3]. The ulcerative stage is characterized by massive necrotic tissue destruction. Lesions are mainly located in the upper and lower limbs (35% and 55%, respectively) while only 10% occur at other parts of the body [3]. Generally, large numbers of extracellular mycobacteria are observed in all, the early, the pre-ulcerative and the ulcerative disease stage without being accompanied by granuloma formation [5]. The ulcers expand over time and can spread over the entire extremities. However, ulceration is

normally not accompanied by pain and fever although those symptoms might be present in severe forms. In 5–10% of all cases, *M. ulcerans* also invades the bone and causes osteomyelitis leading to serious disabilities and severe deformities [4,6]. Although Buruli ulcer itself is rarely life threatening, untreated disease generally results in severe functional and aesthetic squeal [7] and increases the risk for dangerous secondary infections [8].

Buruli ulcer is one of currently 18 neglected tropical diseases (NTDs) according to the WHOs classification and primarily affects children under the age of fifteen. *M. ulcerans* infections have been reported from at least 33 countries, typically in tropical and subtropical regions, and represent a substantial societal and economic burden [9]. Although the vast majority of Buruli ulcer cases has been reported for Western sub-Saharan Africa (especially from Ivory Coast, Benin, Ghana and the Democratic Republic of the Congo), the pathogen is also endemic in South America, the Western Pacific region (incl. Australia) and Asia (e.g., China and Japan). In certain highly endemic regions like the Zou department in southern Benin, the prevalence of Buruli ulcer can even exceed that of tuberculosis or leprosy [10]. Since 2010, the number of reported Buruli ulcer infections worldwide has declined from almost 5000 annual cases to approximately 2000 in 2015 [11,12], but the reasons for this decrease are unknown [3]. However, these numbers have to be treated with care and numerous cases have to be assumed to remain unreported, since only 15 countries regularly report data to the WHO [3]. In addition, infections might often remain unrecognized, due to poor healthcare standards in most of the affected countries [12].

The first suspected case of a *M. ulcerans* infection was reported in the early 1860s by Captain James August Grant in his accounts of his journey with John Hanning Speke on their quest for the source of the White Nile. In his book *A walk across Africa or domestic scenes from my Nile journal* [13] a detailed description of his condition is given that reflects the symptoms of the edematous form of Buruli ulcer as it is occurring in Central and Western Africa [14]. The first clinical description of Buruli ulcer was provided in 1897 by the medical missionary Sir Ruskin Albert Cook in Kampala (Uganda) [15]. More than 50 years later, a seminal report by MacCallumn and co-workers from Bairnsdale hospital (Victoria, Australia) described six patients from rural riverine areas suffering from an unknown ulcerative infection [16]. A "mycobacterium hitherto unrecorded and pathogenic to man" was found in the patients' lesions. Biopsy and microscopic analysis revealed a unique histopathological pattern in all patients that distinctly differed from tuberculosis. However, the germ gave the typical acid-fast stain common to all mycobacteria. As reported by Fenner et al., MacCallum later suggested the name *Mycobacterium ulcerans* [17]. Initial attempts to cultivate the bacterium failed until it was realized that, in contrast to *M. tuberculosis* that can be grown at 37 °C, *M. ulcerans* requires temperatures above 25 °C, but below 37 °C (ideally 32–33 °C) for growth [16]. This might be one of the reasons why *M. ulcerans* infections in humans are primarily limited to cutaneous tissue. Furthermore, low oxygen concentrations were later shown to be beneficial for cultivating this very slow growing mycobacterium [18]. A few years after their initial characterization, infections with *M. ulcerans* were also observed in today's Democratic Republic of Congo [19] and in Uganda [20-22]. The name Buruli ulcer was suggested in relation to case reports from Buruli County in Mengo district (today Nakasongola district) in Uganda [20]. Although Bairnsdale ulcer would be the historically more correct denomination, the WHO approved the name Buruli ulcer.

Despite the long known association of Buruli ulcer with riverine areas and wetlands [22,23], the natural reservoir of *M. ulcerans* is still elusive and due to its obscure route of transmission [12], Buruli ulcer is sometimes referred to as the "mysterious disease" [24]. While *M. ulcerans* is believed to be an environmental pathogen [25], there is putative evidence that it can also be hosted and transmitted by living organisms such as aquatic insects [26], mosquitoes [27], fish and amphibians [28].

Upon infection, *M. ulcerans* is usually concentrated in a small focus surrounded by a larger necrotic area that contains few bacteria. Based on this observation, Connor and Lunn speculated already in 1966 that *M. ulcerans* might excrete a diffusible toxin [21]. In 1974, two reports by Connor and co-workers corroborated this hypothesis by demonstrating that the injection of culture filtrates from different *M. ulcerans* strains into mouse footpads and guinea pig skin caused similar effects as the inoculation with the living organism [29,30]. These studies also suggested that the toxin had a molecular mass of around 100,000 Da and was moderately heat stable. Four years later, in 1978, Krieg and co-workers proposed the toxin to be a phospholipoprotein–polysaccharide complex, based on studies investigating the stability of *M. ulcerans* extracts towards different chemicals and enzymes [31]. The true nature of the toxin, however, remained elusive until 1998, when Small and co-workers identified a polyketide isolated from acetone-soluble *M. ulcerans* lipid extracts as the key virulence factor [32,33]. The initial characterization of the toxin relied on the separation of extract components by thin layer chromatography (TLC) and the biological characterization of the individual bands, a process that revealed a light yellow UV-active component to possess the highest cytopathogenic activity. Further purification of this material by reversed-phase HPLC and subsequent characterization by high-resolution mass spectrometry

and two-dimensional NMR spectroscopy unveiled a 12-membered macrolactone substituted with two polyketide-derived side chains (Figure 1). Based on its mycobacterial origin and its chemical structure, this compound was named mycolactone. It is worth noting that mycolactone represented the first polyketide macrolide isolated from a mycobacterial species and was also the first example of a polyketide acting as the virulence factor of a human pathogen [34].

The purified toxin possessed similar in vitro cytopathogenicity as culture filtrates from *M. ulcerans* and caused essentially the same gross pathological and histopathological changes as a *M. ulcerans* infection. In contrast, a mycolactone-deficient *M. ulcerans* strain was not able to induce those phenotypes [32]. However, chemical complementation with mycolactone restored the typical *M. ulcerans* pathology for mycolactone-deficient strains [35]. Some chemical modifications were performed on the purified extracts showing that peracetylation or exhaustive double bond saturation by hydrogenation resulted in a total loss of cytopathogenicity. Interestingly, washing cells after mycolactone treatment restored cell growth, thus indicating at least a partial reversibility of the toxic effects.

The structural proposal for mycolactone that was offered by Small and co-workers in the context of their original report on the isolation of the toxin was only cursory. A complete two-dimensional structure was reported shortly thereafter, although both the absolute and relative stereochemistry of the molecule remained unassigned at the time [36]. Importantly, an NMR spectroscopic analysis showed that the isolated "mycolactone" in fact consisted of a 3:2 mixture of two isomeric compounds that were distinct by the configuration of the C4'–C5' double bond in the C5 ("lower") side chain. These isomers were consequently named mycolactone A (*Z*-isomer, **1a**) and B (*E*-isomer, **1b,** Figure 1). Although separable by reversed-phase HPLC, neither of the isomers could be isolated in pure form, presumably due to rapid (re)equilibration during or after separation. Indeed, this presumption was later proven to be true by the (attempted) targeted total synthesis of each isomer; as part of this work, mycolactones A and B were shown to rapidly equilibrate under standard laboratory conditions [37]. The prevalence of the *Z*-$\Delta^{4',5'}$ isomer at equilibrium can be rationalized by the allylic strain [38] induced by the methyl groups attached to C4' and C6', respectively. The relative and absolute stereochemistry of mycolactone was then established in 2001 by Kishi and co-workers [39,40], using a combination of model compound synthesis and exploitation of an NMR database [41,42]. The correctness of the assignment was subsequently verified by total synthesis (vide infra) [43].

After the discovery of mycolactones A/B (**1a,b**), eight congeners (mycolactones C (**2**), D (**3**), E (**6**) and its minor oxo-metabolite (**7**), F (**8**) and *dia*-F (**9**), S1 (**4**) and S2 (**5**)) (Figure 2) were discovered in extracts from different *M. ulcerans* strains and closely related mycobacteria. Given their close genetic relationship [44], it has been suggested that all currently known mycolactone-producing bacteria should be reclassified as *M. ulcerans* [45]. Within this review, however, the originally proposed species names (*M. marinum*, *M. ulcerans* ecovar *liflandii*, *M. pseudoshottsii*, *M. ulcerans* subsp. *shinshuense*) will be used.

It should also be noted at this point that the nomenclature used for mycolactones is not consistent throughout the literature. In this review, we will use the term "mycolactone A/B" to refer to the equilibrated mixture of mycolactone A and mycolactone B; in contrast, and following common literature practice, all other mycolactones (vide infra) are denoted by appending a single letter to the name mycolactone, although preparations of these different variants that are obtained either by isolation or by total synthesis are mixtures of double bond isomers and used as such in biological experiments. As for atom numbering, the carbon atoms in the 12-membered macrolactone ring are designated as C1–C11 (with the carbonyl carbon of the lactone ester group as

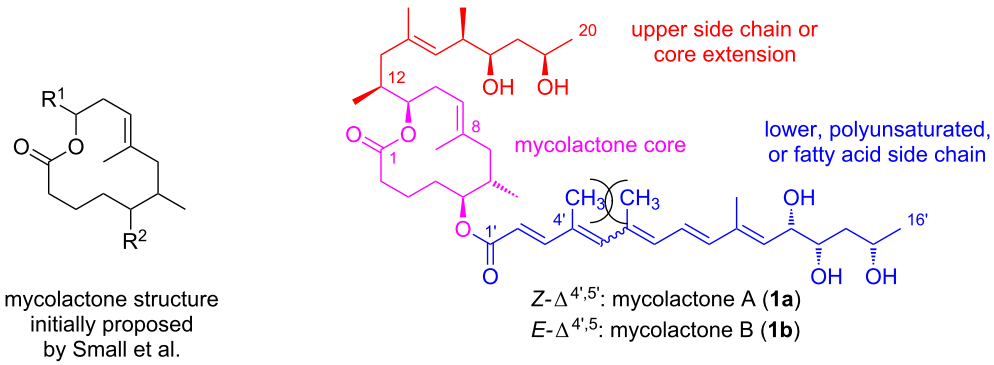

Figure 1: Initial proposal for the core macrolactone structure (left) and the established complete structure of mycolactones A (**1a**) and B (**1b**) (right).

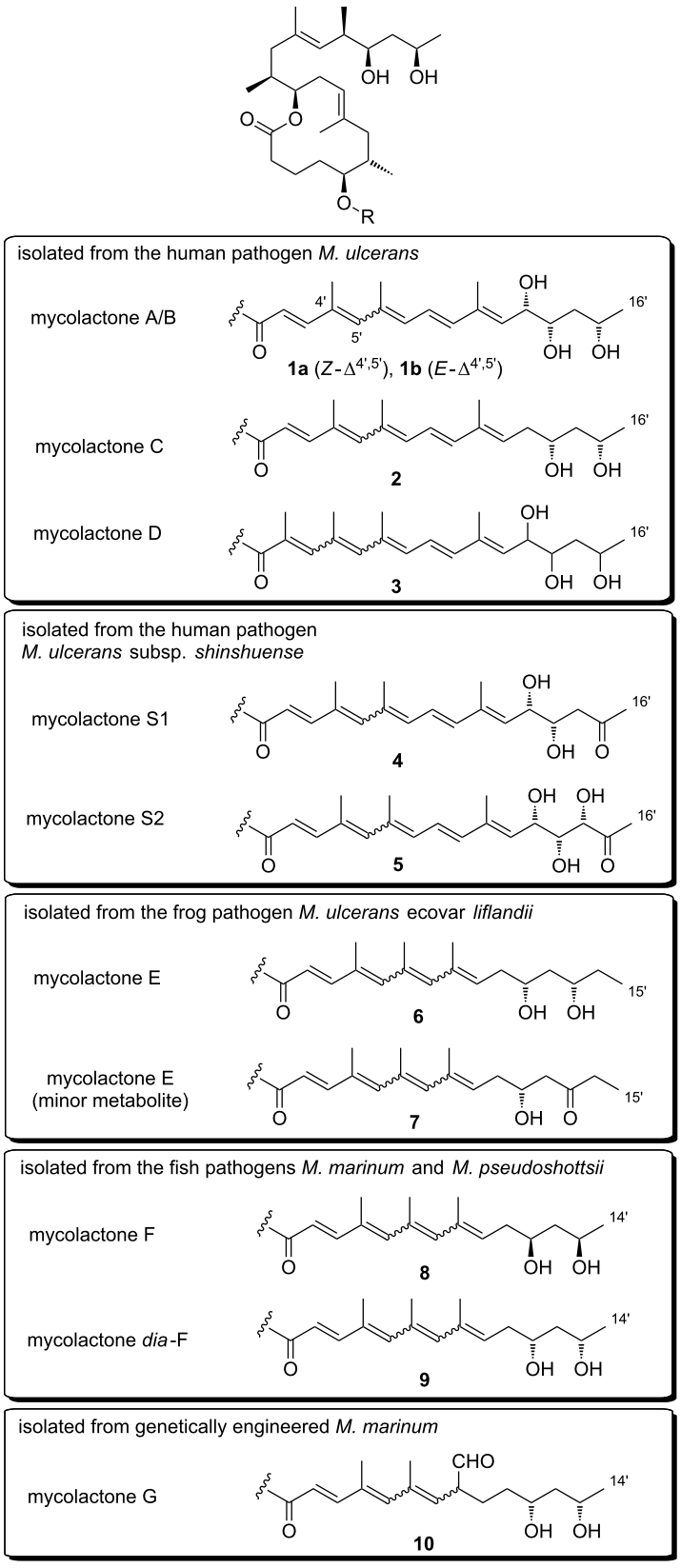

Figure 2: Mycolactone congeners and their origins.

C1), those in the carbon-linked ("upper") side chain as C12–C20 and those of the oxygen-linked ("lower") side chain as C1'–C16' (with the carbonyl carbon of the exocyclic ester group as C1'). Finally, in our terminology, the term "mycolactone core" refers to the C1–C11 macrolactone ring (including the OH group on C5) without the C12–C20 side chain, while the term "extended core" encompasses the entire C1–C20 segment. Consequently, the upper side chain comprising C12–C20 will be referred to as "core extension."

The discovery of mycolactones other than mycolactone A/B (**1a**,**b**) was initially triggered by the observation that *M. ulcerans* strains from Asia, Mexico, and Australia were apparently less virulent than African strains [46]. Intriguingly, these differences seem to translate into differences in the specific pathology of *M. ulcerans* infections [46]. For example, osteomyelitis, a pathology regularly observed in association with *M. ulcerans* infections in Benin [6] is absent in Australia or Mexico. Likewise, the plaque form of Buruli ulcer which is also found in Benin has not been reported in Australia [47]. Finally, Asian strains seem to be less virulent than their African complements [48-50]. These observations led the Small group to analyze partially purified mycolactones from *M. ulcerans* isolates of different geographical origin by TLC, (LC–)MS and in a cytopathogenicity assay [47,51]. These studies suggested the presence of at least two additional mycolactone congeners, with the dominant mycolactone variant found in Australian strains lacking one oxygen atom. Importantly, this compound, which was termed mycolactone C (**2**), had a lower cytopathogenic activity than mycolactone A/B (**1a**,**b**), thus offering a rationale for the lower virulence of Australian *M. ulcerans* strains. Asian strains contained significant amounts of a variant that was denominated mycolactone D (**3**) and which was hypothesized to contain an additional oxygen atom; in addition, the presence of minor amounts of the (non-acylated) extended mycolactone core was demonstrated. These findings were subsequently confirmed by Spencer et al. employing LC−sequential mass spectrometry (LC–MS^n) analysis, which suggested that the various mycolactone congeners only differ in the exact structure of the polyunsaturated side chain. More specifically, they concluded that mycolactone C (**2**) is distinct from mycolactone A/B (**1a**,**b**) by a lack of the hydroxy group at C12' [52], a proposal that was finally verified by Kishi and co-workers by means of total synthesis (vide infra) [53]. The structure of mycolactone D (**3**) was later re-investigated by Leadlay and co-workers applying LC−sequential and high-resolution mass spectrometry in combination with deuterium exchange experiments [54]. Instead of the additional hydroxy group proposed by the Small group, these studies provided strong evidence for mycolactone D (**3**) to feature an extra methyl group at the C2'-position. However, ultimate proof for the structure of mycolactone D (**3**) is still elusive.

More recently, it was discovered that not only *M. ulcerans* but also the fish pathogens *M. marinum* and *M. pseudoshottsii* and the frog pathogen *M. ulcerans* ecovar *liflandii* are capable of producing mycolactones. In contrast to *M. ulcerans*, those organisms cause systemic infections [50,55], probably enabled by the lower body temperature of their poikilothermic hosts. In 2005, the Small [50] and the Leadlay [56] group independently discovered mycolactone E (**6**) from *M. ulcerans* ecovar *liflandii*, a pathogen that causes lethal infections in *Xenopus* frogs. This congener differs from mycolactone A/B (**1a**,**b**) in the lower side chain by the lack of the C8'–C9' segment, the replacement of the terminal methyl group by ethyl, and the absence of one hydroxy group. A different structure of mycolactone E (**6**) had originally been proposed by the Small group (**11**, Figure 3) after partial TLC purification and subsequent high-resolution mass spectrometry and ^{1}H NMR spectroscopy (although no NMR data are shown in their report) [50]. Shortly afterwards, the Leadlay group proposed structure **6** (Figure 2) based on tandem mass spectrometry in conjunction with oxidative degradation and deuterium exchange experiments [56]. In spite of the challenge posed by the severely limited availability of natural mate-

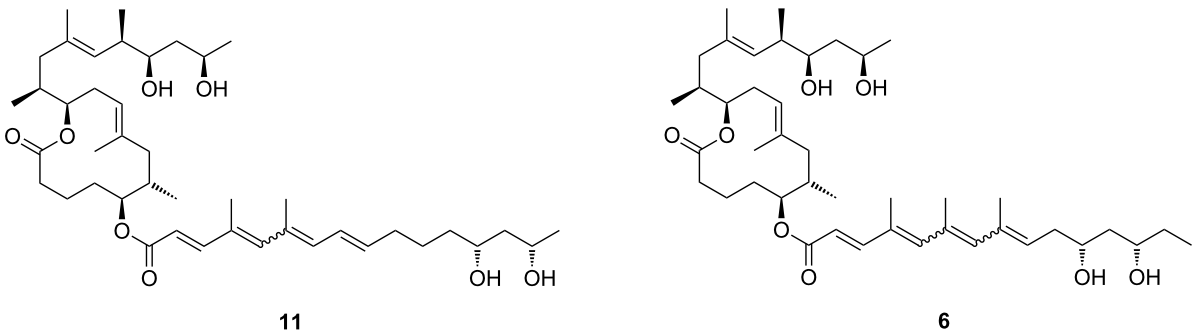

Figure 3: Misassigned mycolactone E structure according to Small et al. [50] (**11**) and the correct structure (**6**) first proposed by Leadlay et al. [56].

rial for structural analysis, Kishi and co-workers later demonstrated by total synthesis (vide infra) that the Leadlay structure was the correct one [57]. Besides mycolactone E (**6**), a minor metabolite (**7**) with a keto group replacing the hydroxy function at the C13'-position was found in *M. ulcerans* ecovar *liflandii* lipid extracts [50,56]. Again, the structure was finally established by Kishi and co-workers using a combination of total synthesis and HPLC on a chiral stationary phase [58]. Of note, the shorter conjugated system in these tetraenoate derivatives causes a different pigmentation of the respective mycobacteria. While *M. ulcerans* colonies generally possess a light yellow color, *M. ulcerans* ecovar *liflandii* colonies are light orange [50].

In 2006, mycolactone F (**8**), a congener found in certain fresh water fish-infesting *M. marinum* strains and in *M. pseudoshottsii*, was first described by Small and co-workers [55]. With its molecular weight of 700 Da, mycolactone F is the smallest member of the mycolactone family known to date. A structure was proposed by the Small group based on mass fragmentation and ^{1}H/2D NMR spectroscopic data. This structure, which features a tetraenoate (lower) side chain with a terminal 1,3-diol motif was once again confirmed by total synthesis in the Kishi laboratory; the relative and absolute stereochemistry of the compound was assigned by NMR in conjunction with HPLC on a chiral stationary phase [59]. Of note, the stereochemistry of the 1,3-diol motif of the polyunsaturated side chain of mycolactone F (**8**) is antipodal to the same motif in all other natural mycolactones with known configuration. Intriguingly, salt water fish-infesting *M. marinum* produces a remote diastereomer [60] of mycolactone F (*dia*-mycolactone F, **9**) that exhibits the regular configuration of the 1,3-diol motif at the end of the lower side chain [61]. Most recently, the Kishi laboratory isolated two new mycolactone family members, mycolactones S1 (**4**) and S2 (**5**), from the Japanese strain *M. ulcerans* subsp. *shinshuense* [62]. Both of these new variants are oxidized derivatives of mycolactone A/B (**1a**,**b**) bearing a keto group at the C15'-position; in addition, mycolactone S2 incorporates an extra hydroxy group at C14'.

The first and currently only mycolactone originating from a genetically engineered biosynthetic pathway was isolated by Leadlay and co-workers in 2007 [63]. Thus, the cloning of a CYP450 hydroxylase gene from a related strain into the *M. marinum* DL045 strain produced a mycolactone F variant with a formyl group attached to C8' and a single bond between C8' and C9' (mycolactone G, **10**).

Due to its unspecific appearance at early stages, the diagnosis of Buruli ulcer is non-trivial and no point-of-care rapid diagnostic test is currently available [64]. Identification of the infection generally relies on the experience of local health professionals. Subsequent laboratory testing to confirm the clinical diagnosis might then be performed by 1) direct smear examination for acid-fast bacilli; 2) in vitro culture; 3) polymerase chain reaction (PCR), targeting the genomic region IS2404; and 4) histopathological examination [64]. Alternatively, serological testing has been proposed and promising results were obtained in a case control study in Ghana [65]. More recently, the detection of mycolactone from patient biopsy samples via LC–MS [66] and RNA aptamer binding [67] has been suggested, but the suitability of these methods for broad application in endemic areas is questionable. The WHO recommends at least two different confirmative tests for a conclusive diagnosis. In clinical practice, however, disease management without microbiological confirmation of the diagnosis is common. To improve this situation, non-invasive diagnostic tools that are cost-efficient, operationally simple and do not require sophisticated laboratory equipment are required. A method that fulfills these requirements and that relies on thin layer chromatography (TLC) for mycolactone separation was recently introduced by Kishi and co-workers [68]. While the UV-based quantification of mycolactones on TLC plates is hampered by a high detection limit (20–30 ng) and requires access to difficult to store reference samples, Kishi and co-workers have devised a more sensitive, specific detection method that is based on the chemical derivatization of mycolactone A/B (**1a**,**b**) with a 2-naphthylboronate-based fluorogenic chemosensor (Figure 4). The latter complexes the 1,3-diol moiety proximal to the pentaene motif of the lower side chain, thus resulting in enhanced fluorescence emission intensity of the mycolactone band upon irradiation with 365 nm UV light. This method allows the detection of as little as 2 ng of mycolactone within a considerably reduced background and it is specific for mycolactones A/B (**1a**,**b**), C (**2**), and D (**3**, no data for mycolactones S1 and S2 available). Mycolactones E (**6**) and F (**7**) do not yield fluorescent spots or bands. The method has been validated for a mouse footpad model of *M. ulcerans* infection [69] and for skin tissue samples from Buruli ulcer patients [70]. With a detection rate of 73%, TLC proved superior to microscopy (30–60%) or culture (35–60%) and comparable to histology (82%), but inferior to PCR (92–98%) [71,72].

Although spontaneous healing may occur in rare cases [73], early and continuous treatment is generally considered crucial for avoiding long-term damage by the Buruli ulcer disease [74]. It is beyond the scope of this review to detail the currently established or exploratory treatment options for Buruli ulcer; this topic has been reviewed elsewhere [75,76]. Suffice it to say that the WHO recommends combination treatment with oral rifampicin (10 mg/kg once daily) and intramuscular streptomycin (15 mg/kg once daily) over eight weeks [75].

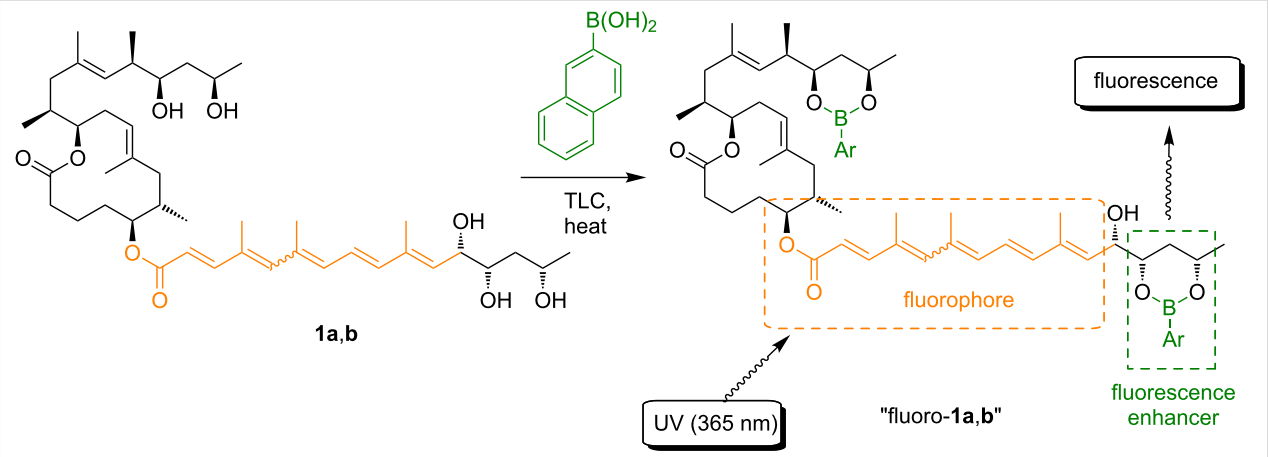

Figure 4: Schematic illustration of Kishi's improved mycolactone TLC detection method exploiting derivatization with 2-napthylboronic acid as a fluorescence enhancer.

II. Biological effects of mycolactones and mechanisms of action

Although Buruli ulcer is associated with extensive fat cell necrosis at the sites of infection, the ulcers are typically accompanied by minimal pain or inflammatory response. These macroscopic observations reflect the cytotoxic [32], immunosuppressive [35,77] and analgesic [78] properties of mycolactones. Although these properties seem fairly general, mycolactone-promoted effects are still multifaceted and strongly depend on the cell line investigated. A detailed discussion of cell-type specific effects can be found in a recent review by Sarfo et al. [79]. Therefore, cellular effects of mycolactones will be discussed here only briefly, while emphasis is placed on their molecular targets.

Even at very low, non-toxic concentrations pure mycolactones or *M. ulcerans* culture supernatants suppress innate and adaptive immune response. For example, mycolactone treatment leads to a marked reduction of cytokine expression levels in human monocytes [77,80] and T-lymphocytes [77], although not all cytokines are affected [81]. In fact, the mycolactone-mediated downregulation of the immune response and prevention of the recruitment of inflammatory cells to the infection site might be crucial for Buruli ulcer pathogenesis [35,81]. With increasing concentrations, the cytotoxic effects of mycolactone become more prominent. These are typically accompanied by a profound structural change in the cytoskeleton followed by cell cycle arrest in the G_0/G_1 phase. Ultimately, cell death, mainly via apoptosis, is observed in vitro and in vivo [32,33,82]. It is worth mentioning that in certain cell types, e.g., adipocytes, cell death via necrosis is dominant over apoptosis [83].

The most commonly used cells to study the cytopathogenicity of mycolactones are murine L929 fibroblasts, which are extremely mycolactone-sensitive. Upon exposure to natural mycolactone A/B concentrations as low as 0.025 ng/mL (0.034 nM), L929 cells show cytoskeletal rearrangements at 12 h, cell rounding within 24 h and a loss of adhesion along with growth arrest after 48 h [32]. At this point, the effect of the toxin seems to be still reversible, since washed cells are capable of regrowth. Upon extended exposure (3 to 5 days), murine L929 fibroblasts undergo apoptosis at mycolactone A/B concentrations as low as 3 ng/mL (4 nM), while very high concentrations (15 µg/mL) cause cell death via necrosis within 4 h [35]. Interestingly, the addition of the pan-caspase inhibitor Boc-Asp(OMe)-fluoromethylketone [84] prevented apoptosis, while a normal cytopathogenic effect and subsequent cell death by necrosis was observed. Mycolactone A/B is also highly cytotoxic to keratinocytes [85], dendritic [81], and endothelial cells [86], while T cells [87,88] and macrophages [80,89] are less sensitive. Strikingly, no toxic potential was observed against human hepatoma HuH7 or human embryonic kidney HEK293 T cells [85]. Intriguingly, mycolactone A/B lacks antimicrobial activity [90], which suggests that the defense against competing microorganisms was not the evolutionary driver for the emergence of the toxin.

It is generally assumed in the literature that mycolactones reach their cellular targets by passive diffusion [91]. Based on competition experiments with the fluorescent, boron-dipyrromethene (BODIPY)-labeled mycolactone analog **12** (Figure 5) which was obtained by chemical modification of natural mycolactone A/B (**1a**,**b**), Synder and Small concluded that mycolactone uptake is non-competitive and non-saturable. The compound quickly penetrated L929 fibroblasts and appeared to be localized in the cytoplasm, without any significant binding to the nucleus, mitochondria or actin being detectable. Similar results were obtained by Blanchard and co-workers with the fully syn-

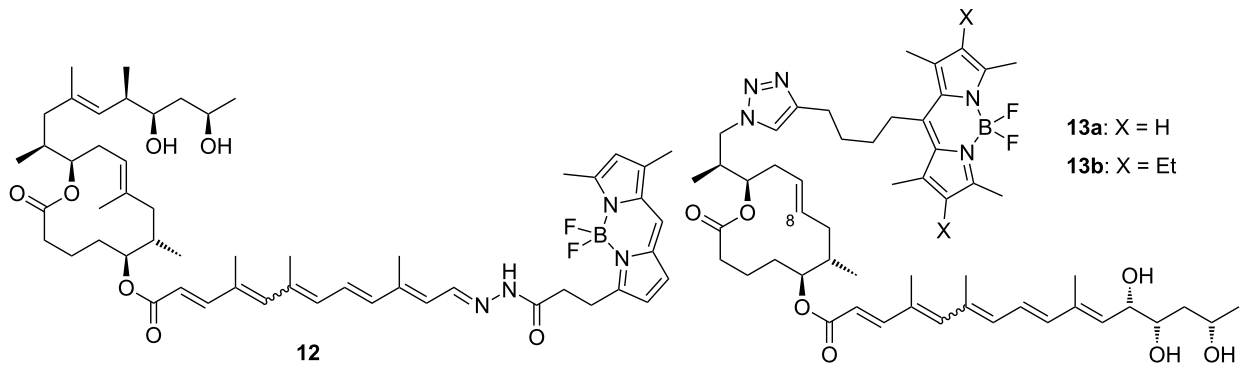

Figure 5: Fluorescent probes derived from natural mycolactone A/B (**1a**,**b**) or its synthetic 8-desmethyl analogs (**13a**,**b**).

thetic 8-desmethylmycolactone analog **13**, which bears a BODIPY tag as a partial replacement for the core extension [92]. According to unpublished data from the Demangel group, corroborative results were obtained in human lymphocytes and epithelial cells exposed to a ^{14}C-labeled form of the toxin [63].

Several molecular targets of mycolactone (A/B) have been identified so far, the first ones being the Wiskott–Aldrich syndrome protein (WASP) and the related neuronal Wiskott–Aldrich syndrome protein (N-WASP) that were discovered by Demangel and co-workers in 2013 based on experiments with a biotinylated mycolactone probe [93]. The WAS family comprises five scaffolding proteins that are crucially involved in the dynamic remodeling of the actin cytoskeleton [94]. While N-WASP is ubiquitously expressed, WASP is only found in cells of the hematopoietic lineage and appears to be critically involved in the regulation of the immune system [95]. WASP and N-WASP exist in a basal auto-inhibited state, a closed conformation in which the C-terminal verprolin homology, cofilin homology, and acidic (VCA) region interacts with a control region located at the N-terminus [96]. Upon cooperative binding of the cell division control protein 42 homolog (CDC42) and phosphatidylinositol 4,5-bisphosphate (PIP2), a conformational change is induced, which allows the (N-)WASP VCA domain to bind to and activate the cytoskeletal organizing complex ARP2/3, which in turn stimulates actin polymerization. Mycolactone A/B was found to bind to the CR1 domain of N-WASP and the CR7 domain of WASP about 100 times more tightly (K_d = 20–70 nM in both cases) than the natural ligand CDC42, thus triggering uncontrolled ARP2/3-mediated assembly of actin. As a consequence, mycolactone A/B causes impaired cell adhesion and defects in the migration of epithelial cells (e.g., increased cell motility accompanied by a loss of directionality). Mycolactone binding to WASP was also demonstrated by means of a fluorescent mycolactone-derived probe, which co-localized with active WASP to a small but significant extent in Jurkat T cells. At the same time, wiskostatin, a known N-WASP inhibitor [97] was found to counteract some of the effects of mycolactone (e.g., impaired cell adhesion in HeLa cells). Wiskostatin also suppressed the thinning of skin caused by mycolactone in a mouse model, thus indicating that N-WASP hyperactivation is indeed critically involved in the epidermal destruction seen in Buruli ulcer. Unfortunately, no X-ray or NMR data on WASP-bound mycolactone are available at this point and the interactions between mycolactone and WASP on a molecular level thus are still elusive.

More recently, Simmonds and co-workers [89,98] have provided evidence for a strong inhibitory effect of mycolactone on the Sec61 translocon. Earlier investigations from this group on human monocytes had indicated that the production of inflammatory mediators such as cytokines (e.g., TNF, IL-1β, IL-6, IL-10, and IP-10), chemokines (e.g., IL-8), and effector molecules like COX-2 was suppressed by subtoxic doses of purified natural mycolactone without any change in the corresponding mRNA levels [80]. A post-transcriptional mechanism was thus suggested to account for the discrepancy between mRNA and protein levels. Similar conclusions were later drawn by Demangel and co-workers [87]; intriguingly, however, mycolactone exposure affected only a subset of the proteome in human monocytes. Subsequent studies on human RAW264.7 macrophages then led to the hypothesis that rather than blocking translation, mycolactone A/B would block translocation of secretory proteins into the endoplasmic reticulum (ER) [89,99]. Nascent secretory proteins that are not translocated into the ER are usually rapidly degraded by the 26S proteasome. Consistent with this, mycolactone treatment in the presence of a proteasome inhibitor restored COX2 and TNF production in RAW264.7 cells and both proteins were found in the cytosol.

Translocation of secretory proteins into the ER is mediated by the Sec61 complex, a protein conducting channel that consists of three monomeric subunits, Sec61α, β and γ. Blockade of the

Sec61 translocon by mycolactone was confirmed in several translocation assays. Of 18 cytokines produced in RAW264.7 cells after LPS stimulation, 17 were almost completely suppressed by mycolactone, generally with IC_{50} values of around 60 nM. Metabolic labeling experiments indicated that mycolactone exposure caused an almost complete blockage of the production of secretory and N-glycosylated proteins, which are generally processed in the ER [100]. In contrast, only minor changes in the levels of cytosolic proteins were detected. Similar results were obtained with human dermal microvascular endothelial cells (HDMVEC), murine L929 fibroblasts and HeLa cells. Mechanistic studies in a cell-free system then showed that mycolactone efficiently inhibited the co-translational translocation of polypeptides into the ER, while the post-translational, ribosome-independent translocation of short secretory proteins (SSPs) is only partially affected. Together with the results of cross-linking experiments, these data indicate that mycolactone interferes with the ribosome–nascent chain (RNC)-Sec61 complex. Similar conclusions were recently derived from an independent study by Demangel and co-workers, who confirmed by global proteome analysis via stable-isotope labeling with amino acids in cell culture (SILAC) [101] in T cells that mycolactone A/B is a broad-spectrum Sec61 inhibitor [102]. The mycolactone binding site on Sec61 appears to be located near a luminal plug of the Sec61α subunit, as the mutation of Arg66 in Sec61α to Gly renders Sec61 insensitive to mycolactone. The expression of this mutant in T cells restored their homing potential and effector functions, while expression in macrophages restored their IFN-γ-mediated bactericidal response, a critical factor for early host defense [103].

Interestingly, based on data from both the Simmonds as well as the Demangel group, WASP does not seem to play a major role for the immunosuppressive effects of mycolactone. Neither did the WASP inhibitor wiskostatin restore the production of secretory proteins nor did the silencing of (N)-WASP by RNA interference alter the suppression of secretory and membrane protein production by mycolactone.

The angiotensin pathway was identified as a third target of mycolactones by Brodin and co-workers in 2014 [104]. It has been known for some time that mycolactone is responsible for the local analgesia and the consequent painlessness of *M. ulcerans* infected lesions [78], a phenomenon that until recently was ascribed to the destruction of nerve bundles [78,105]. However, this assumption seems inconsistent with the fact that nerve damage only occurs at advanced stages of the infection, while lesions are painless from its very onset. In fact, Brodin and co-workers could demonstrate that the injection of either mycolactone A/B (**1a**,**b**) or a GFP-expressing *M. ulcerans* mutant into mouse footpads was associated with a rapid onset of analgesia that was reversible and not accompanied by macroscopic or ultrastructural signs of nerve destruction and hypoesthesia. Subsequent experiments revealed that mycolactone exposure caused hyperpolarization of neurons derived from PC12 cells that was mediated by the TRAAK potassium channel. Finally, screening of a siRNA library targeting 8000 host genes identified the angiotensin type II receptor (AT_2R) as the molecular target of mycolactone, which was confirmed by genetic knockout in vitro and in vivo and by chemical inhibition. In a competition binding assay mycolactone was able to displace the potent radiolabeled agonist [^{125}I]-CGP42,112A (K_d = 0.01 nM) [106,107] with an IC_{50} value of 3 μg/mL (corresponding to 4 μM). Binding of mycolactone A/B to AT_2R was found to trigger the activation of phospholipase A2, resulting in the release of arachidonic acid. The latter can be converted into prostaglandin E2 (PGE2), which was shown to activate TRAAK channels. In line with this mechanistic model, cyclooxygenase (COX) 1 and prostaglandin-E synthase 2, which are central for PGE2 biosynthesis from arachidonic acid, were found to be essential for mycolactone-mediated hyperpolarization; in contrast, genetic or chemical abrogation of COX2-activity was inconsequential. The conclusions of Brodin and co-workers have recently been challenged by Anand and co-workers, who described a destructive effect of mycolactone A/B on human and rat nociceptive dorsal root ganglia (DRG) neurons [108]. Furthermore, mycolactone-treated DRG neurons showed a reversible and dose-dependent decline in capsaicin response, potentially indicating an interaction of mycolactone A/B with the transient receptor potential cation channel subfamily V member 1 (TRPV1, vanilloid receptor 1) [109]. On the other hand, co-treatment with either angiotensin II or the AT_2R antagonist EMA401 [110] did not alter the morphological and functional defects provoked by mycolactone, thus putting into question the proposed role of the angiotensin II receptor in mycolactone-promoted analgesia.

Very recently, the Pluschke laboratory in collaboration with our own group identified the mammalian (more recently: mechanistic) target of rapamycin (mTOR) pathway as a key player in the pathogenesis of Buruli ulcer [111]. As a principal regulator of cell fate decisions, mTOR interacts with different proteins to form the multiprotein complexes mTOR complex 1 and 2 (mTORC 1 and 2), which trigger different downstream signaling cascades. As the core component of these complexes, mTOR exhibits protein kinase activity and phosphorylates a variety of downstream meditators. One of the principal substrates of the mTORC2 complex is the serine/threonine kinase Akt, which gets activated upon phosphorylation at Ser473 [112]. Disruption of the mTORC2 complex or inhibition of its kinase activity causes Akt inactivation via dephosphorylation that results in the dephosphorylation and activation of Akt-

targeted transcription factors including forkhead box O1 and O3 (FoxO1 and FoxO3) [113,114]. Upon translocation to the nucleus, dephosphorylated FoxOs induce the expression of target genes such as *BCL2L11*, which encodes the pro-apoptotic Bcl-2-like protein 11, also referred to as BIM. Moreover, FoxOs can trigger apoptosis via the Fas death receptor signaling pathway [115]. In early investigations, we studied the toxicity of synthetic mycolactone A/B on L929 fibroblasts pre-treated with the pan-caspase inhibitor Z-Val-Ala-Asp-[OMe]-fluoromethyl ketone (Z-VAD-FMK) [116], the autophagy inhibitor 3-methyladenine [117] and necrostatin 1 [118], an inhibitor of programmed necrosis and found that mycolactone-treated cells die by apoptosis. Interestingly, the addition of wiskostatin, which was previously shown to counteract cytotoxic effects of mycolactones [93], even enhanced mycolactone toxicity. By using a real-time PCR (qPCR) screening of 84 genes involved in the regulation of apoptosis, autophagy and necrosis, a strong increase in the mRNA transcripts encoding for the BH3-only protein Bim and the Fas receptor was observed. Both translated into an increase of the respective protein levels and into the emergence of apoptosis markers such as cleaved caspase 3 and 8, which correlated well with the time course of mycolactone-mediated apoptosis. Silencing Bim and Fas by RNA interference proved that Bim is the key driver of mycolactone-mediated apoptosis while Fas upregulation may represent a passive bystander effect. Based on these results and considering the remote similarity of mycolactones with rapamycin, the mTOR pathway was contemplated as a potential molecular target. To put this hypothesis to test, the effect of mycolactone treatment on the phosphorylation of the mTORC1-targeted ribosomal protein S6 (rpS6) and the mTORC2-targeted kinase Akt was investigated in L929 fibroblast and Jurkat T cells. Strikingly, mycolactone treatment abolished both, S6 and Akt phosphorylation. Since mycolactone A/B did not directly interfere with the kinase activity of mTOR and caused a time-dependent gradual loss of mTORC1/2 signaling capacity, it was hypothesized that mycolactone interferes with the mTOR complex assembly. This hypothesis was confirmed by immunoprecipitation of the respective mTOR complexes at different time points after mycolactone treatment. Of note, the blockade of mTORC2 assembly by rapamycin [119] followed a similar time course as observed for mycolactone A/B. Subsequent Western blot analysis of L929 whole cell lysates proved the complete abrogation of FoxO3 phosphorylation at the Akt target site after 12 h of mycolactone treatment, which is in line with the time course of Akt inactivation. In accordance with these results, stable overexpression of constitutively active Akt (Myr-Akt) [120] rescued L929 fibroblasts from mycolactone-promoted apoptosis while silencing FoxO3 by RNA interference was only partially protective. The latter finding might be explained by the compensating effects of other FoxO proteins. Two synthetic mycolactone-derived probes bearing a biotin tag as a substitute of the lower side chain (**15**) or attached at C20 of the core extension (**16,** Figure 6) were used to investigate whether mycolactone supresses mTOR signaling in a similar fashion as rapamycin. The latter is known to bind to the FK506-binding protein

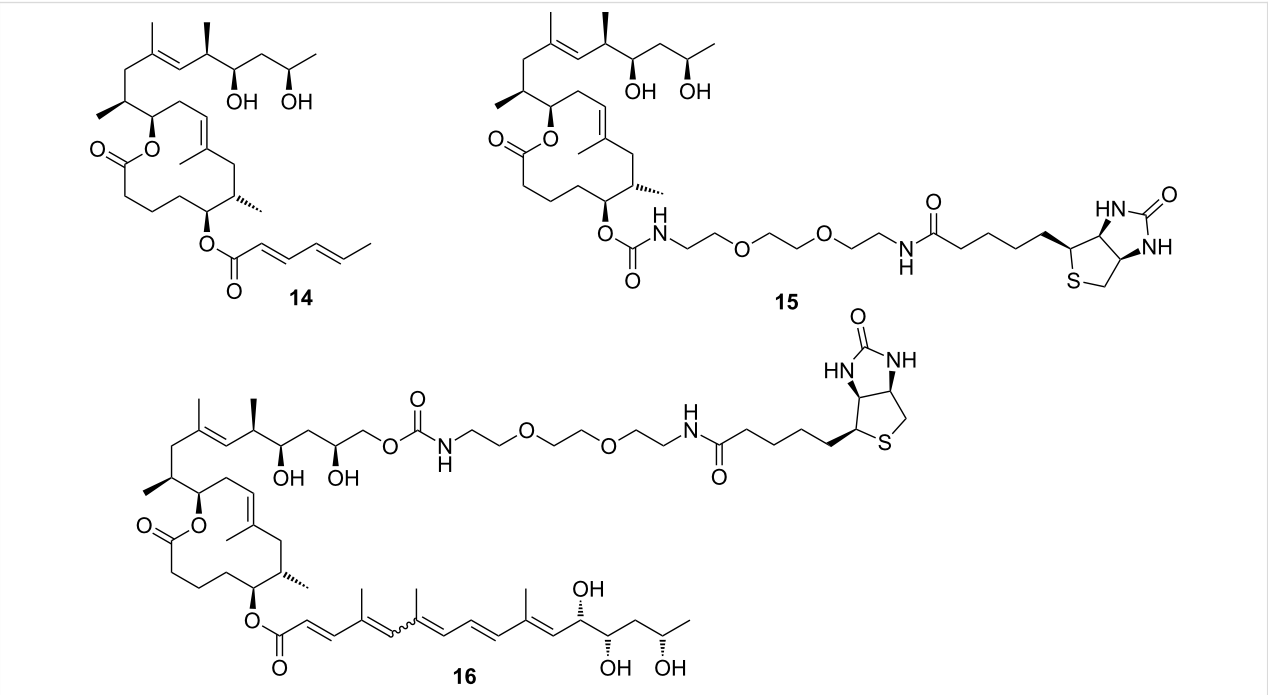

Figure 6: Tool compounds used by Pluschke and co-workers for elucidating the molecular targets of mycolactones.

FKBP12. Strikingly, target fishing in L929 whole cell lysates using these two tool compounds identified FKBP12 in the precipitates obtained with **16**, but not with **15.** In line with those observations and with published SAR (vide infra) [90], the simplified analog **14** with a truncated lower side chain caused neither inhibition of mTORC2 activity nor up-regulation of Bim. Furthermore, the suggested interaction of mycolactone A/B with FKBP12 is supported by the protective effects of an excess of FK506 against mycolactone-induced apoptosis. However, further experimental validation of the mycolactone-FKBP12 interaction, e.g., by SPR, NMR or X-ray crystallography, would be highly appreciable. Finally, we also demonstrated the key role of mycolactone-triggered Bim-mediated apoptosis in vivo. To this end, the food pads of wild-type (WT) and homozygous Bim and Fas knockout mice ($Bim^{-/-}$ and $Fas^{-/-}$) were infected with *M. ulcerans*. Intriguingly, WT and $Fas^{-/-}$ mice showed the typical Buruli ulcer phenotype, while $Bim^{-/-}$ mice were devoid of the typical Buruli ulcer-like symptoms. Moreover, $Bim^{-/-}$ mice were able to contain the *M. ulcerans* infection suggesting that infiltrating phagocytes are able to eliminate *M. ulcerans* if they are not killed by the excreted toxin.

III. Total synthesis of mycolactones

The fascinating biology and the challenging structural features of mycolactones have attracted significant interest from research groups worldwide with a focus on natural product synthesis. In this chapter the synthetic work on mycolactones that has been reported by the groups of Kishi, Negishi, Burkart, Altmann, Aggarwal, Gurjar, Feringa, Minnaard, Blanchard and Dai will be discussed. As a consequence of the enormous amount of work published in the field, not every single aspect of this research can be covered. While trying to be as comprehensive as necessary, we will focus on highlighting conceptual differences between different total syntheses and synthesis plans (even if not fully implemented) and exceptional chemistry that has emerged from these efforts. Moreover, a summary assessing synthetic efficiency by step count and overall yield will be provided for each synthesis. In this context, we will define a "step" as one in which a substrate is converted to a product (irrespective of the number of transformations) without intermediate workup [121]. For detailed information the interested reader is referred to the literature cited.

III.1. Syntheses of the mycolactone core

Currently, all mycolactone partial and total syntheses share the (projected) final esterification of the C5-hydroxy group of the appropriately protected extended mycolactone core with the respective polyunsaturated fatty acid under Yamaguchi conditions (Figure 7). Two principal approaches have been used to establish the 12-membered macrolactone ring, namely (1) ring-closure by macrolactonization, the approach followed by Kishi, Negishi and Aggarwal, or (2) ring-closing olefin metathesis (RCM) to form the C8–C9 double bond, which is part of Burkart's and Altmann's syntheses of the mycolactone core and of Blanchard's synthesis of its 8-desmethyl derivative.

A common element between Kishi's 1st generation approach and Negishi's and Aggarwal's strategies consists in the assembly of the entire linear C1–C20 fragment prior to macrocyclization. For most other syntheses, namely Kishi's 2nd and 3rd generation approaches, Burkart's 3rd generation strategy as well as Altmann's and Blanchard's approaches, full elaboration of the upper (C12) side chain is performed only after formation of the macrocycle. Moreover, the majority of syntheses (all of Kishi's syntheses, Burkart's 3rd generation synthesis, Altmann's and Blanchard's syntheses) relied on the construction of the C13–C14 bond by means of palladium-mediated $C(sp^2)$–$C(sp^3)$ cross-coupling between a C1–C13 and a C14–C20 fragment. As one of two exceptions, Negishi's mycolactone synthesis features the final assembly of the C1–C20 seco acid via formation of the C9–C10 bond by an epoxide-opening reaction with an alkyne-derived alkenyl trialkylaluminate. A distinct strategy was also chosen by the Aggarwal group, which connected the linear C1–C11 fragment to the C12–C20 fragment employing their lithiation–borylation homologation methodology; the required fragments were also obtained by the sequential application of this methodology. Of note, Burkart's 1st generation approach aiming to assemble the cyclized C1–C14 fragment with the C15–C20 extension was unsuccessful, since the keto group located at C14 failed to undergo Wittig, HWE or Julia olefination with the respective C15–C20 fragments.

The most extensive contributions to the synthesis of mycolactones have come from Kishi and co-workers, who pioneered the synthesis of the extended mycolactone core structure. The group's approaches to this problem have evolved over time, leading to three distinct generations of syntheses. The 1st generation synthesis [39] was developed in 2001 with the intention to confirm the mycolactone core structure, including the unambiguous assignment of its relative and absolute stereochemistry. In their 2nd generation approach [122], published in 2007, Kishi and co-workers increased the overall efficiency of the synthesis by reorganizing the assembly of the principal fragments and by optimizing the key $C(sp^2)$–$C(sp^3)$ Negishi cross-coupling reactions as well as the choice of protecting groups. The 3rd generation approach [123], published in 2010 was developed with a main focus on scalability. Alternative access routes to key fragments allowed the efficient synthesis of multigram quantities of late stage intermediates. Finally, 1.3 g of the highly pure extended mycolactone core were prepared.

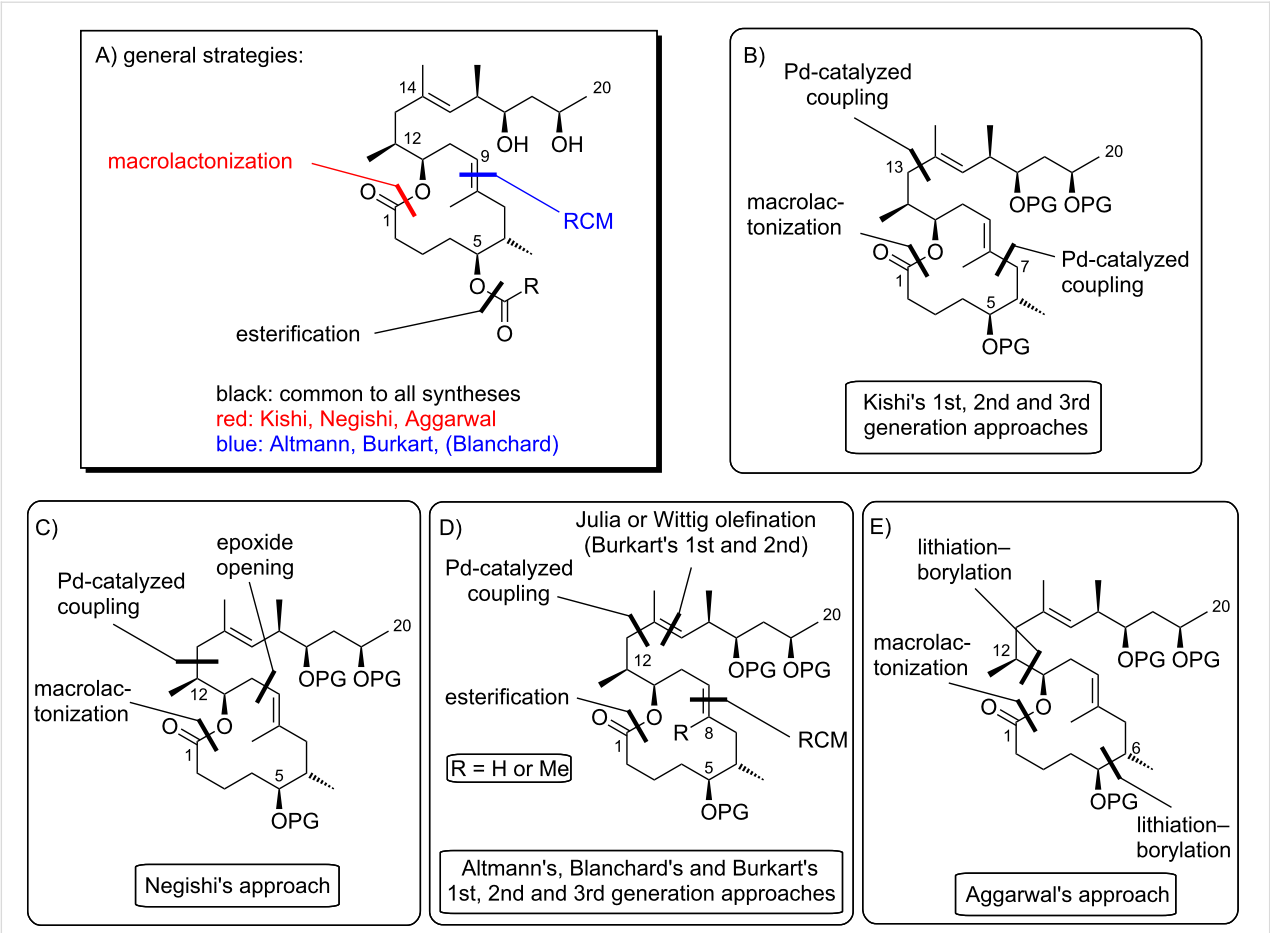

Figure 7: Synthetic strategies towards the extended mycolactone core. A) General strategies. B) Kishi's approaches. C) Negishi's approach. D) Altmann's, Blanchard's and Burkart's approaches. E) Aggarwal's approach. PG = protecting group.

Kishi's 1st generation synthesis of the mycolactone core structure is depicted in Scheme 1. It relied on two consecutive Negishi cross-coupling reactions [124] to construct the linear C1–C20 fragment, which was to be cyclized by macrolactonization [39].

Vinyl iodide **19**, corresponding to the C14–C20 part of the core extension, was synthesized from literature-known aldehyde (*R*)-**17**, which defined the configuration of the C19 stereocenter (mycolactone numbering, see Figure 1). Aldehyde (*R*)-**17** can be easily prepared from commercially available methyl (*R*)-3-hydroxybutyrate ((*R*)-**47**, see Scheme 4) in two steps, namely TBS protection followed by selective reduction with DIBAL-H [125]. Aldehyde (*R*)-**17** was submitted to an asymmetric Brown crotylation reaction [126,127] to establish the C16 and C17 stereocenters. Of note, all four possible C16,C17-diastereomers of **18** were prepared (not shown) by using different combinations of (*E*)- or (*Z*)-butene and either enantiomer of methoxydiisopinocampheylborane (Ipc_2BOMe). These compounds were required to assign the stereochemistry in the core extension by NMR spectroscopy. Homoallylic alcohol **18** was converted into vinyl iodide **19** in a high-yielding six step sequence involving ozonolysis of the double bond, Seyferth–Gilbert homologation [128,129] under Bestmann–Ohira conditions [130,131], a Schwartz hydrozirconation/iodination sequence [132], and appropriate protecting group manipulations.

Vinyl iodide **21**, which comprises the C8–C13 segment was prepared from TBDPS-protected (*R*)-hydroxy-2-methylbut-3-ene **20** that was obtained according to literature procedures [133], thus setting the stereochemistry at C12. The five-step sequence from **20** to vinyl iodide **21** included a (poorly diastereoselective) epoxidation, epoxide opening with a propynyl anion and a hydrozirconation/iodination reaction to generate the vinyl iodide moiety.

The synthesis of alkyl iodide **23** departed from TBS-protected 5-hydroxypentanal **22** and proceeded via an asymmetric Brown crotylation to establish the C5 and C6 stereocenters. Intermediates **21** and **23** were combined under Smith's modified [134]

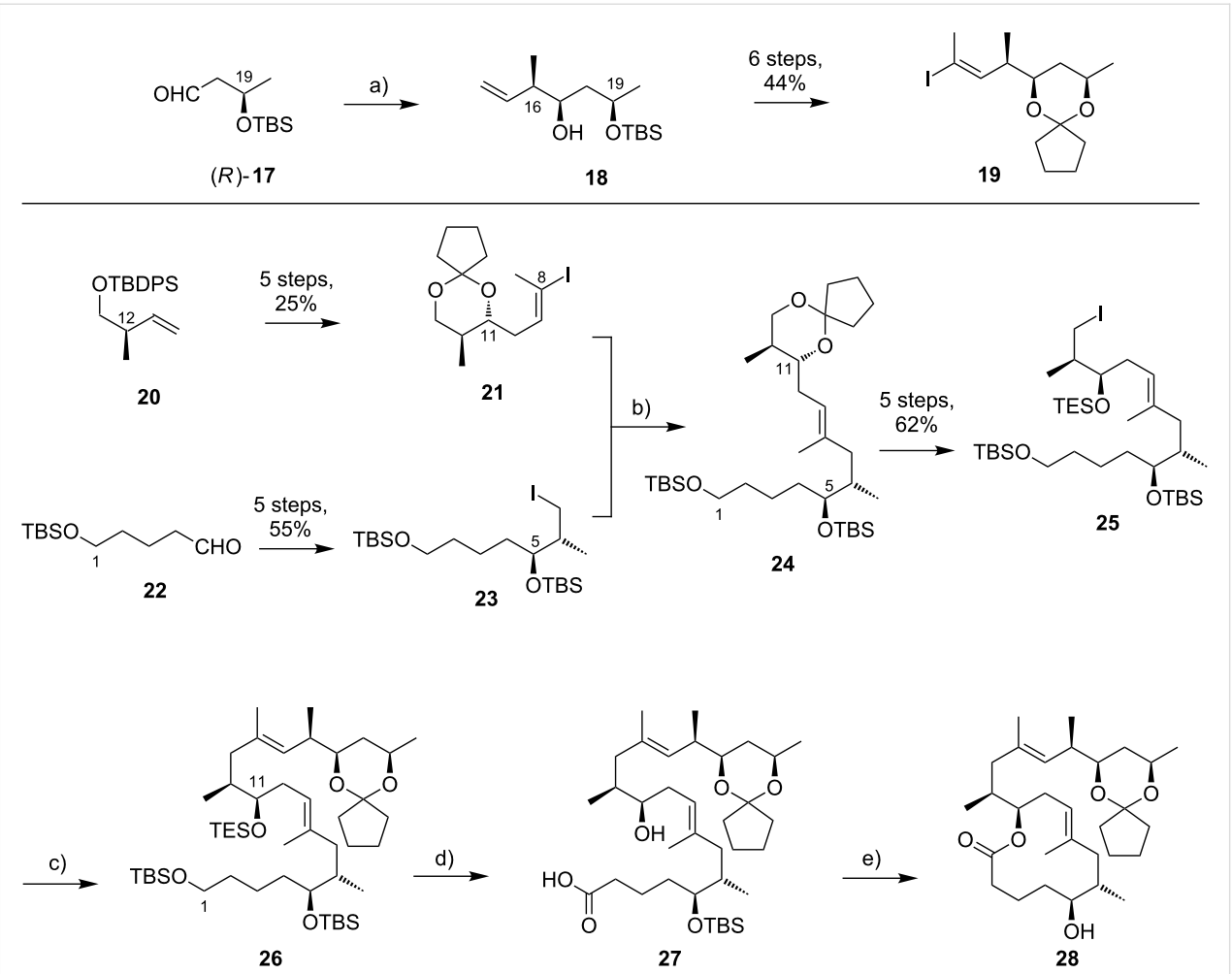

Scheme 1: Kishi's 1st generation approach towards the extended core structure of mycolactones. Reagents and conditions: a) (*Z*)-2-butene, *t*-BuOK, *n*-BuLi, (−)-Ipc$_2$BOMe, $BF_3{\cdot}OEt_2$, −78 °C, then aq H_2O_2 b) **23**, *t*-BuLi, $ZnCl_2$, then **21**, $Pd(Ph_3P)_4$, THF, rt, 60%; c) **25**, *t*-BuLi, $ZnCl_2$, then **19**, $Pd(Ph_3P)_4$, THF, rt, 50%; d) (i) HF·pyridine/pyridine/THF (1:1:4), rt, 72%; (ii) TEMPO, *N*-chlorosuccinimide, Bu_4NCl, CH_2Cl_2/pH 8.6 buffer 1:1, rt, 95%; (iii) $NaClO_2$, NaH_2PO_4, 1,3-dimethoxybenzene, DMSO/*t*-BuOH 1:1, rt, 94%; e) (i) 2,4,6-trichlorobenzoyl chloride, DIPEA, DMAP, benzene, rt, 70%; (ii) CH_2Cl_2/H_2O/TFA 16:4:1, rt, 62%.

Negishi cross-coupling [124] conditions to furnish the protected C1–C13 fragment **24**; the latter was then transformed into alkyl iodide **25** via several functional group interconversions and protecting group manipulations. Negishi cross-coupling of **25** with vinyl iodide **19** then furnished the full length intermediate **26** in moderate yield. Simultaneous removal of the secondary TES and the primary TBS ether protecting groups was followed by selective oxidation of the ensuing primary alcohol to deliver seco acid **27**. The crucial macrolactonization was performed under Yamaguchi conditions [135] in 70% yield and subsequent cleavage of the secondary TBS ether under mildly acidic conditions furnished the acetal-protected extended core structure **28**. In summary, Kishi's 1st generation synthesis provided the extended mycolactone core in a longest linear sequence of 17 steps in 1.3% overall yield from known homoallylic silyl ether **20** [133]; the latter had to be prepared in four additional steps from commercially available (*R*)-Roche ester (*R*)-**70** (cf. Scheme 6, no yields are reported in [133] for the conversion of (*R*)-**70** into **20**).

Upon careful re-analysis of their 1st generation synthesis, Kishi and co-workers recognized that improvements could be made by more efficient strategies to access and assemble the chiral fragments. Moreover, they sought to employ a fully silyl-based protecting group strategy (including protection of the diol motif in the C12–C20 core extension) that would enable global deprotection after attachment of the polyunsaturated side chain. The major conceptual difference between Kishi's 1st and 2nd generation approaches towards the extended mycolactone core structure consists in the fact that macrocyclization in the 2nd generation approach precedes Negishi coupling between a C14–C20 vinyl iodide and a C1–C13 alkyl iodide, thus making the syn-

thesis more convergent. The synthesis of TBS-protected vinyl iodide **35** was realized by the same principle strategy as used for its cyclopentylidene-protected analog **19** in the 1st generation synthesis (cf. Scheme 1), while a distinct approach starting from diethyl (*S*)-malate ((*S*)-**29**) was used for the preparation of vinyl iodide **21**. As illustrated in Scheme 2, the nine-step synthesis of the latter proceeded via key epoxide **30** and comprised a diastereoselective alkylation of diethyl (*S*)-malate according to Seebach and Wasmuth [136] to introduce the C12-methyl group (dr = 8:1). Although being longer than the 1st generation sequence to **21**, the revised approach provided a similar overall yield and proved superior in terms of diastereoselectivity.

As for the synthesis of **23** in the 1st generation approach, alkyl iodide **31** was also prepared from aldehyde **22**. While the sequence leading to **31** was clearly longer than for **23** (10 steps vs 5 steps), the additional steps are accounted for the early adjustment of the final oxidation state at the C1-position and the protecting group change on the C5-hydroxy group from TBS to PMB. However, in terms of overall strategy, the synthesis of **31** resembles that of **23**, with an asymmetric Brown crotylation defining the C5/C6 stereochemistry as the key step.

The generation of an alkylzinc species from **31** in the presence of an ester required metalation with a zinc–copper couple [137] instead of a Li–Zn transmetalation. The efficiency of the Negishi cross-coupling between the intermediate organozinc species and vinyl iodide **21** was increased by the addition of LiCl, which is known to accelerate Stille coupling reactions [138]. Of note, a 1.4-fold excess of the alkyl iodide was needed to obtain the coupling product **32** in 83% yield. Subsequent protecting group manipulations then furnished seco acid **33**, which underwent macrocyclization to the corresponding lactone under Yamaguchi conditions in almost quantitative yield (compared to 70% for the cyclization of **27** in the 1st generation synthesis). After TIPS deprotection and Appel-type iodination [139], the ensuing alkyl iodide **34** was submitted to a second Negishi cross-coupling reaction under the conditions elaborated for the coupling of **21** and **31**, except that an excess of the vinyl iodide **35** (1.5 equivalents) was used in this case. Having

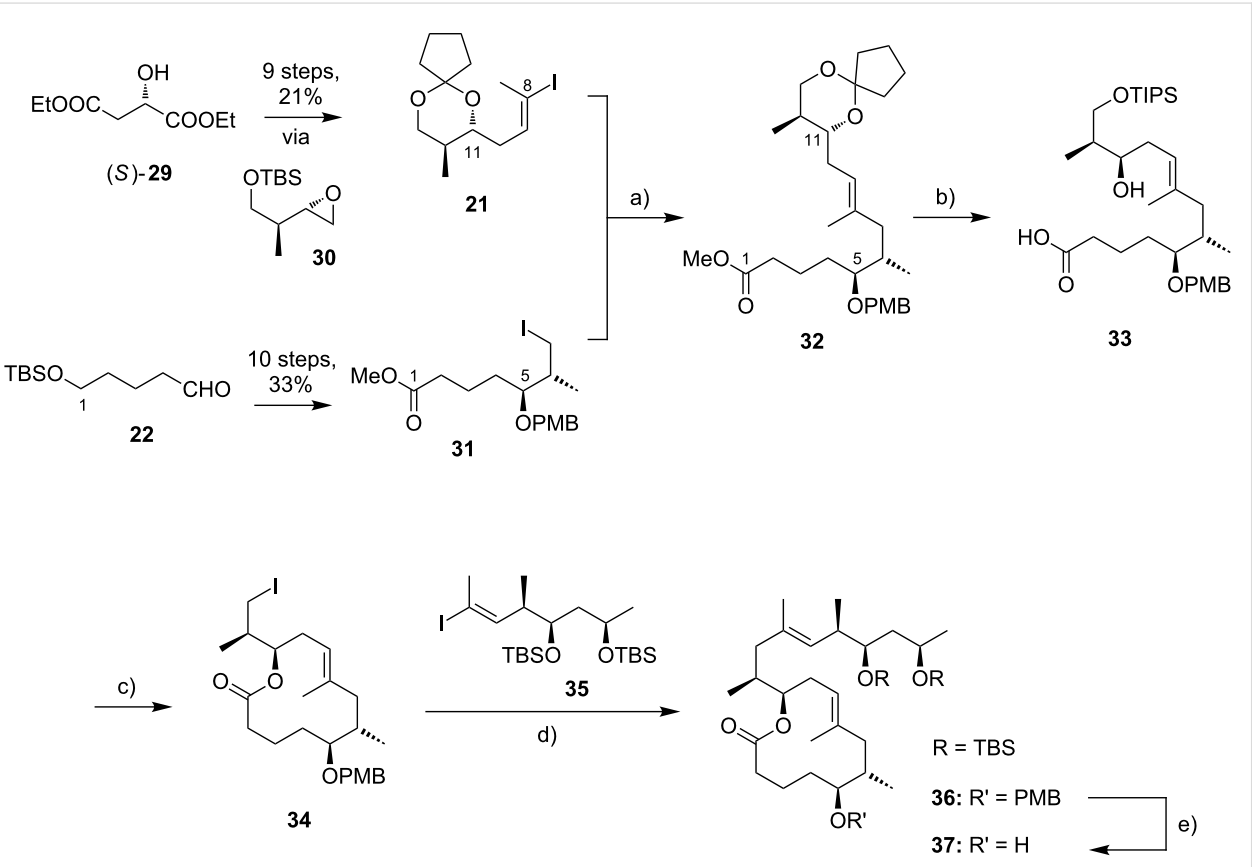

Scheme 2: Kishi's 2nd generation approach towards the extended core structure of mycolactones. Reagents and conditions: a) **31**, Zn/Cu, benzene/DMF 15:1, 55 °C, then **21**, $Pd(PPh_3)_4$, LiCl, NMP, 60 °C, 83%; b) (i) CH_2Cl_2/H_2O/TFA 16:4:1, rt, 90%; (ii) TIPSCl, imidazole, DMF, 0 °C, quant.; (iii) LiOH, THF/MeOH/H_2O 4:1:1, rt, 81%; c) (i) 2,4,6-trichlorobenzoyl chloride, DIPEA, benzene, then DMAP, benzene, rt, 96%; (ii) HF·pyridine/pyridine 1:1, MeCN, 0 °C, 90%; (iii) Ph_3P, imidazole, I_2, CH_2Cl_2, rt, 98%; d) (i) **34**, Zn/Cu, benzene/DMF 15:1, 55 °C, then **35**, $Pd(PPh_3)_4$, LiCl, NMP, 50 °C, 80%; e) DDQ, CH_2Cl_2/H_2O, 0 °C, 91%.

fully protected intermediate **36** in hand, the final DDQ-promoted cleavage of the C5-PMB ether furnished the bis-TBS-protected extended mycolactone core **37** in 20 steps and 12% overall yield from known aldehyde **22** [140]; the latter can be prepared from commercially available 1,5-pentanediol in two additional steps.

Kishi's 3rd generation synthesis of the extended mycolactone core differs from the two previous approaches mainly by employing alternative routes for the synthesis of vinyl iodides **21** and **35** (Scheme 3). Vinyl iodide **35** was prepared from commercially available (*R*)-propylene oxide ((*R*)-**38**), which was opened with deprotonated TMS-acetylene. After TBS protection of the newly formed hydroxy group, iodination with *N*-iodosuccinimide followed by hydroboration/protodeboronation and Sonogashira coupling [141] with propyne gave conjugated enyne **39** in excellent overall yield. Intermediate **39** was stereoselectively epoxidized with hydrogen peroxide in the presence of titanium isopropoxide by using the Katsuki ligand **L1** [142] to give epoxide **40**, thus defining the C16/C17 stereochemistry. The C14–C20 fragment **35** was completed by selective epoxide opening with in situ generated $LiAlMe_4$, TBS protection and installation of the vinyl iodide moiety by hydrozirconation/iodination. Vinyl iodide **21** was prepared from known hepta-2,5-diyn-1-ol (**41**) [143]. Briefly, the selective reduction of the hydroxymethyl-substituted alkyne **41** with $LiAlH_4$ provided an allylic alcohol which underwent the key Sharpless asymmetric epoxidation [144] to furnish epoxide **42** in 69% yield and with excellent enantiomeric purity. Epoxide opening with a higher-order methyl cyanocuprate followed by TBS protection and hydrozirconation/iodination yielded the C8–C13 fragment **21**. Only minor adjustments were made to the synthesis of alkyl iodide **31**.

Starting from known aldehyde **43** [145], possessing the final oxidation state at the C1 atom, the sequence was shortened to six steps while maintaining the previous overall strategy. The connection of the fragments followed the 2nd generation logic and fine tuning of reaction conditions, most notably of the Negishi cross-coupling between **21** and **31**, led to an increased overall yield. In total, Kishi's 3rd generation approach featured a longest linear sequence of 14 steps with an overall yield of 23% from aldehyde **43** [145], which is accessible in two additional steps from δ-valerolactone.

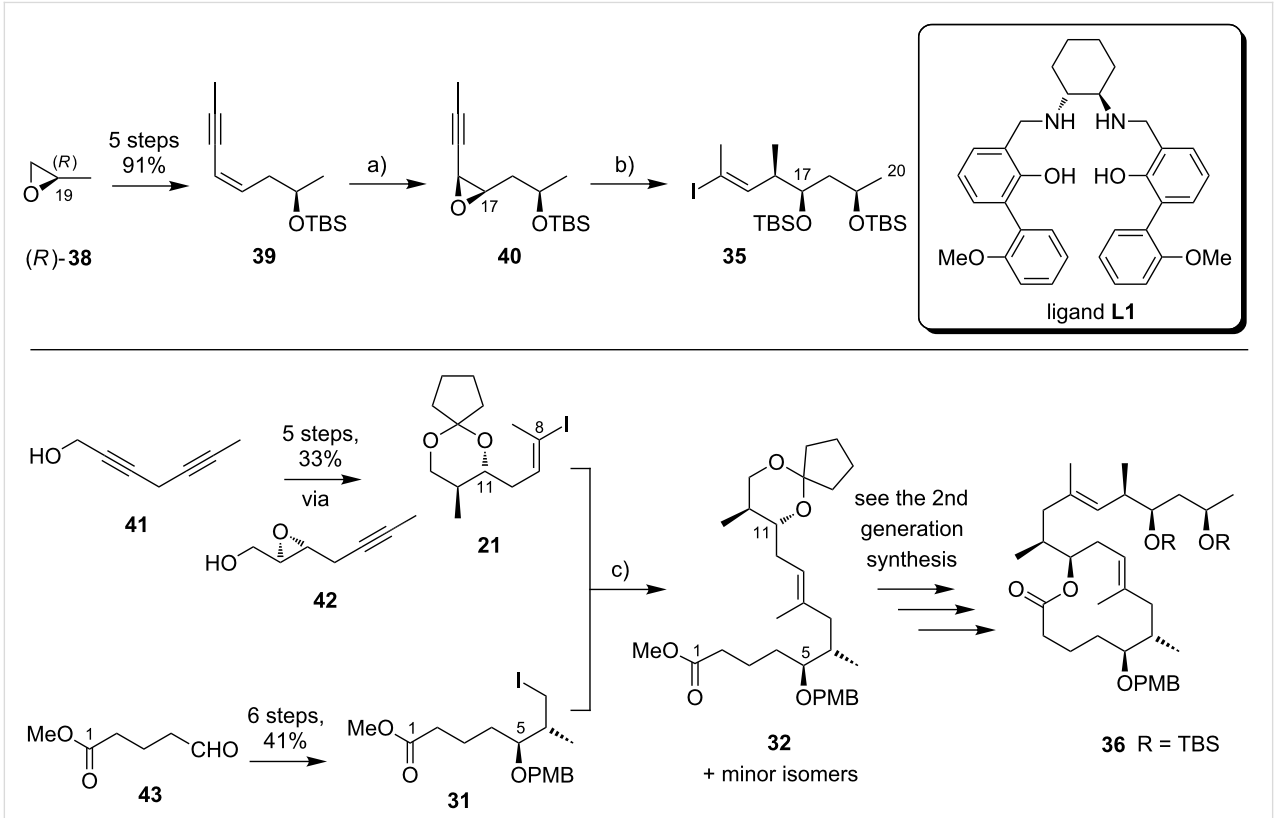

Scheme 3: Kishi's 3rd generation approach towards the extended core structure of mycolactones. Reagents and conditions: (a) **L1**, $Ti(OiPr)_4$, 4,4′-thiobis(6-*tert*-butyl-*m*-cresol), H_2O_2, pH 7.4 phosphate buffer, CH_2Cl_2, 40 °C, 91%, ee > 99% after recrystallization; (b) (i) $LiAlMe_4$, $BF_3{\cdot}OEt_2$, CH_2Cl_2, −78 °C, 87%; (ii) TBSCl, imidazole, DMF, rt, 99%; (iii) $Cp_2Zr(H)Cl$, THF, 50 °C, then I_2, THF, 0 °C, 68%. c) **31**, Zn/Cu, benzene/DMF 15:1, 55 °C, then **21**, $Pd(PPh_3)_4$, LiCl, NMP, 55 °C, 95%.

An alternative approach to the extended mycolactone core that also relied on a late-stage macrolactonization was reported by the group of Negishi in 2011 [37]. They envisaged a strategy that would be heavily branded by methodologies that had been developed in their own laboratories. Moreover, increasing stereoselectivity compared to previous routes was defined as a major objective at the outset of Negishi's work. As shown in Figure 7C, the Negishi strategy as a distinct key step features the formation of the C9–C10 bond by a zirconium-catalyzed methylalumination of alkyne **46** to form a vinyl trialkylalumi-nate that was reacted with epoxide **54** to obtain the linear C1–C20 fragment **55** (Scheme 4).

The synthesis of alkyne **46** followed a similar logic as Kishi's synthesis of alkyl iodide **31**, with the contiguous stereocenters at C5 and C6 being installed by asymmetric Brown crotylation (Scheme 4, intermediate **45**). Subsequent TBS protection of the C5-hydroxy group, hydroboration of the homoallylic double bond followed by oxidation and a Corey–Fuchs reaction [146] sequence delivered stereochemically pure alkyne **46** in a

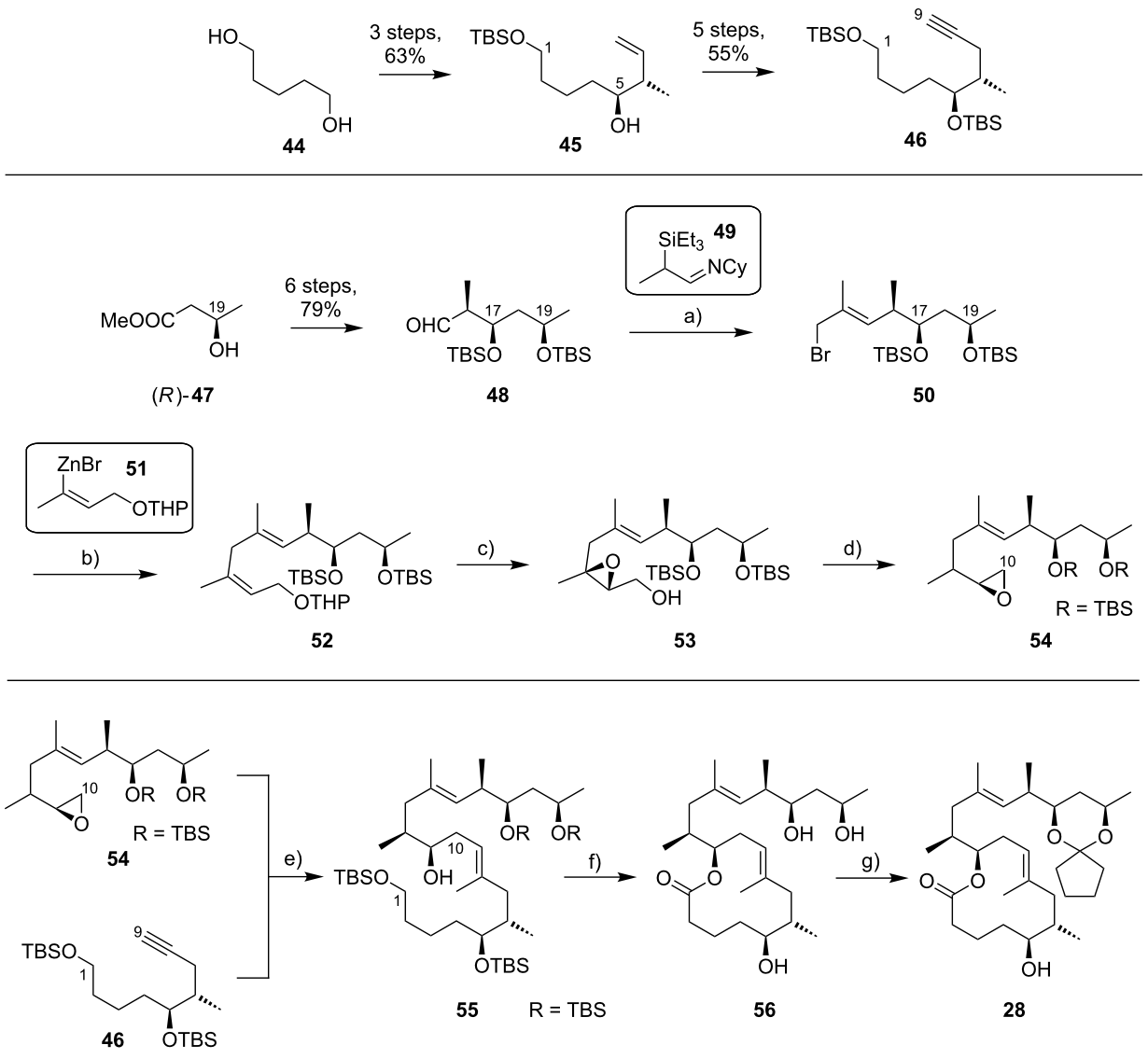

Scheme 4: Negishi's synthesis of the extended core structure of mycolactones. Reagents and conditions: a) (i) *s*-BuLi, THF, −78 °C to −20 °C; (ii) CF_3COOH, THF, 0 °C, 91%; (iii) $NaBH_4$, MeOH, 0 °C; (iv) CBr_4, PPh_3, 2,6-lutidine, CH_2Cl_2, 91% (2 steps); b) $Pd_2(dba)_3$, P(*o*-furyl)$_3$, DMF, 20 °C, 89%; c) (i) $MgBr_2$, Et_2O, 20 °C; (ii) $Ti(OiPr)_4$, (−)-DIPT, *t*-BuOOH, CH_2Cl_2, −78 °C to −23 °C, 76% (2 steps); d) (i) $LiBH_4$, $BF_3{\cdot}OEt_2$, CH_2Cl_2, −40 °C, 75%; (ii) MsCl, 2,4,6-collidine, CH_2Cl_2, 0 °C; (iii) K_2CO_3, MeOH, 87% (2 steps); e) (i) **46**, Cp_2ZrCl_2, $AlMe_3$, H_2O, CH_2Cl_2, −40 °C, then *n*-BuLi, hexane, −78 °C, then **54**, Et_2O, −40 °C to rt, then rt, 83%; f) (i) TBAF, THF, 0 °C, 78%; (ii) TEMPO, [bis(acetoxy)iodo]benzene, CH_2Cl_2/H_2O 2:1, rt; (iii) $NaClO_2$, 2-methyl-2-butene, NaH_2PO_4, *t*-BuOH/H_2O 2:1, rt, 85% (2 steps); (iv) 2,4,6-trichlorobenzoyl chloride, DIPEA, DMAP, benzene, rt, 78%; (v) HF·pyridine, THF, rt, 86%; g) 1,1-dimethoxycyclopentane, PPTS, 80%.

total of eight steps and 35% overall yield from pentane-1,5-diol (**44**).

The preparation of epoxide **54** started from commercially available methyl (*R*)-3-hydroxybutyrate ((*R*)-**47**) setting the stereochemistry at the C19 position. As for the elaboration of **44** into **45**, an asymmetric Brown crotylation was used to install the chiral centers at C16 and C17; after TBS protection of the newly formed hydroxy group, aldehyde **48** was then obtained by oxidative cleavage of the homoallylic double bond using the Upjohn dihydroxylation protocol [147] followed by periodate-mediated diol cleavage [148].

Aldehyde **48** was olefinated with **49** in a highly *E*-selective manner via a Corey, Schlessinger, and Mills (CSM)-modified [149-151] Peterson olefination [152] and the ensuing homologated aldehyde was subsequently converted into alkyl bromide **50** by reduction and Appel reaction. Bromide **50** was then reacted with the vinylzinc bromide **51** in an alkenyl–allyl Negishi coupling reaction [153] to deliver protected allylic alcohol **52**. A Lewis acid-promoted removal of the THP group followed by Sharpless asymmetric epoxidation of the resulting allylic alcohol furnished epoxide **53** in excellent stereochemical purity. The epoxide was then migrated to the terminal position (intermediate **54**) using a three-step procedure, thus setting the stage for the assembly of the principal fragments. In this key step, the alkenylalanate-based epoxide-opening reaction developed by the Negishi group in the 1980s [154,155] was put to test.

Thus, alkyne **46** was treated with an excess of trimethylaluminum in the presence of zirconocene dichloride to furnish the neutral methylaluminated alkene that was transformed into the respective alkenyl trialkylaluminate with *n*-BuLi. The latter selectively opened the epoxide ring in **54** to furnish the isomerically pure linear C1–C20 fragment **55** in high yield (83%). Selective removal of the primary TBS group followed by a TEMPO/Pinnick–Kraus oxidation [156,157] gave the corresponding seco acid that smoothly underwent macrolactonization under Yamaguchi conditions. Global removal of the TBS groups with HF·pyridine yielding triol **56** was followed by acid-catalyzed protection of the 1,3-diol at the core extension as the cyclopentylidene acetal, which finally led to **28**, the partially protected extended mycolactone core. Ultimately, Negishi's synthesis of the extended mycolactone core comprised a longest linear sequence of 23 steps and 8.3% yield from commercially available (*R*)-methyl 3-hydroxybutyrate ((*R*)-**47**).

The preparation of the extended mycolactone core via ring-closing (olefin) metathesis (RCM) [158] was first reported by the Burkart group in 2006 as part of a projected synthesis of mycolactone A/B. In addition to this alternative approach to ring closure, Burkart's overall strategy towards the extended mycolactone core also featured a new concept for the full elaboration of the upper side chain, which was to be based on Wittig [159,160] or Julia–Lythgoe olefination [161,162] between C14 and C15. Of note, a high *E*-selectivity would be necessary in both key reactions.

In Burkart's 1st generation strategy, the C1–C8 fragment **59** was prepared from known aldehyde **57** [163] via an asymmetric Evans aldol reaction [164], providing the C5 and C6 stereocenters in a highly stereoselective manner (Scheme 5). TBS protection of the newly formed hydroxy group, reductive removal of the Evans auxiliary, oxidation of the resulting primary alcohol, and addition of 2-propenylmagnesium bromide to the ensuing aldehyde furnished intermediate **58**. The secondary hydroxy group was acetylated and the acetate was reduced by palladium-catalyzed transfer hydrogenolysis according to a modification of the Tsuji protocol [165]. Selective cleavage of the primary TPDPS group in the presence of a secondary TBS ether was readily achieved with NaOH in refluxing methanol. The primary alcohol was oxidized in a Swern [166]/Pinnick–Kraus oxidation sequence to obtain acid **59** in excellent overall yield.

The synthesis of the C9–C14 segment started from known methyl (*S*)-2-methyl-4-oxopentanoate ((*S*)-**60**) [167], which was protected as the 1,3-dithiane followed by reduction of the ester moiety to the aldehyde stage. The installation of the secondary homoallylic alcohol moiety and thereby the C11 stereocenter was achieved by asymmetric allylboration using a 9-BBD-derived reagent developed by Soderquist et al. [168]. Despite being a mismatched and *anti*-Felkin addition, **61** was obtained with excellent diastereoselectivity, indicating a high level of reagent control. Secondary alcohol **61** and acid **59** were then coupled in high yield employing the Keck modification of the Steglich esterification [169,170], to furnish the crucial RCM precursor **62**. The RCM reaction was accomplished with Grubbs 2nd generation catalyst (5 mol %) [171] to deliver macrolactone **63** in 60% yield after flash-chromatographic removal of the concomitantly formed acyclic dimer and a catalyst-derived benzylidene derivative. The RCM provided the desired product with exceptional *E*-selectivity, as indicated by the lack of a NOE correlation between the C9-proton and the C8-methyl group. Removal of the 1,3-dithiane protecting group with *N*-chlorosuccinimide in the presence of silver nitrate set the stage for the final olefination that had been envisioned to complete the construction of the C1–C20 fragment (vide infra). The longest linear sequence to crystalline macrocyclic ketone **64**, whose structure was confirmed by X-ray crystallography, comprised 14 steps with an overall yield of 19% from known

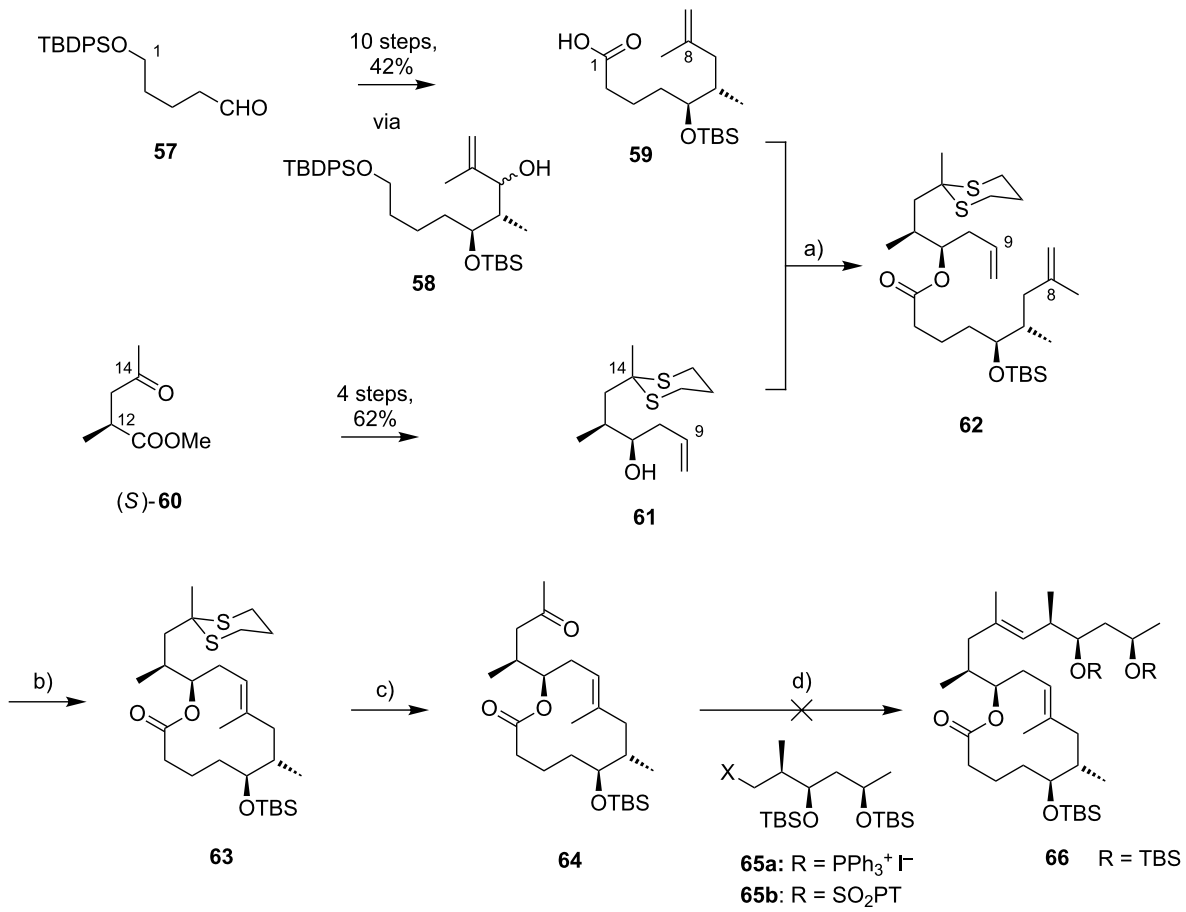

Scheme 5: Burkart's (incomplete) 1st generation approach towards the extended core structure of mycolactones. Reagents and conditions: a) DCC, DMAP, CSA, CH_2Cl_2, rt, 95%; b) Grubbs II (5 mol %), CH_2Cl_2, reflux, 60%; c) *N*-chlorosuccinimide, $AgNO_3$, MeCN/H_2O 4:1, 81%; d) Wittig or Julia–Kocienski olefination (undisclosed reaction conditions).

aldehyde **57** [172]; the latter can be obtained in two additional steps from 1,5-pentanediol.

While Burkart's 2006 paper did not discuss the elaboration of **64** into a protected version of the extended macrolactone core, such attempts were described in a follow-up paper published in 2010 [173]. Due to problems with the originally envisaged extension of **64** at C14 by means of Wittig or Julia-type olefinations, a number of alternative strategies were explored for the elaboration of the C-linked upper side chain (Scheme 6). Initial experiments focused on cross metathesis between alkene **67**, which was accessible from ketone **64** (Scheme 5) by Wittig olefination, and known alkene **68**. A variety of conditions were investigated, all of which led to undesired intramolecular cyclization to cyclohexene ester **69** as the only isolated product, along with several side products (Scheme 6).

An alternative strategy (termed 2nd generation here) was then explored, probing the completion of the core extension by Julia olefination prior to RCM. For this purpose a route toward sulfone **71**, corresponding to the C9–C14 segment was developed. Starting from commercial (*S*)-Roche ester ((*S*)-**70**), a high-yielding seven-step sequence, employing a chelation-controlled Keck-type [174] allylation as the key step, led to **71**.

The anion of sulfone **71** was next reacted with known aldehyde **48** to furnish the Julia-olefination intermediate **72** that could be trapped with benzoyl chloride as a 12:6:1:0.5 mixture of diastereomers. Elimination of **72** to form the corresponding olefin was postponed to a later stage of the synthesis, in order to avoid intramolecular cyclization as it had been observed for **67** during attempted cross metathesis with **68**. Instead, oxidative removal of the PMB group followed by esterification with acid **59** yielded the full-length linear precursor **73** ready for cyclization. RCM to macrolactone **74** with 2nd generation Grubbs catalyst proceeded in excellent yields. Although the *E*/*Z*-selectivity of the RCM was not commented on, one may assume that the *E*-isomer was formed exclusively, based on Burkart's previous results with diene **62**. Treatment of **74** with sodium amalgam then gave a 2:1 mixture of the *E*- and *Z*-olefins, regardless of

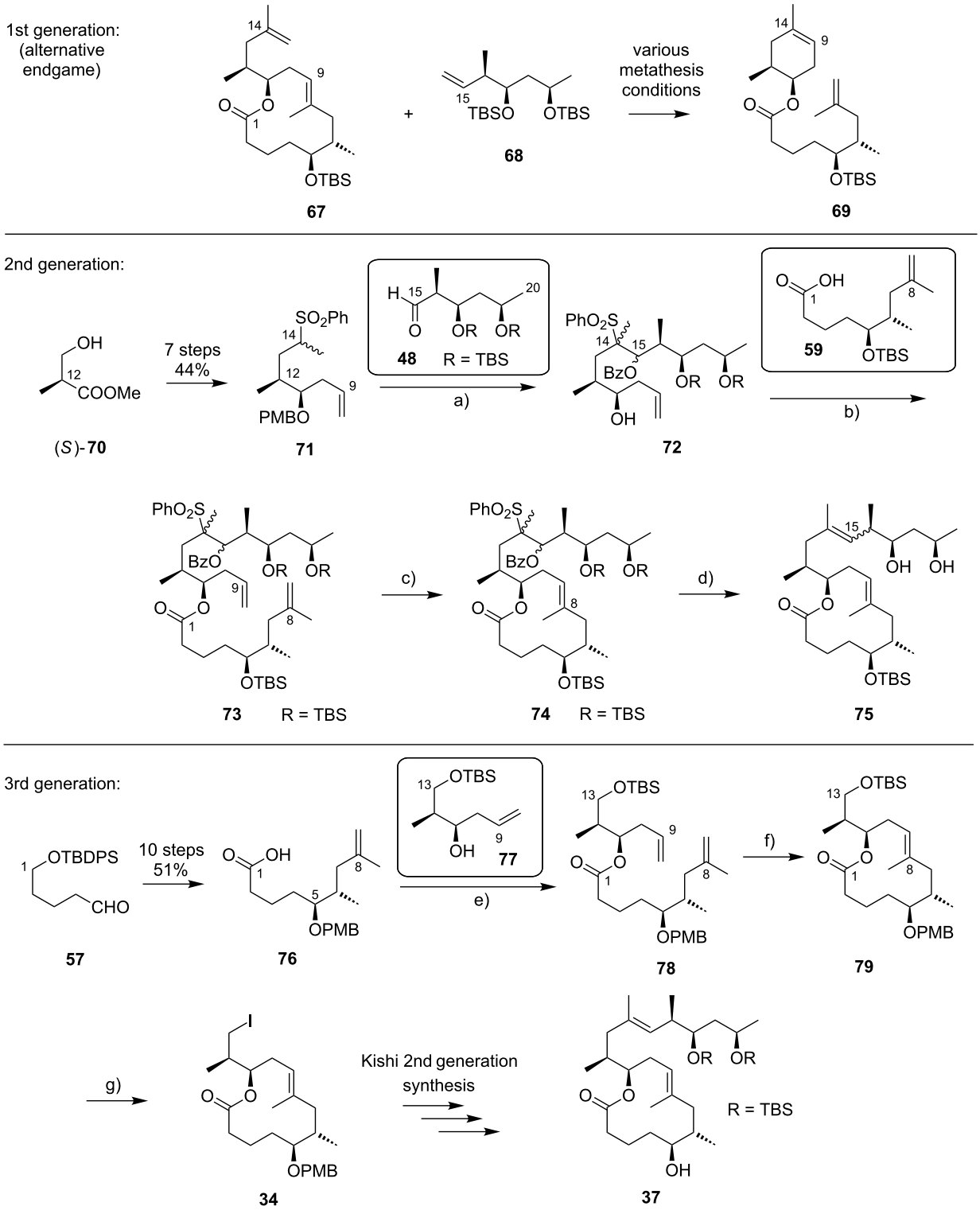

Scheme 6: Burkart's (incomplete) 1st, 2nd and 3rd generation approach towards the extended mycolactone core structure. Reagents and conditions: a) (i) *n*-BuLi, THF, −78 °C to −20 °C, then **48**, THF, −78 °C to −20 °C, then BzCl, −78 °C to rt, 57%; (ii) DDQ, wet CH_2Cl_2, rt, 95%; b) **59**, DCC, DMAP, CSA, CH_2Cl_2, 0 °C to rt, 96%; c) Grubbs II (4.3 mol %), CH_2Cl_2, reflux, 94%; d) (i) Na/Hg, MeOH, −20 °C, 90% (*E*/*Z* 2:1); (ii) TASF, DMF, 42% of *E*-isomer and 19% of *Z*-isomer; e) DCC, DMAP, pyridine, CH_2Cl_2, 0 °C, 87%; f) Grubbs II, CH_2Cl_2, reflux, 78%; g) (i) TBAF, THF, 0 °C to rt, 85%; (ii) I_2, PPh_3, imidazole, toluene, 0 °C, 98%.

the configuration of the starting diastereomer. Finally, removal of the TBS groups at the core extension with tris(dimethylamino)sulfonium difluorotrimethylsilicate (TASF) gave diol **75** in 8.1% yield over 13 steps from (*S*)-Roche ester (*S*)-**70**, while no suitable deprotection method for the C5-TBS ether was found. This is in sharp contrast to results from Kishi [39] who removed the C5-TBS ether under mildly acidic conditions and Negishi [37] and Aggarwal [175] who performed global TBS deprotection of the same intermediate using HF·pyridine in very good yield (see Scheme 1, Scheme 4, Scheme 11). Due to the issues encountered with the cleavage of the C5-TBS ether, the Burkart group developed a 3rd generation RCM-based access to the mycolactone core that relied on PMB protection of the C5-hydroxy group. This strategy was guided by a prior work by Kishi and co-workers, who had already demonstrated that a PMB ether masking the C5-hydroxy group could be readily removed by oxidation with DDQ [122]. To this end, C5-OPMB-protected acid **76** was prepared from aldehyde **57** in 10 steps and 51% yield (Scheme 6). The synthesis was performed in analogy to the approach depicted in Scheme 5, with the notable difference that a Crimmins thiazolidinethione auxiliary was used to enable the selective formation of the C5 and C6 stereocenters in a $TiCl_4$-mediated aldol addition. After Keck-modified Steglich esterification with literature-known alcohol **77** [176], the stage was set for RCM. Cyclization of diene **78** with 2nd generation Grubbs catalyst furnished macrolactone **79** in good yield. The subsequent cleavage of the TBS ether at the C13 position followed by iodination under Appel conditions gave alkyl iodide **34** that was further elaborated into the extended mycolactone core **37** following Kishi's lead [122]. The Burkhart synthesis provided iodide **34** in 14 linear steps and 29% yield from known aldehyde **57**.

In early 2007, shortly after the publication of Burkart's initial work, our own group reported a distinct synthesis of the mycolactone core structure via RCM [177]. The approach delivered alkyl iodide **91** that was further elaborated into the extended mycolactone core and, ultimately, the entire natural product (as reported in 2011) [178].

The synthesis of the C9–C13 fragment started from (*S*)-Roche ester ((*S*)-**70**), thereby setting the stereochemistry at the C12-position (Scheme 7). After PMB protection of the hydroxy group and reduction of the protected ester to the corresponding aldehyde **80**, a chelation controlled Keck-type allylation with allyltributyltin in the presence of tin tetrachloride furnished diol **81** with high diastereoselectivity. Selective tosylation of the C13-hydroxy group completed the synthesis of this fragment (**82**). The C1–C8 fragment containing the carboxylic acid moiety was prepared from 1,5-pentanediol (**83**). In the initial steps this involved mono-PMB protection of **83**, Swern oxidation of the resulting mono-protected diol, and an Oppolzer aldol reaction [179] with the ensuing aldehyde to provide **84** with a dr > 20:1. Reductive removal of the Oppolzer auxiliary followed by selective tosylation of the primary hydroxy group gave tosylate **85**.

Direct substitution of the tosyl group with isopropenyllithium failed, however, and so did the attempted copper-catalyzed reaction with the corresponding iodide. Therefore, a two-step procedure was applied. Upon treatment with sodium hydride, tosylate **85** was cleanly converted into oxetane **86**, a stable intermediate suitable for extended storage periods. Regioselective opening of **86** with isopropenyllithium in the presence of BF_3·etherate gave terminal alkene **87** in excellent yield. After TES protection of the unmasked secondary hydroxy group, PMB cleavage with DDQ followed by a Dess–Martin [180]/Pinnick–Kraus oxidation sequence gave acid **88**. The esterification of **88** with secondary alcohol **82** under Höfle–Steglich conditions [181] proceeded smoothly and gave key diene **89** in very good yield. An RCM was achieved with Grubbs 2nd generation catalyst in refluxing methylene chloride.

Since yields for the RCM reaction varied over a wide range without any changes in reaction conditions (mostly between 50% and 60%), a screening of alternative catalysts and solvents was performed; however, these efforts proved to be futile (Gehringer & Altmann, unpublished). These findings mirror those made in the Blanchard laboratory as part of their work on 8-desmethylmycolactones [182].

The macrocyclic tosylate **90** was then converted into iodide **91** under Finkelstein conditions [183] to enable chain extension by $C(sp^2)$–$C(sp^3)$ cross-coupling. Since the attempted coupling of **91** with the Kishi vinyl iodide **35**, either under modified Suzuki [184] or Negishi conditions did not furnish any of the desired product, an adjustment of the protecting group strategy was made at the stage of the vinyl iodide fragment: The two TBS ethers in **35** were cleaved and a cyclic bis-*tert*-butylsilyl ether was installed to mask the 1,3-diol moiety (**92**) (Scheme 8). Strikingly, the reduced steric hindrance of this protecting group enabled the 9-MeO-9-BBN-promoted $C(sp^2)$–$C(sp^3)$ Suzuki coupling [184] giving rise to the complete extended mycolactone core **93**. Most recently, a more concise route furnishing vinyl iodide **92** from known homoallylic alcohol **18** in six steps and 40% yield was developed (Scheme 8, Gehringer, Bucher & Altmann, unpublished). Moreover, the yields for the Suzuki coupling reaction could be improved to up to 97% (Gehringer & Altmann, unpublished). Cleavage of the secondary TES ether under mildly acidic conditions furnished the key intermediate **94**, ready for acylation with the lower side chain. Up to this point the synthesis comprised a longest linear sequence of

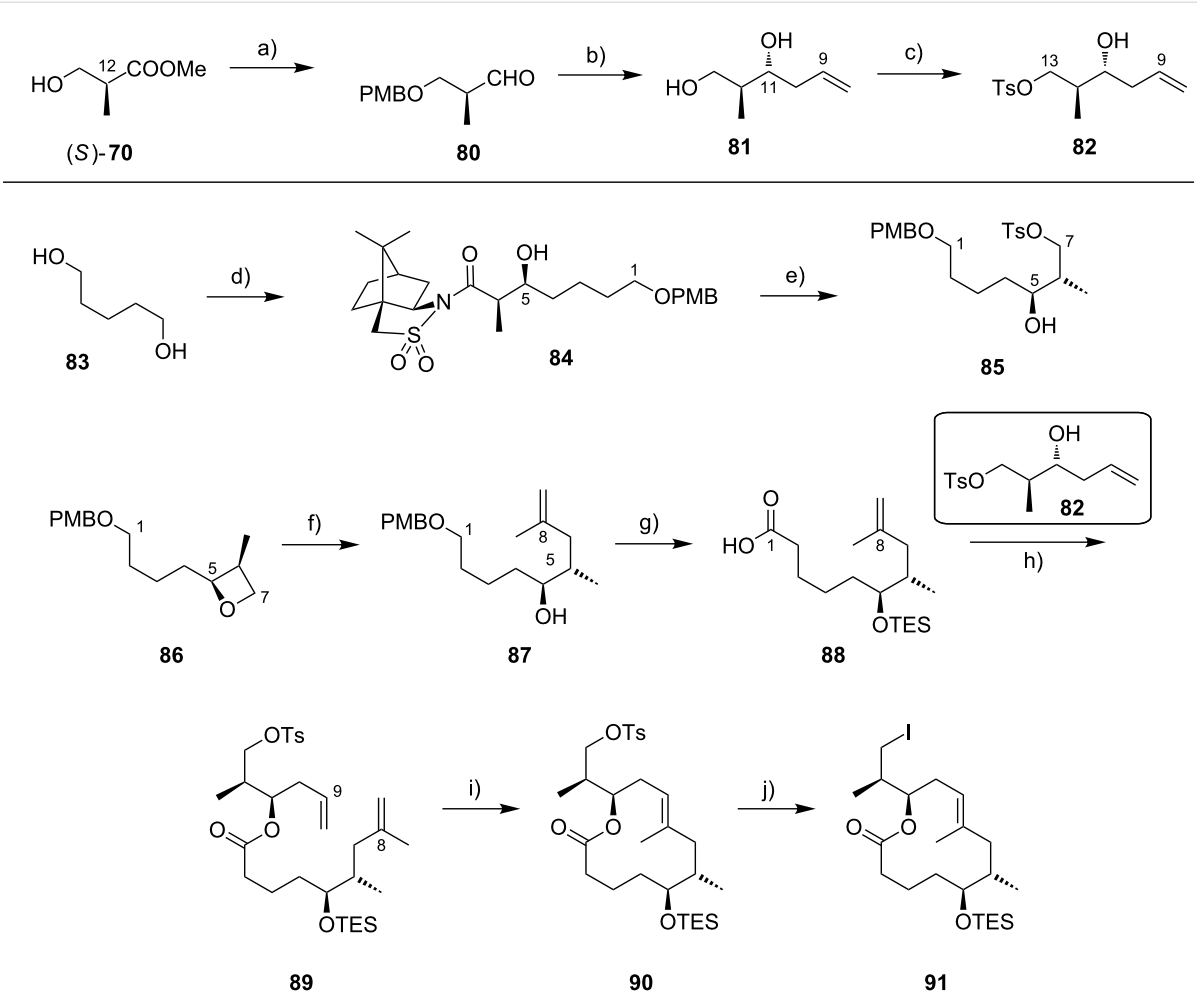

Scheme 7: Altmann's synthesis of alkyl iodide **91**. Reagents and conditions: a) (i) PMB-trichloroacetimidate, TfOH, Et_2O, rt, 58%. (ii) DIBAL-H, CH_2Cl_2, −78 °C, quant.; b) (i) allyl–$SnBu_3$, $SnCl_4$, CH_2Cl_2, −90 °C, 82%, dr > 20:1; (ii) DDQ, H_2O, CH_2Cl_2, rt; (iii) $LiAlH_4$, Et_2O, 0 °C to rt, 76% (2 steps); c) TsCl, Et_3N, DMAP, CH_2Cl_2, 35 °C, 86%; d) (i) PMBCl (0.15 equiv), NaH, benzene, reflux, 97%; (ii) $(COCl)_2$, DMSO, Et_3N, CH_2Cl_2, −78 °C to rt, 99%; (iii) *N*-propionyl-(2*R*)-bornane-(10,2)-sultam, Et_2BOTf, CH_2Cl_2, −5 °C, then addition of aldehyde, −78 °C, 83%, >95% de; e) (i) $LiAlH_4$, THF, 0 °C to rt, 78%; (ii) TsCl, Et_3N, DMAP, CH_2Cl_2, 0 °C to rt, 96%; f) NaH, THF, rt to 40 °C, 98%; g) isopropenyllithium, $BF_3{\cdot}Et_2O$, Et_2O, −78 °C, 90% (optimized: 97%; Gehringer & Altmann, unpublished). g) (i) TESOTf, 2,6-lutidine, CH_2Cl_2, −78 °C to rt, 98%; (ii) DDQ, CH_2Cl_2, buffer pH 7.2, rt, 92%; (iii) DMP, CH_2Cl_2, 0 °C to rt; (iv) $NaClO_2$, 2-methyl-2-butene, NaH_2PO_4, *t*-BuOH/H_2O 9:2, rt, 91% (2 steps); h) DCC, DMAP, CH_2Cl_2, 0 °C to rt, 82%; i) Grubbs II (12 mol %), CH_2Cl_2, reflux, 80%; j) NaI, acetone, rt to 65 °C, 95%.

16 steps and gave **94** in overall yields up to 26%, if the optimized conditions were employed.

The most recent and probably most elegant contribution to the synthesis of the extended mycolactone core has been made by Aggarwal and co-workers [175]. Besides the goal of providing material for biological studies, the Aggarwal group also adopted the synthesis of the extended mycolactone core as a case study to demonstrate the usefulness of their recently developed lithiation–borylation methodology [185,186] in a highly complex molecular setting. The Aggarwal methodology involves three steps [186]: 1) the generation of a chiral lithium carbenoid, typically by enantioselective Hoppe-type lithiation [187] of *N*,*N*-dialkyl carbamates in the presence of (+)- or (−)-sparteine; 2) electrophilic trapping with the organoboron reagent that usually occurs with retention of configuration; and 3) *anti*-1,2-metallate rearrangement substituting the carbamate leaving group by the migrating group on the boron atom (Scheme 9). This methodology enables simple desymmetrization in a largely reagent-controlled manner without any matching issues and it allows to perform iterative homologations to generate consecutive stereocenters.

The Aggarwal synthesis of the extended mycolactone core started from commercially available pent-3-yn-1-ol that was transformed into vinyl boronate **95** by means of a copper-catalyzed regioselective hydroboration followed by protection of the ensuing hydroxy group as the *N*,*N*-diisopropyl carbamate

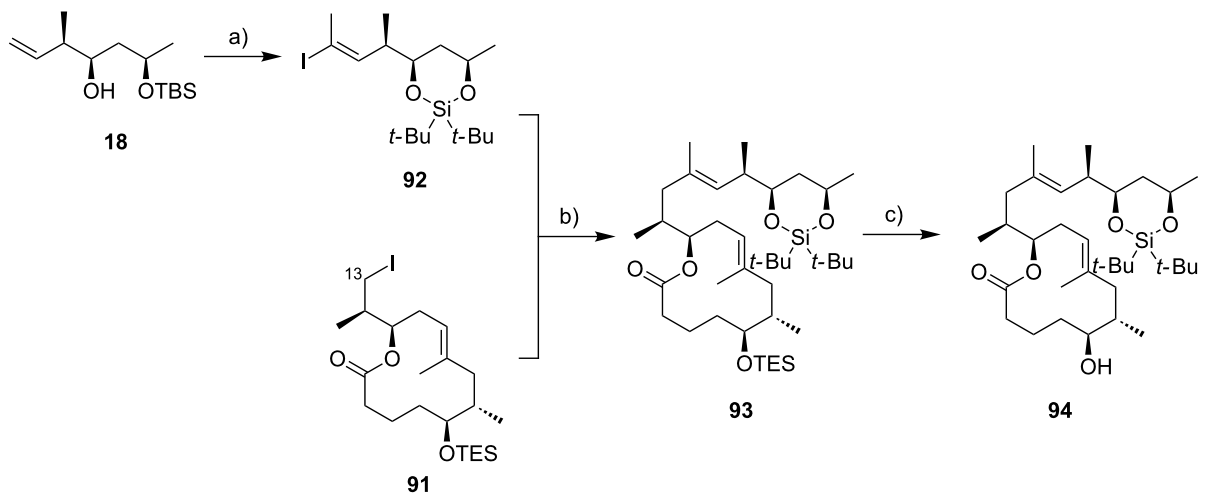

Scheme 8: Final steps of Altmann's synthesis of the extended core structure of mycolactones. Reagents and conditions: a) (i) TBAF, THF, rt, 83%; (ii) *t*-$Bu_2Si(OTf)_2$, pyridine, CH_2Cl_2, 0 °C, 87%; (iii) O_3, CH_2Cl_2, −78 °C, then Me_2S, PPh_3, −78 °C to rt, 84%; (iv) CBr_4, PPh_3, CH_2Cl_2, 0 °C, 88%; (v) *n*-BuLi, MeI, THF, −78 °C, 79%; (vi) $Cp_2Zr(H)Cl$, THF, 45 °C, then I_2, 0 °C, 95% (Gehringer, Bucher & Altmann, unpublished); b) **91**, 9-MeO-9-BBN, *t*-BuLi, Et_2O, THF, −78 °C to rt, then **92**, $[Pd(dppf)Cl_2]$, $AsPh_3$, Cs_2CO_3, DMF, rt, 80% (optimized: 97%; Gehringer & Altmann, unpublished); c) $THF/H_2O/AcOH$ (2:1:1), rt, 90%.

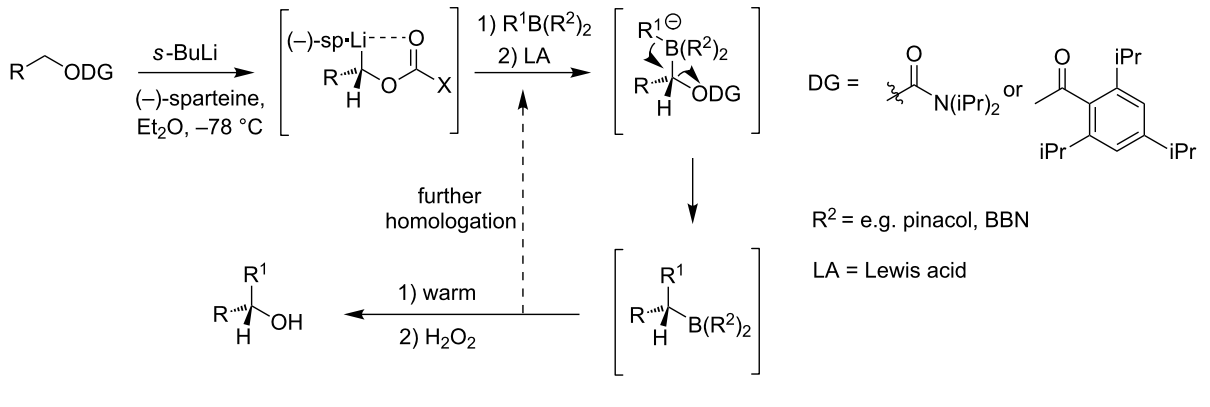

Scheme 9: Basic principles of the Aggarwal lithiation–borylation homologation process [185,186].

(not shown). Matteson one-carbon elongation [188] with in situ generated chloromethyllithium (**96**) then furnished allyl boronate **97** (Scheme 10). Further homologation with asymmetrically lithiated *N,N*-diisopropyl ethyl carbamate **98** elaborated the C6-stereocenter (**99**) in good yield and with excellent enantioselectivity.

The C1–C5 fragment was then introduced by homologation with chiral lithiated carbamate **100** that was accessible from 1,5-pentanediol in a simple two-step protection sequence. The high diastereomeric ratios obtained in this lithiation–borylation step highlight the level of reagent control mediated by lithiated carbamate **100**. Oxidative cleavage of the boronate furnished secondary alcohol **101** and subsequent TBS protection led to key intermediate **102**. Interestingly, the three consecutive homologation reactions from **95** to **101** could also be performed sequentially without intermediate purification (termed "one pot" by the authors) increasing the yield from 63% to 82% over three steps.

Vinyl boronate **103**, corresponding to the C14–C20 segment of mycolactones was prepared via alkene **68** (cf. Scheme 6), which was accessed from methyl (*R*)-3-hydroxybutyrate ((*R*)-**47**) using the Kishi approach [122]. Cross metathesis with isopropenylboronic acid pinacol ester using Hoveyda–Grubbs 2nd generation catalyst [189] under optimized conditions gave **103** in moderate yield (Scheme 11). Matteson one-carbon homologation to **104** followed by another homologation with enantioselectively

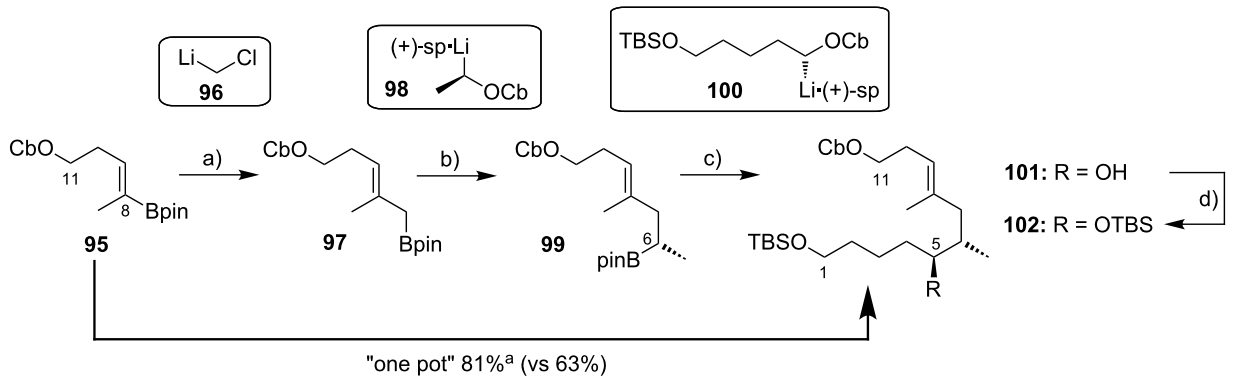

Scheme 10: Aggarwal's synthesis of the C1–C11 fragment of the mycolactone core. Reagents and conditions: a) $ClCH_2I$, *n*-BuLi, Et_2O, −95 °C, 99%; b) EtOCb, (+)-sparteine, *s*-BuLi, Et_2O, −78 °C, then **97**, −78 °C to 40 °C, 83%, er 97:3; c) (i) 5-TBSO-pentyl-OCb, (+)-sparteine, *s*-BuLi, Et_2O, −78 °C, then **99**, −78 °C to 40 °C; (ii) $NaOH/H_2O_2$, THF, 0 °C, 77% (2 steps), dr 94:6; d) TBSCl, imidazole, DMF, 25 °C, 82%. OCb = *N,N*-diisopropyl carbamate. [a]One pot = sequential reactions without intermediate purification.

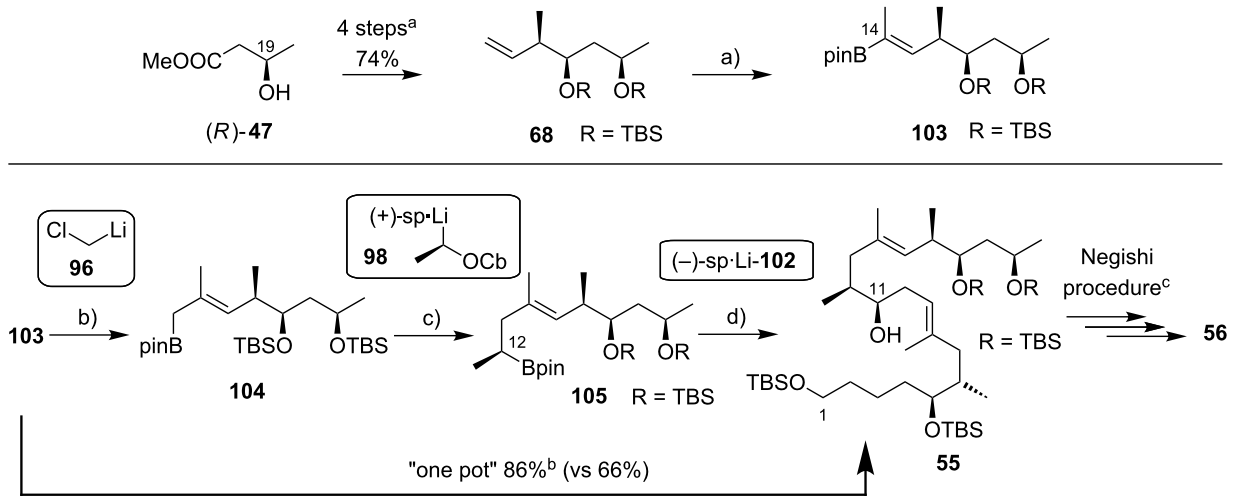

Scheme 11: Aggarwal's synthesis of the linear C1–C20 fragment of the mycolactone core. Reagents and conditions: a) isopropenylboronic acid pinacol ester, Hoveyda–Grubbs II catalyst (10 mol %, sequentially added), CH_2Cl_2, periodic degassing, 60%, *Z*/*E* > 99:1; b) $ClCH_2I$, *n*-BuLi , Et_2O, −95 °C, 99%; c) EtOCb, (+)-sparteine, *s*-BuLi, Et_2O, −78 °C, then **104**, −78 °C to 40 °C, 81%, dr 97:3; d) (i) **102**, (−)-sparteine, *s*-BuLi, Et_2O, −78 °C, then **105**, −78 °C to 40 °C; (ii) $NaOH/H_2O_2$, THF, 0 °C, 82%, (2 steps). [a]Procedure according to [37,39,178]. [b]One pot = sequential reactions without intermediate purification. [c]Procedure according to [37].

lithiated *N,N*-diisopropyl ethyl carbamate **98** produced the C12 stereocenter (**105**) with excellent diastereoselectivity.

Subsequently, **105** was stereoselectively elongated with lithiated key intermediate **102** followed by oxidative cleavage of the boronate to yield the complete linear C1–C20 fragment **55**. Again, performing the reaction sequence from **103** to **55** in "one pot" increased the yield from 66% to 81% over three steps.

With known intermediate **55** in hand, the endgame was realized according to Negishi's approach [37] and gave the unprotected extended mycolactone core in 45% yield over 5 more steps. The Aggarwal synthesis outcompetes the other published syntheses in terms of longest linear sequence (11 or 13 steps, respectively, vs 14 steps [123]) and total step count (15 or 19 steps, respectively, vs 26 steps [173]), but not in terms of overall yield (17% and 13%, respectively, vs 23% [123]). The optional implementation of "one pot" reaction sequences suggest that this synthe-

sis may be performed in a very time-efficient manner. In addition, the synthesis proved to be scalable (950 mg of intermediate **55** were produced in a single batch) and most of the expensive sparteine required for the stereoselective homologations can be recovered.

III.2. Synthesis of the lower mycolactone side chain

A general feature of all syntheses of the mycolactone A/B polyunsaturated side chain is the convergent late stage assembly of two fragments of similar size (Figure 8). The pioneering approach by Gurjar and Cherian connecting the C8'–C9' double bond by HWE olefination was adopted by the groups of Kishi and Altmann, while the Negishi and the Blanchard groups opted for fragment assembly between the C7' and the C8' atoms by $C(sp^2)$–$C(sp^2)$ cross-coupling reactions. A disconnection between the C9' and the C10' atom was envisaged by the groups of Feringa and Minnaard who intended to join their fragments by C(sp)–$C(sp^2)$ cross-coupling followed by selective reduction of the generated internal triple bond.

The western trienoate fragment is usually built up by Wittig two-carbon elongation cycles, with the notable exception of the Negishi approach, which relied exclusively on (hydro/carbo)metalation and cross-coupling reactions. The eastern fragment incorporating the three chiral centers (C12', C13' and C15') was either constructed by chiral pool synthesis from monosaccharides (Gurjar/Cherian, Feringa/Minnaard and Altmann), by a strategy relying solely on asymmetric synthesis (Blanchard) or by mixed approaches (Kishi/Negishi). The convergent strategy based on the assembly of two advanced fragments was also pursued in the synthesis of the pentaenoate chains of mycolactones C, S1 and S2, while the tetraenoate chains in mycolactones E and F were constructed completely by iterative elongation cycles. As an exception, the mycolactone E side chain was prepared by Wang and Dai via connection of the C1'–C7' and the C8'–C15' fragments by Suzuki cross-coupling.

III.2.1. Synthesis of the mycolactone A/B pentaenoate side chain: In 2001, Gurjar and Cherian were the first to complete the synthesis of the protected mycolactone fatty acid side chain [190]. Their retrosynthetic analysis involved a Horner–Wadsworth–Emmons (HWE) [191,192] reaction to assemble the pentaene from a triene harboring the requisite phosphonate and an α,β-unsaturated aldehyde bearing the triol moiety. Due to the unknown stereochemistry at the C12', C13' and C15' position at the beginning of their synthetic endeavor, Gurjar and Cherian needed a flexible approach towards this eastern fragment. They opted for a chiral pool synthesis starting from different 4,6-deoxyhexoses that would eventually define the stereochemistry of the triol moiety.

The western triene fragment was prepared starting from α,β-unsaturated ester **106**, which is readily accessible from ethylene glycol or allyl alcohol in a three-step protection, oxidation, Wittig reaction sequence [193]. The ester **106** was then reduced to the corresponding allylic alcohol with DIBAL-H, oxidized with MnO_2 and the ensuing aldehyde was olefinated with ethyl 2-(triphenylphosphoranylidene)propionate to furnish diene **107** (Scheme 12).

The same three-step homologation procedure was repeated with ethyl (triphenylphosphoranylidene)acetate as the Wittig reagent, giving triene **108** upon TBS deprotection. The transformation of the primary hydroxy group to the respective bromide with PBr_3 was succeeded by conversion to phosphonate **109** in a Michaelis–Arbuzov reaction [194,195] with neat triethyl phosphite.

The synthesis of the eastern fragment started from benzylated methyl 4,6-dideoxy-D-glucose **110**, which was hydrolyzed with sulfuric acid and reduced with sodium borohydride to give the dibenzylated tetraol **111** (Scheme 13). For selective benzylation of the secondary hydroxy group at the C15' position, a three step sequence involving protection and deprotection of the

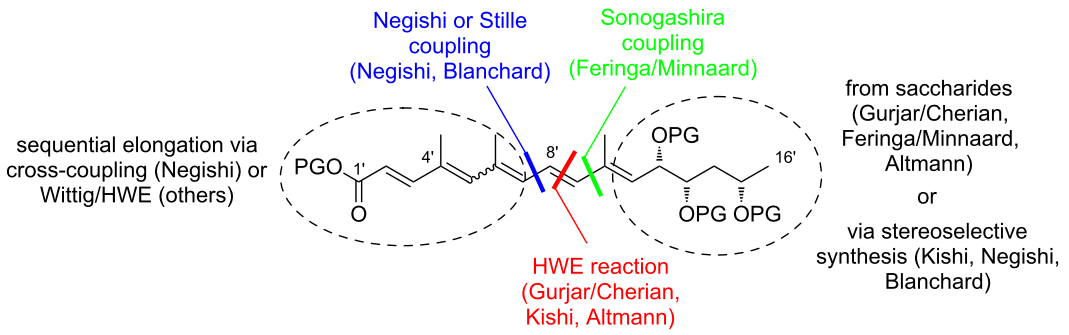

Figure 8: Synthetic strategies towards the mycolactone A/B lower side chain.

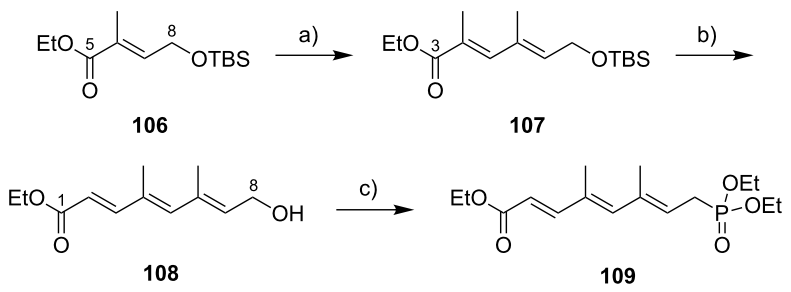

Scheme 12: Gurjar and Cherian's synthesis of the C1'–C8' fragment of the mycolactone A/B pentaenoate side chain. Reagents and conditions: a) (i) DIBAL-H, CH_2Cl_2, −78 °C; (ii) MnO_2, $CHCl_3$, rt; (iii) Ph_3P=C(Me)COOEt, benzene, reflux, 84% (2 steps); b) (i) DIBAL-H, CH_2Cl_2, −78 °C, 92%; (ii) MnO_2, $CHCl_3$, rt; (iii) Ph_3P=CHCOOEt, benzene, reflux, 83% (2 steps); (iv) TBAF, THF, rt, 93%; c) (i) PBr_3, Et_2O, 0 °C; (ii) $P(OEt)_3$, 90 °C, 64% (2 steps).

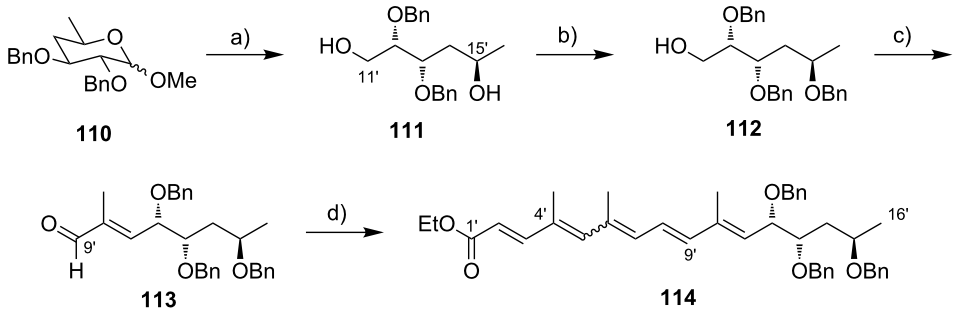

Scheme 13: Gurjar and Cherian's synthesis of the benzyl-protected mycolactone A/B pentaenoate side chain. Reagents and conditions: a) (i) H_2SO_4, dioxane/water 2:1, 100 °C; (ii) $NaBH_4$, MeOH, 0 °C, 54% (2 steps); b) (i) TBSCl, imidazole, CH_2Cl_2, rt; (ii) BnBr, NaH, DMF, rt; (iii) TBAF, THF, rt, 75% (3 steps); c) (i) $(COCl)_2$, DMSO, Et_3N, −78 °C; (ii) Ph_3P=C(Me)COOEt, benzene, reflux, 80%; (iii) DIBAL-H, CH_2Cl_2, −78 °C, 94%; (iv) MnO_2, $CHCl_3$, rt; d) **109**, LDA, THF, −78 °C to 0 °C, 65% (*Z*-$\Delta^{4',5'}$/ *E*-$\Delta^{4',5'}$ 3:2).

primary hydroxy group was required. The resulting alcohol **112** was oxidized under Swern conditions [166] and the resulting aldehyde was submitted to a Wittig reaction with ethyl (triphenylphosphoranylidene)propionate. The subsequent reduction of the ensuing ester with DIBAL-H and oxidation with MnO_2 delivered α,β-unsaturated aldehyde **113**.

At this point, it is worth mentioning that an initial attempt to elaborate the entire pentaene backbone iteratively was hampered by the limited stability of the doubly unsaturated aldehyde obtained from **113** after another two-carbon elongation cycle. The LDA-mediated HWE reaction of **113** with phoshonate **109**, however, proceeded smoothly to provide the fully protected pentaenoate **114** in a longest linear sequence of 10 steps (19 in total) and 20% overall yield from benzylated 4,6-dideoxy-D-glucose **110**. Compound **114** was obtained with a *Z*-$\Delta^{4',5'}$/*E*-$\Delta^{4',5'}$-ratio of 3:2 as demonstrated by NOESY-NMR studies. In accordance with later findings [43,122], the authors reported a slow re-equilibration of the C4'–C5' double bond isomers after separation by HPLC on a chiral stationary phase. However, no conclusions were drawn at that stage with regard to the configuation of the C12', C13' and C15' stereocenters. Although the utility of Gurjar and Cherian's work is confined by the limited availability of methods to selectively remove the benzyl ether protecting groups in the presence of the sensitive pentaenoate system and the stereochemistry at the C15' position that would require to start from expensive L-sugars [196] to furnish the desired epimer, as already alluded to above, their approach was adopted by other groups in their strategies towards mycolactones A/B (vide infra).

Kishi's synthesis of the mycolactone A/B pentaenoate side chain incorporated Gurjar and Cherian's approach towards triene **109** (Scheme 12) with the minor modification of using the methyl ester instead of the ethyl ester at the C1' position [43]. For the eastern C9'–C16' fragment, however, a different strategy was chosen. In Kishi's earlier studies, model compounds were prepared to elucidate the stereochemistry at C12', C13' and C15' by NMR spectroscopy [40]. To enable the determination of the relative configuration at those three proximal stereocenters, a route permitting the synthesis of all possible stereoisomers at the C13' and the C15' position was chosen, while keeping the configuration at C12' invariable. The absolute stereochemistry would then be deduced by compari-

son of NMR spectra of the model compounds with the natural material in chiral solvents. The synthesis of the model compounds started from D-glyceraldehyde acetonide ((*R*)-**115**), which was subjected to Roush allylation [197] with either (*R*,*R*)- or (*S*,*S*)-diisopropyl tartrate-modified allylboronates [176] to separately obtain two diastereomeric homoallylic alcohols (Scheme 14).

After benzyl protection and oxidative cleavage of the double bond, an unselective methyl cuprate addition gave access to a diastereomeric mixture of **116** that could be separated after hydrogenolytic benzyl cleavage. In seven more steps, including a Wittig olefination and several redox and protecting group manipulations, **116** was transformed into α,β-unsaturated ester **117**, and six more steps were required to obtain the four diastereomeric C7'–C16' model dienes exemplified by **118**. As discussed above, comparison of ^{1}H NMR shifts revealed the relative *syn*,*syn*-relationship of the C12', C13' and C15' hydroxy groups and differential ^{1}H NMR profiles in (*R*)- and (*S*)-*N*,α-dimethylbenzylamine (DMBA) unveiled the C12'/C13'/C15' configuration of **118** to be the opposite of natural mycolactone A/B.

Although the route used to prepare the model compounds could have been used to prepare aldehyde **120** (Scheme 15) required for assembly of the lower side chain of natural mycolactone A/B by HWE olefination, Kishi and co-workers pursued an alternative strategy. Even though, not commented on in their report, obvious reasons against the previous strategy include its length and the lack of stereocontrol during the desymmetrization of the C15' atom. Kishi's improved approach commenced with a Wittig reaction to elongate literature known aldehyde (*R*)-**17** (Scheme 15).

The α,β-unsaturated ester obtained was submitted to asymmetric Sharpless dihydroxylation [198] with AD-mix-α [199], which proceeded with a moderate 3.8:1 diastereoselectivity in favor of the desired diastereomer **119**. The undesired diastereomers, however, could be separated chromatographically at a later stage of the synthesis. TBS protection of both hydroxy groups followed by a five-step reduction/oxidation/Wittig reaction sequence furnished key aldehyde **120**. The latter was connected to phosphonate **121** under Gurjar and Cherian's HWE conditions, furnishing full length pentaenoate **122a**,**b**.

Photochemical equilibration gave an inseparable 35:52:4:5 mixture of the all-*E,* the *Z*-$\Delta^{4',5'}$, the *Z*-$\Delta^{6',7}$ and the *Z*-$\Delta^{4',5'}$/*Z*-$\Delta^{6',7'}$ isomers, containing, in addition, 3% of a fifth isomer. After ester hydrolysis, the two major geometric isomers could be separated as a 3:2 mixture of the *Z*-$\Delta^{4',5'}$ and the *E*-$\Delta^{4',5'}$ isomer. The mycolactone side chain was thus obtained in 10 steps and 18% overall yield from aldehyde (*R*)-**17**.

Endeavors towards the synthesis of the polyunsaturated mycolactone A/B side chain were subsequently reported by the groups of Feringa and Minnaard [196]. Although they did not ultimately complete the synthesis, Feringa and Minnaard established a convenient access towards intermediates with the correctly configured C12', C13' and C15' stereocenters by using readily available α-D-glucopyranoside or α-L-rhamnopyranoside as starting materials. Furthermore, the preparation of several key precursors that might be useful for the assembly of (modified) mycolactone A/B side chains was reported, although the connection of these fragments could not be successfully executed at the time. Due to space limitations, only the most significant aspects of this work will be highlighted here.

The preparation of the western C1'–C9' fragment started from known 2,4-dimethylfuran (**123**) [200], which was transformed into keto ester **124** by a rhodium-catalyzed reaction with ethyl diazoacetate [201] (Scheme 16).

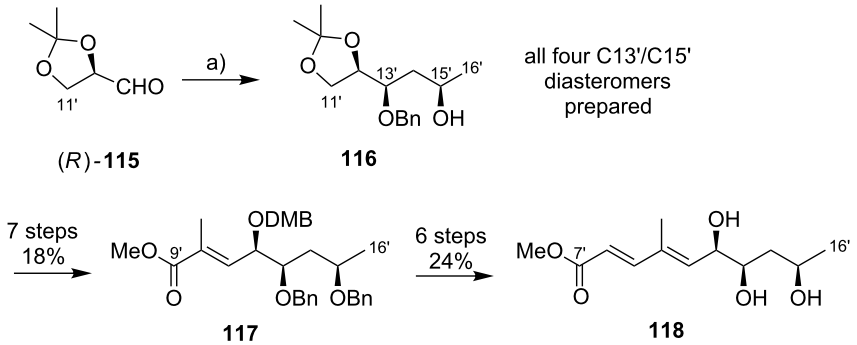

Scheme 14: Kishi's synthesis of model compounds for elucidating the stereochemistry of the C7'–C16' fragment of the mycolactone A/B pentaenoate side chain. Reagents and conditions: a) (i) (*R*,*R*)- and (*S*,*S*)-diisopropyl tartrate-modified allylboronate, 4 Å molecular sieves, toluene, −78 °C, then $NaBH_4$, EtOH, −78 °C; (ii) NaH, BnBr, DMF, 0 °C to rt, 88%; (iii) OsO_4, NMO, DABCO, THF/H_2O 10:1, rt; (iv) $Pb(OAc)_4$, benzene, rt; (v) MeLi, CuI, −20 °C, 83% (3 steps), 1:1 mixture of diastereomers.

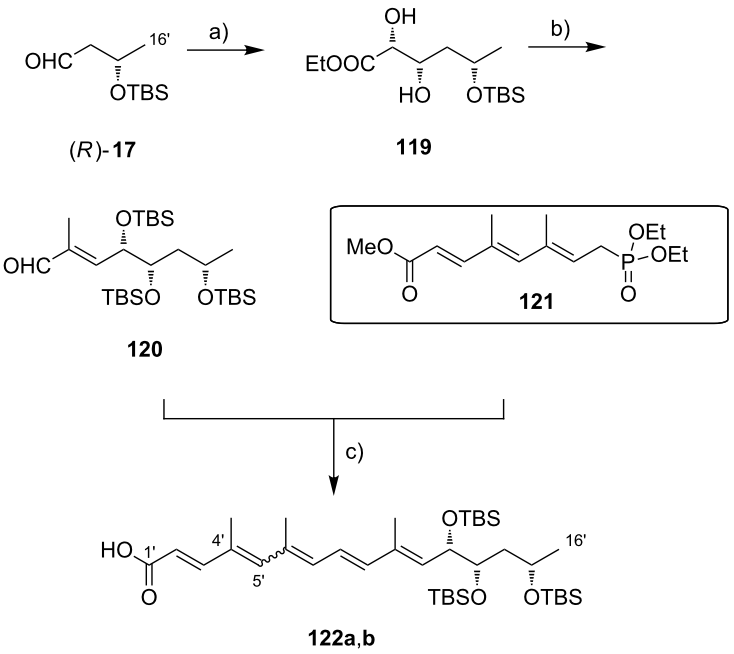

Scheme 15: Kishi's synthesis of the mycolactone A/B pentaenoate side chain. (a) (i) NaH, $(EtO)_2P(O)CH_2CO_2Et$, THF, rt, 64%; (ii) AD-mix-α, $MeSO_2NH_2$, 1:1 *t*-BuOH/H_2O, 0 °C, 70%, dr 3.8:1; (b) (i) TBSOTf, 2,6-lutidine, CH_2Cl_2, 0 °C, 99%; (ii) DIBAL-H, CH_2Cl_2, −78 °C, 89%; (iii) SO_3·pyridine, DIPEA, 3:2 CH_2Cl_2/DMSO, rt; (iv) $Ph_3P{=}C(Me)CO_2Et$, toluene, 110 °C, 83% (2 steps); (v) DIBAL-H, CH_2Cl_2, −78 °C, then separation of diastereomers by flash chromatography; major isomer: 57%; minor isomer: 15%; (vi) SO_3·pyridine, DIPEA, 3:2 CH_2Cl_2/DMSO, rt, quant.; c) (i) LDA, THF, −78 °C to rt, 94% (*E*-$\Delta^{4',5'}$/*Z*-$\Delta^{4',5'}$/other isomers 73:17:10); (e) LiOH, THF/MeOH/H_2O 4:1:1, rt, quant. (*Z*-$\Delta^{4',5'}$/*E*-$\Delta^{4',5'}$ 3:2 + minor isomers).

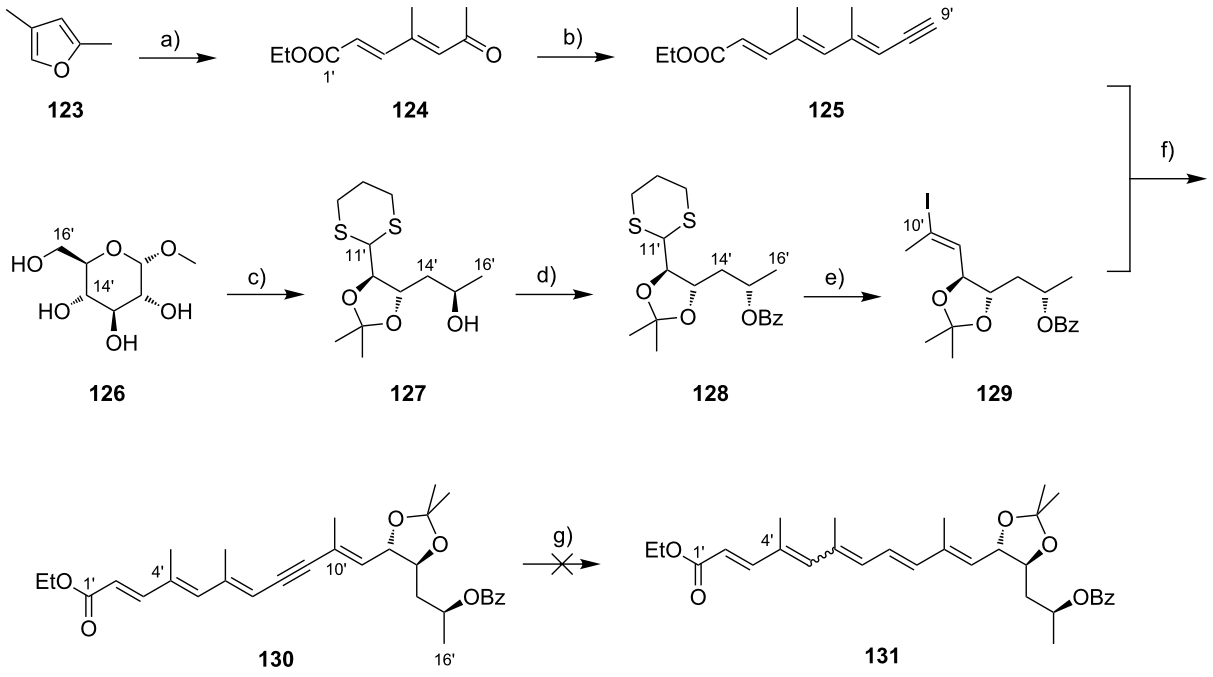

Scheme 16: Feringa and Minnaard's incomplete synthesis of mycolactone A/B pentaenoate side chain. Reagents and conditions: a) (i) $Rh_2(OAc)_4$ (0.4 mol %), CH_2Cl_2, ethyl diazoacetate, rt; (ii) I_2, CH_2Cl_2, rt; b) (i) TMS–C≡C–CH_2–P(O)$(OEt)_2$, *n*-BuLi, THF, 0 °C to rt, 61%; (ii) TBAF, THF, EtOAc, 0 °C, 80%; c) (i) SO_2Cl_2, pyridine, $CHCl_3$, −78 °C to 50 °C, 56%; (ii) Bu_3SnH, AIBN, toluene, reflux, 89%; (iii) 1,3-propanedithiol, conc. HCl, 87%; (iv) acetone, $CuSO_4$, H_2SO_4, 95%; d) PPh_3, BzOH, DEAD, THF, 82%; e) (i) MeI, 2,4,6-collidine, acetone, H_2O, reflux, 89%; (ii) PPh_3, CBr_4, CH_2Cl_2, 0 °C to rt, 72%; (iii) LDA, THF, −78 °C, 88%; (iv) LDA, HMPA, MeI, THF, −78 °C to −10 °C, 88%; (v) $Pd(PPh_3)_2Cl_2$, Bu_3SnH, pentane, 63%; (vi) CH_2Cl_2, I_2, −78 °C to rt, 99%; f) $Pd(PPh_3)_4$, CuI, $iPrNH_2$, 94%; g) H_2, Lindlar catalyst, hexanes, EtOAc, quinoline; or Zn, $Cu(OAc)_2·H_2O$, $AgNO_3$, H_2O, MeOH; or H_2, THF, Elsevier catalyst; or $Ni(OAc)_2·4H_2O$, EtOH, H_2, hydrazine, $NaBH_4$.

A two-carbon elongation was then performed by HWE reaction with TMS-protected diethyl ethynylmethyl phosphonate, and the subsequent TMS cleavage afforded alkyne **125**. The synthesis of the eastern fragment started from α-D-methyl glucopyranoside (**126**), which was converted into partially protected triol **127** by selective chlorination of the C14' and the C16' positions and consecutive reductive removal of the chlorine atoms as the key steps. The configuration at the C15' position was subsequently inverted under Mitsunobu conditions [202] furnishing benzoate ester **128**, which is also a key intermediate in the Altmann synthesis of the mycolactone A/B pentaenoate chain. After dithiane cleavage, the resulting aldehyde was subjected to a Corey–Fuchs reaction [146]/methylation sequence to furnish a methylalkyne that underwent palladium-catalyzed hydrostannylation [203] with moderate regioselectivity (6.3:1 ratio in favor of the desired isomer). Tin–iodine exchange finally delivered vinyl iodide **129** in 16% yield over 10 steps. An alternative synthesis of **129** starting from α-L-rhamnopyranoside proved less cost-efficient and concise. Vinyl iodide **129** was reacted with terminal alkyne **125** in a Sonogashira cross-coupling reaction [141] to produce the full length C1'–C16' fragment **130**. Unfortunately, all conditions screened to selectively reduce the internal triple bond in **130** (e.g., hydrogenation with Lindlar catalyst [204] or Elsevier catalyst [205], reduction with $Ni(OAc)_2/NaBH_4$ [206] or Zn(Cu/Ag) [207]) failed to provide pentaenoate **131**. Moreover, all attempts to convert terminal alkyne **125** into the corresponding *E*-vinyl iodide or stannane that might have been used to assemble the C1'–C16' fragment in a palladium-catalyzed $C(sp^2)$–$C(sp^2)$ cross-coupling reaction were not successful nor was an alternative strategy with a retrosynthetic disconnection at the C7'–C8' double bond.

As noted above, our own group used a hybrid approach that combined access to the C1'–C8' fragment according to Gurjar and Cherian with the synthesis of the chiral C11'–C16' fragment according to Feringa and Minnaard (Scheme 17) [178]. To this end, intermediate **128** from the Feringa/Minnaard synthesis [196] was partially deprotected and reprotected and then elongated to **120** by a Wittig/reduction/oxidation sequence. HWE reaction of **120** with **109** under the conditions elaborated by Gurjar and Cherian gave rise to the full length C1'–C16' fragment; alkaline saponification finally furnished acid **122a**,**b** in 15 steps (longest linear sequence) and 18% overall yield from α-D-methyl glucopyranoside.

A distinct approach selectively providing both the mycolactone A and the mycolactone B pentaenoate chain was followed by the Negishi group [37]. In analogy to their synthesis of the mycolactone core, this strategy was largely driven by the desire to demonstrate the synthetic utility of their (hydro/carbo)metalation and cross-coupling methodologies. In a communication in 2006, Negishi and co-workers reported the stereoselective synthesis of both of the above mycolactone side chains [208]. However, it turned out later that the protecting group strategy chosen in this initial work was not appropriate for the late stage global deprotection envisaged in the total synthesis of mycolactones A and B. Therefore, minor adjustments (replacement of the C12' MOM ether by a TBS ether) were made in the context of the total synthesis. Since the syntheses from both reports are virtually identical, only the 2nd generation approach will be discussed here.

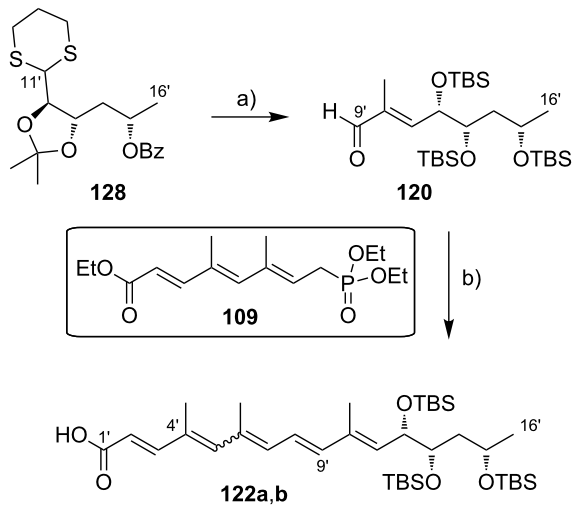

Scheme 17: Altmann's approach towards the mycolactone A/B pentaenoate side chain. Reagents and conditions: a) (i) NaH, MeOH, rt, 95%; (ii) cat. TFA, AcOH, H_2O, rt, quant.; (iii) TBSCl, imidazole, DMF, 70 °C, 96%; (iv) MeI, 2,4,6-collidine, acetone, H_2O, reflux, 97%; (v) Ph_3P=C(Me)COOEt, benzene, reflux, 93%; (vi) DIBAL-H, CH_2Cl_2, −78 °C, 91%; (vii) SO_3-pyridine, DIPEA, CH_2Cl_2/DMSO, rt, 97%; b) (i) **109**, LDA, THF, −78 °C to rt, 90%; (ii) LiOH, THF/H_2O/MeOH (4:1:1), rt, 99%.

The Negishi group provided two different synthetic pathways to prepare the C1'–C7' fragment with a *Z*-configured C4'–C5'-double bond (Scheme 18). The first started from propargyl alcohol (**132**) that was converted into the geminal dibromoolefin **133** [209] by a sequence of TMS protection of the terminal alkyne moiety, Swern oxidation and dibromoolefination of the ensuing aldehyde according to Corey–Fuchs. A highly *E*-selective palladium-catalyzed methylation with $ZnMe_2$ yielded *Z*-bromoolefin **134** that was converted into ynediene **135** by another Negishi-type cross-coupling reaction with (*E*)-(3-((*tert*-butyldimethylsilyl)oxy)prop-1-en-1-yl)zinc bromide followed by global silyl deprotection. Compound **135** was thus obtained in 42% yield over 6 steps.

An alternative route to obtain **135** departed from propyne (**136**) [210] which underwent bromoborylation to **137**, which served

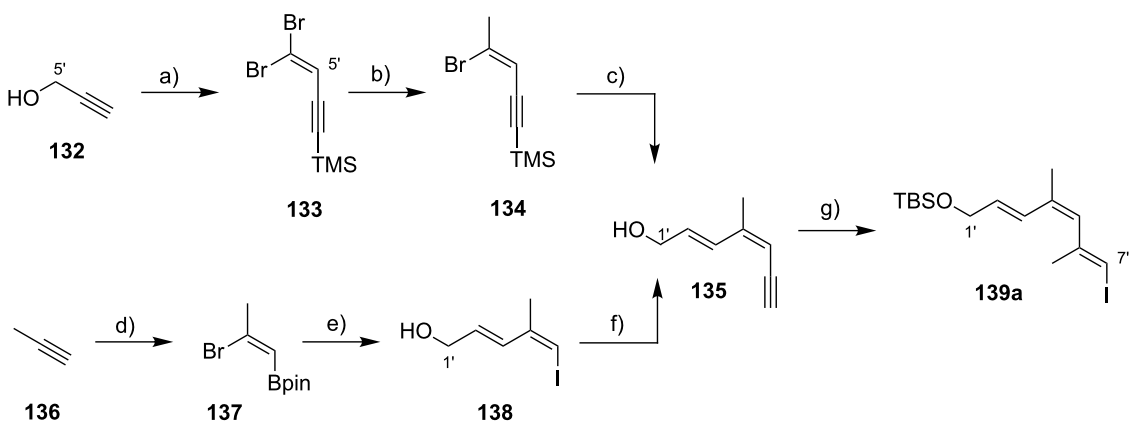

Scheme 18: Negishi's access to the C1'–C7' fragment of mycolactone A. Reagents and conditions: a) (i) *n*-BuLi, TMSCl, then HCl; (ii) $(COCl)_2$, DMSO; (iii) CBr_4, PPh_3, Zn, 90% (3 steps); b) Me_2Zn, Pd(dpePhos)Cl_2 (5 mol %), DMF/THF 1:1, rt, 70%; c) (i) [*trans*-TBSO–CH_2C=C–ZnBr], Pd(dpePhos)Cl_2 (5 mol %), THF/DMF 1:1, rt to 45 °C; (ii) TBAF, THF, rt, 66% (2 steps); d) (i) BBr_3, CH_2Cl_2; (ii) pinacol; e) (i) [*trans*-iBu_2Al–OCH_2C=C–ZnBr], PEPPSI (1 mol %); (ii) I_2, NaOH, THF/H_2O, 77% (2 steps); f) Et_2Zn, then $(HC{\equiv}C)_2$–Zn, Pd(*t*-$Bu_3P)_2$ (0.5 mol %), 94%; g) (i) $AlMe_3$, Cp_2ZrCl_2, CH_2Cl_2, −78 °C to rt, then I_2, THF, −78 °C; (ii) TBSCl, imidazole, DMF, rt, 65% (2 steps).

as the precursor for a Negishi alkenylation and alkynylation reaction, respectively. Of note, this approach relied on a transient protection of the C1' hydroxy group as a diisobutylaluminum complex during cross-coupling. Intermediate **135** was obtained in only three steps and 72% overall yield thereby clearly outcompeting the approach departing from propargylic alcohol both in terms of step count and efficiency. Finally, transformation to *E*,*Z*,*E*-configured trienyl iodide **139a** was achieved in two steps and 65% yield by means of a zirconium-mediated carboalumination/iodination sequence followed by TBS protection [211].

The C1'–C7' fragment with an *E*-configured C4'–C5'-double bond was also prepared from propargyl alcohol (**132**, Scheme 19). Transient protection of the C1' hydroxy group with DIBAL-H followed by hydrozirconation with in situ-generated Schwartz reagent [212] and quenching with iodine yielded an (*E*)-vinyl iodide, that was further processed into enyne **140** by Negishi cross-coupling with bis(ethynyl)zinc. Again, transient hydroxy protection was employed with diethylzinc as the blocking agent. A second zirconium-mediated carboalumination/iodination/cross-coupling sequence then furnished terminal alkyne **141** that was eventually transformed into all-(*E*) vinyl iodide **139b**, again by carboalumination/iodination.

Negishi and co-workers again decided for an independent strategy, when it came to the synthesis of the eastern C8'–C16' fragment. Aldehyde (*S*)-**17** was prepared as previously and submitted to a variant of the Brown allylation [213] employing (+)-(*Z*)-MOM-OCH=$CHCH_2B(Ipc)_2$ (**142**), thus enabling the simultaneous installation of the stereocenters at C12' and C13' (Scheme 20). Although this reaction was highly selective, it came at the cost of requiring a MOM ether protecting group which necessitated further protecting group manipulations, in order to enable late stage global deprotection. Alkene **143** was

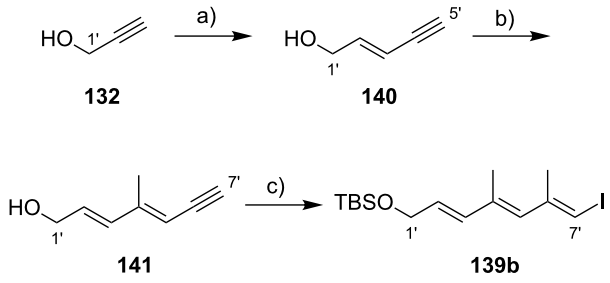

Scheme 19: Negishi's approach to the C1'–C7' fragment of mycolactone B. Reagents and conditions: a) (i) DIBAL-H, THF, 0 °C, then DIBAL-H, Cp_2ZrCl_2, THF, 0 °C to rt, then I_2, THF, −78 °C; (ii) Et_2Zn; then $(HC{\equiv}C)_2$–Zn, Pd(dpePhos)Cl_2 (5 mol %), THF, 0 °C to rt, 58% (2 steps); b) (i) $AlMe_3$/Cp_2ZrCl_2, CH_2Cl_2, −78 °C to rt, then I_2, THF, −78 °C; (ii) $(HC{\equiv}C)_2$–Zn, Pd(dpePhos)Cl_2 (5 mol %), THF, 0 °C to rt, 62% (2 steps); c) (i) $AlMe_3$/Cp_2ZrCl_2, CH_2Cl_2, −78 °C to rt, then I_2, THF, −78 °C; (ii) TBSCl, imidazole, DMF, rt, 63% (2 steps).

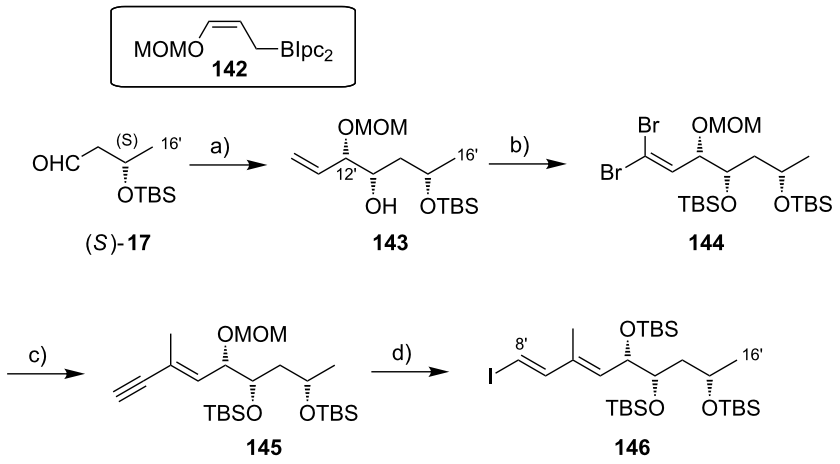

Scheme 20: Negishi's synthesis of the C8'–C16' fragment of mycolactone A/B. Reagents and conditions: a) **142**, $BF_3{\cdot}Et_2O$, Et_2O, −90 °C to 0 °C, then H_2O_2, aq $NaHCO_3$, 91%, dr 94:4; b) (i) TBSOTf, 2,6-lutidine, CH_2Cl_2, 0 °C; (ii) OsO_4 (1 mol %), NMO, THF, H_2O, rt; (iii) $NaIO_4$, THF, H_2O, rt, 95% (3 steps); (iv) PPh_3, CBr_4, 2,6-lutidine, CH_2Cl_2, 0 °C, 96%; c) (i) TMS–C≡C–ZnBr, Pd(dpePhos)Cl_2 (5 mol %), THF, 0 °C; (ii) Me_2Zn, Pd(*t*-$Bu_3P)_2$ (2 mol %), THF, rt; (iii) K_2CO_3, MeOH, rt, 61% (3 steps); d) (i) HCl (3 M in H_2O), MeOH, 55 °C; (ii) TBSOTf, 2,6-lutidine, CH_2Cl_2, rt; (iii) $Cp_2Zr(H)Cl$, THF, rt, then I_2, −78 °C, 55% (3 steps).

cleaved under Upjohn/Lemieux–Johnson [147,148] conditions and conversion of the resulting aldehyde into the geminal vinyl dibromide **144** was achieved by employing the Corey–Fuchs protocol. The more reactive *E*-bromo substituent underwent selective palladium-mediated alkynylation with TMS-ethynylzinc bromide, which was followed by another Negishi-type cross-coupling reaction between the *Z*-bromide and dimethylzinc to furnish enyne **145**. After several protecting group manipulations, a final hydrozirconation/iodination reaction then yielded key dienyl iodide **146** in 28% yield over 11 steps (longest linear sequence from (*S*)-**17**). At this point, it is worth mentioning that dienyl iodide **146** was also prepared using a different route in the course of our own studies and we found this material to be relatively unstable even at −18 °C, thus hampering the storage of this key intermediate (Gehringer & Altmann, unpublished).

With the C1'–C7' and the C8'–C16' fragments in hand, the subsequent assembly was carried out in parallel for the respective precursors of mycolactone A and B. To assemble the polyunsaturated side chain, the trienyl iodides **139a** and **139b** were lithiated with *t*-BuLi. After transmetallation, the corresponding alkenylzinc intermediates were subjected to Pd-mediated Negishi coupling with dienyl iodide **146** (Scheme 21).

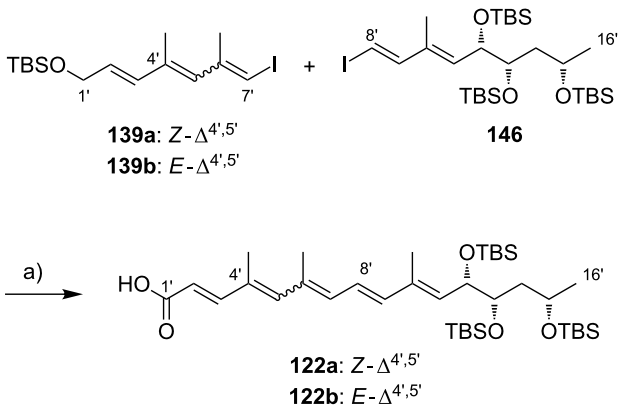

Scheme 21: Negishi's assembly of the mycolactone A and B pentaenoate side chains. Reagents and conditions: a) (i) **139a** or **139b**, *t*-BuLi, then dry $ZnBr_2$, Et_2O, THF, −78°C to rt, then **146**, Pd(dpePhos)Cl_2 (5 mol %), DMF, rt; (ii) TBAF, THF, 0 °C, 61% and 65% (2 steps); (iii) DMP, $NaHCO_3$, CH_2Cl_2, rt; (iv) $NaClO_2$, NaH_2PO_4, 2-methyl-2-butene *t*-BuOH/H_2O 2:1, rt, **122a**: 73%, **122b**: 76% (2 steps).

After selective unmasking of the primary hydroxy group at C1', a Dess–Martin/Pinnick–Kraus oxidation sequence afforded the highly pure (≥98%) side chain acids of mycolactone A (**122a**) and B (**122b**) in 15 steps (longest linear sequence) from (*S*)-**17** in 12% and 14% overall yield, respectively.

Finally, a very distinct approach to the polyunsaturated mycolactone A/B side chain was established by Blanchard and co-workers. With the goal of developing a diverted total synthesis of C8-desmethylmycolactone analogs for SAR studies, the Blanchard group required a general strategy that would give access to different stereoisomers of the lower side chain [92]. Therefore, they adopted a methodology developed by O'Doherty [214] that involves catalytic asymmetric oxidation and subsequent reductive defunctionalization reactions to construct all three stereocenters. The linkage of the C1'–C7' and the C8'–C16' fragments relied on a Stille-type coupling reaction. Starting from readily available *trans*-hexadienal (**147**) (which corresponds to the C11'–C16' segment), a Wittig two-carbon elongation followed by stereoselective Sharpless dihydroxylation (86% ee) of the most electron-rich double bond and subsequent reaction with triphosgene furnished cyclic carbonate **148** (Scheme 22). The C14' position was then defunctionalized to give alcohol **149** by palladium-catalyzed allylic reduction using triethylammonium formate as the hydride donor [214]. A second Sharpless dihydroxylation and subsequent TBS protection afforded fully protected triol **150** with the correctly configured stereocenters at C12', C13', and C15' in place. Ester reduction and allylic oxidation with MnO_2 followed by chromium-mediated one-carbon elongation with $Bu_3SnCHBr_2$ [215] led to dienyl stannane **151**, the precursor for the Stille cross-coupling.

The partner for this coupling reaction, vinyl iodide **152**, was obtained from known (*E*)-3-iodo-2-methylprop-2-en-1-ol [216] by two Wittig elongation cycles. Instead of using traditional Stille conditions, Blanchard and co-workers relied on the palladium-free copper(I) thiophene-2-carboxylate (CuTC)-promoted variant developed by Allred and Liebeskind [217]. Coupling proceeded rapidly at ambient temperature in the presence of tetra-*n*-butylammonium diphenylphosphinate as tin scavenger [218], but only moderate yields were obtained, which somewhat limits the overall efficiency of the synthesis. Final ester hydrolysis and photochemical equilibration furnished the mycolactone A/B pentaenoate side chain acid in 12 steps (longest linear sequence) and 7.4% overall yield from *trans*-hexadienal (**147**). Ultimately, a set of 4 stereoisomers (vide infra) was prepared via this route (as pairs of *E*/*Z* isomers at C4',C5', including **122a**,**b**).

III.2.2 Synthesis of the polyunsaturated side chains of other natural mycolactones: The most extensive contributions to the synthesis of the polyunsaturated side chains of other natural mycolactones were again made by the Kishi laboratory. After having completed the total synthesis of mycolactone A/B, Kishi and co-workers devised strategies for the synthesis of mycolactones C, E, F, S1 and S2 and the photochemical decomposition products of mycolactone A/B ("photo-mycolactones"). Contributions from other groups include the approach to the mycolactone E side chain developed by Wang and Dai and Blanchard's

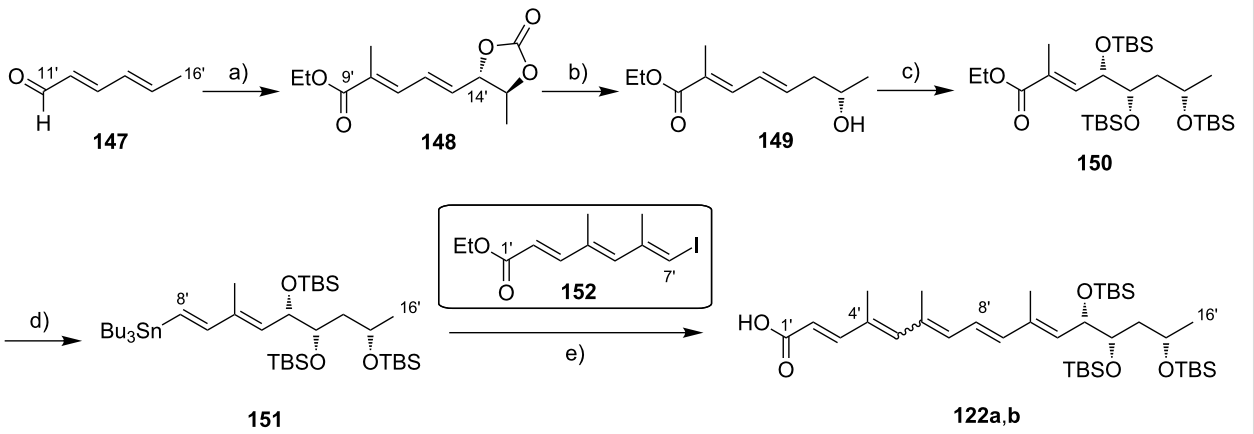

Scheme 22: Blanchard's approach to the mycolactone A/B pentaenoate side chain. a) (i) $Ph_3P{=}C(Me)COOEt$, CH_2Cl_2, rt, 99%; (ii) AD-mix α, $K_2OsO_4{\cdot}2H_2O$ (0.6 mol %), $MeSO_2NH_2$, *t*-BuOH, H_2O, 0 °C, 70%, 86% ee; (iii) triphosgene, pyridine, CH_2Cl_2, rt, 79%; b) $Pd_2(dba)_3{\cdot}CHCl_3$ (0.5 mol %), HCO_2H, Et_3N, THF, rt, 63%; c) (i) TBSCl, imidazole, DMAP, DMF, rt, 93%; (ii) AD-mix α, $K_2OsO_4{\cdot}2H_2O$ (2 mol %), $MeSO_2NH_2$, *t*-BuOH, H_2O, 0 °C, 70%; (iii) TBSCl, imidazole, DMAP, DMF, rt, 83%; d) (i) DIBAL-H, CH_2Cl_2, −78 °C, 97%; (ii) MnO_2, CH_2Cl_2, 94%; (iii) $CrCl_2$, *n*-$Bu_3SnCHBr_2$, LiI, THF/DMF 20:1, rt; e) (i) **152**, CuTC, $Ph_2P(O)OBu_4N$, NMP, rt, 48% (2 steps); (ii) LiOH, THF, H_2O, 92%; (iii) *hv*, acetone, rt, quant.

synthesis of the mycolactone C side chain, as well as our own unpublished work on the latter.

III.2.2.1. Synthesis of the pentaenoate side chain of mycolactone C: At the time when Kishi and co-workers initiated their work on mycolactone C, only a gross structure had been proposed for the compound by the Small [47] and the Leadlay groups [52] (vide supra). Having a suitable route to the mycolactone core in hand, a flexible approach enabling the synthesis of all four possible stereoisomers of the proposed 1,3-diol motif in the pentaenoate side chain was required for Kishi to synthesize mycolactone C and establish its exact structure. Kishi's work departed from the two enantiomers of TBS-protected 3-hydroxybutyraldehyde **17**. The second stereocenter was introduced by Brown asymmetric allylation with allylmagnesium bromide [219] in the presence of (+)- or (−)-Ipc$_2$BOMe, respectively (Scheme 23) [53]. After TBS-protection of the resulting secondary alcohols and ozonolysis of the homoallylic double bond, a two-carbon chain extension was performed by Wittig chemistry to obtain α,β-unsaturated ester **153** (and all of the corresponding stereoisomers). The ester was further processed according to Gurjar and Cherian's protocol to deliver all four C13'/C15' stereoisomers of the putative mycolactone C side chain as 1:1 mixtures of *Z*-$\Delta^{4',5'}$ and *E*-$\Delta^{4',5'}$-isomers. As an example, Scheme 23 shows that the 13'*R*,15'*S*-isomer **154** was obtained in 48% overall yield for the 8-step sequence from (*S*)-3-hydroxybutyraldehyde ((*S*)-**17**).

An alternative, as yet unpublished approach to the mycolactone C fatty acid side chain was recently developed in our own laboratories [220]. The synthesis started with the allylation of 1,3-dithiane (**155**) with allyl bromide (Scheme 24). Deprotonation of the resulting allylated dithiane and quenching with (*S*)-propylene oxide ((*S*)-**38**) yielded (*S*)-configured alcohol **156**.

Unmasking the keto group with iodine under slightly basic conditions followed by a chelation-controlled 1,3-*syn* reduction with $NaBH_4$ in the presence of Et_2BOMe [221] provided a 1,3-diol that was converted into the cyclic di-*tert*-butylsilyl ether **157**. Cleavage of the double bond by ozonolysis followed by a two-carbon elongation via Wittig olefination with 2-(triphenylphosphoranylidene)propanal yielded aldehyde **158**, which was to be submitted to HWE reaction with phosphonate **109**. The HWE reaction, however, proved to be more difficult than for the analogous step in the synthesis of the mycolactone A/B side chain. After some experimentation, it was found that a two-fold excess of deprotonated phosphonate **109** was necessary to consume most (>80%) of the aldehyde **158**. Fortunately, the starting materials could be recovered, yielding 70% of the ethyl pentaenoate as an inseparable 4:1 mixture of the *E*-$\Delta^{4',5'}$ and the *Z*-$\Delta^{4',5'}$-isomers along with 4% of a minor isomer. The ethyl ester smoothly underwent saponification with LiOH to yield acid **159** in 95% yield as a 72:22:6 mixture of the *E*-$\Delta^{4',5'}$-isomer, the *Z*-$\Delta^{4',5}$-isomer and other minor isomers, respectively. This product was obtained from 1,3-dithiane (**155**) in 7 steps and 14% overall yield.

Yet an alternative approach towards the mycolactone C side chain was reported by Blanchard and co-workers in the context of their work on C8-desmethylmycolactone analogs [92]. The synthesis relied on the same logic as their synthesis of the mycolactone A/B side chain (cf. Scheme 22). Briefly, intermediate **149** was protected and stereoselectively dihydroxylated with AD-mix α at the γ,δ-double bond (Scheme 25). The resulting diol **160** was converted into the corresponding cyclic carbonate, defunctionalized in the allylic position with triethylammonium formate/palladium(0) and TBS-protected to provide ester **161**. Transformation of **161** into vinylstannane **162** was achieved by reduction to the corresponding aldehyde followed

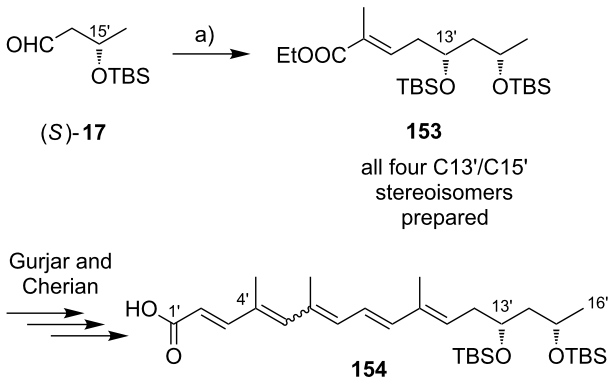

Scheme 23: Kishi's approach to the mycolactone C pentaenoate side chain exemplified for the 13'*R*,15'*S*-isomer **154**. Reagents and conditions: a) (i) (+)-Ipc$_2$BOMe, allylmagnesium bromide, Et_2O, −78 °C, 67%, dr 8:1; (ii) TBSCl, imidazole, DMF, rt; (iii) O_3, CH_2Cl_2, −78 °C, then PPh_3; (iv) Ph_3P=C(Me)COOEt, toluene, 110 °C, 84% (3 steps).

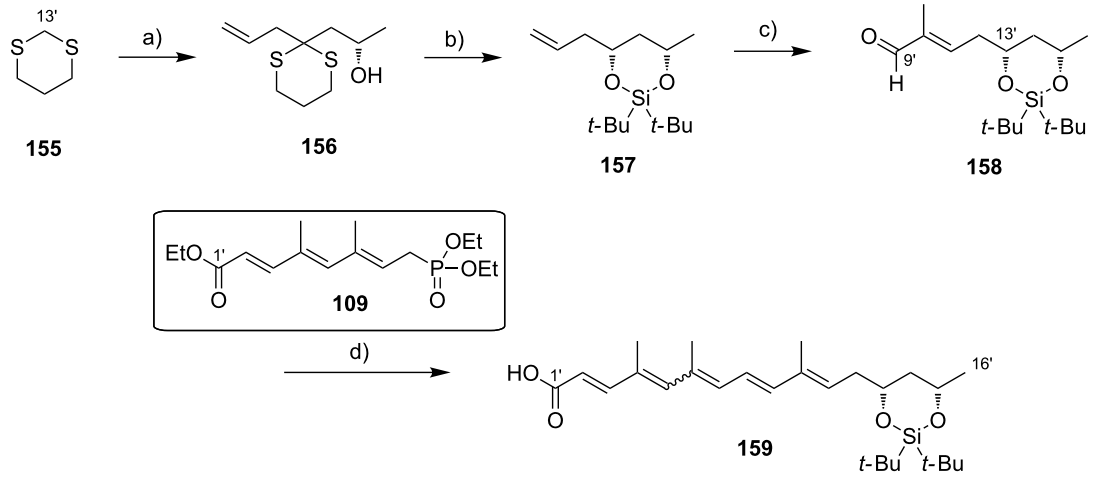

Scheme 24: Altmann's (unpublished) synthesis of the mycolactone C pentaenoate side chain. Reagents and conditions: a) (i) *n*-BuLi, THF, −78 °C, then allyl bromide, −78 °C to rt, 97%; (ii) *n*-BuLi, THF, −10 °C, then (*S*)-propylene oxide, −10 °C, 74%; b) (i) I_2, $NaHCO_3$, MeCN/H_2O 2:1, 0 °C, 85%; (ii) Et_2BOMe, $NaBH_4$, THF, MeOH, −78 °C, 71%, dr 17:1; (iii) *t*-$Bu_2Si(OTf)_2$, pyridine, CH_2Cl_2, 0 °C, 85%; c) (i) O_3, CH_2Cl_2, −78 °C, then PPh_3, 76%; (ii) Ph_3P=C(Me)CHO, benzene, reflux, 77%; d) (i) **109**, LDA, THF, −78 °C to rt, 70%, (*E*-$\Delta^{4',5'}$/*Z*-$\Delta^{4',5'}$ 4:1); (ii) LiOH, THF/H_2O/MeOH 4:1:1, rt, 95% (*E*-$\Delta^{4',5'}$/*Z*-$\Delta^{4',5'}$/minor isomers 72:22:6).

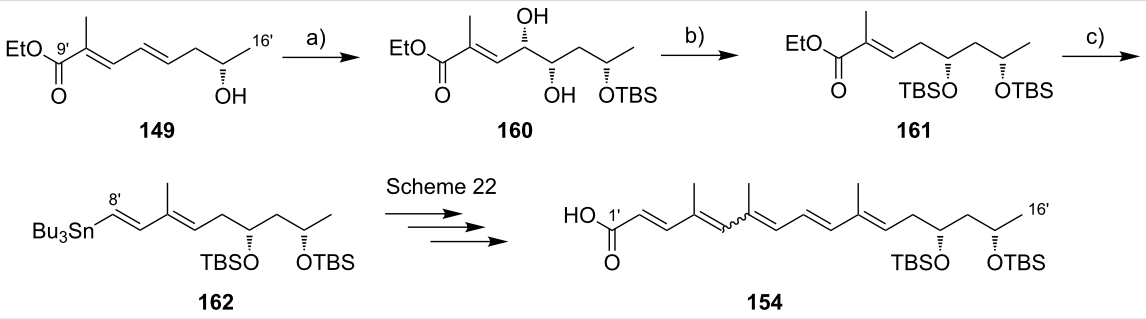

Scheme 25: Blanchard's synthesis of the mycolactone C pentaenoate side chain. Reagents and conditions: a) (i) TBSCl, imidazole, DMAP, DMF, rt, 93%; (ii) AD-mix α, $K_2OsO_4{\cdot}2H_2O$ (2 mol %), $MeSO_2NH_2$, *t*-BuOH/H_2O, 0 °C, 70%; b) (i) triphosgene, pyridine, CH_2Cl_2, 0 °C, 84%; (ii) $Pd_2(dba)_3{\cdot}CHCl_3$ (0.4 mol %), HCO_2H, Et_3N, THF, rt, 95%; (iii) TBSCl, imidazole, DMAP, DMF, rt, 87%; c) (i) DIBAL-H, CH_2Cl_2, 0 °C, 81%; (ii) MnO_2, CH_2Cl_2, reflux, 93%; (iii) $CrCl_2$, CHI_3, THF, rt, 59%; (iv) *n*-BuLi, Et_2O, −78 °C, then *n*-Bu_3SnCl, −78 °C to rt.

by Takai-olefination [222], lithiation and quenching of the vinyllithium intermediate with tributyltin chloride. Intermediate **162** was further processed according to Scheme 22 to obtain the complete lower side chain acid **154** in 15 steps (longest linear sequence) and 0.8% overall yield from *trans*-hexadienal.

III.2.2.2. Synthesis of the tetraenoate side chain of mycolactone F: Kishi and co-workers have also addressed the total synthesis of mycolactone F (**8**) [59], another mycolactone congener, whose gross structure had been inferred from mass spectrometry data, while the relative and absolute configuration of the lower side chain could not be assigned. The Kishi group assumed a *syn*-relationship of the 1,3-diol moiety in analogy to the structures that had been previously established for other mycolactone variants [40,43,53]. Consequently, only the two enantiomers with an *S*,*R* or *R*,*S*-configuration, respectively, at the C11'- and C13'-positions were to be prepared (exemplified by **163**, Scheme 26). Again, the two enantiomers of aldehyde **17** served as starting points for the syntheses, which were identical for both enantiomers. Aldehyde **17** was reacted with allyl bromide in an asymmetric variant of the Nozaki–Hiyama–Kishi coupling reaction [223,224] using ligand **L2**, which had previously been developed by the Kishi group [225]. Interestingly, a Cr/Zr/Mn system was used to promote coupling, which likely improves the overall efficiency of the Nozaki–Hiyama–Kishi reaction [226,227] compared to the Fe/Cr or Co/Cr-mediated variants described in Kishi's initial report. Of note, a subsequent TBS ether cleavage was necessary to remove the minor diastereomer from the allylation step. Reprotection of the diol **163** as the bis-TBS ether and ozonolysis of the homoallylic double bond provided the starting aldehyde for four (almost

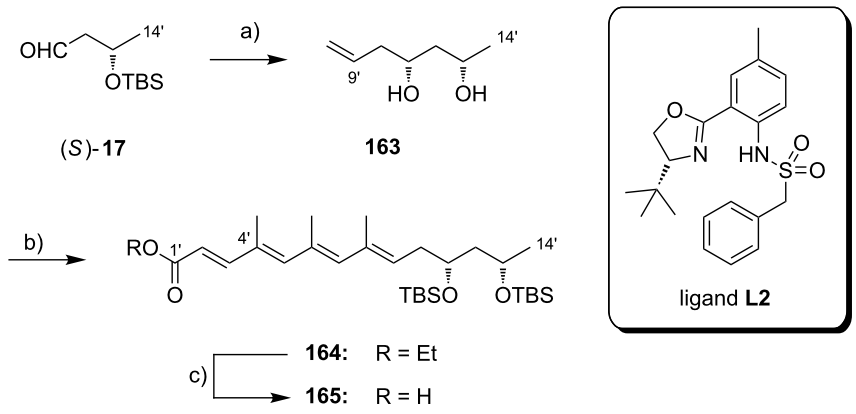

Scheme 26: Kishi's synthesis of the tetraenoate side chain of mycolactone F exemplified by enantiomer **165**. Reagents and conditions: a) (i) $CrCl_3$·3THF, ligand **L2**, Mn, Et_3N, THF, then 2,6-lutidine, allyl bromide, Cp_2ZrCl_2, rt, 83%, dr 14:1; (ii) TBAF, 84% after separation of the minor diastereomer; b) (i) TBSCl, imidazole, DMF, rt, quant.; (ii) O_3, CH_2Cl_2, −78 °C, PPh_3, 83%; (iii) $(EtO)_2P(O)CH(Me)COOEt$, *n*-BuLi, THF, 0 °C; (iv) DIBAL-H, CH_2Cl_2, −78 °C; (v) MnO_2, CH_2Cl_2, 72% (3 steps); (vi) $(EtO)_2P(O)CH(Me)COOEt$, *n*-BuLi, THF, 0 °C; (vii) DIBAL-H, CH_2Cl_2, −78°C; (viii) MnO_2, CH_2Cl_2, 62% (3 steps); (ix)–(xi) repeat steps vi–viii, 36% (3 steps); (xii) $(EtO)_2P(O)CHCOOEt$, *n*-BuLi, THF, 0 °C, 90%; c) LiOH, THF/MeOH/H_2O 4:1:1, rt, 89%.

identical) HWE elongation cycles, leading to ethyl tetraenoate **164**. Base-mediated saponification then smoothly furnished acid **165** in 15 linear steps and 7.8% overall yield from aldehyde (*S*)-**17**.

In contrast to the pentaenoate series, the predominant product (>98%) of ethyl tetraenoate **164** was the all-*E* isomer, which was stable under the ester hydrolysis conditions. However, **164** could be equilibrated to a 4:3:3 mixture with its *Z*-$\Delta^{4',5'}$ and the *Z*-$\Delta^{6',7'}$-isomers by irradiation at 300 nm. Of note, the two minor geometric isomers of ester **164** were also prepared separately via a similar route using the Ando modification of the HWE reaction [228] to construct the *Z*-double bonds.

III.2.2.3. Synthesis of the tetraenoate side chain of mycolactone E and its minor metabolite: When Kishi and co-workers initiated their work on mycolactone E (**7**), two possible gross structures differing in the constitution of the polyunsaturated side chain (cf. Figure 2) had been proposed, again by the groups of Small [50] and Leadlay [56]. After re-examination of the available analytical data the Kishi group favored Leadlay's structure, which only differed from the gross structure of mycolactone F (**8**) by the replacement of a methyl by an ethyl group at the terminal position of the polyunsaturated side chain [57]. Consequently, a similar synthesis strategy was chosen as for the mycolactone F fatty acid side chain. Although a *syn*-relationship of the 1,3-diol moiety was assumed, the absolute configuration was again unknown. Therefore, the Kishi group prepared both enantiomers of this tetraenoate. The synthesis was launched by a copper(I)-promoted regioselective opening of either enantiomer of 1,2-butylene oxide (**166**) with vinylmagnesium bromide**,** thus defining the stereochemistry at the C13' position (exemplified in Scheme 27 by the synthesis of **169**).

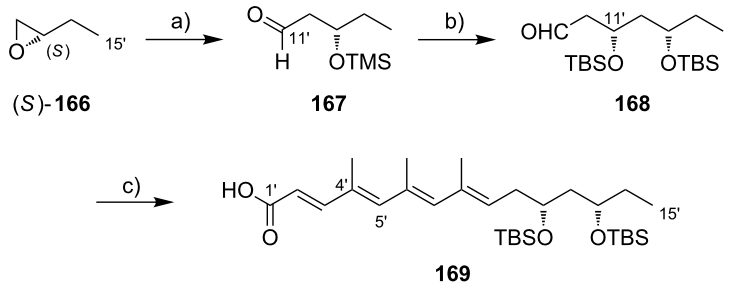

Scheme 27: Kishi's synthesis of the mycolactone E tetraenoate side chain. Reagents and conditions: a) (i) CH_2=CHMgBr, CuI, Et_2O, −30 °C to −20 °C; then TMSCl, DIPEA, −20 °C to 0 °C; (ii) OsO_4, NMO, H_2O, rt; (iii) $Pb(OAc)_4$, benzene, rt, 67% (3 steps); b) (i) ligand **L2***, $CrBr_3$, Mn, Et_3N, THF, 42 °C, then 2,6-lutidine, rt, then allyl bromide, aldehyde, Cp_2ZrCl_2, 0 °C; then 0.5 N HCl, rt, 55%, dr 95:5; (ii) TBSCl, imidazole, DMF, rt, 86%; (iii) OsO_4, NMO, H_2O, rt; (iv) $Pb(OAc)_4$, benzene, rt, 93% (2 steps); c) (i) $(EtO)_2P(O)CH(Me)COOEt$, *n*-BuLi, LiBr, THF, 0 °C, 95%; (ii) DIBAL-H, CH_2Cl_2, −78 °C, 89%; (iii) MnO_2, CH_2Cl_2, rt, 94%; (iv)–(ix) 2× repeat steps i–iii, 40% (6 steps); (x) $(EtO)_2P(O)CHCOOEt$, *n*-BuLi, THF, 0 °C to rt, 87%; (xi) LiOH, THF/MeOH/H_2O 4:1:1, rt, 96%.

Subsequent TMS protection of the resulting alcohol and oxidative cleavage of the double bond afforded aldehyde **167**which was subjected to the Cr/Zr/Mn-mediated Nozaki–Hiyama–Kishi coupling reaction, in analogy to the synthesis of the mycolactone F side chain (using a slightly modified version of ligand **L2** (not shown here)). After TMS cleavage and global TBS protection of the resulting diol, oxidative double bond cleavage delivered aldehyde **168**. The latter was then elaborated into tetraenoate **169** by the same sequence of transformations as in the synthesis of mycolactone F. **169** was obtained as the all-*E*-isomer in 18 linear steps and 7.9% overall yield starting from (*S*)-1,2-butylene oxide ((*S*)-**166**).

An alternative route to prepare the mycolactone E tetraenoate side chain acid was recently reported by Wang and Dai [229]. They aimed to provide a more convergent strategy that would combine a western triene fragment with an alkene bearing the chiral 1,3-diol moiety via Suzuki–Miyaura cross-coupling [230,231] thereby demonstrating the utility of their Aphos-$Pd(OAc)_2$ catalyst system [232]. The synthesis of the trienyl bromide fragment **172** started from methyl methacrylate (**170**) that was transformed into the corresponding *E*-vinyl bromide via a bromination/elimination sequence (Scheme 28). $LiAlH_4$ reduction to the alcohol, allylic oxidation with MnO_2 and Wittig olefination of the ensuing aldehyde afforded dienyl bromide **171**. Another reduction/oxidation sequence followed by HWE olefination with trimethyl phosphonoacetate furnished trienyl bromide **172** in seven steps and 41% yield from methyl methacrylate. Only a single intermediate in this sequence required purification. The eastern fragment was accessed from methyl (*S*)-3-hydroxyvalerate ((*S*)-**173**), which was homologated to **174** in a four-step sequence involving a HWE olefination. The second hydroxy group was diastereoselectively introduced by intramolecular conjugate addition of the hemiacetal-derived alkoxide formed from **174** and benzaldehyde in the presence of potassium *tert*-butoxide [233]. After replacing the benzaldehyde acetal in **175** by a cyclic di-*tert*-butylsilyl ether, the selective reduction of the methyl ester to the corresponding alde-

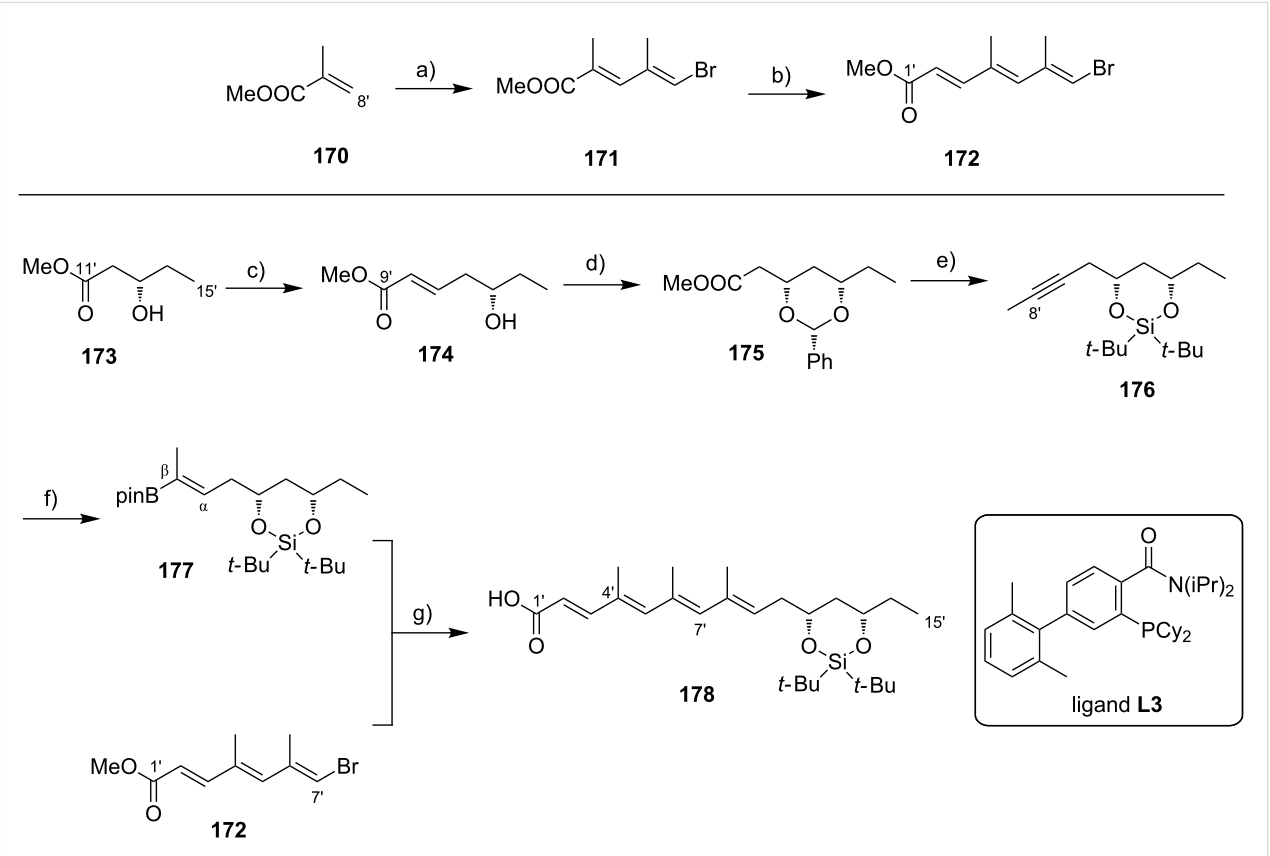

Scheme 28: Wang and Dai's synthesis of the mycolactone E tetraenoate side chain. Reagents and conditions: a) (i) Br_2, CCl_4, rt, then DBU, CCl_4, rt; (ii) $LiAlH_4$, CH_2Cl_2, 0 °C; (iii) MnO_2, CH_2Cl_2, rt; (iv) $Ph_3P{=}C(Me)COOEt$, CH_2Cl_2, 0 °C to rt, 63% (4 steps); b) (i) DIBAL-H, CH_2Cl_2, 0 °C; (ii) MnO_2, CH_2Cl_2, rt; (iii) $(MeO)_2P(O)CH_2COOMe$, NaH, THF, −78 °C, 65% (3 steps); c) (i) TBSCl, imidazole, CH_2Cl_2, rt, 98%; (ii) DIBAL-H, CH_2Cl_2, 0 °C, 85%; (iii) DMP, CH_2Cl_2, $NaHCO_3$, rt, 86%; (iv) $(MeO)P(O)CH_2COOMe$, NaH, THF, −78 °C, 85%, 9:1 *E*/*Z*; (v) PPTS, MeOH, 50 °C, 85%; d) PhCHO, *t*-BuOK, THF, 0 °C, 65%; e) (i) H_2, $Pd(OH)_2$, MeOH, rt, 90%; (ii) *t*-$Bu_2Si(OTf)_2$, 2,6-lutidine, DMF, rt, 85%; (iii) DIBAL-H, CH_2Cl_2, −78 °C, 92%; (iv) CBr_4, PPh_3, Et_3N, CH_2Cl_2, 93%; (v) *n*-BuLi, −78 °C, THF, then MeI, rt, 90%; f) $B_2(pin)_2$, CuCl (10 mol %), PCy_3, *t*-BuONa, MeOH, toluene, rt, 75%, α:β 92.5:7.5; g) (i) $Pd(OAc)_2$ (5 mol %), ligand **L3**, K_3PO_4, THF/H_2O, 35 °C, 85%; (ii) LiOH, $THF/MeOH/H_2O$ 4:1:1, rt, 90%.

hyde followed by a Corey–Fuchs alkynylation/methylation sequence furnished alkyne **176**. The stereo- and regioselective transformation of **176** into trisubstituted alkenyl boronate **177** was accomplished using a [Cu(I)PCy_3]-catalyzed borylation [234]. The key Suzuki–Miyaura cross-coupling reaction was performed in 85% yield using the Aphos-Y ligand (**L3**) [232] under conditions that had been carefully optimized with a model substrate. The resulting methyl tetraenoate could be readily hydrolyzed to acid **178**. The latter was obtained in a longest linear sequence of 13 steps in 11% overall yield from (*S*)-**173**.

When Kishi and co-workers set out to synthesize the minor oxo-metabolite of mycolactone E, its structure had not been unambiguously assigned [58] and the structural proposal [56] still needed to be confirmed by other means. Kishi and co-workers developed a synthesis relying on multicomponent anion relay chemistry [235] and iterative Horner–Wadsworth–Emmons elongation cycles. Starting from (*R*)-epichlorohydrin ((*R*)-**179**), epoxide opening with vinylmagnesium bromide in the presence of catalytic amounts of copper iodide followed by base-promoted intramolecular nucleophilic substitution of the ensuing chlorohydrin furnished epoxide **180** (Scheme 29). One-pot tandem alkylation of 2-TBS-1,3-dithiane with epoxide **180** and ethyl iodide exploiting an anion-relay mechanism, followed by oxidative cleavage of the terminal double bond gave aldehyde **181**, which was elaborated into α,β-unsaturated ester **182** by HWE chemistry.

Three subsequent reduction/oxidation/HWE-elongation cycles yielded ethyl tetraenoate **183** which was saponified to obtain acid **184**. The latter, which corresponds to the 1,3-dithiane and TBS-protected lower side chain of the mycolactone E minor metabolite, was obtained in 16 linear steps and 18% overall yield from (*R*)-epichlorohydrin ((*R*)-**179**).

III.2.2.4. Synthesis of the pentaenoate side chains of mycolactones S1 and S2: The synthesis of mycolactones S1 (**4**) and S2 (**5**) was reported by the Kishi group in 2012 [62]. After identification of those congeners from *M. ulcerans* subsp. *shinshuense* extracts by using their fluorogenic TLC method (vide supra), structural hypotheses were generated on the basis of (HR) MS/MS profiles. While mycolactone S1 (**4**) was assumed to be the C15' keto analog of mycolactone A/B (**1a**,**b**), mycolactone S2 (**5**) was speculated to possess the C15' keto group along with an additional hydroxy group at the C14' position. In analogy to Kishi's approach to the mycolactone E fatty acid side chain, the synthesis of the putative mycolactone S1 pentaenoate chain departed from (*S*)-propylene oxide ((*S*)-**38**), which was opened by copper(I)-mediated addition of vinylmagnesium bromide (Scheme 30). α,β-Unsaturated ester **185** was then obtained by PMB protection of the newly formed hydroxy group and subsequent Lemieux–Johnson oxidation [148] of the homoallylic double bond followed by a HWE olefination. Stereoselective introduction of the vicinal *syn*-diol by Sharpless dihydroxylation followed by TBS protection gave ester **186**. A subsequent reduction/oxidation/Wittig elongation cycle furnished the corresponding α,β-unsaturated ester. After PMB removal, several redox manipulations finally provided keto-aldehyde **187** in 12 steps and 28% overall yield from commercially available (*S*)-**38**. Compound **187** was elaborated into the full length side chain acid **188** using the same strategy as in the synthesis of the mycolactone A/B side chain (see Scheme 15). In the case of mycolactone S2, both C14'-epimers

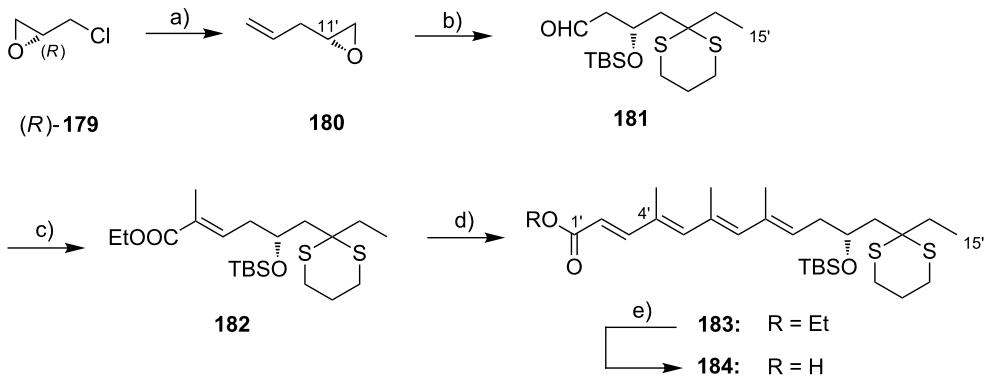

Scheme 29: Kishi's synthesis of the dithiane-protected tetraenoate side chain of the minor oxo-metabolite of mycolactone E. Reagents and conditions: a) (i) CH_2=CHMgBr, cat. CuI, Et_2O, −78 °C to −40 °C, 92%, ee >95% as determined by Mosher ester analysis [236]; (ii) KOH, distillation, 91%; b) (i) *t*-BuLi, 2-TBS-1,3-dithiane, Et_2O, then EtI, HMPA, −78 °C to −25 °C, 64%; (ii) OsO_4, $K_3Fe(CN)_6$, DABCO, $MeSO_2NH_2$, *t*-BuOH/H_2O, 0 °C; (iii) $Pb(OAc)_4$, benzene, 0 °C, 57% (two steps); c) (i) $(EtO)_2P(O)CH(Me)COOEt$, *n*-BuLi, LiBr, MeCN, 0 °C to rt, 94%, *E*/*Z* 94:6; d) three HWE elongation cycles: (i) DIBAL-H, CH_2Cl_2, −78 °C; (ii) MnO_2, CH_2Cl_2, rt; (iii) $(EtO)_2P(O)CH(Me)COOEt$ or $(EtO)_2P(O)CH_2COOEt$, *n*-BuLi, THF, 0 °C to rt, 72–95% over three steps, *E*/*Z* between 95:5 and 98:2; e) LiOH, THF/MeOH/H_2O, 4:1:1 rt, quant.

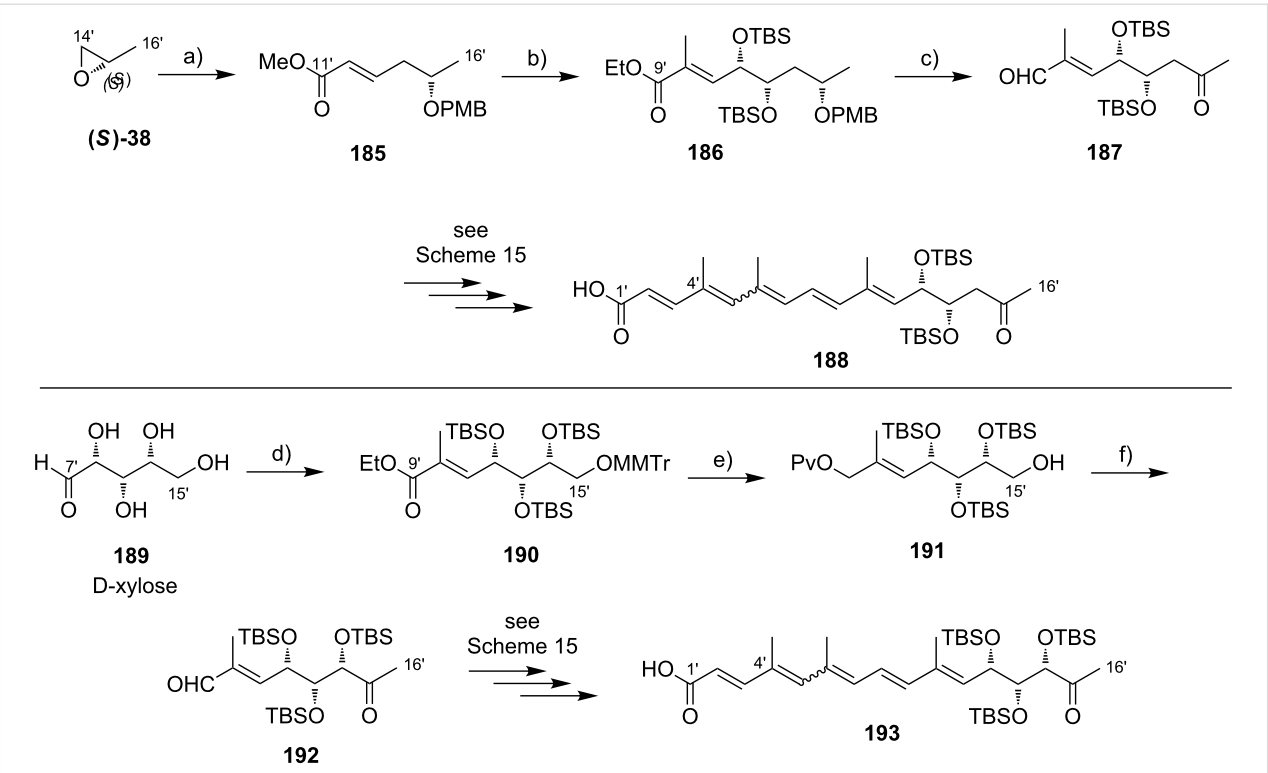

Scheme 30: Kishi's synthesis of the mycolactone S1 and S2 pentaenoate side chains. Reagents and conditions: a) (i) CH_2=CHMgBr, CuI (10 mol %), Et_2O, −30 °C to −20 °C; (ii) PMBBr, NaH, THF, DMF, 0 °C to rt, 87% (2 steps); (iii) OsO_4 (1 mol %), $NaIO_4$, 2,6-lutidine, dioxane, H_2O, rt; (iv) Ph_3P=CHCOOMe, toluene, 80 °C, 70% (2 steps); b) (i) AD mix-α, $MeSO_2NH_2$, dioxane, H_2O, 0 °C, dr 8:1; (ii) TBSCl, $AgNO_3$, pyridine, DMF, rt, 87% (2 steps); c) (i) DIBAL-H, CH_2Cl_2, −78 °C, 80% (major diastereomer); (ii) SO_3·pyridine, DIPEA, DMSO, CH_2Cl_2, rt, 95%; (iii) Ph_3P=C(Me)COOEt, toluene, 90 °C; (iv) DIBAL-H, CH_2Cl_2, −78 °C, 78% (2 steps); (v) DDQ, CH_2Cl_2, H_2O, 0 °C, 94%; (vi) DMP, $NaHCO_3$, CH_2Cl_2, rt, 90%; d) (i) $EtO_2CCH(Br)Me$, Zn, *n*-Bu_3P, 1,4-dioxane, 100 °C, 56%, 3:1 *E*/*Z*; (ii) MMTrCl, pyridine, 0 °C, 70% (*E*-isomer); (iii) TBSCl, $AgNO_3$, pyridine, DMF, rt, quant.; e) (i) DIBAL-H, CH_2Cl_2, −78 °C; (ii) PvCl, pyridine, DMAP, CH_2Cl_2, 0 °C, 98% (2 steps); (iii) HCO_2H, Et_2O, rt, 88%; f) (i) SO_3·pyridine, DIPEA, DMSO, CH_2Cl_2, rt, 95%; (ii) MeMgCl, Et_2O, THF, 0 °C to rt, 93%; (iii) DMP, $NaHCO_3$, CH_2Cl_2, rt, 84%.

were prepared since the local stereochemistry could not be deduced from the preliminary mass spectrometric analysis. The C14' α-epimer, which is exemplified in Scheme 30, was accessed from D-xylose (**189**), which already incorporates the correctly configured C12'–C14' stereotriad. Two-carbon elongation by zinc-mediated coupling with ethyl bromopropionate [237] followed by 4-methoxytrityl protection (MMTr) of the primary hydroxy group and subsequent TBS protection of the remaining alcohol groups furnished the α,β-unsaturated ester **190**. Reduction to the primary alcohol followed by protection with pivaloyl chloride and acid-mediated cleavage of the MMTr ether furnished **191**, bearing a free primary hydroxy group at the C15' position. Swern oxidation to the corresponding aldehyde was succeeded by the addition of methylmagnesium chloride, with concurrent cleavage of the pivaloyl ester. The resulting diastereomeric mixture of diols was oxidized to key ketoaldehyde **192** again being processed according to the procedure presented in Scheme 15 to deliver pentaenoate **193** in 11 steps and 12% overall yield from **189**. The C14' β-epimer was prepared from L-arabinose in similar yields using the same strategy.

III.3. Total synthesis of natural mycolactones

So far, total syntheses have been successfully completed for mycolactones A/B, C, E, (*dia*)-F, S1 and S2. All of the syntheses feature the same general endgame, including Yamaguchi-type esterification of the C5-hydroxy group with the respective, protected polyunsaturated side chain acid followed by protecting group removal. If a global TBS-protection strategy was employed, deprotection with TBAF as the fluoride source was performed in a single step. If the hydroxy groups at the core extension (upper side chain) were protected as a cyclopentylidene ketal (cf. structure **28**), initial removal of the side chain TBS groups with TBAF was followed by ketal cleavage under mildly acidic conditions to complete the synthesis.

Specifically, Kishi's 1st generation approach towards mycolactone A/B (**1a,b**) [43] relied on TBS protection of the lower side chain hydroxy groups, while the 1,3-diol at the core extension was protected as a cyclopentylidene ketal (Scheme 31). The same protecting group strategy was also part of Negishi's projected individual syntheses of mycolactone A (**1a**) and mycolactone B (**1b**) [37], while in the mycolactone total synthe-

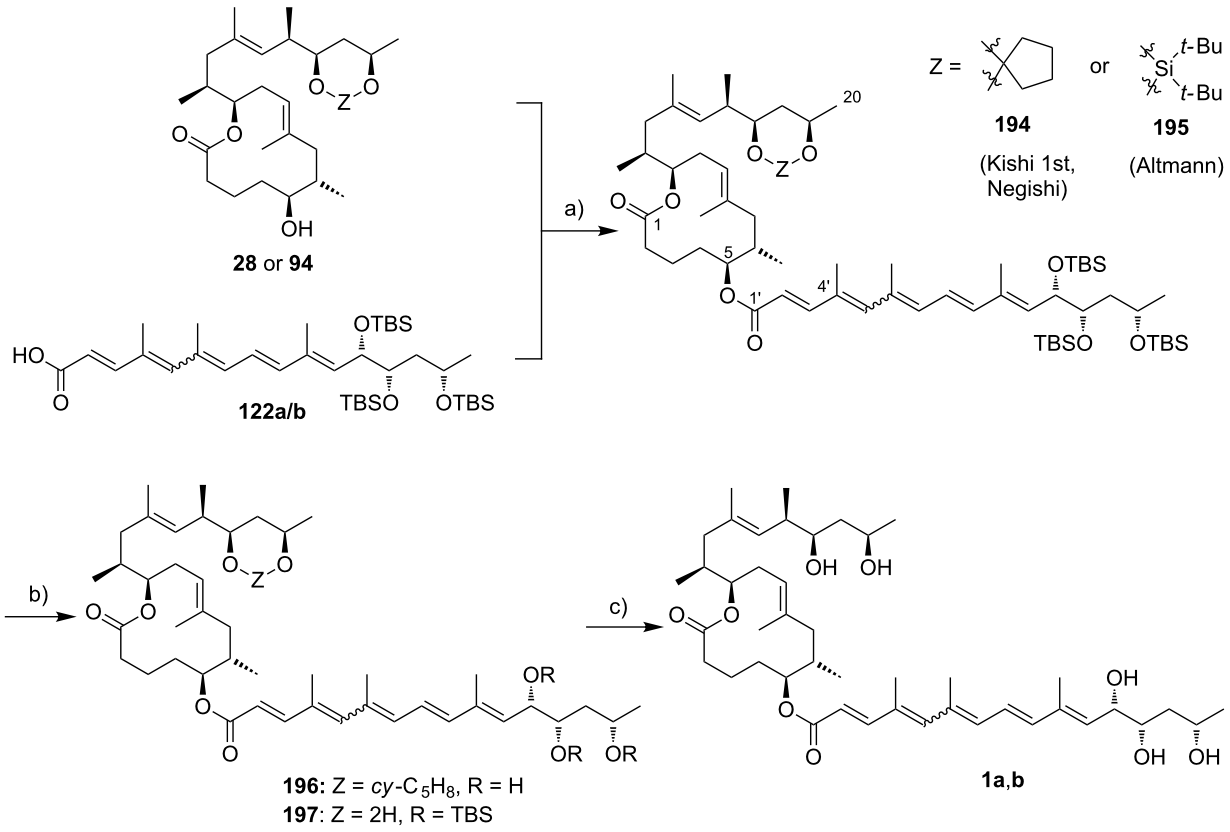

Scheme 31: Kishi's 1st generation and Altmann's total synthesis of mycolactone A/B (**1a**,**b**) and Negishi's selective synthesis of protected mycolactone A and B and their isomerization upon deprotection. Reagents and conditions: Kishi 1st generation approach*:* a) 2,4,6-trichlorobenzoyl chloride, DIPEA, DMAP, benzene, rt, 90%; b) TBAF, THF, rt, 81%; c) THF/HOAc/H_2O, 2:2:1, rt, and the recovered starting material was recycled (once), 67% (*E*/*Z*-$\Delta^{4',5'}$ 2:3). Negishi's synthesis starting from *Z*-$\Delta^{4',5'}$-**122**: a) 2,4,6-trichlorobenzoyl chloride, DIPEA, DMAP, benzene, rt, 6 h, 67%, >98% isomeric purity; b) TBAF, THF, rt, 71%, (*E*/*Z*-$\Delta^{4',5'}$ ca. 1:4); c) THF/HOAc/H_2O, 2:2:1, rt, 11 h and the recovered starting material was recycled (once), 59% (*E*/*Z*-$\Delta^{4',5'}$ ca. 3:4). Negishi's synthesis starting from *E*-$\Delta^{4',5'}$-**122***:* a) 2,4,6-trichlorobenzoyl chloride, DIPEA, DMAP, benzene, rt, 73%, >98% isomeric purity; b) TBAF, THF, rt, 70% (*E*/*Z*-$\Delta^{4',5'}$ ca. 2:5); c) THF/HOAc/H_2O, 2:2:1, rt, and the recovered starting material was recycled (once), 64% (*E*/*Z*-$\Delta^{4',5'}$ ca. 4:5). Altmann's approach*:* a) 2,4,6-trichlorobenzoyl chloride, DIPEA, DMAP, THF, rt, 89%; b) HF·pyridine, THF/pyridine 4:1, rt, 84%; c) TBAF, THF, rt, 85% (*E*/*Z*-$\Delta^{4',5'}$ ca. 1:1, 10% minor isomers).

ses from our own laboratory used a cyclic bis-*tert*-butylsilyl ether was used to mask the 1,3-diol motif at the core extension. In all cases, Yamaguchi esterification of the partially protected extended core structure proceeded smoothly to give the fully protected mycolactones **194** or **195**. While the polyunsaturated side chain acid in Kishi's case was a 2:3 *E*/*Z* mixture at the C4'–C5' double bond, Negishi employed the pure *E*- and *Z*-$\Delta^{4',5'}$ isomers, which had been obtained in separate syntheses (vide supra). The isomeric state of the side chain was maintained during the esterification reaction and in all three cases TBS deprotection with TBAF typically proceeded in good yield. However, despite the exclusion of light, partial isomerization of the C4'–C5' double bond took place under these conditions, leading to isomeric product mixtures, even for the isomerically homogenous protected versions. Final removal of the cyclopentylidene ketal with acetic acid generally afforded the free mycolactones **1a**,**b** in moderate yield and further isomerization of the C4'–C5' double bond was observed by Negishi. In summary, Kishi's 1st generation approach employed a total of 20 steps for the longest linear sequence (from known **20**) and gave mycolactone A/B (**1a,b**) in 0.63% yield. Negishi's total synthesis departed from (*R*)-methyl 3-hydroxybutyrate ((*R*)-**47**) and comprises 26 steps for the longest linear sequence. The mycolactones A/B were obtained and 2.8% overall yield, when using the *E*-$\Delta^{4',5'}$-isomer of the lower side chain acid in the esterification step.

For our own total synthesis of mycolactone A/B (**1a,b**), the final deprotection involved first the cleavage of the bis-*tert*-butylsilyl ether in **195** with pyridine-buffered HF·pyridine followed by TBAF-mediated removal of the TBS protecting groups from the lower side chain (Scheme 31) [178]. This two-step sequence furnished mycolactone A/B as a 1:1 mixture of the *E*-$\Delta^{4',5'}$ and the *Z*-$\Delta^{4',5'}$ isomer containing ca. 10% of minor isomers. The

two-step procedure was required since extended treatment of **195** with buffered HF·pyridine, as it was required for TBS cleavage, caused partial decomposition, while TBAF alone did not efficiently remove the cyclic silyl-ether protecting group. More recently, however, we have found that the sequential addition of TBAF followed by an excess of ammonium fluoride allowed for efficient, one-pot global deprotection [111]. Overall, our synthesis comprises a longest linear sequence of 19 steps and produced the target structure in 13% overall yield according to [178]. The synthesis, thus, is significantly more efficient than either Kishi's 1st generation approach or the Negishi synthesis although recent unpublished optimizations (vide supra) were not considered.

In contrast to his first generation synthesis, Kishi's 2nd generation approach to mycolactone A/B (**1a,b**) incorporated a global TBS-protection strategy that was also maintained in his 3rd generation approach towards the mycolactone core and in all syntheses of other mycolactone congeners (Scheme 32). Global TBS deprotection of **198** with TBAF furnished the typical mixture of mycolactones A and B.

Interestingly, and contrary to the observations by Negishi and co-workers, the Kishi group found *E*/*Z* isomerization of the C4'–C5' double bond under their TBAF deprotection conditions to be less pronounced. Thus, deprotection of a chromatographically enriched mixture of **198** predominantly containing the *Z*-$\Delta^{4',5'}$-isomer (10:1) yielded a 6:1 mixture of **1a** and **1b**, if light was carefully excluded. With a longest linear sequence of 21 steps and an overall yield of 8.9%, Kishi's 2nd generation synthesis of mycolactone A/B represented a significant advance over his 1st generation approach.

Kishi's syntheses of other natural mycolactones uniformly relied on the 2nd generation strategy developed for the synthesis of mycolactones A/B (**1a,b**) and will therefore not be discussed here in detail. Briefly, mycolactone C (**2**) was prepared in two steps from the partially TBS-protected mycolactone core **37** and the TBS-protected mycolactone C side chain **154** as an equimolar mixture of *Z*-$\Delta^{4',5'}$ and *E*-$\Delta^{4',5'}$-isomers in 76% yield [53]. The same two-step procedure gave mycolactones E (**6**) and *dia*-F (*dia*-**8**) in 62% and 56% yield, respectively [57,59]. Both, mycolactone E and mycolactone *dia*-F, were obtained as 100:4:4 mixtures of the all-*E*, the *Z*-$\Delta^{4',5'}$ and the *Z*-$\Delta^{6',7'}$ isomers, respectively. The minor metabolite of mycolactone E was prepared in a similar manner using side chain acid **184**; however, dithiane deprotection mediated by *N*-chlorosuccinimide and silver nitrate had to be performed prior to global TBAF-promoted silyl ether cleavage. The latter was relatively inefficient (44% yield) and product **7** was finally obtained in 3 steps and 35% yield [58]. Another minor modification of the strategy had to be made to prepare the two oxidized congeners mycolactones S1 (**4**) and S2 (**5**) [62]. While Yamaguchi esterification with the respective side chain acids uneventfully provided the protected mycolactones, TBAF-mediated deprotection resulted in a complex mixture of products. Ultimately, buffering the TBAF solution with imidazole hydrochloride cleanly furnished the desired products, although extended reaction times (5 d) were necessary. Mycolactones S1, S2-14'α and S2-14'β were obtained as the typical $\Delta^{4',5'}$*E*/*Z* mixtures in 58%, 74% and 94% yield, respectively (over two steps). Finally, natural mycolactone S2 was proven to be equivalent to S2-14'α.

Our own approach towards mycolactone C (**2**) also relied on Yamaguchi esterification of the mycolactone core with the

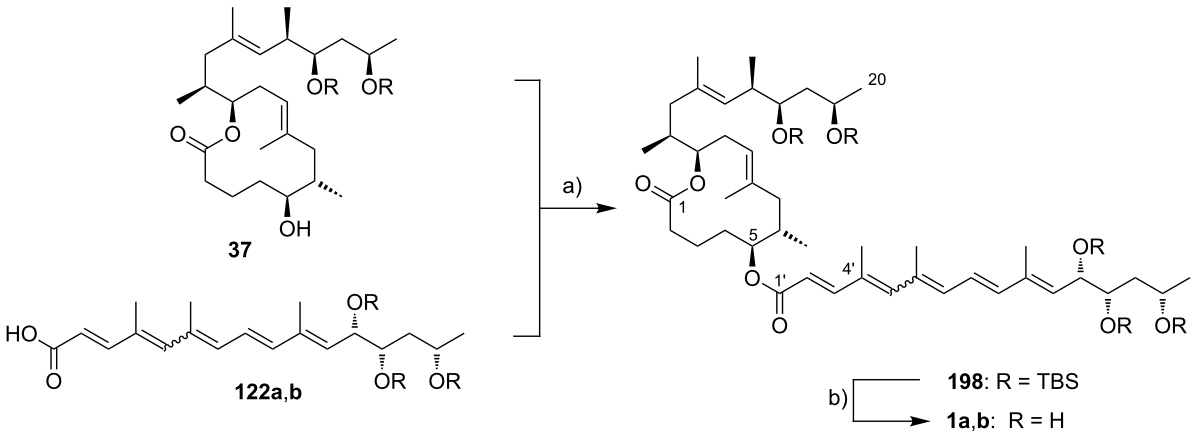

Scheme 32: Kishi's 2nd generation total synthesis of mycolactone A/B (**1a**,**b**). Reagents and conditions: a) 2,4,6-trichlorobenzoyl chloride, DIPEA, DMAP, benzene, rt, 90%; b) TBAF, THF, rt, 80% (*E*/*Z*-$\Delta^{4',5'}$ 2:3).

mycolactone C fatty acid side chain, both being protected as cyclic bis-*tert*-butylsilyl ethers. In contrast to the lower mycolactone A/B side chain, the mycolactone C pentaenoate chain was tolerant to pyridine-buffered HF·pyridine, thus enabling smooth global deprotection. Mycolactone C (**2**) was obtained in 59% yield over two steps as a 66:27:7 mixture of isomers (E-$\Delta^{4',5'}$/Z-$\Delta^{6',7'}$/minor).

IV. Synthesis of mycolactone analogs

IV.1. Modifications of the extended mycolactone core

In 2011, Blanchard and co-workers reported a synthesis of the extended C8-desmethylmycolactone core, which is strategically related to our own approach towards the analogous "natural" fragment (Scheme 33, cf. Scheme 7 and Scheme 8). The key steps in Blanchard's synthesis of the 8-desmethylmycolactone core include the closure of the macrolactone ring by RCM and the attachment of the C14−C20 core extension to the C13 atom via C(sp^2)–C(sp^3) cross-coupling. The synthesis started from (*S*)-Roche ester (*S*)-**70**, which was tosylated and converted into aldehyde **199**. The latter served as the substrate for a subsequent asymmetric Brown allylation that was performed either with (−)- or (+)-Ipc_2B(allyl)borane to furnish *syn*- and *anti*-**200**, respectively. The *syn*-diastereomer was TBS protected and subjected to cross metathesis with acrylic acid in methylene chloride under microwave heating using Grubbs 2nd generation catalyst. The double bond of the resulting acrylate **201** was reduced by hydrogenation in the presence of Pearlman's catalyst and the tosylate was converted to the corresponding iodide under Finkelstein conditions. By applying Cossy's iron-mediated C(sp^2)–C(sp^3) cross-coupling methodology [238], alkyl iodide **202** was fused with vinylmagnesium bromide to produce alkene **203**. Interestingly, no protection of the carboxylic acid moiety was required in the presence of an excess of vinylmagesium bromide. Acid **203** was activated with DCC and esterified with *anti*-**200** under Steglich conditions to produce diene **204**. This diene readily underwent RCM-mediated cyclization with Grubbs 2nd generation catalyst again in overheated methylene chloride. After cyclization, the C13 tosylate was transformed into the corresponding alkyl iodide **205** under Finkelstein conditions, which was then connected with known vinyl iodide **35** by Negishi cross-coupling.

Treatment of the coupling product with HF·pyridine only led to cleavage of the C5-TBS ether (producing **206**), while global silyl ether cleavage to **207** occurred only after extended reac-

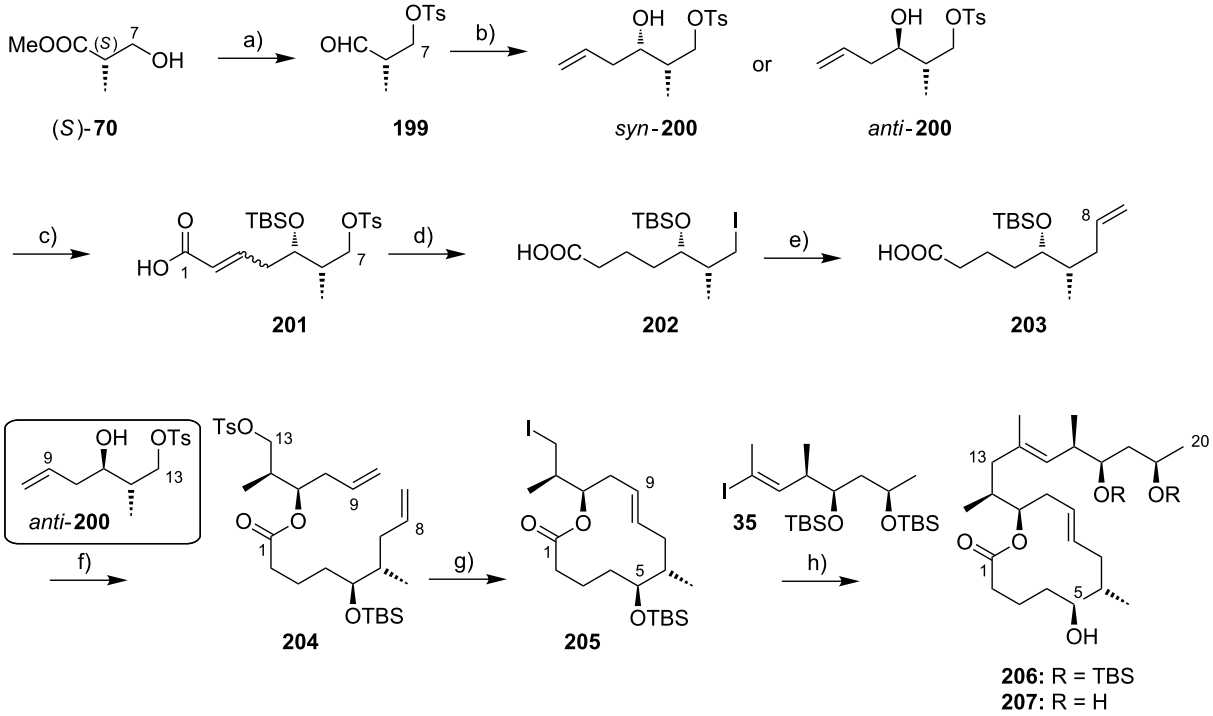

Scheme 33: Blanchard's synthesis of the 8-desmethylmycolactone core. Reagents and conditions: a) (i) TsCl, TEA, DMAP, CH_2Cl_2, 0 °C to rt; (ii) DIBAL-H, toluene, −78 °C to rt, 87% (2 steps); (iii) TEMPO (10 mol %), $PhI(OAc)_2$, CH_2Cl_2, 10 °C to rt; b) (−)- or (+)-$Ipc_2Ballyl$, Et_2O, −78 °C, then $NaBO_3{\cdot}4H_2O$, 70%, dr > 97:3 for *syn*-**200** and 76%, dr > 97:3 for *anti*-**200**; c) (i) TBSCl, imidazole, CH_2Cl_2, rt, 95%; (ii) acrylic acid, Grubbs II (3 mol %), CH_2Cl_2, 90 °C (μw); d) (i) H_2, $Pd(OH)_2$, EtOAc, 79% (2 steps); (ii) NaI, acetone, reflux, 90%; e) (i) vinylmagnesium bromide, $FeCl_3$ (20 mol %), TMEDA, THF, 0 °C, 51%; f) *anti*-**200**, DCC, DMAP, CH_2Cl_2, 0 °C to rt, 82%; g) (i) Grubbs II (10 mol %), CH_2Cl_2, 90 °C (μw), 83%; (ii) NaI, acetone, reflux, 92%; h) (i) Li, naphthalene, $ZnCl_2$, THF, rt, then **205**, benzene/DMF 15:1, rt, then **35**, $Pd(PPh_3)_4$ (13 mol %), LiCl, NMP, 55 °C, 63%; (ii) HF·pyridine, pyridine, THF, 0 °C, 4 h (yields **206**) or 15 h (yields **207**), **206**: 42% or **207**: 81%.

tion times. The extended C8-desmethylmycolactone core was prepared in 14 steps (longest linear sequence) and 6.7% overall yield from (*S*)-Roche ester ((*S*)-**70**).

A modified version of the extended mycolactone core with a hydroxy tag at the C20 position was designed in our own group [90,111]. The additional hydroxy group enables the attachment of various residues for SAR and target elucidation studies. The synthesis started from commercially available (*R*)-glycidol ((*R*)-**208**), thus immediately setting the configuration of the C19 stereocenter (Scheme 34). PMB protection of the primary hydroxy group followed by regioselective copper(I)-mediated epoxide opening with vinylmagnesium bromide furnished homoallylic alcohol **209** that was TBS protected and subjected to oxidative double bond cleavage under Upjohn/Lemieux–Johnson conditions. The ensuing aldehyde **210** was subjected to an asymmetric Evans aldol addition to simultaneously establish the stereochemistry at the C16 and C17 positions in **211**.

Replacement of the TBS protecting group by a cyclic di-*tert*-butylsilyl ether blocking the 1,3-diol followed by reductive removal of the Evans auxiliary with $NaBH_4$ then gave primary alcohol **212** that was transformed into the corresponding aldehyde with Dess–Martin periodinane. Application of the two-step Corey–Fuchs protocol and trapping of the alkynyllithium intermediate with methyl iodide provided alkyne **213**. Hydrozirconation followed by a zirconium–iodine exchange then furnished key vinyl iodide **214** (Gersbach, Gehringer, Bucher & Altmann, unpublished). $C(sp^2)$–$C(sp^3)$ Suzuki coupling with the mycolactone core (**91**) proceeded smoothly in almost quantitative yield under optimized conditions (Gehringer & Altmann, unpublished). A replacement of the C20 PMB protecting group was necessary to enable an orthogonal deprotection of the C20 hydroxy group in the presence of the mycolactone lower side chain at a later stage [111]. Therefore, the PMB ether was cleaved with DDQ followed by DMAP-promoted acetylation of the liberated hydroxy group with acetic anhydride. Finally, cleavage of the C5-TES ether furnished the adequately pro-

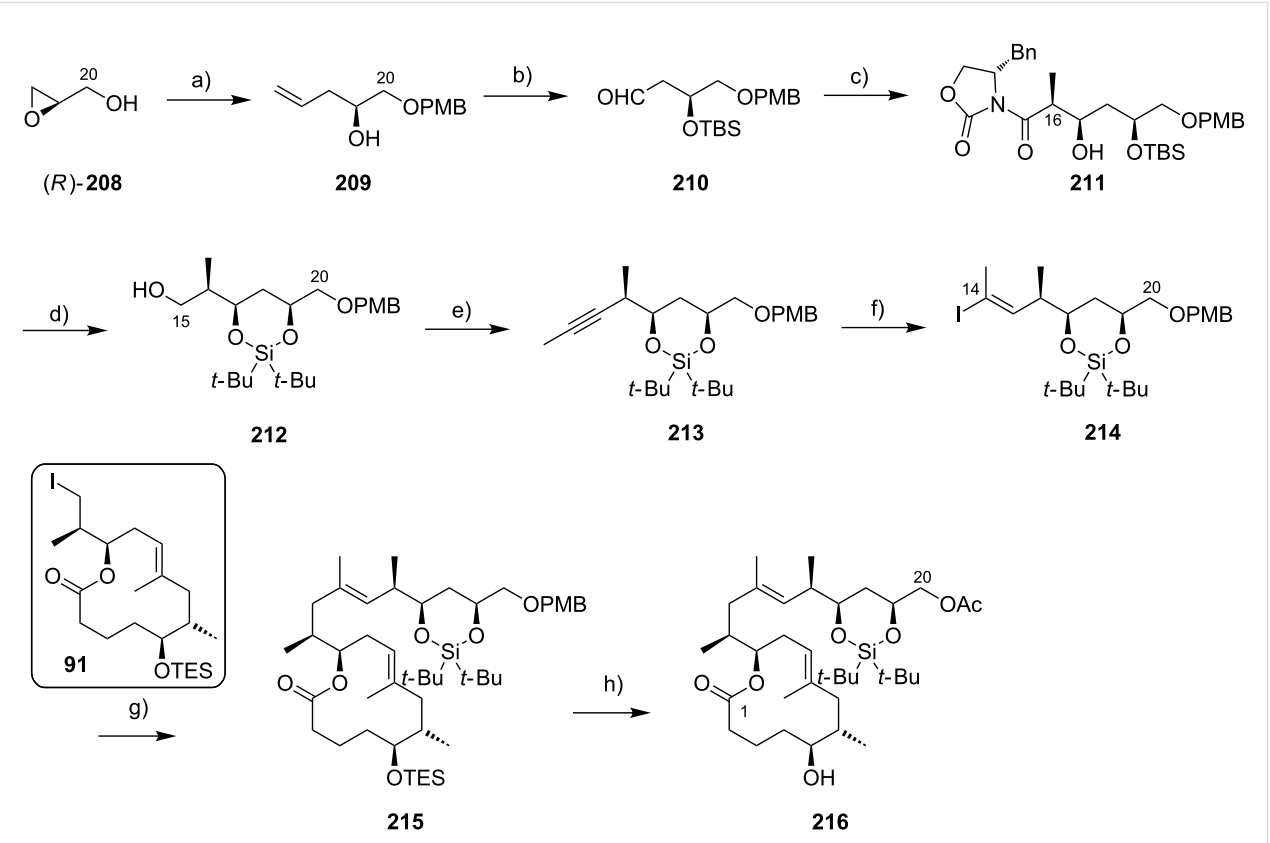

Scheme 34: Altmann's (partially unpublished) synthesis of the C20-hydroxylated mycolactone core. Reagents and conditions: a) (i) NaH, PMBCl, cat. TBAI, DMF, rt, 79%; (ii) vinylmagnesium bromide, CuI, THF, −20 °C, 97%; b) (i) TBSCl, imidazole, CH_2Cl_2, reflux, 97%; (ii) $K_2OsO_4{\cdot}2H_2O$, NMO, acetone/H_2O 9:1, rt; (iii) $NaIO_4$, THF/H_2O 4:3, rt, 98% (2 steps); c) (*S*)-4-benzyl-3-propionyloxazolidin-2-one, Et_2BOTf, DIPEA, CH_2Cl_2, 0 °C; then **210**, −78 °C to 0 °C, 77%, de 20:1; d) (i) HF·pyridine, THF, rt, 98%; (ii) *t*-$Bu_2Si(OTf)_2$, pyridine, CH_2Cl_2, rt, 98%; (iii) $NaBH_4$, THF/water 4:1, rt, 91%; e) (i) DMP, $NaHCO_3$, CH_2Cl_2, rt, 92%; (ii) CBr_4, PPh_3, 0 °C, 96%; (iii) *n*-BuLi, THF, −78 °C, then MeI, −78 °C to rt, 92%; f) $Cp_2Zr(H)Cl$, THF, 40 °C, then I_2, 0 °C, 90%; g) **91**, *t*-BuLi, 9-MeO-9-BBN, Et_2O, THF, −78 °C to rt, then **214**, $Pd(dppf)Cl_2$ (10 mol %), $AsPh_3$, Cs_2CO_3, DMF, H_2O, rt, 98%; h) (i) DDQ, CH_2Cl_2/H_2O 5:1, rt, 99%; (ii) Ac_2O, DIPEA, DMAP, CH_2Cl_2, rt, quant.; (iii) THF/H_2O/HOAc 3:1:1, rt, quant.

tected modified mycolactone core **216** in 17 steps and 35% overall yield from (*R*)-glycidol ((*R*)-**208**).

In order to assess the importance of the upper side chain for biological activity, we have also prepared simplified mycolactones lacking the C14–C20 part of the core extension [178]. In an initial attempt, we investigated the synthesis of the truncated extended core structure **220** by RCM of diene **219** (Scheme 35).

However, the latter proved to be resistant to ring closure under the conditions that had proven effective for the cyclization of **89** and any other of the conditions screened, including the use of different metathesis catalysts (Grubbs 1st generation [239], Grubbs 2nd generation [171], or Hoveyda–Grubbs 2nd generation [189]) and solvents (CH_2Cl_2 or toluene).

This observation is in line with results from the Burkart [173,240] and the Blanchard [182] groups, showing that the successful closure of the 12-membered ring is sensitive to subtle changes of the substituent at the C13 position. As an alternative to the RCM-based cyclization of **219**, lactone **220** could eventually be obtained in good yields by reduction of tosylate **90** with an excess of $NaBH_4$ in DMSO at 100 °C followed by the removal of the TES protecting group under slightly acidic conditions. The synthesis of the 8-desmethyl analog of **220**, i.e., **221** has been reported by Blanchard and co-workers starting from iodide **205** [92]. An iodine–zinc exchange with Rieke zinc [241] followed by aqueous quenching smoothly reduced the C13 position and subsequent cleavage of the C5-TBS ether by pyridine-buffered HF·pyridine uneventfully yielded the free alcohol **221**.

Blanchard also prepared a saturated analog of **221** via tosylate **222** [242]. Hydrogenation of this intermediate over Pearlman's catalyst, followed by Finkelstein iodination, metalation/protonation, and TBS-ether cleavage with buffered HF·pyridine finally gave **223** in 27% overall yield from **222** (Scheme 36).

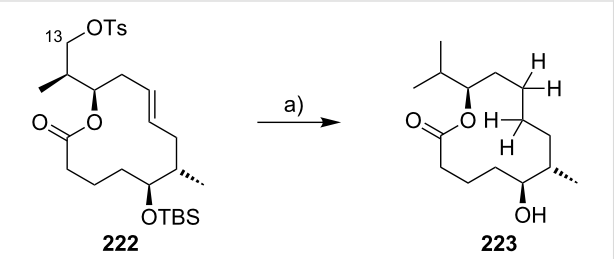

Scheme 36: Blanchard's synthesis of the saturated variant of the C11-isopropyl-8-desmethylmycolactone core. Reagents and conditions: a) (i) H_2 (1 atm), $Pd(OH)_2$, EtOAc, rt, 77%; (ii) NaI, acetone, reflux, 80%; (iii) Zn, LiCl, TMSCl, $BrCH_2CH_2Br$, THF, rt, then alkyl iodide, rt, then aq NH_4Cl, 75%; (iv) HF·pyridine, pyridine, THF, 0 °C to 40 °C, 59%.

IV.2 Modifications of the lower mycolactone side chain

In a recent publication, the Kishi group reported the synthesis of non-natural mycolactones that they have termed photo-myco-

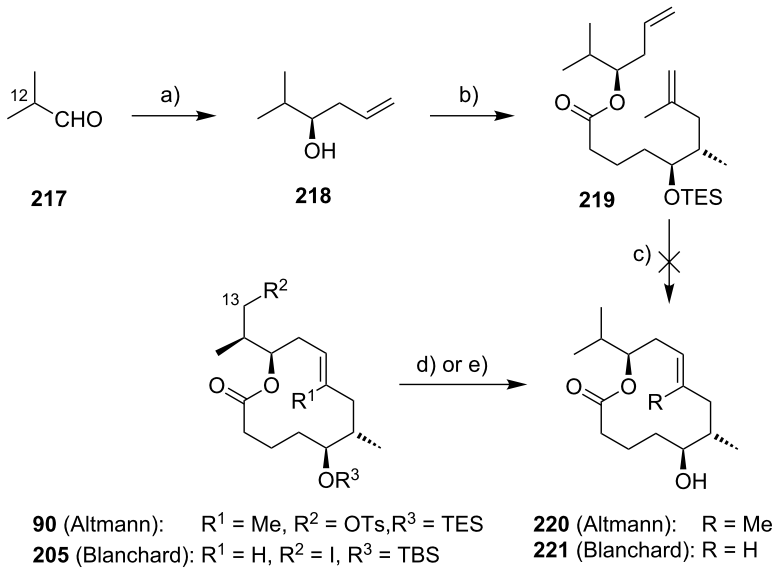

Scheme 35: Altmann's and Blanchard's approaches towards the 11-isopropyl-8-desmethylmycolactone core. Reagents and conditions: **220**: a) $AllylSnBu_3$, $Ti(OiPr)_4$, (*S*)-(−)-1,1'-bi-2-naphthol, CH_2Cl_2, 4 Å molecular sieves, −78 °C to −18 °C, 47%, single isomer; b) **88**, EDCI, DMAP, CH_2Cl_2, rt, 71%; c) Grubbs II, Grubbs I or Hoveyda–Grubbs II catalyst; CH_2Cl_2 or toluene; d) (i) $NaBH_4$, DMSO, 100 °C, 76%; (ii) HOAc/THF/H_2O 2:2:1, rt, 98%. **221**: e) (i) Li, naphthalene, $ZnCl_2$ THF, rt, then **205**, benzene/DMF 15:1, rt, then aq NH_4Cl, 60%; (ii) HF·pyridine, pyridine, 40 °C, 89%.

lactones [243]. This work was triggered by the fact that mycolactone A/B completely loses its activity against keratinocytes after 30 min of exposure to light [244]. Earlier findings of the Kishi group had already shown that synthetic mycolactone A/B upon light exposure was cleanly transformed into four closely related compounds that were denominated as photo-mycolactones A1, A2, B1 and B2 [244]. These compounds were isomeric to mycolactone A/B, but they could not be properly separated. Thus, the Kishi group started to study the photochemical behavior of the isolated, protected mycolactone A/B pentaenoate side chain and its tetraenoate analog. The photoproducts in the tetraenoate series (**225**) were separable into two groups (A and B) containing two compounds each (Scheme 37). Upon TBS deprotection, the two constituents of each group could be finally separated by HPLC on a chiral stationary phase. Oxidative diol cleavage of those products gave two matching pairs of levorotatory and dextrorotatory aldehydes ((+)-/(−)-**226** and (+)-/(−)-**227**, Scheme 37).

Strikingly, the synthesis of the tri-*p*-bromobenzoate variants of compound **225** furnished a crystalline product that was analyzed by X-ray crystallography. The crystallographic data showed the photoproducts to be bicyclo[3.1.0]cyclohexene derivatives, which was in line with the structural proposal that had already been derived by NMR spectroscopy. Based on further experiments and literature data, the Kishi group proposed a concerted $[4\pi_s + 2\pi_a]$ cycloaddition as the mechanism for the cyclization. In a seven-step sequence, they then converted the four photoproducts prepared from the tetraenoate series into their pentaenoate-derived analogs that were subsequently attached to the mycolactone core, to yield the complete photo-mycolactones. The synthetic photo-mycolactones were found to be identical with the compounds obtained by direct photocyclization of mycolactone A/B. Since all mycolactone side chains presented in the following section were attached to the mycolactone core and deprotected according to the same general methodologies as presented in the total synthesis section (i.e., Yamaguchi esterification with the C5-hydroxy group and subsequent silyl ether cleavage by different fluoride sources), these steps will not be discussed. The interested reader is referred to the cited literature.

Following the structure elucidation of photo-mycolactones, the Kishi laboratory embarked on the total synthesis of these compounds [243]. The envisaged key step was an intramolecular LiTMP-promoted Hodgson cyclopropanation [245,246], that would transform a chiral 1,2-epoxy-5-ene into the desired bicyclo[3.1.0]cyclohexene skeleton in a stereocontrolled fashion. Starting from (*R*)-glycidol ((*R*)-**208**, exemplified in Scheme 38) or (*S*)-glycidol, TBDPS protection followed by base-promoted epoxide opening with diethyl methylmalonate and intramolecular transesterification furnished γ-lactone **228** as an inseparable mixture of diastereomers. After selective hydrolysis of the exocyclic ester group, an acid activation/reduction sequence furnished a 3:2 mixture of the diastereomeric primary alcohols **229** and *dia*-**229** that was separable by column chromatography. Similarly, (*S*)-**208** furnished the corresponding enantiomers *ent*-**229** and *ent-dia*-**229** and every single stereoisomer was processed separately. As an example, **229** was then elaborated into epoxyaldehyde **230** in an eight-step sequence that involved reductive opening of the lactone, selective tosylation of the primary hydroxy group and subsequent base-promoted epoxide formation as the key transformations. The aldehyde was converted into diene **233** by a one-pot Julia olefination [247,248] with **232**; the latter was easily prepared from known precursor **231** in a Mitsunobu reaction/*S*-oxidation sequence. Following the same route, all four stereoisomers varying in the configuration of C4' and the C6' were prepared.

Epoxide **233** was then subjected to LiTMP-mediated Hodgson cyclopropanation, to deliver hydroxylated bicyclo[3.1.0]cyclohexane **234** with excellent stereoselectivity, but in relatively

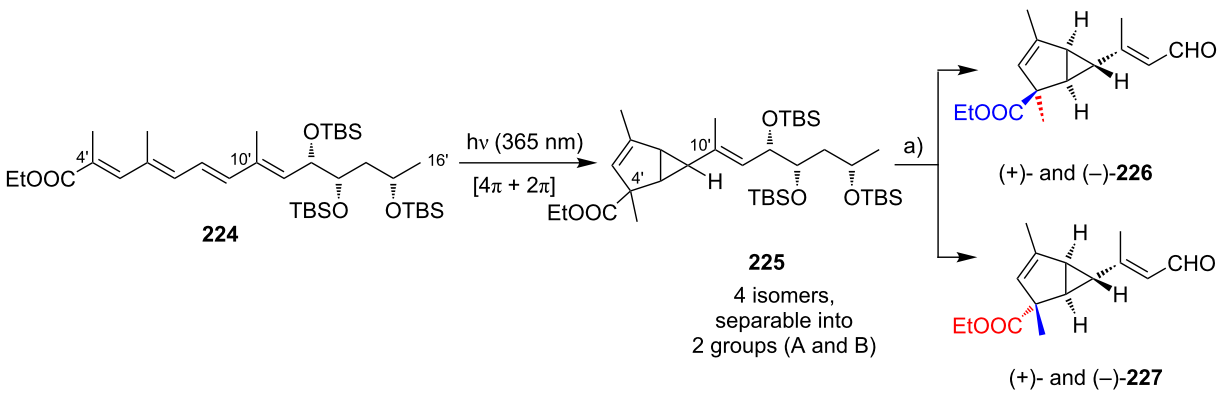

Scheme 37: Structure elucidation of photo-mycolactones generated from tetraenoate **224**.

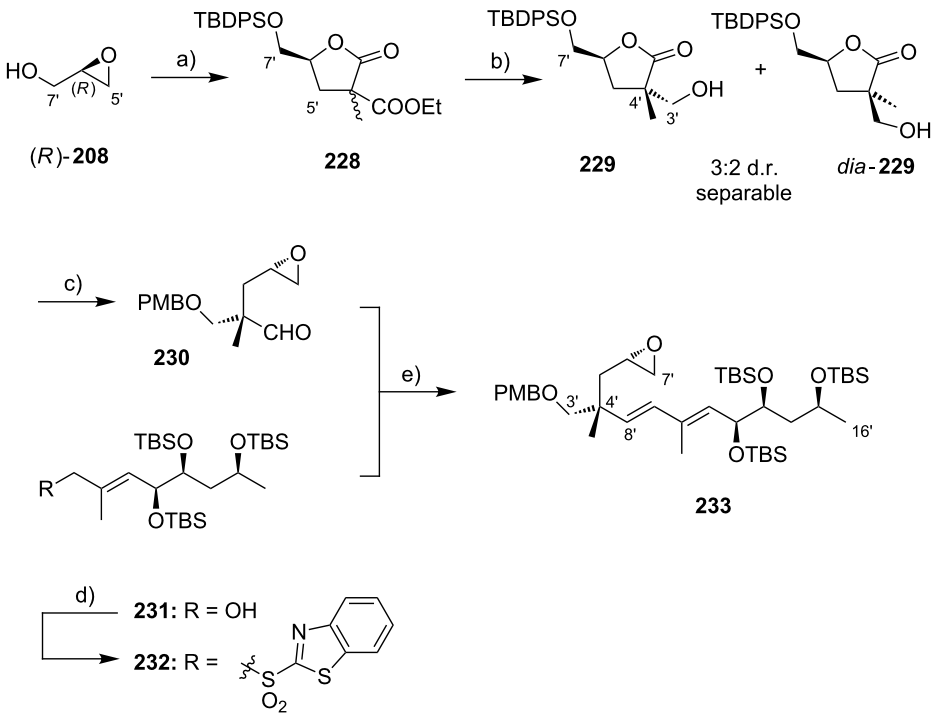

Scheme 38: Kishi's synthesis of the linear precursor of the photo-mycolactone B1 lower side chain. Reagents and conditions: a) (i) TBDPSCl, imidazole, CH_2Cl_2, rt; (ii) $MeCH(CO_2Et)_2$, LiHMDS, $AlEt_3$, THF, −78 °C, then *p*-TsOH, 88%; b) (i) KOH, EtOH, H_2O, 0 °C, 99%; (ii) $ClCO_2Et$, TEA, THF, 0 °C, then $NaBH_4$, iPrOH, rt, 38% (**229**) and 31% (*dia*-**229**); c) (i) PMB-trichloroacetimidate, $La(OTf)_3$, toluene, 0 °C to rt, 87%; (ii) $LiBH_4$, MeOH, THF, 0 °C, 98%; (iii) TIPSCl, imidazole, DMF, rt, 93%; (iv) NaOH, MeOH, H_2O, 60 °C, 69%; (v) TsCl, TEA, *n*-Bu_2SnO, CH_2Cl_2, rt; (vi) K_2CO_3, MeOH, rt, 88% (2 steps); (vii) TBAF, THF, rt; (viii) TEMPO, $NaClO_2$, KBr, $NaHCO_3$, CH_2Cl_2, H_2O, −10 °C, 86% (2 steps); d) (i) benzothiazole-2-thiol, PPh_3, DIAD, THF, 0 °C to rt, 98%; (ii) H_2O_2, $(NH_4)_6Mo_7O_{24}{\cdot}4H_2O$, EtOH, 0 °C to rt, 86%; e) LiHMDS, THF, −78 °C, 86%.

low yields; although most of the starting material could be recovered (Scheme 39). Of note, yields could be significantly increased (65% vs 34%) by replacing the PMB protecting group with a 2-methoxyethoxymethyl (MEM) group and changing the solvent to diethyl ether. The oxidation of **234** to the corresponding ketone under Ley–Griffith conditions [249] followed by enol triflate formation and subsequent coupling with lithium dimethylcopper ("Gilman reagent") [250] introduced the C6'-methyl group. The cleavage of the PMB ether with DDQ then furnished primary alcohol **235** in 19 steps and 1.2% overall yield from (*R*)-glycidol ((*R*)-**208**). Alcohol **235** was processed to α,β-unsaturated acid **236** in a three-step oxidation/Wittig

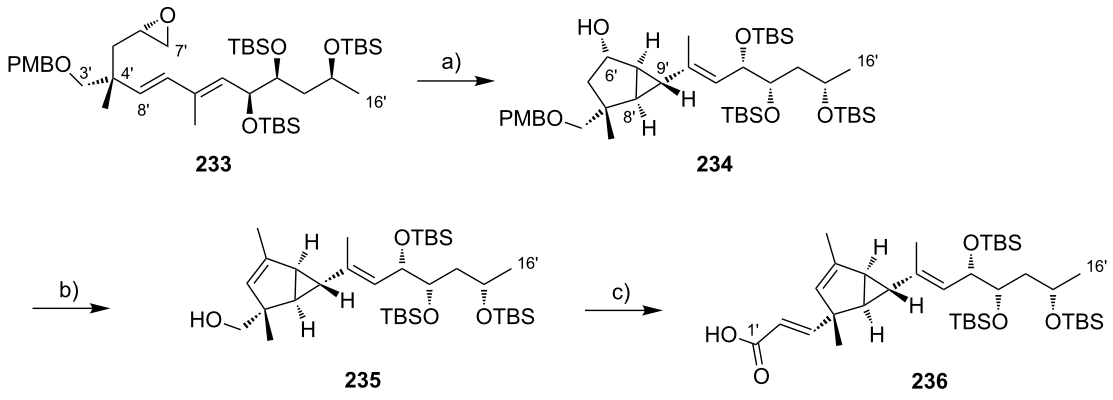

Scheme 39: Kishi's synthesis of the photo-mycolactone B1 lower side chain. Reagents and conditions: a) LiTMP, MTBE, −10 °C, 34%, single diastereomer; b) (i) TPAP, NMO, CH_2Cl_2, H_2O, rt, 72%; (ii) LDA, 5-Cl-2-$PyNTf_2$, THF, −78 °C; (iii) $LiCuMe_2$, THF, −15 °C, 81% (2 steps); (iv) DDQ, CH_2Cl_2, *t*-BuOH, phosphate buffer pH 7.0, rt, 51%; c) (i) DMP, CH_2Cl_2, rt, 84%; (ii) $Ph_3P{=}CHCOOMe$, toluene, 90 °C, 87%; (iii) NaOH, THF/MeOH/H_2O 4:1:1, rt, 90%.

olefination/saponification sequence, according to Kishi's first report on photo-mycolactones [244] (66% yield). The other three photo-mycolactone side chain acids were prepared in the same manner from *dia*-**229**, *ent*-**229** and *ent-dia*-**229**.

In their latest contribution to mycolactone chemistry, Kishi and co-workers reported mycolactone analogs with a partially saturated lower side chain [251]. Motivated by their studies on the photochemical behavior of mycolactones [243,244], they sought to stabilize the lower side chain by saturating the central double bond of the pentaene system. Since the saturation generates a stereocenter at C6', a novel stereoselective synthesis strategy was required. This route is exemplified in Scheme 40 for the (*R*)-C6' epimer **243**. Starting from (*S*)-glycidol ((*S*)-**208**), TBDPS protection and regioselective epoxide opening by the anion of *tert*-butyl propionate in the presence of $AlEt_3$ furnished secondary alcohol **237** as an epimeric mixture at the C6' position. Acid treatment then induced the formation of the corresponding five-membered lactone, which was deprotonated with LDA and re-protonated under kinetic control with 2,6-di-*tert*-butylphenol to provide lactone **238** in high diastereomeric purity after recrystallization.

Reductive lactone opening and selective protection of the ensuing primary hydroxy group as the pivalate followed by TBDPS cleavage afforded vicinal diol **239**, which was subjected to periodate-mediated diol cleavage. Reduction of the resulting aldehyde and protection with TBS chloride yielded orthogonally protected diol **240**, with the C6'-stereocenter in place. The pivaloyl group was removed reductively and two subsequent Wittig-elongation cycles gave the C1'–C8' fragment **241**. Conversion into the corresponding 1-phenyl-1*H*-tetrazol-5-yl sulfone **242** was achieved in a three-step deprotection/Mitsunobu/oxidation sequence and **242** was then reacted with aldehyde **120** under Julia–Kocienski conditions. The ensuing full length C1'–C16' fragment was saponified with lithium hydroxide to finally yield acid **243** in 21 linear steps and 15% overall yield. The C6'-(*S*)-epimer was prepared via the same route.

The influence of the hydroxylation pattern at the lower side chain on the biological activity of C8-desmethylmycolactones has been thoroughly investigated by the Blanchard group. For those studies, they devised flexible strategies towards the lower mycolactone A/B and C side chains (cf. Scheme 23 and Scheme 25), which enabled the synthesis of several analogs differing in the number and configuration of the hydroxy-substituted carbons [92,242]. As illustrated by the general reaction scheme in Scheme 41A, all syntheses proceeded via the respective ethyl (*E*)-2-methyloct-2-enoate, which was transformed into the corresponding dienyl stannane in analogy to the syntheses shown in Scheme 22 and Scheme 25. CuTC-mediated Stille-

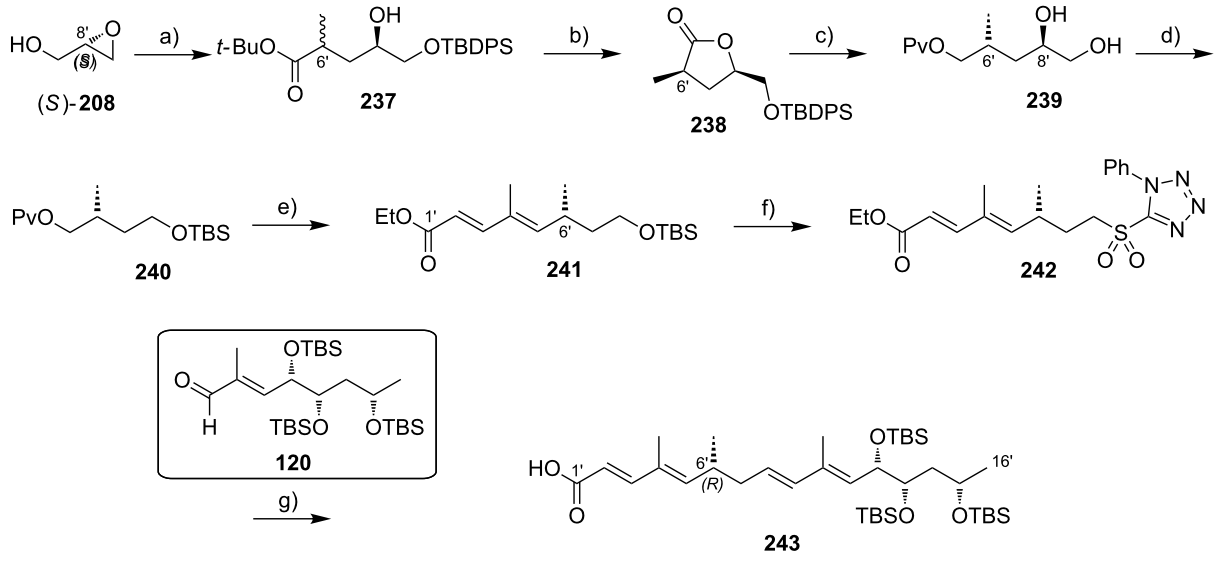

Scheme 40: Kishi's synthesis of a stabilized lower mycolactone side chain. Reagents and conditions: a) (i) TBDPSCl, imidazole, CH_2Cl_2, rt, 96%; (ii) $MeCH_2COO$-*t*-Bu, LiHMDS, $AlEt_3$, THF, −78 °C, 95%; b) (i) PTSA, $CHCl_3$, reflux, 96%; (ii) LDA, THF, −78 °C, then 2,6-di-*tert*-butylphenol, −78 °C, dr 8–10:1, then recrystallization, 65%, dr 50–100:1; c) (i) $LiBH_4$, THF, MeOH, 0 °C, 97%; (ii) PvCl, pyridine, CH_2Cl_2, 0 °C to rt, 90%; (iii) TBAF, THF, rt, 96%; d) (i) $NaIO_4$, THF, H_2O, 0 °C, 93%; (ii) $NaBH_4$, MeOH, 0 °C, 96%; (iii) TBSCl, imidazole, CH_2Cl_2, rt, 94%; e) (i) DIBAL-H, CH_2Cl_2, −78 °C, 92%; (ii) SO_3·pyridine, DIPEA, DMSO, CH_2Cl_2, 0 °C to rt, 90%; (iii) $Ph_3P{=}C(Me)COOEt$, CH_2Cl_2, rt, 90%; (iv) DIBAL-H, CH_2Cl_2, −78 °C, 94%; (v) MnO_2, CH_2Cl_2, rt, 92%; (vi) $(EtO)_2P(O)CH_2COOEt$, *n*-BuLi, THF, 0 °C to rt, 93%; f) (i) PPTS, EtOH, rt, 90%; (ii) 1-phenyl-1*H*-tetrazole-5-thiol, DIAD, PPh_3, THF, 0 °C, 94%; (iii) H_2O_2, $(NH_4)_6Mo_7O_{24}{\cdot}4H_2O$, EtOH, 0 °C to rt, 90%; g) (i) KHMDS, THF, −78 °C, 90%; (ii) LiOH, THF/MeOH/H_2O 4:1:1, rt, 92%. Using the same reaction sequence the C6'-(*S*) epimer of **242** was prepared from (*R*)-glycidol ((*R*)-**208**).

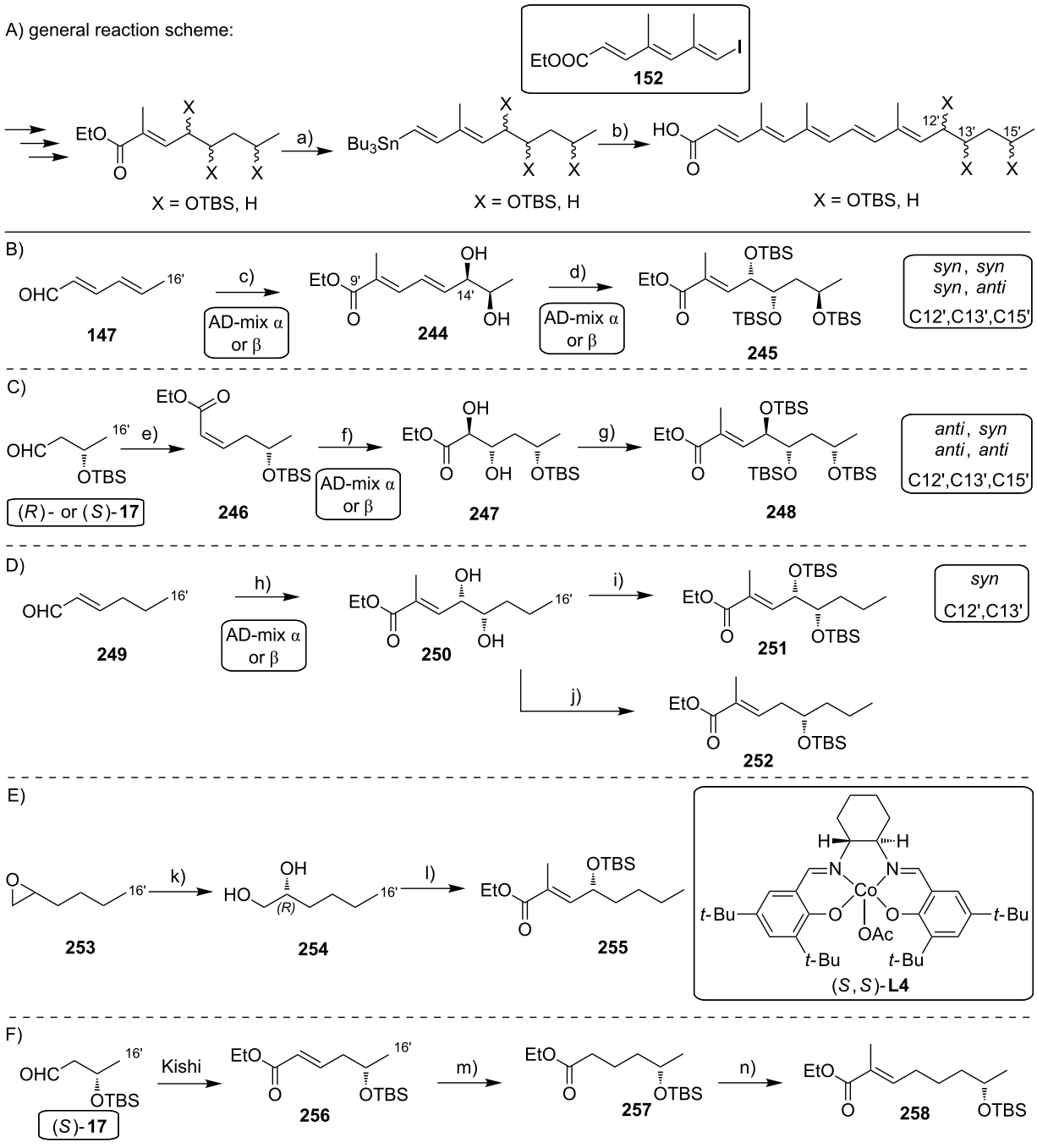

Scheme 41: Blanchard's variation of the C12',C13',C15' stereocluster. Reagents and conditions: a) (i) DIBAL-H, CH_2Cl_2, 0 °C; (ii) MnO_2, CH_2Cl_2, reflux; (iii) $CrCl_2$, CHI_3, THF, rt; (iv) *n*-BuLi, Bu_3SnCl, Et_2O, −78 °C; b) (i) CuTC, $Ph_2P(O)ONBu_4$, NMP, rt; (ii) LiOH, THF, MeOH, H_2O, rt; c) (i) $Ph_3P{=}C(Me)COOEt$, CH_2Cl_2, rt, 99%; (ii) AD-mix α, $K_2OsO_4{\cdot}2H_2O$ (0.6 mol %), $MeSO_2NH_2$, *t*-BuOH, H_2O, 0 °C, 70%; d) (i) triphosgene, pyridine, CH_2Cl_2, rt, 63%; (ii) $Pd_2(dba)_3{\cdot}CHCl_3$ (0.5 mol %), HCO_2H, Et_3N, THF, rt, 80%; (iii) TBSCl, imidazole, DMAP, DMF, rt, 83%; (iv) AD-mix α, $K_2OsO_4{\cdot}2H_2O$ (2 mol %), $MeSO_2NH_2$, *t*-BuOH, H_2O, 0 °C, 73%; (v) TBSCl, imidazole, DMAP, DMF, rt, 82%; e) $(o\text{-Tol})_2P(O)CH_2COOEt$, NaI, NaH, THF, −78 °C, 75%; f) AD-mix α, $K_2OsO_4{\cdot}2H_2O$ (0.6 mol %), $MeSO_2NH_2$, *t*-BuOH, H_2O, 0 °C, 62%, dr 9:1; g) (i) TBSCl, imidazole, DMAP, DMF, rt, 63%; (ii) DIBAL-H, CH_2Cl_2, 0 °C, 73%; (iii) TEMPO, $PhI(OAc)_2$, CH_2Cl_2, rt; (iv) $Ph_3P{=}C(Me)COOEt$, $ClCH_2CH_2Cl$, 70 °C, 65% (2 steps); h) (i) $Ph_3P{=}C(Me)COOEt$, CH_2Cl_2, rt, 98%; (ii) AD-mix α, $K_2OsO_4{\cdot}2H_2O$ (0.6 mol %), $MeSO_2NH_2$, *t*-BuOH, H_2O, 0 °C, 95%, ee >99%; i) TBSCl, imidazole, DMAP, DMF, rt, 97%; j) (i) triphosgene, pyridine, CH_2Cl_2, rt, 76%; (ii) $Pd_2(dba)_3{\cdot}CHCl_3$ (0.5 mol %), HCO_2H, Et_3N, THF, rt, 76%; (iii) TBSCl, imidazole, DMAP, DMF, rt, 98%; k) (*S*,*S*)-**L4** (0.05 mol %), AcOH (20 mol %), H_2O, THF, 46%, er > 99:1; l) (i) TBSCl, imidazole, DMAP, DMF, rt, 98%; (ii) TBAF, THF, rt, 49%; (iii) TEMPO, $PhI(OAc)_2$, CH_2Cl_2, rt; (iv) $Ph_3P{=}C(Me)COOEt$, CH_2Cl_2, reflux, 79% (2 steps); m) H_2 (1 atm), $Pd(OH)_2$, rt, 83%; n) (i) DIBAL-H, CH_2Cl_2, 0 °C; (ii) TEMPO, $PhI(OAc)_2$, CH_2Cl_2, rt; (iii) $Ph_3P{=}C(Me)COOEt$, CH_2Cl_2, rt, 63% (3 steps).

type coupling then furnished the full length C1'–C16' fragments. Different strategies were pursued to provide the hydroxylated ethyl (*E*)-2-methyloct-2-enoates (Scheme 41B–F). C12',C13',C15'-trihydroxylated variants with a *syn*,*syn*- or a *syn*,*anti*-configuration at the triol motif were prepared via the same dihydroxylation/partial defunctionalization approach as in Blanchard's synthesis of the mycolactone A/B lower side chain (exemplified in Scheme 41B). By using different combinations of AD-mix α or AD-mix β in the first and the second dihydroxylation step, respectively, all four possible isomers of **245** with *syn*,*syn* or *syn*,*anti* stereochemistry were prepared. The corresponding *anti*,*anti*- or *anti*,*syn*-C12',C13',C15'-stereocluster was prepared from known aldehydes (*R*)- or (*S*)-**17** by Ando–HWE reaction, furnishing, e.g., α,β-unsaturated ester **246** with a *Z*-configuration (Scheme 41C). The latter was dihydroxylated with AD-mix α, subsequent protection and two-carbon elongation by Wittig chemistry then furnished **248** with an *anti*,*syn*-arrangement of the three hydroxy groups. Furthermore, both enantiomers of the *syn*-diastereomer of the C15'-dehydroxy mycolactone A/B polyenoate chain were prepared (Scheme 41D). Starting from (*E*)-hex-2-enal (**249**) ethyl (2*E*,4*E*)-2-methylocta-2,4-dienoate was prepared by Wittig olefination and the γ,δ-double bond was selectively dihydroxylated, either with AD-mix α or AD-mix β, to obtain **250** or its enantiomer.

TBS protection then furnished *syn*-C12',C13'-dihydroxylated intermediate **251**, while palladium-mediated allylic reduction of the corresponding carbonate and subsequent TBS protection gave the C13'-monohydroxylated analog **252** (only the (*S*)-enantiomer was prepared in this case). The (*R*)-C12'-monohydroxylated derivative was prepared from racemic 1-hexene oxide (**253**) by selective hydrolysis of the (*S*)-enantiomer using Jacobsen's catalytic kinetic resolution protocol for terminal epoxides (Scheme 41E) [252]. TBS protection of both ensuing hydroxy groups followed by selective cleavage of the primary TBS ether gave the free primary alcohol, which was oxidized to the aldehyde stage and converted into key intermediate **255** by Wittig olefination. Finally, the (*S*)-C15'-hydroxylated derivative **258** was again prepared from aldehyde (*S*)-**17** by Wittig two-carbon elongation using the Kishi procedure [43] and subsequent hydrogenolytic reduction of the α,β-unsaturated ester intermediate followed by another Wittig elongation cycle (Scheme 41F).

The Blanchard group has also reported the synthesis of mycolactone analogs with partially rigidized lower side chains, by incorporating phenyl moieties at different positions in the polyenoate chain (**262**–**264**). To this end, dienyl or trienyl stannanes **151** or **261**, possessing the hydroxylation pattern of natural mycolactone A/B, were coupled to *meta*-brominated benzoic acid (**259**) or cinnamic acid esters (**260**) under classical, palladium-based Stille conditions (Scheme 42). Yields were typically high and the ensuing esters were cleaved under the usual conditions.

IV.3. Fluorescent and biotinylated mycolactone analogs

Mycolactone analogs featuring a fluorescent BODIPY or a biotin label at the lower side chain have been prepared through semisynthesis by Small [91] and Demangel [93], respectively. Starting from natural mycolactone A/B (**1a**,**b**), both groups exploited a periodate-mediated cleavage of the 1,2-diol moiety in the polyunsaturated side chain to afford the extensively conjugated aldehyde **265** (Scheme 43). Condensation with BODIPY or biotin hydrazide furnished the labeled mycolactone analogs **266** and **267** (no yield given) that were purified by RP-HPLC.

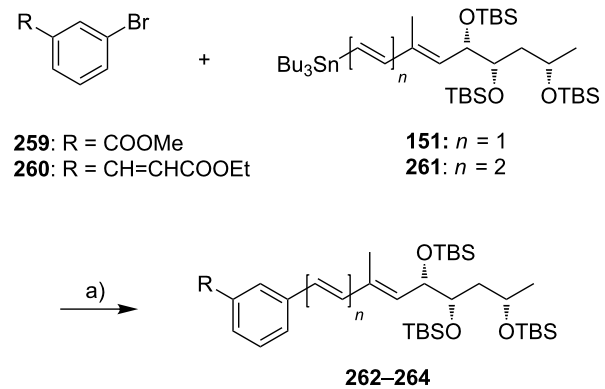

Scheme 42: Blanchard's synthesis of aromatic mycolactone polyenoate side chain analogs. Reagents and conditions: a) $Pd(PPh_3)_4$ (4 mol %), toluene, 110 °C, 86% (**262**: *n* = 1, R = –COOMe) or 92% (**263**: *n* = 1, R = –CH=CHCOOEt), or 81% (**264**: *n* = 2, R = –COOMe).

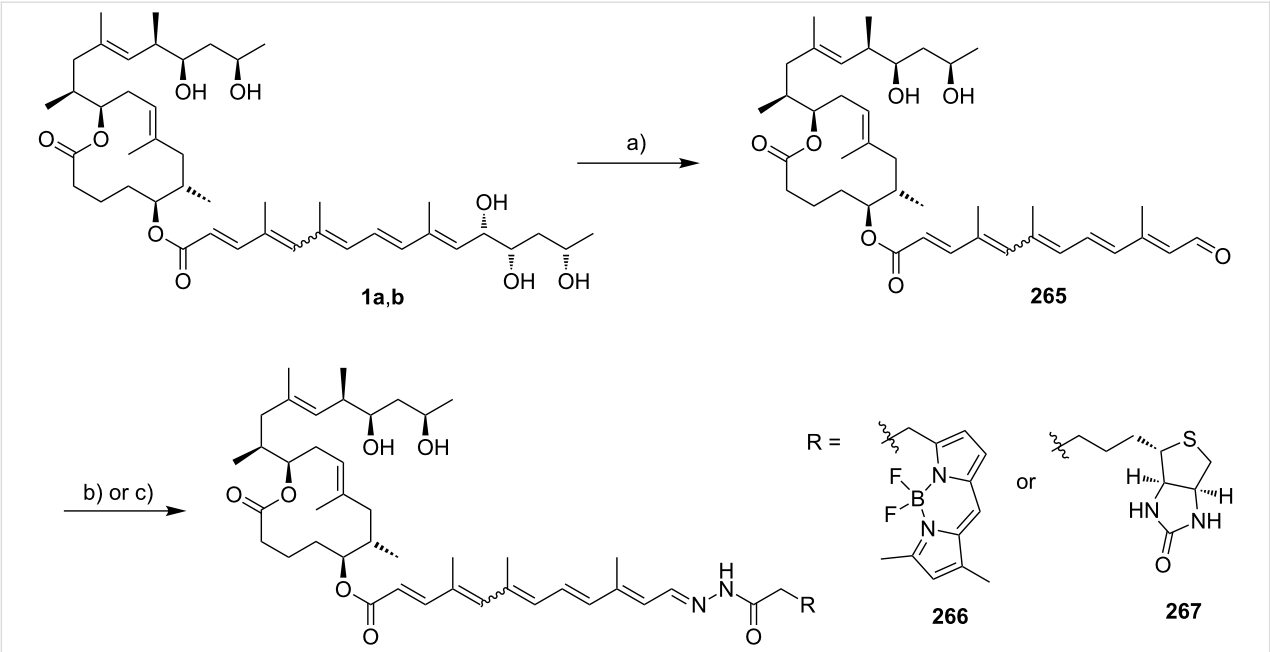

Scheme 43: Small's partial synthesis of a BODIPY-labeled mycolactone derivative and Demangel's partial synthesis of a biotinylated mycolactone analog. Reagents and conditions: a) Small: HCl (0.1 M), HIO_4 (0.01 M), EtOH, 37 °C; Demangel: $NaIO_4$ (0.01 M), THF/H_2O 1:1, rt; b) BODIPY hydrazide, $CHCl_3$/MeOH 2:1, rt, then HPLC purification; c) biotin hydrazide, $CHCl_3$/MeOH 2:1, DMSO, rt, HPLC purification.

C8-desmethylmycolactone analogs tagged with two different BODIPY fluorophores replacing part of the C12–C20 core extension have been disclosed by the Blanchard group (Scheme 44) [92,242]. In order to introduce the fluorescent dye, the tosylate **205** was converted into an azide as a handle for the introduction of various residues by copper-catalyzed Huisgen–Meldal–Sharpless azide–alkyne cycloaddition [253-255]. Subsequently, the lower side chain was introduced by Yamaguchi esterification and deprotected with TBAF, yielding triol **269**. Functionalized BODIPY dyes bearing terminal alkyne groups were prepared according to literature procedures [256] and were clicked on the azide-functionalized mycolactone core equipped with the fully deprotected lower side chain (**269**). This strategy furnished the green and red-fluorescent derivatives **13a** and **13b**, respectively. Non-fluorescent triazoles such as **270** and **271** were also prepared for SAR studies.

Very recently, our own group reported two biotinylated mycolactone-derived probes, which were used to gain insight into mycolactones' molecular mechanism of action within the mTor pathway (cf. Figure 6) [111]. Probe **15** possessing a biotin-substituted triethylene glycol-derived linker as a replacement of the lower side chain was prepared starting from secondary alcohol **94**, which was reacted with CDI to give the respective imidazolyl carbamate (Scheme 45).

After quenching unreacted CDI with water, the addition of a large excess of 1,2-bis(2-aminoethoxy)ethane gave carbamate **272**. Cleavage of the cyclic silyl ether with pyridine-buffered HF·pyridine followed by PyBOP-promoted acylation of the terminal amino group with biotin finally yielded **15**. Probe **16**, which has the biotin linked to C20 of the core extension via the same linker was prepared from secondary alcohol **216** bearing an acetoxy group at C20. Yamaguchi esterification of the C5-hydroxy group with the TBS-protected mycolactone A/B pentaenoate side chain acid and subsequent saponification of the C20-acetoxy group led to primary alcohol **273**. The linker was again introduced via the formation of an imidazolyl carbamate, which was reacted with 1,2-bis(2-aminoethoxy)ethane to give carbamate **274**. Global silyl ether deprotection was achieved by one-pot sequential treatment with TBAF and ammonium fluoride and the ensuing pentol was acylated with biotin at the terminal amino function of the linker using PyBOP as the coupling agent.

V. Structure–activity relationship (SAR) studies

Although there have been numerous reports on the biological activity of mycolactones, systematic structure–activity relationship (SAR) studies are sparse. The only systematic assessment of analogs with a natural core was conducted by the groups of Altmann and Pluschke [90], while the Blanchard and the Demangel groups have investigated a diverse set of C8-desmethylmycolactones for cytopathogenic activity [92], (N)-WASP inhibition [242] and anti-inflammatory properties [257]. The mutual comparability of these studies is limited,

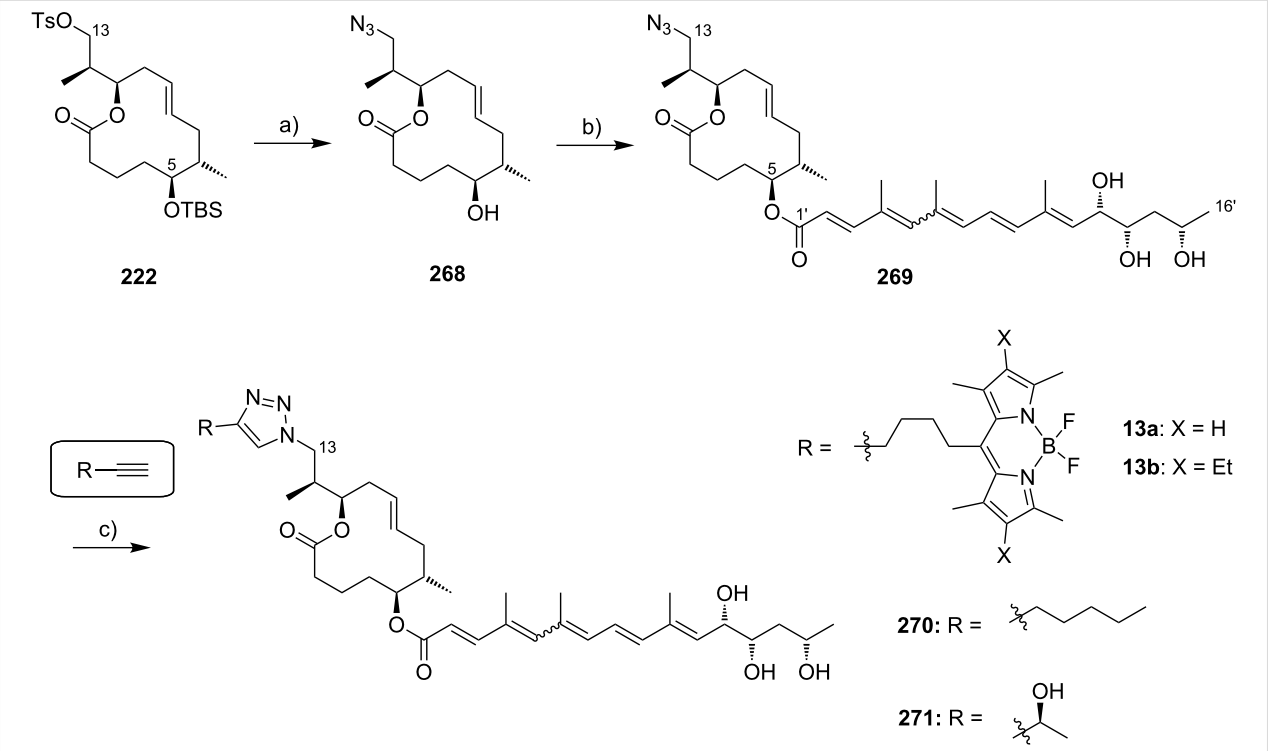

Scheme 44: Blanchard's synthesis of the BODIPY-labeled 8-desmethylmycolactones. Reagents and conditions: a) (i) NaN_3, DMF, 75 °C, 79%; (ii) TBAF, THF, 74%; b) (i) **122a**,**b**, 2,4,6-trichlorobenzoyl chloride, DIPEA, DMAP, benzene, 85%; (ii) TBAF, THF, 93%; c) alkyne, $Cu(OAc)_2{\cdot}H_2O$, sodium ascorbate, *t*-BuOH/H_2O 5:3, 60 °C (μw), 50% (**270**), 22% (**271**), 35% (**11a**) or 35% (**11b**), *E*-$\Delta^{4',5'}$/*Z*-$\Delta^{4',5}$ ca. 1:1.

however, since different cell lines (e.g., murine L929 fibroblasts, Jurkat T cells or human cancer cell lines) and readouts (e.g., cell rounding, cytokine production or flow cytometric parameters) were used. In some cases, no complete description of the experimental details is provided, thereby further complicating quantitative comparisons between the studies. Moreover, many studies rely on the determination of activity at a single concentration or give activity thresholds instead of providing IC_{50} or LC_{50} data. Due to the delayed kinetics of mycolactone action (see chapter I), the time point of data collection is of major importance and not consistent between studies. Most studies employed purified natural mycolactones as the standard and the results should thus be treated with care due to potential variations in the degree of purity of the material used. However, results obtained with synthetic mycolactones may also be biased, since mycolactones tend to be very sensitive to light exposure and might even decompose partially when stored at −20 °C for extended time periods [251,258]. Consequently, caution needs to be exercised when comparing results from different reports has to be handled with care.

V.1. Natural mycolactones

The cytopathogenic effect (CPE) of mycolactones was first described by Krieg and colleagues who fractionated cell cultures and tested the individual fractions on L929 mouse fibroblasts [29]. The first quantification of the CPE of natural mycolactone A/B (**1a**,**b**) was provided by Small and co-workers in their seminal work from 1999 [32]. According to their data, mycolactone A/B caused cell rounding in murine L929 fibroblasts after 24 h at concentrations as low as 25 pg/mL (34 pM); in addition, detachment of cells from the culture plate accompanied by a growth arrest was observed after 48 h [32]. Cell death via apoptosis was only observed at concentrations of 4 nM or above after 72 h (L929 and J774 cells) [82] and no pronounced effect of inhibitors like genistein (TK inhibitor [259]), PD150606 (calpain inhibitor [260]), mastoparan or and suramin T (G-protein inhibitors [261,262]) or wortmannin (PI3K inhibitor [263]) on cytopathogenicity could be detected [91]. Interestingly, concomitant treatment of cells with a caspase inhibitor prevented apoptosis, but not the cytopathogenic phenotype, indicating that apoptosis might be a secondary effect [82]. In a more recent detailed analysis of the biological activity of synthetic mycolactone A/B on L929 fibroblasts, Pluschke and co-workers observed a similar time-dependent phenotype as had been reported in this earlier work. Based on DNA staining with 4',6',-diamidino-2-phenylindole (DAPI) [264] and by using a fluorescent derivative of the selective F-actin-binding peptide phalloidin [265] they could also show that the morphological changes were accompanied by DNA fragmentation and depolymerization of the actin cytoskeleton [90,178]. Mycolactone con-

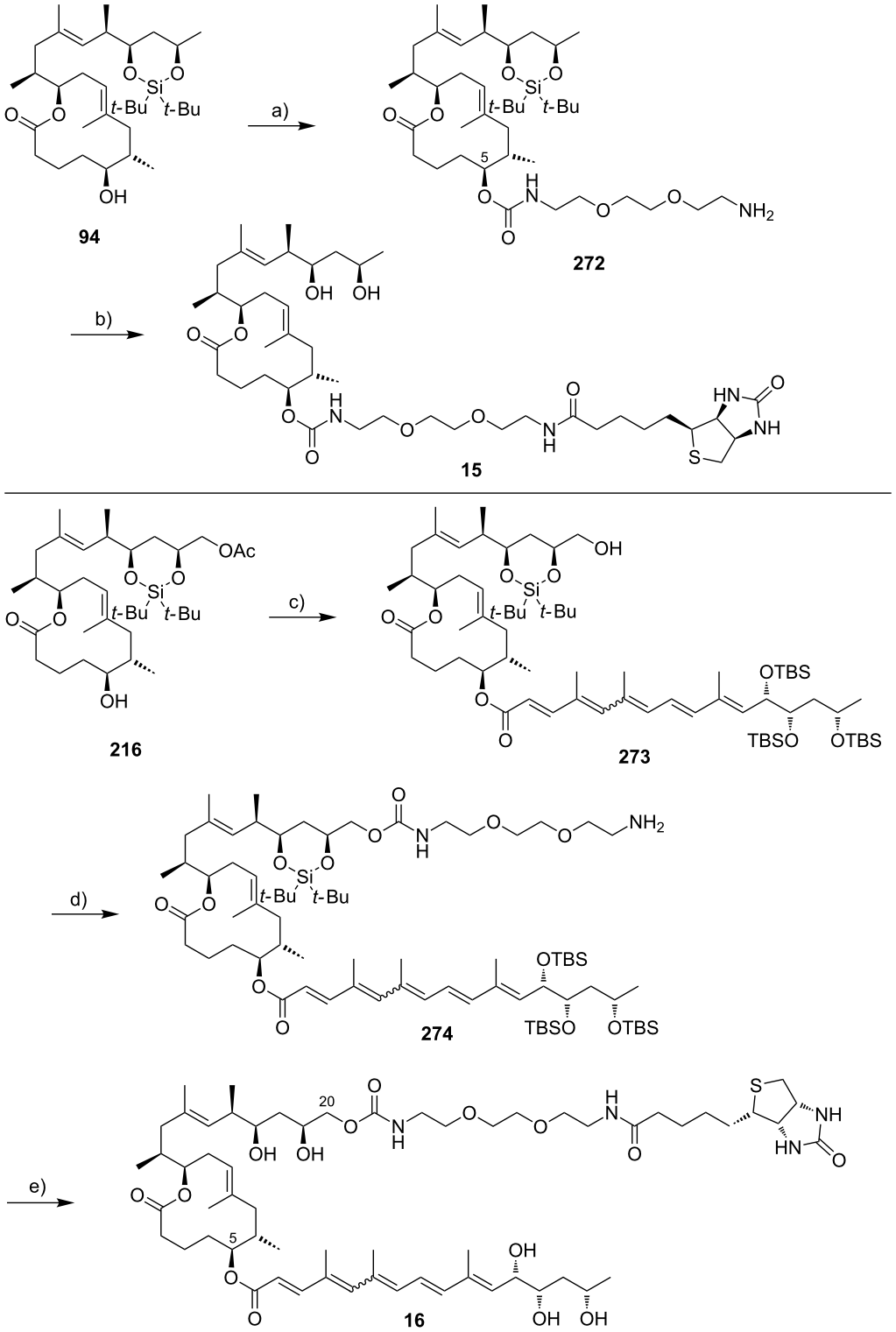

Scheme 45: Altmann's synthesis of biotinylated mycolactones. Reagents and conditions: a) (i) CDI, THF, rt, 2 d, then H_2O, rt, 45 min, then 1,2-bis(2-aminoethoxy)ethane, rt, 1 d, 81%; b) (i) HF·pyridine, THF/pyridine 4:1, rt, 2 h, 96%; (ii) (+)-biotin, PyBOP, DIPEA, DMF, rt, 30 min, 54%; c) (i) **122a,b**, 2,4,6-trichlorobenzoyl chloride, DIPEA, DMAP, rt, 16 h, 88%; *E*-$\Delta^{4',5'}$/*Z*-$\Delta^{4',5'}$ 4.3:1; (ii) K_2CO_3, MeOH, rt, 3 h, 90%; *E*-$\Delta^{4',5'}$/*Z*-$\Delta^{4',5'}$ 4:1; d) (i) CDI, THF, rt, 5 h, then H_2O, rt, 30 min, then 1,2-bis(2-aminoethoxy)ethane, rt, 90 min, 87%, *E*-$\Delta^{4',5'}$/*Z*-$\Delta^{4',5'}$ 3:1; e) (i) TBAF, THF, rt, 4 h, then NH_4F, rt, 17 h, quant., *E*-$\Delta^{4',5'}$/*Z*-$\Delta^{4',5'}$ 3:1; (ii) (+)-biotin, DIPEA, PyBOP, DMF, rt, 30 min, 63% *E*-$\Delta^{4',5'}$/*Z*-$\Delta^{4',5'}$/other isomers 63:29:8.

centrations ≥10 nM were found to be cytotoxic after 48 h and 72 h, respectively, while no effect was observed at 5 nM, independent of the duration of treatment. After exposure to mycolactone concentrations of 20 nM for 48 h, more than 90% of the cells displayed either apoptotic (A^+/PI^-) or necrotic (A^+/PI^+) properties as determined via flow cytometry after annexin-V-FITC (A) [266] and propidium iodide (PI) staining (see also Table 2) [267]. Furthermore, cellular metabolic activity was strongly inhibited by mycolactone A/B (IC_{50} = 5 nM) as determined by AlamarBlue® (resazurin) staining/flow cytometry and a complete shutdown of proliferation was observed in L929 cells at concentrations of 81 nM [90]. Using a panel of 39 human tumor cell lines, the Kishi group found selective cytotoxicity of mycolactone A/B (LC_{50} = 89 nM) against human LOX-IMVI melanoma cells, while no other cell line was significantly affected below 10 μM (no experimental details were provided) [268]. The groups of Leadlay and Demangel further demonstrated that mycolactone A/B suppresses cytokine production in Jurkat T cells [63,93] and several other immune cell lines [257], with IC_{50} values in the low nanomolar range. In contrast, no antimicrobial activity of mycolactone A/B against *Streptococcus pneumoniae* (Gram positive), *Escherichia coli* (Gram negative), *Saccharomyces cerevisiae*, or *Dictyostelium discoideum* was detected [90].

Already in 2003, Small and co-workers recognized the importance of the hydroxy groups at the lower side chain of mycolactone A/B for activity and they concluded that the cytopathogenicity of mycolactones declines with decreasing polarity [47]. In the same study it was shown that mycolactone C (**2**), which was later shown to lack the C12'-hydroxy group [53], caused the typical cytopathogenic mycolactone A/B phenotype in murine L929 fibroblasts, albeit at much higher concentrations (8×10^5-fold) [47]. Of note, this conclusion is based on a CPA of 0.01 ng/mL (0.014 nM) of mycolactone A/B. In subsequent studies from the same group the CPA of mycolactone A/B was reported as 1 ng/mL. Contrary to these earlier findings, Pluschke and co-workers showed by flow cytometry that synthetic mycolactone C (LC_{50} = 186 nM, IC_{50} = 122 nM, see Table 2) was only 16 times less cytopathogenic than synthetic mycolactone A/B [90], while Leadlay and co-workers found a significantly decreased suppression of phorbol 12-myristate-13-acetate (PMA)/ionomycin (IO)-stimulated IL-2 production in Jurkat T cells compared with mycolactone A/B [63]. Similarly to mycolactone C (**2**), natural mycolactone E (**6**) caused an identical cytopathogenic phenotype as mycolactone A/B at approximately 100-fold higher concentrations, when tested in the same L929 cell assay system (135 nM vs. 1.4 nM) [50]. Moreover, **6** showed a stronger suppression of PMA/IO-stimulated IL-2 production (EC_{50} ca. 130–270 nM) than mycolactone C (**2**), F (**8**), and G (**10**) [63]. For synthetic mycolactone E (**6**), a GI_{50} of approximately 15 nM was reported by Kishi and co-workers on L929 fibroblasts, but no details on the assay conditions were provided in the corresponding publication [58]. Under the same (unspecified) conditions, the synthetic minor C13'-oxo metabolite of mycolactone E (**7**) was shown to be equipotent (GI_{50} = 15 nM) with the parent compound [58]. Natural mycolactone F (**8**) also caused the typical cytopathogenic phenotype in L929 cells at 14 nM [55]; LC_{50} and IC_{50} values of 29 nM and 9 nM, respectively, have been reported for the synthetic compound (see Table 2) [90]. This potent activity is remarkable, considering that mycolactone F (**8**) has a shortened tetraenoate side chain with an inverted stereochemistry at the C11'–C13' diol moiety. Similar to mycolactone A/B [35], natural mycolactone F (**8**), was found to cause necrosis in L929 fibroblasts at 20 μM after a 4 h treatment, while substantial apoptosis was detected after 24 h at 100-fold lower concentrations [55]. The suppression of stimulated IL-2 production caused by mycolactone F was slightly lower than for mycolactone E (**7**) [63]. Synthetic mycolactone *dia*-F (**9**) has been reported to possess a similar biological profile as mycolactone F (**8**), albeit with 1000-fold reduced potency; details on the effects of mycolactone *dia*-F (**9**) remain to be published [61]. Of note, neither mycolactone A/B nor mycolactones C, E, F or G caused detectable apoptosis in Jurkat T cells at 1.4 μM after 24 h [63]. Within this set of compounds, mycolactone G (**10**) was the weakest suppressor of IL-2 production with an EC_{50} above 700 nM [63]. Currently, no data on the biological activity of mycolactones D (**3**), S1 (**4**) and S2 (**5**) are available.

V.2. Synthetic and semisynthetic mycolactones with an unmodified core

Early SAR data on chemically modified natural mycolactone A/B (**1a**,**b**) were reported by the Small group, including peracetylated and fully saturated analogs (obtained by exhaustive hydrogenation of double bonds). These modifications caused complete ablation of cytopathogenic activity [32]. In a later study, Small and Snyder, hypothesizing that the trihydroxy motif was simply an "inactive hydrophilic portion of the toxin", reported the oxidative cleavage of the C12',C13' diol motif and used the resulting aldehyde to introduce a fluorescent BODIPY dye by means of hydrazone formation (vide supra). Interestingly, both the aldehyde **265** and the fluorescent derivative **266** (Scheme 43) maintained substantial cytopathogenic activity, which was only reduced by a factor 6–10 compared to the natural product [91]. The extended core lactone, obtained by base hydrolysis of natural mycolactone A/B, also induced a nearly identical cytopathogenic phenotype, but only at 10^6-fold higher concentrations [47] (again, this conlusion was based on CPA for mycolactone A/B of 0.01 ng/mL). A C12'-biotinylated derivative from Demangel and co-workers, which was also obtained from aldehyde **265**, displayed only slightly de-

creased cytotoxicity on HeLa cells and suppressed induced IL-2 production in Jurkart T cells with comparable potency as natural mycolactone A/B [93]. In 2011, Kishi reported an isolated example of a synthetic mycolactone derivative with an elongated lower side chain (C1'–C18') bearing a terminal *n*-butyl carbamoyl group (**275**, Figure 9) [268].

The compound was cytotoxic at 30 nM against L929 mouse fibroblasts, corresponding to a three-fold decrease relative to mycolactone A/B. This indicates that an extension of the lower side chain is well tolerated. Unfortunately, no details on assay conditions were provided in Kishi's paper.

The Kishi group has also reported that photo-mycolactones possess significantly reduced toxicity, but details were only reported for photo-mycolactone A1 (**276**); the latter was tested against five human and murine cell lines (Table 1). Due to the 100–1000-fold drop in activity, compared to mycolactone A/B, the detoxification of mycolactones by light was suggested, and the idea of stabilizing mycolactones by partial saturation of the conjugated double bond system evolved. Two such compounds, α-**277** and β-**277**, which differ from mycolactone A/B by the saturation of the C6'–C7' double bond were reported by Kishi and co-workers in a very recent paper [251]. Indeed, both epimers exhibit significantly increased stability against light, heat, acid, and base, while preserving some cytotoxicity. The antiproliferative activity of these compounds was assessed against three human cancer lines and L929 mouse fibroblasts (Table 1).

Most notably, the β-epimer exhibited almost the same activity against human embryonic kidney (HEK) 293 cells as mycolac-

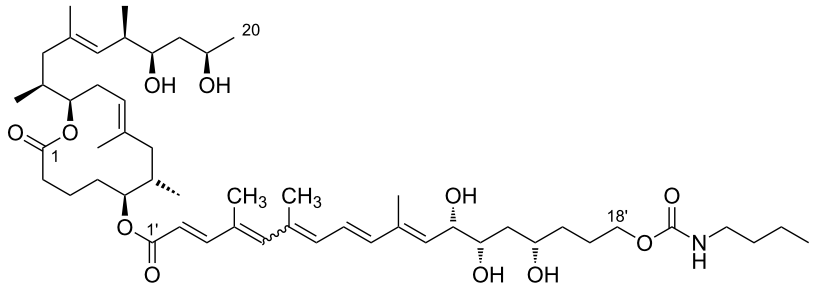

275

Figure 9: Kishi's elongated *n*-butyl carbamoyl mycolactone A/B analog.

Table 1: Antiproliferative activities of photo-mycolactone A1 and C6'–C7' dihydromycolactones (IC_{50} or GI_{50} values [nM]).

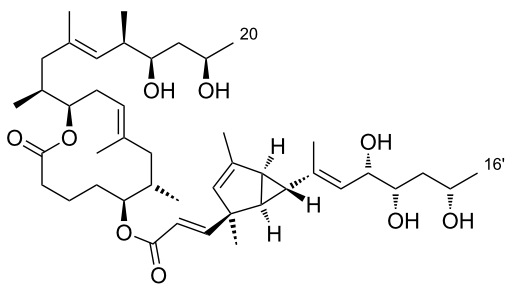

276
(photo-mycolactone A1)

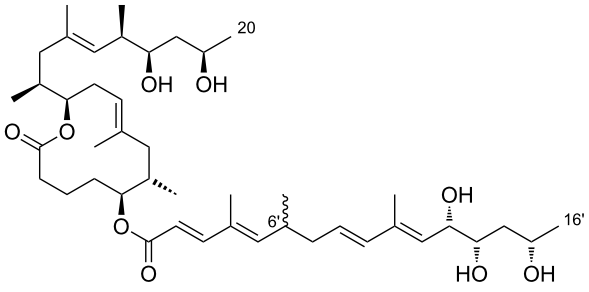

6'-(*R*): α–**277**
6'-(*S*): β–**277**

Mycolactone	L929	HEK-293	LOX-IMVI[a]	A-549	SK-MEL-5[b]	SK-MEL-28[b]
1a/b	13[a,b]	3.2[a]/3.3[b]	6.9	0.77[a]/4.7[b]	12	4.5
276	2020[b]	2510[b]	–	3820[b]	3600	470
α-**277**	63[a]	83[a]	129	400[a]	–	–
β-**277**	53[a]	3.0[a]	29	77[a]	–	–-

[a]Cytotoxicity (IC_{50}) according to [251]. [b]Growth inhibition (GI_{50}) according to [244].

tone A/B, but was significantly less potent against the other three cell lines. Generally, the cytotoxicity of the α-epimer was approximately 3–30-fold decreased compared to the β-epimer, with the exception of the mouse L929 fibroblasts cell line, where both epimers were almost equipotent.

In two studies on synthetic mycolactone analogs, Altmann, Pluschke, and co-workers reported on the effects of modifications at the lower side chain and the core extension while leaving the core structure unchanged (Table 2) [90,178]. Biological activity on L929 fibroblasts was evaluated by flow cytometry (A/PI and AlamarBlue® staining) and fluorescence microscopy (DAPI and phalloidin staining as described above). For all compounds, except the C5–O sorbate ester **278**, concentrations required to induce cytotoxicity, reduction of metabolic activity, rearrangements in the actin cytoskeleton and the nuclear morphology were in the same range. Generally, a significant reduction in biological activity was observed if the lower side chain was truncated. For example, both, the C5–O acetyl-capped mycolactone core **279** and analog **280**, which incorporates a C1'–C16' pentaenoate side chain lacking all three hydroxy groups showed little effects up to concentrations in the

Table 2: Biological activities of mycolactones A/B, C, F, and of mycolactone analogs.

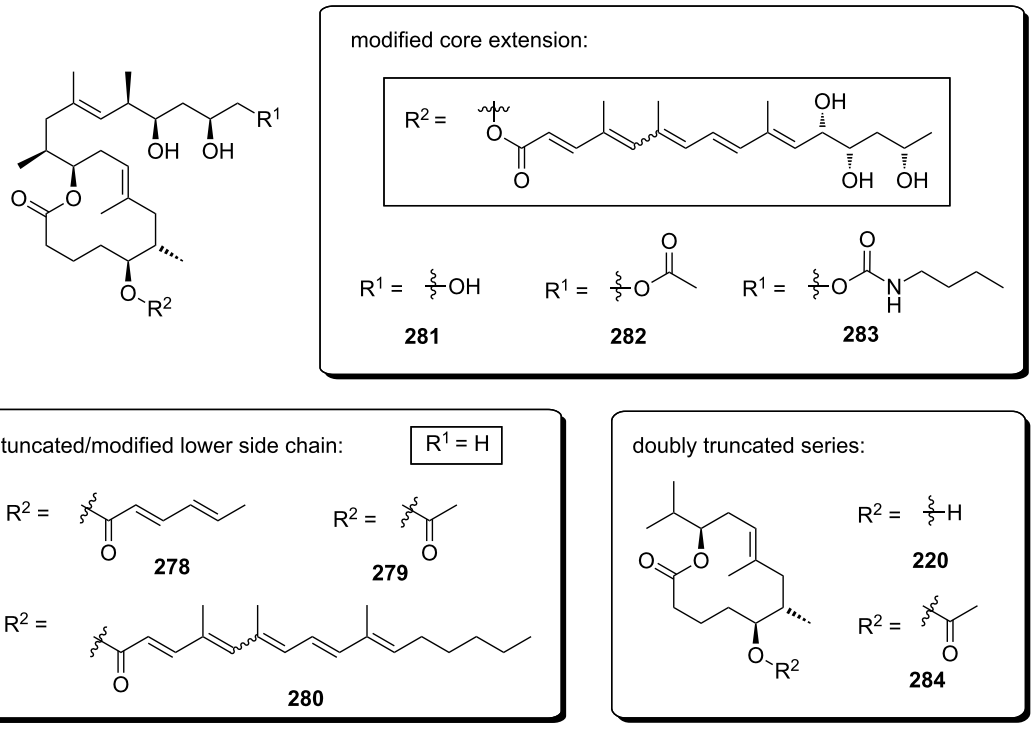

Mycolactone	LC_{50} [nM][a]	IC_{50} [nM][b]	LC_{50}/IC_{50}
1a/b	12	5	2.4
2	186	122	1.5
8	29	9	3.2
278	3426	171	20
279	>>5000	>>5000	n.a.
280	4550	1439	3.2
281	15	5	3.0
282	45	20	2.3
283	50	16	3.1
220	inactive	n.d.	n.a.
284	inactive	n.d.	n.a.

[a]Cytotoxicity (LC_{50}) determined after 48 h by flow cytometry employing annexin-V-FITC (A) and propidium iodide (PI) staining. [b]Reduction of metabolic activity (IC_{50}) analyzed by AlamarBlue® staining. All experiments were carried out with L929 mouse fibroblasts.

low micromolar range. Interestingly, analog **278** was only moderately cytotoxic (LC_{50} = 3426 nM), while being a potent inhibitor of metabolism (IC_{50} = 171 nM). The antiproliferative activity of **278** was significantly lower than for mycolactone A/B, but higher than for **279**, which did not show any measurable antiproliferative activity up to the highest concentration tested (5 μM).

Derivatives modified at the C20 position of the core extension were generally equipotent (**281**) or only slightly less active (**282**, **283**) than mycolactone A/B (**1a**,**b**). Since even an *n*-butyl carbamoyl substituent at C20 atom (**283**) was well tolerated, it can be assumed that this position is well suited for the introduction of tags enabling the deconvolution of mycolactones' cellular fate and its targets. Simultaneous truncation of the core extension and the lower side chain was deleterious to activity; thus, both **220** (see also Scheme 35) and **284** were devoid of measurable cytopathogenic or apoptosis-inducing effects [178].

V.3. Synthetic mycolactones with a C8-desmethylmycolactone core

Extensive work on the SAR of C8-desmethylmycolactones was performed in a joint effort by the groups of Blanchard and Demangel. In an initial study, the Blanchard group prepared a series of seven C8-desmethylmycolactone derivatives for studying the effects of different substitution patterns at the C12',C13',C15'-stereocluster, as well as the removal of the C14–C20 part of the core extension and/or the lower side chain [92]. Cytopathogenicity was analyzed at 10 μM and 50 μM and the minimum concentration required to induce 90% cell rounding was determined for natural mycolactone A/B (**1a**,**b**, 40 nM) and the synthetic C8-desmethyl analog **285** (5000 nM). Although the computationally predicted 3D conformations of the C8-desmethyl and the unmodified mycolactone core were virtually identical [182], a 125-fold drop in cytopathogenic activity was observed when removing the C8-methyl group. Therefore, the comparison of activities between mycolactones possessing an unmodified and a C8-desmethyl core, respectively, is hardly conclusive and it cannot be ruled out that C8-desmethyl analogs engage a different set of targets in vivo. Consequently, those SAR are treated separately in this review.

For Blanchard's first set of C8-desmethylmycolactones, significant changes in cytopathogenicity were observed when the C12',C13',C15'-stereocluster was modified (Table 3) [92].

Inverting the stereochemistry at the C15'-hydroxy group (**286**) maintained full cytopathogenicity (100%) at both tested concentrations, while inversion of the configuration of the entire C12',C13',C15'-stereocluster (**287**) decreased cytopathogenic activity to 10% at 10 μM; at 50 μM full cytopathogenic activity was retained. Removal of the C12'-hydroxy group (**288**) also decreased cytopathogenicity, albeit to a lower extent (49% at 10 μM). Interestingly, the removal of the C15'-hydroxy group (**289**) had a higher impact on the cytopathogenic activity, which was reduced to 40% at 10 μM [182,242]. The truncation of the core extension (**290**) had a similar effect as the removal of the C12'-hydroxy group, leading to 53% cytopathogenicity at 10 μM, while maintaining full cytopathogenic activity at 50 μM. A slightly more pronounced drop in cytopathogenic activity was seen if the lower side chain was removed, while keeping the core extension (**291**, 27% at 10 μM and 100% at 50 μM). Removing both the core extension and the polyenoate side chain (**221**, see also Scheme 35) was detrimental to activity. Similarly, the isopropyl ester of the lower side chain acid **292** was virtually inactive. Interestingly, the click chemistry-derived fluorescent analog **13a** (see Scheme 44 and Figure 5) had a cytopathogenic activity of 90% at 10 μM, thus maintaining most of the cytopathogenicity of the parent compound **285**.

In a subsequent study, the Blanchard and Demangel groups investigated the binding of a series of 27 C8-desmethylmycolactone analogs to (N)-WASP [242]. Due to the amount of work presented in [242], not every single analog will be discussed here. Based on the experiments described in this paper, natural mycolactone A/B (**1a**,**b**) binds to N-WASP with an approximate K_d value of 170 nM, as estimated indirectly by measuring the dependence of the increase in the maximal rate of actin assembly on mycolactone concentration. The binding affinity (K_d) of natural mycolactone A/B to the CR1 domain of WASP and the CR7 domain of N-WASP was reported to be 20 nM and 66 nM, respectively [93,182]. Binding of C8-desmethylmycolactone analogs was assessed by displacement of the C12'-biotinylated mycolactone A/B derivative **267** (see Scheme 43) from immobilized isolated (N)-WASP mycolactone binding domains (MBDs), as they had been defined previously [93]. Data are reported in [93] only for binding to the WASP-MBD, but comparable results were also obtained with the corresponding N-WASP domain (that is not shown in the paper). The IC_{50} value of mycolactone A/B in this displacement assay was 32 μM (Table 4) [242]. Compared to the 125-fold reduced cytopathogenicity of C8-desmethylmycolactone analog **285** [92], only a three-fold reduction in affinity was observed for the WASP-MBD (IC_{50} = 98 μM). Similarly, C8-desmethylmycolactone derivatives **286**, **287**, and **289**, with modifications in the C12',C13',C15' stereocluster (for structures cf. Table 3) had IC_{50} values in the range between 30 μM and 70 μM. Thus, the influence of the stereochemistry and substitution pattern at the C12', C13', and C15'-positions on WASP affinity seems to be less pronounced than on cytopathogenicity. Similar observations were made with compounds from the series devoid of the

Table 3: Cytopathogenic activities of C8-desmethylmycolactone analogs.

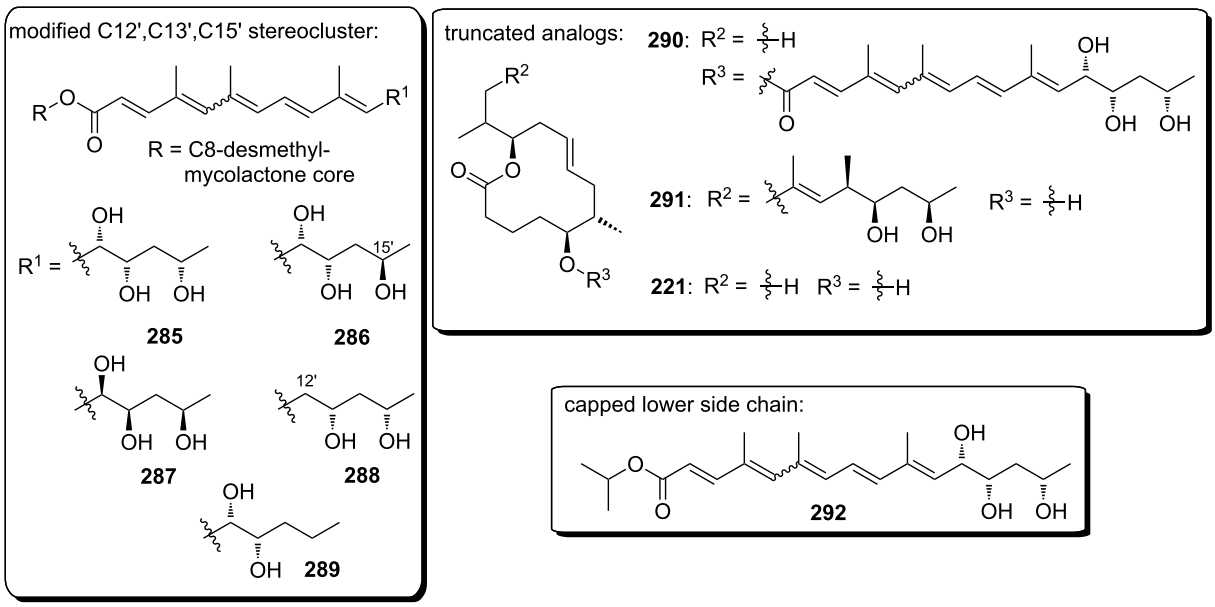

Mycolactone	% Cell rounding at 10 μM[a]	% Cell rounding at 50 μM[a]
1a/b[b]	100	100
285[c]	100	100
286	100	100
287	10	100
288	49	100
289[d]	40	n.d.
290	53	100
291	27	100
221	10	20
292	5	15
13a[e]	90	n.d.

[a]Cytopathogenicity determined after 48 h as the number of rounded cells compared to the total number of cells. [b]Minimum concentration required for 90% cell rounding after 24 h: 40 nM. [c] Minimum concentration required for 90% cell rounding: 5 μM. [d]Data from [242] and [182]. [e]No cell rounding was detectable at 0.5 μM, the concentration at which cellular uptake was assessed.

larger part of the core extension. Interestingly, derivative **290**, which lacks the C14–C20 segment of the core extension, showed an IC_{50} of 22 μM and, thus, was more potent than mycolactone A/B. This observation is in conflict with the original cytopathogenicity data that have been reported for this compound [92], which showed a profound drop in activity upon removal of the core extension. Both, the truncated and the extended C8-desmethylmycolactone core (**291** and **221**, respectively) with a free C5-hydroxy group showed no displacement of the reporter under the conditions tested (IC_{50} > 1000 μM). In contrast, full cytopathogenic activity was observed for **291** at 50 μM (cf. Table 3) [92]. Among all analogs with a truncated core extension that have been investigated so far, the most potent representative was found to be **295**, which features an inverted configuration at the C13’ atom and which showed an IC_{50} of 10 μM in the displacement assay. The affinity of compound **293** (IC_{50} = 34 μM), which comprises the all-epi mycolactone A/B side chain differed only slightly from the natural stereoisomer **290** (IC_{50} = 22 μM) and a similar affinity was observed for the C15’-epimer **294** (IC_{50} = 44 μM). While the removal of the C15’-hydroxy group in analog **296**, with the natural stereochemistry for the two other hydroxy-bearing stereocenters remaining unchanged, was detrimental to binding (IC_{50} = 250 μM), the inversion of both the C12’ and the C13’-stereocenters (**297**, IC_{50} = 27 μM) completely rescued affinity.

In contrast, analog **298**, possessing a C13’,C15’-dihydroxy substitution pattern with the natural configuration was highly active

Table 4: Biological activities of C8-desmethylmycolactone analogs on WASP.

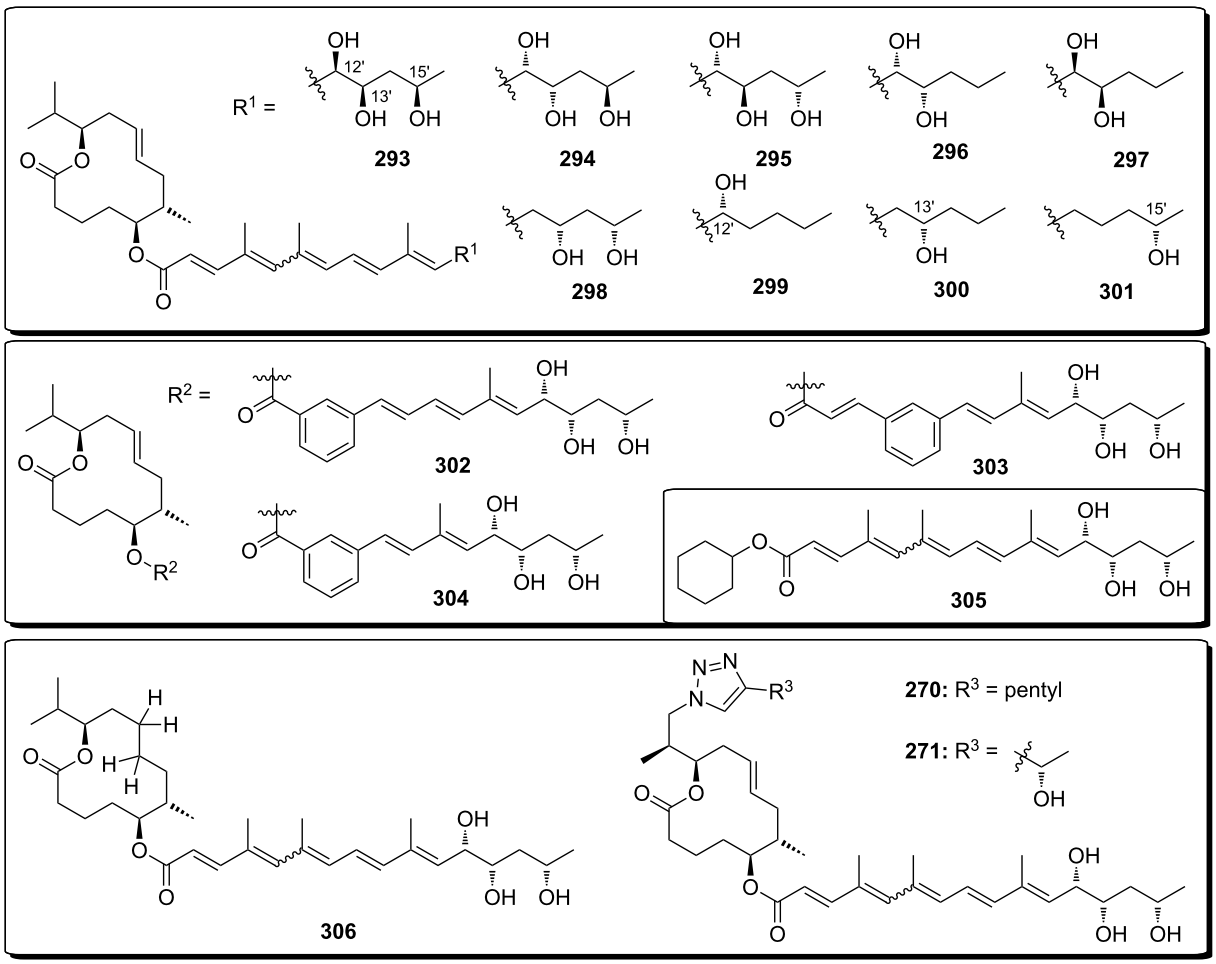

Mycolactone	IC_{50} [μM][a]	Mycolactone	IC_{50} [μM][a]
1 a/b	32	**297**	27
285	98	**298**	28
286	41	**299**	350
287	33	**300**	23
289	70	**301**	75
290	22	**302**	60
291	>1000	**303**	35
221	>1000	**304**	70
293	34	**305**	135
294	44	**306**	65
295	10	**270**	35
296	250	**271**	170

[a]IC_{50} values were determined as the capacity to displace biotinylated mycolactone **267** (1 μM) from immobilized GST-fused WASP mycolactone binding domains (amino acids 200–313). Testing compounds were used in concentrations between 0 μM and 10 μM (intervals were not defined).

(IC_{50} = 28 μM) in spite of the missing C12'-hydroxy group. Intriguingly, compound **300** which bears a single hydroxy group at the C13' position (IC_{50} = 23 μM) was even more potent than natural mycolactone A/B. The removal of both, the C13' and the C15'-hydroxy groups (**299**), led to a strong erosion of affinity (IC_{50} = 350 μM), while removal of the C12' and C13' hydroxy groups in derivative **301** had a much lower impact (IC_{50} = 75 μM). With IC_{50} values between 35 μM and

70 μM, derivatives **302–304**, which incorporate a *meta*-substituted phenyl ring as a rigid diene bioisostere retained similar activity as natural mycolactone A/B. Quite remarkably, the cyclohexyl ester of the mycolactone A/B lower side chain (**305**) preserved significant activity. With an IC_{50} of 135 μM, an approximately four-fold reduction in affinity was observed compared to the parent compound **1a**,**b**. This observation stands in sharp contrast to the almost complete loss in cytopathogenic activity of the corresponding isopropyl ester **292** (cf. Table 3). Saturation of the C8–C9 double bond in the truncated 8-desmethylmycolactone core was well tolerated and the activity of compound **306** (IC_{50} = 65 μM) was only three-fold lower than for its C8–C9 unsaturated counterpart **290**. The effect of a 4-substituted 1,2,3-triazole moiety attached to the C13 position was strongly dependent on the nature of the substituent. While an unsubstituted pentyl chain was well tolerated (**270**, for structures see also Scheme 44, IC_{50} = 35 μM), an (*S*)-2-hydroxyethyl substituent caused a substantial drop in activity (**271**, see also Scheme 44, IC_{50} = 170 μM). Compound **290**, the closest structural analog of the natural toxin from the series lacking the C14–C20 part of the core extension, was analyzed for its capability to disrupt the (N)-WASP-VCA interaction. It was shown that **290** displaces the VCA domain from an immobilized GST-fused version of the WASP mycolactone binding domain in a dose dependent manner. IC_{50} values for both, mycolactone A/B and **290** were in the low micromolar range as determined by electrophoresis of the pulled down products. Similar observations were made for N-WASP (no data provided in [242]). The adhesion capacity of HeLa cells was also reduced by **290** albeit at much higher concentrations as with the natural toxin (16 μM vs 26 nM). Of note, the unsubstituted extended mycolactone core **291**, which is devoid of WASP binding affinity, did not alter cell adhesion at the same concentrations (no data shown in [242]).

Collectively, it can be concluded from these SAR studies that neither the core extension nor the C8-methyl group of mycolactone A/B are required for (N)-WASP binding, while the lower side chain is crucial. The impact of the stereochemistry at the C12', the C13', and the C15'-positions on (N)-WASP affinity is much less pronounced than would have been expected on the basis of earlier cytopathogenicity studies. In fact, the effects on WASP affinity are sometimes opposite to the changes in cytopathogenicity observed for the same modifications [59,90,92]. Even the removal of one or two hydroxy groups, including the C12'-hydroxy group, which had been found to be of crucial importance in other studies [47,50,63,92], was tolerated in certain cases. Likewise, the inclusion of a *meta*-substituted phenyl ring in the lower side chain and the replacement of the core extension by a 4-alkyl-substituted 1,2,3-triazole is tolerated. Overall, the SAR for WASP binding were relatively flat and significantly more pronounced effects of modifications causing relatively minor changes in WASP binding had been observed in previous studies using cellular readouts [47,63,90,92]. Since cytopathogenic activity and (N)-WASP binding hardly correlate and the concentrations of **290** used in confirmatory cellular experiments were very high, it can be debated to which extent the interaction with (N)-WASP contributes to the cellular mycolactone phenotypes. In this context, it is worth noting that the involvement of mycolactone-promoted WASP activation in the blockage of proinflammatory cytokine production has recently been questioned [89,111].

In their most recent contribution to the SAR of mycolactones, the groups of Blanchard and Demangel have dissected the immunosuppressive and cytotoxic properties of selected representatives from the set of C8-desmethylmycolactone analogs discussed above [257]. Notably, all of the molecules included in this recent study were devoid of the C14–C20 segment of the core extension. As shown in Table 5, immunosuppressive activity of mycolactone analogs was determined as the ability to block PMA/IO-induced IL-2 production in Jurkat T cells (expressed as IC_{50}), while cytotoxicity was determined as the capacity to provoke detachment-induced cell death in HeLa cells (in %) after 48 h at a fixed concentration (16 μM). As expected, all variants were less active than natural mycolactone A/B, which killed >80% of the cells at 16 μM and suppressed IL-2 production with an IC_{50} of 40 nM (Table 5). Unsurprisingly, the free extended core structure with a truncated upper side chain (**221**) and the cyclohexyl ester of lower mycolactone A/B side chain acid (**305**) exhibited no IL-2 suppressive activity up to 4 μM, the maximum concentration tested.

The SAR of the remaining compounds cannot be easily rationalized and there was no obvious correlation between IL-2 suppressive activity and WASP affinity. For example, C8-desmethylmycolactone A/B **285**, the structurally closest analog of the natural compound within this set, was inactive at 4 μM. In contrast, its close analog **290**, which lacks the C14–C20 segment of the core extension, was the most potent derivative with an IC_{50} of 1.5 μM. The effects of configurational changes at the C12', the C13', and the C15' stereocenters were rather ambiguous and IC_{50} values (in the narrow range) between 1.5 μM and >4 μM were determined for different trihydroxylated derivatives. All derivatives bearing only a single hydroxy substituent at the lower side chain (**299**–**301**) were inactive at 4 μM, while all dihydroxylated derivatives (**296**–**298**) had IC_{50} values between 2.5 μM and 4 μM. Likewise, derivatives incorporating a phenyl residue as part of the lower side chain were found to display a range of potencies; while compound **303** was among the most immunosuppressive derivatives tested ($IC_{50} \approx 1.7$ μM), **302** was only moderately

Table 5: Cytotoxicity and immunosuppressive properties of C8-desmethylmycolactones.

Mycolactone	% Cytotoxicity at 16 μM[a,b]	IC_{50} [μM] (IL-2 production)[b,c]
1a,**b**[d]	85	0.040[e]
285	80	>4
290	50	1.5
221	10	>4
296	60	2.7
297	80	2.8
298	40	3.7
299	30	>4
300	43	>4
301	40	>4
302	57	3.2
303	70	1.7
304	65	>4
305	45	>4
306	80	1.7
270	80	1.7

[a]Cell viability in HeLa cells after 48 h at a mycolactone concentration of 16 μM. [b]All numbers represent approximate values that have been manually extracted from a plot since no numerical data was given. [c]Suppression of PMA/IO-induced IL-2 production in Jurkat T cells.[d]Natural mycolactone A/B was used in this study. [e]Data from [87].

active (IC_{50} ≈ 3.2 μM) and **304** belonged to the group of inactive analogs (IC_{50} > 4 μM). Most notably, derivative **306**, which features a saturated C8-desmethyl C1–C13 mycolactone core and 4-pentyltriazolyl-substituted derivative **270** were among the most potent suppressors of IL-2 production, both with IC_{50}'s around 1.7 μM. At the same time, the latter compounds belong to the most cytotoxic analogs within this series (80% reduction in cell viability at 16 μM). In this context, it is worth mentioning that the IL-2 suppressive properties of all compounds investigated are significantly less pronounced than immunosuppressive effects of mycolactone E (**6**) or F (**8**) that have been determined under similar assay conditions by Leadlay and co-workers [63]. The comparability of the cytotoxicity data within the compound set is hampered by the fact that only a single concentration was tested. Despite these constraints, it is interesting to note that only a limited correlation could be observed between the immunosuppressive activity and cytotoxicity. For example, 8-desmethylmycolactone A/B (**285**) was relatively cytotoxic (≈80% reduction in cell viability at 16 μM), while being weakly immunosuppressive (IC_{50} > 4 μM). In contrast, truncated 8-desmethylmycolactone A/B **290** was less cytotoxic (≈50% reduction in cell viability at 16 μM), but a more potent immunosuppressant (IC_{50} = 1.5 μM). Similarly, no clear correlation between structure and activity was found. The only clear trend was that low cytotoxicity (<50% at 16 μM) was associated with the presence of a single hydroxy group at the lower side chain (**299**–**301**); this was also observed for ester **305** or the isolated (partially extended) C1–C13 core (**221**).

Despite the relatively flat SAR, derivative **290** was selected for further investigations, since it provided the best ratio between the suppression of IL-2 production and cytotoxicity. Compound **290** was tested for its capability to suppress stimulated TNFα, IL-2 or INF-γ production in polymorphonuclear neutrophils (PMN), monocyte-derived macrophages (MDM) and in $CD4^+$ T cells. Cytotoxicity against MDM cells and primary human dermal fibroblasts (HDF) as well as AT_2R binding in AT_2R-transfected HEK cells were also assessed (Table 6). IC_{50} values for **290** were generally in the low micromolar range in all assays, while values in the low nanomolar range were typically observed for mycolactone A/B.

A notable exception was AT_2R binding, where mycolactone A/B and **290** showed similar potency (16 μM vs 9 μM, respectively) for displacing the peptidic agonist radioligand [^{125}I]-CGP42,112A. Furthermore, while **290** was between 160- and 320-fold less potent than mycolactone A/B (**1a**,**b**) as an inhibitor of cytokine production, a roughly 500- and 2000-fold decreased toxicity against MDM and HDF cells, respectively, was observed, suggesting a slightly increased selectivity window for **290**. However, both mycolactone A/B and **290** were non-toxic to PMN and $CD4^+$ cells at immunosuppressive concentrations. In a mouse model for PMA-induced chronic skin inflammation,

Table 6: Diverse biological activities of mycolactone A/B (**1a**,**b**) and **290** (IC_{50} [nM]).

Mycolactone	TNFα[a]	TNFα[b]	Cell viability[c]	IL-2[d]	INF-γ[e]	AT_2R binding[f]
1a,**b**	13	12	18/6	12	7	9200
290	2000	3500	9000/12000	3900	1800	16000
IC_{50} ratio	162	285	514/1910	320	268	2

[a]Suppression of PMA-induced TNFα production in PMN cells. [b]Suppression of LPS-induced TNFα production in MDM cells. [c]Cell viability assessed by an MTT reduction assay after 72 h of incubation (MDM/HDF cells). [d]Suppression of PMA/IO-induced IL-2 production in $CD4^+$cells. [e]Suppression of PMA/IO-induced IFN-γ production $CD4^+$ cells. [f]Competitive binding to human AT_2R against 0.01 nM of the agonist radioligand [^{125}I]-CGP42,112A (K_d = 0.01 nM) in transfected HEK cells.

injection of mycolactone A/B showed a marked reduction in inflammatory response at 0.5 mg/kg, while a less pronounced effect was observed for 5 mg/kg of **290**. In contrast, 5 mg/kg of **290** were similarly effective as 0.5 mg/kg of mycolactone A/B in relieving inflammatory pain. Both compounds had little effect on acute pain in a mouse model relying on formalin injection. A mouse model for rheumatoid arthritis also demonstrated a moderate anti-rheumatic effect of natural mycolactone A/B, while **290** was not tested in this model. The observation that the cytotoxicity of mycolactones can at least be partially dissociated from their immunosuppressive and pain-relieving properties is interesting. However, its significantly reduced potency and the still narrow range between desired and undesired activities in combination with the complexity of **290** will likely prevent its (preclinical) development.

Conclusion

The complex structure of mycolactones has inspired many chemistry groups to develop elegant approaches towards the conserved extended mycolactone core structure and the variable lower side chain. Until now, all known natural mycolactones except mycolactone D were prepared by means of total synthesis and their structures have been validated. Moreover, the fascinating biology of mycolactones, which possess cytotoxic, immunosuppressive and analgesic properties, has stimulated the synthesis of modified analogs, that have been used to study structure–activity relationships and to decipher the molecular targets of these polyketides. Numerous natural mycolactones and synthetic derivatives have been tested for their biological activities in a variety of assay systems and fluorescent probes have unveiled the cellular localization of mycolactones. It has been shown that the effect of mycolactone exposure varies substantially between different cell lines and is highly dependent on the particular read-out employed. These observations may point to the involvement of several molecular targets in mycolactone bioactivity, in addition, those targets may have different expression levels and/or functions in different cell types. Four of these targets, namely (N)-WASP, the AT_2R receptor, the Sec61 translocon and the mTOR signaling pathway have been identified to date. However, so far, only the effects on (N)-WASP have been addressed by systematic SAR studies. Generally, the activity of mycolactones is highly sensitive to even minor structural changes at certain hotspots. This is impressively highlighted by the 125-fold drop in cytopathogenic activity upon removal of a single methyl group in the C8 position of the mycolactone core. Likewise, subtle changes in the hydroxylation pattern and the stereochemistry of the C5–O-linked lower side chain can have a major (lowering) impact on biological activity. In contrast to the lower side chain, the core extension seems to be more amenable to biologically tolerated modifications. For example, extensions at the C20 position can be introduced without appreciable effects on cytotoxicity and even the almost complete removal of the core extension is tolerated with regard to AT_2R receptor binding. The complex structure of mycolactones still leaves room for a plethora of structural modifications that will hopefully allow a further dissociation of the desired anti-inflammatory and pain-relieving properties from the pro-apoptotic effects considered responsible for Buruli ulcer pathology. To achieve this goal, further specific SAR studies on all known (and potential, unknown) molecular mycolactone targets would be highly desirable. The quest for a mycolactone-based therapy, however, is complicated by the enormous complexity even of simplified mycolactone analogs. Furthermore, the metabolically labile ester bond connecting the macrolactone core to the pharmacologically highly relevant lower side chain might hamper systemic application of such compounds and might necessitate bioisosteric replacement. However, even if endeavors towards mycolactone-derived therapeutics remain futile, the detailed knowledge on the molecular mycolactone targets, the underlying pathways and how these are linked to biological effects might stimulate the search for novel, drug-like molecules modulating those networks, thereby fueling the drug pipeline.

Acknowlegements

The authors are grateful to Lukas Leu, Barbara Stoessel, Jennifer Mueller, Simon Glauser and Adriana Edenharter for proofreading. Moreover, we want to thank Dr. Philipp Gers-

bach, Dr. Claudio Bomio, Dr. Jun Li, Amina Salihovic and Pascal Bucher for their contributions to the (unpublished) syntheses of mycolactones presented in this review.

References

1. Weir, E. *Can. Med. Assoc. J.* **2002,** *166,* 1691.
2. WORLD HEALTH ORGANIZATION Geneva. *Wkly. Epidemiol. Rec.* **2008,** *83,* 145–156.
3. Fact sheet Buruli ulcer. WHO, http://www.who.int/mediacentre/factsheets/fs199/en/ (accessed Jan 9, 2017).
4. Walsh, D. S.; Portaels, F.; Meyers, W. M. *Clin. Microbiol. Newsl.* **2009,** *31,* 119–127. doi:10.1016/j.clinmicnews.2009.07.004
5. Hayman, J.; McQueen, A. *Pathology* **1985,** *17,* 594–600. doi:10.3109/00313028509084759
6. Vincent, Q. B.; Ardant, M.-F.; Adeye, A.; Goundote, A.; Saint-André, J.-P.; Cottin, J.; Kempf,, M.; Agossadou, D.; Johnson, C.; Abel, L.; Marsollier, L.; Chauty, A.; Alcaïs, A. *Lancet Global Health* **2014,** *2,* e422–e430. doi:10.1016/S2214-109X(14)70223-2
7. Van der Werf, T. S.; Stienstra, Y.; Johnson, C. R.; Phillips, R.; Ohene, A.; Fleischer, B.; Wansbrough-Jones, M.; Johnson, P. D. R.; Portaels, F.; Van der Graaf, W. T. A.; Asiedu, K. *Bull. W. H. O.* **2005,** *83,* 785–791.
8. Yeboah-Manu, D.; Kpeli, G. S.; Ruf, M.-T.; Asan-Ampah, K.; Quenin-Fosu, K.; Owusu-Mireku, E.; Paintsil, A.; Lamptey, I.; Anku, B.; Kwakye-Maclean, C.; Newman, M.; Pluschke, G. *PLoS Negl. Trop. Dis.* **2013,** *7,* e2191. doi:10.1371/journal.pntd.0002191
9. Asiedu, K.; Etuaful, S. *Am. J. Trop. Med. Hyg.* **1998,** *59,* 1015–1022. doi:10.4269/ajtmh.1998.59.1015
10. Debacker, M.; Aguiar, J.; Steunou, C.; Zinsou, C.; Meyers, W. M.; Guédénon, A.; Scott, J. T.; Dramaix, M.; Portaels, F. *Emerging Infect. Dis.* **2004,** *10,* 1391–1398. doi:10.3201/eid1008.030886
11. Global Health Observatory (GHO) data on Buruli ulcer. WHO, http://apps.who.int/neglected_diseases/ntddata/buruli/buruli.html (accessed Jan 26, 2017).
12. Pluschke, G.; Röltgen, K. *Res. Rep. Trop. Med.* **2015,** *6,* 59–73. doi:10.2147/RRTM.S62026
13. Grant, J. A. *A walk across Africa or Domestic scenes from my Nile journal;* W. Blackwood and sons: Edinburgh, London, 1864.
14. Phanzu, D. M.; Ablordey, A.; Imposo, D. B.; Lefevre, L.; Mahema, R. L.; Suykerbuyk, P.; Meyers, W. M.; Portaels, F. *Am. J. Trop. Med. Hyg.* **2007,** *77,* 1099–1102.
15. B. M. J. *Br. Med. J.* **1970,** *2,* 378–379. doi:10.1136/bmj.2.5706.378-a
16. MacCallum, P.; Tolhurst, J. C.; Buckle, G.; Sissons, H. A. *J. Pathol. Bacteriol.* **1948,** *60,* 93–122. doi:10.1002/path.1700600111
17. Fenner, F.; Leach, R. H. *Aust. J. Exp. Biol. Med. Sci.* **1952,** *30,* 1–10. doi:10.1038/icb.1952.1
18. Palomino, J. C.; Obiang, A. M.; Realini, L.; Meyers, W. M.; Portaels, F. *J. Clin. Microbiol.* **1998,** *36,* 3420–3422.
19. Jannsens, P. G.; Quertinmont, M. J.; Sieniawski, J.; Gatti, F. *Trop. Geogr. Med.* **1959,** *11,* 293–312.
20. Clancey, J. K.; Dodge, O. G.; Lunn, H. F.; Oduori, M. L. *Lancet* **1961,** *278,* 951–954. doi:10.1016/S0140-6736(61)90793-0
21. Connor, D. H.; Lunn, H. F. *Arch. Pathol.* **1966,** *81,* 183–199.
22. Lunn, H. F.; Connor, D. H.; Wilks, N. E.; Barnley, G. R.; Kamunvi, F.; Clancey, J. K.; Bee, J. D. *East Afr. Med. J.* **1965,** *42,* 275–288.
23. Epidemiology of Mycobacterium ulcerans infection (buruli ulcer) at Kinyara, Uganda. *Trans. R. Soc. Trop. Med. Hyg.* **1971,** *65,* 763–775. doi:10.1016/0035-9203(71)90090-3
24. Merritt, R. W.; Walker, E. D.; Small, P. L. C.; Wallace, J. R.; Johnson, P. D. R.; Benbow, M. E.; Boakye, D. A. *PLoS Negl. Trop. Dis.* **2010,** *4,* e911. doi:10.1371/journal.pntd.0000911
25. Hayman, J. *Int. J. Epidemiol.* **1991,** *20,* 1093–1098. doi:10.1093/ije/20.4.1093
26. Marsollier, L.; Robert, R.; Aubry, J.; André, J.-P. S.; Kouakou, H.; Legras, P.; Manceau, A.-L.; Mahaza, C.; Carbonnelle, B. *Appl. Environ. Microbiol.* **2002,** *68,* 4623–4628. doi:10.1128/AEM.68.9.4623-4628.2002
27. Johnson, P. D. R.; Azuolas, J.; Lavender, C. J.; Wishart, E.; Stinear, T. P.; Hayman, J. A.; Brown, L.; Jenkin, G. A.; Fyfe, J. A. M. *Emerging Infect. Dis.* **2007,** *13,* 1653–1660. doi:10.3201/eid1311.061369
28. Willson, S. J.; Kaufman, M. G.; Merritt, R. W.; Williamson, H. R.; Malakauskas, D. M.; Benbow, M. E. *Infect. Ecol. Epidemiol.* **2013,** *3,* No. 19946. doi:10.3402/iee.v3i0.19946
29. Krieg, R. E.; Hockmeyer, W. T.; Connor, D. H. *AMA Arch. Dermatol.* **1974,** *110,* 783–788. doi:10.1001/archderm.1974.01630110073023
30. Read, J. K.; Heggie, C. M.; Meyers, W. M.; Connor, D. H. *Infect. Immun.* **1974,** *9,* 1114–1122.
31. Hockmeyer, W. T.; Krieg, R. E.; Reich, M.; Johnson, R. D. *Infect. Immun.* **1978,** *21,* 124–128.
32. George, K. M.; Chatterjee, D.; Gunawardana, G.; Welty, D.; Hayman, J.; Lee, R.; Small, P. L. C. *Science* **1999,** *283,* 854–857. doi:10.1126/science.283.5403.854
33. George, K. M.; Barker, L. P.; Welty, D. M.; Small, P. L. C. *Infect. Immun.* **1998,** *66,* 587–593.
34. Rohr, J. *Angew. Chem., Int. Ed.* **2000,** *39,* 2847–2849. doi:10.1002/1521-3773(20000818)39:16<2847::AID-ANIE2847>3.0.CO;2-0
35. Adusumilli, S.; Mve-Obiang, A.; Sparer, T.; Meyers, W.; Hayman, J.; Small, P. L. C. *Cell. Microbiol.* **2005,** *7,* 1295–1304. doi:10.1111/j.1462-5822.2005.00557.x
36. Gunawardana, G.; Chatterjee, D.; George, K. M.; Brennan, P.; Whittern, D.; Small, P. L. C. *J. Am. Chem. Soc.* **1999,** *121,* 6092–6093. doi:10.1021/ja990017l
37. Wang, G.; Yin, N.; Negishi, E.-i. *Chem. – Eur. J.* **2011,** *17,* 4118–4130. doi:10.1002/chem.201002627
38. Hoffmann, R. W. *Chem. Rev.* **1989,** *89,* 1841–1860. doi:10.1021/cr00098a009
39. Benowitz, A. B.; Fidanze, S.; Small, P. L. C.; Kishi, Y. *J. Am. Chem. Soc.* **2001,** *123,* 5128–5129. doi:10.1021/ja0105414
40. Fidanze, S.; Song, F.; Szlosek-Pinaud, M.; Small, P. L. C.; Kishi, Y. *J. Am. Chem. Soc.* **2001,** *123,* 10117–10118. doi:10.1021/ja011824z
41. Kobayashi, Y.; Lee, J.; Tezuka, K.; Kishi, Y. *Org. Lett.* **1999,** *1,* 2177–2180. doi:10.1021/ol9903786
42. Kobayashi, Y.; Hayashi, N.; Kishi, Y. *Org. Lett.* **2001,** *3,* 2253–2255. doi:10.1021/ol010110q
43. Song, F.; Fidanze, S.; Benowitz, A. B.; Kishi, Y. *Org. Lett.* **2002,** *4,* 647–650. doi:10.1021/ol0172828
44. Röltgen, K.; Stinear, T. P.; Pluschke, G. *Infect., Genet. Evol.* **2012,** *12,* 522–529. doi:10.1016/j.meegid.2012.01.018
45. Pidot, S. J.; Asiedu, K.; Käser, M.; Fyfe, J. A. M.; Stinear, T. P. *PLoS Negl. Trop. Dis.* **2010,** *4,* e663. doi:10.1371/journal.pntd.0000663

46. Van der Werf, T. S.; Van der Graaf, W. T.; Tappero, J. W.; Asiedu, K. *Lancet* **1999,** *354,* 1013–1018. doi:10.1016/S0140-6736(99)01156-3
47. Mve-Obiang, A.; Lee, R. E.; Portaels, F.; Small, P. L. C. *Infect. Immun.* **2003,** *71,* 774–783. doi:10.1128/IAI.71.2.774-783.2003
48. Faber, W. R.; Arias-Bouda, L. M. P.; Zeegelaar, J. E.; Kolk, A. H. J.; Fonteyne, P.-A.; Toonstra, J.; Portaels, F. *Trans. R. Soc. Trop. Med. Hyg.* **2000,** *94,* 277–279. doi:10.1016/S0035-9203(00)90320-1
49. Kazumi, Y.; Ohtomo, K.; Takahashi, M.; Mitarai, S.; Sugawara, I.; Izumi, J.; Andoh, A.; Hasegawa, H. *Kekkaku* **2004,** *79,* 437–441. doi:10.11400/kekkaku1923.79.437
50. Mve-Obiang, A.; Lee, R. E.; Umstot, E. S.; Trott, K. A.; Grammer, T. C.; Parker, J. M.; Ranger, B. S.; Grainger, R.; Mahrous, E. A.; Small, P. L. C. *Infect. Immun.* **2005,** *73,* 3307–3312. doi:10.1128/IAI.73.6.3307-3312.2005
51. Cadapan, L. D.; Arslanian, R. L.; Carney, J. R.; Zavala, S. M.; Small, P. L. C.; Licari, P. *FEMS Microbiol. Lett.* **2001,** *205,* 385–389. doi:10.1111/j.1574-6968.2001.tb10977.x
52. Hong, H.; Gates, P. J.; Staunton, J.; Stinear, T.; Cole, S. T.; Leadlay, P. F.; Spencer, J. B. *Chem. Commun.* **2003,** 2822–2823. doi:10.1039/b308163j
53. Judd, T. C.; Bischoff, A.; Kishi, Y.; Adusumilli, S.; Small, P. L. C. *Org. Lett.* **2004,** *6,* 4901–4904. doi:10.1021/ol0479996
54. Hong, H.; Spencer, J. B.; Porter, J. L.; Leadlay, P. F.; Stinear, T. *ChemBioChem* **2005,** *6,* 643–648. doi:10.1002/cbic.200400339
55. Ranger, B. S.; Mahrous, E. A.; Mosi, L.; Adusumilli, S.; Lee, R. E.; Colorni, A.; Rhodes, M.; Small, P. L. C. *Infect. Immun.* **2006,** *74,* 6037–6045. doi:10.1128/IAI.00970-06
56. Hong, H.; Stinear, T.; Skelton, P.; Spencer, J. B.; Leadlay, P. F. *Chem. Commun.* **2005,** 4306–4308. doi:10.1039/b506835e
57. Aubry, S.; Lee, R. E.; Mahrous, E. A.; Small, P. L. C.; Beachboard, D.; Kishi, Y. *Org. Lett.* **2008,** *10,* 5385–5388. doi:10.1021/ol802233f
58. Spangenberg, T.; Aubry, S.; Kishi, Y. *Tetrahedron Lett.* **2010,** *51,* 1782–1785. doi:10.1016/j.tetlet.2010.01.105
59. Kim, H.-J.; Kishi, Y. *J. Am. Chem. Soc.* **2008,** *130,* 1842–1844. doi:10.1021/ja7111838
60. Kobayashi, Y.; Tan, C.-H.; Kishi, Y. *Helv. Chim. Acta* **2000,** *83,* 2562–2571. doi:10.1002/1522-2675(20000906)83:9<2562::AID-HLCA2562>3.0.CO;2-Z
61. Kim, H.-J.; Jackson, K. L.; Kishi, Y.; Williamson, H. R.; Mosi, L.; Small, P. L. C. *Chem. Commun.* **2009,** 7402–7404. doi:10.1039/b917014f
62. Hande, S. M.; Kazumi, Y.; Lai, W. G.; Jackson, K. L.; Maeda, S.; Kishi, Y. *Org. Lett.* **2012,** *14,* 4618–4621. doi:10.1021/ol302072b
63. Hong, H.; Stinear, T.; Porter, J.; Demangel, C.; Leadlay, P. F. *ChemBioChem* **2007,** *8,* 2043–2047. doi:10.1002/cbic.200700411
64. Portaels, F. *Laboratory diagnosis of buruli ulcer: A manual for health care providers;* WHO: Geneva, 2014.
65. Okenu, D. M. N.; Ofielu, L. O.; Easley, K. A.; Guarner, J.; Spotts Whitney, E. A.; Raghunathan, P. L.; Stienstra, Y.; Asamoa, K.; van der Werf, T. S.; van der Graaf, W. T. A.; Tappero, J. W.; Ashford, D. A.; King, C. H. *Clin. Diagn. Lab. Immunol.* **2004,** *11,* 387–391. doi:10.1128/CDLI.11.2.387-391.2004
66. Sarfo, F. S.; Phillips, R. O.; Zhang, J.; Abass, M. K.; Abotsi, J.; Amoako, Y. A.; Adu-Sarkodie, Y.; Robinson, C.; Wansbrough-Jones, M. H. *BMC Infect. Dis.* **2014,** *14,* 202. doi:10.1186/1471-2334-14-202
67. Sakyi, S. A.; Aboagye, S. Y.; Otchere, I. D.; Liao, A. M.; Caltagirone, T. G.; Yeboah-Manu, D. *PLoS Negl. Trop. Dis.* **2016,** *10,* e0004950. doi:10.1371/journal.pntd.0004950
68. Spangenberg, T.; Kishi, Y. *Chem. Commun.* **2010,** *46,* 1410–1412. doi:10.1039/b924896j
69. Converse, P. J.; Xing, Y.; Kim, K. H.; Tyagi, S.; Li, S.-Y.; Almeida, D. V.; Nuermberger, E. L.; Grosset, J. H.; Kishi, Y. *PLoS Negl. Trop. Dis.* **2014,** *8,* e2618. doi:10.1371/journal.pntd.0002618
70. Wadagni, A.; Frimpong, M.; Phanzu, D. M.; Ablordey, A.; Kacou, E.; Gbedevi, M.; Marion, E.; Xing, Y.; Babu, V. S.; Phillips, R. O.; Wansbrough-Jones, M.; Kishi, Y.; Asiedu, K. *PLoS Negl. Trop. Dis.* **2015,** *9,* e0004247. doi:10.1371/journal.pntd.0004247
71. Siegmund, V.; Adjei, O.; Nitschke, J.; Thompson, W.; Klutse, E.; Herbinger, K. H.; Thompson, R.; Van Vloten, F.; Racz, P.; Fleischer, B.; Loescher, T.; Bretzel, G. *Clin. Infect. Dis.* **2007,** *45,* 68–75. doi:10.1086/518604
72. Phillips, R.; Horsfield, C.; Kuijper, S.; Lartey, A.; Tetteh, I.; Etuaful, S.; Nyamekye, B.; Awuah, P.; Nyarko, K. M.; Osei-Sarpong, F.; Lucas, S.; Kolk, A. H. J.; Wansbrough-Jones, M. *J. Clin. Microbiol.* **2005,** *43,* 3650–3656. doi:10.1128/JCM.43.8.3650-3656.2005
73. Gordon, C. L.; Buntine, J. A.; Hayman, J. A.; Lavender, C. J.; Fyfe, J. A.; Hosking, P.; Johnson, P. D. R. *PLoS Negl. Trop. Dis.* **2011,** *5,* e1290. doi:10.1371/journal.pntd.0001290
74. WHO. *Treatment of Mycobacterium Ulcerans Disease (Buruli Ulcer): Guidance for Health Workers;* WHO: Geneva, 2012.
75. Converse, P. J.; Nuermberger, E. L.; Almeida, D. V.; Grosset, J. H. *Future Microbiol.* **2011,** *6,* 1185–1198. doi:10.2217/fmb.11.101
76. Huang, G. K. L.; Johnson, P. D. R. *Expert Rev. Anti-Infect. Ther.* **2014,** *12,* 855–865. doi:10.1586/14787210.2014.910113
77. Pahlevan, A. A.; Wright, D. J. M.; Andrews, C.; George, K. M.; Small, P. L. C.; Foxwell, B. M. *J. Immunol.* **1999,** *163,* 3928–3935.
78. En, J.; Goto, M.; Nakanaga, K.; Higashi, M.; Ishii, N.; Saito, H.; Yonezawa, S.; Hamada, H.; Small, P. L. C. *Infect. Immun.* **2008,** *76,* 2002–2007. doi:10.1128/IAI.01588-07
79. Sarfo, F. S.; Phillips, R.; Wansbrough-Jones, M.; Simmonds, R. E. *Cell. Microbiol.* **2016,** *18,* 17–29. doi:10.1111/cmi.12547
80. Simmonds, R. E.; Lali, F. V.; Smallie, T.; Small, P. L. C.; Foxwell, B. M. *J. Immunol.* **2009,** *182,* 2194–2202. doi:10.4049/jimmunol.0802294
81. Coutanceau, E.; Decalf, J.; Martino, A.; Babon, A.; Winter, N.; Cole, S. T.; Albert, M. L.; Demangel, C. *J. Exp. Med.* **2007,** *204,* 1395–1403. doi:10.1084/jem.20070234
82. George, K. M.; Pascopella, L.; Welty, D. M.; Small, P. L. C. *Infect. Immun.* **2000,** *68,* 877–883. doi:10.1128/IAI.68.2.877-883.2000
83. Dobos, K. M.; Small, P. L.; Deslauriers, M.; Quinn, F. D.; King, C. H. *Infect. Immun.* **2001,** *69,* 7182–7186. doi:10.1128/IAI.69.11.7182-7186.2001
84. Callus, B. A.; Vaux, D. L. *Cell Death Differ.* **2006,** *14,* 73–78. doi:10.1038/sj.cdd.4402034
85. Bozzo, C.; Tiberio, R.; Graziola, F.; Pertusi, G.; Valente, G.; Colombo, E.; Small, P. L. C.; Leigheb, G. *Microbes Infect.* **2010,** *12,* 1258–1263. doi:10.1016/j.micinf.2010.08.005
86. Ogbechi, J.; Ruf, M.-T.; Hall, B. S.; Bodman-Smith, K.; Vogel, M.; Wu, H.-L.; Stainer, A.; Esmon, C. T.; Ahnström, J.; Pluschke, G.; Simmonds, R. E. *PLoS Pathog.* **2015,** *11,* e1005011. doi:10.1371/journal.ppat.1005011
87. Boulkroun, S.; Guenin-Macé, L.; Thoulouze, M.-I.; Monot, M.; Merckx, A.; Langsley, G.; Bismuth, G.; Bartolo, V. D.; Demangel, C. *J. Immunol.* **2010,** *184,* 1436–1444. doi:10.4049/jimmunol.0902854

88. Guenin-Macé, L.; Carrette, F.; Asperti-Boursin, F.; Bon, A. L.; Caleechurn, L.; Bartolo, V. D.; Fontanet, A.; Bismuth, G.; Demangel, C. *Proc. Natl. Acad. Sci. U. S. A.* **2011,** *108,* 12833–12838. doi:10.1073/pnas.1016496108
89. Hall, B. S.; Hill, K.; McKenna, M.; Ogbechi, J.; High, S.; Willis, A. E.; Simmonds, R. E. *PLoS Pathog.* **2014,** *10,* e1004061. doi:10.1371/journal.ppat.1004061
90. Scherr, N.; Gersbach, P.; Dangy, J.-P.; Bomio, C.; Li, J.; Altmann, K.-H.; Pluschke, G. *PLoS Negl. Trop. Dis.* **2013,** *7,* e2143. doi:10.1371/journal.pntd.0002143
91. Snyder, D. S.; Small, P. L. C. *Microb. Pathog.* **2003,** *34,* 91–101. doi:10.1016/S0882-4010(02)00210-3
92. Chany, A.-C.; Casarotto, V.; Schmitt, M.; Tarnus, C.; Guenin-Macé, L.; Demangel, C.; Mirguet, O.; Eustache, J.; Blanchard, N. *Chem. – Eur. J.* **2011,** *17,* 14413–14419. doi:10.1002/chem.201102542
93. Guenin-Macé, L.; Veyron-Churlet, R.; Thoulouze, M.-I.; Romet-Lemonne, G.; Hong, H.; Leadlay, P. F.; Danckaert, A.; Ruf, M.-T.; Mostowy, S.; Zurzolo, C.; Bousso, P.; Chrétien, F.; Carlier, M.-F.; Demangel, C. *J. Clin. Invest.* **2013,** *123,* 1501–1512. doi:10.1172/JCI66576
94. Takenawa, T.; Suetsugu, S. *Nat. Rev. Mol. Cell Biol.* **2007,** *8,* 37–48. doi:10.1038/nrm2069
95. Miki, H.; Takenawa, T. *J. Biochem.* **2003,** *134,* 309–313. doi:10.1093/jb/mvg146
96. Prehoda, K. E.; Scott, J. A.; Mullins, R. D.; Lim, W. A. *Science* **2000,** *290,* 801–806. doi:10.1126/science.290.5492.801
97. Peterson, J. R.; Bickford, L. C.; Morgan, D.; Kim, A. S.; Ouerfelli, O.; Kirschner, M. W.; Rosen, M. K. *Nat. Struct. Mol. Biol.* **2004,** *11,* 747–755. doi:10.1038/nsmb796
98. McKenna, M.; Simmonds, R. E.; High, S. *J. Cell Sci.* **2016,** *129,* 1404–1415. doi:10.1242/jcs.182352
99. Benham, A. M. *Cold Spring Harbor Perspect. Biol.* **2012,** *4,* a012872. doi:10.1101/cshperspect.a012872
100. Breitling, J.; Aebi, M. *Cold Spring Harbor Perspect. Biol.* **2013,** *5,* a013359. doi:10.1101/cshperspect.a013359
101. Ong, S.-E.; Blagoev, B.; Kratchmarova, I.; Kristensen, D. B.; Steen, H.; Pandey, A.; Mann, M. *Mol. Cell. Proteomics* **2002,** *1,* 376–386. doi:10.1074/mcp.M200025-MCP200
102. Baron, L.; Paatero, A. O.; Morel, J.-D.; Impens, F.; Guenin-Macé, L.; Saint-Auret, S.; Blanchard, N.; Dillmann, R.; Niang, F.; Pellegrini, S.; Taunton, J.; Paavilainen, V. O.; Demangel, C. *J. Exp. Med.* **2016,** *213,* 2885–2896. doi:10.1084/jem.20160662
103. Bieri, R.; Bolz, M.; Ruf, M.-T.; Pluschke, G. *PLoS Negl. Trop. Dis.* **2016,** *10,* e0004450. doi:10.1371/journal.pntd.0004450
104. Marion, E.; Song, O.-R.; Christophe, T.; Babonneau, J.; Fenistein, D.; Eyer, J.; Letournel, F.; Henrion, D.; Clere, N.; Paille, V.; Guérineau, N. C.; Saint André, J.-P.; Gersbach, P.; Altmann, K.-H.; Stinear, T. P.; Comoglio, Y.; Sandoz, G.; Preisser, L.; Delneste, Y.; Yeramian, E.; Marsollier, L.; Brodin, P. *Cell* **2014,** *157,* 1565–1576. doi:10.1016/j.cell.2014.04.040
105. Goto, M.; Nakanaga, K.; Aung, T.; Hamada, T.; Yamada, N.; Nomoto, M.; Kitajima, S.; Ishii, N.; Yonezawa, S.; Saito, H. *Am. J. Pathol.* **2006,** *168,* 805–811. doi:10.2353/ajpath.2006.050375
106. Timmermans, P. B.; Wong, P. C.; Chiu, A. T.; Herblin, W. F.; Benfield, P.; Carini, D. J.; Lee, R. J.; Wexler, R. R.; Saye, J. A.; Smith, R. D. *Pharmacol. Rev.* **1993,** *45,* 205–251.
107. Pelegrini-da-Silva, A.; Martins, A. R.; Prado, W. A. *Neuroscience* **2005,** *132,* 453–463. doi:10.1016/j.neuroscience.2004.12.046
108. Anand, U.; Sinisi, M.; Fox, M.; MacQuillan, A.; Quick, T.; Korchev, Y.; Bountra, C.; McCarthy, T.; Anand, P. *Mol. Pain* **2016,** *12,* 1–11. doi:10.1177/1744806916654144
109. Caterina, M. J.; Schumacher, M. A.; Tominaga, M.; Rosen, T. A.; Levine, J. D.; Julius, D. *Nature* **1997,** *389,* 816–824. doi:10.1038/39807
110. Rice, A. S. C.; Dworkin, R. H.; McCarthy, T. D.; Anand, P.; Bountra, C.; McCloud, P. I.; Hill, J.; Cutter, G.; Kitson, G.; Desem, N.; Raff, M. *Lancet* **2014,** *383,* 1637–1647. doi:10.1016/S0140-6736(13)62337-5
111. Bieri, R.; Scherr, N.; Ruf, M.-T.; Dangy, J.-P.; Gersbach, P.; Gehringer, M.; Altmann, K.-H.; Pluschke, G. *ACS Chem. Biol.* **2017,** *12,* 1297–1307. doi:10.1021/acschembio.7b00053
112. Laplante, M.; Sabatini, D. M. *Cell* **2012,** *149,* 274–293. doi:10.1016/j.cell.2012.03.017
113. Guertin, D. A.; Stevens, D. M.; Thoreen, C. C.; Burds, A. A.; Kalaany, N. Y.; Moffat, J.; Brown, M.; Fitzgerald, K. J.; Sabatini, D. M. *Dev. Cell* **2006,** *11,* 859–871. doi:10.1016/j.devcel.2006.10.007
114. Janes, M. R.; Limon, J. J.; So, L.; Chen, J.; Lim, R. J.; Chavez, M. A.; Vu, C.; Lilly, M. B.; Mallya, S.; Ong, S. T.; Konopleva, M.; Martin, M. B.; Ren, P.; Liu, Y.; Rommel, C.; Fruman, D. A. *Nat. Med.* **2010,** *16,* 205–213. doi:10.1038/nm.2091
115. Fu, Z.; Tindall, D. J. *Oncogene* **2008,** *27,* 2312–2319. doi:10.1038/onc.2008.24
116. Slee, E. A.; Zhu, H.; Chow, S. C.; MacFarlane, M.; Nicholson, D. W.; Cohen, G. M. *Biochem. J.* **1996,** *315,* 21–24. doi:10.1042/bj3150021
117. Wu, Y.-T.; Tan, H.-L.; Shui, G.; Bauvy, C.; Huang, Q.; Wenk, M. R.; Ong, C.-N.; Codogno, P.; Shen, H.-M. *J. Biol. Chem.* **2010,** *285,* 10850–10861. doi:10.1074/jbc.M109.080796
118. Degterev, A.; Hitomi, J.; Germscheid, M.; Ch'en, I. L.; Korkina, O.; Teng, X.; Abbott, D.; Cuny, G. D.; Yuan, C.; Wagner, G.; Hedrick, S. M.; Gerber, S. A.; Lugovskoy, A.; Yuan, J. *Nat. Chem. Biol.* **2008,** *4,* 313–321. doi:10.1038/nchembio.83
119. Sarbassov, D. D.; Ali, S. M.; Sengupta, S.; Sheen, J.-H.; Hsu, P. P.; Bagley, A. F.; Markhard, A. L.; Sabatini, D. M. *Mol. Cell* **2006,** *22,* 159–168. doi:10.1016/j.molcel.2006.03.029
120. Watanabe, S.; Umehara, H.; Murayama, K.; Okabe, M.; Kimura, T.; Nakano, T. *Oncogene* **2006,** *25,* 2697–2707. doi:10.1038/sj.onc.1209307
121. Cernijenko, A.; Risgaard, R.; Baran, P. S. *J. Am. Chem. Soc.* **2016,** *138,* 9425–9428. doi:10.1021/jacs.6b06623
122. Song, F.; Fidanze, S.; Benowitz, A. B.; Kishi, Y. *Tetrahedron* **2007,** *63,* 5739–5753. doi:10.1016/j.tet.2007.02.057
123. Jackson, K. L.; Li, W.; Chen, C.-L.; Kishi, Y. *Tetrahedron* **2010,** *66,* 2263–2272. doi:10.1016/j.tet.2010.02.010
124. Negishi, E.; Okukado, N.; King, A. O.; Van Horn, D. E.; Spiegel, B. I. *J. Am. Chem. Soc.* **1978,** *100,* 2254–2256. doi:10.1021/ja00475a059
125. Paterson, I.; Craw, P. A. *Tetrahedron Lett.* **1989,** *30,* 5799–5802. doi:10.1016/S0040-4039(00)76201-0
126. Brown, H. C.; Bhat, K. S. *J. Am. Chem. Soc.* **1986,** *108,* 293–294. doi:10.1021/ja00262a017
127. Brown, H. C.; Bhat, K. S. *J. Am. Chem. Soc.* **1986,** *108,* 5919–5923. doi:10.1021/ja00279a042
128. Seyferth, D.; Marmor, R. S.; Hilbert, P. *J. Org. Chem.* **1971,** *36,* 1379–1386. doi:10.1021/jo00809a014
129. Gilbert, J. C.; Weerasooriya, U. *J. Org. Chem.* **1982,** *47,* 1837–1845. doi:10.1021/jo00349a007
130. Ohira, S. *Synth. Commun.* **1989,** *19,* 561–564. doi:10.1080/00397918908050700

131. Müller, S.; Liepold, B.; Roth, G. J.; Bestmann, H. J. *Synlett* **1996,** *1996,* 521–522. doi:10.1055/s-1996-5474
132. Hart, D. W.; Schwartz, J. *J. Am. Chem. Soc.* **1974,** *96,* 8115–8116. doi:10.1021/ja00833a048
133. Murakami, N.; Wang, W.; Aoki, M.; Tsutsui, Y.; Higuchi, K.; Aoki, S.; Kobayashi, M. *Tetrahedron Lett.* **1997,** *38,* 5533–5536. doi:10.1016/S0040-4039(97)01194-5
134. Smith, A. B., III; Qiu, Y.; Jones, D. R.; Kobayashi, K. *J. Am. Chem. Soc.* **1995,** *117,* 12011–12012. doi:10.1021/ja00153a030
135. Inanaga, J.; Hirata, K.; Saeki, H.; Katsuki, T.; Yamaguchi, M. *Bull. Chem. Soc. Jpn.* **1979,** *52,* 1989–1993. doi:10.1246/bcsj.52.1989
136. Seebach, D.; Wasmuth, D. *Helv. Chim. Acta* **1980,** *63,* 197–200. doi:10.1002/hlca.19800630118
137. LeGoff, E. *J. Org. Chem.* **1964,** *29,* 2048–2050. doi:10.1021/jo01030a529
138. Han, X.; Stoltz, B. M.; Corey, E. J. *J. Am. Chem. Soc.* **1999,** *121,* 7600–7605. doi:10.1021/ja991500z
139. Appel, R. *Angew. Chem., Int. Ed. Engl.* **1975,** *14,* 801–811. doi:10.1002/anie.197508011
140. Marshall, J. A.; Shearer, B. G.; Crooks, S. L. *J. Org. Chem.* **1987,** *52,* 1236–1245. doi:10.1021/jo00383a012
141. Sonogashira, K.; Tohda, Y.; Hagihara, N. *Tetrahedron Lett.* **1975,** *16,* 4467–4470. doi:10.1016/S0040-4039(00)91094-3
142. Matsumoto, K.; Sawada, Y.; Katsuki, T. *Synlett* **2006,** 3545–3547. doi:10.1055/s-2006-956496
143. Langille, N. F.; Jamison, T. F. *Org. Lett.* **2006,** *8,* 3761–3764. doi:10.1021/ol0613721
144. Katsuki, T.; Sharpless, K. B. *J. Am. Chem. Soc.* **1980,** *102,* 5974–5976. doi:10.1021/ja00538a077
145. Marples, B. A.; Saint, C. G.; Traynor, J. R. *J. Chem. Soc., Perkin Trans. 1* **1986,** 567–574. doi:10.1039/P19860000567
146. Corey, E. J.; Fuchs, P. L. *Tetrahedron Lett.* **1972,** *13,* 3769–3772. doi:10.1016/S0040-4039(01)94157-7
147. VanRheenen, V.; Kelly, R. C.; Cha, D. Y. *Tetrahedron Lett.* **1976,** *17,* 1973–1976. doi:10.1016/S0040-4039(00)78093-2
148. Pappo, R.; Allen, D. S., Jr.; Lemieux, R. U.; Johnson, W. S. *J. Org. Chem.* **1956,** *21,* 478–479. doi:10.1021/jo01110a606
149. Corey, E. J.; Enders, D.; Bock, M. G. *Tetrahedron Lett.* **1976,** *17,* 7–10. doi:10.1016/S0040-4039(00)71308-6
150. Schlessinger, R. H.; Poss, M. A.; Richardson, S.; Lin, P. *Tetrahedron Lett.* **1985,** *26,* 2391–2394. doi:10.1016/S0040-4039(00)94835-4
151. Desmond, R.; Mills, S. G.; Volante, R. P.; Shinkai, I. *Tetrahedron Lett.* **1988,** *29,* 3895–3898. doi:10.1016/S0040-4039(00)80374-3
152. Peterson, D. J. *J. Org. Chem.* **1968,** *33,* 780–784. doi:10.1021/jo01266a061
153. Matsushita, H.; Negishi, E. *J. Am. Chem. Soc.* **1981,** *103,* 2882–2884. doi:10.1021/ja00400a074
154. Negishi, E.; Baba, S.; King, A. O. *J. Chem. Soc., Chem. Commun.* **1976,** 17–18. doi:10.1039/C39760000017
155. Kobayashi, M.; Valente, L. F.; Negishi, E.; Patterson, W.; Silveira, A., Jr. *Synthesis* **1980,** *1980,* 1034–1035. doi:10.1055/s-1980-29313
156. Bal, B. S.; Childers, W. E., Jr.; Pinnick, H. W. *Tetrahedron* **1981,** *37,* 2091–2096. doi:10.1016/S0040-4020(01)97963-3
157. Kraus, G. A.; Taschner, M. J. *J. Org. Chem.* **1980,** *45,* 1175–1176. doi:10.1021/jo01294a058
158. Villemin, D. *Tetrahedron Lett.* **1980,** *21,* 1715–1718. doi:10.1016/S0040-4039(00)77818-X
159. Wittig, G.; Schöllkopf, U. *Chem. Ber.* **1954,** *87,* 1318–1330. doi:10.1002/cber.19540870919
160. Wittig, G.; Haag, W. *Chem. Ber.* **1955,** *88,* 1654–1666. doi:10.1002/cber.19550881110
161. Julia, M.; Paris, J.-M. *Tetrahedron Lett.* **1973,** *14,* 4833–4836. doi:10.1016/S0040-4039(01)87348-2
162. Kocienski, P. J.; Lythgoe, B.; Waterhouse, I. *J. Chem. Soc., Perkin Trans. 1* **1980,** 1045–1050. doi:10.1039/p19800001045
163. Murphy, J. A.; Rasheed, F.; Roome, S. J.; Scott, K. A.; Lewis, N. *J. Chem. Soc., Perkin Trans. 1* **1998,** 2331–2340. doi:10.1039/a802971g
164. Evans, D. A.; Bartroli, J.; Shih, T. L. *J. Am. Chem. Soc.* **1981,** *103,* 2127–2129. doi:10.1021/ja00398a058
165. Tsuji, J.; Yamakawa, T. *Tetrahedron Lett.* **1979,** *20,* 613–616. doi:10.1016/S0040-4039(01)86016-0
166. Mancuso, A. J.; Huang, S.-L.; Swern, D. *J. Org. Chem.* **1978,** *43,* 2480–2482. doi:10.1021/jo00406a041
167. Hoffman, R. V.; Kim, H.-O. *J. Org. Chem.* **1995,** *60,* 5107–5113. doi:10.1021/jo00121a031
168. Burgos, C. H.; Canales, E.; Matos, K.; Soderquist, J. A. *J. Am. Chem. Soc.* **2005,** *127,* 8044–8049. doi:10.1021/ja043612i
169. Neises, B.; Steglich, W. *Angew. Chem., Int. Ed. Engl.* **1978,** *17,* 522–524. doi:10.1002/anie.197805221
170. Boden, E. P.; Keck, G. E. *J. Org. Chem.* **1985,** *50,* 2394–2395. doi:10.1021/jo00213a044
171. Scholl, M.; Ding, S.; Lee, C. W.; Grubbs, R. H. *Org. Lett.* **1999,** *1,* 953–956. doi:10.1021/ol990909q
172. Keller, V. A.; Martinelli, J. R.; Strieter, E. R.; Burke, S. D. *Org. Lett.* **2002,** *4,* 467–470. doi:10.1021/ol0172368
173. Ko, K.-S.; Alexander, M. D.; Fontaine, S. D.; Biggs-Houck, J. E.; Clair, J. J. L.; Burkart, M. D. *Org. Biomol. Chem.* **2010,** *8,* 5159–5165. doi:10.1039/c0ob00540a
174. Keck, G. E.; Abbott, D. E. *Tetrahedron Lett.* **1984,** *25,* 1883–1886. doi:10.1016/S0040-4039(01)90066-8
175. Brown, C. A.; Aggarwal, V. K. *Chem. – Eur. J.* **2015,** *21,* 13900–13903. doi:10.1002/chem.201503122
176. Roush, W. R.; Palkowitz, A. D.; Palmer, M. J. *J. Org. Chem.* **1987,** *52,* 316–318. doi:10.1021/jo00378a041
177. Feyen, F.; Jantsch, A.; Altmann, K.-H. *Synlett* **2007,** 415–418. doi:10.1055/s-2007-967943
178. Gersbach, P.; Jantsch, A.; Feyen, F.; Scherr, N.; Dangy, J.-P.; Pluschke, G.; Altmann, K.-H. *Chem. – Eur. J.* **2011,** *17,* 13017–13031. doi:10.1002/chem.201101799
179. Oppolzer, W.; Blagg, J.; Rodriguez, I.; Walther, E. *J. Am. Chem. Soc.* **1990,** *112,* 2767–2772. doi:10.1021/ja00163a045
180. Dess, D. B.; Martin, J. C. *J. Org. Chem.* **1983,** *48,* 4155–4156. doi:10.1021/jo00170a070
181. Höfle, G.; Steglich, W.; Vorbrüggen, H. *Angew. Chem., Int. Ed. Engl.* **1978,** *17,* 569–583. doi:10.1002/anie.197805691
182. Blanchard, N.; Chany, A.-C.; Tresse, C.; Casarotto, V.; Bréthous, L.; Saint-Auret, S. A Walk Across Africa with Captain Grant: Exploring Mycobacterium ulcerans Infection with Mycolactone Analogs. In *Strategies and Tactics in Organic Synthesis;* Harmata, M., Ed.; Academic Press, 2015; Vol. 11, pp 85–117.
183. Finkelstein, H. *Ber. Dtsch. Chem. Ges.* **1910,** *43,* 1528–1532. doi:10.1002/cber.19100430257

184. Seidel, G.; Fürstner, A. *Chem. Commun.* **2012,** *48,* 2055–2070. doi:10.1039/c2cc17070a
185. Stymiest, J. L.; Dutheuil, G.; Mahmood, A.; Aggarwal, V. K. *Angew. Chem., Int. Ed.* **2007,** *46,* 7491–7494. doi:10.1002/anie.200702146
186. Leonori, D.; Aggarwal, V. K. *Acc. Chem. Res.* **2014,** *47,* 3174–3183. doi:10.1021/ar5002473
187. Hoppe, D.; Hintze, F.; Tebben, P. *Angew. Chem.* **1990,** *102,* 1457–1459. doi:10.1002/ange.19901021218
188. Sadhu, K. M.; Matteson, D. S. *Organometallics* **1985,** *4,* 1687–1689. doi:10.1021/om00128a038
189. Garber, S. B.; Kingsbury, J. S.; Gray, B. L.; Hoveyda, A. H. *J. Am. Chem. Soc.* **2000,** *122,* 8168–8179. doi:10.1021/ja001179g
190. Gurjar, M. K.; Cherian, J. *Heterocycles* **2001,** *55,* 1095–1103. doi:10.3987/COM-01-9199
191. Horner, L.; Hoffmann, H.; Wippel, H. G. *Chem. Ber.* **1958,** *91,* 61–63. doi:10.1002/cber.19580910113
192. Wadsworth, W. S.; Emmons, W. D. *J. Am. Chem. Soc.* **1961,** *83,* 1733–1738. doi:10.1021/ja01468a042
193. Enders, D.; Schüßeler, T. *Synthesis* **2002,** 2280–2288. doi:10.1055/s-2002-34949
194. Michaelis, A.; Kaehne, R. *Ber. Dtsch. Chem. Ges.* **1898,** *31,* 1048–1055. doi:10.1002/cber.189803101190
195. Arbusow, B. A. *Pure Appl. Chem.* **2009,** *9,* 307–336. doi:10.1351/pac196409020307
196. Van Summeren, R. P.; Feringa, B. L.; Minnaard, A. J. *Org. Biomol. Chem.* **2005,** *3,* 2524–2533. doi:10.1039/b505980a
197. Roush, W. R.; Hoong, L. K.; Palmer, M. A. J.; Park, J. C. *J. Org. Chem.* **1990,** *55,* 4109–4117. doi:10.1021/jo00300a031
198. Jacobsen, E. N.; Marko, I.; Mungall, W. S.; Schroeder, G.; Sharpless, K. B. *J. Am. Chem. Soc.* **1988,** *110,* 1968–1970. doi:10.1021/ja00214a053
199. Sharpless, K. B.; Amberg, W.; Bennani, Y. L.; Crispino, G. A.; Hartung, J.; Jeong, K. S.; Kwong, H. L.; Morikawa, K.; Wang, Z. M. *J. Org. Chem.* **1992,** *57,* 2768–2771. doi:10.1021/jo00036a003
200. Morel, T.; Verkade, P. E. *Recl. Trav. Chim. Pays-Bas* **1949,** *68,* 619–638. doi:10.1002/recl.19490680706
201. Wenkert, E.; Khatuya, H.; Klein, P. S. *Tetrahedron Lett.* **1999,** *40,* 5171–5174. doi:10.1016/S0040-4039(99)01007-2
202. Mitsunobu, O.; Yamada, M. *Bull. Chem. Soc. Jpn.* **1967,** *40,* 2380–2382. doi:10.1246/bcsj.40.2380
203. Zhang, H. X.; Guibe, F.; Balavoine, G. *J. Org. Chem.* **1990,** *55,* 1857–1867. doi:10.1021/jo00293a035
204. Lindlar, H. *Helv. Chim. Acta* **1952,** *35,* 446–450. doi:10.1002/hlca.19520350205
205. Van Laren, M. W.; Elsevier, C. J. *Angew. Chem., Int. Ed.* **1999,** *38,* 3715–3717. doi:10.1002/(SICI)1521-3773(19991216)38:24<3715::AID-ANIE3715>3.0.CO;2-O
206. Brown, C. A.; Ahuja, V. K. *J. Org. Chem.* **1973,** *38,* 2226–2230. doi:10.1021/jo00952a024
207. Boland, W.; Schroer, N.; Sieler, C.; Feigel, M. *Helv. Chim. Acta* **1987,** *70,* 1025–1040. doi:10.1002/hlca.19870700415
208. Yin, N.; Wang, G.; Qian, M.; Negishi, E. *Angew. Chem., Int. Ed.* **2006,** *45,* 2916–2920. doi:10.1002/anie.200600012
209. Uenishi, J.; Kawahama, R.; Yonemitsu, O.; Tsuji, J. *J. Org. Chem.* **1996,** *61,* 5716–5717. doi:10.1021/jo961013r
210. Wang, C.; Xu, Z.; Tobrman, T.; Negishi, E. *Adv. Synth. Catal.* **2010,** *352,* 627–631. doi:10.1002/adsc.200900766
211. Negishi, E.; Van Horn, D. E.; Yoshida, T. *J. Am. Chem. Soc.* **1985,** *107,* 6639–6647. doi:10.1021/ja00309a036
212. Huang, Z.; Negishi, E. *Org. Lett.* **2006,** *8,* 3675–3678. doi:10.1021/ol061202o
213. Brown, H. C.; Jadhav, P. K.; Bhat, K. S. *J. Am. Chem. Soc.* **1988,** *110,* 1535–1538. doi:10.1021/ja00213a029
214. Hunter, T. J.; O'Doherty, G. A. *Org. Lett.* **2001,** *3,* 1049–1052. doi:10.1021/ol0156188
215. Hodgson, D. M.; Boulton, L. T.; Maw, G. N. *Tetrahedron* **1995,** *51,* 3713–3724. doi:10.1016/0040-4020(95)00086-N
216. Baker, R.; Castro, J. L. *J. Chem. Soc., Perkin Trans. 1* **1990,** 47–65. doi:10.1039/p19900000047
217. Allred, G. D.; Liebeskind, L. S. *J. Am. Chem. Soc.* **1996,** *118,* 2748–2749. doi:10.1021/ja9541239
218. Srogl, J.; Allred, G. D.; Liebeskind, L. S. *J. Am. Chem. Soc.* **1997,** *119,* 12376–12377. doi:10.1021/ja9726926
219. Brown, H. C.; Jadhav, P. K. *J. Am. Chem. Soc.* **1983,** *105,* 2092–2093. doi:10.1021/ja00345a085
220. Gersbach, P. R. *Total synthesis of natural mycolactones and of mycolactone analogs and conjugates for structure-toxicity-relationship studies and the selection of antibodies*. Ph.D. Thesis, ETH Zürich, Switzerland, 2012.
221. Chen, K.-M.; Hardtmann, G. E.; Prasad, K.; Repič, O.; Shapiro, M. J. *Tetrahedron Lett.* **1987,** *28,* 155–158. doi:10.1016/S0040-4039(00)95673-9
222. Takai, K.; Nitta, K.; Utimoto, K. *J. Am. Chem. Soc.* **1986,** *108,* 7408–7410. doi:10.1021/ja00283a046
223. Jin, H.; Uenishi, J.; Christ, W. J.; Kishi, Y. *J. Am. Chem. Soc.* **1986,** *108,* 5644–5646. doi:10.1021/ja00278a057
224. Takai, K.; Tagashira, M.; Kuroda, T.; Oshima, K.; Utimoto, K.; Nozaki, H. *J. Am. Chem. Soc.* **1986,** *108,* 6048–6050. doi:10.1021/ja00279a068
225. Kurosu, M.; Lin, M.-H.; Kishi, Y. *J. Am. Chem. Soc.* **2004,** *126,* 12248–12249. doi:10.1021/ja045557j
226. Fürstner, A.; Shi, N. *J. Am. Chem. Soc.* **1996,** *118,* 12349–12357. doi:10.1021/ja9625236
227. Namba, K.; Cui, S.; Wang, J.; Kishi, Y. *Org. Lett.* **2005,** *7,* 5417–5419. doi:10.1021/ol052084s
228. Ando, K. *J. Org. Chem.* **1997,** *62,* 1934–1939. doi:10.1021/jo970057c
229. Wang, Y.; Dai, W.-M. *Eur. J. Org. Chem.* **2014,** 323–330. doi:10.1002/ejoc.201301484
230. Miyaura, N.; Yamada, K.; Suzuki, A. *Tetrahedron Lett.* **1979,** *20,* 3437–3440. doi:10.1016/S0040-4039(01)95429-2
231. Miyaura, N.; Suzuki, A. *J. Chem. Soc., Chem. Commun.* **1979,** 866–867. doi:10.1039/c39790000866
232. Ye, N.; Dai, W.-M. *Eur. J. Org. Chem.* **2013,** 831–835. doi:10.1002/ejoc.201201602
233. Evans, D. A.; Gauchet-Prunet, J. A. *J. Org. Chem.* **1993,** *58,* 2446–2453. doi:10.1021/jo00061a018
234. Moure, A. L.; Gómez Arrayás, R.; Cárdenas, D. J.; Alonso, I.; Carretero, J. C. *J. Am. Chem. Soc.* **2012,** *134,* 7219–7222. doi:10.1021/ja300627s
235. Smith, A. B., III; Wuest, W. M. *Chem. Commun.* **2008,** 5883–5895. doi:10.1039/b810394a
236. Hoye, T. R.; Jeffrey, C. S.; Shao, F. *Nat. Protoc.* **2007,** *2,* 2451–2458. doi:10.1038/nprot.2007.354
237. Le Mignot, V.; Lièvre, C.; Fréchou, C.; Demailly, G. *Tetrahedron Lett.* **1998,** *39,* 983–984. doi:10.1016/S0040-4039(97)10721-3
238. Guérinot, A.; Reymond, S.; Cossy, J. *Angew. Chem., Int. Ed.* **2007,** *46,* 6521–6524. doi:10.1002/anie.200702206

239. Schwab, P.; France, M. B.; Ziller, J. W.; Grubbs, R. H. *Angew. Chem., Int. Ed. Engl.* **1995,** *34,* 2039–2041. doi:10.1002/anie.199520391
240. Alexander, M. D.; Fontaine, S. D.; Clair, J. J. L.; DiPasquale, A. G.; Rheingold, A. L.; Burkart, M. D. *Chem. Commun.* **2006,** 4602–4604. doi:10.1039/b609408b
241. Rieke, R. D.; Li, P. T.-J.; Burns, T. P.; Uhm, S. T. *J. Org. Chem.* **1981,** *46,* 4323–4324. doi:10.1021/jo00334a056
242. Chany, A.-C.; Veyron-Churlet, R.; Tresse, C.; Mayau, V.; Casarotto, V.; Le Chevalier, F.; Guenin-Macé, L.; Demangel, C.; Blanchard, N. *J. Med. Chem.* **2014,** *57,* 7382–7395. doi:10.1021/jm5008819
243. Li, X.; Babu, V. S.; Kishi, Y. *Tetrahedron Lett.* **2015,** *56,* 3220–3224. doi:10.1016/j.tetlet.2014.12.024
244. Xing, Y.; Hande, S. M.; Kishi, Y. *J. Am. Chem. Soc.* **2012,** *134,* 19234–19239. doi:10.1021/ja309215m
245. Hodgson, D. M.; Chung, Y. K.; Paris, J.-M. *J. Am. Chem. Soc.* **2004,** *126,* 8664–8665. doi:10.1021/ja047346k
246. Hodgson, D. M.; Chung, Y. K.; Nuzzo, I.; Freixas, G.; Kulikiewicz, K. K.; Cleator, E.; Paris, J.-M. *J. Am. Chem. Soc.* **2007,** *129,* 4456–4462. doi:10.1021/ja0672932
247. Baudin, J. B.; Hareau, G.; Julia, S. A.; Ruel, O. *Tetrahedron Lett.* **1991,** *32,* 1175–1178. doi:10.1016/S0040-4039(00)92037-9
248. Bellingham, R.; Jarowicki, K.; Kocienski, P.; Martin, V. *Synthesis* **1996,** 285–296. doi:10.1055/s-1996-4184
249. Griffith, W. P.; Ley, S. V.; Whitcombe, G. P.; White, A. D. *J. Chem. Soc., Chem. Commun.* **1987,** 1625–1627. doi:10.1039/c39870001625
250. Gilman, H.; Jones, R. G.; Woods, L. A. *J. Org. Chem.* **1952,** *17,* 1630–1634. doi:10.1021/jo50012a009
251. Babu, V. S.; Zhou, Y.; Kishi, Y. *Bioorg. Med. Chem. Lett.* **2017,** *27,* 1274–1277. doi:10.1016/j.bmcl.2017.01.036
252. Tokunaga, M.; Larrow, J. F.; Kakiuchi, F.; Jacobsen, E. N. *Science* **1997,** *277,* 936–938. doi:10.1126/science.277.5328.936
253. Huisgen, R. *Proc. Chem. Soc., London* **1961,** 357–396. doi:10.1039/PS9610000357
254. Tornøe, C. W.; Christensen, C.; Meldal, M. *J. Org. Chem.* **2002,** *67,* 3057–3064. doi:10.1021/jo011148j
255. Rostovtsev, V. V.; Green, L. G.; Fokin, V. V.; Sharpless, K. B. *Angew. Chem., Int. Ed.* **2002,** *41,* 2596–2599. doi:10.1002/1521-3773(20020715)41:14<2596::AID-ANIE2596>3.0.CO;2-4
256. Verdoes, M.; Hillaert, U.; Florea, B. I.; Sae-Heng, M.; Risseeuw, M. D. P.; Filippov, D. V.; van der Marel, G. A.; Overkleeft, H. S. *Bioorg. Med. Chem. Lett.* **2007,** *17,* 6169–6171. doi:10.1016/j.bmcl.2007.09.025
257. Guenin-Macé, L.; Baron, L.; Chany, A.-C.; Tresse, C.; Saint-Auret, S.; Jönsson, F.; Le Chevalier, F.; Bruhns, P.; Bismuth, G.; Hidalgo-Lucas, S.; Bisson, J.-F.; Blanchard, N.; Demangel, C. *Sci. Transl. Med.* **2015,** *7,* 289r. doi:10.1126/scitranslmed.aab0458
258. Marion, E.; Prado, S.; Cano, C.; Babonneau, J.; Ghamrawi, S.; Marsollier, L. *PLoS One* **2012,** *7,* e33600. doi:10.1371/journal.pone.0033600
259. Akiyama, T.; Ishida, J.; Nakagawa, S.; Ogawara, H.; Watanabe, S.; Itoh, N.; Shibuya, M.; Fukami, Y. *J. Biol. Chem.* **1987,** *262,* 5592–5595.
260. Wang, K. K.; Nath, R.; Posner, A.; Raser, K. J.; Buroker-Kilgore, M.; Hajimohammadreza, I.; Probert, A. W., Jr.; Marcoux, F. W.; Ye, Q.; Takano, E.; Hatanaka, M.; Maki, M.; Caner, H.; Collins, J. L.; Fergus, A.; Lee, K. S.; Lunney, E. A.; Hays, S. J.; Yuen, P. *Proc. Natl. Acad. Sci. U. S. A.* **1996,** *93,* 6687–6692. doi:10.1073/pnas.93.13.6687
261. Igarashi, M.; Strittmatter, S. M.; Vartanian, T.; Fishman, M. C. *Science* **1993,** *259,* 77–79. doi:10.1126/science.8418498
262. Freissmuth, M.; Boehm, S.; Beindl, W.; Nickel, P.; Ijzerman, A. P.; Hohenegger, M.; Nanoff, C. *Mol. Pharmacol.* **1996,** *49,* 602–611.
263. Wymann, M.; Arcaro, A. *Biochem. J.* **1994,** *298,* 517–520. doi:10.1042/bj2980517
264. Kapuscinski, J. *Biotech. Histochem.* **1995,** *70,* 220–233. doi:10.3109/10520299509108199
265. Cooper, J. A. *J. Cell Biol.* **1987,** *105,* 1473–1478. doi:10.1083/jcb.105.4.1473
266. Logue, S. E.; Elgendy, M.; Martin, S. J. *Nat. Protoc.* **2009,** *4,* 1383–1395. doi:10.1038/nprot.2009.143
267. Riccardi, C.; Nicoletti, I. *Nat. Protoc.* **2006,** *1,* 1458–1461. doi:10.1038/nprot.2006.238
268. Kishi, Y. *Proc. Natl. Acad. Sci. U. S. A.* **2011,** *108,* 6703–6708. doi:10.1073/pnas.1015252108

License and Terms

BEILSTEIN JOURNAL OF ORGANIC CHEMISTRY

18-Hydroxydolabella-3,7-diene synthase – a diterpene synthase from *Chitinophaga pinensis*

Jeroen S. Dickschat*[1], Jan Rinkel[1], Patrick Rabe[1], Arman Beyraghdar Kashkooli[2] and Harro J. Bouwmeester[3]

Full Research Paper

Open Access

Address:
[1]Kekulé-Institute of Organic Chemistry and Biochemistry, University of Bonn, Gerhard-Domagk-Straße 1, 53121 Bonn, Germany, [2]Laboratory of Plant Physiology, Wageningen University, Droevendaalsesteeg 1, 6708 PB Wageningen, The Netherlands, and [3]Swammerdam Institute for Life Sciences, University of Amsterdam, Sciencepark 904, 1098 XH Amsterdam, The Netherlands

Email:
Jeroen S. Dickschat* - dickschat@uni-bonn.de

* Corresponding author

Keywords:
biosynthesis; *Chitinophaga pinensis*; *Nicotiana benthamiana*; structure elucidation; terpenes

Beilstein J. Org. Chem. **2017,** *13,* 1770–1780.
doi:10.3762/bjoc.13.171

Received: 21 June 2017
Accepted: 09 August 2017
Published: 23 August 2017

This article is part of the Thematic Series "Lipids: fatty acids and derivatives, polyketides and isoprenoids".

Associate Editor: A. Kirschning

Abstract

The product obtained in vitro from a diterpene synthase encoded in the genome of the bacterium *Chitinophaga pinensis*, an enzyme previously reported to have germacrene A synthase activity during heterologous expression in *Escherichia coli*, was identified by extensive NMR-spectroscopic methods as 18-hydroxydolabella-3,7-diene. The absolute configuration of this diterpene alcohol and the stereochemical course of the terpene synthase reaction were addressed by isotopic labelling experiments. Heterologous expression of the diterpene synthase in *Nicotiana benthamiana* resulted in the production of 18-hydroxydolabella-3,7-diene also in planta, while the results from the heterologous expression in *E. coli* were shown to be reproducible, revealing that the expression of one and the same terpene synthase in different heterologous hosts may yield different terpene products.

Introduction

Terpene synthases convert a handful of simple linear and achiral oligoprenyl diphosphates in just one enzymatic step into a remarkable diversity of usually polycyclic structurally complex lipophilic terpenes with multiple stereogenic centres. In their active sites type I terpene synthases contain the highly conserved aspartate-rich motif DDXX(X)(D,E) and the NSE triad NDXXSXX(R,K)(E,D), modified to a DTE triad in plants, for binding of the Mg^{2+} cofactor that forms a trinuclear $(Mg^{2+})_3$ cluster to which the diphosphate portion of the substrate binds. Upon substrate binding the active site closes, resulting in hydrogen bonds between the substrate's diphosphate and the pyrophosphate sensor, a highly conserved arginine located

43 amino acids upstream of the NSE triad, and the RY dimer, a highly conserved motif at the C-terminus. The substrate is ionised by extrusion of diphosphate, yielding a highly reactive allyl cation that can react in a cyclisation cascade by attack of olefinic double bonds to the cationic centre, hydride shifts and Wagner–Meerwein rearrangements. The process is usually terminated by deprotonation or attack of water to yield a lipophilic terpene hydrocarbon or alcohol. Among the first investigated terpene synthases were the (+)- and (−)-bornyl diphosphate synthases from the plants *Salvia officinalis* and *Tanacetum vulgare* forming a more polar product by the unusual termination via reattack of diphosphate [1], the trichodiene synthase from the fungus *Trichothecium roseum* [2], and pentalenene synthase from *Streptomyces exfoliatus* [3]. Recently, the first terpene synthases were reported from a eukaryotic soil microorganism, the social amoeba *Dictyostelium discoideum* [4,5]. With respect to bacterial enzymes, many terpene synthases have been identified and their products have been structurally characterised (reviewed in [6], following reports: [7-14]). One possible method to investigate the products of terpene synthases is the expression of terpene synthase genes in a heterologous host, as was recently performed for a large number of bacterial enzymes in an engineered *Streptomyces avermitilis* strain from which the biosynthesis genes for all other natural products were deleted, allowing a relatively easy purification of the terpene synthase products from culture extracts [15,16]. The heterologous expression of terpene synthase genes in *Escherichia coli* is also frequently successful, resulting in the production of volatile terpenes by this bacterium that can be detected in headspace extracts [17,18]. In one of these previous reports [17] we have described a terpene synthase from *Chitinophaga pinensis* DSM 2588 (accession number WP_012789469) as a sesquiterpene synthase for germacrene A (**1**), which was based on the identification of this compound and its Cope rearrangement product β-elemene (**2**) formed by the thermal impact during GC–MS analysis [19] in *E. coli* headspace extracts under heterologous expression of the terpene synthase gene (Scheme 1). Here we present the diterpene synthase activity of this enzyme in in vitro experiments and the first heterologous expression of a bacterial terpene synthase gene in a plant, *Nicotiana benthamiana*.

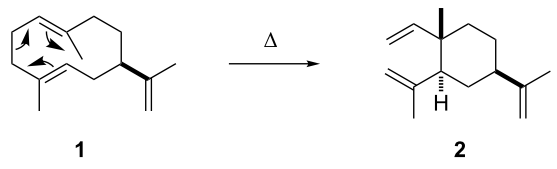

Scheme 1: Germacrene A (**1**) and its Cope rearrangement to β-elemene (**2**).

Results and Discussion

Characterisation of a diterpene synthase from *Chitinophaga pinensis* in vitro

The terpene synthase from *C. pinensis* was heterologously expressed in *E. coli* as a recombinant protein with a C-terminal polyhistidine tag using a previously reported pET28c-based expression construct [17] and purified by Ni-NTA affinity chromatography (Figure S1, Supporting Information File 1). The purified enzyme was tested in in vitro experiments for mono-, sesqui- and diterpene activity by incubation with geranyl (GPP), farnesyl (FPP) and geranylgeranyl diphosphate (GGPP) as substrates, which yielded a single product **3** only from GGPP, but no products from FPP and GPP as demonstrated by GC–MS analysis (Figure 1). The mass spectrum of **3** showed a molecular ion at m/z = 290 pointing to a diterpene alcohol and a base peak ion at m/z = 59 indicative of a 2-hydroxyisopropyl group that frequently occurs in terpene alcohols. Both findings, i.e., no production of sesquiterpenes from FPP in in vitro experiments with recombinant purified enzyme as well as the emission of sesquiterpenes by *E. coli* during heterologous expression, were fully reproducible (Figure S2, Supporting Information File 1).

The compound **3** obtained from the in vitro incubation of GGPP was purified and its structure was elucidated by extensive one- and two-dimensional NMR spectroscopic methods (Table 1, Figures S3–S9, Supporting Information File 1). The ^{13}C NMR spectrum showed five signals for methyl groups, seven aliphatic CH_2 groups, two aliphatic and two olefinic CH groups, and four signals for quarternary carbons including one connected to oxygen and two olefinic carbons, suggesting the structure of a bicyclic diterpene alcohol. The $^{1}H,^{1}H$-COSY spectrum revealed three contiguous spin systems for C2–C3, C5–C6–C7, and C9–C10–C11–C12–C13–C14 (Scheme 2). Key HMBC correlations from H19 and H20 to C12 and C18 placed the 2-hydroxyisopropyl group at C12, while HMBC correlations from H17 to C6, C7, C8 and C9 located the C8–C17 fragment between C7 and C9. HMBC crosspeaks between H16 and C3, C4 and C5 indicated the C3–C4–C5 connection, and HMBC correlations between H15 and C1, C2 and C14, and between H11, C1 and C2 established the bonds between the quarternary carbon C1 and its four neighbours. Diagnostic NOESY correlations between H11 and H2β, H3 and H7, between H12 and H2β, and between H10α and H15 established the relative configuration of **3**, resulting in the structure of (1*R**,3*E*,7*E*,11*S**,12*S**)-18-hydroxydolabella-3,7-diene and identifying the terpene synthase from *C. pinensis* as 18-hydroxydolabella-3,7-diene synthase (HdS).

The proposed cyclisation mechanism from GGPP to **3** is likely a concerted one-step process with 1,11- and 10,14-cyclisation and concomittant attack of water at C15 (Scheme 2). We have

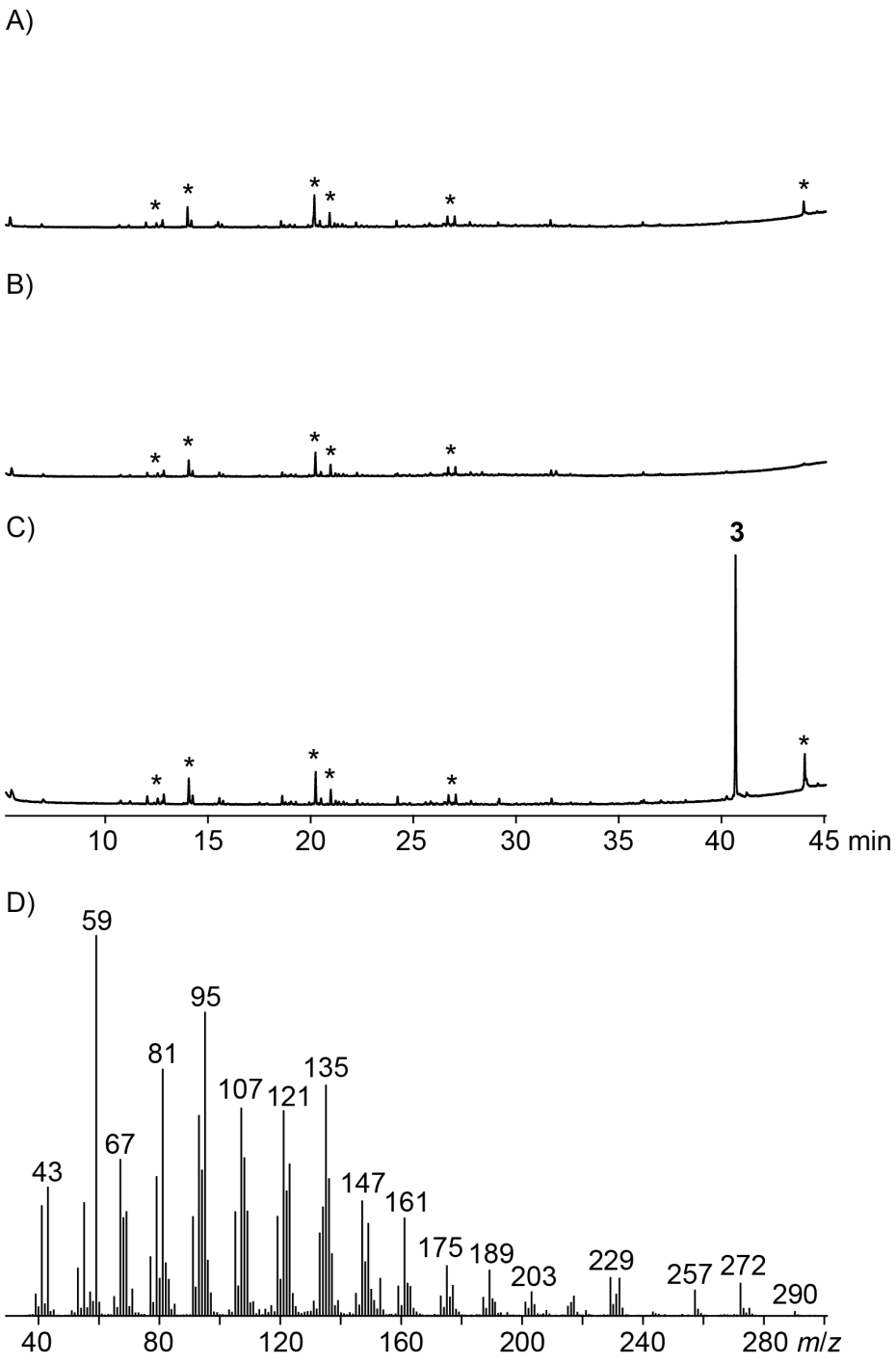

Figure 1: In vitro terpene synthase activity of the investigated recombinant enzyme from *C. pinensis*, showing no formation of monoterpenes from GPP (A) and no formation of sesquiterpenes from FPP (B), but formation of a single diterpene alcohol **3** from GGPP (C) with the mass spectrum depicted in (D). Asterisks indicate non-terpenoid contaminants such as plasticisers.

recently shown that the absolute configurations of terpenes can be determined by enzymatic conversion of stereoselectively deuterated terpene precursors, because the problem of determining the absolute configuration of the terpene under investigation is simplified to a problem of delineating the relative orientation of its stereocentres to the known absolute configuration at the deuterated carbon [12,13]. This approach was used to determine the absolute configuration of **3** using both enantiomers of (*R*)- and (*S*)-(1-^{13}C,1-^{2}H)GGPP [14], (*R*)- and (*S*)-(1-^{13}C,1-^{2}H)FPP, and (*R*)- and (*S*)-(1-^{13}C,1-^{2}H)GPP [12] in which

Table 1: NMR data of **3** recorded in C_6D_6.

C[a]	^{13}C (δ)[b]	^{1}H (δ, m, *J*, int)[c]
1	47.5 (C_q)	–
2	42.6 (CH_2)	2.19 (m, 1H, Hβ) 1.71 (dd, *J* = 6.2, *J* = 13.8, 1H, Hα)
3	126.5 (CH)	5.16 (dd, *J* = 9.7, *J* = 5.8, 1H)
4	134.0 (C_q)	–
5	40.2 (CH_2)	2.12 (m, 1H) 2.06 (m, 1H)
6	25.0 (CH_2)	2.22 (m, 1H, Hβ) 2.05 (m, 1H, Hα)
7	128.2 (CH)	4.87 (dd, *J* = 10.0, *J* = 4.3, 1H)
8	134.0 (C_q)	–
9	39.2 (CH_2)	2.27 (m, 1H, Hα) 2.14 (m, 1H, Hβ)
10	23.7 (CH_2)	2.13 (m, 1H, Hβ) 1.23 (m, 1H, Hα)
11	42.1 (CH)	1.84 (m, 1H)
12	53.7 (CH)	1.84 (ddd, *J* = 10.4, *J* = 7.4, *J* = 7.4, 1H)
13	26.0 (CH_2)	1.53 (m, 1H) 1.53 (m, 1H)
14	41.3 (CH_2)	1.47 (m, 1H, Hα) 1.39 (m, 1H, Hβ)
15	24.9 (CH_3)	1.08 (s, 3H)
16	16.6 (CH_3)	1.59 (s, 3H)
17	16.0 (CH_3)	1.47 (s, 3H)
18	72.1 (C_q)	–
19	30.8 (CH_3)	1.11 (s, 3H)
20	30.7 (CH_3)	1.18 (s, 3H)

[a]Carbon numbering as shown in Scheme 2. [b]Chemical shifts δ in ppm and assignment of carbons by ^{13}C-DEPT135 spectroscopy.
[c]Chemical shifts δ in ppm, multiplicity m (s = singlet, d = doublet, t = triplet, m = multiplet), coupling constants *J* are given in Hertz.

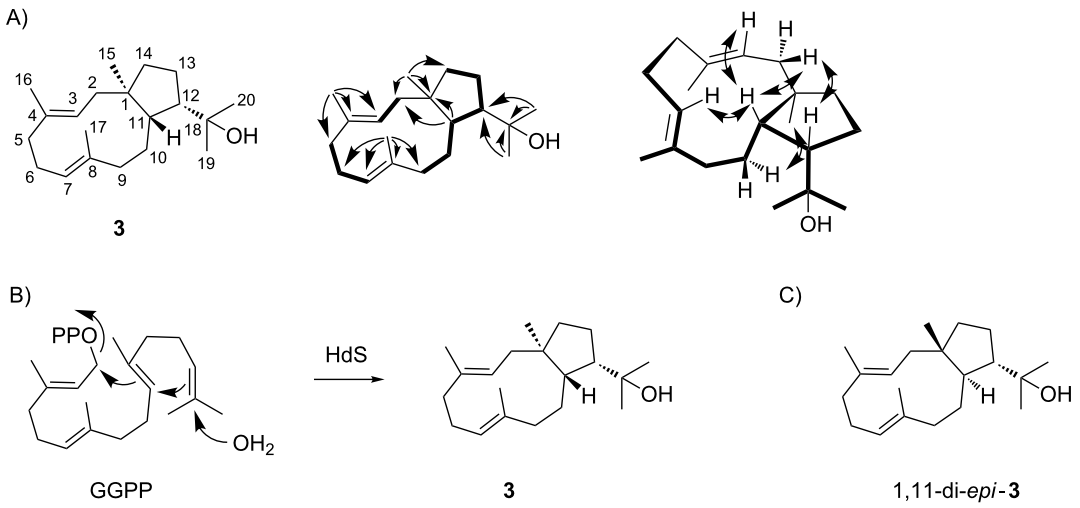

Scheme 2: Product obtained from the diterpene synthase from *C. pinensis*. (A) Structure of (1*R*,3*E*,7*E*,11*S*,12*S*)-18-hydroxydolabella-3,7-diene (**3**), contiguous $^{1}H,^{1}H$-COSY spin systems (bold), and diagnostic HMBC and NOESY correlations (single and double headed arrows). (B) Cyclisation mechanism for the conversion of GGPP into **3** by HdS. (C) Structure of the known stereoisomer 1,11-di-*epi*-**3**.

the additional ^{13}C labels were introduced to increase sensitivity in the HSQC analysis of the obtained terpene products. Incubation of (*R*)-(1-^{13}C,1-^{2}H)GGPP with HdS resulted in the specific incorporation of the deuterium labelling into the 2α position as indicated by a deminished crosspeak in the HSQC spectrum, while the crosspeak for H2β was strongly enhanced because of the ^{13}C labelling of C2 (Figure 2). Consistently, the substrate (*S*)-(1-^{13}C,1-^{2}H)GGPP gave a product with specific incorporation of the deuterium label into the 2β position. Assuming inversion of configuration at C1 for the cyclisation of GGPP to

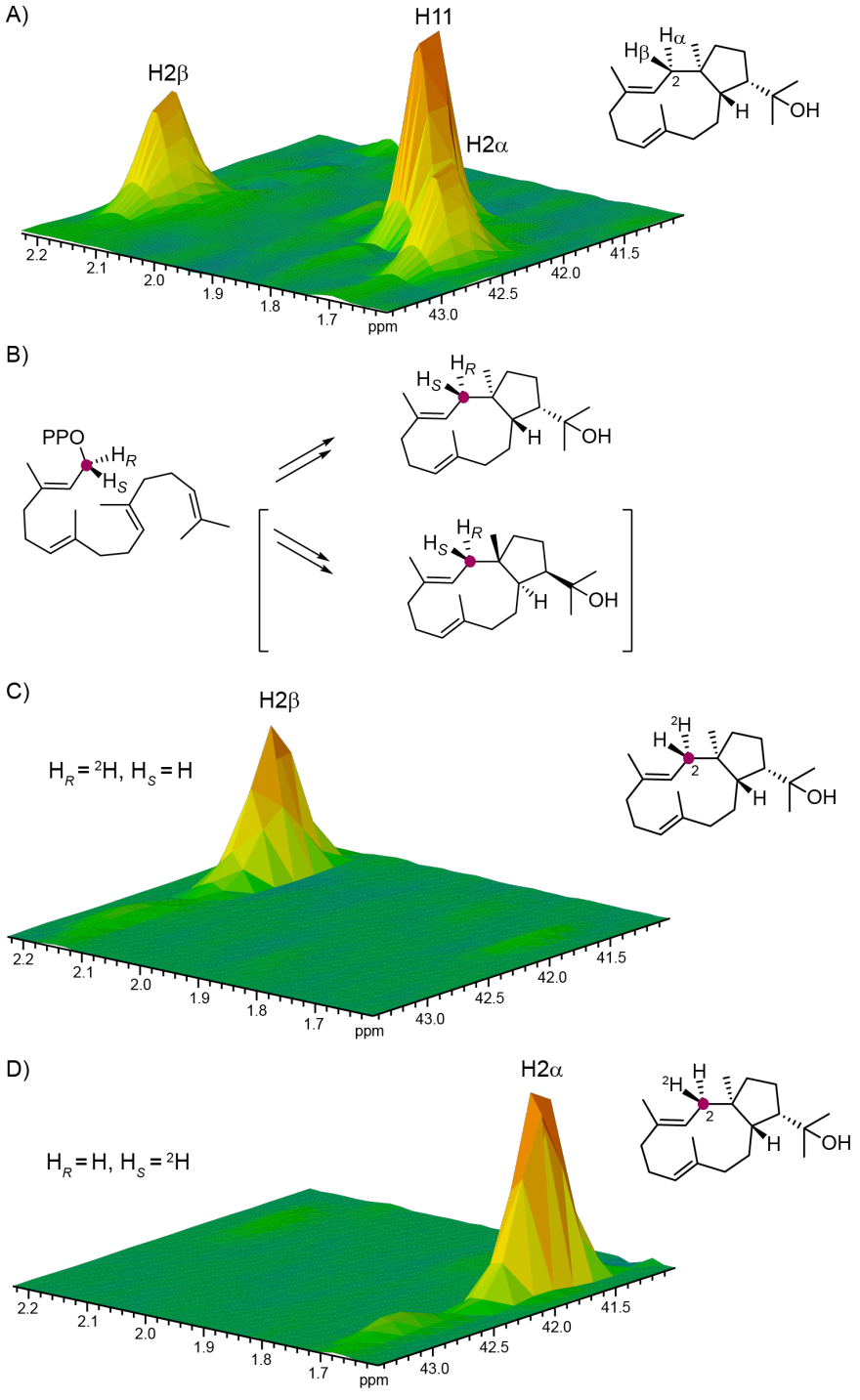

Figure 2: Determination of the absolute configuration of **3**. (A) Partial HSQC spectrum of unlabelled **3** showing the region for C2, (B) cyclisation of GGPP to the two possible enantiomers of **3**, (C) partial HSQC spectrum of the product obtained from (*R*)-(1-^{13}C,1-^{2}H)GGPP, and (D) partial HSQC spectrum of the product obtained from (*S*)-(1-^{13}C,1-^{2}H)GGPP. Purple dots indicate ^{13}C-labelled carbons.

3 as reported for several other terpene synthases [13,20-22], these findings point to the absolute configuration of (1*R*,3*E*,7*E*,11*S*,12*S*)-18-hydroxydolabella-3,7-diene.

For the incubation experiments with (*R*)- and (*S*)-(1-^{13}C,1-^{2}H)GPP, the terpene monomer IPP, HdS and the GGPP synthase (GGPPS) from *S. cyaneofuscatus* [12] were added to the reaction mixtures for an enzymatic elongation of the GPP isotopomers to the corresponding GGPPs. It is well established that the elongations of oligoprenyl diphosphates with IPP by type I oligoprenyl diphosphate synthases proceeds with inversion of configuration at C1 [23,24]. The conversion of the obtained labelled GGPPs by HdS gave a stereospecific incorporation of the deuterium labelling into H10α from (*R*)-(1-^{13}C,1-^{2}H)GPP and into H10β from (*S*)-(1-^{13}C,1-^{2}H)GPP (Figure 3), which pointed to the same absolute configuration for **3** as

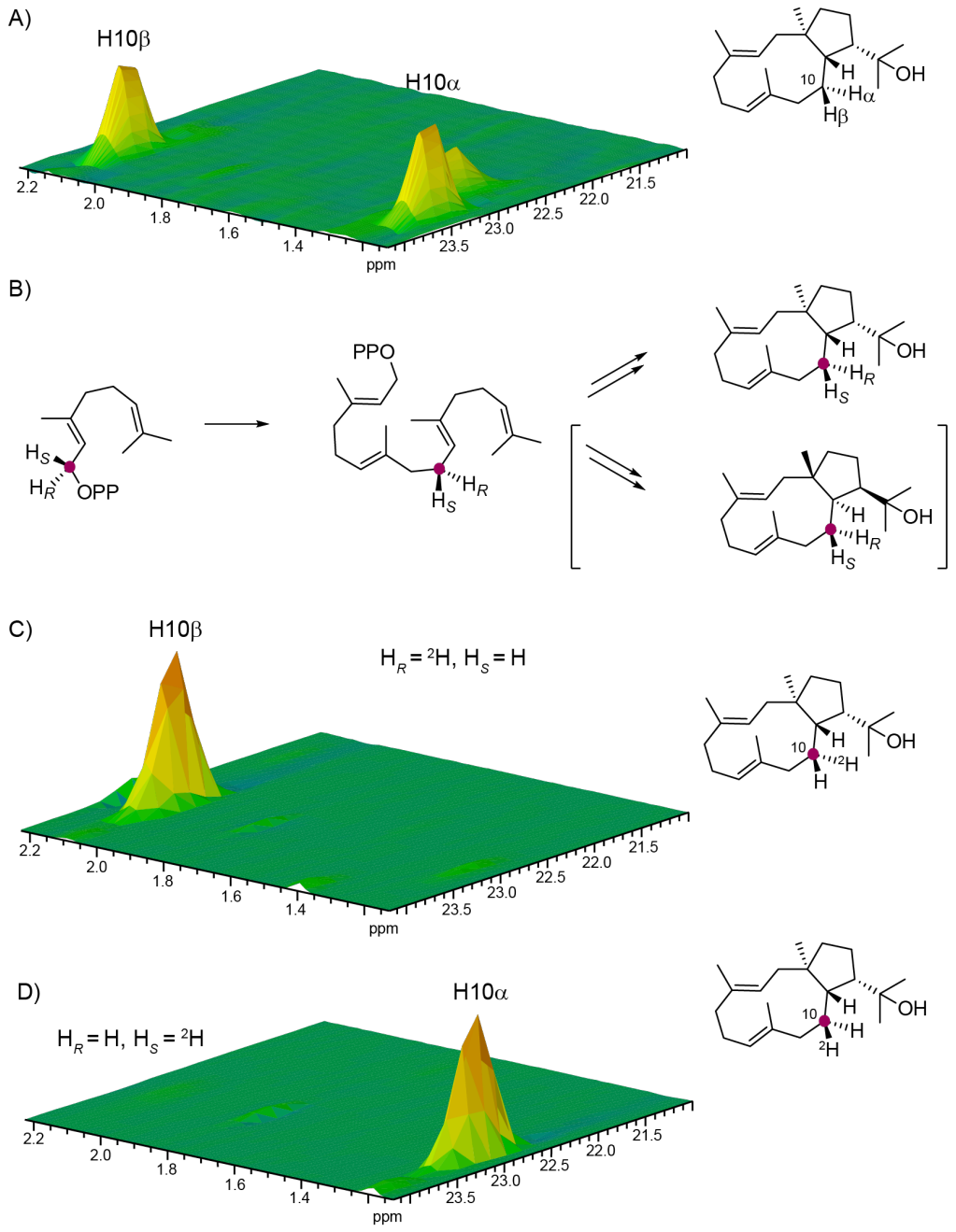

Figure 3: Determination of the absolute configuration of **3**. (A) Partial HSQC spectrum of unlabelled **3** showing the region for C10, (B) elongation of GPP with IPP to GGPP and cyclisation to the two possible enantiomers of **3**, (C) partial HSQC spectrum of the product obtained from (*R*)-(1-^{13}C,1-^{2}H)GPP, and (D) partial HSQC spectrum of the product obtained from (*S*)-(1-^{13}C,1-^{2}H)GPP. Purple dots indicate ^{13}C-labelled carbons.

deduced from the experiments with the two enantiomers of (1-^{13}C,1-^{2}H)GGPP.

Similar incubation experiments were performed with (*R*)- and (*S*)-(1-^{13}C,1-^{2}H)FPP, IPP, GGPPS and HdS, resulting in the stereospecific incorporation of deuterium labelling into the hydrogens at C6 of **3** (Figure 4). These experiments could not be used to confirm the absolute configuration of the diterpene, because the signals for H6α and H6β could not be unambiguously assigned from the NMR spectra of the unlabelled com-

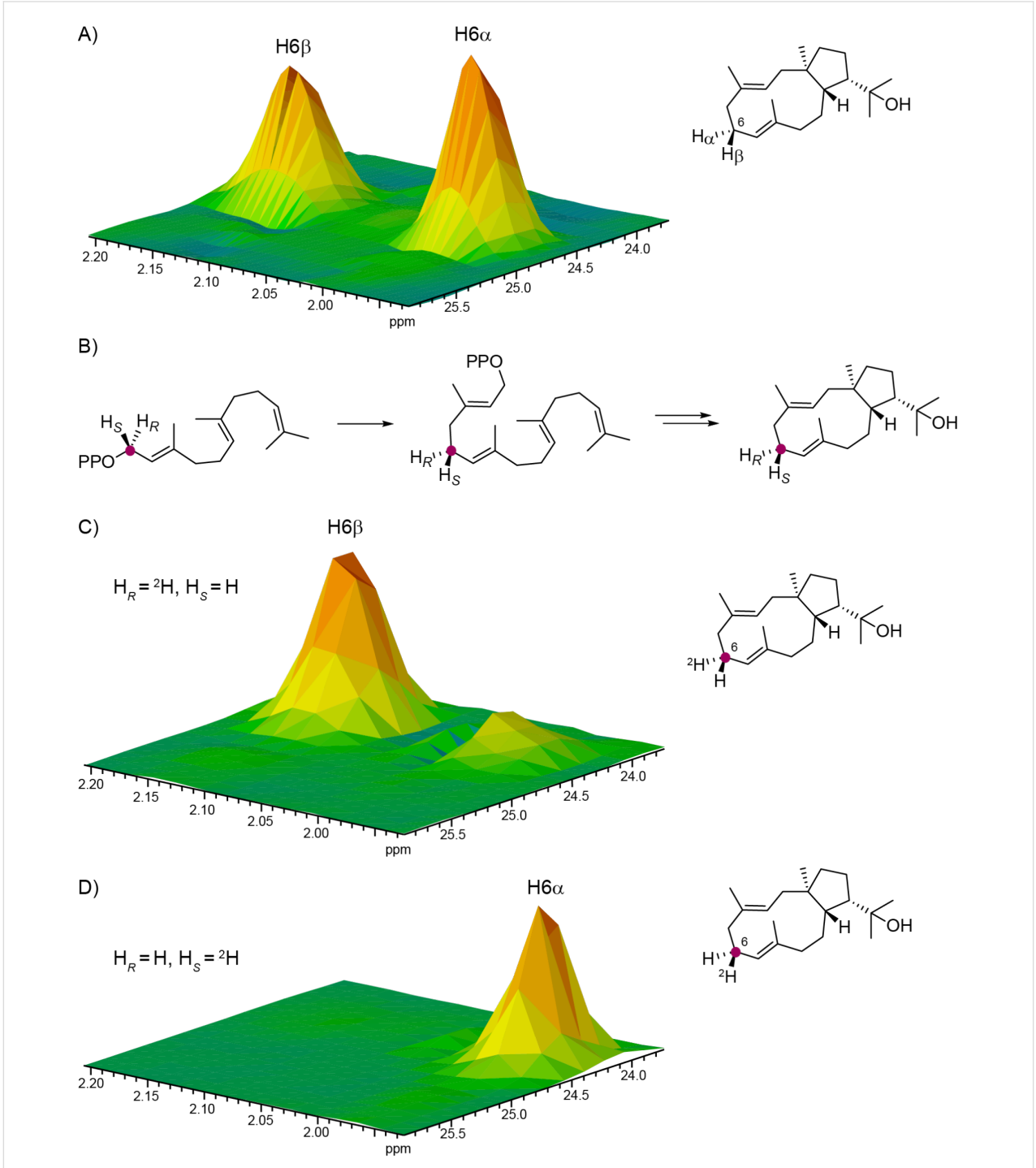

Figure 4: Assignment of H6α and H6β of **3**. (A) Partial HSQC spectrum of unlabelled **3** showing the region for C6, (B) elongation of FPP with IPP to GGPP and cyclisation to **3**, (C) partial HSQC spectrum of the product obtained from (*R*)-(1-^{13}C,1-^{2}H)FPP, and (D) partial HSQC spectrum of the product obtained from (*S*)-(1-^{13}C,1-^{2}H)FPP. Purple dots indicate ^{13}C-labelled carbons.

pound. Instead, the results from these incubation experiments were used for this assignment.

HdS exhibited a defined stereochemical course with respect to the methyl groups in the hydroxyisopropyl group of **3**, as was indicated by conversion of (12-^{13}C)FPP and (13-^{13}C)FPP [25] with IPP by GGPPS and HdS that resulted in the specific incorporation of labelling into the carbon atoms absorbing at 30.8 ppm and 30.7 ppm, respectively (Figure 5).

Functional characterisation of bacterial diterpene synthase in planta

To test the catalytic activity of HdS in planta, its corresponding gene was transiently expressed in *N. benthamiana*. Since we have shown before that the mitochondria are a suitable subcellular compartment for the heterologous production of terpenes [26], and it is known that one of the multiple GGPP synthases in plants are targeted to the mitochondria [27], we decided to attempt the expression of HdS with mitochondrial targeting (HdS-mit). A construct without targeting signal (HdS; resulting in cytoplasmic localisation) and an empty vector were used as controls. A *p19* construct [28] was co-infiltrated in all treatments to suppress endogenous silencing of *N. benthamiana* upon agroinfiltration. No difference was found by GC–MS in EtOAc extracts of *N. benthamiana* leaves expressing an empty vector or HdS, while the chromatogram of an extract obtained from HdS-mit expressing leaves revealed an additional major compound (Figure 6). This compound (retention time of 21.08 min) was identified as 18-hydroxydolabella-3,7-diene by GC–MS, using the diterpene alcohol obtained by the in vitro incubations of GGPP with HdS as an authentic standard. A preparative scale isolation of **3** from plant leaves expressing HdS-mit yielded 26.2 mg of the pure diterpene alcohol from 100 g of fresh leaves (0.03% of fresh leaf weight). The obtained material was identical to **3** obtained by in vitro incubation of GGPP with recombinant HdS by ^{1}H and ^{13}C NMR spectroscopy.

A compound with the same structure as determined from our experiments for (1*R*,3*E*,7*E*,11*S*,12*S*)-18-hydroxydolabella-3,7-diene (**3**), but with different NMR data, was recently reported from the brown alga *Dilophus spiralis* [29]. In this study, a revision for the previously reported structure of (1*S*,3*E*,7*E*,11*R*,12*S*)-18-hydroxydolabella-3,7-diene (1,11-di-*epi*-**3**) for a compound isolated from the brown alga *Dictyota dichotoma* [30] was suggested (Scheme 2C). The same natural

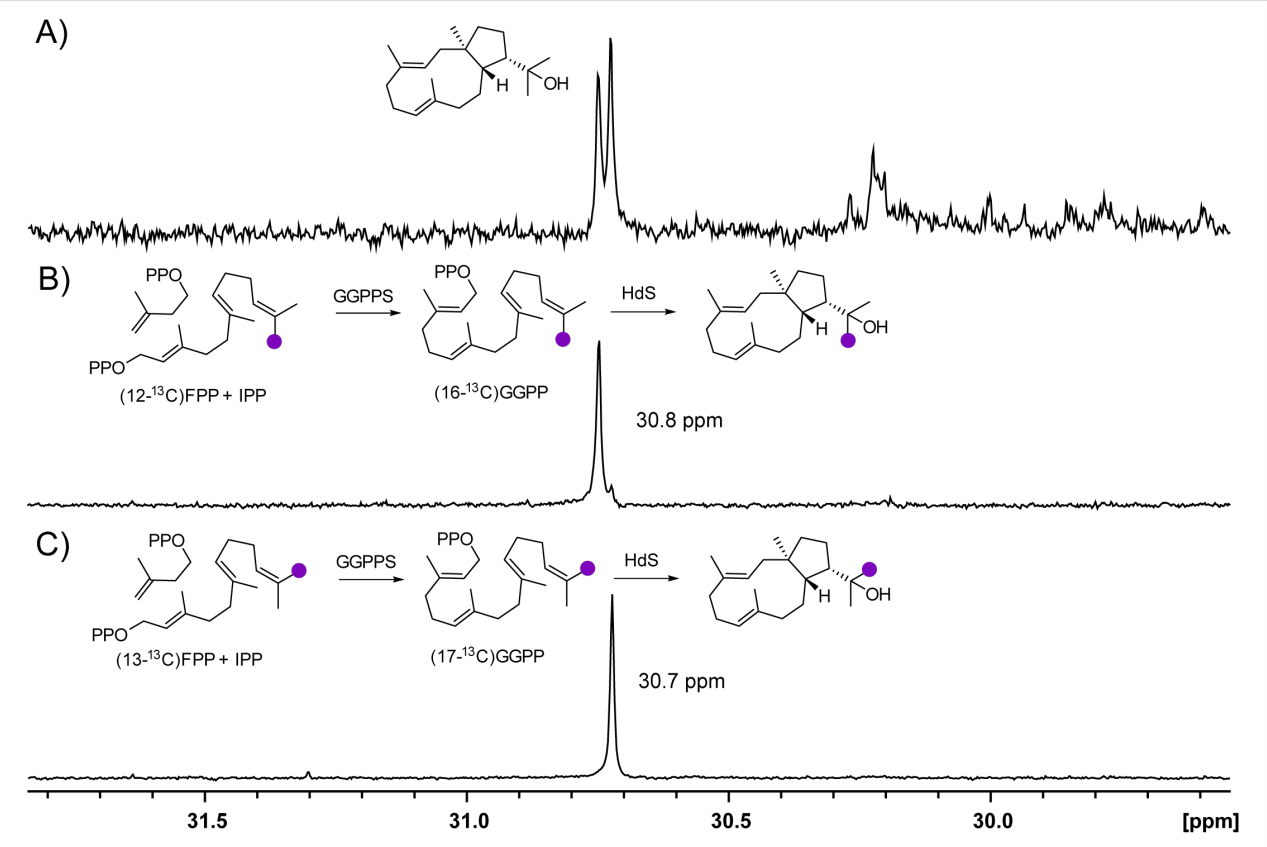

Figure 5: Partial ^{13}C NMR spectra of A) unlabeled **3**, B) ($^{13}C_1$)-**3** arising from incubation of HdS and GGPPS with (12-^{13}C)FPP + IPP, and C) ($^{13}C_1$)-**3** arising from incubation of HdS and GGPPS with (13-^{13}C)FPP + IPP. Labelled carbons are indicated by purple dots.

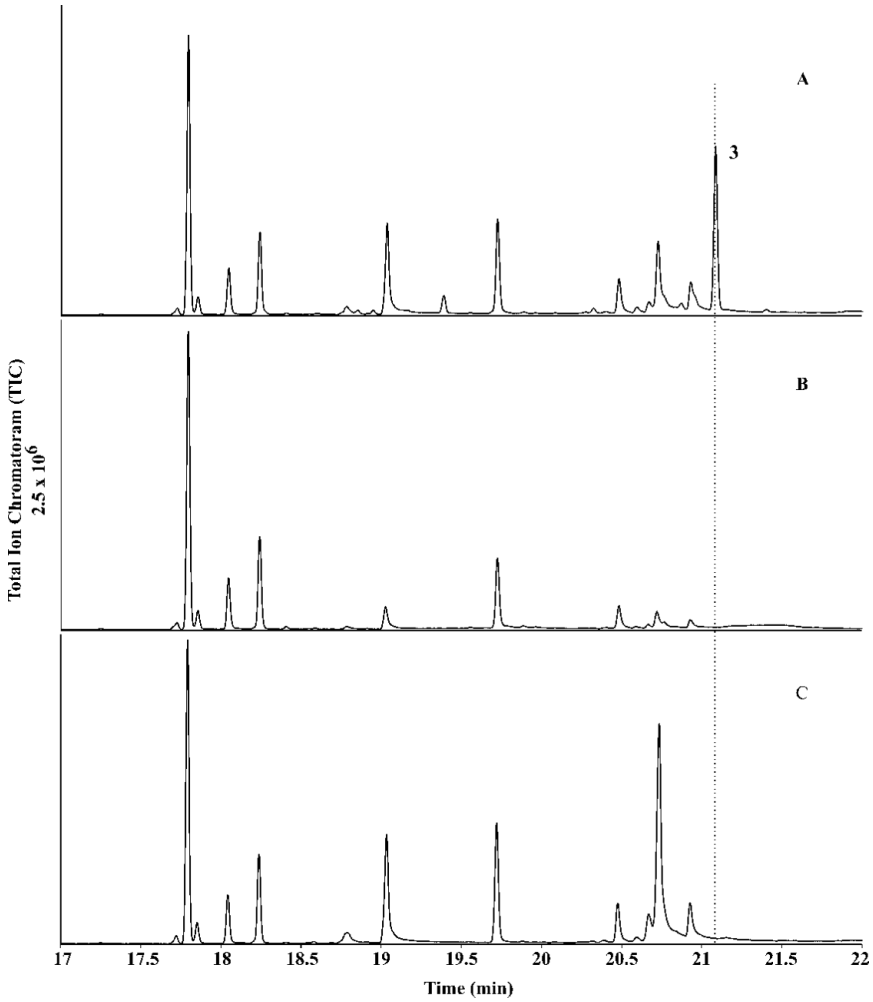

Figure 6: Transient expression of 18-hydroxydolabella-3,7-diene synthase (HdS) in *Nicotiana benthamiana*. Total ion chromatograms of GC–MS analyses of *N. benthamiana* leaf extracts. A) HdS-mit (HdS expressed with mitochondrial targeting signal) showing the production of **3** in planta, B) HdS (expression without targeting signal) and C) empty vector.

product is known from the higher plant *Aglaia odorata* [31], but in this case the reason for the assignment of the reported absolute configuration is unclear, because no optical rotation has been included in this study. It is difficult to judge what the correct structure for the compounds isolated from the brown algae and from *A. odorata* is, but the NMR data and isotopic labelling experiments presented here clearly point to the structure of **3** for the material obtained by us from the diterpene synthase from *C. pinensis*.

Conclusion

In this study we have reinvestigated a terpene synthase from *Chitinophaga pinensis* that was previously characterised as germacrene A synthase by heterologous expression in *E. coli*. While this result could be reproduced during the course of the present study, the recombinant purified enzyme surprisingly only showed diterpene synthase activity (it did not produce any product from GPP nor FPP) and the obtained product was identified as (1*R*,3*E*,7*E*,11*S*,12*S*)-18-hydroxydolabella-3,7-diene. Notably, heterologous expression in the plant *Nicotiana benthamiana* and targeting to the mitochondria resulted in the production of the same diterpene alcohol. Although the mitochondria of *N. benthamiana* also produce FPP [32], again no germacrene D was detected. Taken together, these experiments demonstrate that the expression of one and the same terpene synthase in different organisms may lead to the formation of different products and even an altered substrate specificity. Indeed, it has been shown before that small alterations in the conditions such as a change of the metal cofactor can result in a switch from FPP to GPP synthase activity for an oligoprenyl diphosphate synthase from the beetle *Phaedon cochleariae* [33]. Similar small changes of the conditions, e.g., of the pH or the presence of different metal cofactors, may also change the product profile of a terpene synthase in different heterologous hosts.

Changes in the product profile of terpene synthases depending on the host that was used to express the gene have been reported by Ginglinger et al., who have shown that *Arabidopsis* TPS10 produced mainly linalool when expressed in yeast and *N. benthamiana*, while the *E. coli* expressed protein catalysed the formation of mainly β-myrcene and β-ocimene [34]. The authors suggested different cofactor availabilities and biochemical conditions in the different hosts as the reason for their findings. Also Fischer et al. pointed out the effect that the host can have on the product specificity of terpene synthases [35]. In this context substrate availability is another issue to be considered: While no GGPP synthase is known in *E. coli*, this diterpene precursor is produced in the mitochondria of *N. benthamiana*. The yield of 18-hydroxydolabella-3,7-diene in planta of 26.2 mg per 100 g of fresh leaves is useful for the preparative scale production of the diterpene alcohol that can easily be isolated by extraction and column chromatography, which underpins the potential of plants, besides the recently reviewed microbial hosts for the sustainable production of diterpenes [36], as expression systems for secondary metabolite genes. The function of the investigated terpene synthase from *C. pinensis* in its natural context remains elusive, since neither (1*R*,3*E*,7*E*,11*S*,12*S*)-18-hydroxydolabella-3,7-diene nor germacrene A or its Cope rearrangement product β-elemene could be detected in laboratory cultures [37].

Supporting Information

Supporting Information File 1

Experimental details for gene expression and enzyme incubation experiments, NMR spectra of (1*R*,3*E*,7*E*,11*S*,12*S*)-18-hydroxydolabella-3,7-diene, and heterologous expression in *Nicotiana benthamiana*.
[http://www.beilstein-journals.org/bjoc/content/supplementary/1860-5397-13-171-S1.pdf]

Acknowledgements

This work was funded by the DFG (DI1536/7-1) and by the Fonds der Chemischen Industrie.

References

1. Croteau, R.; Felton, N. M.; Wheeler, C. J. *J. Biol. Chem.* **1985,** *260,* 5956–5962.
2. Cane, D. E.; Swanson, S.; Murthy, P. P. N. *J. Am. Chem. Soc.* **1981,** *103,* 2136–2138. doi:10.1021/ja00398a063
3. Cane, D. E.; Pargellis, C. *Arch. Biochem. Biophys.* **1987,** *254,* 421–429. doi:10.1016/0003-9861(87)90120-2
4. Rabe, P.; Rinkel, J.; Nubbemeyer, B.; Köllner, T. G.; Chen, F.; Dickschat, J. S. *Angew. Chem., Int. Ed.* **2016,** *55,* 15420–15423. doi:10.1002/anie.201608971
5. Chen, X.; Köllner, T. G.; Jia, Q.; Norris, A.; Santhanham, B.; Rabe, P.; Dickschat, J. S.; Shaulsky, G.; Gershenzon, J.; Chen, F. *Proc. Natl. Acad. Sci. U. S. A.* **2016,** *113,* 12132–12137. doi:10.1073/pnas.1610379113
6. Dickschat, J. S. *Nat. Prod. Rep.* **2016,** *33,* 87–110. doi:10.1039/C5NP00102A
7. Rabe, P.; Rinkel, J.; Klapschinski, T. A.; Barra, L.; Dickschat, J. S. *Org. Biomol. Chem.* **2016,** *14,* 158–164. doi:10.1039/C5OB01998B
8. Schifrin, A.; Khatri, Y.; Kirsch, P.; Thiel, V.; Schulz, S.; Bernhardt, R. *Org. Biomol. Chem.* **2016,** *14,* 3385–3393. doi:10.1039/C6OB00130K
9. Klapschinski, T. A.; Rabe, P.; Dickschat, J. S. *Angew. Chem., Int. Ed.* **2016,** *55,* 10141–10144. doi:10.1002/anie.201605425
10. Rabe, P.; Schmitz, T.; Dickschat, J. S. *Beilstein J. Org. Chem.* **2016,** *12,* 1839–1850. doi:10.3762/bjoc.12.173
11. Rinkel, J.; Rabe, P.; Garbeva, P.; Dickschat, J. S. *Angew. Chem., Int. Ed.* **2016,** *55,* 13593–13596. doi:10.1002/anie.201608042
12. Rabe, P.; Rinkel, J.; Dolja, E.; Schmitz, T.; Nubbemeyer, B.; Luu, T. H.; Dickschat, J. S. *Angew. Chem., Int. Ed.* **2017,** *56,* 2776–2779. doi:10.1002/anie.201612439
13. Rabe, P.; Samborskyy, M.; Leadlay, P. F.; Dickschat, J. S. *Org. Biomol. Chem.* **2017,** *15,* 2353–2358. doi:10.1039/C7OB00234C
14. Rinkel, J.; Rabe, P.; Chen, X.; Köllner, T. G.; Chen, F.; Dickschat, J. S. *Chem. – Eur. J.* **2017,** *23,* 10501–10505. doi:10.1002/chem.201702704
15. Yamada, Y.; Kuzuyama, T.; Komatsu, M.; Shin-ya, K.; Omura, S.; Cane, D. E.; Ikeda, H. *Proc. Natl. Acad. Sci. U. S. A.* **2015,** *112,* 857–862. doi:10.1073/pnas.1422108112
16. Yamada, Y.; Arima, S.; Nagamitsu, T.; Johmoto, K.; Uekusa, H.; Eguchi, T.; Shin-ya, K.; Cane, D. E.; Ikeda, H. *J. Antibiot.* **2015,** *68,* 385–394. doi:10.1038/ja.2014.171
17. Rabe, P.; Dickschat, J. S. *Angew. Chem., Int. Ed.* **2013,** *52,* 1810–1812. doi:10.1002/anie.201209103
18. Dickschat, J. S.; Pahirulzaman, K. A. K.; Rabe, P.; Klapschinski, T. A. *ChemBioChem* **2014,** *15,* 810–814. doi:10.1002/cbic.201300763
19. de Kraker, J.-W.; Franssen, M. C. R.; de Groot, A.; König, W. A.; Bouwmeester, H. *J. Plant Physiol.* **1998,** *117,* 1381–1392. doi:10.1104/pp.117.4.1381
20. Cane, D. E.; Oliver, J. S.; Harrison, P. H. M.; Abell, C.; Hubbard, B. R.; Kane, C. T.; Lattman, R. *J. Am. Chem. Soc.* **1990,** *112,* 4513–4524. doi:10.1021/ja00167a059
21. Cane, D. E.; Prabhakaran, P. C.; Salaski, E. J.; Harrison, P. H. M.; Noguchi, H.; Rawlings, B. J. *J. Am. Chem. Soc.* **1989,** *111,* 8914–8916. doi:10.1021/ja00206a022
22. Wang, C.-M.; Hopson, R.; Lin, X.; Cane, D. E. *J. Am. Chem. Soc.* **2009,** *131,* 8360–8361. doi:10.1021/ja9021649
23. Cornforth, J. W.; Cornforth, R. H.; Donninger, C.; Popjak, G. *Proc. R. Soc. London, Ser. B* **1966,** *163,* 492–514. doi:10.1098/rspb.1966.0004
24. Thulasiram, H. V.; Poulter, C. D. *J. Am. Chem. Soc.* **2006,** *128,* 15819–15823. doi:10.1021/ja065573b
25. Rabe, P.; Barra, L.; Rinkel, J.; Riclea, R.; Citron, C. A.; Klapschinski, T. A.; Janusko, A.; Dickschat, J. S. *Angew. Chem., Int. Ed.* **2015,** *54,* 13448–13451. doi:10.1002/anie.201507615
26. Liu, Q.; Majdi, M.; Cankar, K.; Goedbloed, M.; Charnikhova, T.; Verstappen, F. W. A.; de Vos, R. C. H.; Beekwilder, J.; van der Krol, S.; Bouwmeester, H. J. *PLoS One* **2011,** *6,* e23255. doi:10.1371/journal.pone.0023255
27. Okada, K.; Saito, T.; Nakagawa, T.; Kawamukai, M.; Kamiya, Y. *Plant Physiol.* **2000,** *122,* 1045–1056. doi:10.1104/pp.122.4.1045

28. Voinnet, O.; Rivas, S.; Mestre, P.; Baulcombe, D. *Plant J.* **2003,** *33,* 949–956. doi:10.1046/j.1365-313X.2003.01676.x
29. Ioannou, E.; Quesada, A.; Rahman, M. M.; Gibbons, S.; Vagias, C.; Roussis, V. *J. Nat. Prod.* **2011,** *74,* 213–222. doi:10.1021/np1006586
30. Amico, V.; Currenti, R.; Oriente, G.; Piattelli, M.; Tringali, C. *Phytochemistry* **1981,** *20,* 848–849. doi:10.1016/0031-9422(81)85196-5
31. Cai, X.-H.; Luo, X.-D.; Zhou, J.; Hao, X.-J. *Helv. Chim. Acta* **2005,** *88,* 2938–2943. doi:10.1002/hlca.200590236
32. Kappers, I. F.; Aharoni, A.; van Herpen, T. W. J. M.; Luckerhoff, L. L. P.; Dicke, M.; Bouwmeester, H. J. *Science* **2005,** *309,* 2070–2072. doi:10.1126/science.1116232
33. Frick, S.; Nagel, R.; Schmidt, A.; Bodemann, R. R.; Rahfeld, P.; Pauls, G.; Brandt, W.; Gershenzon, J.; Boland, W.; Burse, A. *Proc. Natl. Acad. Sci. U. S. A.* **2013,** *110,* 4194–4199. doi:10.1073/pnas.1221489110
34. Ginglinger, J. F.; Boachon, B.; Höfer, R.; Paetz, C.; Köllner, T. G.; Miesch, L.; Lugan, R.; Baltenweck, R.; Mutterer, J.; Ullmann, P.; Beran, F.; Claudel, P.; Verstappen, F.; Fischer, M. J. C.; Karst, F.; Bouwmeester, H.; Miesch, M.; Schneider, B.; Gershenzon, J.; Ehlting, J.; Werck-Reichhart, D. *Plant Cell* **2013,** *25,* 4640–4657. doi:10.1105/tpc.113.117382
35. Fischer, M. J. C.; Meyer, S.; Claudel, P.; Perrin, M.; Ginglinger, J. F.; Gertz, C.; Masson, J. E.; Werck-Reinhardt, D.; Hugueney, P.; Karst, F. *J. Biotechnol.* **2013,** *163,* 24–29. doi:10.1016/j.jbiotec.2012.10.012
36. Kemper, K.; Hirte, M.; Reinbold, M.; Fuchs, M.; Brück, T. *Beilstein J. Org. Chem.* **2017,** *13,* 845–854. doi:10.3762/bjoc.13.85
37. Citron, C. A.; Gleitzmann, J.; Laurenzano, G.; Pukall, R.; Dickschat, J. S. *ChemBioChem* **2012,** *13,* 202–214. doi:10.1002/cbic.201100641

License and Terms

BEILSTEIN JOURNAL OF ORGANIC CHEMISTRY

Sulfation and amidinohydrolysis in the biosynthesis of giant linear polyenes

Hui Hong, Markiyan Samborskyy, Katsiaryna Usachova, Katharina Schnatz and Peter F. Leadlay*

Full Research Paper

Open Access

Address:
Department of Biochemistry, University of Cambridge, Cambridge CB2 1GA, UK

Email:
Peter F. Leadlay* - pfl10@cam.ac.uk

* Corresponding author

Keywords:
amidinohydrolase; clethramycin; mediomycin; polyketide synthase; sulfotransferase

Beilstein J. Org. Chem. **2017,** *13,* 2408–2415.
doi:10.3762/bjoc.13.238

Received: 02 June 2017
Accepted: 13 October 2017
Published: 13 November 2017

This article is part of the Thematic Series "Lipids: fatty acids and derivatives, polyketides and isoprenoids".

Guest Editor: J. S. Dickschat

Abstract

Clethramycin from *Streptomyces malaysiensis* DSM4137, and mediomycins (produced together with clethramycin from *Streptomyces mediocidicus*), are near-identical giant linear polyenes apparently constructed from, respectively, a 4-guanidinobutanoate or 4-aminobutanoate starter unit and 27 polyketide extender units, and bearing a specific *O*-sulfonate modification at the C-29 hydroxy group. We show here that mediomycins are actually biosynthesised not by use of a different starter unit but by direct late-stage deamidination of (desulfo)clethramycin. A gene (*slf*) encoding a candidate sulfotransferase has been located in both gene clusters. Deletion of this gene in DSM4137 led to accumulation of desulfoclethramycin only, instead of a mixture of desulfoclethramycin and clethramycin. The mediomycin gene cluster does not encode an amidinohydrolase, but when three candidate amidinohydrolase genes from elsewhere in the *S. mediocidicus* genome were individually expressed in *Escherichia coli* and assayed, only one of them (*medi4948*), located 670 kbp away from the mediomycin gene cluster on the chromosome, catalysed the removal of the amidino group from desulfoclethramycin. Subsequent cloning of *medi4948* into DSM4137 caused mediomycins A and B to accumulate at the expense of clethramycin and desulfoclethramycin, respectively, a rare case where an essential biosynthetic gene is not co-located with other pathway genes. Clearly, both desulfoclethramycin and clethramycin are substrates for this amidinohydrolase. Also, purified recombinant sulfotransferase from DSM4137, in the presence of 3'-phosphoadenosine-5'-phosphosulfate as donor, efficiently converted mediomycin B to mediomycin A in vitro. Thus, in the final steps of mediomycin A biosynthesis deamidination and sulfotransfer can take place in either order.

Introduction

Bacterial modular polyketide synthases (PKSs) follow an assembly-line paradigm for enzyme catalysis, in which each round of chain extension requires a different set, or module, of enzymatic activities [1-4]. Among the more remarkable natural products derived by this pathway is the giant linear polyene clethramycin (**1a**, Scheme 1), originally isolated as an anti-

fungal and as an inhibitor of pollen tube outgrowth from a plant-associated *Streptomyces hygroscopicus* strain [5]. Clethramycin (together with desulfoclethramycin (**1b**)) is also a product of the prolific strain *Streptomyces malaysiensis* DSM4137 (formerly *Streptomyces violaceusniger* DSM4137) [6] and it co-occurs with the closely-related antifungal mediomycins A (**1c**) and B (**1d**, Scheme 1) in *Streptomyces mediocidicus* ATCC 23936 [7]. Mediomycins are also produced by *Streptomyces blastmyceticus* [8]. The genes for the assembly-line PKS for mediomycin from *S. blastmyceticus* have been recently reported, encoding a separate extension module for all 27 cycles of chain extension [8]. These systems are attractive targets for knowledge-based engineering to produce novel antifungal compounds. A member of this class of polyketides, tetrafibricin from *Streptomyces neyagawaensis* (Scheme 1), is a potent inhibitor of the fibrinogen receptor, which suggests an even wider potential utility for such compounds [8,9].

We have previously shown that in the biosynthesis of giant macrocyclic antifungal polyketides (so-called marginolactones) compounds bearing a terminal amino moiety are formed by specific final-stage deamidination of a precursor bearing a guanidino substituent at this position [10]. The aim of the present study was to test whether the same "protective group" strategy is operating in the biosynthesis of the giant linear mediomycins. If true, then mediomycin A formation involves quite distinctive late-stage processing: both an *O*-sulfonation step and a deamidination step. *O*-Sulfonation in particular is a rare and interesting modification seen in diverse microbial natural products (Scheme S1, Supporting Information File 1) including the non-glycosylated teicoplanin-related antibacterial A47934 [11], the engineered trisubstituted sulfoteicoplanin aglycone G [12], the echinocandin-like FR901379 [13]; and the sulfated carbapenem MM4550 [14]. A specific amidinohydrolase has been found encoded in the respective biosynthetic gene clusters for the marginolactone antibiotics primycin and desertomycin [10] but not in the reported cluster for mediomycin in *S. blastmyceticus* [8], so the enzyme hypothesised to be responsible for this step in mediomycin biosynthesis has not been identified until now. We present here the characterisation of the *med* biosynthetic gene cluster, the successful identification of a specific

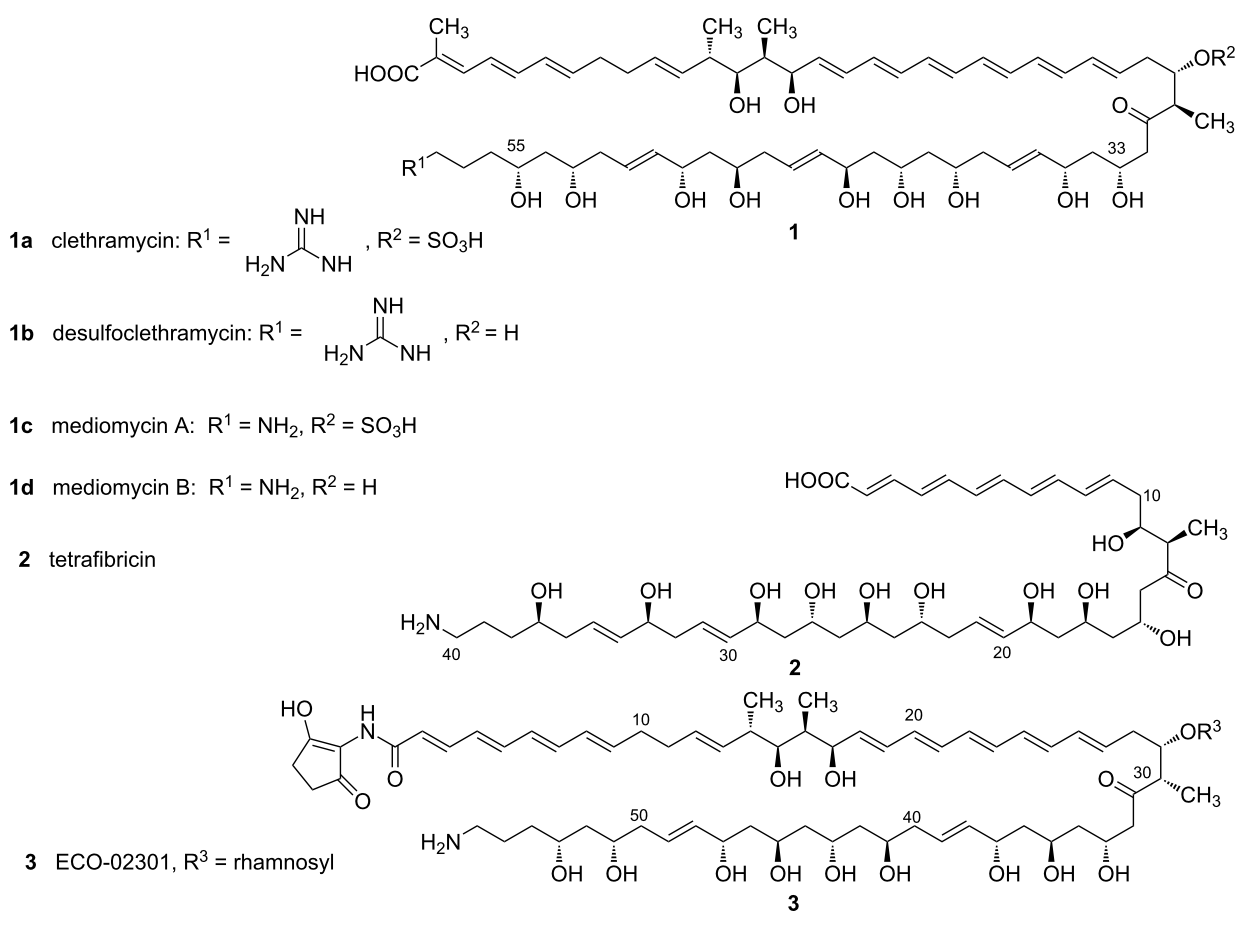

Scheme 1: The structures of clethramycin, mediomycins and related linear polyenes.

mediomycin amidinohydrolase encoded at a location on the genome remote from the *med* cluster, and genetic and biochemical evidence for the respective roles played by these sulfotransferase and amidinohydrolase enzymes in the production of mediomycins.

Results and Discussion

We have previously [10] sequenced the biosynthetic gene cluster for clethramycin from *S. malaysiensis* DSM4137 (*cle*); and we have now also sequenced the cluster for mediomycins A and B from *S. mediocidicus* (*med*), by whole-genome sequencing of the strain. Clethramycin and desulfoclethramycin were not previously known to be produced by *S. malaysiensis* DSM4137, but the identity of these metabolites in cell extracts was readily confirmed by high-resolution mass analysis (Figure S1, Supporting Information File 1). The properties of the genes and proteins in the *med* cluster and *cle* cluster are summarised in Table S4 (Supporting Information File 1). Both gene clusters encode a giant modular PKS housing 27 extension modules, distributed across nine PKS subunits (Scheme 2). This is exactly the number of extension modules predicted on the basis of the known structures of **1a**–**d**. Detailed comparison of our amino acid sequences for the Cle PKS [10] and the Med PKS with the sequence recently reported for the Med PKS of *S. blastmyceticus* [8] showed in each case a high degree of amino acid sequence identity across the entire PKS (≈96% identity) and essentially perfect conservation of sequence in each of the characteristic active site sequence motifs for the ketosynthase (KS), acyltransferase (AT), ketoreductase (KR), dehydratase (DH), and enoylreductase (ER) domains of each of the 27 extension modules, including the newly-recognised YGP motif of active DH domains [8] between the three PKS multienzymes. The stereochemistry of **1a**–**d** shown in Scheme 1 is that predicted from the biosynthetic analysis; and is in full agreement with the experimentally-determined relative configuration of stereocentres in mediomycin [7,8]. The flanking genes are also for the most part near-identical, including a sulfotransferase (*slf*) gene that appears to mark one boundary of the cluster. However, in the *cle* cluster there are additional putative regulatory and export genes, as well as, remarkably, a set of six genes interpolated into the cluster that are predicted to govern lantibiotic biosynthesis (Scheme 2).

The key difference expected between the *cle* and the *med* clusters was the presence of an essential amidinohydrolase gene, encoding an enzyme that would act at a late stage in the pathway to unmask the primary amino group of the mediomycins, as we have previously described for the biosynthesis of aminomarginolactone antibiotics [10]. However, careful scrutiny of the open reading frames flanking the PKS in the *med* biosynthetic gene cluster failed to reveal any whose product could be plausibly construed to be an amidinohydrolase. The reported

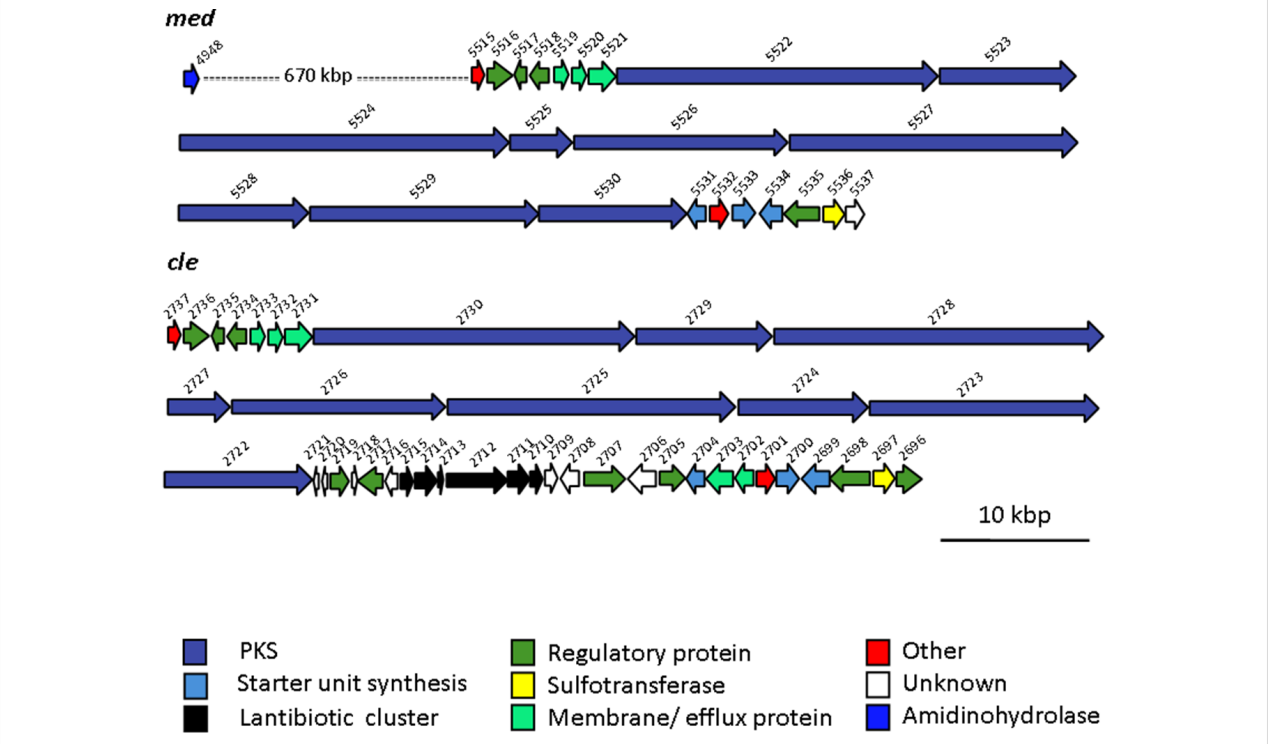

Scheme 2: The biosynthetic gene clusters for mediomycin (*med*) from *Streptomyces mediocidicus* and clethramycin (*cle*) from *S. malaysiensis* DSM4137. The numbers refer to the position of each orf in the genome sequence.

S. blastmyceticus med cluster also lacks the expected amidinohydrolase [8]. We therefore sought to locate the "missing" amidinohydrolase by BLAST analysis [15] of our near-complete genome sequence of *S. mediocidicus* using as a probe the protein sequence of a putative amidinohydrolase (Orf32) from the biosynthetic gene cluster of the linear polyene ECO-02301 (Scheme 1) [16]. The analysis returned two strong matches, Medi4948 (80% identity, 93% similarity) and Medi2865 (82% identity, 92% similarity), both provisionally annotated as agmatinases (the numbers quoted refer to the position of the respective orf in the genome sequence). The next best match was a further agmatinase Medi0234 (41% identity, 57% similarity). Each of these three genes was cloned and expressed in *Escherichia coli* as an *N*-terminally histidine-tagged protein as described in the Experimental section, and purified by chromatography on a Ni-NTA column. The putative amidinohydrolases Medi2865 and Medi0234 were wholly inactive when incubated with desulfoclethramycin (**1b**) purified from DSM4137 extracts, although Medi2865 did show metal-dependent amidinohydrolase activity against 4-guanidinobutyrate to yield 4-aminobutanoate. In contrast, recombinant Medi4948 upon brief incubation gave essentially complete conversion of purified **1b** into mediomycin B (**1d**, see later). The gene encoding this enzyme is located 670 kbp distant from the *med* gene cluster on the *S. mediocidicus* chromosome (Scheme 2), a rare but not unprecedented [17] example of an apparently essential gene being located far from the relevant gene cluster. Because the *S. mediocidicus* strain proved highly resistant to introduction of cloned DNA, we were unable to obtain formal proof that this gene is essential for mediomycin biosynthesis by mutating *medi4948* and seeing accumulation of **1a** and/or **1b**. Instead, we introduced the *medi4948* gene, cloned in expression vector pIB139 [18] into DSM4137. As shown in Figure 1B, in extracts of the culture pellet of this recombinant the normal products of this strain **1a** and **1b** were absent, and replaced by mediomycins **1c** and **1d**, fully consistent with the proposed function of the

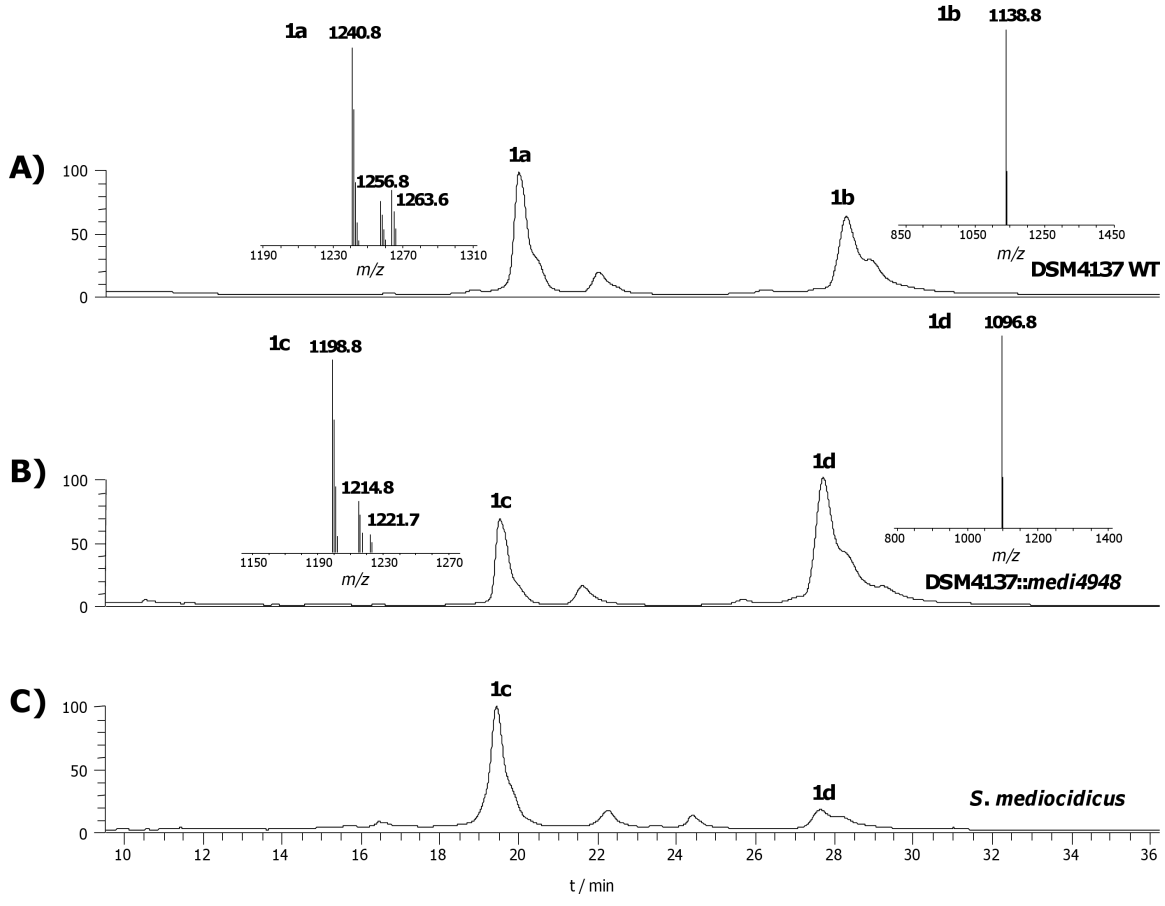

Figure 1: HPLC–UV–MS analysis of polyenes. A) LC–UV (360 nm) trace of mycelium methanol extract from DSM4137 wild type, showing the production of clethramycin (**1a**) and desulfoclethramycin (**1b**) at *m/z* 1240.8 ($[M + Na]^+$) and 1138.8 ($[M + H]^+$) , respectively. B) LC–UV (360 nm) trace of mycelium methanol extract from DSM4137 complemented with amidinohydrolase gene *medi4948* from *S. mediocidicus*, showing clethramycin (**1a**) and desulfoclethramycin (**1b**) are fully converted to the corresponding amino forms, mediomycin A (**1c**) and mediomycin B (**1d**) at *m/z* 1198.8 ($[M + Na]^+$) and 1096.8 ($[M + H]^+$), respectively. C) LC–UV (360 nm) trace of mycelium methanol extract from *S. mediocidicus*, showing the production of mediomycin A (**1c**) and mediomycin B (**1d**).

amidinohydrolase encoded by gene *medi4948*. In contrast, when an authentic amidinohydrolase from the *Streptomyces olivaceus* Tü4018 strain producing the macrocyclic polyene desertomycin [10] was similarly cloned and expressed in *S. malaysiensis* DSM4137, it had no effect on the production of **1a** and **1b** (Figure S6, Supporting Information File 1), implying that these amidinotransferases operating on linear and macrocyclic polyenes do not have overlapping substrate specificities. Sequence alignment of amidinohydrolase Medi4948 with authentic ureohydrolases in the Protein Data Bank (PDB) (Figure S2, Supporting Information File 1) revealed that it contains the sequence motifs xGGDH, DAHxD, and SxDxDxxDPxxxP (where x = any amino acid), which are conserved in this enzyme superfamily and are implicated in cation binding and catalysis [19-22].

Our finding that amidinohydrolase encoded by the *medi4948* gene acts on both desulfoclethramycin (**1b**) and clethramycin (**1a**) in vivo raised the question of whether there is a preferred or even obligatory order of events in the late-stage tailoring of the mediomycins in *S. mediocidicus*. In order to resolve this question we sought to characterise the putative sulfotransferase encoded by the polyene-cluster associated *slf* gene in both *S. malaysiensis* DSM4137 and *S. mediocidicus* (Table S4, Supporting Information File 1). The polyene cluster-associated *slf* gene in *S. malaysiensis* DSM4137 (*smala2697*) was specifically deleted in-frame as described in the Experimental section. The resulting mutant strain, under conditions where the wild type produces both **1a** and **1b**, only produced **1b** (Figure 2B) showing that the *slf* gene is uniquely responsible for the conversion of desulfoclethramycin into clethramycin. Complementation of the mutant was carried out with either a wild type copy of *slf* from DSM4137 (*smala2697*, or its counterpart from *S. mediocidicus* (*medi5536*). In each case, co-production of **1a** was fully restored (Figure 2C and 2D).

These in vivo results together establish that Medi4948 is capable of deprotection of both **1a** and **1b** and that the sulfotransferase SMALA_2697 (or Medi5536) is responsible for converting **1b** into **1a,** as indicated in Scheme 3.

What remained unclear was whether the sulfotransferase is capable of acting on both **1b** and **1d**, which would mean that there are two independent routes to forming mediomycin A. We

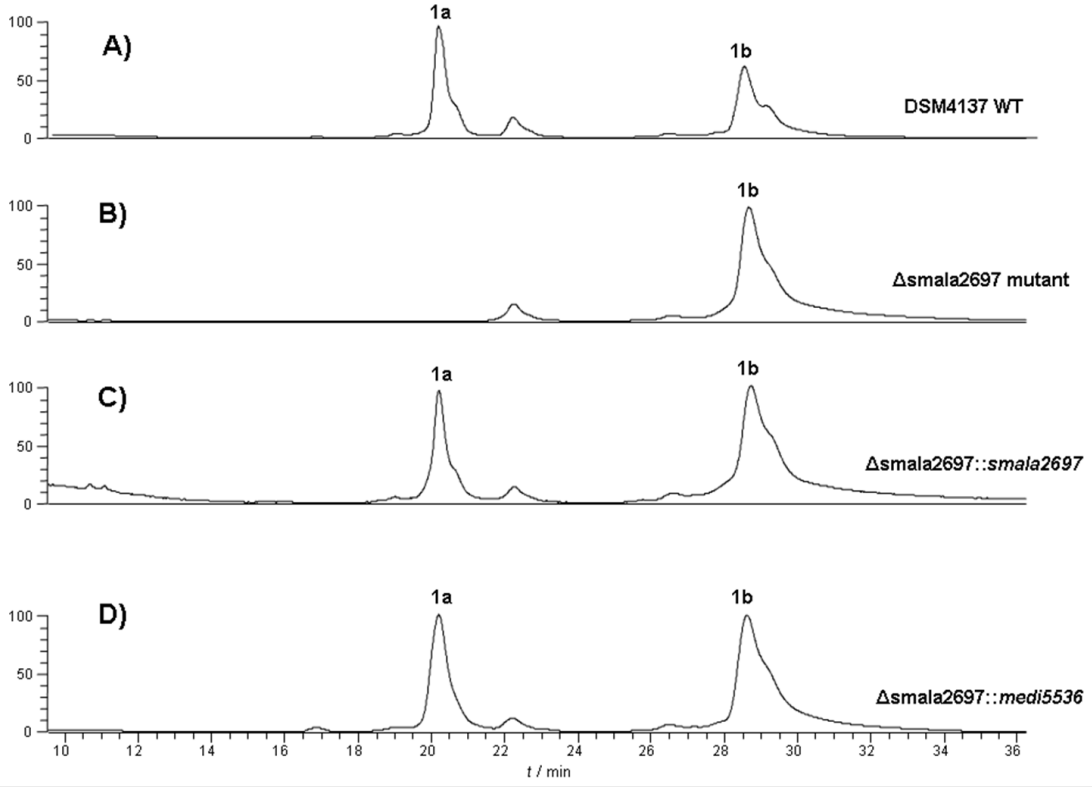

Figure 2: HPLC–UV–MS analysis of polyenes from DSM4137 wild type and mutants. A) LC–UV (360 nm) trace of mycelium methanol extract from DSM4137 wild type, showing the production of clethramycin (**1a**) and desulfoclethramycin (**1b**). B) LC–UV (360 nm) trace of mycelium methanol extract from the Δsmala2697 deletion mutant. In the mutant, production of **1a** was completely abolished. C) LC–UV (360 nm) trace of mycelium methanol extract from the Δsmala2697 deletion mutant complemented with *smala2697* from DSM4137. D) LC–UV (360 nm) trace of mycelium methanol extract from the Δsmala2697 deletion mutant complemented with the polyene cluster-associated *slf* gene (*medi5536*) from *S. mediocidicus*. Both complementations restored the production of sulfonated polyene **1a**.

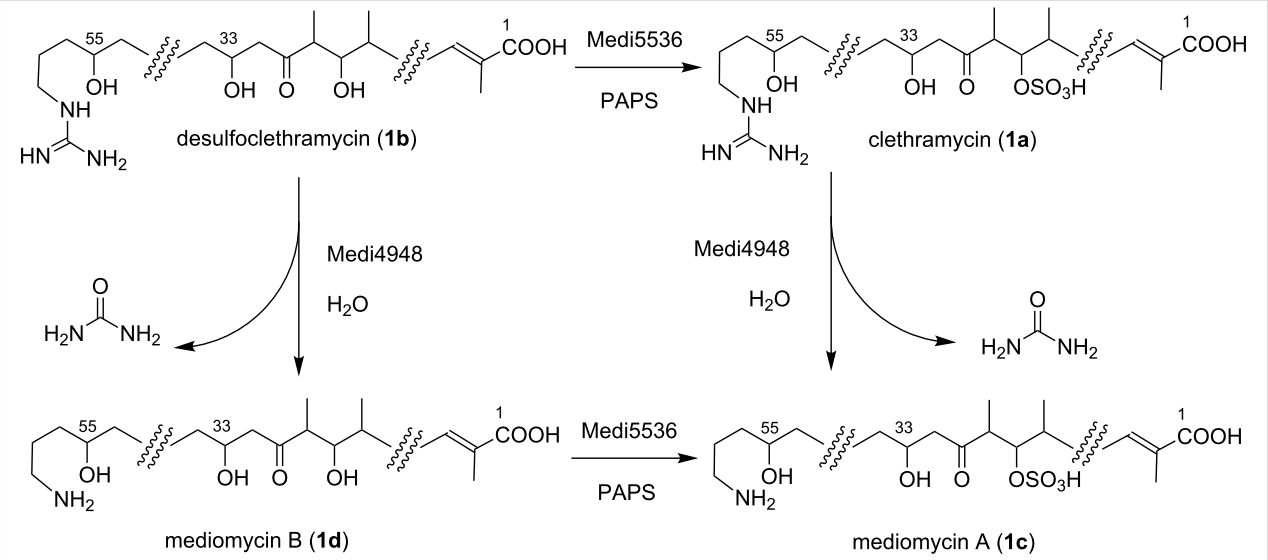

Scheme 3: The parallel pathways for the biosynthesis of mediomycin A.

first confirmed that when purified recombinant Slf from DSM4137 (SMALA_2697) was incubated with **1b**, in the presence of the cofactor 3′-phosphoadenosine-5′-phosphosulfate (PAPS), **1a** was formed (Figure 3C). Then, **1b** was pre-incubated with amidinohydrolase Medi4948, to convert it fully into mediomycin B **1d**, as monitored by HPLC–MS (Figure 3B).

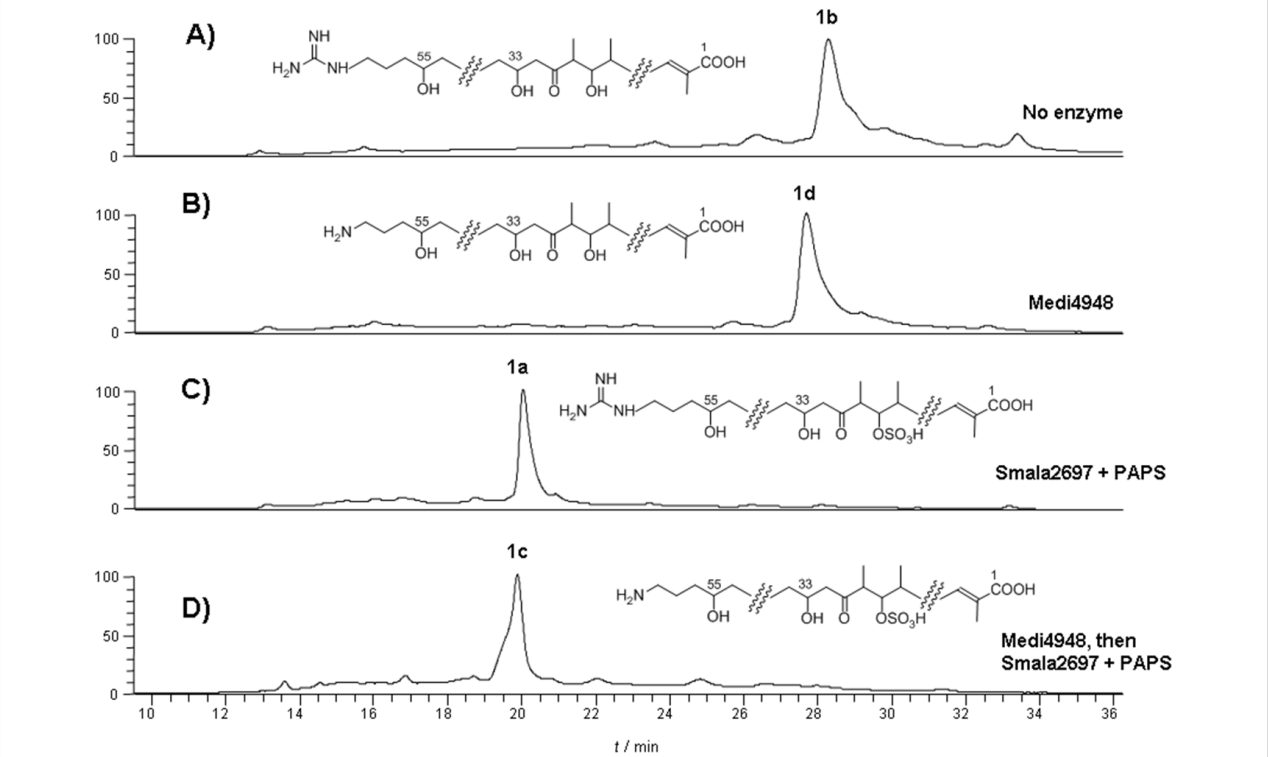

Figure 3: HPLC–UV–MS analysis of in vitro assays with amidinohydrolase Medi4948 and sulfotransferase Slf from *S. malaysiensis* DSM4137 (SMALA_2697). A) LC–UV (360 nm) trace of control assay, where purified **1b** at *m/z* 1138.8 ($[M + H]^+$) was incubated without enzyme. B) LC–UV (360 nm) trace of **1b** incubated with amidinohydrolase Medi4948, showing complete convertion of desulfoclethramycin (**1b**) to its amino form mediomycin B (**1d**) at *m/z* 1096.8 ($[M + H]^+$). C) LC–UV (360 nm) trace of **1b** incubated with sulfotransferase SMALA_2697 and PAPS, showing complete convertion of desulfoclethramycin (**1b**) to its sulfonated form clethramycin (**1a**) at *m/z* 1240.8 ($[M + Na]^+$). D) LC–UV (360 nm) trace of **1b** incubated with amidinohydrolase Medi4948 to generate mediomycin B (**1d**) in situ, followed by addition of sulfotransferase SMALA_2697 and PAPS to convert mediomycin B (**1d**) to mediomycin A (**1c**) at *m/z* 1198.8 ($[M + Na]^+$).

Then, Slf from DSM4137 (SMALA_2697) was added to the reaction mixture together with PAPS. As shown in Figure 3D, **1d** was efficiently converted into **1c** under these conditions. Therefore parallel pathways do exist (Scheme 3) for the formation of mediomycin A (**1c**) from desulfoclethramycin (**1b**), which is the full-length initial product of the assembly-line PKS in both clethramycin and mediomycin biosynthesis. The sulfotransferases from the *cle* and *med* clusters appear essentially identical in their catalytic activity.

The co-location of the *slf* gene with the gigantic 27-extension module PKS of clethramycin or mediomycin suggested that the Slf protein sequence might be a useful probe to uncover further examples of strains producing these or closely-related compounds. BLAST analysis of public databases using the protein sequence of the Slf of DSM4137 as a probe sequence uncovered multiple candidate Slf sequences (see sequence alignment in Figure S3, Supporting Information File 1) all of which bear the conserved sequence motifs for binding of the sulfo-donor PAPS. Some, but by no means all, of the genes for these Slf sequences are indeed co-located with giant PKS genes (these are coloured green) in the phylogenetic tree of Slf sequences presented in Figure S3 (Supporting Information File 1). This analysis shows that *slf* genes associated with remarkable biosynthetic gene clusters harbouring 27-module PKS genes are distributed quite widely among *Streptomyces* strains. Because the mediomycin amidinohydrolase gene is not located anywhere near the *med* biosynthetic gene cluster, it is presently not possible to distinguish with confidence, on sequence comparisons alone, between clethramycin and mediomycin clusters.

Conclusion

The accelerating speed and ever-decreasing cost of sequencing of microbial genomes has spurred our interest in a genome-led approach to the uncovering of novel enzymology in the biosynthetic pathways to antibiotic natural products [23-26]. Here, we have used in-house whole-genome sequencing to characterise the closely-related gene clusters to the sulfated antifungal linear polyenes clethramycin and mediomycin A. Further, it has enabled a successful search for the key amidinohydrolase enzyme required for late-stage deprotection of clethramycins to mediomycins, the gene for which is found 670 kbp distant from the *med* gene cluster. We have also shown that the amidinohydrolase can act either before or after the specific sulfonation step. The sequence of the sulfotransferase is a useful probe to uncover related gene clusters in public sequence databases.

Sulfonation remains a rare and relatively poorly understood modification in natural product biosynthesis [27-30]. As our understanding of their specificity improves, sulfotransferases have been deployed to increase the structural diversity of several classes of natural products [31-33]. The *slf* genes of polyene biosynthesis reported here represent an additional starting point for such natural product diversification. Sulfonation has been suggested as a novel approach to block the development of antibiotic resistance [33,34] while the discovery of the sulfated metabolite FR901379 was a critical breakthrough in the successful clinical development of micafungin to combat systemic fungal infections [12].

Supporting Information

Supporting Information File 1

Experimental part and additional Figures and Schemes.
[http://www.beilstein-journals.org/bjoc/content/supplementary/1860-5397-13-238-S1.pdf]

Acknowledgements

We gratefully acknowledge the joint support, for part of this work, of Syngenta and the Biotechnology and Biological Sciences Research Council (U.K., strategic LoLa award BB/K002341/1). K. U. thanks the Darwin Trust of Edinburgh for a studentship, and the Herchel Smith Chair of Biochemistry Fund for additional support. We thank Shilo Dickens and colleagues (Nextgen Sequencing Facility, Department of Biochemistry, University of Cambridge) for help with genome sequencing, and Professor Kohei Kamiya for useful discussions.

References

1. Staunton, J.; Weissman, K. J. *Nat. Prod. Rep.* **2001,** *18,* 380–416. doi:10.1039/a909079g
2. Fischbach, M. A.; Walsh, C. T. *Chem. Rev.* **2006,** *106,* 3468–3496. doi:10.1021/cr0503097
3. Smith, S.; Tsai, S.-C. *Nat. Prod. Rep.* **2007,** *24,* 1041–1072. doi:10.1039/b603600g
4. Hertweck, C. *Angew. Chem., Int. Ed.* **2009,** *48,* 4688–4716. doi:10.1002/anie.200806121
5. Igarashi, Y.; Iwashita, T.; Fujita, T.; Naoki, H.; Yamakawa, T.; Yoshida, R.; Furumai, T. *J. Antibiot.* **2003,** *56,* 705–708. doi:10.7164/antibiotics.56.705
6. Hong, H.; Fill, T.; Leadlay, P. F. *Angew. Chem., Int. Ed.* **2013,** *52,* 13096–13099. doi:10.1002/anie.201308136
7. Cai, P.; Kong, F.; Fink, P.; Ruppen, M. E.; Williamson, R. T.; Keiko, T. *J. Nat. Prod.* **2007,** *70,* 215–219. doi:10.1021/np060542f
8. Zhang, L.; Hashimoto, T.; Qin, B.; Hashimoto, J.; Kozone, I.; Kawahara, T.; Okada, M.; Awakawa, T.; Ito, T.; Asakawa, Y.; Ueki, M.; Takahashi, S.; Osada, H.; Wakimoto, T.; Ikeda, H.; Shin-ya, K.; Abe, I. *Angew. Chem., Int. Ed.* **2017,** *56,* 1740–1745. doi:10.1002/anie.201611371
9. Kobayashi, Y.; Czechtizky, W.; Kishi, Y. *Org. Lett.* **2003,** *5,* 93–96. doi:10.1021/ol0272895
10. Hong, H.; Samborskyy, M.; Lindner, F.; Leadlay, P. F. *Angew. Chem., Int. Ed.* **2016,** *55,* 1118–11123. doi:10.1002/anie.201509300

11. Pootoolal, J.; Thomas, M. G.; Marshall, C. G.; Neu, J. M.; Hubbard, B. K.; Walsh, C. T.; Wright, G. D. *Proc. Natl. Acad. Sci. U. S. A.* **2002,** *99,* 8962–8967. doi:10.1073/pnas.102285099
12. Banik, J. J.; Brady, S. F. *Proc. Natl. Acad. Sci. U. S. A.* **2008,** *105,* 17273–17277. doi:10.1073/pnas.0807564105
13. Fujie, A. *Pure Appl. Chem.* **2007,** *79,* 603–614. doi:10.1351/pac200779040603
14. Li, R.; Lloyd, E. P.; Moshos, K. A.; Townsend, C. A. *ChemBioChem* **2014,** *15,* 320–331. doi:10.1002/cbic.201300319
15. Altschul, S. F.; Gish, W.; Miller, W.; Myers, E. W.; Lipman, D. J. *J. Mol. Biol.* **1990,** *215,* 403–410. doi:10.1016/S0022-2836(05)80360-2
16. McAlpine, J. B.; Bachmann, B. O.; Piraee, M.; Tremblay, S.; Alarco, A.-M.; Zazopoulos, E.; Farnet, C. M. *J. Nat. Prod.* **2005,** *68,* 493–496. doi:10.1021/np0401664
17. Lazos, O.; Tosin, M.; Slusarczyk, A. L.; Boakes, S.; Cortés, J.; Sidebottom, P. J.; Leadlay, P. F. *Chem. Biol.* **2010,** *17,* 160–173. doi:10.1016/j.chembiol.2010.01.011
18. Wilkinson, C. J.; Hughes-Thomas, Z. A.; Martin, C. J.; Böhm, I.; Mironenko, T.; Deacon, M.; Wheatcroft, M.; Wirtz, G.; Staunton, J.; Leadlay, P. F. *J. Mol. Microbiol. Biotechnol.* **2002,** *4,* 417–426.
19. Elkins, J. M.; Clifton, I. J.; Hernández, H.; Doan, L. X.; Robinson, C. V.; Schofield, C. J.; Hewitson, K. S. *Biochem. J.* **2002,** *366,* 423–434. doi:10.1042/bj20020125
20. Lee, S. J.; Kim, D. J.; Kim, H. S.; Lee, B. I.; Yoon, H.-J.; Yoon, J. Y.; Kim, K. H.; Jang, J. Y.; Im, H. N.; An, D. R.; Song, J.-S.; Kim, H.-J.; Suh, S. W. *J. Struct. Biol.* **2011,** *175,* 329–338. doi:10.1016/j.jsb.2011.05.002
21. D'Antonio, E. L.; Hai, Y.; Christianson, D. W. *Biochemistry* **2012,** *51,* 8399–8409. doi:10.1021/bi301145n
22. Dowling, D. P.; Di Costanzo, L.; Gennadios, H. A.; Christianson, D. W. *Cell. Mol. Life Sci.* **2008,** *65,* 2039–2055. doi:10.1007/s00018-008-7554-z
23. Sun, Y.; Hahn, F.; Demydchuk, Y.; Chettle, J.; Tosin, M.; Osada, H.; Leadlay, P. F. *Nat. Chem. Biol.* **2010,** *6,* 99–101. doi:10.1038/nchembio.285
24. Kanchanabanca, C.; Tao, W.; Hong, H.; Liu, Y.; Hahn, F.; Samborskyy, M.; Deng, Z.; Sun, Y.; Leadlay, P. F. *Angew. Chem., Int. Ed.* **2013,** *52,* 5785–5788. doi:10.1002/anie.201301680
25. Rabe, P.; Samborskyy, M.; Leadlay, P. F.; Dickschat, J. S. *Org. Biomol. Chem.* **2017,** *15,* 2353–2358. doi:10.1039/C7OB00234C
26. Yurkovich, M. E.; Jenkins, R.; Sun, Y.; Tosin, M.; Leadlay, P. F. *Chem. Commun.* **2017,** *53,* 2182–2185. doi:10.1039/C6CC09934C
27. Kaysser, L.; Eitel, K.; Tanino, T.; Siebenberg, S.; Matsuda, A.; Ichikawa, S.; Gust, B. *J. Biol. Chem.* **2010,** *285,* 12684–12694. doi:10.1074/jbc.M109.094490
28. Bick, M. J.; Banik, J. J.; Darst, S. A.; Brady, S. F. *Biochemistry* **2010,** *49,* 4159–4168. doi:10.1021/bi100150v
29. Gu, L.; Wang, B.; Kulkarni, A.; Gehret, J. J.; Lloyd, K. R.; Gerwick, L.; Gerwick, W. H.; Wipf, P.; Håkansson, K.; Smith, J. L.; Sherman, D. H. *J. Am. Chem. Soc.* **2009,** *131,* 16033–16035. doi:10.1021/ja9071578
30. Hossain, M. M.; Moriizumi, Y.; Tanaka, S.; Kimura, M.; Kakuta, Y. *Mol. Cell. Biochem.* **2012,** *361,* 97–104. doi:10.1007/s11010-011-1093-x
31. Lamb, S. S.; Patel, T.; Koteva, K. P.; Wright, G. D. *Chem. Biol.* **2006,** *13,* 171–181. doi:10.1016/j.chembiol.2005.12.003
32. Yan, Y.; Zhang, L.; Ito, T.; Qu, X.; Asakawa, Y.; Awakawa, T.; Abe, I.; Liu, W. *Org. Lett.* **2012,** *14,* 4142–4145. doi:10.1021/ol301785x
33. Thaker, M. N.; Wright, G. D. *ACS Synth. Biol.* **2015,** *4,* 195–206. doi:10.1021/sb300092n
34. Kalan, L.; Perry, J.; Koteva, K.; Thaker, M.; Wright, G. *J. Bacteriol.* **2013,** *195,* 167–171. doi:10.1128/JB.01617-12

License and Terms